

NASA  
CP  
2127  
c.1

NASA Conference Publication 2127

LOAN COPY: RE  
AFWL TECHNICAL  
KIRTLAND AFB,

0099342



TECH LIBRARY KAFB, NM

# 14th Aerospace Mechanisms Symposium

Proceedings of a symposium held at  
NASA Langley Research Center,  
Hampton, Virginia, May 1-2, 1980

**NASA**



**Lockheed**



NASA Conference Publication 2127

# 14th Aerospace Mechanisms Symposium

Proceedings of a symposium sponsored  
by National Aeronautics and Space Administration,  
the California Institute of Technology, and  
Lockheed Missiles and Space Company, Inc.,  
and held at NASA Langley Research Center,  
Hampton, Virginia, May 1-2, 1980

**NASA**

National Aeronautics  
and Space Administration

**Scientific and Technical  
Information Office**

1980



## PREFACE

The proceedings of the 14th Aerospace Mechanisms Symposium held at Langley Research Center on May 1-2, 1980, are in this NASA Conference Publication. The symposium was co-sponsored by the National Aeronautics and Space Administration, the California Institute of Technology, and Lockheed Missiles & Space Company, Inc.

The purpose of the symposium was to provide a forum for the interchange of information among those active in the field of mechanism technology. To that end, 26 papers were presented on aeronautics and space flight, with special emphasis on actuators and aerospace applications for ground systems. The papers were authored by engineers from a broad aerospace spectrum including the U.S. aerospace industry, the university community, NASA, and several European participants.

The efforts of the review committee, session chairmen, and speakers contributing to the technical excellence and professional character of the conference are especially appreciated.

The use of trade names or names of manufacturers in this publication does not constitute an official endorsement of such products or manufacturers, either expressed or implied, by the National Aeronautics and Space Administration.



## ORGANIZING AND REVIEWING COMMITTEE

The papers presented at the symposium were selected and reviewed by the Organizing Committee. Responsibility for content and technical accuracy lies with each respective author. The committee included the following members:

Charles W. Coale: General Chairman, Lockheed Missiles & Space Co., Inc.  
Alfred L. Rinaldo: Operations Chairman, Lockheed Missiles & Space Co., Inc.  
David F. Welch: Executive Co-Chairman, California Institute of Technology  
James H. Parks (ret.): Host Chairman, NASA Langley Research Center  
Tom F. Bonner, Jr.: Technical Program Chairman and Symposium Organizer,  
NASA Langley Research Center  
Paul W. Bomke: Jet Propulsion Laboratory  
Aleck C. Bond: NASA Johnson Space Center  
H. Mervin Briscoe: European Space Technology Center  
Kenneth S. Bush: NASA Langley Research Center  
Kenneth C. Curry: Jet Propulsion Laboratory  
Charles R. Darwin: NASA Marshall Space Flight Center  
David F. Anglebert: NASA Ames Research Center  
Angelo Giovannetti: NASA Ames Research Center  
Harvey H. Horiuchi: Jet Propulsion Laboratory  
Thomas P. Isbell: NASA Marshall Space Flight Center  
Allen J. Louviere: NASA Johnson Space Center  
Frank T. Martin: NASA Goddard Space Flight Center  
Bowden W. Ward: NASA Goddard Space Flight Center



## CONTENTS

PREFACE . . . . .	iii
ORGANIZING AND REVIEWING COMMITTEE . . . . .	v
1. MECHANISMS TO DEPLOY THE TWO-STAGE IUS FROM THE SHUTTLE CARGO BAY . . . . . H. Theron Haynie	1
2. MANNED MANEUVERING UNIT LATCHING MECHANISM . . . . . Charles S. Allton	9
3. ORBITER DOOR CLOSURE TOOLS . . . . . William R. Acres	19
4. ORBITER EMERGENCY CREW ESCAPE SYSTEM . . . . . William W. Lofland	33
5. FLUID CIRCULATING PUMP OPERATED BY SAME INCIDENT SOLAR ENERGY WHICH HEATS ENERGY COLLECTION FLUID . . . . . Earl R. Collins	47
6. THE ECCENTUATOR - A NEW CONCEPT IN ACTUATION . . . . . Robert G. Musgrove	57
7. THE ACTUATED LATCH PIN AND ITS DEVELOPMENT . . . . . Patrick J. Lawlor	69
8. BALL BEARING VERSUS MAGNETIC BEARING REACTION AND MOMENTUM WHEELS AS MOMENTUM ACTUATORS . . . . . W. Auer	79
9. CENTRIFUGAL REGULATOR FOR CONTROL OF DEPLOYMENT RATES OF DEPLOYABLE ELEMENTS . . . . . J. C. Vermalle	93
10. MECHANISMS OF UK RADIOMETERS FLOWN ON NIMBUS 5 AND 6 WITH PARTICULAR REFERENCE TO BEARINGS, PIVOTS AND LUBRICATION . . . . . H. Hadley	101
11. TRIPLE-AXIS COMMON-PIVOT ARM WRIST DEVICE FOR MANIPULATIVE APPLICATIONS . . . . . Leendert Kersten and J. Dwight Johnston	111
12. DESIGN AND DEVELOPMENT OF THE QUAD REDUNDANT SERVOACTUATOR FOR THE SPACE SHUTTLE SOLID ROCKET BOOSTER THRUST VECTOR CONTROL . . . . . James M. Lominick	125
13. A PRECISION BEARING GIMBAL SYSTEM FOR THE TEAL RUBY PROGRAM . . . . . Charles H. Lowry	143

14. FUEL/HYDRAULIC TRANSFER VALVE IMPROVES RELIABILITY OF ATLAS SPACE LAUNCH VEHICLE . . . . .	155
M. Ogman	
15. KU BAND DEPLOYED ASSEMBLY AND GIMBAL . . . . .	163
T. E. Deal	
16. EMERGENCY IN-FLIGHT EGRESS OPENING FOR GENERAL AVIATION AIRCRAFT . .	173
Laurence J. Bement	
17. A SPIN-RECOVERY PARACHUTE SYSTEM FOR LIGHT GENERAL-AVIATION AIRPLANES . . . . .	195
Charles F. Bradshaw	
18. F100 EXHAUST NOZZLE AREA CONTROL MECHANISM . . . . .	211
Joseph R. Kozlin	
19. AIRPLANE WING LEADING EDGE VARIABLE CAMBER FLAP . . . . .	225
James B. Cole	
20. A MECHANICAL ADAPTER FOR INSTALLING MISSION EQUIPMENT ON LARGE SPACE STRUCTURES . . . . .	237
A. LeFever and R. S. Totah	
21. AUTOMATED BEAM BUILDER . . . . .	247
Walter K. Muench	
22. THE MAGSAT MAGNETOMETER BOOM . . . . .	267
James F. Smola, Wade E. Radford, and Marcus H. Reitz	
23. DRAWER DRIVE FOR SPACE SHUTTLE VACUUM CANISTER . . . . .	279
Kenneth E. Werner	
24. DESIGN OF AN ATMOSPHERIC SOUNDING RADIOMETER FOR THE GOES METEOROLOGICAL SATELLITE SYSTEM . . . . .	289
Robert G. Jensen	
25. A POLARIMETER FOR THE HIGH RESOLUTION ULTRAVIOLET SPECTROMETER/POLARIMETER . . . . .	303
John A. Calvert	
26. THE DESIGN AND APPLICATION OF AN ANTENNA POSITIONER MECHANISM FOR INTELSAT-V SERIES COMMUNICATION SATELLITE . . . . .	311
Big Szeto	
27. THE MECHANISMS OF THE SAMS EXPERIMENT FLOWN ON NIMBUS 7 WITH PARTICULAR REFERENCE TO THE 2 AXIS SCANNING MIRROR . . . . .	323
H. Hadley	

# MECHANISMS TO DEPLOY THE TWO-STAGE IUS FROM THE SHUTTLE CARGO BAY<sup>1</sup>

H. Theron Haynie, PE  
Boeing Aerospace Company

## SUMMARY

The Inertial Upper Stage (IUS) is a two-stage or three-stage booster used to transport spacecraft from the space shuttle orbit to synchronous orbit or on an interplanetary trajectory. The mechanisms discussed in this paper were designed specifically to perform the two-stage IUS required functions while contained within the cargo bay of the space shuttle during the boost phase and while in a low Earth orbit. This paper describes the requirements, configuration, and operation of the mechanisms with particular emphasis on the tilt actuator and the mechanism for decoupling the actuators during boost to eliminate redundant load paths.

## INTRODUCTION

The mechanisms required to function during the space shuttle orbiter boost and IUS separation sequence were designed and selected to meet the challenge of remote deployment. The environment is hostile and exceeds the capabilities of many of the materials considered standard in the aircraft industry.

The IUS cradle assembly is the airborne support equipment (ASE), which interfaces between the IUS flight vehicle and the space shuttle orbiter cargo bay. The cradle structure consists of (1) an aft support frame that provides support structure for IUS X, Y, Z, Mx and Mz loads and (2) a forward support frame that provides support for IUS Y and Z loads during boost. A keel pin between the forward frame and the IUS carries the Y loads and may be loaded at deployment due to thermal distortions of the orbiter. The aft frame pivots during deployment to elevate the IUS out of the shuttle cargo bay. All mechanisms are a part of these two major structural elements. Figure 1 shows the space shuttle and its relationship to the IUS cradle assembly.

After orbit has been achieved, the forward frame latches are opened to allow the aft frame tilt actuators (AFTA) to erect the IUS and its payload to a checkout position and, finally, the separation position. The Super\*Zip<sup>2</sup> linear explosive fractures the support structure, allowing self-deployment spring assemblies to eject the IUS and its payload at a velocity that is adequate to obtain a safe separation distance before firing the IUS first-stage boost motor.

<sup>1</sup>Work performed on contract F04701-78-C-0040, HQ. Space Division (AFSC).

<sup>2</sup>Lockheed Missiles and Space Company.

## DESIGN REQUIREMENTS

All mechanisms share certain general requirements relative to the space environment, such as the following:

- a. Complete 100 flights and last for 10 years.
- b. Operate in zero gravity.
- c. Survive temperatures as low as  $-84^{\circ}\text{C}$  ( $-120^{\circ}\text{F}$ ).
- d. Have an operating temperature range of  $-23^{\circ}\text{C}$  to  $+52^{\circ}\text{C}$  ( $-10^{\circ}\text{F}$  to  $+125^{\circ}\text{F}$ ).
- e. Provide redundancy for any operating mechanism.
- f. Be contained within the allowable payload dynamic envelope.
- g. Use materials and finishes that will not outgas.

Tilt system specific design requirements are:

- a. Rotate the aft frame at an angular rate of  $12 \pm 6$  degrees per minute.
- b. Elevate the IUS to  $29^{\circ}$  for checkout and to  $58^{\circ}$  for separation.
- c. Provide the capability to elevate the IUS to  $90^{\circ}$ .
- d. Retract the aft frame to the stowed position with the IUS attached.
- e. Retract the aft frame to the landing lock position ( $-6^{\circ}$ ) without the IUS attached.
- f. Provide redundant drive systems.
- g. No intentional load paths during boost.
- h. Decouple a failed drive system.

## AFT FRAME TILT ACTUATOR

Rotation of the IUS about the trunnion in the aft support frame is powered by the aft frame tilt actuator (AFTA), an electrically driven jack screw. The design is similar to the thrust vector control actuator described in reference 1. The power is provided by a reversible rare-Earth dc torque motor and tachometer mounted directly to a recirculating ball nut. The controller electronics are mounted on the aft support frame. The operation performance characteristics and the actuator assembly are shown in figure 2.

The lower curve of the performance diagram describes the worst case resistance torques. These include trunnion friction, electrical cable bending between the shuttle and the aft frame, IUS keel pin friction and two umbilical plug lanyards. The curve shows a margin in excess of 1 as required by specification DOD-A-83577A(USAF). Cable bending loads and umbilical plug forces have been verified in full scale development tests. Keel pin friction test results are shown in table 1 and cable bending loads are shown in table 2.

The AFTA system consists of the jackscrew, motor, tachometer, potentiometer, and electronic control assembly. The hollow machined screw is 98.8 cm (38.9 in) long and is supported on both ends by guide bushings. The ball nut is supported to the housing by a combination radial and thrust ball bearings. Position control for power off mission functions is provided by two meshing lock gears that mesh with a gear integral with the ball nut. With solenoids unpowered, return springs inside the solenoids hold the lock gears in mesh with the ball nut gear. When energized, the solenoids withdraw two gears from the ball nut gear, allowing the torque motor to drive. The locking gears operate independently and will perform their lock-unlock function even if one solenoid fails to operate.

The lead of the ball screw is .254 cm (0.10 in) and the normal rotational rate of the ball nut is 18 r/min. A linear potentiometer and wiper provide position information and switch signals to the controller. A tachometer provides the rate data to the controller. The rod end of the actuator connects to a slip-ring assembly mounted on the aft frame.

### SLIP RING

The slip ring shown coupled to the AFTA in figure 3 provides the means to decouple the AFTA during boost. The requirement results from the two-stage aft frame mounting to the shuttle cargo bay longerons. A 1.83 m (6 ft) long spreader spring supports each end of the aft frame. Deflections of the spring would create a load path through the AFTA if coupled during boost or landing.

An engage pin mounted within the aft frame structure is spring loaded and offset from the mating hole in the slip ring. As the spreader spring deflects under IUS oscillations in boost, the engage pin moves along the slip ring approaching but never entering the engage hole. A redundant load path through the tilt actuator is avoided.

Engagement of the actuator and slip ring to the aft frame to erect for launch of the IUS is accomplished when the actuator is extended until the mating hole is aligned with the engage pin. A signal at the crew station confirms engagement.

The tilt actuator and slip-ring system is completely redundant. The primary AFTA is located on the right-hand side of the shuttle with the alternate system located on the left side on the opposite end of the aft support frame. During operation of the primary actuator, the alternate system engage pin slides along the alternate slip ring, never aligning with the engage hole. A

failure of the primary actuator system stops the erection cycle and will require the astronaut to remotely extend the alternate actuator until the alternate engage pin enters the slip ring hole. At that time, the pin puller of the primary system is fired, using two NSI cartridges to release the primary actuator from the aft frame. A spring cartridge rotates the primary actuator out of engagement to prevent any physical interference as the aft frame rotates back to lock for landing.

#### KEEL PIN EXTRACTOR SPRING

During the erection cycle of the IUS from the shuttle, the keel pin at the forward frame to IUS interface must be withdrawn. This is normally a simple matter unless the shuttle has assumed a distorted shape because of differential heating of the two sides of the cargo bay. The resulting Y loads on the keel pin could overload the tilt actuator since this friction is applied at a moment arm of about 3.35 m (11 ft) from the aft frame pivot.

The keel pin is shown in figure 3. The pin is machined from 4330M steel and chrome plated. The IUS keel pin socket is machined from 6Al-4V titanium and coated with Vitrolube<sup>2</sup> dry film lubricant. Selection of this material combination was made after completion of a simulated keel pin friction test summarized on table 1. The test objective was to find materials with a consistent coefficient of friction of less than 0.1 at very low loads. The objective was not met which resulted in a decision to design a spring assist system to ensure successful keel pin extraction under the worst expected keel pin side loads. The spring has 4 coils rated at 445 N each (100 lbf). In terms of aft frame rotation moment applied at an arm of 3.35 m, we have 5330 N·m (47174 lbf·in). This moment will overcome a keel pin initial side load of 4450 N (1000 lbf) with a margin of 1 if the coefficient of friction is 0.2 or less. The keel pin is disengaged after 2.3 cm (0.90 in) of travel. The spring leaves the IUS after about 3 cm of travel and is not reactivated throughout the remainder of the mission.

#### DEPLOYMENT SYSTEM DESCRIPTION

The block diagram and time line of figure 4 is a schematic description of the system. The power control panel is mounted in the shuttle crew station and contains all control switching except the payload retention latch actuator (PRLA) which remains on the shuttle A6 panel. The power control unit and the two AFTA controllers are located on the ASE cradle aft support frame.

In a typical mission after the space shuttle is in orbit, the flight crew orients the shuttle and opens the cargo bay doors. The primary AFTA is extended until the slip ring engage pin enters its mating hole and signals engagement. The latches on the forward support frame are opened and the IUS spacecraft is elevated to an angle of 29 degrees for completion of the spacecraft electrical

<sup>2</sup>National Process Industries

checkout through the IUS-to-shuttle umbilical cables. After verification of spacecraft flight readiness, the crew disconnects the umbilical plugs and the umbilical cable tray moves away from the IUS for deployment clearance.

The AFTA is again extended to an IUS-spacecraft angle of 58 degrees with the space shuttle center, the Super\*Zip is fired, the IUS separates structurally from the aft support frame, and the separation springs provide the impulse to separate the IUS from the space shuttle.

Once separated, the AFTA is retracted to return the aft support frame to its original position plus 6 degrees to engage landing locking pins and to capture the umbilical boom to a latch located on the forward support frame. The pin puller is fired to disengage the AFTA and eliminate a redundant load path. The payload bay doors are closed for reentry or repositioning of the space shuttle for operation with other payloads.

The tilt mechanism system contains built-in redundancy by providing two actuators, two controllers, two power supplies, two switching systems, and two slip ring mechanisms.

#### CONCLUDING REMARKS

The AFTA and slip ring mechanisms meet the established design requirements for operation in a near Earth orbit.

A test program is planned to gain confidence that the system will successfully perform as required. The IUS and aft support frame will be statically balanced about a single tree and sling support. A counterweight will exactly balance the test article. During the rotation test, measurements will be made to verify that the required drive margins are present.

#### REFERENCES

1. G. E. Conner: IUS Thrust Vector Control (TVC) Servo System, 13th Aerospace Mechanisms Symposium, NASA CP-2081, 1979.

TABLE 1.- KEEL PIN FRICTION TEST

MATERIAL/FINISH (TEST CONDUCTED AT ROOM TEMPERATURE)	LOAD, N	DYNAMIC* FRICTION COEFFICIENT
TITANIUM/CANADIZE AGAINST 4130 STL/CHROME	1333	.29
	2000	.31
	2667	—
TITANIUM/VITROLUBE AGAINST 15-5 PH/VITROLUBE	1300	.16
	2000	.15
	2667	.17
TITANIUM/VITROLUBE AGAINST 4130 STL/CHROME (SELECTED)	1300	.14
	2000	.14
	2667	.15
TITANIUM/EVERLUBE 620 AGAINST 4130 STL/CHROME	1300	.22
	2000	.24
	2667	.28
TITANIUM/PLASMA SPRAYED Cr <sub>2</sub> O <sub>2</sub> AND EVERLUBE 620 AGAINST 4130 STL/CHROME	1300	.19
	2000	.23
	2667	.23

\* CONSTANT VELOCITY OF .38 cm/sec.

TABLE 2.- ELECTRICAL CABLE TORQUE TESTS

ANGLE	UMBILICAL CABLE IN BENDING (90° TO 0°)		UMBILICAL CABLE IN TORSION	
	*TORQUE (21°C), N·m	TORQUE (-51°C), N·m	TORQUE (21°C), N·m	TORQUE (-51°C), N·m
22.5°	1.7	4.1	1.4	3.8
45°	1.4	3.6	1.4	5.0
67.5°	2.6	3.3	3.1	6.2
90°	1.9	3.3	3.1	6.2
POWER AND CONTROL CABLE BENDING				
ANGLE	TORQUE (21°C)*, N·m	TORQUE (-51°C)*, N·m	TORQUE (21°C)▲, N·m	TORQUE (-51°C)▲, N·m
0°	-6.8	-1.4	17.6	15.6
30°	1.4	19.0	7.5	5.4
60°	3.4	20.3	4.2	3.4
90°	12.9	29.8	12.9	1.4

● ERECT CYCLE 0° TO 90°

▲ RESTOW CYCLE 90° - 0°

\*1 N·m = .73756 lbf·ft

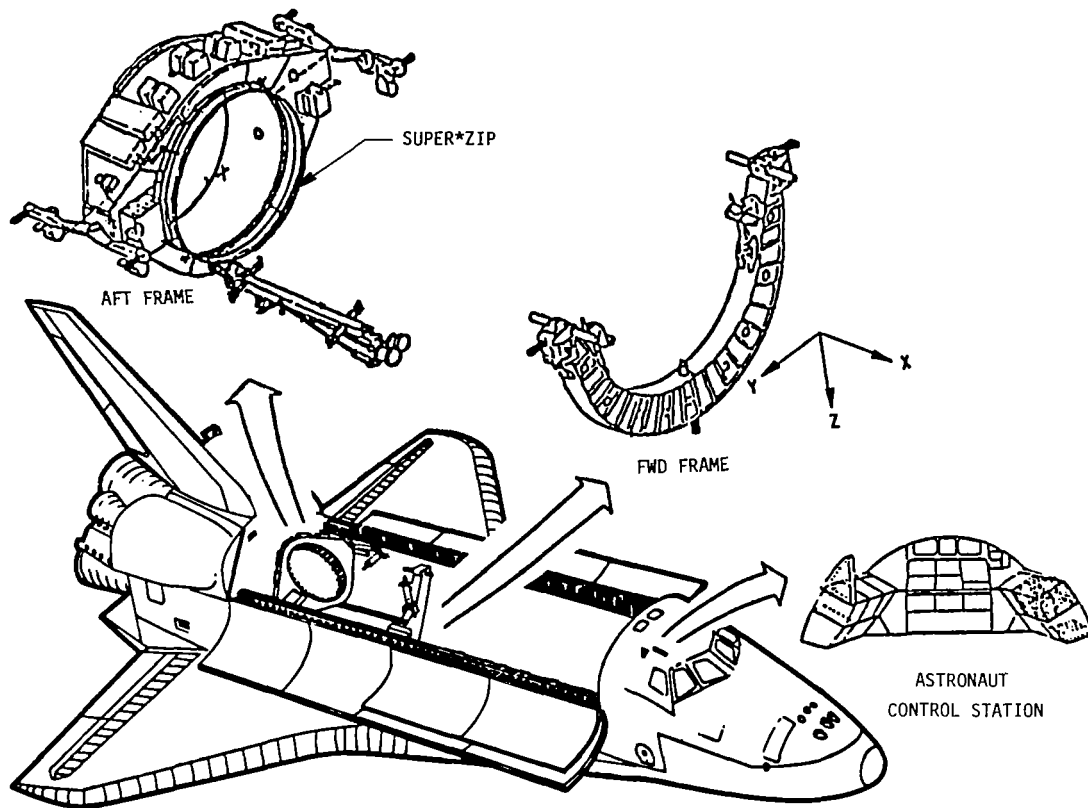


Figure 1.- IUS airborne support equipment.

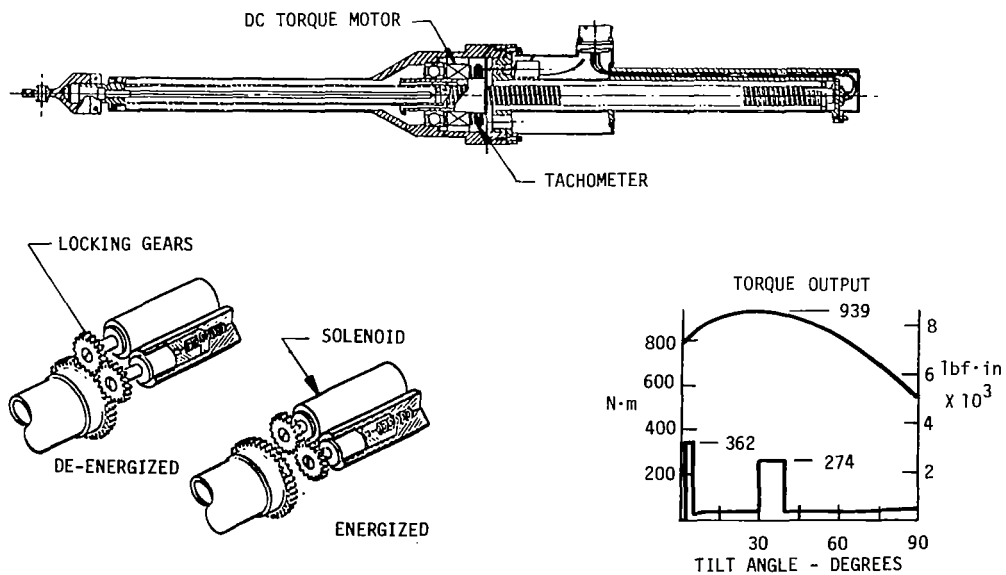


Figure 2.- Tilt actuator and performance characteristics.

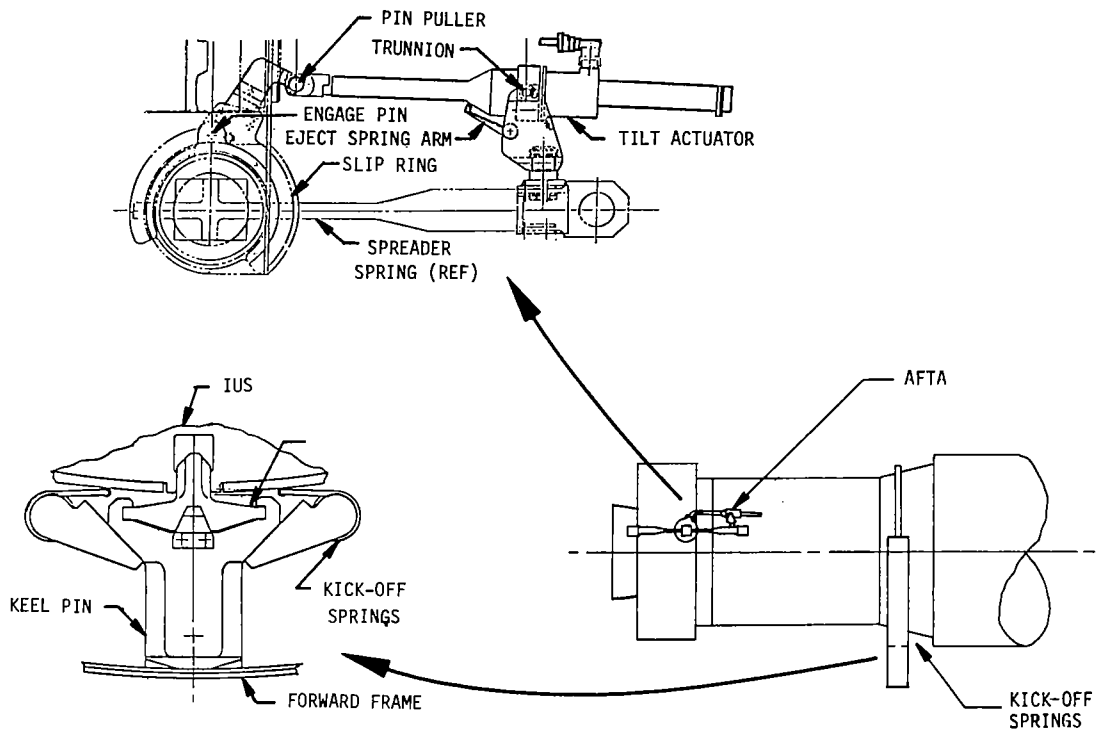


Figure 3.- Tilt mechanisms.

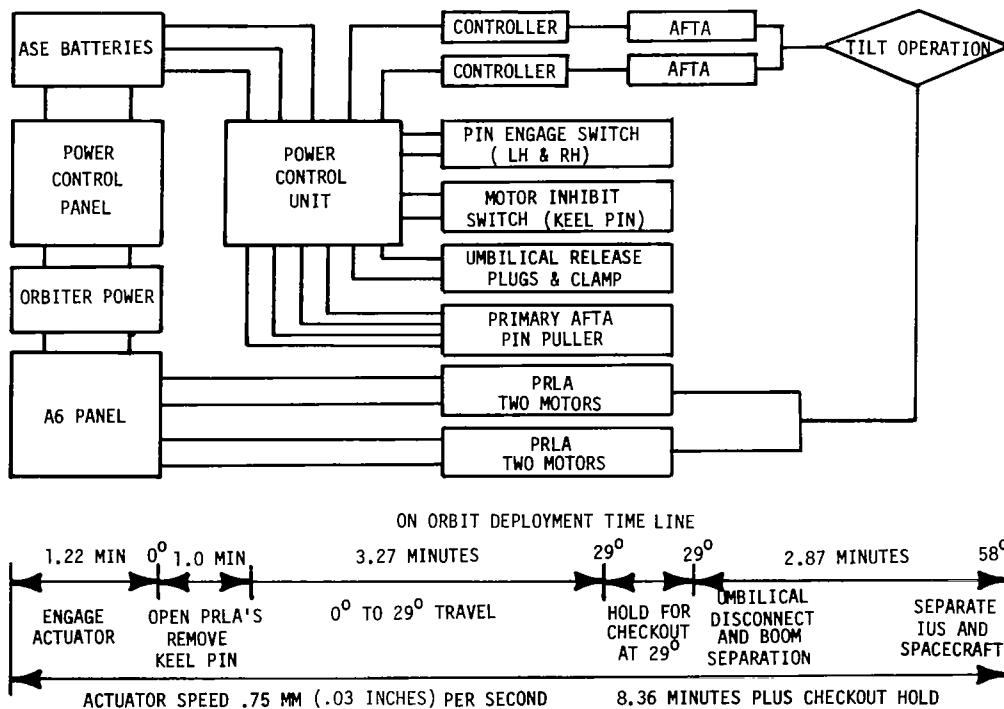


Figure 4.- Block diagram and time line description of deployment system.

## MANNED MANEUVERING UNIT LATCHING MECHANISM\*

Charles S. Allton  
NASA Johnson Space Center

### INTRODUCTION

The Manned Maneuvering Unit (MMU) is a thruster type propulsion device which is being developed to provide maneuvering capability for an astronaut in the near vicinity of the Shuttle spacecraft. The device is worn on the astronaut's back just behind the Portable Life Support System (PLSS) backpack as shown in figure 1. The MMU can propel the wearer in any of three translational directions (fore and aft, left and right, and up and down) and any of three rotational directions (pitch, roll, and yaw). With this maneuverability, an astronaut can move away from the spacecraft beyond the reach of short tethers without relying on unmanageably long lifelines. This freedom will permit carrying out numerous tasks such as rendezvous and inspection of orbiting satellites as depicted in figure 2.

Such tasks will be feasible only if the MMU can demonstrate an acceptable degree of safety and reliability in performing its missions. But even more critical than reliability during a mission is the ability to remove the MMU when the mission is over. This is due to the fact that the spacecraft hatches are not large enough for an astronaut to pass through while wearing the MMU. The attachment latching mechanism must release with failsafe reliability so that re-entry to the spacecraft can be accomplished when breathing air in the PLSS is expended.

In addition to the demanding requirement to both retain and release the MMU with failsafe reliability, the latching mechanism is required to perform its function under adverse environmental conditions. Temperature ranges encountered in orbit force the mechanism to accept dimensional variations due to differential expansion at all MMU/PLSS interfaces. Thermal differences also necessitate some control of heat transfer rates through the interface points. The hard vacuum of space permits cold welding or increased adhesion of parts in contact. Vibration and impact during operation tend to wedge clamping parts more tightly together. In addition, the astronaut is confined to a restrictive space suit which limits hand and arm movements and field of vision.

### DESCRIPTION OF LATCHING MECHANISM

The latching mechanism which has been developed to overcome the difficulties described above is a spring-loaded cam segment with a variable ratio pulley and cable release. The spring-loaded cam segment is functionally similar to an

\*A portion of this work - the release actuator - was performed under contract to Pan American by Mr. Sonne L. Hooper.

ordinary household door latch. As shown in figure 3, it is mounted in the MMU and retracts against a torsion spring when a striker plate on the PLSS moves past. As the PLSS approaches its proper position, the contact surface of the segment rotates into the striker plate until contact is made, locking the PLSS in place. Since the contact surface of the segment is cammed, some variation in relative position of striker plate and segment is allowed. This permits reasonable tolerances in the manufacture of both PLSS and MMU while still providing the needed rigidity between the two units when they are connected. The take-up characteristic of the cam surface is important in maintaining complete interchangeability among all PLSS units and all MMU units.

The striker plate, detailed in figure 4, is a hardened rectangular block with an open-ended slot facing forward. One striker plate is mounted in each side of the PLSS in a recess in the side face. The contact surface is machined at the appropriate angle to make contact with the cam segment contact surface. The striker plate/cam segment interface functions as a retention mechanism to prevent relative motion of the PLSS in a forward direction and in the side-to-side and up-and-down directions. The PLSS is seated against an MMU surface at its back face so that the striker plate does not have to provide retention of the PLSS for backward movement.

The release actuator consists of a variable ratio pulley connected by a cable to the cam segment. The variable ratio feature is achieved by bolting together two separate pulleys, each of which has a cammed drum surface as shown in figure 5. The pulley ratios are such that an approximate five-to-one mechanical advantage exists at the beginning of the release action to give the astronaut extra force for disengaging the cam segment in case it is jammed. When the initial friction has been overcome and fast rotation of the cam segment is desired, the variable ratio decreases smoothly until it reaches approximately one-to-one. This provides more travel of the cam segment for each increment of actuation motion. The configuration at the beginning and end of the release motion is shown schematically in figure 6. It can be seen that the tangent point of the cable on the driver cam is at a distance  $r_1$  from the center and that this distance is roughly five times the distance  $r_2$  of the tangent point of the cable on the driven cam at the beginning of rotation. At the end of the rotation, distances  $r_1$  and  $r_2$  are approximately equal.

Figure 7 shows the complete latching mechanism with cam segment and variable ratio pulley. Also shown are the small pulley, the tensioner link, and the pull ring which actuates the release. The small pulley located near the cam segment serves only to turn the cable. The tensioner link located between the small pulley and the cam segment permits the cam segment to be depressed without loss of tension on the retraction cable. The tensioner link has its own torsion spring so that its motion is independent of the cam segment. The retraction cable is connected directly to the tensioner link, not the cam segment. The cam segment can rotate back through the tensioner link without moving it but when the tensioner link is retracted by the retraction cable it pulls the cam segment along with it. This is significant when the PLSS is in the process of entering the MMU. At that time, the cam segment can be depressed back out of the way without creating slack loops in the retraction cable.

The pull ring located near the variable ratio pulley is sized to receive the astronaut's gloved finger. A ramped relief pocket behind the pull ring provides a guided clearance surface for easier access and also permits the pull ring to be partially recessed to minimize inadvertent snagging. The back side of the pull ring is attached to two pull cables which maintain the horizontal alignment of the ring when it returns to its seated position. To receive the two pull cables, two driver pulleys are used on the variable ratio pulley rather than one. However, only one driven pulley is required. The variable ratio pulley is spring loaded by a torsion spring so that the pull ring returns to its seated position.

A complete latching mechanism with all the above described components is installed on each side of the MMU. Both mechanisms must be engaged to secure the MMU for operations and both segments would normally be disengaged to release the MMU. If one mechanism should jam or fail in any way to release, the astronaut can still remove the MMU by releasing only one mechanism and rolling out of the MMU in a side-to-side rotation, bypassing the jammed latch.

This rollout option is only one of several design precautions taken to reduce the risk or the consequences of a possible jam at the cam segment/striker plate interface. Other precautions include the variable ratio pulley release actuator, hard spring bearing points, and a nonstandard set of material selection criteria. The variable ratio pulley, described earlier, attempts to mechanically overcome a jam after it occurs. Hard spring bearing points are mounted in the MMU where the back side of the PLSS makes contact. These bearing points remain stationary under normal clamping loads, but yield slightly if a maximum established load is reached due to thermal expansion or vibration. This yielding effectively limits the buildup of forces at the cam segment/striker plate interface. Material selection was carried out with the objective of precluding excessive adhesion or cold welding of the cam segment to the striker plate.

#### MATERIAL SELECTION

Adhesion or cold welding is a concern since the cam segment and striker plate are in direct contact with each other, loaded with a substantial clamping force, and required to separate by tangential sliding. Candidate materials were chosen which were expected to have some resistance to cold welding. The susceptibility to cold welding is determined by such parameters as hardness, melting point, shear strength, effect of coatings and corrosion films, effect of alloying elements, response to load, and response to contact duration. Once the candidate materials were selected, they were subjected to friction testing in various combinations. Friction testing was necessary since a high coefficient of friction between cam segment and striker plate would constitute an adhesion problem.

Results of the friction testing are charted on figure 8 where coefficients of friction are plotted for eight materials in sixty-four combinations. Each combination consists of a pair of materials, one of which would be used for the cam segment and the other for the striker plate. As the graph shows, coefficients ranged from 0.18 to 0.47. The higher values were undesirable because

they would result in higher forces required to disengage the cam segment. Extremely low values, however, were also undesirable since coefficients approaching 0.10 would result in a tendency for the cam segment to slip out of the latched position. This slippage would be due to a small tangential component of the clamping force which occurs on a ramped surface. A certain amount of surface friction is necessary to hold the cam segment in place. Friction coefficients within the range 0.18 to 0.20 were considered ideal and, as can be seen from the graph, 15 pairs of materials fell within the ideal range.

To further narrow the field of candidate pairs of materials, other design considerations were used in addition to the adhesion or friction characteristics. These considerations included thermal conductivity, weight, machinability, cost, and wear. Of these factors, only thermal conductivity proved to have any real influence - this due to a concern over thermal leakage between the MMU and the PLSS. Other interface points are insulated to some extent, but the cam segment/striker plate contact surface has to be metal-to-metal contact. A low thermal conductivity for at least one member of the pair is an advantage in reducing thermal leakage problems. Of the candidate materials, titanium had a significantly lower conductivity and the friction testing showed that, used as striker plate material, titanium was a member of several pairs in the ideal range. The cam segment material, stainless steel 17-4 PH, was selected based on factors enhancing the resistance to cold welding.

#### OBLIQUE ENTRY WEDGING PROBLEM

Although no instances of cold welding, adhesion or friction have occurred as yet, a wedging problem was recognized early in the development of the cam segment. As illustrated in figure 9, an oblique entry into the MMU can result in only one cam segment engaging at first. Further entry requires rotation of the PLSS in the clockwise direction which results in wedging. This could prevent adequate engagement of the opposite cam segment or it could result in too great a clamping force at the wedged side of the PLSS.

The problem was overcome by the addition of hard springs to the bearing points. The springs limit the wedge force that can be built up at the end of the PLSS positioning motion. As mentioned earlier, the hard spring bearing points were found to also serve as clamping load limiters for thermal expansion or vibration induced wedging action, but they were originally added to solve the oblique entry wedging problem.

#### MECHANISM TESTING

The oblique entry wedging problem was discovered during routine tests on a two-dimensional mockup of the latching mechanism. Extensive testing in the form of higher fidelity mockups has also been conducted in order to thoroughly evaluate the functioning of the mechanism. A high fidelity MMU mockup has been manufactured which contains cam segments made of the correct material and several

prototype PLSS units exist which have striker plates also of the correct material. These units have been fit and function tested using both test subjects and astronauts in spacesuits in donning and doffing tests. Ambient conditions consisted of normal earth air pressure, temperature, and gravity in most cases, but some testing has been done in simulated zero gravity.

Two methods are available for simulating the weightless aspects of zero gravity. One is flight in a specially rigged KC-135 aircraft along a parabolic flight path and the other is underwater neutral buoyancy testing. The latching mechanism has been tested by both methods. In the aircraft, periods of near zero gravity are limited to 30-45 seconds but a fairly realistic donning or doffing procedure can be completed. Vacuum and temperature conditions such as would be found in orbit are not simulated on the aircraft. Underwater neutral buoyancy testing is carried out in a large water tank with special underwater versions of the MMU and PLSS. There is no time limitation on these tests, but friction characteristics are not realistic with the surrounding water acting as a possible lubricant. And some fluid drag can be expected to alter slightly the dynamics of moving parts such as spring returns. In addition, vacuum and temperature conditions are again not simulated in underwater testing.

In fact, no testing has as yet been done which does simulate the hard vacuum or the extreme temperatures which would be present in orbit. However, all testing and evaluation of the latching mechanism which has been conducted thus far has been considered successful. The current materials may be changed if further testing indicates a risk of adhesion problems under orbital conditions.

#### CONCLUSION

The astronaut/Manned Maneuvering Unit interface has presented a challenging set of requirements for a latching mechanism. The mechanism must hold reliably and release on demand to avoid jeopardizing the safety of the astronaut. It must perform its function under adverse environmental and operational conditions. The spring loaded cam segment with variable ratio pulley release actuator has been developed to meet these demanding requirements. To preclude jamming of the mechanism special precautions have been taken such as spring loaded bearing points and careful selection of materials to resist cold welding. The mechanism has successfully passed a number of tests which partially simulated orbital conditions.

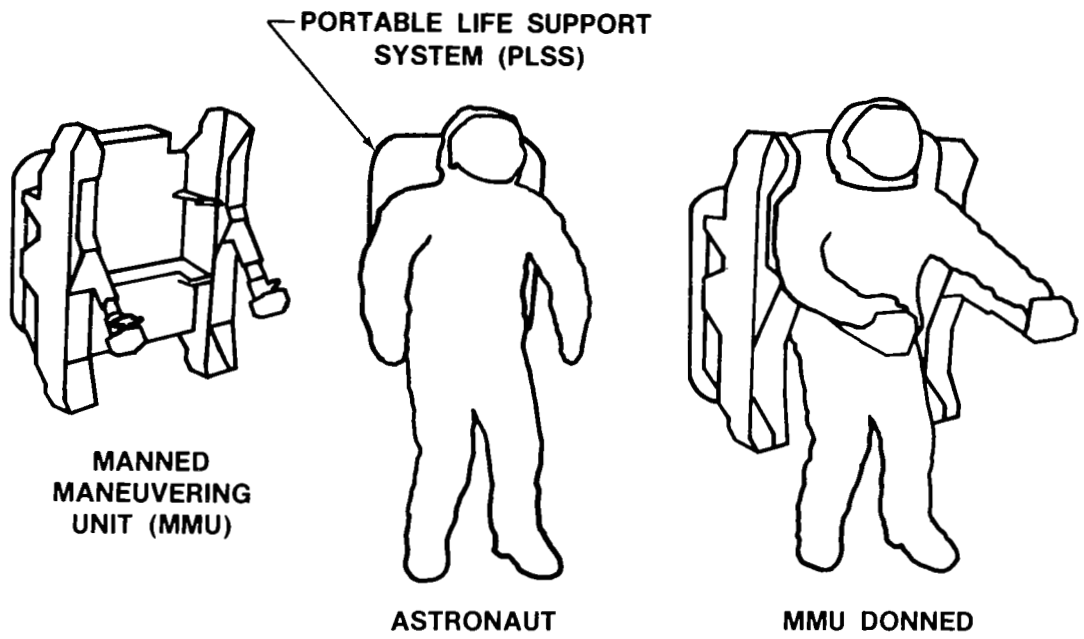


Figure 1.- Manned Maneuvering Unit.

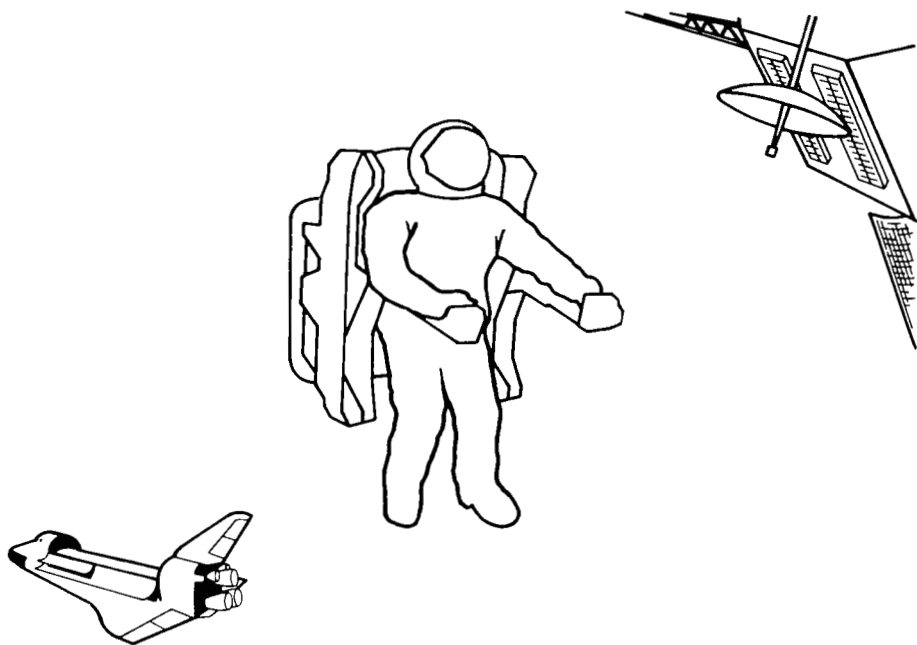


Figure 2.- Operational use of the Manned Maneuvering Unit.

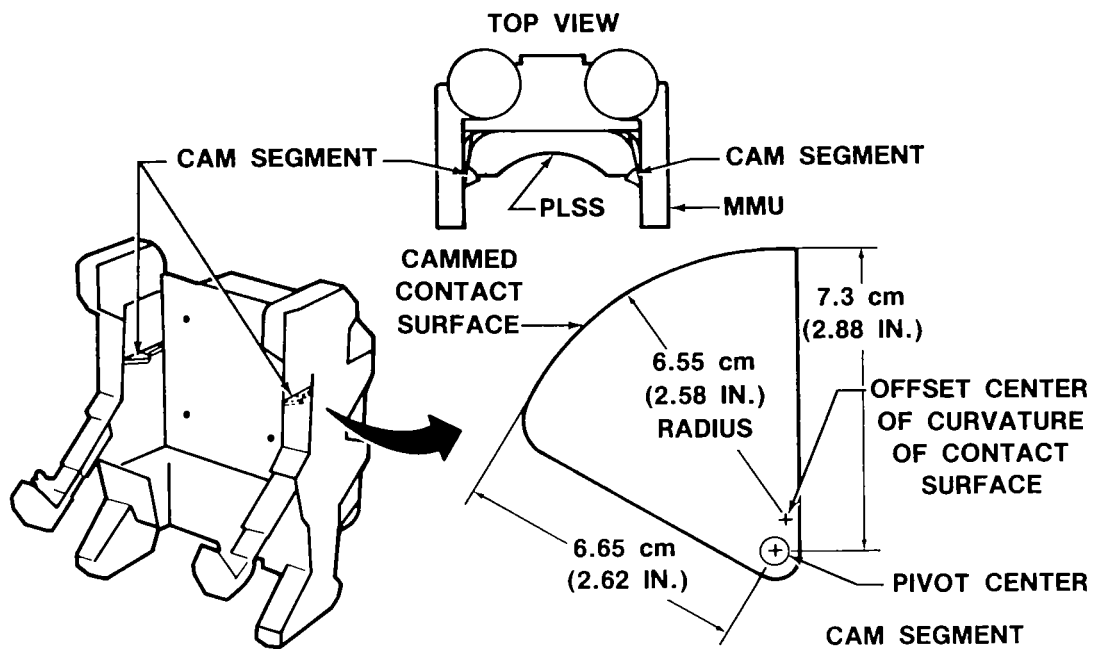


Figure 3.- Cam segment.

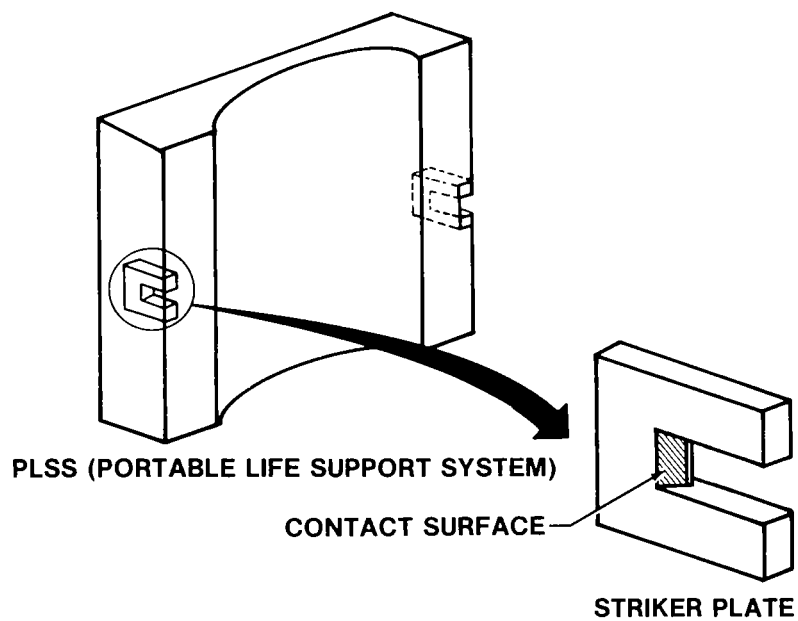


Figure 4.- Striker plate.

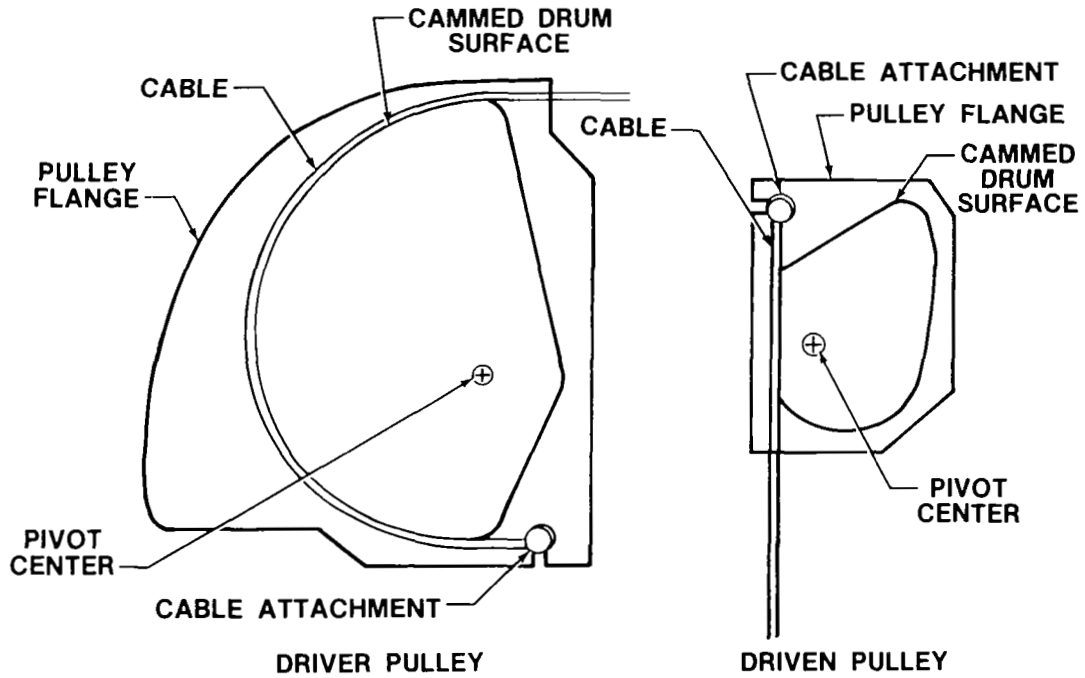


Figure 5.- Release actuator driver and driven pulleys.

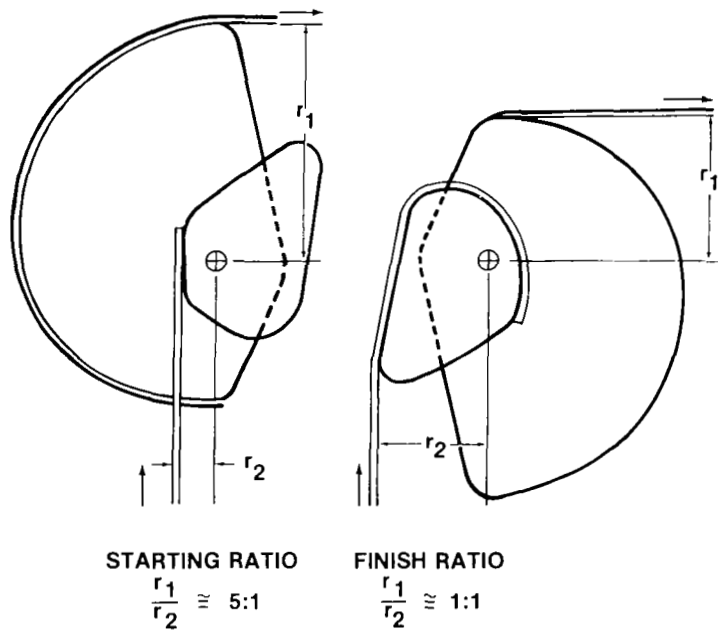


Figure 6.- Release actuator ratio variation.

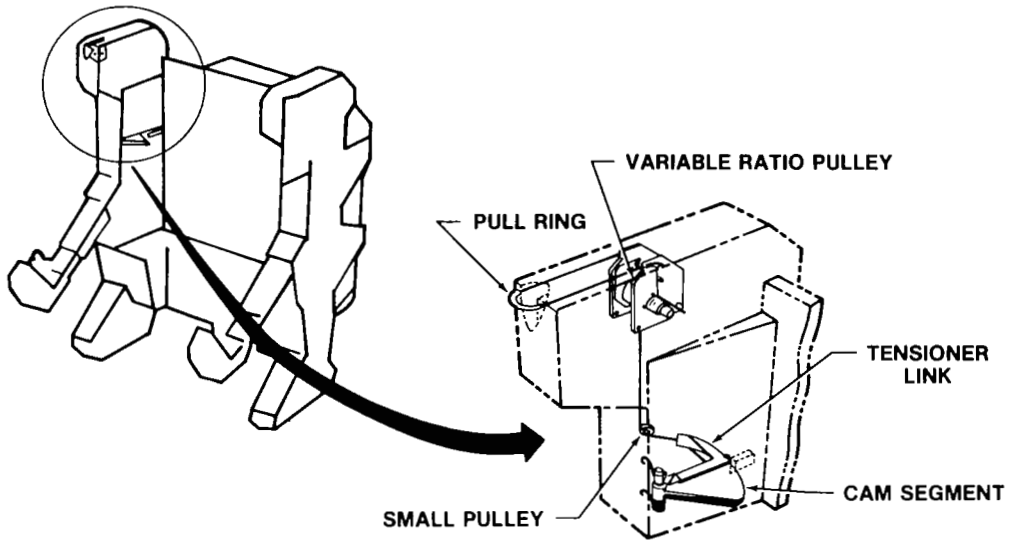


Figure 7.- Latching mechanism with release actuator.

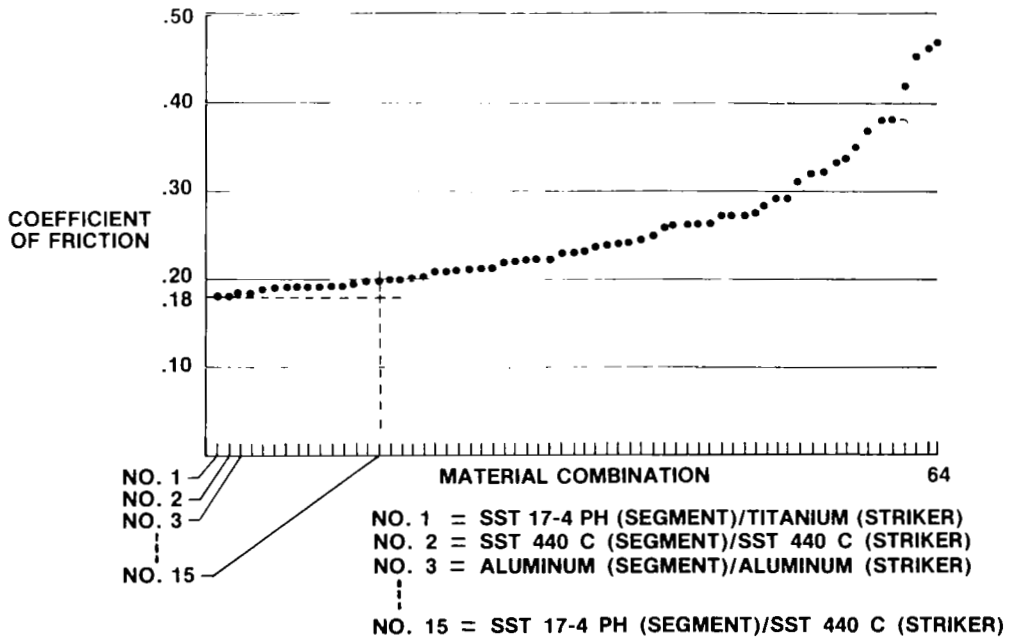


Figure 8.- Friction coefficients of material combinations.

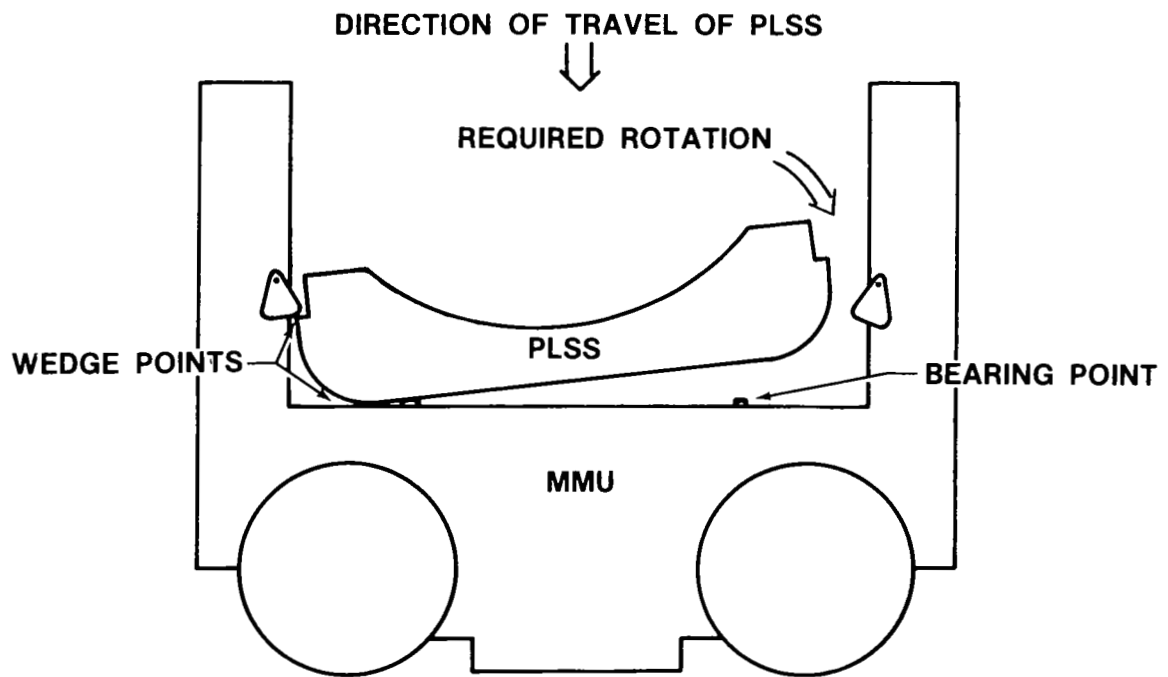


Figure 9.- Wedging problem due to oblique entry.

## ORBITER DOOR CLOSURE TOOLS

William R. Acres  
Lyndon B. Johnson Space Center

### SUMMARY

Safe reentry of the Shuttle Orbiter requires that the payload bay doors be closed and securely latched. Since a malfunction in the door drive or bulkhead latch systems could make safe reentry impossible, the requirement to provide tools to manually close and secure the doors has been implemented. These tools would disconnect a disabled door or latch closure system and close and secure the doors if the normal system failed. The tools required to perform these tasks have evolved into a set that consists of a tubing cutter, a winch, a latching tool, and a bolt extractor.

Use of the tools requires that a crewmember enter the payload bay in a pressurized suit and manually complete door closure. Therefore, it is highly desirable that the tools be operable with one hand, leaving the other free for positioning and for counteracting the force required to operate the tool. Controls, handgrips, operating forces, and procedures must all be within the capabilities of a partially restrained, suited crewmember in a zero-g environment. The extravehicular-activity (EVA) door closure tools designed, developed, and tested at the Johnson Space Center meet these requirements.

### INTRODUCTION

The complex payload bay door system (fig. 1) was discussed in detail at the 13th Aerospace Mechanisms Symposium in a report entitled "Space Shuttle Orbiter Payload Bay Door Mechanisms" (ref. 1). A review of that report will help to understand the need and use of the EVA tool set.

The payload bay doors are closed by a drive system that moves the doors to a designated position by two actuator systems, one on either side of the payload bay. Each system drives one 18.3-meter (60 foot) door and consists of an electromechanical actuator that drives six gear boxes interconnected by torque tubes. The gear box output is transmitted through drive linkage to the door as shown in figure 2.

The forward edges of the doors are connected to the bulkhead by latch mechanisms mounted on the doors and mating hook rollers mounted on the bulkhead (fig. 3). The latch mechanisms consist of a right-hand and a left-hand gang of four latches, one on each door, that operate sequentially. Each gang of latches is driven by an electromechanical rotary actuator. The aft edges of the doors are secured to the aft bulkhead in a manner similar to that used on the forward edge except that a fore/aft shear tie at each latch, identified

as a passive roller in figure 4, is used to control the distance between the door and the bulkhead.

During normal operation, each door is closed by the door drive system to within 5.1 centimeters (2 inches) of the number 1 bulkhead latch. The ganged latches are activated and provide a zippering effect whereby the number 1 latch first engages the door and then pulls it to a position within reach of the number 2 latch. The number 2 latch continues to pull the door further closed until it is within the reach of the number 3 latch and so on until all four latches have fully closed and secured the doors.

A failure in any actuator system could require a manual operation using one or more of the tools described in this paper to complete the door closure and latching process. The basic types of failures that could occur, the causes, and the required EVA actions are described in table I.

### TUBING CUTTER

In the event the door drive system fails such that the door can neither be opened or closed, the upper or lower drive tubes (fig. 2) must be disconnected from the door to allow manual door closure. Cutting these six tubes has proved to be the quickest and easiest way to accomplish this task.

Design criteria required that the cutter be operable with one hand, be installed on a tube that is attached at both ends, and be able to cut a tube that is 5.0 centimeters (1.97 inches) from an obstruction. The cutter must be able to cut a tube that ranges from 1.27 to 2.54 centimeters (0.500 to 1.000 inch) outside diameter and is made of 718 Inconel with a wall thickness of 0.16 centimeter (0.063 inch) and with a hardness from 36 to 38 RC. It must also withstand side loads introduced by a crewmember in zero-g conditions.

Designing a cutting wheel that would satisfy these requirements proved to be a real challenge. The material selected was AISI Type 0 tool steel heat-treated to 60 RC. Various cutting angles and wheel thicknesses were tried until a combination that could withstand the side loads and the cutting loads was found.

The tubing cutter (fig. 5) consists of the housing, the body that contains two fixed rollers, a spring-loaded roller, and the cutting wheel/screw ratchet assembly. The body is turned in one direction within the housing by three pawls mounted in the housing. By alining openings in the housing and the body, the tool can be installed anywhere along the tube. The tool is retained in position by a spring-loaded roller until the cutting wheel can be forced against the tube by the screw ratchet. Once a load is applied on the cutting wheel, the handle on the housing is ratcheted back and forth, causing the body to turn around the tube. After the body has made one complete revolution around the tube, the cutting wheel is again advanced against the tube with the screw ratchet. This procedure is continued until the tube has been cut.

After the tube is cut, the tool is removed from the tube and reset for the next cut by alining the openings in the housing and body, reversing the control lever, and retracting the cutting wheel with the screw ratchet until the next tube to be cut will move into position in the tool. The control lever is returned to the original position and the cutting wheel is forced against the second tube by the screw ratchet. This procedure is repeated until all six drive tubes on the affected door have been cut. The door is then ready to be manually closed by using the winch to pull the disabled door to a position where the bulkhead latching system can be actuated.

#### WINCH

Two EVA winches, one mounted to each bulkhead, are provided to manually close the doors to a position where the bulkhead latching system can be actuated or the three-point latch tool can be installed.

The winch assembly (fig. 6) is made up of a housing, a reel, a ratchet handle, and a mounting adapter. The housing encloses the reel and the mechanism that turns and controls it. A rope guide assembly mounted on the housing guides the rope over a set of rollers to prevent fraying. The mounting adapter also attaches to the housing. A reel powered by a negator spring houses 7.3 meters (24 feet) of 0.95-centimeter (0.375 inch) diameter Kevlar rope with a hook attached to the free end. Load is transmitted to the reel and rope by the ratchet handle through a gear system. A ratchet control lever selects the function of the ratchet between the handle and gear system and has reverse, neutral, and engage positions. A second ratchet system controls movement of the reel; ratchet-in, ratchet-out, reel-out, and gear-release functions can be selected with its control handle. The complete winch assembly is attached to the bulkhead handrails by the adapter.

After all apparent obstructions to free door movement have been removed, the crewmember routes the rope over the number 4 hook roller and attaches the rope hook to the number 4 latch bellcrank at the tip of the door. The rope can be pulled from the winch with a 4.45-newton (1 pound) force by placing the control handle momentarily to GEAR RELEASE to release the load on the reel ratchet and then to REEL OUT, and moving the ratchet control lever to the NEUTRAL position. The rope can be extended but will not automatically retract with the controls in this position. When the crewmember returns to the winch, slack rope is automatically retracted by placing the controls to RATCHET OUT and NEUTRAL. A load of 2669 newtons (600 pounds) can be applied on the rope by placing the controls to RATCHET IN and ENGAGE and either cranking or ratcheting the ratchet handle. When that load is reached, a torque limiter incorporated in the handle allows it to "collapse" approximately 15°. This is verified by misalignment of indicator marks on the handle and also by feeling the handle suddenly give way. If this occurs, the crewmember finds the obstruction to door movement, removes it, and completes closing the door.

The rope can be safely extended under load by placing the controls in the RATCHET OUT and ENGAGE positions and applying a load on the ratchet handle and then releasing it. This allows the reel to back up one tooth of its

ratchet. Repeating this process will extend the rope until the load has been relieved.

After the door has been fully closed by this method, the bulkhead latching system is actuated to secure the door, the rope hook is removed from the latch bellcrank, and the rope is completely retracted by placing the controls in the RATCHET OUT and NEUTRAL positions. If the bulkhead latching system works properly, the crewmember returns to the crew module.

### THREE-POINT LATCH TOOL

If a gang of latches on either end of one or both doors fails to complete door closure, the door must be secured to the bulkhead by some other means. The three-point latch tool was designed for this purpose. Eight of these tools (enough to bypass two gangs of latches) will be carried on the first Orbiter flight.

Design criteria for this tool required that the tool must fit all 16 latches, must be able to be installed and close a door that is 5.1 centimeters (2 inches) open with the number 1 latch hook  $37^\circ$  or more from being closed, must withstand design reentry loads on the latch, must transmit these loads into the latch pivot points with similar magnitudes and directions as the latch mechanisms, and must retain itself in position while being used by the crewmember.

The three-point latch tool (fig. 7) consists of a frame of two parallel plates, a compensator that pivots in the frame and attaches to the nut, a screw turned by a ratchet, and a bellcrank. The ratchet handle hinges to conserve stowage space. The force required to retain the tool in place is supplied by a spring-loaded telescoping pivot held in the compressed position by a release catch. The trigger to release this catch is mounted on the handle, requiring that the rod that releases the catch also hinge at the same point as the handle. The catch also incorporates a means to lock the ratchet handle offset  $30^\circ$  on either side of the tool to aid in installing the tool. Releasing the telescoping pivot also releases the ratchet handle positioning lock; however, a position release button is provided to reposition the handle in the desired position.

The tool is installed by first straightening the handle and offsetting it to the desired side (fig. 7(a)). The hook portion of the frame is fitted on the latch hook pivot shaft (fig. 7(b)) with the frame plates straddling the latch hook, which may be in any position greater than  $37^\circ$  from the closed position. The frame is then rotated until it contacts the bellcrank pivot. The telescoping pivot is released (fig. 7(c)), forcing the tool bellcrank against the hook roller, and the nut forces the compensator against the bellcrank pivot. In this configuration, the tool will hold itself in position while the crewmember extends the screw by means of the ratchet until a force is exerted on the hook roller, closing and securing the door (fig. 7(d)).

One tool is installed on each latch in the disabled gang in the same manner, starting with number 1 and proceeding in order to the number 4 latch, closing the door at each position before proceeding to the next latch. After installing the last required three-point latch tool, the crewmember is ready to enter the crew module.

#### BOLT EXTRACTOR

If the actuator of a gang of bulkhead latches fails such that a latch hook prevents installation of the three-point latch tool, the gang linkage must be disconnected from the disabled actuator. The bolt extractor (fig. 8) was designed for this task.

The linkage is attached to the actuator through a clevis joint using a shoulder bolt as the connecting pin. Removal of the bolt is required to disconnect the linkage. A force can be expected to be transmitted across the joint at the time of removal.

The bolt extractor consists of an expanding frame that straddles the clevis, a socket that turns the bolt, and an extractor that pulls the bolt free after the nut is removed. To operate the tool, the nut retaining slot in the frame is fitted completely on the nut and held in place while the tool is squeezed at points A and B. This compresses the frame until the socket contacts the bolthead. With pressure still being applied at points A and B, the bolthead socket handle is turned to align the socket with the bolthead and the tool can be fully installed on the bolthead.

The nut retainer keeps the nut from turning and also holds it against the clevis while the bolt is unscrewed. When the bolt threads have cleared the nut, the bolthead has been pushed into the socket past the extractor hooks. The bolt removal ratchet is then ratcheted back and forth to force the extractor away from the clevis and pull the bolt out. The tool will then slip off the clevis and the bolt can be removed from the socket.

Three bolt extractors will be taken on Shuttle flights, normally making it unnecessary to reset the tool for further use. The tool can be reset in flight if required, however, by holding the frame at point A and lifting up on the ratchet latches and point B simultaneously. The reset disk is turned to move the extractor and socket into position against the upper part of the frame. The same procedure is followed to remove any other bolts necessary to prepare the latch system to accept the three-point latch tool.

With the required bolts removed from the clevis joints, the latch gangs can be manually moved to rotate the latch hooks, thus allowing the three-point latch tool to be installed and door closure to be completed.

## TEST PROGRAM

Each of the door closure tools has undergone a period of development and evaluation by crewmembers and NASA officials and has repeatedly been used with success in the Neutral Buoyancy Facility at the Johnson Space Center. The flight tools have been delivered and are ready for the first Shuttle flight.

## CONCLUDING REMARKS

The door drive and bulkhead latch systems are reliable mechanical systems; however, like any mechanical system, they are subject to malfunctions that could cause an unsafe reentry of the Orbiter. This set of backup door closure tools provides the extra degree of safety needed for the Shuttle Program.

## REFERENCE

1. McAnally, Bill M.: Space Shuttle Orbiter Payload Bay Door Mechanisms. Proceedings of the 13th Aerospace Mechanisms Symposium, NASA CP-2081, 1979, pp. 261-269.

TABLE I.- DOOR CLOSURE FAILURES

Type of failure	Cause	Action
One or both doors will not close	Door drive system failure	Attach the winch hook to the affected door and manually close the door. Actuate the bulkhead latch system.
	Door drive system failure and jam	Cut the six drive tubes on the affected door with the tubing cutter and manually close the door using the winch. Actuate the bulkhead latch system.
Bulkhead latch system fails with the latch hook greater than 37° from the closed position	Latch actuator fails or jams	Install the three-point latch tool on the end of the affected door starting with the number 1 latch. Proceed in order to the number 4 latch, closing the door at each position before proceeding to the next latch.
Bulkhead latch system fails with the latch hook less than 37° from the closed position	Latch actuator fails or jams	Remove the connector bolt from the actuator linkage with the bolt extractor. Manually backdrive the latch hooks until the three-point latch tool can be installed on the number 1 latch; proceed in order to the number 4 latch, closing the door at each position before proceeding to the next latch.

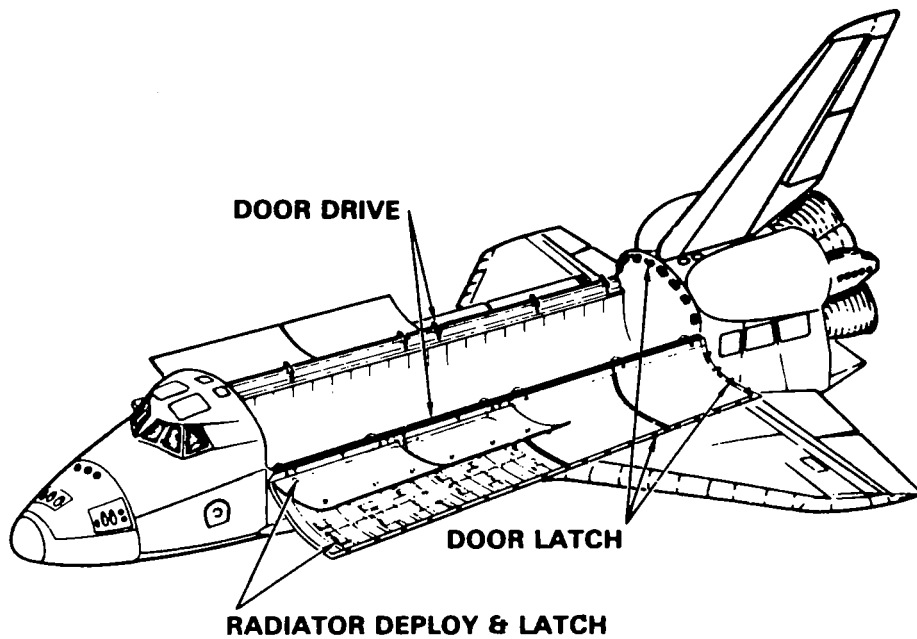


Figure 1.- Payload bay door system (from ref. 1).

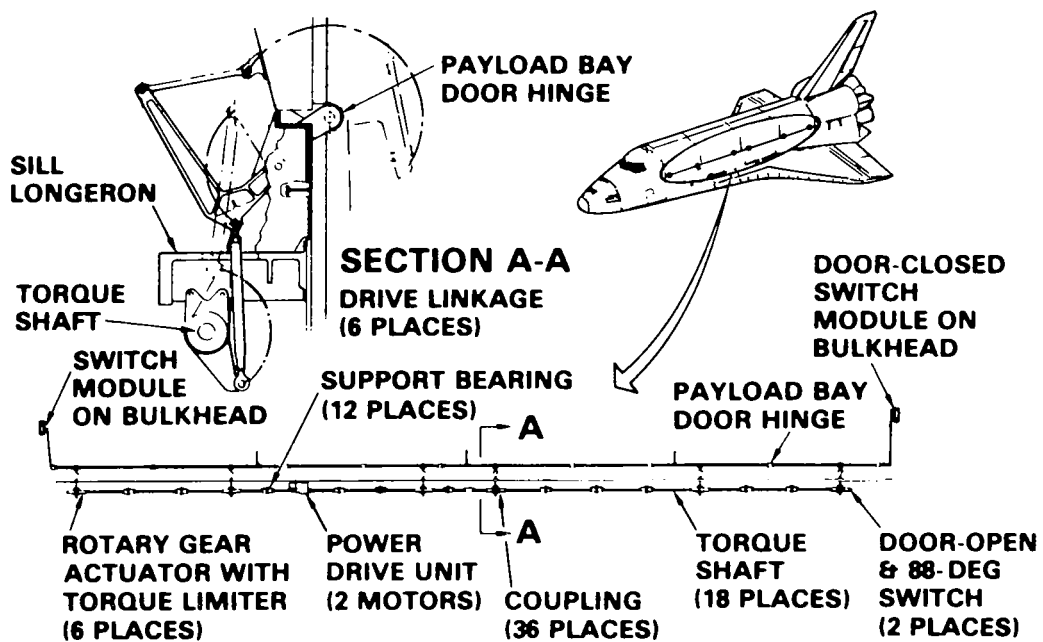


Figure 2.- Payload bay door drive system (from ref. 1).

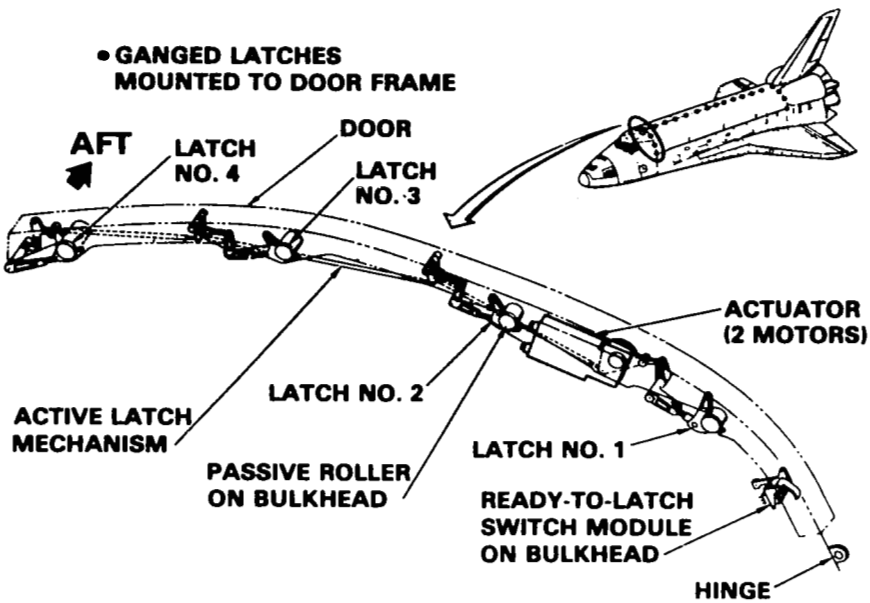


Figure 3.- Forward bulkhead circular latch system (from ref. 1).

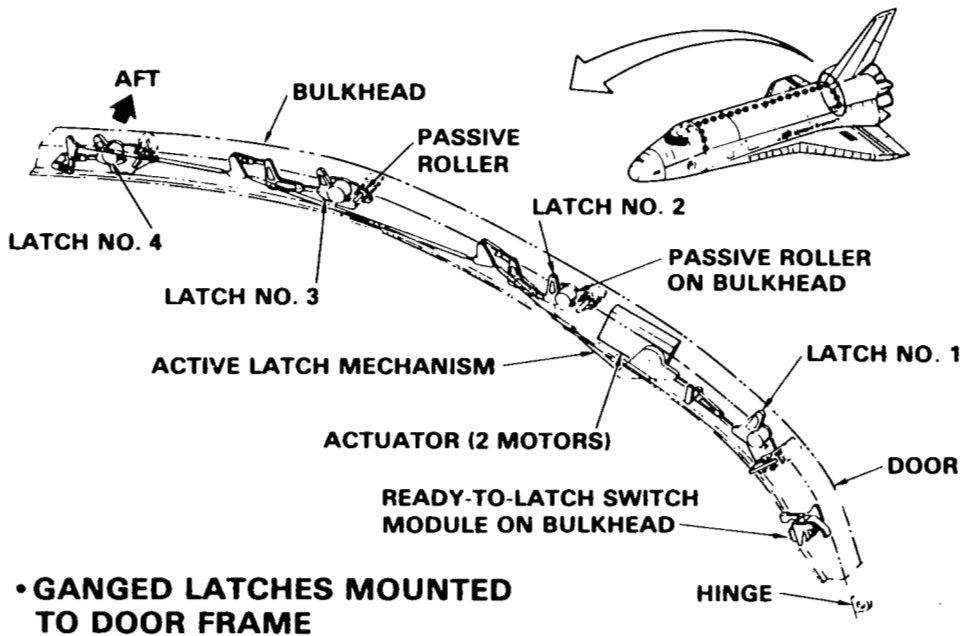


Figure 4.- Aft bulkhead circular latch system (from ref. 1).

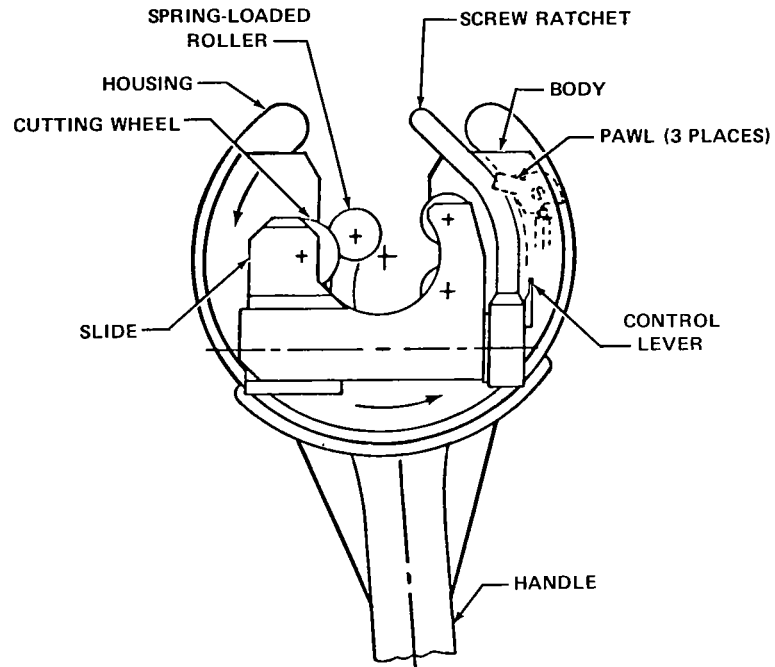


Figure 5.- Tubing cutter.

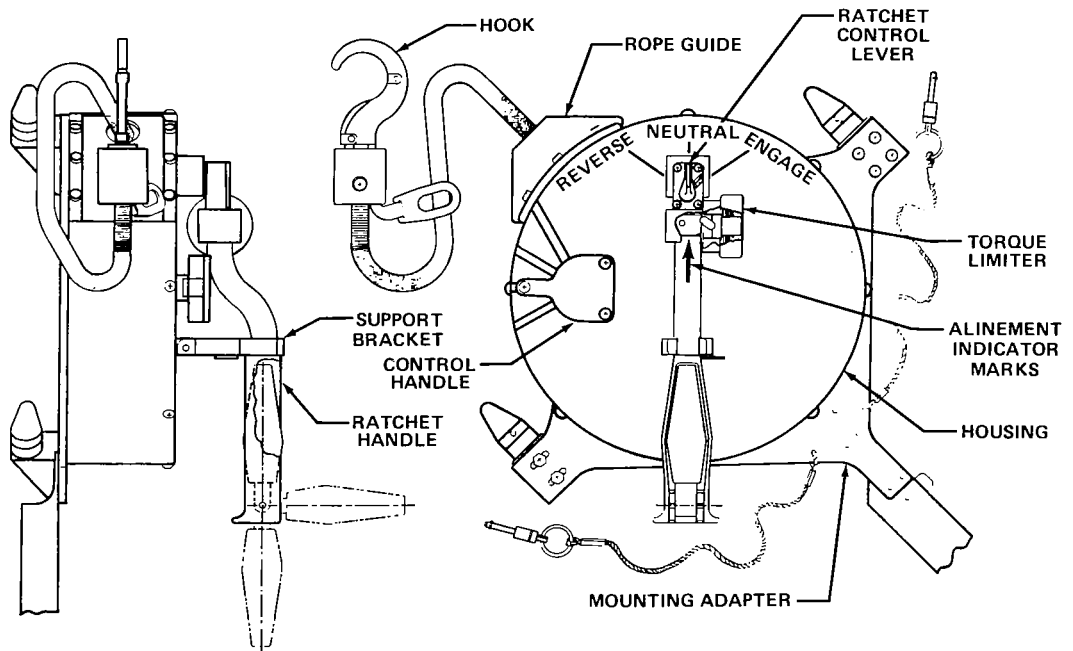
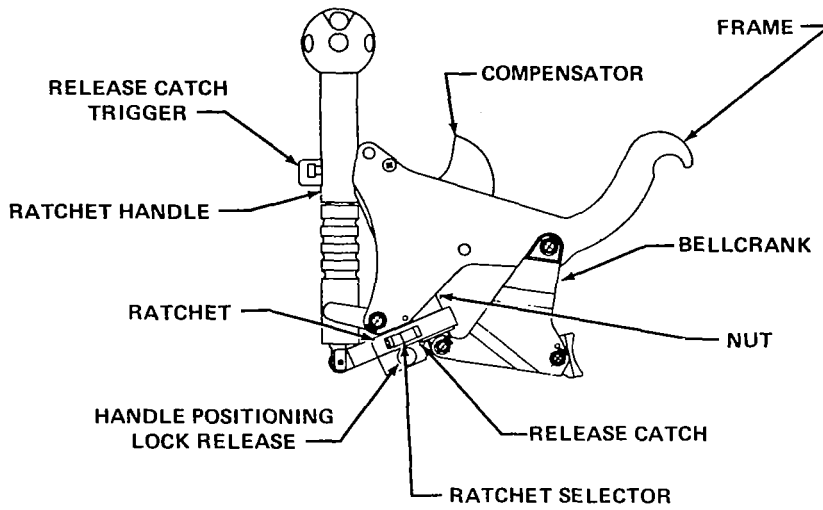
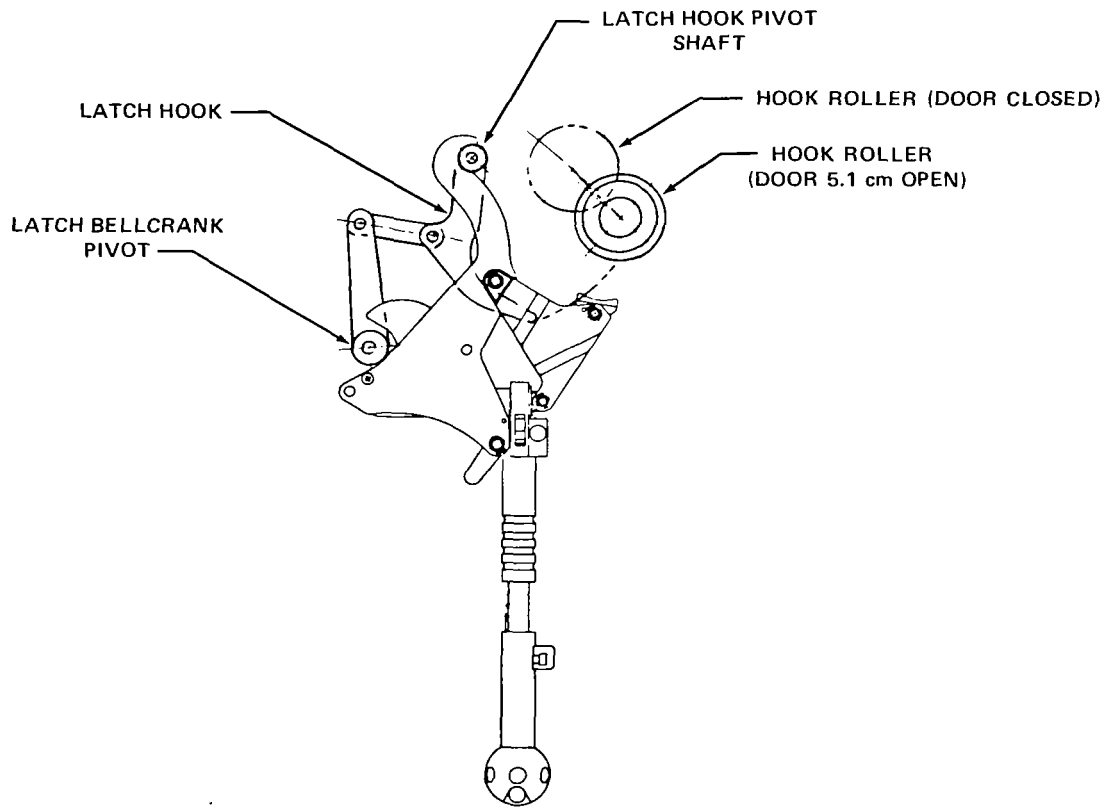


Figure 6.- Winch.

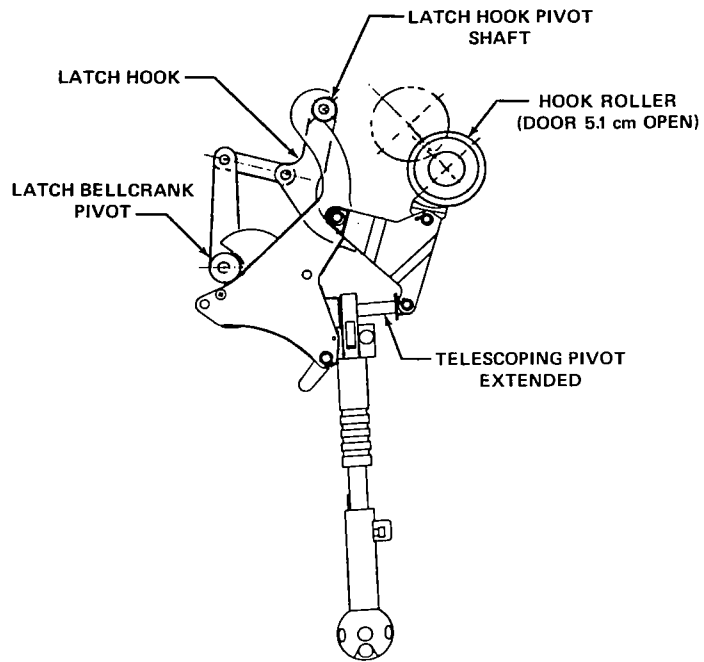


(a) Stowed.

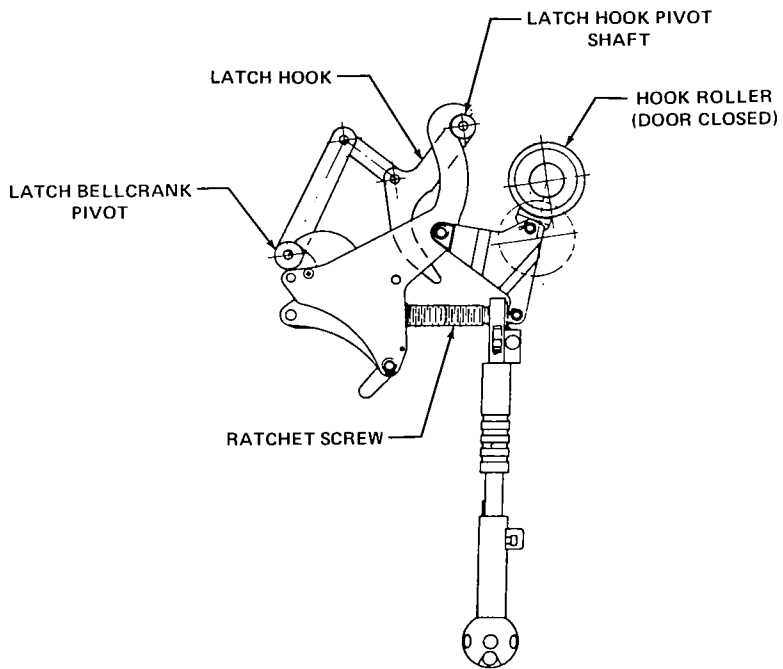


(b) Installed.

Figure 7.- Three-point latch tool.



(c) Retained by telescoping pivot.



(d) Expanded - door closed and secured.

Figure 7.- Concluded.

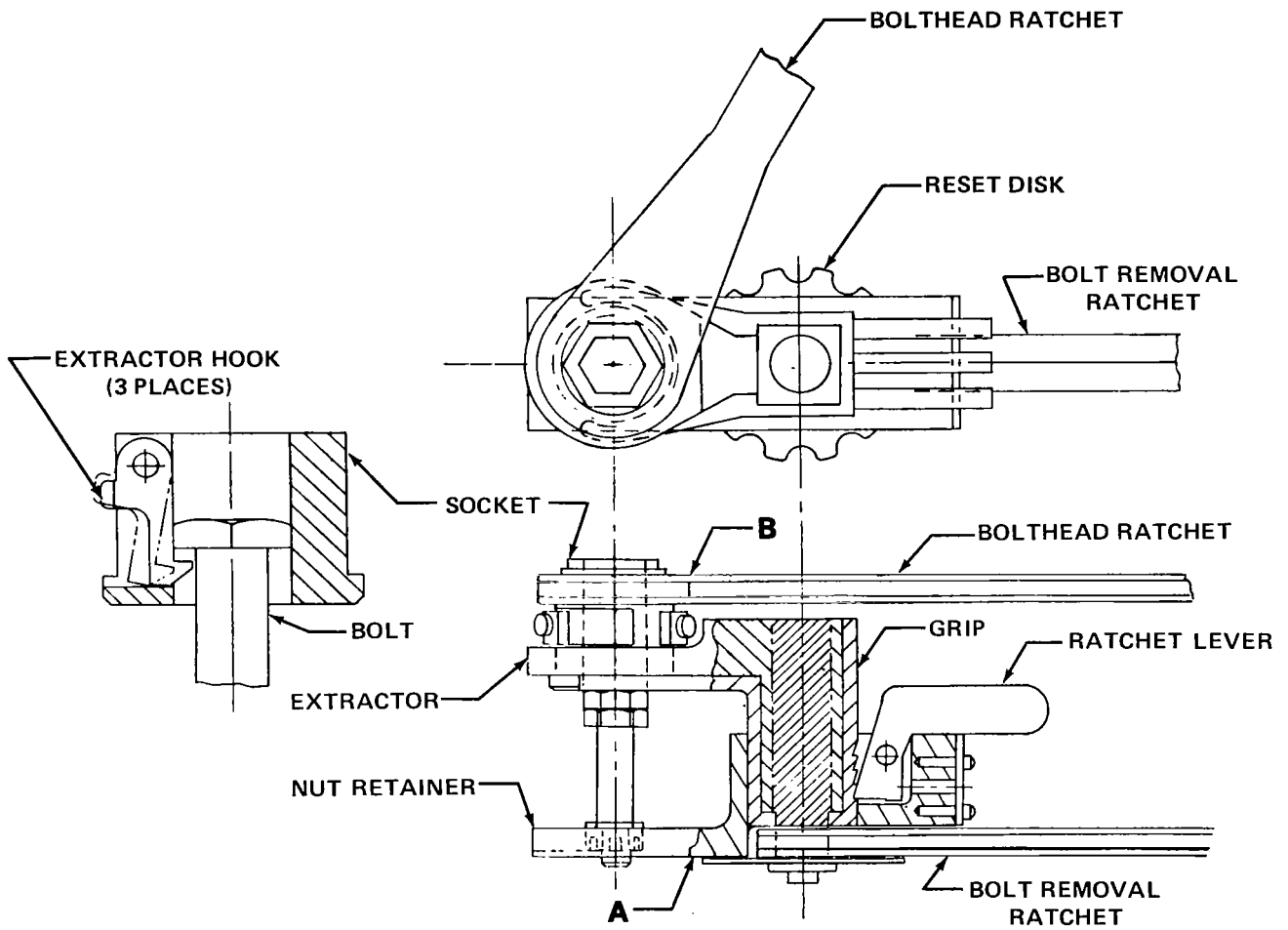


Figure 8.- Bolt extractor.



## ORBITER EMERGENCY CREW ESCAPE SYSTEM

William W. Lofland  
Lyndon B. Johnson Space Center

### SUMMARY

Two conventional ejection seats have been incorporated into the first two Orbiter vehicles to provide the crew with emergency ejection capability during the flight test programs. To avoid extensive development and test costs, existing ejection seats were selected and minimum modifications were made to accommodate the Orbiter application. The new components and modifications were qualified at the component level, and a minimum sled test program was conducted to verify the Orbiter installation and validate the six-degree-of-freedom analysis. The system performance was certified and the orbital flight test capability was established by analysis.

### INTRODUCTION

The Orbiter incorporates an "intact abort" philosophy. Problems during launch that compromise the mission success or safety will result in termination of the normal flight plan and return of the Orbiter to the launch site runway or another designated contingency runway. The Orbiter is a high-technology aircraft operating in a range of extreme environments and will have a crew of only two for the first few flights. Therefore, it is prudent and practical to incorporate an individual emergency crew escape capability to protect against those problems or failures that might render the Orbiter incapable of landing safely on a runway.

Originally, ejection seats were added to the first Orbiter vehicle to provide escape capability only for the horizontal flight test program. Off-the-shelf ejection seats were to be used; however, before their selection, it was decided to provide escape capability for portions of the orbital flight test program to be conducted with the second Orbiter. The ejection seats will primarily enhance crew safety during the first demonstrations of launch and landing. Following the orbital flight test programs, the seats will be replaced with operational seats similar to those in commercial air transport vehicles.

The orbital flight test requirement led to the selection of the ejection seat used in the SR 71 aircraft because of its demonstrated high-altitude capability. This ejection seat had been qualified for velocities of 230 m/sec (450 knots equivalent air speed) for the Air Force application and had demonstrated ejection capability at speeds greater than Mach 3 at an altitude of 24 kilometers (78 000 feet). These capabilities exceed the orbital flight test environments for ascent and reentry below approximately 30.5 kilometers (100 000 feet). Early centrifuge tests proved the crewman must be positioned

in a tilted-forward attitude during ascent to reach and see all the required controls and displays; however, during ejection, physiological limits require the seat to be in the normal aft position. Although the selected seats would provide escape capability for the horizontal flight test and the entry portions of the orbital flight test programs, the results from the centrifuge test necessitated the addition of a back-angle device to support launch and ascent. Orbiter flammability and toxicity requirements also necessitated a few material changes.

The ejection seat had been qualified to Air Force requirements and installed in their aircraft for some time. The Air Force qualification of the basic seat was accepted as satisfactory for the Orbiter application. The energy transfer and sequencing system and the modifications to the ejection seats were each qualified at the component level and in breadboard tests. Finally, the complete system operation was verified and the six-degree-of-freedom (DOF) analysis program was validated during a minimum sled test program. The crew escape system was then certified by evaluation of the results of the six-DOF analysis. Likewise, system performance under adverse conditions and during ascent was established using this analysis.

#### SYSTEM DESCRIPTION

Since the Orbiter was not designed specifically to accommodate ejection seats, several unique features had to be incorporated to facilitate the Crew Escape System installation (fig. 1). A structure was added between the floor and the ceiling of the inner crew station to support the ejection rails. Both the inner structure and the outer skin must be severed, without injuring the crew, and then thrust clear before the seats are ejected. To allow ejection at higher altitudes, an Air Force-type pressure suit was included for the orbital flight tests and the supporting ventilation and oxygen supply was incorporated into the Orbiter.

The Orbiter Crew Escape System consists of ejection seats; the ejection escape suit; guide rails and support structures; the escape-panel severance and jettison system; and the energy transfer and sequencing system. Operation of the escape system is accomplished through state-of-the-art pyrotechnic devices, many of which are off the shelf or only slightly modified for the Orbiter application. The pre-ejection functions of crew positioning (including the back-angle change) and restraint and the post-ejection functions of drogue deployment, seat/man separation, and main parachute deployment are accomplished through a self-contained gas-operated pyrotechnic system. The energy transfer and sequencing system controls the ejection from the Orbiter and consists of shielded mild detonating cord (SMDC), confined detonating cord (CDC) initiators, time delays, inner and outer panel severance systems, thrusters, safe and arm sequencers, and gas generators. A schematic of the Crew Escape System is shown in figure 2.

## Ejection Seat

A conventional ejection seat from the SR 71 aircraft was procured off the shelf for use in the Orbiter. This system includes the rocket catapult, seat adjustment actuator, survival kit container, crew restraint, stabilization drogue parachute, recovery parachute, and Orbiter interface components. To accommodate the unique application in the Orbiter of launching in the vertical position, remaining in orbital flight for some time, and then gliding to a more or less conventional landing, the ejection seat had to satisfy the requirements for positioning of the crew while fitting in a limited space in the Orbiter. These requirements, together with considerations of material flammability and toxicity for spacecraft applications, necessitated the following changes to the basic ejection seat.

1. A two-position seat-back subsystem was added to provide a crewman back angle of  $2^{\circ}$  forward of vertical ( $X_0$  axis) for launch to improve reach and vision. The seat back was mechanized to return to the aft position automatically before ejection or manually for the on-orbit and approach-and-landing mission phases.

2. The ejection seat vertical adjustment was changed to be compatible with Orbiter physical and anthropometric requirements.

3. The cushions were revised to improve comfort and positioning during prelaunch and launch but still satisfy ejection safety requirements.

4. Material changes were made and shielding was added to meet Orbiter fire protection requirements.

5. Parachute holddown straps and survival kit forward-edge holddown clips were added to reduce upward movement of the seat occupant during the prelaunch and launch phases.

6. The timing of the seat drogue deployment and of seat/man separation was changed to improve stabilization and seat/man separation trajectories.

7. Oil damping was added to the crew positioning inertial reel to reduce acceleration during repositioning.

8. To improve ascent survivability, the aneroids were changed to initiate the low-altitude mode below 3 kilometers (10 000 feet) rather than at 4.5 kilometers (15 000 feet).

A survival kit, packaged in a fiberglass box assembly, is installed in the ejection seat pan. The survival kit contains an emergency supply of breathing oxygen in the back compartment and worldwide survival equipment in the front compartment.

The Orbiter ejection seat has two modes of operation that are automatically selected by the aneroids depending on altitude. If ejection occurs below 3 kilometers (10 000 feet), seat/man separation and main parachute deployment occur immediately after separation from the Orbiter. If ejection

occurs above 3 kilometers (10 000 feet), seat/man separation is inhibited and the crewman descends on a drogue parachute to 3 kilometers (10 000 feet) altitude, at which time separation occurs and the main parachute deploys. The sequence of events during ejection is shown in table I. For emergency ground egress, either the flight crew or the ground crew can jettison the escape panels without ejecting the seats.

The salient features of the Orbiter ejection seat are shown in figure 3.

### Ejection Escape Suit

The ejection escape suit (EES) is a modified off-the-shelf Air Force full-pressure suit. The Air Force unit has been modified by adding medical monitoring of the crewman and anti-g protection for the entry phase of the orbital flight test program.

The EES (fig. 4) consists of a torso assembly, separable helmet, gloves, retainer assembly, urine collection system, anti-g protection, and biomedical monitoring. The suit has separate breathing and ventilation gas inlets, each with independent plumbing and ducting systems. When the helmet visor is down, a dual demand breathing regulator supplies breathing oxygen to the helmet face area, which is separated from the rest of the suit assembly by the face barrier. Ventilation air is supplied to the torso assembly for body cooling during pressurized cabin flight. The differential pressure is controlled by a valve that regulates the exhaust of the ventilation air from the EES. This valve also controls the pressure after ejection, and makeup pressure for the exhausted air comes from the oxygen that escapes from the face area barrier into the torso assembly.

Suit ventilation system.- Two ventilator assemblies, each including a compressor, the associated electronics, and a check valve, are enclosed in a housing located immediately behind each ejection seat. Conditioned air is pulled from the environmental control life-support system duct and discharged from each compressor into a common manifold assembly. Two manifold discharge ports are each connected to a plenum located under each ejection seat. Each plenum in turn is connected to the pressure suit by a flexible hose that supplies the ventilation air. The air flows through the suit to provide body cooling and then is returned to the cabin atmosphere. Either ventilator assembly can provide adequate cooling for the crew.

Regulated oxygen system.- The regulated oxygen system uses a dual oxygen regulator to convert the  $5860\text{-kN/m}^2$  (850 psi) oxygen to the  $414\text{- to }620\text{-kN/m}^2$  (60 to 90 psi) oxygen required for the pressure suit and the anti-g suit. The regulator assembly also has an  $862\text{-kN/m}^2$  (125 psig) relief valve downflow from the regulator. The regulated oxygen is delivered to manifolds located on the right side of the rail support structure and then through the survival kit to the EES.

## Guide Rails and Support Structures

Since the Orbiter is primarily designed to operate similarly to a commercial air transport with four crewmembers on the flight deck, the flight deck area is open and there is no bulkhead on which to mount the ejection seat guide rails in the conventional manner. Therefore, a special support structure with integral guide rails (fig. 5) was incorporated to provide ejection seat support during normal operations and guidance during ejection. This structure also transmits both the normal flight loads and the loads from the panel jettison and ejection into the Orbiter structure. Components from the pyrotechnic system, the interface wire harness for seat adjustment power, communications, biomedical monitoring, the oxygen system manifold, suit ventilation system blowers, and ducting are also mounted on this structure.

## Escape Panel Severance and Jettison

The outer structure of the Orbiter is designed to carry flight loads; it also provides a mounting surface for the thermal protection system tiles. The pressure vessel that provides the habitable workspace and living area for the crew is supported within the outer structure of the Orbiter. This arrangement does not provide the normal canopy or hatch arrangements to facilitate emergency ground egress or ejection. Therefore, a panel severance and jettison system was incorporated to cut openings in the surfaces above each seat and thrust the panels clear of the Orbiter during emergency procedures. The escape panels are shown in figure 6.

The outer structure is severed by mild detonating fuse (MDF) as is done in numerous other aircraft and spacecraft applications. The MDF system severs the panel primarily by shock effects. To protect the crew from dangerous hot gases and debris, the inner structure is severed by an expanding tube assembly (XTA). The XTA consists of one strand of MDF encased in lead and inserted in a stainless steel tube. The assembly is flattened and fitted to the structure around each inner panel, and the voids around the XTA are filled with silicone rubber. Upon firing, the tube expands and severs the panel from the crew module structure in a prescribed section around each panel. The XTA is retained in the support structure by stainless steel straps that do not inhibit its expansion.

As the panels are severed, thrusters mounted between each seat support structure and the inner panels provide propulsion for jettison of the panels. Both cabin pressure and aerodynamic forces assist panel jettison under some conditions. The energy applied to the inner panels by the thrusters is transmitted to the outer panels through a system of attenuator pads and cable attenuators as shown in figure 6. The expended thruster barrel is removed from the ejection path by the thruster retractor and guillotines sever the panel-to-Orbiter wire harnesses. The escape panels are automatically jettisoned during ejection but can be manually jettisoned from the center console or the lower right side of the Orbiter for emergency ground egress.

## Energy Transfer and Sequencing System

The energy transfer and sequencing system controls the sequencing and initiation of each element of the Crew Escape System. The initiation signal is transmitted to the various elements by the energy transfer system, which uses SMDC between fixed paths and CDC between elements requiring relative motion. Both the SMDC and the CDC use MDF for transmission of the initiation signal. Since the ejection seat incorporates a hot-gas system, initiators and hot-gas generators are used to transmit the signal to and from the seat system. Through-bulkhead initiators transmit the signal between the pressurized and unpressurized compartments, and one-way transfer devices prevent the initiation of the ejection seat when the escape panels are jettisoned with either of the manual controls.

The energy transfer system provides the initiation signals to the Crew Escape System elements so fast that several of the operations cannot be completed without additional time delays. One-half-second delay initiators are included to delay the ejection of the right seat to allow time for the jettisoned panels to clear; another is included to delay the ejection of the left seat to avoid collision with the right seat. Safe and arm sequencing devices are provided to ensure that the escape panels have been jettisoned before the actuation of the ejection seats. These sequences require a pyrotechnic input from the energy transfer system and a mechanical signal from the rotating inner panel before the initiation signal is transmitted to the ejection seat propulsion system.

### TEST PROGRAM

To reduce development costs, maximum utilization of off-the-shelf components was made throughout the Crew Escape System. Where necessary, existing items were modified to meet the Orbiter requirements; only as a last resort were new items developed. For example, the basic ejection seat is used in the SR 71 aircraft and the one-way transfer device is used in the F-14 aircraft, but the inner panel XTA severance system was developed for the Orbiter. Maximum use of previous test data and qualification test experience was made in the certification of the Orbiter Crew Escape System. The new hardware and the modified existing hardware were first qualified at the component level and then portions of the system were operated in breadboard tests. Finally, the installation of the system was verified in a minimum sled test program.

The ejection seats, rail support structures, overhead panel structures, and energy transfer and sequencing system were installed in a sled vehicle that simulated the Orbiter crew module. The system was then realistically tested throughout the Orbiter velocity range. The sled test program consisted of the following tests.

1. Two panel-jettison tests using previously severed panels
2. One panel severance and jettison test

3. One dual-ejection test with a complete system at zero velocity

4. Four dynamic tests at various velocities throughout the flight envelope (two complete dual-ejection tests and two single-ejection tests)

The sled test program verified the installation and operation of the Crew Escape System in the Orbiter. The six-DOF analysis developed to predict system performance was updated during the sled test program such that it gave excellent correlation between the predicted and actual system performance. As a result, the six-DOF analysis was validated during this program.

#### PERFORMANCE

The capabilities of the Crew Escape System during each phase of the orbital flight test program were established using the six-DOF analysis. During ascent, the plumes from the Space Shuttle main engines (SSME) and the solid rocket booster engines and reasonable deviation of the Orbiter from its nominal trajectory in pitch, roll, and yaw were considered. Based on this analysis, the system will provide escape capability from approximately 3 seconds after launch to about 3.7 kilometers (12 000 feet) altitude. From approximately 3.7 to 9 kilometers (12 000 to 30 000 feet), the crew will intersect the SSME plumes at a location where the temperature and/or dynamic pressure exceed human limits. From approximately 9 to 30.5 kilometers (30 000 to 100 000 feet), the crew will pass through the plumes at a location where the environment is acceptable. During descent, escape capability exists from approximately 30.5 kilometers (100 000 feet) through landing and rollout. The estimated and demonstrated ejection seat capabilities for the orbital flight test ascent and reentry conditions are shown in figure 7.

This analysis considered adverse Orbiter body rates about a nominal trajectory but did not consider such factors as the actual body rate resulting from anomalies, vehicle breakup and explosion, or engine-out conditions. When anomalous vehicle performance is considered, the performance capabilities will change.

#### CONCLUDING REMARKS

The Orbiter Crew Escape System, initially installed to provide escape capability during horizontal flight, has made maximum use of existing components and prior qualification programs. The system has been qualified at the component level and verified at the system level, and the analysis has been validated. The analysis indicates that the system also offers substantial escape system capabilities during portions of the ascent phase and of the descent and landing phases during the orbital flight program.

TABLE I.- ESCAPE SYSTEM SEQUENCE<sup>a</sup>

Time from initiation, sec	Sequence of events below 3 km (10 000 ft)	Sequence of events above 3 km (10 000 ft)
0.0	D-ring pulled, escape panels jettison, shoulder harness reel and foot actuators retract, back positioner retracts, <sup>b</sup> faceplate heater activated	Same
0.5	Sequencers ignite the catapult	Same
0.7	Drogue gun deploys drogue parachute	Same
0.95	Drogue parachute full open	Same
1.2	Rocket burns out	Same
1.5	Separation occurs; lap belt releases; shoulder straps, foot cables, and D-ring cable cut; separator actuates	Separation initiator armed but blocked by aneroid device
1.8	Upper drogue parachute risers cut	
2.1	Drogue gun deploys main parachute	
3.6	Main parachute full open	
11.5	Lower drogue parachute risers cut	Lower drogue parachute risers cut  Aneroid unblocks, initiating complete separation sequence, deploying main parachute 0.6 sec later and cutting upper drogue parachute risers after 0.3 sec

<sup>a</sup>The sequence shown is for the right seat; the sequence for the left seat is the same except there is an 0.5-sec time delay before the sequencers ignite the catapult.

<sup>b</sup>During launch only; already retracted during reentry.

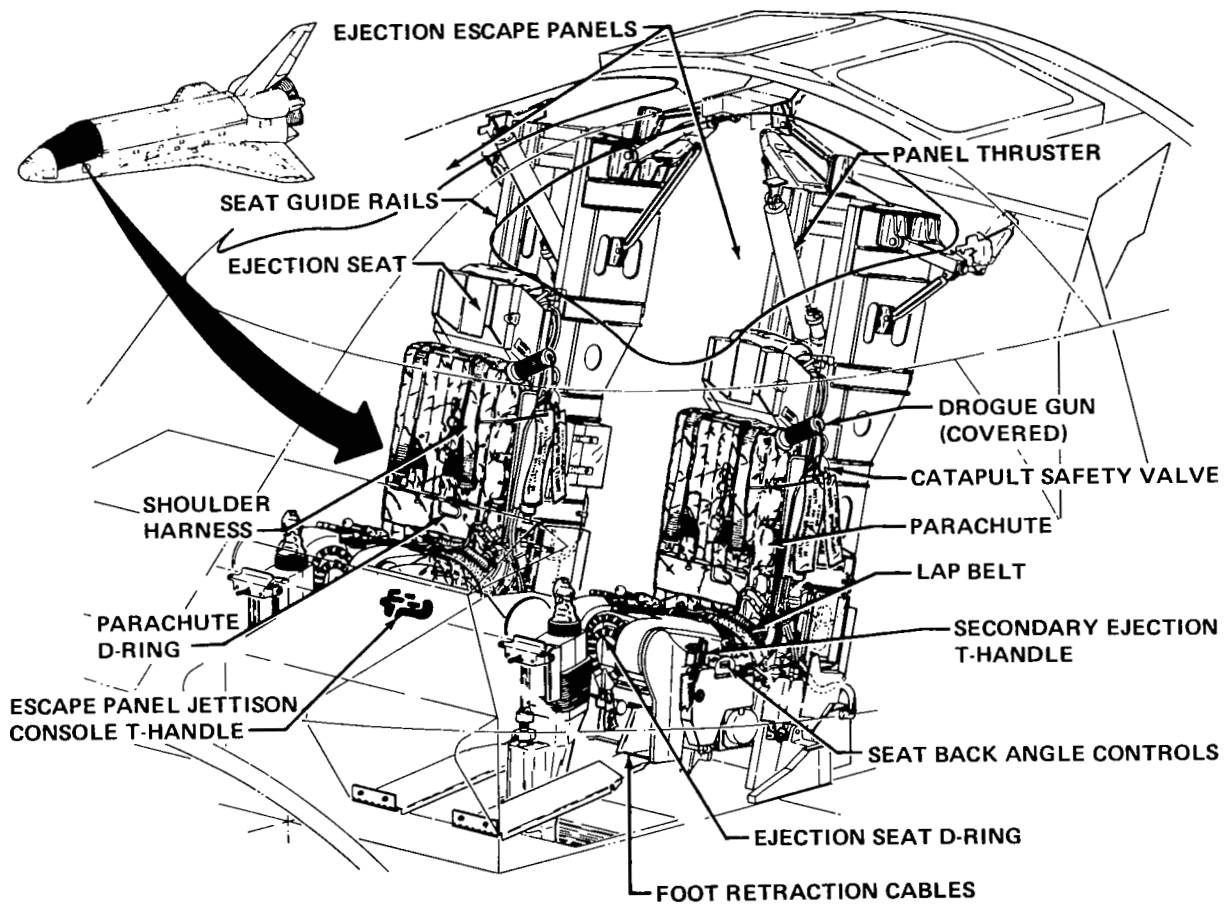


Figure 1.- General arrangement of the Crew Escape System.

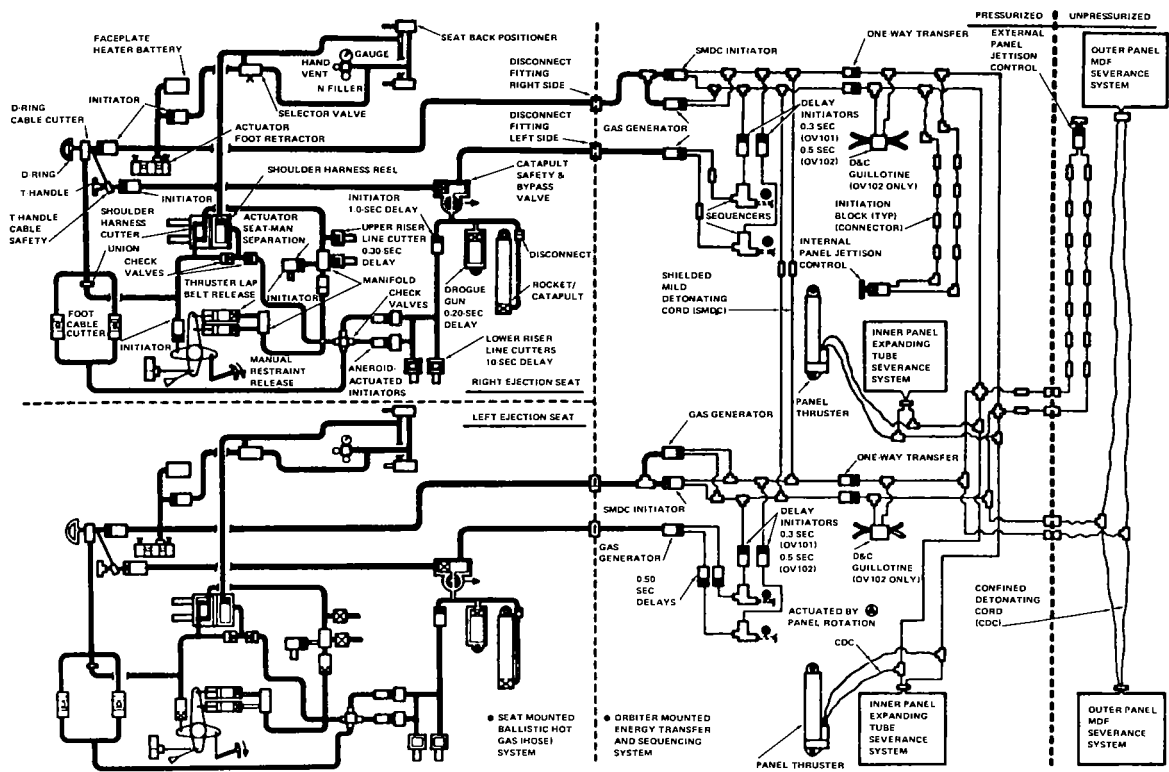


Figure 2.- Crew Escape System schematic.

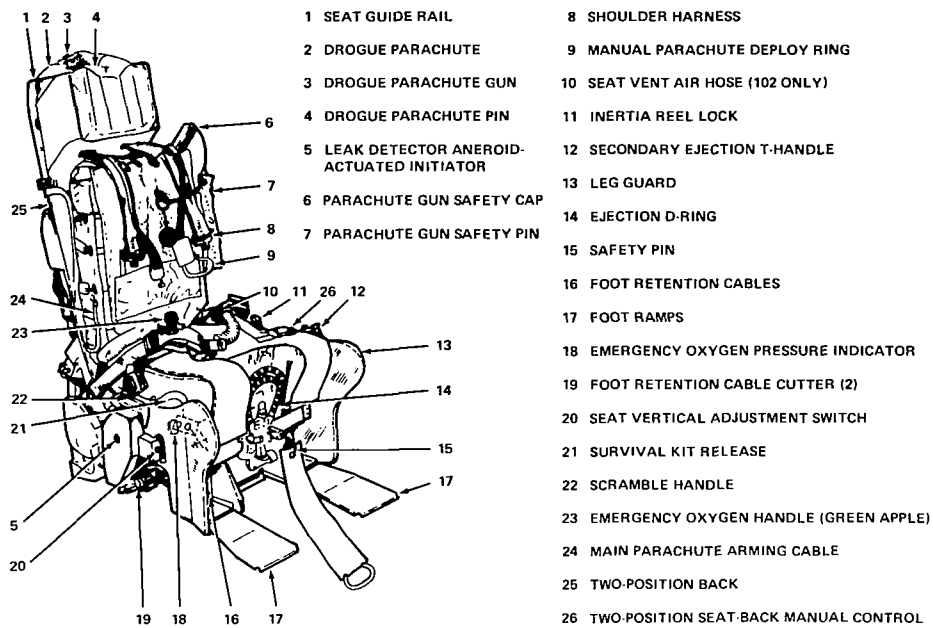


Figure 3.- Orbiter ejection seat.

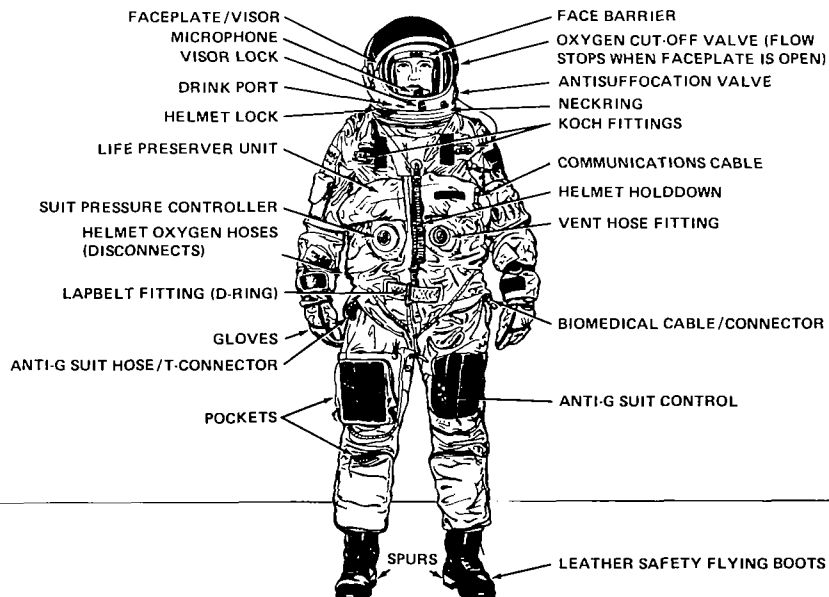
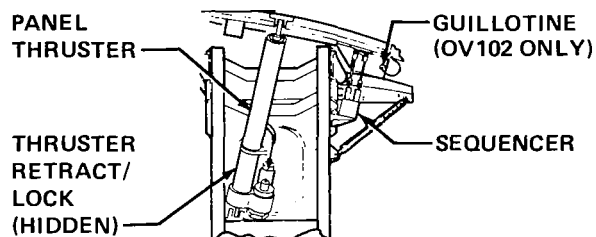
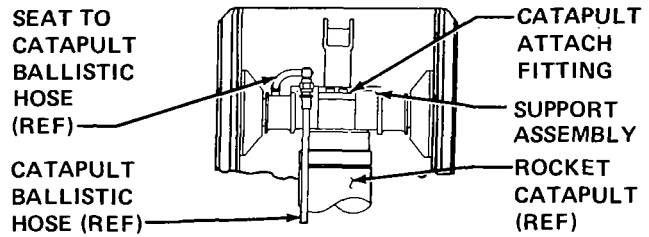


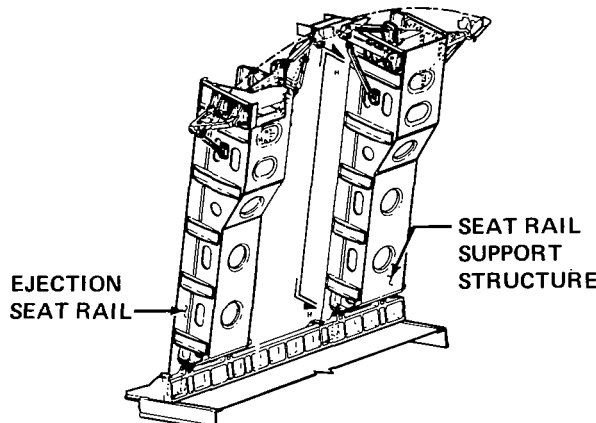
Figure 4.- Ejection escape suit (modified Air Force pressure suit).



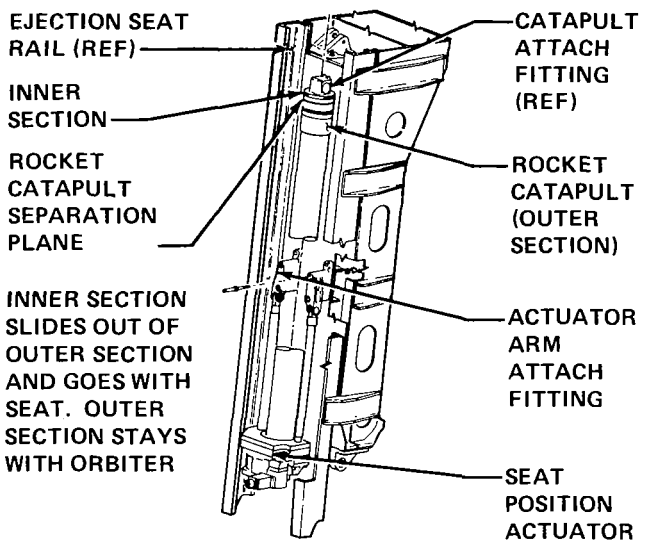
ESCAPE PANEL THRUSTER INSTALLATION



ROCKET CATAPULT/SEAT INTERFACE (DROGUE PARACHUTE BRIDLE AND COVER OMITTED FOR CLARITY)



SEAT RAIL SUPPORT STRUCTURE



SEAT ROCKET CATAPULT INSTALLATION

Figure 5.- Guide rails and support structure.

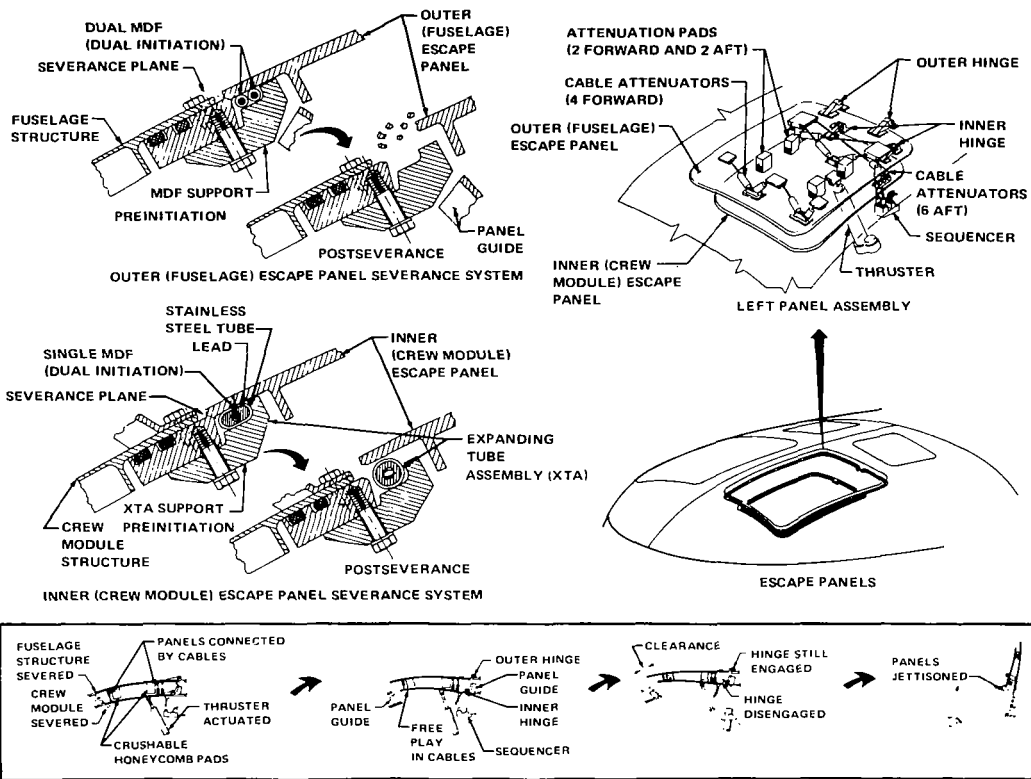


Figure 6.- Escape panel severance and jettison system.

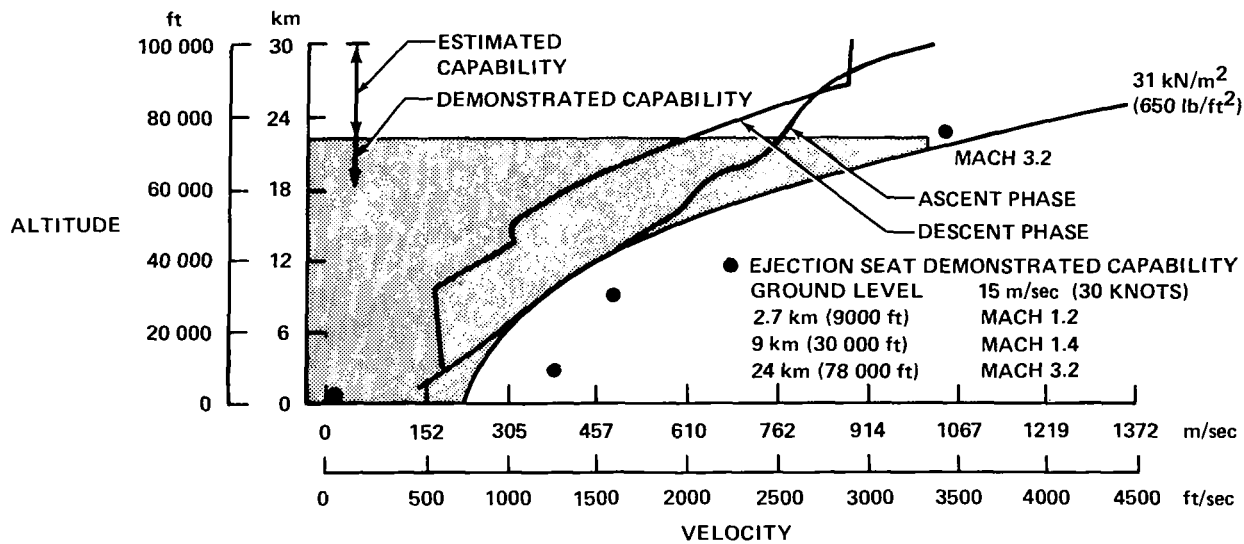


Figure 7.- Ejection seat capability.

FLUID CIRCULATING PUMP OPERATED BY SAME INCIDENT  
SOLAR ENERGY WHICH HEATS ENERGY COLLECTION FLUID<sup>1</sup>

Earl R. Collins  
Jet Propulsion Laboratory  
California Institute of Technology

ABSTRACT

This paper describes how a concept or idea for a solar-powered pump for spacecraft may be applied terrestrially to reduce or eliminate the need for fossil-fuel generated electricity for domestic solar hot water systems. A breadboard prototype model was constructed utilizing bimetals to convert thermal energy into mechanical motion by means of a toggle operated shutter mechanism. Although it did not meet expected thermal efficiency, the prototype model was sufficient to demonstrate the mechanical concept.

INTRODUCTION

If a domestic hot water system has a rooftop solar thermal energy collector, it will likely require some method or means for pumping the solar heated fluid to the heat exchanger, storage tank, or other work-extracting device. Existing fluid pumps are usually operated by electricity which is generated mainly by burning fossil fuels. Most pumps require only a small amount of electrical power to operate the individual collectors. However, in view of the expected increase in rooftop solar energy collectors, the total annual power consumption in the aggregate may become significantly large enough to warrant considering any means of reducing the need in the United States for scarce costly fossil fuel generated electrical power.

A flow diagram for a rooftop solar thermal energy collection system is shown in Figure 1. A desired power source would be the same incident solar energy which is, during daylight hours, irradiating and heating the fluid in

---

<sup>1</sup>This paper presents one phase of research conducted at the Jet Propulsion Laboratory, California Institute of Technology, under Contract NAS7-100, sponsored by the National Aeronautics and Space Administration.

the rooftop collector. In a typical installation, the solar heater is mounted higher than the storage tank, and the pump is essential to move the hot water, which is less dense than the cold water, to the heat exchanger (eg, room heater), to the storage tank, or to another heat-extracting device (eg, air conditioning unit).

#### SYMBOLS AND ABBREVIATIONS

Values and calculations are given in both the International System (SI) and US Customary units.

D	deflection of element in cm (in.)
m	specific deflection
P	load or force in N (ozf)
$\Delta T$	temperature change in K ( $^{\circ}\text{F}$ )
t	thickness of element in cm (in.)
$K_{\text{DS}}$	strip deflection constant per K ( $^{\circ}\text{F}$ )
$K_{\text{PS}}$	strip torque constant, $\text{N}/\text{m}^2$ ( $\text{oz}/\text{in.}^2$ )
$d_o$	diameter of disk in cm (in.)
$d_i$	diameter of hole in disk in cm (in.)

#### BACKGROUND OF PUMP CONCEPT

A pumping system, originally conceived as an aerospace method for circulating a cooling fluid to control temperatures within electronic bays of outer planet spacecraft, may be terrestrially applied (in accordance with the NASA Technology Utilization Program) to domestic solar hot water installations.

The basic concept underlying the solar pumping system was not using electrical energy, but instead converting the heat energy obtained from sunlight into mechanical work or kinetic energy. For space purposes, it was necessary for the spacecraft coolant fluid to be routed between the interior of the electronic bay and the thermal radiator on the shadow side of the spacecraft. The spacecraft approach, as evaluated and adopted, was an alternating thermodynamic cycle operation in which a heat absorber is first exposed to solar energy and then shielded (cooled) from Sun energy in order to produce a reciprocating motion or mechanical work. The spacecraft concept provided a self-starting demand pumping system completely independent of the

conventional onboard spacecraft power systems which were subjected to widely varying power requirements and demands. The concept as proposed for a terrestrial device will result in an automated system (i.e., when the water is being heated, it is being pumped; and, conversely, when it is not being heated, it is not being pumped). A device of this type could operate a pump from the same incident solar radiation that is heating the water for a domestic solar water heater. The description below follows the original concept proposed as a solution to the outer planet spacecraft internal temperature-cooling circulation problem.

#### DESIGN THEORY AND APPROACH

The solar pump concept essentially is an application (Reference 1) based upon the difference in radiant energy between a thermal heat source and a thermal cold sink, which may be one and the same at different times. This may be understood if the pump is thought of as a sink being exposed to a source. Then, after the absorption of heat, the pump is alternatively considered as the heat source. The concept or idea for using the thermal difference between source and sink posed three problems: first, developing a system to convert the radiant energy to mechanical energy; second, selecting a suitable material for the source-sink; and third, providing a method for a self-starting control of the source-sink. The first problem involves, of course, the fact that heat as a form of energy obeys the principle of energy conservation and may be transferred into mechanical work (and vice versa). The system to convert heat into work makes use of the transformation accomplished by heating a material and causing the material to do work as it expands. Several materials were considered for the energy conversion source-sink unit, such as solids, liquids, and gases used singly, hybridized, and, when appropriate, combined with the change of state. Examples of substances considered are alcohol, paraffin, Freon, ammonia, and bimetal.

The selection of a material was closely associated with the consideration of a mechanical configuration. Among the configurations evaluated were bellows, Bourdon tubes, helixes, springs, spiral coils, U- and S-shapes, and others which produce mechanical motion as a result of changes in temperature either directly or indirectly. A thermostatic bimetal was selected because of its heat flow characteristics, thermal properties (Table 1, Reference 2), mechanical configurations or shapes, the availability of the material, and the convenience for fabricating a breadboard prototype model. The most important characteristic of thermostatic bimetal is that it bends or deflects proportionally with temperature change within a broad operating range (i.e., the bimetal is a linear transducer). Such a bimetal temporarily changes shape when heat is absorbed and reverts to the original shape when cooled. Another broadly useful property of thermostatic bimetal is its ability to develop a force when deflection is inhibited. A bimetal element thus can produce both force and deflection and thereby perform mechanical work.

The third or control problem was solved by developing an over-the-center toggle device which would provide self-starting and full-on/full-off cycling of the source-sink system fields of view.

### PUMP SYSTEM FUNCTION

The mechanical approach for converting heat energy into reciprocating motion utilizes a series of bimetal elements that are alternately exposed to and shielded from sunlight. The bimetal elements will change shape when heated by the Sun, then return to their original shape when cooled. For this application, the Sun is the source; the pump elements are the sink. As the pump elements cool, they are now the source radiating the solar heat previously absorbed. Thus, the pump becomes a sink-source or source-sink, as the situation may be, and the alternations create a reciprocating motion that could power a pump.

From a functional standpoint, since the device converts the heat from solar radiation directly into reciprocating mechanical motion, the working cycle may be defined as composed of a power stroke and a return stroke. During the power stroke the pump elements pile is exposed to the heat source, thereby resulting in its expansion. The power stroke performs three functions: provides power for the pump, preloads the shutter escapement mechanism, and stores energy for the return stroke. At the end of the power stroke, the shutter escapement mechanism releases, thereby shuttering the solar radiation from the pump elements pile and initiating the return stroke. During the return stroke, the pump pile radiates its heat, returns to its initial position, triggers the shutters escapement mechanism, and commences the cycle again.

### CONFIGURATION

The solar-powered pump developed at the Jet Propulsion Laboratory, Pasadena, California, is composed of a series of bimetallic disk elements or units mounted on a metal spindle or brass rod (see Figure 2). The spindle is the heat-into-motion rod onto which are placed the Belleville units made of thermostatic bimetal individually formed in the shape of Belleville springs (Figure 3) with the low expanding side on the concave side. The disks are installed alternating on the rod, concave to concave and convex to convex. The perimeters of adjacent disks may be welded or snapped together with clips to form unitary elements. The left end of the disk assembly is anchored to a fixed rigid pump system frame structure, and the right is secured to a locking collar on the sliding spindle or drive rod adjacent to the return spring (see Figure 4). The diameter of the hole (see Figure 3) in the Belleville disk, 0.953 cm (0.375 in.), allows enough clearance, and the disk hole has been deburred so as to slide freely upon the center slide rod or spindle.

The action of the disk pile assembly is such that straight line reciprocating motion is effectively gotten from the expansion and contraction of the circular bimetallic element units. The thermal deflection of the disk pile assembly may be determined for the entire solar power unit. In order to provide a force of 26.7 N (newton) (96 ozf) over a temperature range of 338.7 K (150°F) to 366.5 K (200°F) and assuming the specific deflection  $m$  is 0.5 to provide for a minimum bimetal volume, the thickness of each disk  $t$  may be calculated, where  $K_{DS}$  is  $138.6 \times 10^{-7}/K$  ( $0.000076/°F$ ),  $K_{PS}$  is  $4.31 \times 10^{10} \text{ N/m}^2$  ( $100\,000\,000 \text{ ozf/in}^2$ ),  $\Delta T$  is 27.8 K (50°F), and  $P$  is 26.7 N (96 ozf):

$$t = \sqrt{\frac{P}{4K_{DS}K_{PS}\Delta T(1 - m)}} \quad (1)$$

$$= 0.0903 \text{ cm (0.0355 in.)}$$

The thermal deflection per each 0.0903-cm (0.0355 in.) thick disk under the design force may be calculated from

$$D \text{ per disk} = \frac{K_{DS}\Delta T (d_o^2 - d_i^2)m}{5t} \quad (2)$$

For the breadboard prototype model,  $d_o$  is 3.81 cm (1.5 in.) and  $d_i$  is 0.95 cm (0.375 in.). Therefore,  $D = 0.00573 \text{ cm (0.00226 in.)}$  per disk.

If the design total deflection for the stacked disk assembly is 0.76 cm (0.3 in.), then the

$$\begin{aligned} \text{Total number of disks} &= \frac{\text{Total deflection required}}{\text{Deflection per disk}} \quad (3) \\ &= \frac{0.76 \text{ cm}}{0.00573 \text{ cm}} \\ &= 133 \text{ disks.} \end{aligned}$$

The straight-line reciprocating motion drive rod slides and actuates both a diaphragm pump system and an over-the-center toggle flip-flop system which controls the shutter-drive for temperature cycling, and compresses a return spring.

As discussed in design theory and approach, the pump is alternately a sink and then a source. This temperature alternating cycle is controlled or produced by a movable aperture shutter/shield arrangement shown in Figure 5. Aperture shutter control is maintained by the over-the-center toggle device, with the drive rod or slide bar providing input to the toggle arm attached to the interconnected reflector surfaces. The over-the-center toggle device provides full-on/full-off cycling without a dead zone. The shutter reflectors are open to the function required (i.e., absorb or reject heat), and they will continue that function until reversal. Delay due to wear or increase in hysteresis will be accommodated by the overtravel inherent in the design. The aperture shutter/shield has a parabolic cross section of polished stainless steel (shim stock) for a reflective surface. The shutter reflector in the open heating (solid lines) position is receiving solar heat and directing it to the bimetal Belleville disks. The shutters in the cooling position (dotted lines) act as a thermal insulator from the Sun and serve as a reflector to re-radiate heat from the pile. The insulation is, in fact, a polyurethane styrofoam-type material which, when in the shuttered cooling position, blocks incoming radiation to the disk pile assembly so that it, in rapidly cooling, becomes a source of heat. The temperature differential causes the Belleville material to contract and expand, resulting in work motion.

#### PROTOTYPE BREADBOARD MODEL

The JPL prototype breadboard model contains 132 disks, 3.81 cm (1.5 in.) in diameter; each are free sliding on a brass slide bar which actuates a diaphragm pump. The other end of the spindle bar is attached to the toggle mechanism that drives the shutter reflectors. The disk stack was preloaded with a return spring calculated to return the mechanism to the cold position and to provide pumping action on the return cycle. The reflectors are of a modified vee-trough type with a parabolic shape. The rotational axis was located through the longitudinal center of gravity of each reflector half. The breadboard model was configured with an opening aperture 12.7 cm (5 in.) wide and 45.7 cm (18 in.) long.

#### PERFORMANCE ANALYSIS

The analysis of the Belleville disk thermopile incorporated the parameters of pump requirements, toggle and reflector operation, and mechanical efficiencies based on anticipated friction losses. The breadboard model was constructed to provide a proof of concept demonstration. While the model did demonstrate the thermal powered toggle actuated cycling operation, it fell short of the analytical performance, providing but half the output expected. A disassembly and inspection revealed several of the disks locking up rather than sliding on the spindle drive rod, reducing the pump's performance.

Figures 4 and 5 show side and end views of the breadboard model. The small model-size prototype contained all primary elements described together

with an associated diaphragm-type water pump mounted on one end and driven by the slide spindle bar. Operating at a frequency of one complete cycle every 40 minutes, the model demonstrated the mechanical concept.

### CONCLUSION

The pumping concept, as originally proposed for maintaining thermal equilibrium within a spacecraft, has possible wide terrestrial application. As demonstrated by a breadboard prototype model, the integration of the solar-powered pump within a domestic solar hot water system may be a desirable method for pumping heated water from roof-mounted collectors to the storage tanks, reducing or eliminating America's need for fossil-fuel generated energy for this facility. It is felt that further R&D will improve the model's performance.

### REFERENCES

1. National Aeronautics and Space Administration. NASA Tech Briefs, "Solar-Powered Hot-Water System," Vol. 3, No. 3, Fall 1978, pp. 349-350.
2. Design Highlights. An Introduction to Thermostatic Bimetal Applications for Designers and Engineers. W. M. Chace Company, 1630 Beard Avenue, Detroit, Michigan 48209.

TABLE 1. PROPERTIES OF CHACE THERMOSTATIC BIMETALS<sup>a</sup>

Type	Useful Deflection Range K (°F)	Maximum Sensitivity Range K (°F)	Deflection Constant Through Maximum Sensitivity Range Strips (K <sub>DS</sub> )/K (/°F)	Torque Constant Strips (K <sub>PS</sub> ) N/m <sup>2</sup> (ozf/in. <sup>2</sup> )
Chase #2400	200 to 644 (-100 to 700)	255 to 422 (0 to 300)	.00001386 (.0000076)	4.3 × 10 <sup>10</sup> (100 000 000)

<sup>a</sup>Selected from Reference 2.

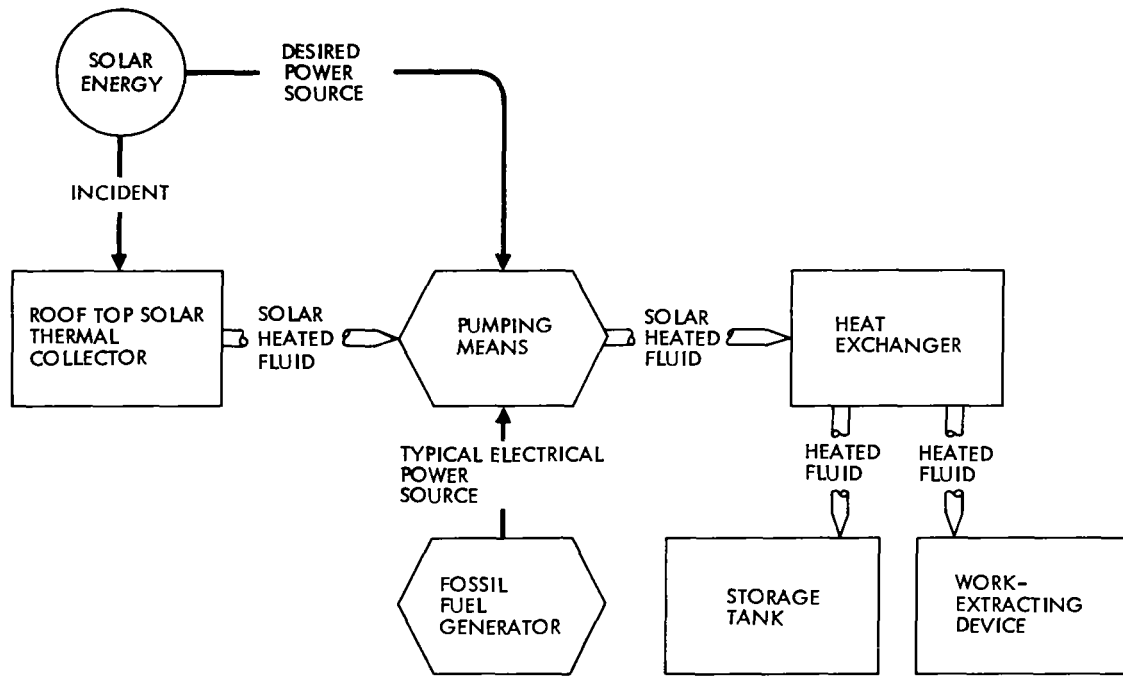


Figure 1.- Flow diagram for rooftop solar thermal energy collection system.

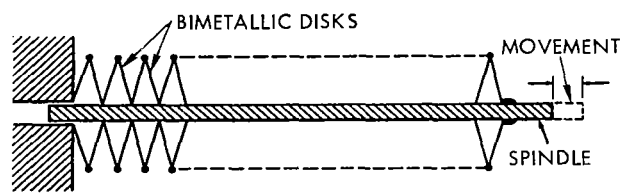


Figure 2.- Bimetallic disks linked together and joined to a spindle.

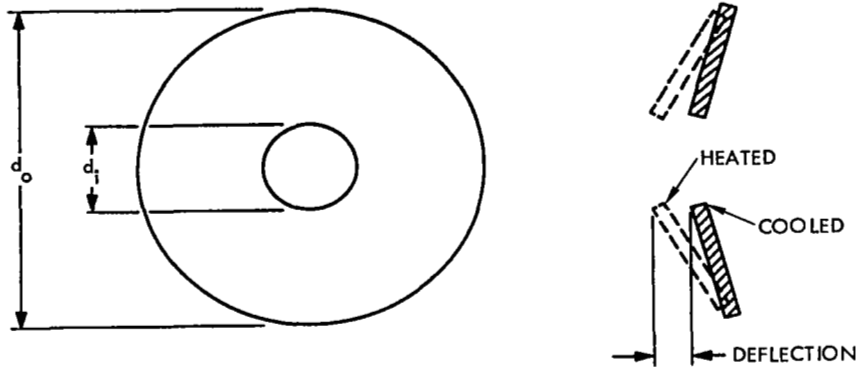


Figure 3.- Belleville spring disk deflection.

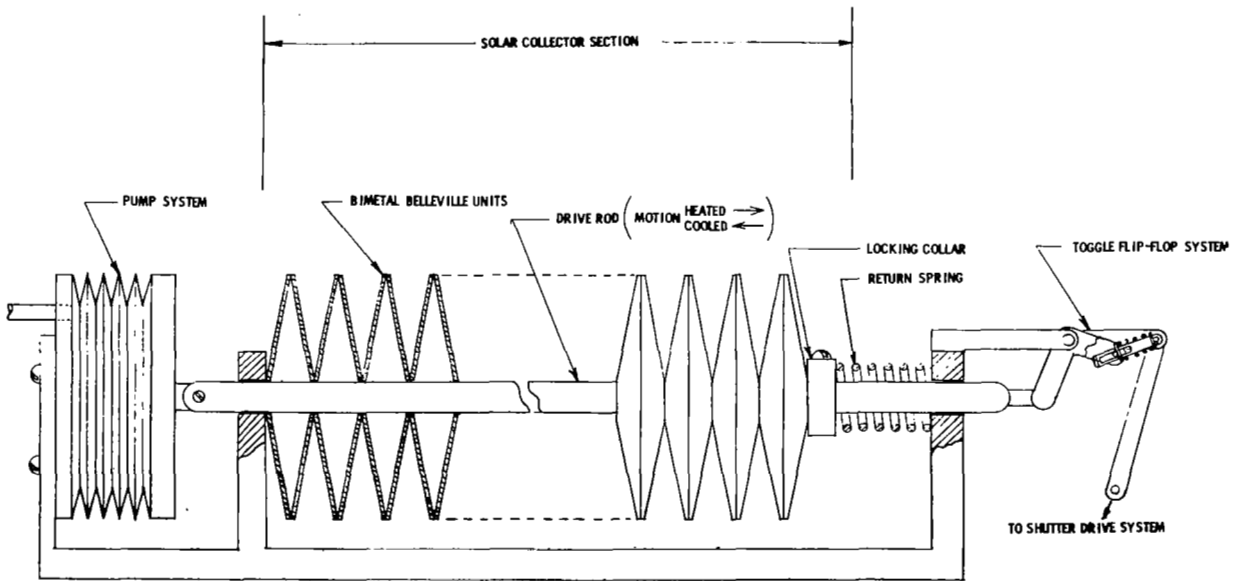


Figure 4.- Thermal pump side view, shutters removed.

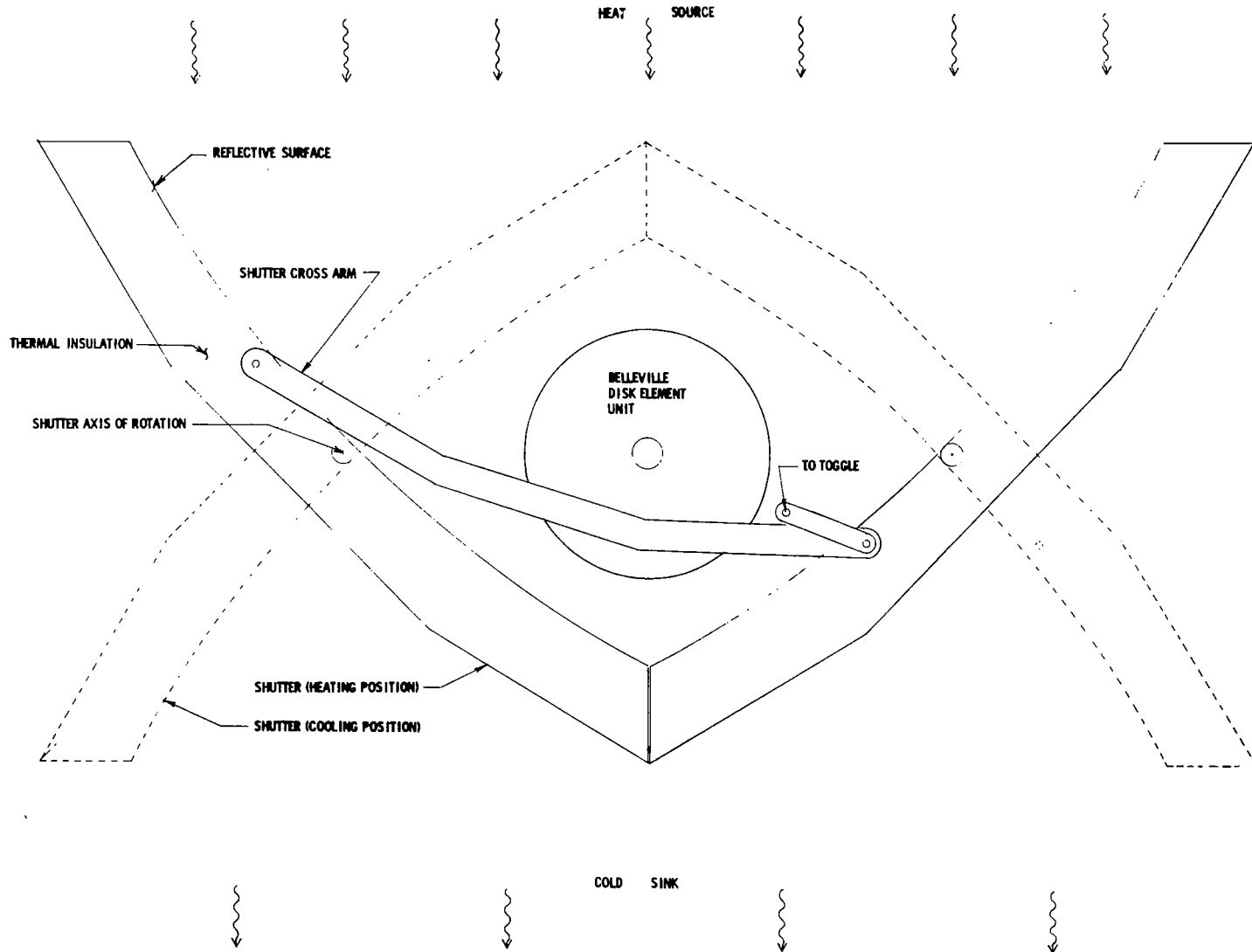


Figure 5.- Thermal pump solar collector system, end view.

## THE ECCENTUATOR - A NEW CONCEPT IN ACTUATION

Robert G. Musgrove  
Vought Corporation

### ABSTRACT

A new concept in actuation for aerospace mechanisms is presented. This actuator, called an Eccentuator, features unique output characteristics, installation and envelope efficiencies, and relative simplicity. The actuator can be powered by either hydraulic or mechanical inputs. Potential applications of the Eccentuator and development efforts are discussed.

### INTRODUCTION

The new actuation concept was discovered during research for methods of actuating variable camber surfaces on supercritical wings. The supercritical contour in the region of the control surface hinge line is thinner than a conventional airfoil contour. The aft air loading of the supercritical contour causes large hinge moments on the control surfaces. The thin contours and large hinge moments coupled with an aerodynamic requirement to keep both the upper and lower surfaces free from protuberances created a need for an actuation system which did not resolve the hinge moments with a force couple parallel to the surface reference plane. The actuation system also had to be mechanically and hydraulically stiff and have good positioning resolution.

An attractive possibility for such a system was a bent beam situated along the surface reference plane and supported in the wing by a two bearing socket. Rotation of the bent beam in the wing socket would cause angular motion of the free end of the beam about a hinge line. However, attachment of the flap to the free end of the beam with an acceptable bearing structure presented a problem. The free end of the beam not only moved in an arcuate motion about the hinge line, but it also had lateral motion along the hinge line. Previous use of bent beam actuators employed rollers on the beam in spanwise tracks in the flap to accommodate this lateral motion.

The Eccentuator is a bent beam actuator that compensates for the lateral motion of the beam with an eccentric bearing on the support end of the beam. A unique indexing gear arrangement employed with the bent beam and the eccentric bearing keeps the free end of the beam in a plane normal to the hinge line. Not only does the bent beam/eccentric bearing combination result in planar arcuate motion, but the arcuate motion is twice that achievable by rotating the bent beam alone.

The Eccentuator actuator exhibits load carrying capabilities much like a straight, fixed-end beam between the flap and the wing. For small surface deflection angles around  $24^{\circ}$ , the Eccentuator carries 90%-100% of the hinge moment through its structural elements depending on the deflection position.

The remaining 10%-0% hinge moment is reacted by an actuation system. This reduced actuation force requirement is a result of the inherent variable mechanical advantage in the Eccentuator. The Eccentuator system can therefore be thought of as variable geometry structure.

The large inherent mechanical advantage which results in a low actuation requirement allows several unique actuation concepts. A small integral rotary hydraulic actuator can be placed between the two moving parts and apply actuator forces directly to the load carrying members. For mechanical drive systems, the inherent mechanical advantage reduces the load on the drive gears allowing these to be smaller. The inherent mechanical advantage reduces the effect of gear freeplay on the surface.

The drawing in figure 1 illustrates a basic single-ended hydraulic Eccentuator. The eccentric support bearing is called a carrier. The indexing ring gear is mounted onto the grounded support housing while the indexing gear is fixed to the beam.

#### CONCEPT SIMPLICITY

The drawing in figure 2 illustrates the basic motion of the Eccentuator. In figure 2(a) the motion generated by rotating the beam alone is shown. The angular output is twice the beam bend angle. The lateral motion along the hinge line is also noted. Figure 2(b) shows the carrier location with respect to the hinge line and illustrates with a theoretical straight beam the effect on a beam of rotating the carrier in the opposite direction from that of the beam. The free end of the theoretical beam moves in the same angular direction as the bent beam, but the lateral movement is in the opposite direction. The eccentric bearing centerline is displaced from the carrier centerline such that it generates an angle with respect to the carrier centerline equal to the bend angle of the beam. Figure 2(c) illustrates that when the bent beam is combined with the carrier, and the two are rotated in opposite directions, the carrier's lateral displacement compensates for the beam's lateral displacement and the angular motion adds to produce a total planar angular displacement of four times the beam bend angle.

#### ENVELOPE EFFICIENCY

One of the principal features of the Eccentuator concept is its installed envelope efficiency. Figure 3 compares the Eccentuator installation with that of a linear actuator in a flap configuration. The Eccentuator is centered about the hingeline and lies along the centerline of the contour. Hinge moments are resolved normal to the wing reference plane rather than parallel to the reference plane as in most actuation concepts. The moment arm is therefore not a function of the wing thickness.

## ACTUATION LOADS

The basic structural advantage of the Eccentuator is that the hinge moment of the moving surface is transferred to the supporting structure primarily through structure. The positioning actuator therefore must react only a small percent of the load. The flap hinge moment ( $M_H$ ) is resolved as shown in figure 4, into a couple load on the flap end of the beam and transferred in bending through the beam to a reaction couple on the support side. The couple reaction on the beam by the carrier in the mid-travel position shown is not on the centerline of the Eccentuator assembly by the amount of eccentricity in the carrier. This eccentric loading causes a rotational torque on the beam in one direction and an equal and opposite torque on the carrier. The actuation torque ( $M_A$ ) on either the beam or carrier is

$$M_A = M_H \tan \theta \cos \phi \quad (1)$$

Where:

$\theta$  = beam bend angle

$\phi$  = rotation angle from mid-travel position

When the beam is in the mid-travel position, the actuation torque requirements are greatest. At the actuator travel extremes where  $\phi$  is  $90^\circ$ , the actuation torque requirements diminish to zero. Small beam bend angles, such as  $6^\circ$  which produce actuator outputs of  $24^\circ$ , require a maximum actuation torque on both the beam and the carrier of only approximately one tenth of the hinge moment. As the Eccentuator is positioned away from the mid-travel setting, the actuation torque requirement decreases for a given hinge moment.

## INHERENT MECHANICAL ADVANTAGE

The reduced actuation torque requirements are a result of an inherent mechanical advantage. This mechanical advantage varies from a maximum value of infinity at the actuator travel extremes to a minimum value at the mid-travel position. The inherent mechanical advantage is calculated by the following equation:

$$\text{Mechanical Advantage} = \frac{1}{\tan \theta \cos \phi} \quad (2)$$

From this relation it can be seen that the mechanical advantage doubles, from its minimum value at mid-travel, when the beam and carrier have been rotated  $60^\circ$  from the mid-travel position. Full actuator travel and an infinite mechanical advantage occur at  $90^\circ$  rotation from mid-travel. Figure 5 is a typical mechanical advantage curve for a 6 degree beam bend angle.

This inherent mechanical advantage can be applied to reduce the input torque requirement at the travel extremes when encountering a constant hinge moment load, or produce an ever increasing output torque, with a constant input torque, as the actuator is positioned away from center.

## OUTPUT MOTION CHARACTERISTICS

The output deflection angle ( $\beta$ ) as a function of the rotation of either the beam or the carrier is given by the following equation of motion:

$$\beta = 2\theta (1 - \sin \phi) \quad (3)$$

Large angular motion of the beam and carrier at the ends of travel produce little output motion. Therefore, avoidance of these areas of very large mechanical advantage will not produce significant output motion loss.

## DRIVE SYSTEMS

The Eccentuator can be actuated by an integral hydraulic actuator or by external power sources through a unique gear drive system. Figure 6 illustrates these two drive systems. Both of these systems operate on the action-reaction principle where the force that produces the torque to turn the beam also produces the torque to turn the carrier.

### Hydraulic Eccentuator

The hydraulic Eccentuator is produced by incorporating a rotary hydraulic actuator between the beam and the carrier as shown in figure 6(a). The beam becomes the shaft of the actuator and has one of the vanes attached. The carrier extension forms the actuator housing with a vane.

Section A-A of figure 6(a) shows that introduction of fluid under pressure into the actuator housing between the vanes produces a force on the beam vane and an equal and opposite force on the carrier. The hydraulic Eccentuator produces a surface installation which is very stiff hydraulically. The surface hydraulic stiffness is a function of the square of the mechanical advantage between the surface and the hydraulic chamber. Thus, a 24 degree output Eccentuator with its 10:1 inherent mechanical advantage will appear to be 100 times as stiff as it would be if the actuator were operating directly on the hinge line. Since the rotary actuator is one tenth the size required at the hinge line, the stiffness increase offered by the Eccentuator over a rotary actuator is approximately tenfold. This factor increases as the mechanical advantage increases for position away from the mid-travel setting.

### Mechanical Eccentuator

The preferred mechanical system utilizes a gear on the beam and a pinion gear mounted on the carrier as shown in figure 6(b). The gear set operates as a planetary system with the pinion gear being the sun gear. The system gear ratio is the product of the inherent mechanical advantage and that of the planetary gear set as follows:

$$\text{Gear Ratio} = \text{Inherent Mech Adv} \times \left( \frac{N_g}{N_p} + 1 \right) \quad (4)$$

Where:  $N_g$  = Number of gear teeth  
 $N_p$  = Number of pinion teeth

The inherent mechanical advantage amplifies the system gear ratio and minimizes the effect of any gear freeplay on the driven surface.

Other mechanical systems are indicated by the fact that rotation of either the beam or the carrier will transmit operational torque to the other member through the indexing gears. Driving through only one part requires inputting twice as much torque as is required by the preferred system described above since the torque of the beam and the carrier are additive.

#### INSTALLATION FLEXIBILITY

The Eccentuator can be installed in a number of different configurations. The three shown in figure 7 differ with each other only at the hinge line bearing on the fixed structure side. The arrangement in figure 7(a) shows the structure side hingeline bearing to be a part of the carrier. Another bearing between the carrier and the beam, which is skewed to the outer bearing, allows the beam to rotate as well as pivot within the structure.

The configuration in figure 7(b) allows the beam to rotate and pivot by use of a spherical bearing.

The configuration of figure 7(c) provides the same functions as the two above, and allows for the elimination of one bearing on the beam. The hinge structure on either side of the beam provides the loadpath from the support structure reaction to the flap beam reaction bearing. The elimination of the bearing on the structure side allows the beam to be larger in the high bending load area. The actuation friction associated with turning the beam is reduced.

The concepts in figure 7 (a) and (b) are structural hinges and a hinge is not required for the surface.

#### CONFIGURATION FLEXIBILITY

The Eccentuator concept discussed has been that of a single-ended basic Eccentuator. Two of these basic units can be joined at the pivot point to form a double-ended Eccentuator. These two concepts are depicted in figure 8. The double-ended unit will allow twice as much deflection as a single-ended unit with the same design beam angle. This double-ended arrangement allows the hydraulic Eccentuator to have dual hydraulic chambers, each of which can drive the unit full-travel with half of the load capability.

Shown in figure 8 are multiple units. The tandem arrangement has two beams and a common carrier. This system has two hinge lines. Multiple hinge lines can be achieved with multiple carriers and beams.

#### CAPABILITIES

The double-ended hydraulic Eccentuator with a design angle of 6 degrees (48 degrees total output motion) can operate against a 4868.5 newton-meter

(100000 lb-in) ultimate moment load and be housed within an estimated cylindrical envelope 10.4 cm (4.1 in) in diameter and 43 cm (17 in) long. The envelope will increase in size as the design deflection angle increases because of the necessary growth of the rotary actuator. The double-ended Eccentuator has a practical angular motion capability of around 90 degrees.

A single-ended mechanical Eccentuator with an output angle of 64 degrees has been prototyped for commercial use. However, to take advantage of the inherent mechanical advantage of the Eccentuator to reduce the size of the drive system and thus the installed envelope in an aircraft, the design output angle should be limited to around 30 degrees for a single-ended unit and 60 degrees for the double-ended Eccentuator. The Eccentuator concept offers numerous trade-off parameters which allow tailoring the design to various requirements.

#### INSTALLATION ADVANTAGES

Typical installation of a mechanical Eccentuator in a leading edge flap application is illustrated in figure 9. In the flap up position the Eccentuator is in an overcenter position and all of the cruise flight loads are transmitted through the structural elements of the Eccentuator leaving the gear drive systems unloaded. This condition also occurs in the flap down position.

Figure 10 illustrates a typical double-ended hydraulic Eccentuator in a trailing edge surface application. The Eccentuator is in the mid-travel position in the control surface neutral position. As deflection of the surface occurs on either side of neutral, the Eccentuator's variable inherent mechanical advantage increases the integral rotary hydraulic actuator output as the airloads increase. This characteristic allows the Eccentuator to be designed to lower actuating loads than the normal maximum deflection airloads.

#### CONCLUDING REMARKS

Studies have found the Eccentuator to be applicable to many other actuation problems on aircraft in addition to the thin wing surfaces. Other aerospace mechanisms on missiles, helicopters and space vehicles also present application opportunities. The joints of space and industrial robots have been identified as potential uses for the Eccentuator. Many agricultural and industrial applications have been forecast.

A working model of a double-ended hydraulic Eccentuator has been modeled in both a unit surface and a rudder application. It is demonstrated by using pressurized Freon. An electric motor powered Eccentuator missile fin control model demonstrates electro-mechanical operation. Vehicle steering with a manual Eccentuator system has been modeled and prototyped on a late model automobile. Other applications are being either modeled or prototyped in the process of developing the Eccentuator concept into a mature actuation system that will meet the demanding requirements of the aerospace industry.

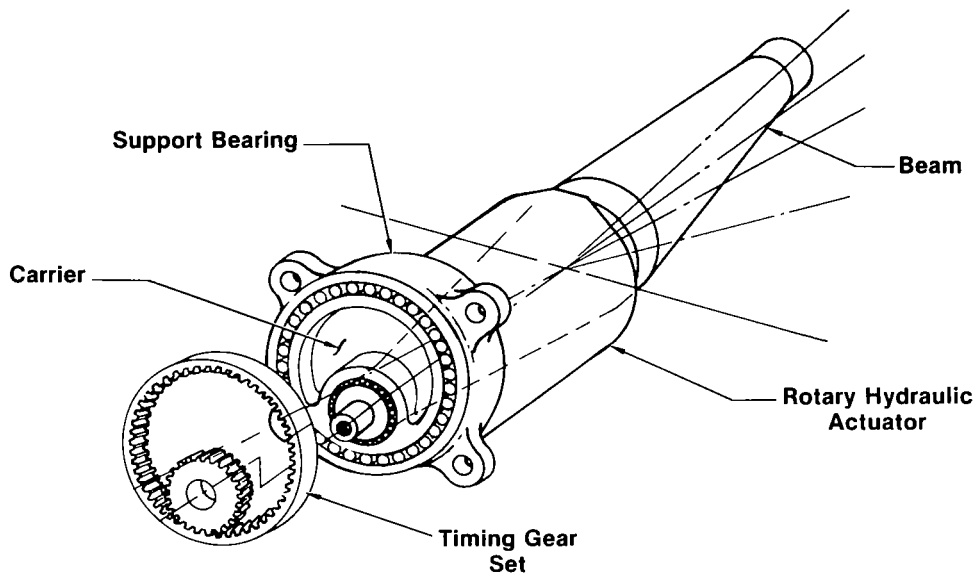


Figure 1.- Single-ended Eccentuator.

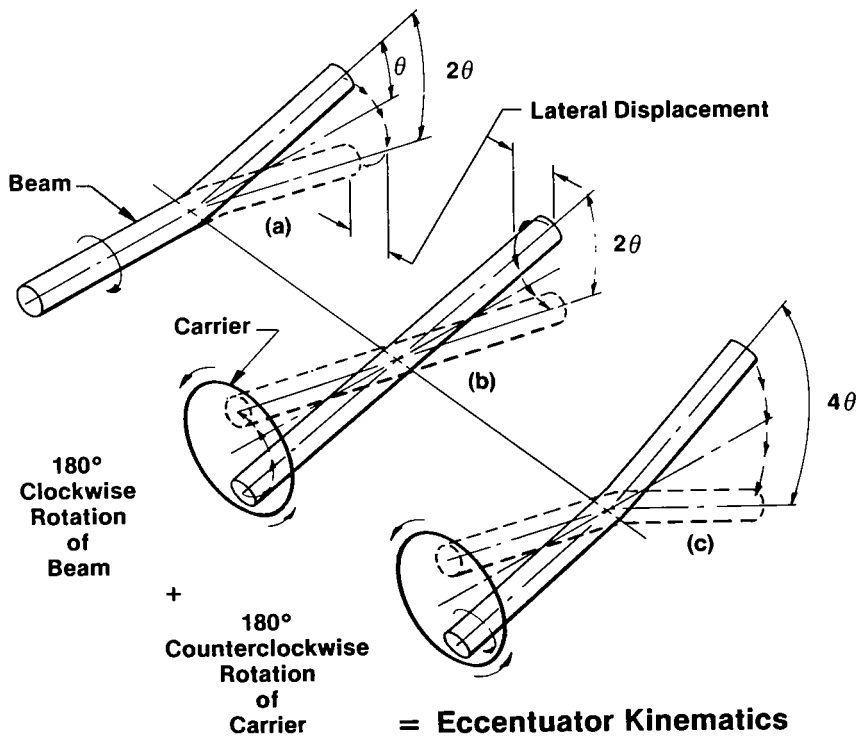


Figure 2.- Eccentuator kinematics.

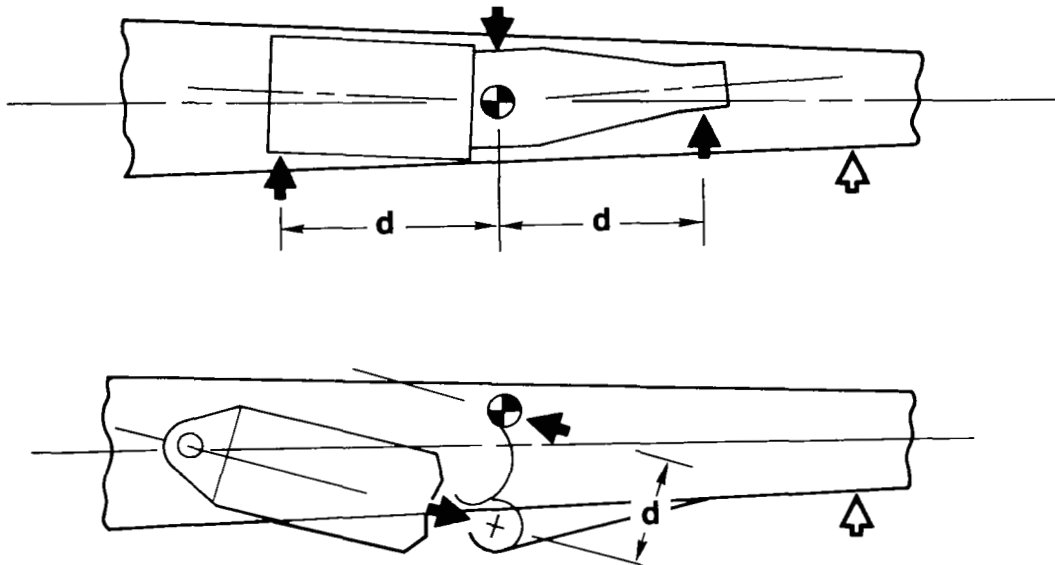


Figure 3.- Installation envelope efficiency.

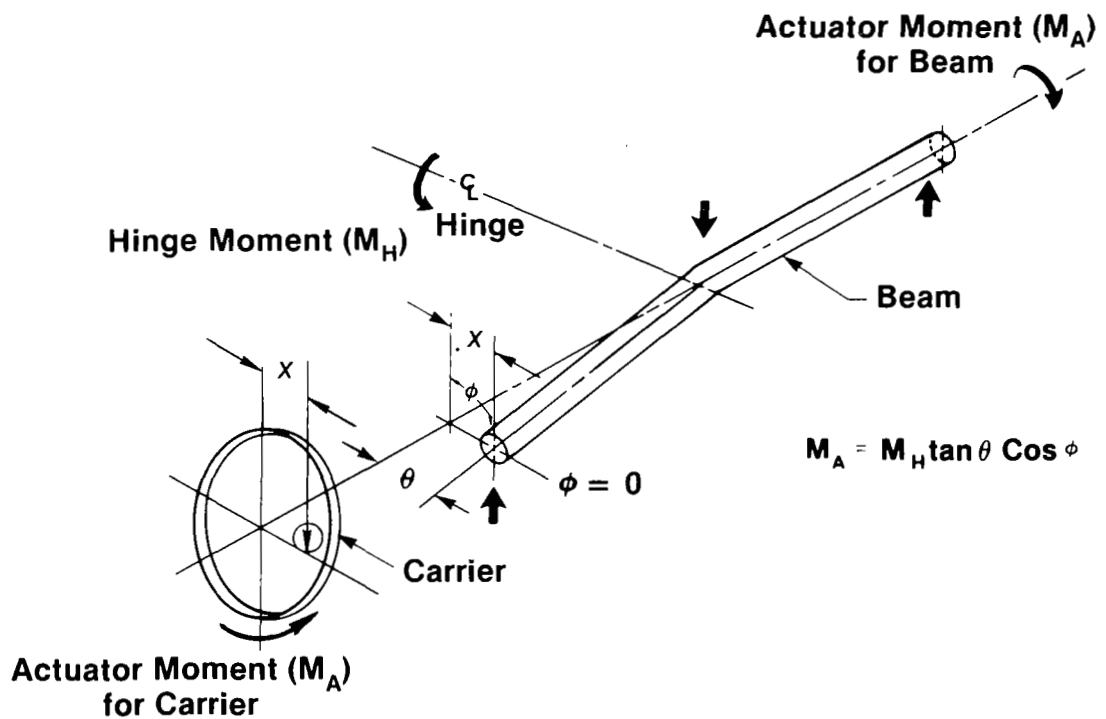


Figure 4.- Actuation loads analysis.

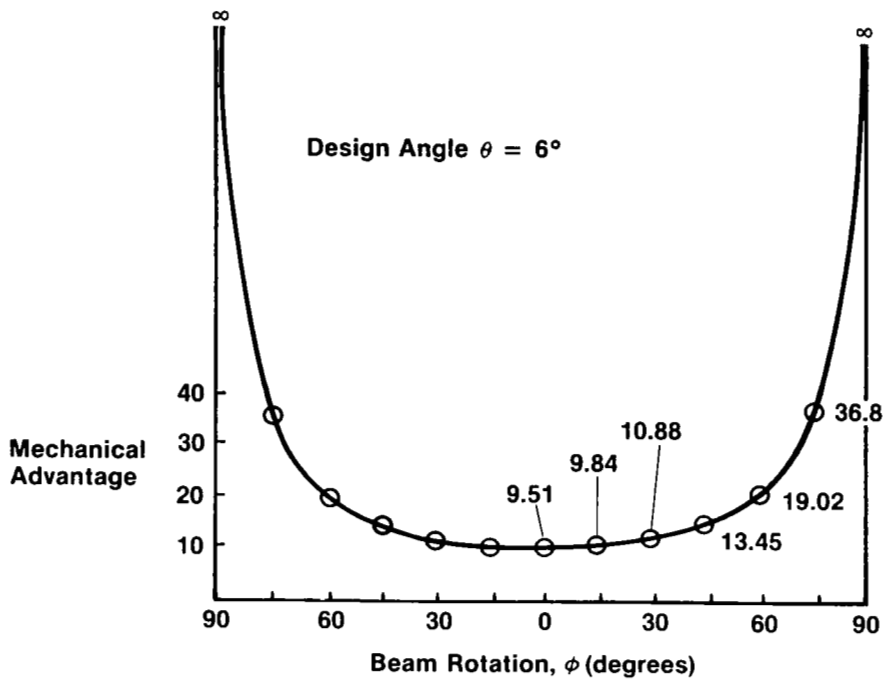


Figure 5.- Inherent mechanical advantage.

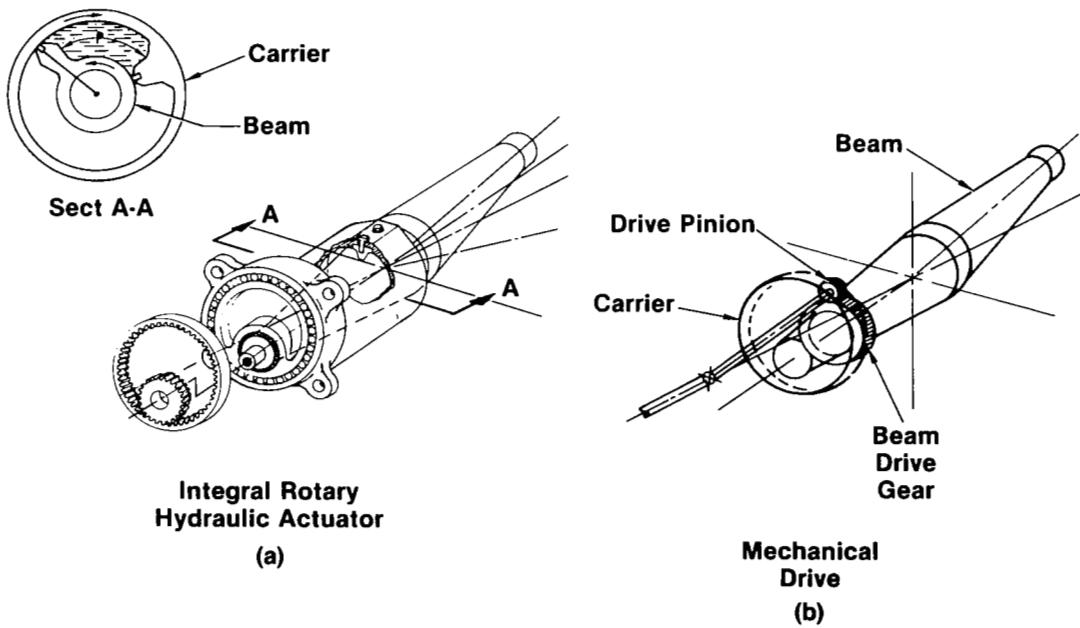


Figure 6.- Drive systems.

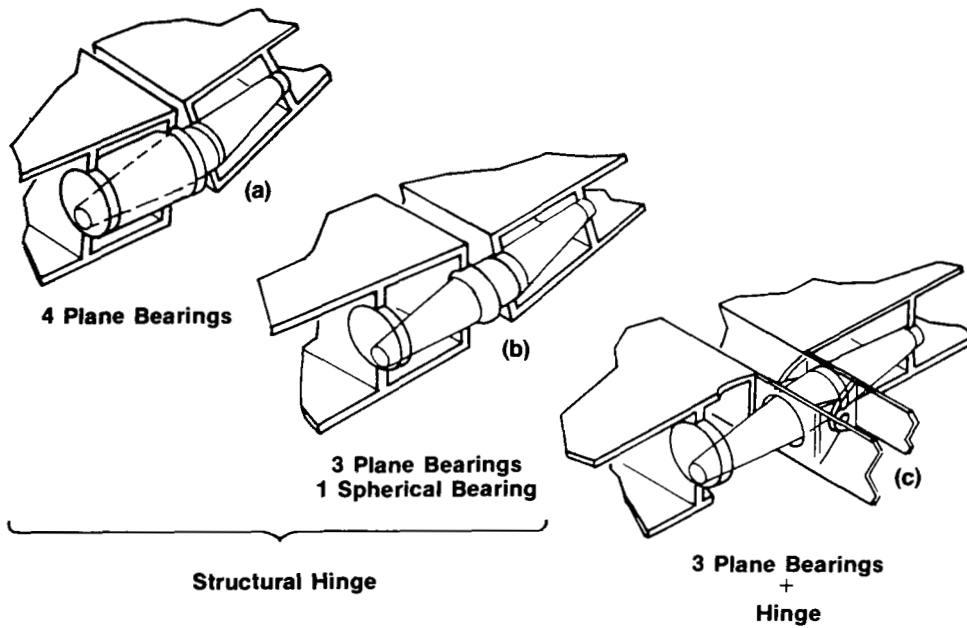


Figure 7.- Installation flexibility.

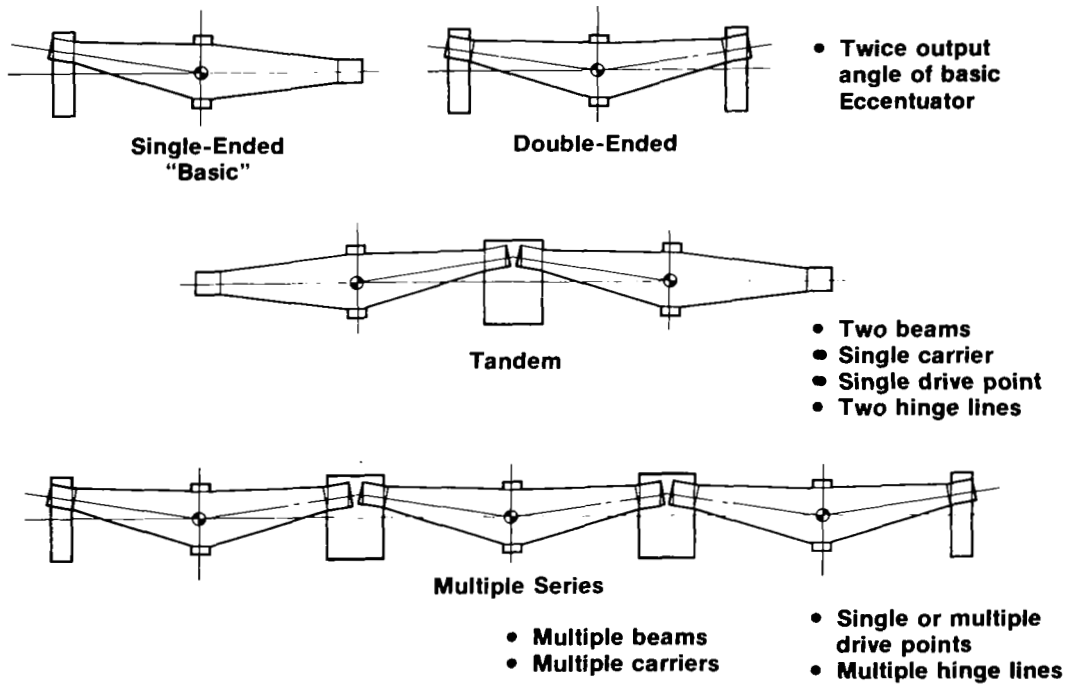


Figure 8.- Configuration flexibility.

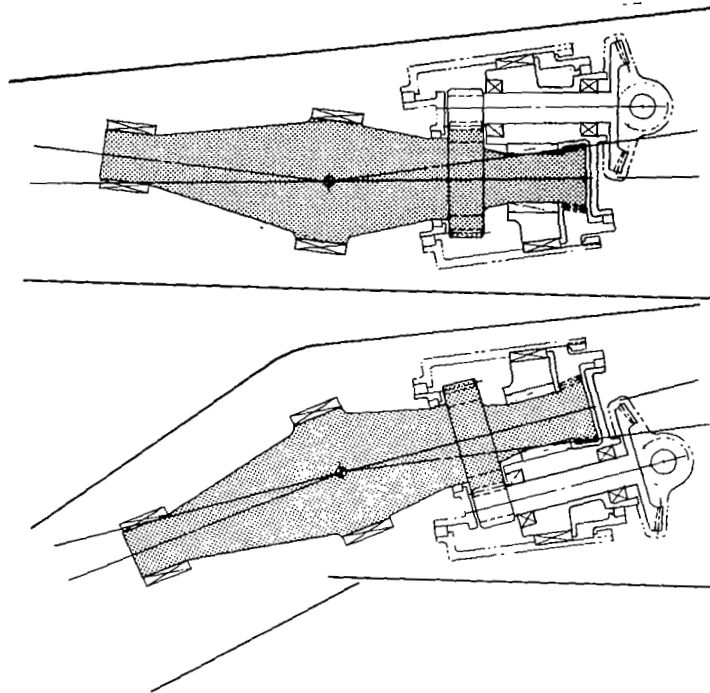


Figure 9.- Leading edge installation.

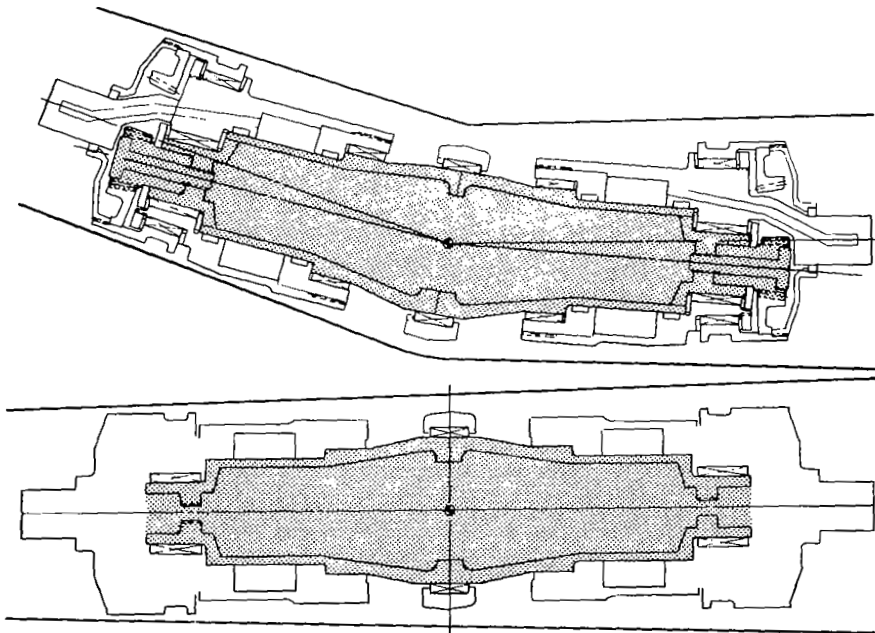


Figure 10.- Trailing edge installation.



# THE ACTUATED LATCH PIN AND ITS DEVELOPMENT

PATRICK J. LAWLOR

Institute for Industrial Research & Standards.

DUBLIN, IRELAND.

## ABSTRACT

An actuated latch pin has been developed to meet the need for a reusable locking device. The unit can function as a pin puller or as a pin pusher latch. Initial prototype testing demonstrated the feasibility of the device with the unit being driven from a 28 V d.c. supply and using 15 W to drive a 12 mm diameter pin through a stroke of 10 mm with a side load of 100 N in 120 ms.

High wear rates with the MOS<sub>2</sub> lubrication on the ballscrew and angular contact bearings have necessitated the reduction in the duty cycle from 1000 cycles in air and vacuum to 100 in air and 1000 in vacuum.

## REASON FOR DEVELOPMENT

The Actuated Latch Pin (ALP) has been developed to meet the need for a reusable locking device suitable for use in a hard vacuum of the order of  $10^{-7}$  torr. Currently, locking and unlocking devices which need to be remotely controlled utilize pyrotechnics to achieve movements; however, these components have several drawbacks including one or two shot operations and the inability to be repositioned once activated.

Specifically the development of the ALP was initiated by the European Space Research and Technology Centre (ESTEC) as there was a need for a device to restrain the piston of the pneumatic ejection system of the Spin Up and Ejection Mechanism (S.U.E.M.), which was to be used to launch spacelab sub-satellites. This device was to retract to permit firing of the piston and to extend to lock the piston after it had been retracted.

## SPECIFICATION

The ALP requirements were based on the ESTEC specification and the major requirements are tabulated in Table 1.

A close look at the specification revealed several potential problem areas. The basic requirement of mass, envelope, power strength and side load indicated that high efficiency components would be required and it was doubtful if indeed this could be achieved. However, the major potential

problem related to the duty cycle of running in air and a vacuum and only being allowed to use dry lubricants. Therefore, there was a requirement for a dry lubricant which could perform in air and a vacuum. Since the wear rates on lead lubricated components are very high in air, it was decided that another form of dry lubrication would be necessary. After discussions with several manufacturers and the National Centre of Tribology at Risley, England, it was decided that the  $\text{MOS}_2$  sputtered process should be used as the lubricant. (See ref. 1.)

TABLE 1.- ALP FUNCTIONAL REQUIREMENTS

Mass	500 gms
Envelope	34 mm x 34 mm x 80 mm
Stroke	10 mm repeatable to 0.1 mm
Retraction Force	25 N over whole of travel above any friction
Side force sensitivity	Meet requirements with side load of 100 N
Duty Cycle - Ground Orbit	10,000 cycles in air 1,000 cycles in vacuum harder than $10^{-7}$ torr
Alignment	Maintained with its nominal axis within $\pm 0.05$ degrees under all conditions
Stiffness	Greater than $10^5 \frac{\text{Nm}}{\text{Rad}}$
Ultimate Strength	$1.8 \times 10^4$ N Radial force on pin top
Proof Strength	$1 \times 10^4$ N Radial force on pin top
Power	Operating power not to exceed 15 W Average power not to exceed 1 W
Voltage	28 V $\pm$ 4 V dc
Time to Retract or Extend.	120 ms

## CONCEPTUAL DESIGN

There were several possible ways of achieving the design requirement but two approaches were singled out for more detailed study, these were solenoid and motor ballscrew configurations. Initially, the solenoid characteristics looked eminently suitable for the design but on closer inspection it was found that several major problems would have to be overcome if a satisfactory design was to be achieved. These problems were associated with the size, weight and power consumption of a solenoid device which would meet the force criteria of the specification. There were additional problems of cost and timescale quoted by several manufacturers and these were outside the scope of the ALP contract.

The motor ballscrew configuration looked more attractive in terms of meeting the power requirements but the problems of switching the motor off and actually stopping the device at the end of its stroke had to be overcome. The approach of solving these problems was to use reed switches, potted in a suitable compound, to act as the switching and indicating device and to use buffers to absorb the surplus energy at the end of the stroke to prevent bounce.

## FIRST PROTOTYPE DEVELOPMENT

### Description

The first prototype consisted of a samarium cobalt permanent d.c. motor driving a precision ballscrew to move the latch pin in or out (fig. 1). The direction of the latch pin is a function of the applied voltage polarity. The latch pin slides on a dry plain bearing with pin rotation being prevented by a guide located in the nose cap.

Detent action was by permanent magnets which moved with the pin and were located at each end. Located at either end of the stroke path are reed switches which serve the dual function of indicating latch pin status and acting as a limit switch for the motor.

The complete mechanism is located in a stainless steel housing. The end cap is adapted to enable a simple tool to be used for manual override. The nose cap is threaded to enable the ALP to be screwed into a suitable housing. However, alternative nose cap designs could be evolved for various mounting configurations. Electrical power is supplied via an external socket.

### Operation

When extend or retract is selected the motor rotates approximately six times and peak velocity of the motor is about 3600 r.p.m.

### Testing

Test results achieved with the first prototype are tabulated in Table 2.

TABLE 2.- FIRST PROTOTYPE TESTING

Test	Result	Specification Target
Ground Duty 10,000 cycles	ALP Functional for 10,000 cycles	ALP functioning ALP meeting performance requirements after cycling
Sample Functioning Test	ALP Functioned	ALP Functioning
Stroke - Movement (No sideload)	6.78 mm	10 mm
Stroke - Repeatability	0.5 mm	0.1 mm
Retaining Force	44.7 N	2.5 N
Peak Power	Limited to 14 W	15 W
Passive Sensitivity-location	0.645 mm	1.0 mm
Passive Sensitivity-Movement	0.01 mm	No movement
Retraction Force	37.7 N	25 N
Operating Time - Retraction	119 msec	120 msec
Operating Time - Extension	113 msec	120 msec
Alignment - Angle, degrees Linear	< 0.02 < 0.005 mm	<+0.05 < 0.005 mm

## PROBLEMS WITH FIRST PROTOTYPE

### Detent

During initial functioning testing it became apparent that permanent magnet detents were not suitable as it was found impossible to align all the magnets simultaneously. Also, the pin which was to prevent rotation caused a considerable increase in friction when a side load was imposed. Thus, a further development was carried out and a cantilever spring detent, which located on a Delrin housing, was chosen. This Delrin housing also incorporated the anti-rotation device. This set-up proved highly successful with a retaining force of 30 N being achieved. This approach is currently incorporated in the design.

### Energy Absorbing Device

There was a requirement for the ALP to move through a distance of 10 mm and be repeatable to within 0.1 mm with a side load of 100 N. The maximum energy input to the ALP was related to that energy required to achieve performance with sideload. The problem then arose as to how to dissipate this energy when the side load was removed. It was decided to remove the surplus energy with an energy absorbent material. At this time, several materials have been tried and the best results have been achieved with a fibrous nylon.

## ENGINEERING MODEL

The engineering model was constructed using components of a type suitable for use in a vacuum. Modifications found necessary during testing of the first prototype were also incorporated.

### Basic Test Requirement

The engineering model test programme was to consist of testing in air and clocking up 1000 cycles and then testing in a vacuum of  $10^{-7}$  torr and interface temperature of  $-30^{\circ}$  C to  $60^{\circ}$  C.

### Test Programme in Air

Testing was conducted in a clean room of class 100,000 with a mean temperature of  $20^{\circ}$  C and relative humidity of 45%.

## PROBLEMS WITH ENGINEERING MODEL

### Energy Absorbing Device

As the results in Table 3 indicate the improved energy absorbing device did not meet the full requirements. However, further investigations are going on to try and find a suitable space qualifiable material which will meet this requirement.

### Brush Gear Failure

After the initial testing, the ALP was set up for cyclic testing. The cycle time was set to 10 seconds. The cycle operation was set in motion and proceeded without fault until 710 cycles had been clocked up; then the ALP ceased to function. Tests on the drive electrics and switch gear indicated that they were functioning satisfactorily. Thus, it was decided to strip down the ALP for investigation. On strip down it was revealed that one of the motor brushes had broken off. The brush gear and broken off brush were removed and sent to ESTEC for a failure investigation. The resulting failure investigation report has been sent to the motor manufacturer for comment, but at this time none has been received.

### Failure of $\text{MOS}_2$ Lubrication on the Ballscrew

The ALP was reassembled with another set of brush gears and cyclic testing continued after initial functional testing. After 100 extra cycles the retraction and extension times started to increase. Further running showed that the rate of slow down was accelerating. Initially it was thought that the brush gear was again causing trouble so the ALP was stripped down and the space qualifiable motor was replaced with the standard prototype motor. This combination was then run but the results showed no improvement. The ballscrew was then removed and tests showed that the friction in the ballscrew had increased. This increase in friction was not determined quantitatively but a comparison test was carried out to compare the ballscrew ability to back-drive itself. A study of the ballscrew under a microscope at x 40 magnification showed indications of wear on the lubricative surface. Thus, it was decided to return the ballscrew to the manufacturer for investigation.

### Test Results

Test results achieved with the engineering model in air are tabulated in Table 3.

TABLE 3.- ENGINEERING MODEL TEST RESULTS

TEST	RESULT	SPECIFICATION TARGET
Simple functioning test	ALP functioned	ALP functioning
Stroke <sup>I</sup> - Movement	9.31 mm	10 mm
- Repeatability	0.4 mm	0.1 mm
Retaining Force	39.3 N	2.5 N
Peak Power - 1st 10 ms	53 W*	15 W
after 10 ms	12 W	15 W
Approx. Average Power for stroke	9 W	15 W
Passive Sensitivity - Location	Zero	1.0 mm
Passive Sensitivity - Movement	Zero	No movement
Retraction Force	32.4 N	25 N
Operating Time - Retraction	112 ms	120 ms
" " - Extension	100 ms	120 ms
Alignment - Angle	< 0.02 <sup>0</sup>	< 0.05 <sup>0</sup>
- Linear	< 0.005 mm	< 0.05 mm

I No sideload

\* Instantaneous Power

## MANUFACTURERS REPORT

The manufacturers indicated that  $\text{MOS}_2$  sputtered coat had worn away along the rolling area of the ball to the thread, i.e. there was metal to metal contact. It was also suggested that a possible cause of the increased friction within the ballscrew was the breakaway debris of  $\text{MOS}_2$ . They also pointed out that the  $\text{MOS}_2$  coat thickness of 0.2 micrometre was compatible with the ballscrew surface finish which had a C.L.A. of 0.05 to 0.1 micrometre and the balls which had a C.L.A. of 0.02 micrometre.

## IMPLICATIONS OF FAILURES

The failures incurred during the design of the ALP were catastrophic in nature; thus, satisfactory answers must be found to account for them. The brush gear failure is being thoroughly investigated and it is hoped that the cause of the failure will be ascertained. However, the failure of the  $\text{MOS}_2$  sputtered coating leads one to wonder if this approach is suitable for the type of duty cycle required by the ALP, i.e., of relatively high speed and operation in air and in vacuum. Some researchers (ref. 2) have obtained good results under laboratory conditions, but there was some doubt as to the performance at high speeds and operation in air. Thus, it would be pertinent for these areas to be investigated further as certainly there is a requirement for a lubrication technique which will meet the requirements as specified for the ALP.

## NEXT STEP IN ALP DEVELOPMENT

After discussions with ESA and the National Tribology Centre, Risley, it was decided that the number of cycles specified for the ALP was too great considering the duty cycle and the environment. Thus, ESA decided to relax the number of cycles from 1000 to 100 cycles in air while retaining 1000 cycles in a vacuum.

They also decided that the balls of the ballscrew should also be coated with  $\text{MOS}_2$ .

## RECOMMENDATIONS FOR FURTHER ALP DEVELOPMENT

Future trends in Space Technology indicate that reusable components must now be designed. The ALP is a fundamental mechanism which meets this criteria and should find use in a considerable number of varied functions. The current work was aimed at developing a locking device of a particular size. However, the ALP design could be thought of in terms of a family of devices covering a range of sizes. A further interesting development would be the incorporation of a stepper motor. This would add an inching capability to the device which would considerably increase its usefulness as it could be used to control other components such as valves, etc. Thus it can be seen that further development of the mechanism is essential as it fulfills a fundamental requirement and can be considered a basic reusable building block in the field of space mechanisms.

The shortcoming of the  $\text{MOS}_2$  lubrication process indicates that further work be carried out as there is certainly a requirement for improvement in this area.

## REFERENCES

- (1) Talivaldis Spalvins, Bearing Endurance Tests in Vacuum for Sputtered Molybdenum Disulfide Films. NASA TMX-3193, 1975.
- (2) Lammer, J., Niederhauser, P., Hinterman H. E.,  $\text{MOS}_2$  Thin Layers Deposited by R.F. Sputtering. International Conference on Plating and Allied Techniques, London, July 1979, Proceeding 1 Pat 79, pp. 204-210.

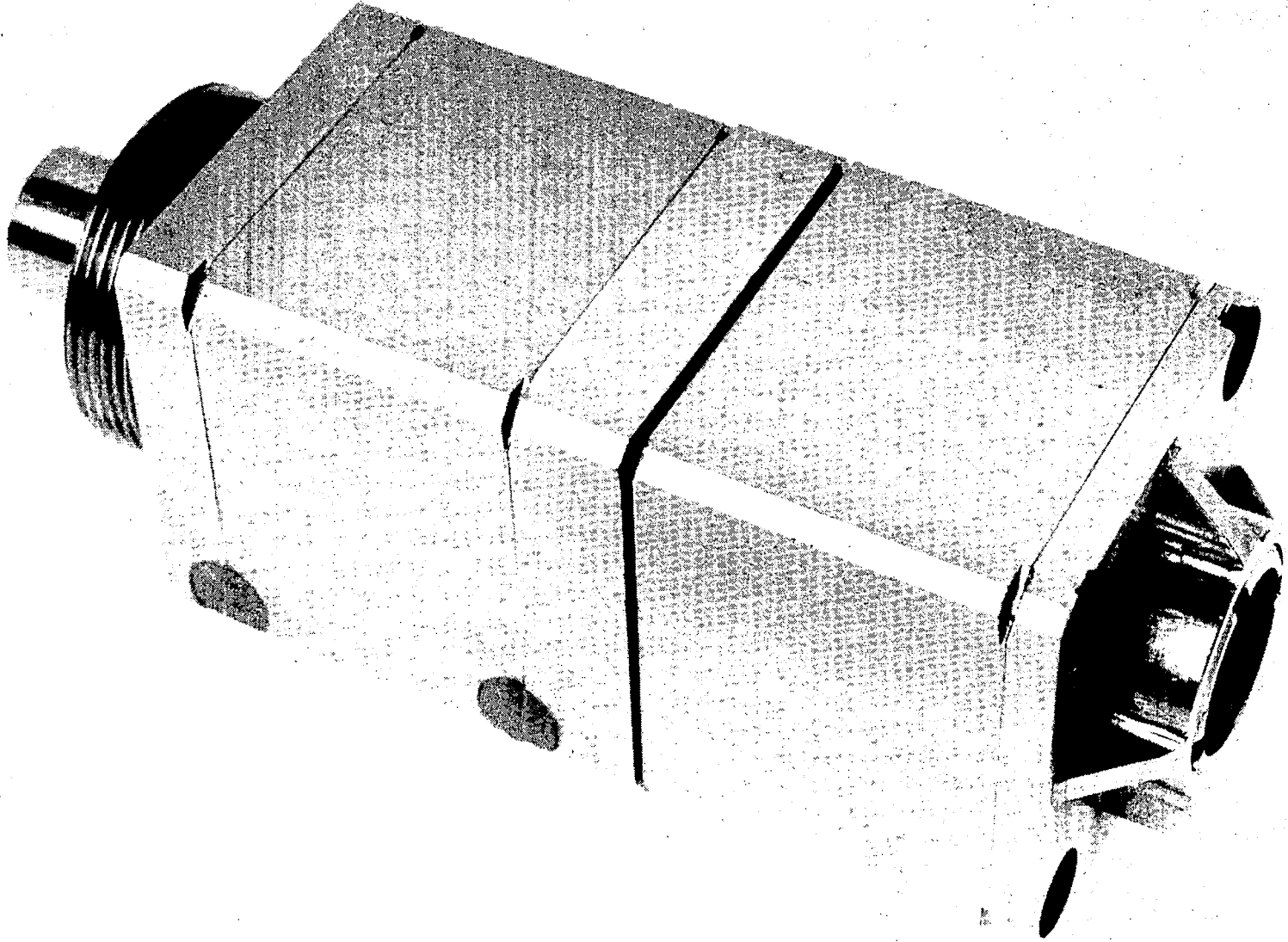


Figure 1.- First prototype.

BALL BEARING VERSUS MAGNETIC BEARING REACTION  
AND MOMENTUM WHEELS AS MOMENTUM ACTUATORS

W. Auer  
TELDIX GmbH  
Heidelberg  
Germany

SUMMARY

For the attitude control of satellites, momentum actuators with different bearing technologies are available. After a short familiarization with the subject, an attempt is made to establish a guideline for the selection of the suitable momentum actuators or momentum actuator configurations to meet given mission goals with high reliability and low cost.

INTRODUCTION

For 3-axis body stabilized satellites, momentum actuators serve, for instance, as a means of averaging out periodical disturbance torques or to turn a spacecraft so as to pinpoint its instruments accurately to different objects. Common to all applications is the goal to save fuel and employ as far as possible electrical energy generated from the sun's radiation.

The discussion about the relative merits of different bearing approaches and technologies of momentum actuators gained has high interest. To establish a basis, some examples of ball bearing and magnetic bearing momentum actuators are first described, together with some typical specifications.

MOMENTUM ACTUATORS

Designs, Configurations and Performance

For the following designs and configurations the main parameters are shown in table I:

1. Ball Bearing Momentum Wheel, BMW
2. Ball Bearing Reaction Wheel, BBRW
3. Magnetic Bearing Momentum Wheel, MBMW 5, with 5 actively controlled degrees of freedom
4. Magnetic Bearing Momentum Wheel, MBMW 1, with 1 actively controlled degree of freedom
5. Magnetic Bearing Reaction Wheel, MBRW 2, with 2 actively controlled degrees of freedom

6. Magnetic Bearing Reaction Wheel, MBRW 1, with 1 actively controlled degree of freedom
7. T-Configuration: 1 Momentum Wheel + 1 Reaction Wheel with their spin axes perpendicular to each other
8. V-Configuration: 2 Momentum Wheels with an angle on the order of 20 deg between their spin axes
9.  $\Delta$ -Configuration: 2 Momentum Wheels + 1 Momentum Wheel with cw/ccw running capability, spin axis in the plane of the two others and perpendicular to their momentum vector sum
10. Tripod-Configuration: 3 Reaction Wheels with orthogonal-oriented spin axes
11. Quadruple-Configuration: 4 Reaction Wheels, 3 of which are orthogonally oriented, the 4th inclined to each of the 3
12. Double Gimbal Momentum Wheel, DGMW, with 1 or 2 Momentum Wheels mounted in a gimbal system.

For 1: Flight proven BBMW designs of different suppliers are available. Modern concepts need no load relief or caging mechanisms to survive launch loads. Wheels equipped with well preloaded and lubricated ball bearing pairs and automatic lubrication applicators achieve a life of more than 7 years with a 2% failure probability. The conservatively calculated fatigue life of properly lubricated bearing pairs for a 1% failure probability is more than 20 years. No zero g - 1 g and slew rate problems should be expected (ref. 1). Figure 1 shows the cross section of a BBMW.

For 2: BBRW's are also offered by different suppliers. Newer designs avoid any kind of caging or load relief mechanisms. By appropriate bearing and lubrication selection, an adequate lubrication film can be achieved even at very low speeds. Typically, at normal room temperatures, balls and races are already separated by the lubricant at 1 revolution per second. Therefore, long life with high probability is the consequence. A problem may be the step in the reaction torque caused by friction when the speed is crossing zero. Figure 2 gives an example of a BBRW, which may be equipped with an ac asynchronous or a brushless dc motor.

For 3: Magnetic bearings have been well known for many years. Due to the slogan "no contact between moving and nonmoving members, therefore no wear," one is inclined to expect a high lifetime with an extremely high reliability.

Table I shows reliability figures for a complete wheel with 5 actively controlled degrees of freedom, including motor and nonredundant bearing electronics of 93%, with redundant bearing electronics of 98% for a 7-year life (ref. 2).

The stiffness of an MBMW 5 around the lateral axes is comparable with that of a BBMW. A distinct advantage could be the possibility of tilting the

momentum vector of the rotor simply by adding signals to the corresponding control loops. This "vernier gimbaling" capability may be used for fine pointing or oscillation (nutation) damping of a spacecraft. In figure 3, an MBMW 5 developed for COMSAT is shown. The emergency ball bearings are able to withstand launch loads without caging.

For 4: Two main approaches of a mainly passive MBMW 1 are known. One utilizes radial repulsive forces of permanent magnet rings, and the other secondary radial forces generated by axial attracting magnets (refs. 3 and 4). Despite the fact that only one control loop (along the spin axis) is necessary, the reliability of a complete wheel, including motor and bearing electronics, is only on the order of 96% for a 7-year life. This can be raised to 99% with redundant bearing electronics.

Because of the low stiffness of these bearings about lateral axes, the transfer of rotational energy of a wheel to the body of a satellite - resulting in nutational motions - is possible and must be counteracted by adequate means (ref. 5).

For 5: One design for an MBRW 2 is shown in figure 4. Actively controlled are the two lateral degrees of freedom. This approach offers simple assembly procedures and a low volume.

The reaction torque noise and ripple as well as the zero speed crossing are mainly influenced not by the bearing but by the motor.

For 6: The design of an MBRW 1 is similar to that of an MBMW 1 but the means for nutation damping are less sophisticated. The reaction torque characteristic is the same as with the MBRW 2.

For 7: This configuration offers active spacecraft attitude control along 2 axes and, in a sequence, probably also about 3 axes.

To achieve higher reliability figures, a TT-configuration is generally necessary.

For 8: This configuration has essentially the same attitude control performance and reliability as the T-configuration; therefore, a VV-configuration must also be taken into consideration.

For 9: In the  $\Delta$ -configuration, only 2 out of 3 wheels are in operation, and these actively control 2 axes of a spacecraft.

The primary mode is identical with that of the V-configuration. If one of the momentum wheels fails, the third momentum wheel which is capable of running in cw/ccw direction, is switched on in the appropriate sense of rotation to maintain the momentum vector sum direction.

For 10: This system is able to control a spacecraft actively about all 3 axes. Under steady state conditions, all 3 reaction wheels operate at speeds near to or at zero. Therefore, this system belongs to the "zero momentum

systems." For high pointing accuracy performance MBRW's could be advantageous, but BBRW's also allow good results when they are kept spinning at low speed during an observation period.

For 11: This configuration is also a zero momentum system. Normally, all 4 wheels are running at a moderate speed, which offers high pointing accuracy.

If one out of the 4 wheels fails, the speeds of the other wheels are adjusted to maintain a zero momentum system.

For 12: This configuration is especially suited for 3-axis active control of geosynchronous spacecraft.

Figure 5 shows an example. Two momentum wheels, which could be operated at the same time, are mounted in a gimbal system. The gimbal axes could be driven by motors (or torquers). Both gimbal axes are equipped with two motors and pick-offs. Therefore, this system is redundant along all 3 axes.

#### MISSION AND MOMENTUM ACTUATORS

After this brief description of the different momentum actuators, an attempt will be made to relate their capabilities to mission and budgetary requirements. Two mission types are taken into account: communication/tv satellites and observation/navigation/research satellites.

##### Communication/TV Satellites

These satellites are assumed to be of the geostationary type.

First of all, the pointing accuracy required should be treated as a function of mass for different actuators (fig. 6). The nominal values for SYMPHONIE, OTS, INTELSAT V, ECS and TV-SAT are indicated.

It is evident that from a mass point of view the MBMW 1 has no advantage over the respective BBMW. On the contrary, special measures against nutational instability must be considered. The MBMW 5 shows as a benefit a higher pointing accuracy potential, essentially that of the DGMW. It should be born in mind, however, that a DGMW has a gimbaling capability of about 50 times that of an MBMW 5 (about 7.5 deg to 0.17 deg).

Other interesting relationships can be deduced from figure 7. For a 1 degree-of-freedom system (1 DOF) it is interesting to compare the BBMW cost trends with those of the MBMW with and without redundant electronics. One MBMW with redundant electronics costs about the same as two BBMW's, but the reliability of the first one is so low that generally two MBMW's would be needed.

The 2 DOF approaches,  $\Delta$ , T, TT, V and VV configurations allow the following interpretation. Single T and V arrangements should not be taken into consideration because reliability is so low. The  $\Delta$  configuration and the TT/VV configuration are comparable in reliability, but the costs of the latter are higher.

In the  $\Delta$  configuration the nominal total angular momentum can vary between 1 and 2 depending on which 2 wheels out of the 3 are in operation. This is, of course, not the case with the TT/VV configuration where the nominal total angular momentum is the same in the primary and redundant mode.

A 3 DOF control can be achieved with 1 DGMW or with 1 or 2 MBMW 5. A certain compensation for the higher cost and the lower reliability of the 2-MBMW 5 solution could be the higher potential of attitude accuracy.

In figure 8 an attempt is made to estimate the mass of different actuator assemblies for different classes of satellites represented by their masses. For communication satellites of up to the 1000-kg class the 2 BBMW configuration is most suitable. If, however, a higher pointing accuracy is required, and/or only a limited north/south station keeping capability is implemented, the  $\Delta$  BBMW configuration can meet the specifications.

For TV satellites of up to the 2000-kg class, the most attractive configuration seems to be the DGMW approach. The MBMW arrangements result in a higher mass, but offer a higher angular momentum capability.

The DGMW and the MBMW 5 can both provide active damping of satellite oscillations.

#### Observation/Navigation/Research Satellites

For these satellites, reaction wheel arrangements are of interest.

A good overall view, giving the reliability/cost relation, is shown in figure 9 for 3, 4 and 6 BBRW's, and MBRW's with and without redundant electronics. For the 2 to 5 N·m/s reaction wheel class, somewhat higher cost of MBRW's compared with BBRW's is assumed.

It is interesting to note that a quadruple configuration of 4 MBRW's with redundant electronics gives a higher reliability than can be achieved with redundant tripod configurations of 6 BBRW's.

Of course, reaction wheel configurations also may be employed in communication satellites.

#### CONCLUSIONS

After weighing the essential parameters it is believed that the following selection guide can be proposed:

For communication satellites:

With 0.2-deg pointing accuracy:

2 BBMW's, parallel spin axes

With 0.1-deg pointing accuracy:

3 BBMW's  $\Delta$  configuration, or

4 BBRW's quadruple, or

4 MBRW's quadruple (with redundant electronics)

For TV satellites of:

Medium mass:

1 DGMW, or

4 BBRW's, or

4 MBRW's (with redundant electronics)

High mass:

The same as medium mass plus MBMW configurations

For observation/navigation/research satellites:

Short time missions:

3 BBRW's

3 MBRW's

Long time missions:

4 BBRW's

4 MBRW's (with redundant electronics)

The comparison between ball bearing and magnetic bearing momentum actuators shows that given mission requirements can be economically met by employing the ball bearing technology without decreasing reliability and lifetime.

However, for some special mission requirements, such as "zero friction at zero speed," fine pointing (met by vernier gimbaling), and/or active damping, magnetic bearings may be advantageous.

This makes evident that magnetic bearing technology will not replace ball bearing technology for momentum actuators, but will supplement it for some special mission requirements.

## REFERENCES

1. Auer, W. F.: Design and Lubrication of Ball Bearing Units for Flywheels. European Space Tribology Symposium, Frascati, April 9-11, 1975.
2. Sindlinger, R. S.: Magnetic Bearing Momentum Wheels With Magnetic Gimballing Capability for 3-Axis Active Attitude Control and Energy Storage. 11th Aerospace Mechanisms Symposium, Greenbelt, Maryland, April 28-29, 1977.
3. Poubeau, P. C.: Development of a Satellite Flywheel Family Operating on One Active Axis Magnetic Bearings. 11th Aerospace Mechanisms Symposium, Greenbelt, Maryland, April 28-29, 1977.
4. Harrison, A. J.: An Optimized 50 Nms Momentum Wheel Utilizing Magnetic Repulsion Bearing. Attitude and Orbit Control Systems Conference, Noordwijk, October 3-6, 1977.
5. Reinhoudt, J. P.: On the Stability of Rotor and Bearing Systems and on the Calculation of Sliding Bearings. Thesis 1972, TU Delft.

TABLE I.- MOMENTUM ACTUATORS

	Angular momentum, N·m/s	Nominal speed, $10^3 \text{ min}^{-1}$	Output torque, N·m	Power, steady state, W	Power, max., W	Reliability, 7 years, %	Starting torque, $10^{-4} \text{ N·m}$	Dimensions, $\phi \times h$ , mm	Mass, kg
BBMW	20-70	3.0-6.0	$\pm 0.1$	6-20	50-100	98.6	50	350×120	5-8
BBRW	2-25	$\pm 2.0-6.0$	$\pm 0.1$	6-20	50-100	97.5	30	205×77 350×120	2.4-4 5-6
MBMW 5	30-150	5.0-8.0	$\pm 0.1$	10-15	70-120	93/98*	1	350×150	12-17**
MBMW 1	50-100	7.7-24.0	$\pm 0.1$	15-20	120-190	96/99*	1	350×220	12-17**
MBRW 2	1-5	$\pm 1.5-3.5$	$\pm 0.1$	3-5	20-40	96/99*	1	220×90	3-3.5**
MBRW 1	2	$\pm 3.0$	$\pm 0.1$	3	47	96/99*	1	250×120	3**
T-Conf.	1 BBMW / 1 BBRW					96.1	TT	99.85	
V-Conf.	2 BBMW					97.2	VV	99.92	
$\Delta$ -Conf.	3 BBMW					99.9			
Tripod	3 BBRW					92.7	Double Tripod	99.8	
	3 MBRW					88.5	Double Tripod	99.5	
	3 MBRW*					97.0	Double Tripod	99.97	
Quadruple	4 BBRW					99.6			
	4 MBRW					99.0			
	4 MBRW*					99.94			
DGMW	2 BBMW + Gimbal system (redundant motors and pick-up's)					99.8			

\*With redundant electronics.

\*\*Including electronics.

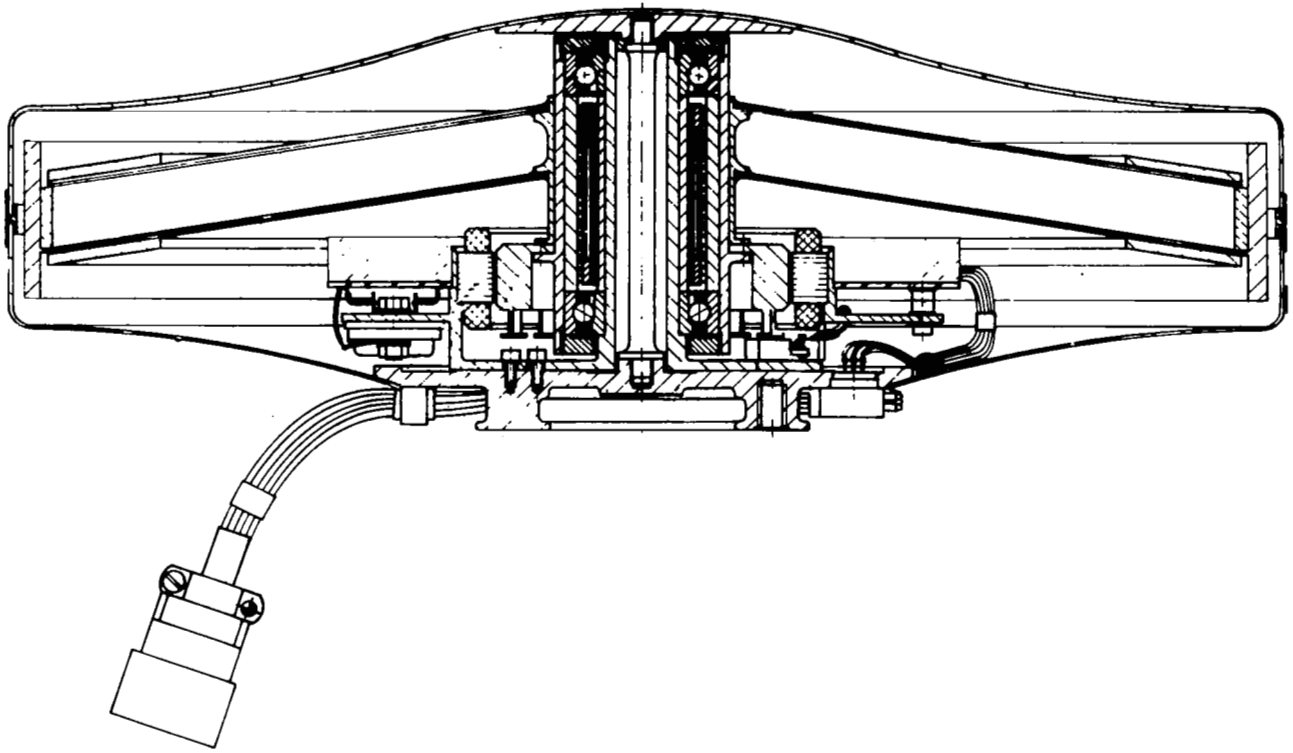


Figure 1.- Cross section of a BMW.

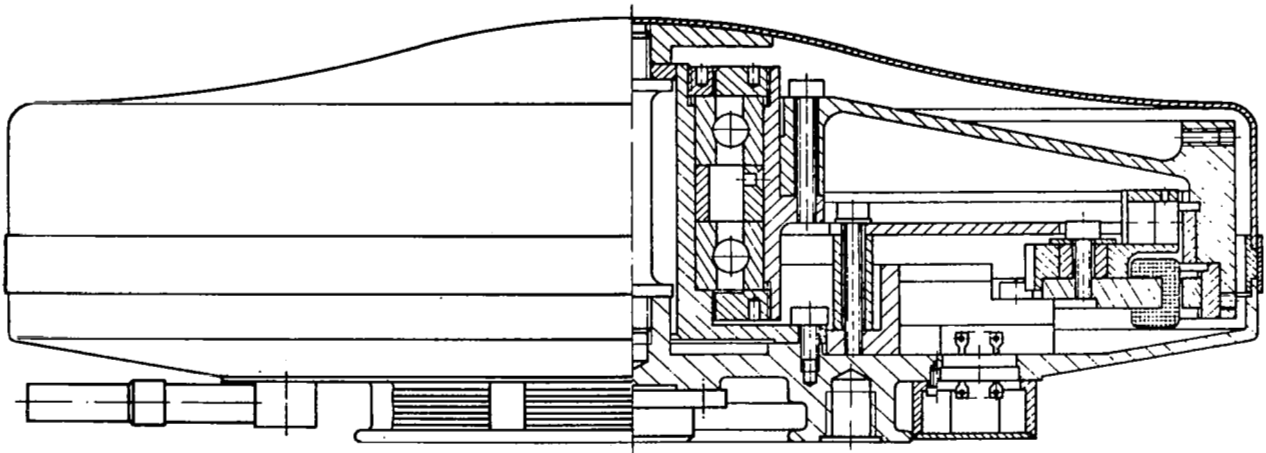


Figure 2.- Cross section of a BBRW.

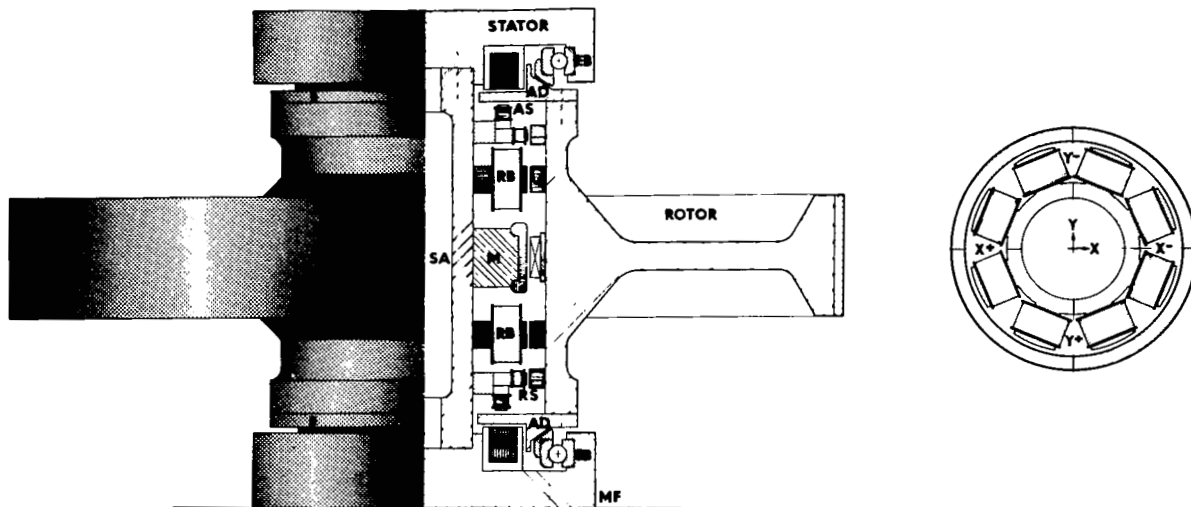


Figure 3.- Cross section of an MBMW 5.

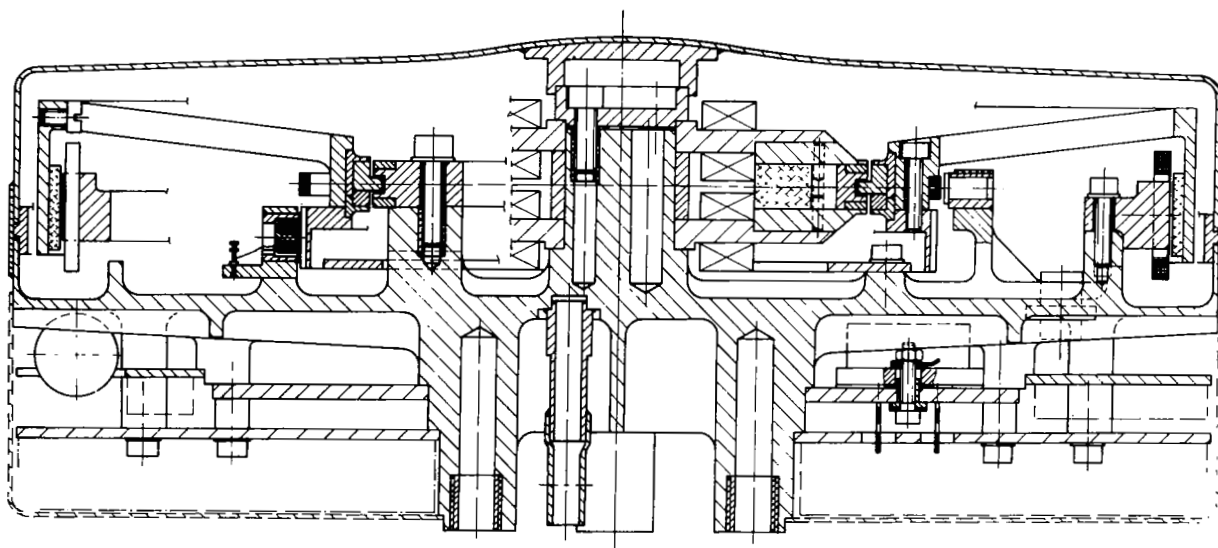


Figure 4.- Cross section of an MBRW 2.

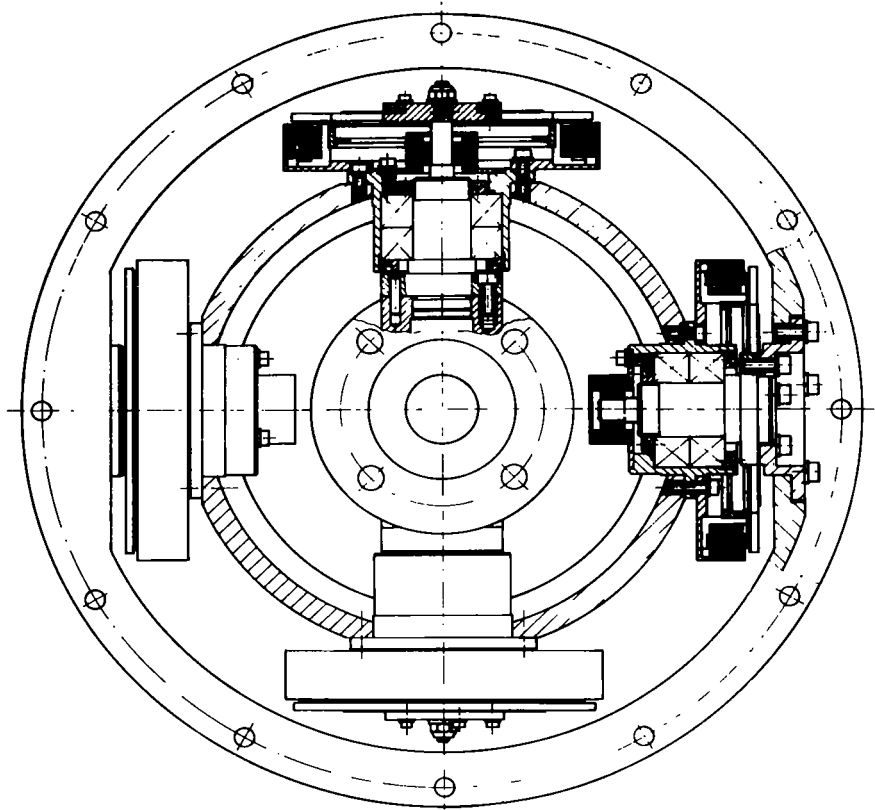
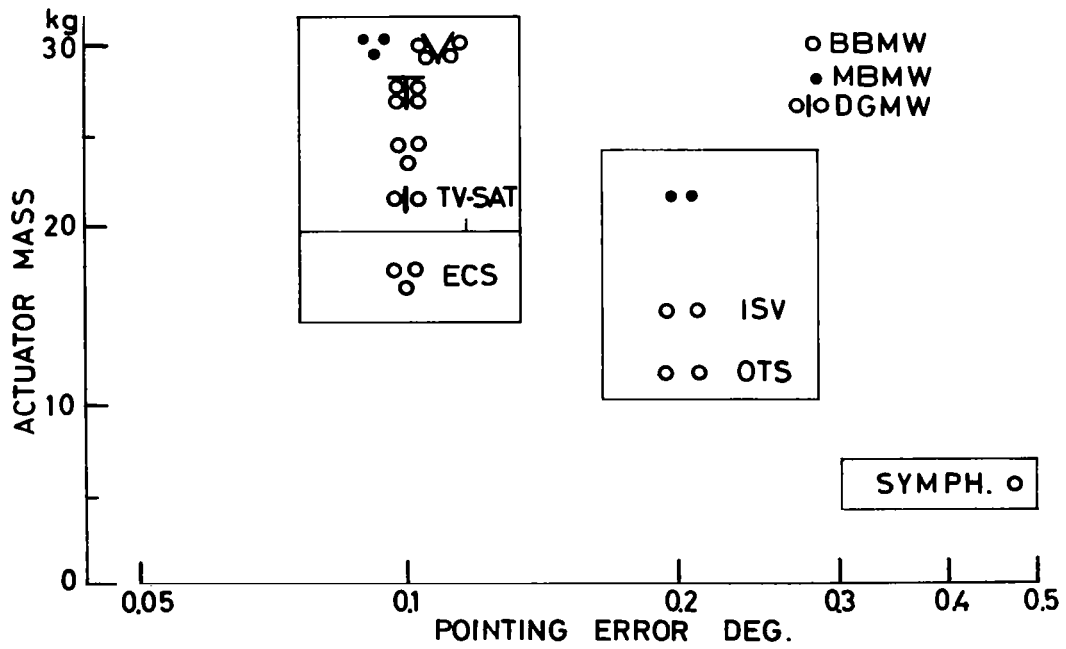


Figure 5.- Cross section of a DGMW.



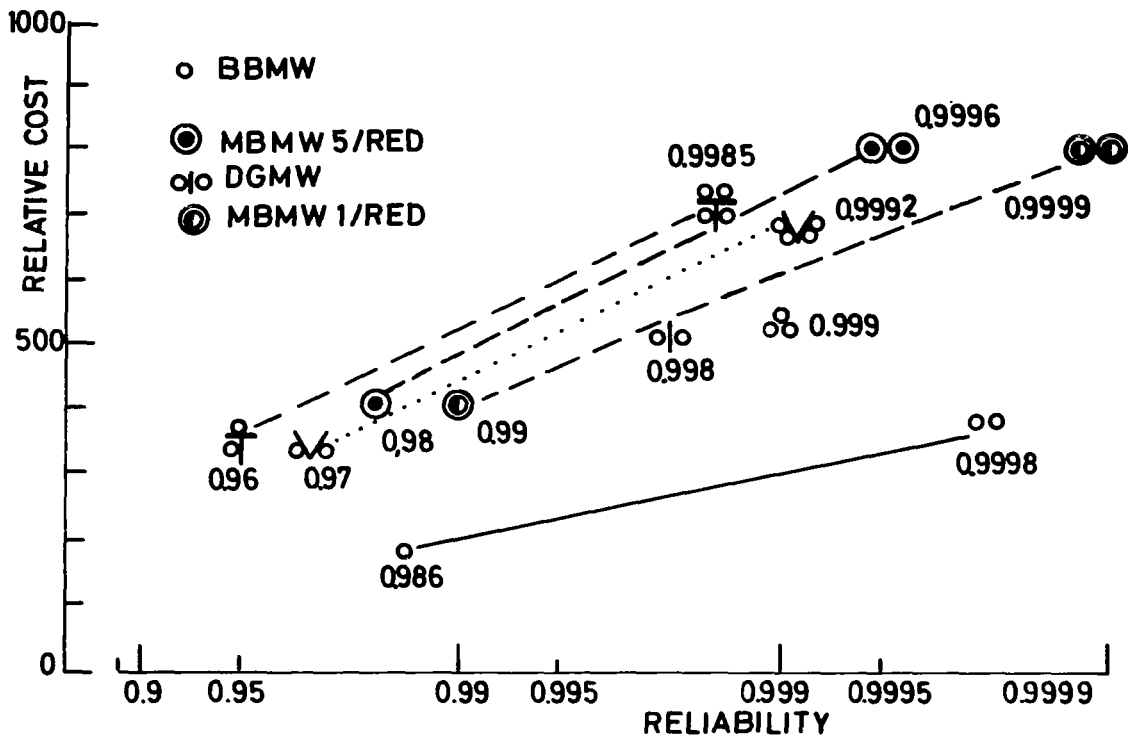


Figure 7.- Relative cost vs. reliability - momentum wheels.

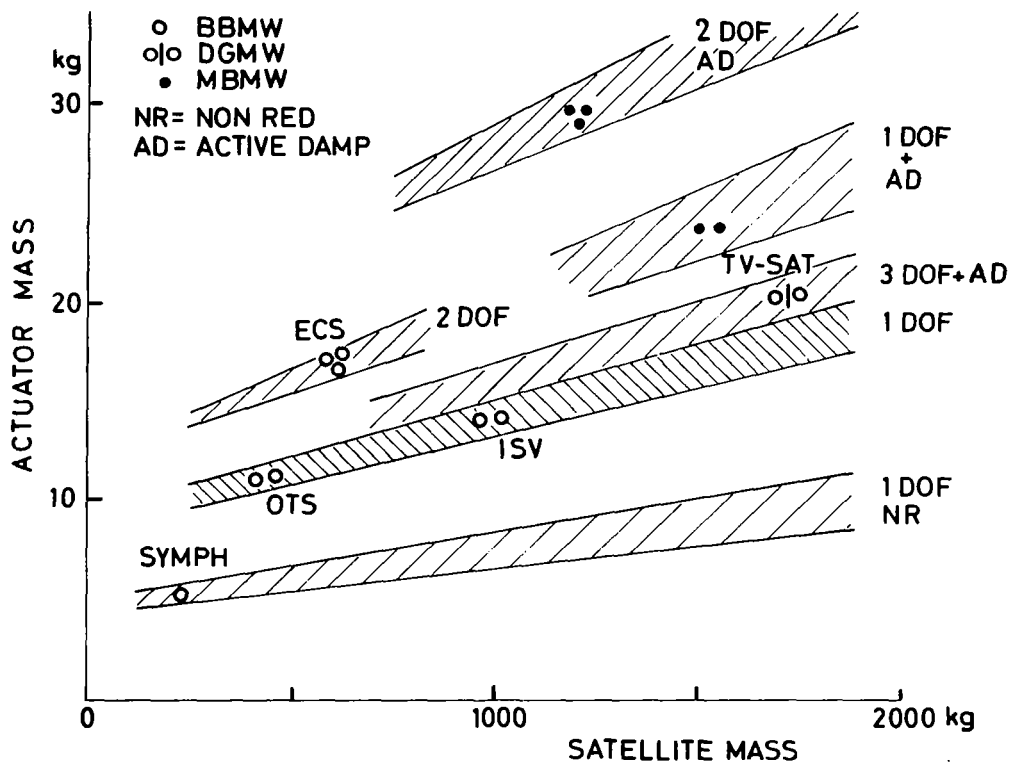


Figure 8.- Actuator/satellite mass.

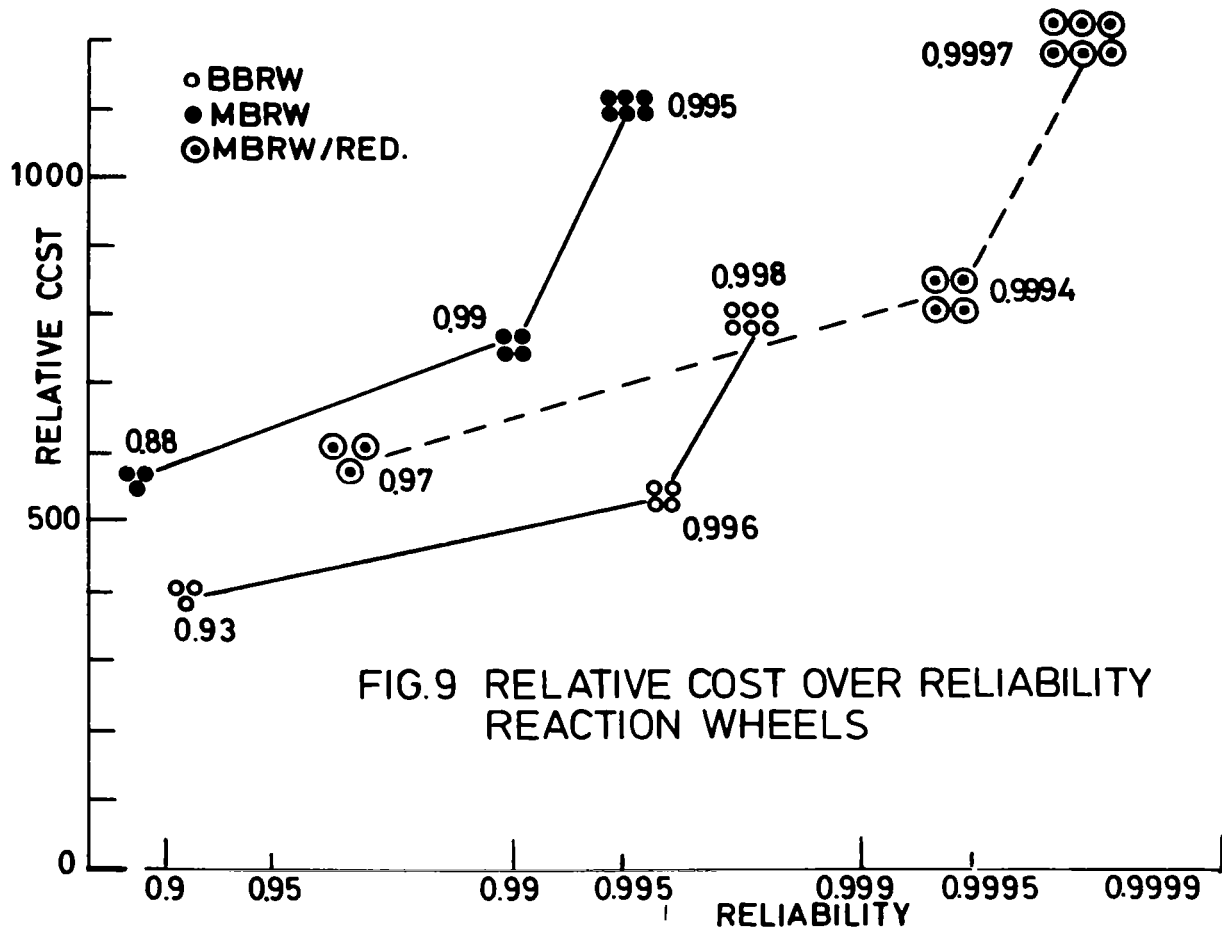


Figure 9.- Relative cost vs. reliability - reaction wheels.



# CENTRIFUGAL REGULATOR FOR CONTROL OF DEPLOYMENT

## RATES OF DEPLOYABLE ELEMENTS

J. C. Vermalle  
Aerospatiale

### ABSTRACT

Centrifugal brakes or clutches are currently used in a number of mechanisms. This paper describes the requirements, design, and performance of a centrifugal regulator aimed at limiting deployment rates of deployable elements.

This mechanism, which uses centrifugal force to produce friction of studs, has been designed, manufactured, and tested to specification for the IUE (see "Acknowledgement") solar array.

### INTRODUCTION

Deployment of the IUE solar array is characterized by a complex motion which can be broken into elementary rotations and translation.

The deployment is initiated by a pyrotechnic device, and the various operations are fulfilled in automatic sequence to final lockup. The motion is controlled by a centrifugal regulator driven by a cable continuously pulled out throughout all phases of deployment.

This solution was selected in view of the following factors:

1. Limiting end of travel shocks to values compatible with mechanical strength of the frame and spacecraft attachment
2. Low sensitivity to the operating temperature range (in contrast to a hydraulic system, which is sensitive to the variation of viscosity)
3. Good cleanliness and, in particular, low outgassing without seal problems
4. Availability of a large number of parameters which are easily adjustable during tests

## MAIN REQUIREMENTS OF THE DESIGN

The main requirements of the design are given in the following table:

Unwound length, m . . . . .	0.75
Nominal load, N . . . . .	40
Maximum load, N . . . . .	100
Nominal unwinding cable rate (corresponding to $10^0/\text{sec}$ ), mm/sec . . . . .	36
Operating threshold, N . . . . .	2
Passive mechanism	
Temperature range, °C . . . . .	$-75 < T < 75$
Mass including cable and attachment, kg . . . . .	0.15

## DESCRIPTION

### General Description

A general description of the centrifugal regulator is given in figures 1, 2, and 3. The overall mechanism is comprised of 4 distinct functional parts in a machined housing:

1. The centrifugal brake device, which checks the payout of the cable
2. The reducing gear, which produces the spin rate necessary for the braking device
3. The payout device, which allows the unwinding of the cable
4. The locking device, which prevents untimely unwinding

The centrifugal regulator is set into operation by a threshold tension of the cable which unlocks the mechanism and allows unwinding. The pulley of the windout device drives the centrifugal brake with the help of the reducing gear.

The centrifugal force pushes aside weights that produce friction of the studs in a cylindrical housing.

### Centrifugal Braking Device

The centrifugal braking device (fig. 3) revolves within a cylindrical bore through the housing; the bore's walls serve as a braking track for the device which consists of

1. One flail, rotating idly about the driving axis
2. Two weights hinged to the flail equipped with friction studs
3. One spring for return of the weights
4. One drive bar pinned on to the axis and directly acting on the weight

Pressure of the brake blocks upon the braking track is the result of three combined forces: (1) centrifugal force on the weights, (2) driving torque, and (3) counteraction by the spring.

#### Reducing Gear

This is of two stages and gives an overall multiplication ratio of  $6.5 \times 6.5 = 42.25$ .

#### The Windout Device

This consists of a helical throat pulley in which the cable is held within the throats by a cylindrical shell integrated to the housing. A slot allows windout for the cable.

The windout device is linked to the driving hub of the reduction gear through a torsion spring lodged within the pulley. This spring, which provides flexible linkage, is aimed at limiting cable tension as well as dynamic loads transmitted to the regulating device. A cable-guide bogie allows the windout for various positions of the cable.

#### The Blocking Device

The blocking device is intended to avoid untimely unwinding of the cable. It blocks the centrifugal brake when the cable's tension is below the operating threshold. This acts through axial pressure of the primary gear's shaft on the spindle of the braking device. Such pressure is applied by a torsion spring, producing differential rotation of both driving hub and shaft.

The axial motion is initiated by a pin engaged through the two helical slots of the hub. As soon as the applied torque exceeds the value of the spring's initial tension, the device releases the centrifugal brake. The reduction gear is then driven from stop position of the spin at the end of the helical slots. As soon as the cable's tension is slackened, the spring's action causes immediate blocking of the centrifugal regulator.

#### TEST RESULTS

During tests, the plastic bearing was replaced by bronze pads because expansion of the plastic led to excessive clearance with respect to the toothed gears. The nominal unwinding cable rate was obtained by adjustment of the weight return spring.

The mechanism behaved well at qualification temperature and vibrations.

## PERFORMANCE

The main performance data are given in the following table:

Unwinding length <sup>1</sup> , m . . . . .	0.75
Operating threshold, N . . . . .	2
Nominal load, N . . . . .	40
Maximum load, N . . . . .	100
Nominal cable payout rate, mm/sec . . . . .	36
Nominal brake rotation rate, rad/sec . . . . .	60
Operating temperature, °C . . . . .	-75 < T < 120
Mass, kg . . . . .	0.135

<sup>1</sup>To control the deployment speed of the Aerospatiale designed GSE solar array, the length of the cable has been increased to 6 m in the same housing. All other characteristics are identical.

## CONCLUDING REMARKS

The reason for interest in centrifugal regulators is obvious since they allow the deployment control of solar arrays, antennas, booms and telescopic booms actuated by springs, compressed gas, etc. . . .

A most attractive aspect is that all the mechanical characteristics are packaged within a very small volume and mass (0.135 kg).

The use of the mechanism allows (1) mass saving, the deployment sequence not being considered as a determinating calculation case, and (2) very good reliability, since the safety factor is not a compromise between the minimum energy needed for deployment and the maximum acceptable end of travel shock.

In addition, a large number of parameters are easily adjustable, including (1) diameter of pulley, (2) weight of tip masses, (3) calibration of weight return spring, and (4) calibration of initial tension for threshold spring.

Many adaptations of the mechanism can be envisaged. These include (1) increase of the energy absorbed by increasing the cable length or the nominal and maximum loads and (2) modification of the cable payout rate.

## ACKNOWLEDGEMENT

(1) International ultraviolet Explorer was a cooperative research program between:

- The UK Science Research Center Council which provided flight TV camera system
- The European Space Agency which provided the solar array (Aerospatiale) and the European ground observatory
- The US National Aeronautics and Space Administration which provided the spacecraft, launch vehicle, and the US ground observatory. (The spacecraft was launched in January 1978 from Kennedy Space Center.)

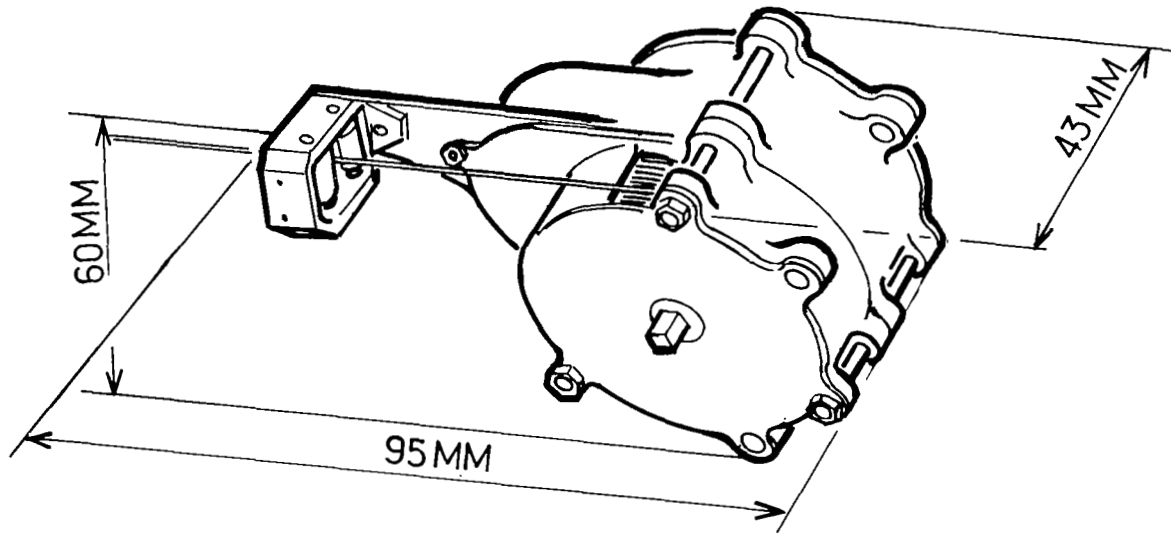


Figure 1.- General view of centrifugal regulator.

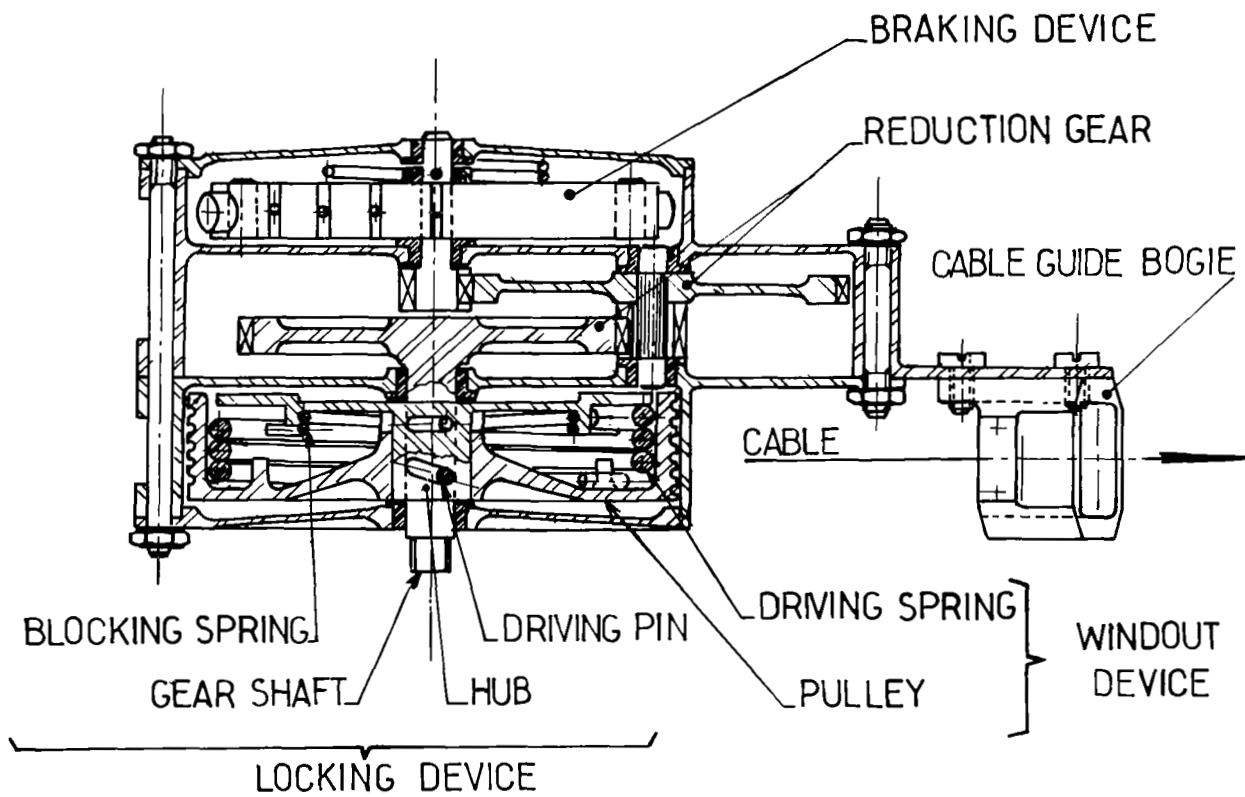


Figure 2.- Cross-sectional view of centrifugal regulator.

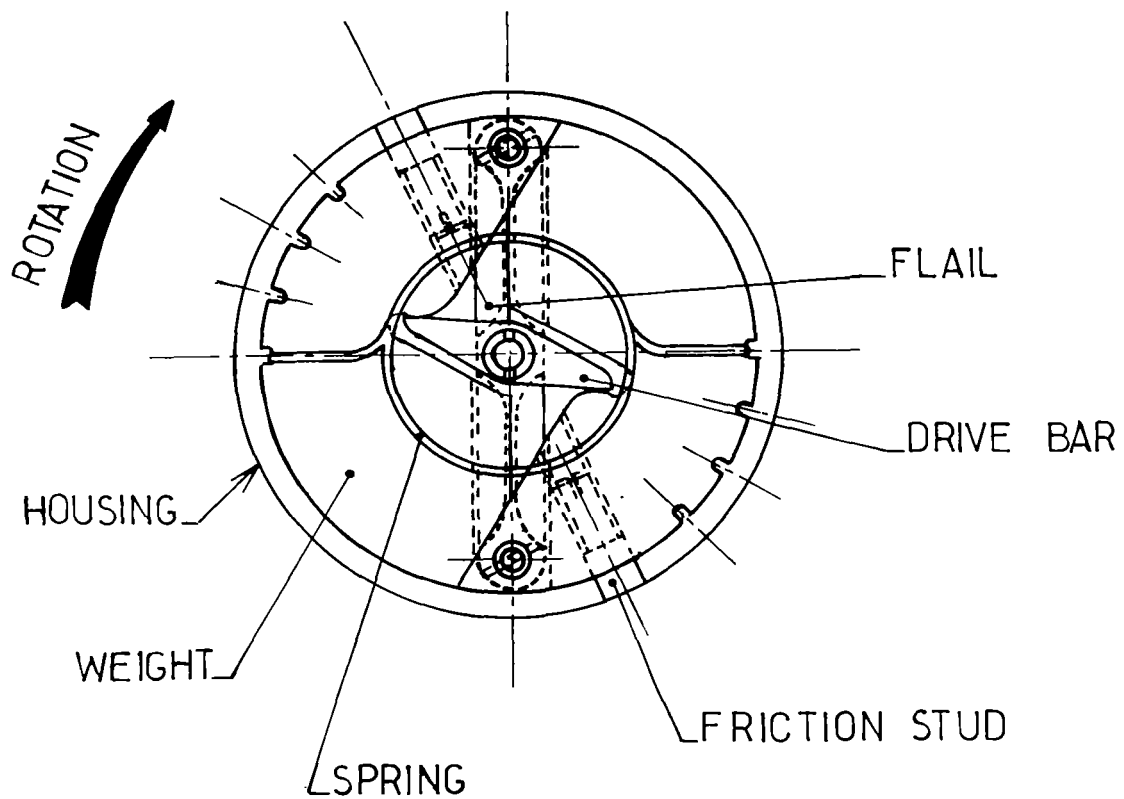


Figure 3.- Centrifugal regulator braking device.



## MECHANISMS OF UK RADIOMETERS FLOWN ON NIMBUS 5 AND 6

### WITH PARTICULAR REFERENCE TO BEARINGS, PIVOTS AND LUBRICATION

H. Hadley

Rutherford and Appleton Laboratories  
Science Research Council U.K.

#### SUMMARY

The mechanisms incorporated in these two experiments which were launched on Nimbus 5 in 1972 and on Nimbus 6 in 1975 are currently still working perfectly. The experiments described are vertical sounding infrared radiometers mainly for measurement of temperature profiles. Both use dry lubricants.

The Nimbus 5 Radiometer includes a rotating chopper driven via a carbon fibre-acetal resin gearwheel. The driving motor runs at 2000 rpm and has completed over  $7 \times 10^9$  revolutions. Four gear driven filter wheels powered by stepper motors have each completed  $2 \times 10^8$  changes. The input calibration mirror mechanism and its field of view compensation mechanisms are also described. All 25 ball races used in the experiment are of the film transfer type.

The Nimbus 6 Radiometer includes two cells. Each contains a piston supported on diaphragm springs and driven electromagnetically to modulate the pressure of CO<sub>2</sub> gas in the optical path. The pistons are 6 cm in diameter with a stroke of 1 cm and are driven at their mechanical resonant frequency of  $\approx 15$  Hz. The calibrating mirrors rotate periodically to view a target, Earth, and space, with the earth view scanned along the satellite track. The support pivots are synthetic sapphire ring stones with separate end thrust stones. The problems of mounting these stones to withstand vibration loads is described.

#### INTRODUCTION

The two experiments described in this paper are infrared vertical sounding instruments to measure the temperature profiles of the atmosphere. They were devised by the Department of Atmospheric Physics, Oxford University, under Professor J. T. Houghton with the engineering design and project management support being provided by the Rutherford Laboratory of the Science Research Council. The flight models were made by Marconi Space and Defence Systems.

These experiments are of interest since they all involve some innovation in the use of lubricants in small mechanisms in space and have proved highly successful in application. At the time of writing, they are all still

working as perfectly as when they were launched. These lubrication aspects are the use of carbon-fibre acetal resin gears in the Selective Chopper Radiometer (SCR) on Nimbus 5 (launched 1972) and the use of synthetic sapphire ring and thrust bearings in the Pressure Modulated Radiometer (PMR) on Nimbus 6 (launched 1975). A companion paper (ref. 1) describes the mechanisms used on the Stratospheric and Mesospheric Sounder (SAMS) on Nimbus 7 (launched 1978) in which lead lubricated recirculating ball screws are used.

#### NIMBUS 5 SCR MECHANISMS

This experiment (ref. 2) is a 16 channel vertically sounding radiometer ( $\lambda = 15 \mu\text{m}$  to  $100 \mu\text{m}$ ) and its 8 main channels measure the temperature profile of the atmosphere up to 45 km in height. As shown in figure 1, the incoming radiation is directed by the calibration mirror to a 13-cm-diameter off-axis paraboloid mirror and focused to pyroelectric detectors. Interposed before the detector is a double sided reflecting chopper set at  $45^\circ$  which chops and directs the field of view (FOV) into two paths; a dichroic beam splitter is placed in each path to feed 4 detectors in total and in front of each detector is a four position filter wheel, thus providing the 16 channels. A view to space is arranged opposite the chopper so that when the through view is chopped the rear face of the chopper directs the detector view to space and when the through view is clear the other detectors look to space through the chopper gap. The chopper is 12.7-cm-diameter, 0.25-cm-thick aluminium, diamond cut and gold plated with 2 cut-outs of  $90^\circ$  and is driven at 1200 rpm to give a 40-Hz signal chopped between atmosphere and space.

#### Chopper

The driving motor is a standard 400-Hz, 8000-rpm hysteresis motor (Muirhead Type 11M18F1) but with the bearings replaced by "BarTemp" bearings (Barden Corpn.) which are deep groove instrument ball bearings with a cage of glass fibre reinforced PTFE loaded with  $\text{MoS}_2$ . The balls transfer the lubricating film from the cage to the raceways. The motor is driven from the spacecraft 100-Hz two-phase supply at 2000 rpm, thus requiring a gear reduction. A stainless steel gear is coupled by a splined driving plate with the outrigger bearing supporting a flywheel of "Heavimet" (Tungsten-copper alloy) to compensate the angular momentum of the chopper disc. The 60T meshing gear is made of chopped carbon fibre (25%) and "Delrin" (Du Pont's acetal homopolymer of formaldehyde) in which the carbon fibre limits the wear and the "Delrin" provides the lubrication. See figure 2 and reference 3. This chopper was rotating during launch to prevent "Brinelling" of the ball race tracks.

The two phase motor windings are each split into two halves and each is powered independently to give complete redundancy and in fact once up to speed the motor will run on one of its four windings. The full power dissipated is 6 watts.

#### Filter Wheels

The filter wheels are also gear driven from stepper motors to reduce the effects of inertia so that a  $90^\circ$  motion of the filter wheel can be completed accurately in less than 150 ms and repeated every second allowing a signal

integration period of 820 ms. The four filters on each wheel are glued into titanium holders and set into an aluminium wheel with the outer rim supporting the teeth of a standard machine cut delrin gear wheel. Two sizes of wheel are used, each with 120 teeth 40 DP and 48 DP. The largest wheel supports four gas cells with a 0.3-cm path length between 2.3-cm-diameter germanium windows filled with CO<sub>2</sub> at various pressures up to a maximum of 350 mbar. The permanent-magnet 90° stepper motors are IMC type 011-804-1 (IMC Magnetics Corp.) which is a space qualified component using "BarTemp" bearings. To the shaft is clamped a 15 tooth stainless steel pinion, thus providing a programme of 8 steps. These steps are at 10-ms intervals with the last pulse delayed to 20 ms and quadrature damping applied by a negative impedance circuit. This, together with the inertias and other system parameters, calculations and measurements, is shown in reference 4. The four filter wheels are driven in step, and should any filter be out of position at the beginning of the 4-second cycle, they all wait until the late filter catches up. To do this, a slow stepping sequence is applied to any filter wheel not in the number one position. Positioning is by opto-transducers from reflecting tracks.

Each filter wheel is encased in an isothermal temperature controlled shroud and figure 3 shows one of the smaller wheels with the cover and input port removed.

#### Calibration Mirror

The calibration mirror is a plane, diamond-cut, aluminium mirror of elliptical form, 20 cm x 14 cm, set at 45° to the nadir. It rotates 90° to view an internal black body and then a further 180° to view space. This occurs twice per orbit. The drive motor is a 90° stepper motor, type IMC 015-802, which is energised with triangular waveforms to provide a smooth torque and to limit the current demand from the spacecraft supply to the permitted rate of rise. This assembly is also pivoted about its centre of gravity so that the mirror is able to scan backwards along the line of the spacecraft motion so the same field of view is seen by each filter for the 4 seconds necessary. The return scan takes place during the 150 ms of the last filter change. The pivot bushes that support this assembly are made of "Vespel" type SP3 (Du Pont's polyimide resin). The field of view compensation mechanism is a long arm connected to a linear motor producing 0.75° mirror movement. This motor consists of a ferrite ring permanent magnet with pole pieces and coil, as in a loudspeaker, with two coil-support diaphragm springs of beryllium copper and a flexible beryllium copper connection to the lever arm. The coil is supplied with the appropriate sawtooth waveform and its movement is monitored by means of redundant sets of gallium arsenide light sources and silicon diode detectors, as are all the other mechanisms used in these radiometers. The position of the calibration mirror in the de-energised positions is held by the normal 'detent' of the stepper motor assisted by permanent magnet pairs and, in the extreme positions of normal vertical viewing and space viewing, the detent magnets are offset to hold the mirror against fixed stops. (See fig. 4 for a sectional view of the mirror and its FOV compensation).

Some 25 ball races were used on this radiometer all "BarTemp" types used well within the manufacturers recommendations and all pre-loaded by separate coil springs or in the case of the motors by spring washers. The pre-loads

are between 1-2N. The application of these bearings is also well within the performance guide for self lubricating bearings in air published in 1976 by the National Centre of Tribology at Risley. (Ref. 5).

The complete radiometer is 31 x 20 x 43 cm, weighs 14 kg, and consumes 15 watts. It is suspended under the spacecraft and was qualified by vibration testing to 7.5g (5 Hz to 2000 Hz) sine wave and 15g rms (20 Hz to 2000 Hz) random (0.11 g<sup>2</sup>/Hz). A separate electronics module, 15 x 17 x 22 cm, weighing 5 kg provides the power converters and the electronic drive systems. This radiometer has now completed 60 000 hours of operation (over 2 x 10<sup>8</sup> filter movements per wheel and 7 x 10<sup>9</sup> revolutions of the copper motor, which must be approaching the theoretical predictable ball race life (ref. 6).

#### NIMBUS 6 PRESSURE MODULATOR RADIOMETER MECHANISMS

This instrument is also a vertical sounding radiometer with 2 channels to measure the temperature profile of the atmosphere from 40 km - 60 km (channel 1) and 60 km to 90 km (channel 2). Each channel has its own pressure modulated cell and calibration mirror system and measurements are confined to the 15 μm band. (Ref. 7).

#### Calibration Mirror System

The calibration mirrors operate in a similar manner to that of the SCR instrument except the mirror is only 7 x 5 cm and is mounted directly onto the shaft of an IMC 008-845 stepper motor. The image motion compensation of the SCR instrument was extended to give a direction of view  $\pm 15^\circ$  from the nadir along the direction of flight. This introduces a varying Doppler shift which varies the optical depth and, hence, the altitude being sounded. The mechanism for this is an actuator consisting of a curved fixed magnet with a moving coil which can move over an arc of  $\pm 7.5^\circ$  and is restrained mechanically only at its end stops. An inductive position pick-off signals the actuator to follow a saw-tooth ramp waveform. The time for a single doppler scan is 85 seconds.

The pivot bearings for this motion were a problem. "BarTemp" bearings need a larger movement for the balls to lay down a lubricated track, polyimide resin sleeve bearings tended to judder for such small slow movements, and suitable flexural pivot bearings require more power at the extremes of motion than the actuator could give.

However, tests were done on a possible flexi-pivot as had also been done previously for the SCR mirror pivots, but again the vibration loads were too great. If larger flexi-pivots were used, the spring loads to be overcome would need more power than could be provided from the drive servo. The limitation with crossed spring flexi-pivots is their rigidity to axial loads which cause the spring leaves to buckle. One way to overcome this problem without using stiffer, stronger flexi-pivots is to relieve the pivot of all axial loads or to clamp during launch.

The decision, after much testing, was to use synthetic sapphire ring bearings with separate thrust end stones. However for these to withstand

vibration testing, they had to be pressed into a titanium ring, mounted in silicon rubber, and off-loaded so that metal-metal contact occurred within 0.01 cm of movement. The 0.2-cm-dia shaft of the bearing is a hard stainless steel, since normal stainless steels are not hard enough to stand the wear. 9% Chromium stainless steel (Firth-Vickers 520B Hardness Rockwell C46) was found to be suitable. Hardened AISI 440 stainless steel would also be suitable. This worked very smoothly with minimum power from the servo system (See Fig. 5 and Ref. 8). The end stones were fixed, with the shaft ends radiused to 0.4 cm and polished with 0.005 cm axial clearance. The ring stones were 0.5 cm o.d. and 0.125 cm thick. The bore was not parallel but olive shaped (radius, 0.2 cm), which allows for misalignment and the removal of wear debris. The shafts were lapped to fit so that they could be angled 3° min to 5° max. (i.e. clearances of 3 to 8 μm). The total weight supported was 0.15 kg, and test vibration levels were 10 g (sinusoidal) and 13.4 g r.m.s. (random excitation).

### Pressure Modulated Cell

This is a very elegant concept compared to the mechanics of the selective chopper radiometer. Instead of a rotating chopper, a piston is driven up and down modulating the pressure of CO<sub>2</sub> in a cell. To change the mean pressure, the temperature of a molecular sieve is changed, instead of switching cells in front of the detector. The cylinder and cell are made of titanium 130 which has excellent outgassing characteristics and is sufficiently hard to allow good permanent seals using 0.05-cm-diameter gold 'O' ring seals on demountable flanges. The piston is 6-cm dia and is made of titanium 679 which has 11% tin and does not scuff or pick up the titanium 130 of the cylinder. The radial clearance is 0.005 cm and the total stroke is 1 cm. The mechanical arrangement is shown also in Fig. 5 with the piston mounted on a shaft with a permanent magnet set in the centre and flat beryllium copper spider springs of constant stress cross section providing the support. The tail end of the shaft carried a position pick-off ferrite rod, and the position was sensed by an externally mounted coil. Drive electromagnets outside the cylinder are servo controlled to drive the piston at constant amplitude at its mechanical resonant frequency of about 15 Hz.

The pressure control is achieved by thermostating a small quantity (2gm) of molecular sieve material which will absorb CO<sub>2</sub> (a zeolite from Union Carbide type 4A XH/2). The equilibrium pressure above the sieve is only a function of temperature for a given filling of CO<sub>2</sub>, for the volume and quantity of sieve material chosen. The pressure in channel 1 (1-cm-long cell) is changed from 0.5 mbar at 30°C to 3 mbar at 80°C and in channel 2 (6-cm-long cell) is 1 to 6 mbar over these temperatures. Five values can be selected on command. A position of maximum temperature was switched in during launch to provide maximum damping to the piston system from vibration and the spring stops are shaped to progressively limit the spring movement and thereby change the natural frequency once the 1-cm amplitude has been exceeded.

The measurement of gas pressure is deduced from the frequency of oscillation of the piston assembly which changes by nearly 10% per mbar pressure change. A 10 bit counter, reset every 32 seconds, allows the data system to record this to 1% accuracy.

The complete PMR radiometer is 23 x 18 x 41 cm, is made integral with its electronics module, weighs 13 kg, and consumes 5 watts. This unit is mounted inside the sensory ring of the spacecraft so the vibration levels are only 50% of the SCR levels. It has completed over 4 years operation in orbit and is operating perfectly, but recently data have only been recorded periodically as an economy in ground control and data handling. At present, however, it is operating continually for comparison with the Nimbus 7 SAMS instrument.

#### CONCLUSION

In the design of these experiments we have conscientiously avoided the use of oil or grease to reduce the risk of contamination of optical components. For the chopper gearbox, a design using labyrinth seals with a grease lubricant was tested, but it was not satisfactory in this respect.

The use of ball races with film transfer lubrication from the cage (such as the "BarTemp" types) has proved ideal in these experiments where they are used well within the guidelines. The life of nearly  $10^{10}$  revolutions in the chopper gearbox is outstanding for any lubricant. The limitation of the lubricating method means that angular rotation to lay down a track must exceed  $30^\circ$  or so.

For limited movements, diaphragm springs and flexible connections have given very good service. The design, however, must incorporate mechanical stops to prevent distortion of the joint under working, launch, and test conditions and stress so that the fatigue life is many times the experiment lift.

The use of jewel bearings as pivots has been demonstrated and, over the 4 years in orbit, each mirror has totalled nearly one million scans of  $15^\circ$  total movement. However, the friction of these stone ring bearings is greater than that of film transfer bearings and should be considered only where use of the latter is not possible.

#### COMPONENT SUMMARY

Hysteresis motor	Muirhead Ltd Beckenham, Kent	Type 11M18F1, 2ph., 400 Hz, split winding.
Film Transfer Bearings	Barden Corpn. Bracknell, Berks	"BarTemp" instrument ball bearings
Carbon Fibre-Delrin	RAE Farnborough(originally) AERE Harwell, Oxon	Production now at AERE for Contract stock for ESTEC
"Vespel" SP3	E.I. du Pont de Nemours Wilmington, DE 19898	Polyimide self-lubricating resin material (loaded)
Stepper Motors	IMC Magnetics Corpn. Maywood, Calif. 90270	Permanent Magnet $90^\circ$ Stepper Motors (Size 8,11&15)
Sapphire Jewel Bearings	Fred Lee & Co(Coventry)Ltd Coventry. CV4 9BJ	Ring Stones and thrust stones (Stockist)
Opto transducers	Texas Instruments Ltd Slough, Berks	Gallium Arsenide Source TIL23 Silicon light sensor LS616
LINDE Molecular Sieve	Union Carbide Corpn. East Chicago Indiana 46312	4A XH/2 $\frac{1}{8}$ " dia beads (sodium metal alumino-silicate)
"Heavimet" heavy alloy	Osram(GEC) Wembley Middx	Copper-Tungsten, Density 18

## REFERENCES

1. Hadley, H.: The Mechanisms of the SAMS Experiment Flown on Nimbus 7. 14th Aerospace Mechanisms Symposium, NASA CP-2127, 1980 (Paper 27 of this compilation).
2. Ellis, P.; Holah, G.; Houghton, J.T. FRS,; Jones, T.S.; Peckham, G.; Peskett, G.D.; Pick, D.R.; Rodgers, C.D.; Roscoe, H.; Sandwell, R.; Smith, S.D.; and Williamson, E.J.: Remote sounding of atmospheric temperature from satellites IV. The selective chopper radiometer for Nimbus 5. Proc. R. Soc. Lond. A. 334, 149-170 (1973).
3. Harris, G.L.; and Wyn-Roberts, D.: Wear of Carbon Fibre Reinforced Polymers in a high vacuum environment. Nature Vol. 217, 981-982. (1968).
4. Ellis, P.J.: Analysis and Control of Permanent Magnet Stepper Motor. The Radio & Electronic Engineer. Vol. 41, 302-308. (1971).
5. Performance Guide for Self-Lubricated Bearings. N.C.T. Risley (1976).
6. Patrick, J.J.: Stepper Motor experience in Space instrumentation. ESA-SP111. 143-147 (1975).
7. Curtis, P.D.; Houghton, J.T. FRS; Peskett, G.D.; and Rodgers, C.D.: Remote sounding of atmospheric temperature from satellites V. The pressure modulator radiometer for Nimbus F. Proc. R. Soc. Lond. A. 337, 135-150 (1974).
8. Dokuchalova, V.V.; Uskova, S.G.; and Khandelsman, Yn. M.: Design of Ring Jewel Bearings for Small Frictional Torques. Translated from Russian in Instrument Construction No. 2. 15-18 (1963).

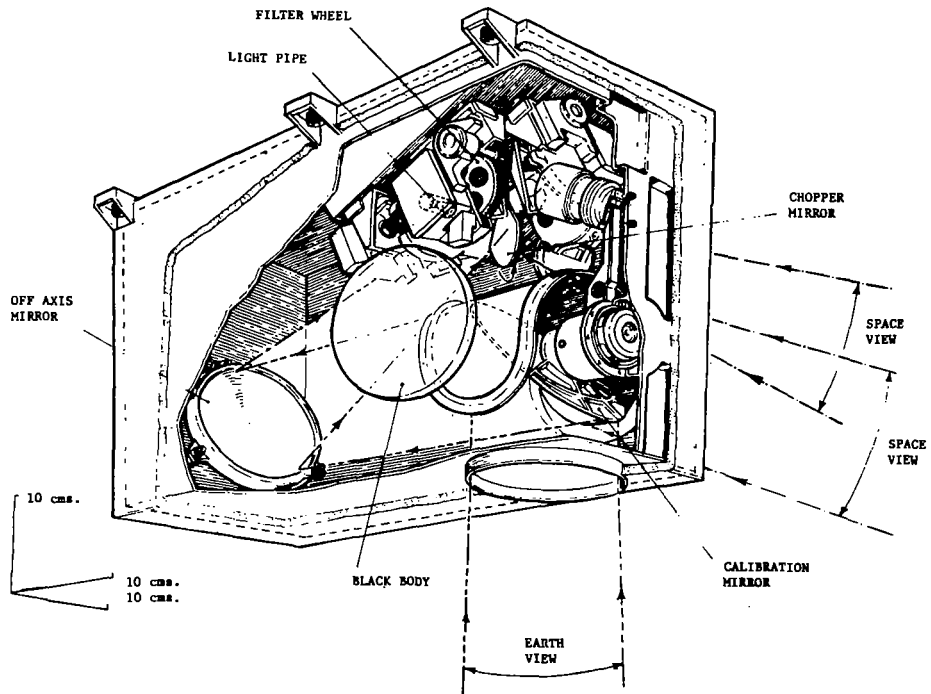


Figure 1.- Selective chopper radiometer on Nimbus 5.

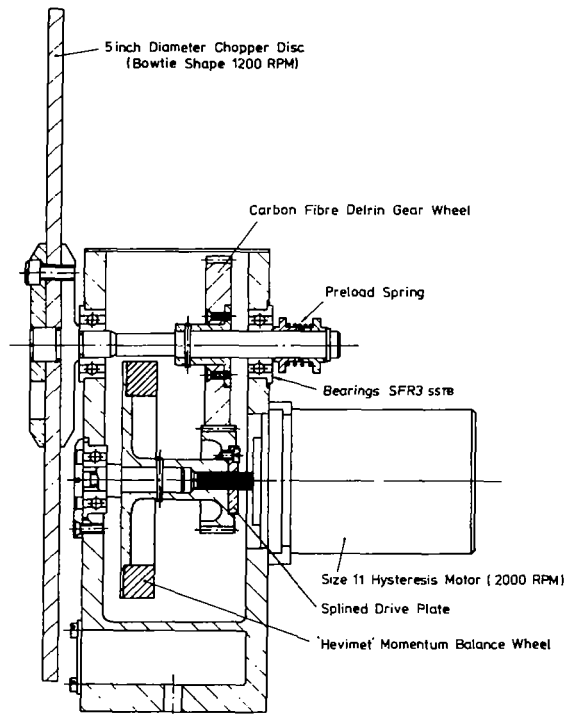


Figure 2.- Chopper gearbox for S.C.R.

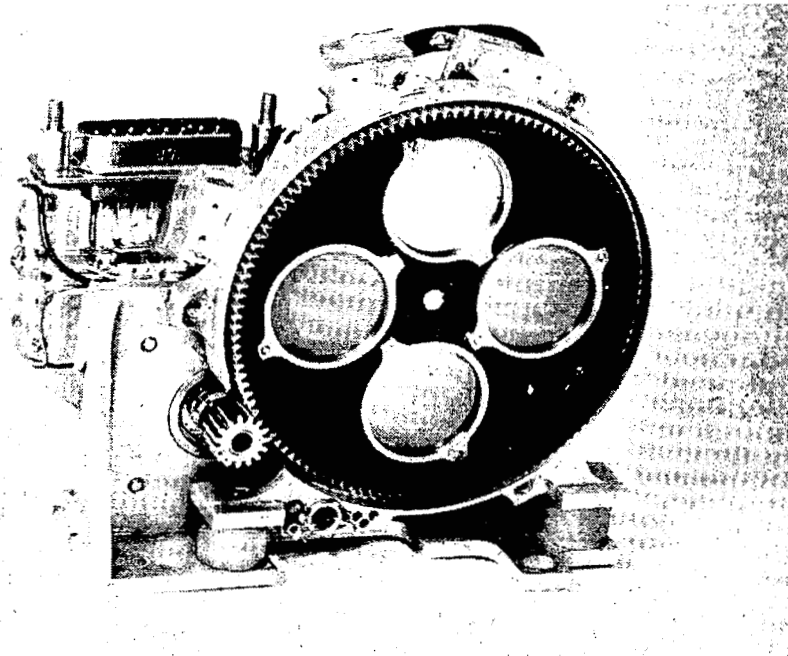


Figure 3.- Filter wheel assembly for S.C.R. (eng. model with cover removed).

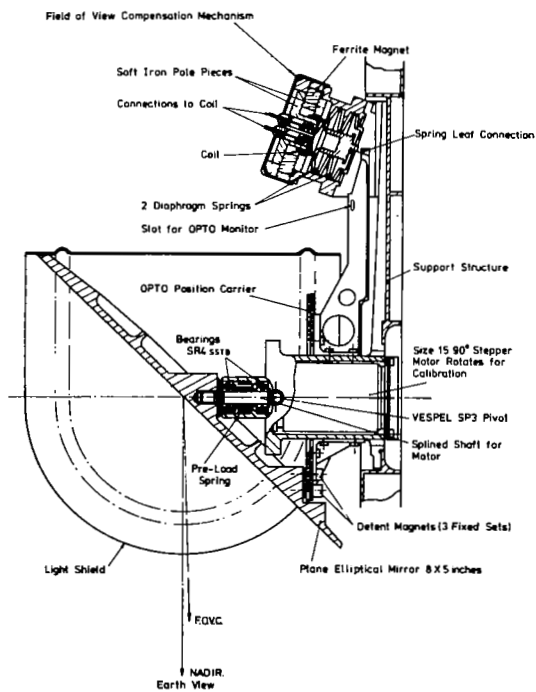


Figure 4.- Calibration mirror mechanism for S.C.R.

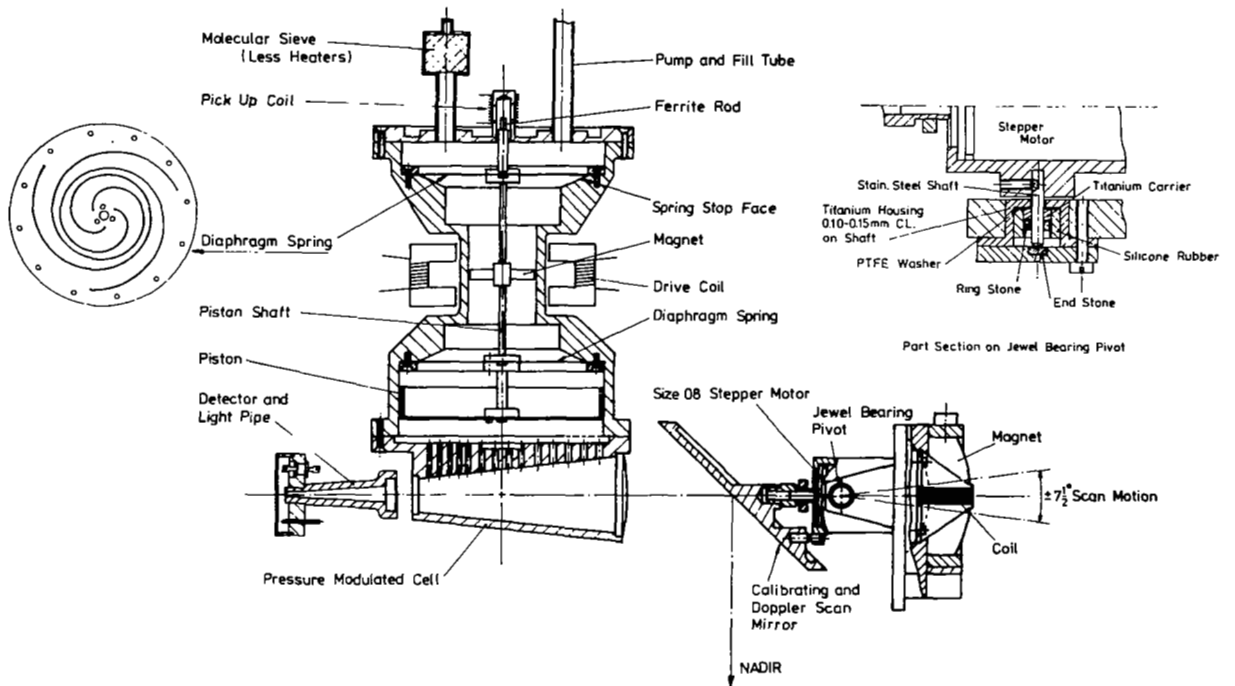


Figure 5.- Pressure modulator radiometer (one channel only) on Nimbus 6.

TRIPLE-AXIS COMMON-PIVOT ARM WRIST DEVICE  
FOR MANIPULATIVE APPLICATIONS

Leendert Kersten  
Associate Professor of Engineering Mechanics  
University of Nebraska-Lincoln

J. Dwight Johnston  
Marshall Space Flight Center

SUMMARY

A new concept in manipulator development to overcome the "weak wrist syndrome" is presented in this paper and is known as a Triple-Axis Common-Pivot Arm Wrist (TACPAW). It contains the usual torque motors for actuation, tachometers for measuring rate and resolvers for position measurements. Furthermore, it provides three degrees of freedom, i.e. pitch, yaw, and roll, in a single manipulator joint. The advantages of this development are increased strength, compactness and simplification of controls. Designed to be compatible with the protoflight manipulator arm (PFMA), the joints of TACPAW are back-driveable with  $\pm 90^\circ$  rotation in pitch,  $\pm 45^\circ$  in yaw and continuous roll in either direction while delivering 20.5 N-m (15 ft-lb) torque in each of the three movements.

BACKGROUND

Mechanical manipulator arms terminating in some type of mechanical hand or gripping device (end-effector) are commonly employed on space vehicles for performing planetary explorations, satellite and space shuttle operations, as well as on 'Earth-bound' robotic assembly or manufacturing device.

During the past several years an increased effort in manipulator design has been directed chiefly to the guidance and control systems, with some work in the area of actual hardware design. It should not be forgotten, however, that the degree of joint sophistication directly influences the degree of

control sophistication. Because of the high level of control-guidance research in the years 1973-1975, with little or no concern for the joint research and design, a "weak wrist syndrome" appeared on the scene. Past joint design resulted in several configurations of small physical shape with externally applied drives and mechanisms; these nullify the objective of improved visibility around the joint which is crucial for space work, especially in the shadow-side where auxiliary illumination is required. (See Figures 1 and 2.)

In many present-day designs of manipulator arms, the wrist-joint configuration has been simplified to the degree that not three but two motions occur in the wrist joint, with the third motion supplied by the shoulder (see Figure 3), or completely ignored. For those arms that have three degrees of freedom in the wrist joint, the actual configurations produce, in some instances, a very bulky joint with external wire loops and not providing the needed visibility.

The design effort relating to wrist joints, therefore, needs to be directed to conformity of sound kinematic manipulator design, elimination of wiring harnesses as loops outside the joint, and reduction of physical lengths (distances) between axes of rotation; one such effort is the Triple-Axis Common-Pivot Arm Wrist (TACPAW).

#### DESIGN CONCEPT

The third rule of good kinematic manipulator design states that

"the last three degrees of freedom of the manipulator shall be as close as possible to the terminus (end-effector) and shall have mutually perpendicular axes."

To comply with this rule and to meet the specific design criteria of a FFTS (Free Flying Teleoperator System) configuration which can be tested in a TOBE (teleoperator experiment on shuttle) program, the concept of TACPAW was born as an application of the three-axis system of a sphere.

In keeping the center as a fixed pivot point (with the X-plane as its platform), the total freedom of motion relative to this pivot point can be observed. (See Figure 4a.) Thus, allowing rotation about the Z-axis produces YAW, about the Y-axis creates PITCH, and about the X-axis ROLL is accomplished; hence, three degrees of freedom, three axes mutually perpendicular and zero physical distance between these axes (this latter item provides for simplification of the mathematical location of a point on the terminus work sphere).

The immediate question now is how to implement this concept into an actual piece of hardware. To create the YAW motion, a disc segment, which is solidly attached to the lower arm and hence considered a fixed body, will allow two hemispheres (coupled together) to rotate about their common (Z) axis which is also the axis of the disc. (See Figure 4b<sup>1</sup>.)

Another shell can be made to move around the initial sphere to supply the PITCH motion. A flat surface, provided on each of the hemispheres, allows for linking the two hemispheres together into a single unit and establishes a pivot axis for the pitch motion. (See Figure 4c.) Around this pivot (Y) axis, a body B as shown in Figure 4d, can provide the second degree of freedom pitch motion. Thus the YAW (X-axis) and PITCH (Y-axis) motions are at right angles to each other and the third (X-axis) motion, i.e. ROLL, can now be obtained easily: a body rotating about or within part B.

This concludes the TACPAW concept, which has been fully disclosed and is patented under U.S. Patent Nr 4,068,763, issued to J.C. Fletcher (NASA), invention by Leendert Kersten and James D. Johnston, on January 17, 1978. (See also Reference 1.)

---

<sup>1</sup>The two hemispheres were (later in the development stage) changed to a 'marriage' of two cylinder halves (Figure 5).

## DESIGN AND DEVELOPMENT OF TACPAW

To demonstrate the feasibility of the concept, a wooden, full-size, mock-up was made and is shown in Figure 6.

Issuance of Contract NAS8-31897 required the analysis and design of the prototype TACPAW.

### Task Description

To produce and manufacture a new manipulator wrist required the establishment of design criteria, specifications and preparations of all necessary detail and assembly drawings, with the added stipulation that this wrist shall be made compatible with existing manipulators ESAM and PFMA at the Marshall Space Flight Center.

This resulted in the necessity for the following steps to be taken to complete the task:

1. design of a new drive system, other than shown in the patent, but within the framework of the conceptual configuration
2. inclusion of tack-generators, resolvers, and brakes within the established configuration
3. design of the wiring harnesses such that all wiring will be internal whenever and wherever possible; this required utilization of the reliable "polytwist" slipping assemblies to avoid looping for the reduction of noise-levels and elimination of line-breakage
4. establishment of a simulated mathematical model for reference in thermal behavior

### Performance Characteristics and Requirements

The unique design of TACPAW shall allow for the following characteristics in motion:

- a: YAW \_\_\_\_\_ approx.  $\pm 45^{\circ}$  ( $90^{\circ}$  total = 1.6 rad)
- b: PITCH \_\_\_\_\_ approx.  $\pm 90^{\circ}$  ( $180^{\circ}$  total = 3.2 rad)
- c: ROLL \_\_\_\_\_ continuous either direction

The drive system employs a back-driveable gear train (Figure 7), allowing for a 20.5 N-m (15 ft-lb) torque delivery in each of the joint movements. Within the limits of the gear tooth strength, the anticipated maximum torque is designed for 35 N-m (25 ft-lb).

Thermal analysis shows that for full solar exposure the unit may exceed the functional parameters of the internal components. Therefore, full exposure in a fixed position should be avoided through shielding or rotation in space. The cold environment in shadow positions require the addition of heaters to stabilize the working range of component temperatures. These conditions prevail for the entire arm and are therefore not unique to the wrist design or its configuration. The hardware design and interfacing of parts and components were detailed in Phase I of the investigation.

#### BUILDING THE PROTOTYPE TACPAW

A continuation of contract NAS8-31897 required the actual manufacturing of the previously established parts and the complete assembly of all components in a prototype of the manipulator wrist TACPAW. Aside from the stock items, such as the DC torque motors, resolvers, brakes, tack generators, wiring connectors, etc., all machined parts were produced locally (Lincoln, Nebraska) by a tool and die firm. The assembly of the various components and the fabrication of the wiring harnesses were performed by students in the department of engineering mechanics at the University of Nebraska. (See Figures 8, 9, 10 and 11.)

The addition of a full rotational slipping in the roll mode allows for a total of 21 terminal leads; 10 of which are for signal transmission, 9 for power transmission and 2 for the control of the end-effector; see Figure 12 where it is to be noted that these 21 leads are terminated in the adapter ring by means of a polarized MDB1-21 Cannon connector.

A full description of parts and components can be found in NAS8-31897 (August 1977) report as well as the November 1978 report (Phase II).

With the unique capability of producing a torque of (at least) 20.5 N-m (15 ft-lb) in each of the joints, yet weighing only 9 kg (20 lbs) and measuring some 355 mm (14 inches), the TACPAW wrist configuration is recommended for all sizes of remote controlled manipulation.

The Earth-bound capabilities are also extremely interesting. It should be recognized however that the gravitational environment reduces the torque capabilities in the "outward" motions by a factor equivalent to lift the joint-weight. With the over design of a maximum 35 N-m (25 ft-lb) torque capabilities in the "outward" motions by a factor equivalent to lifting the prosthetics, medical equipment (scanner positioning), industrial robotic applications, high-risk or high-danger environmental task performances, delicate and precise placement of assembly components, etc. Some streamlining of the outside cosmetics, due to different selection of poly-twist modules in the yaw-axis, is easily accomplishable and will greatly enhance the looks of the new wrist TACPAW.

#### REFERENCE

1. 1975 NASA/ASEE Summer Faculty Fellowship Research Program - Final Administrative Report. BER. Rep. No. 199-94, Univ. of Alabama, Sept. 1975. (Available as NASA TM X-72500.)

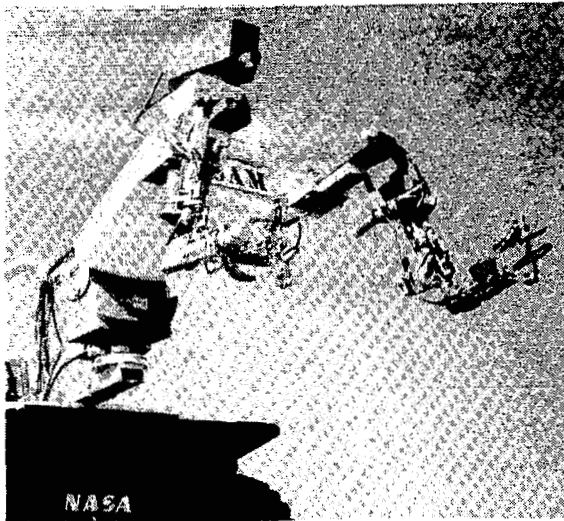


Figure 1.- NASA's application of the Rancho Antropomorphic Manipulator (RAM-M12) for test purposes as a Space Arm Manipulator (SAM).

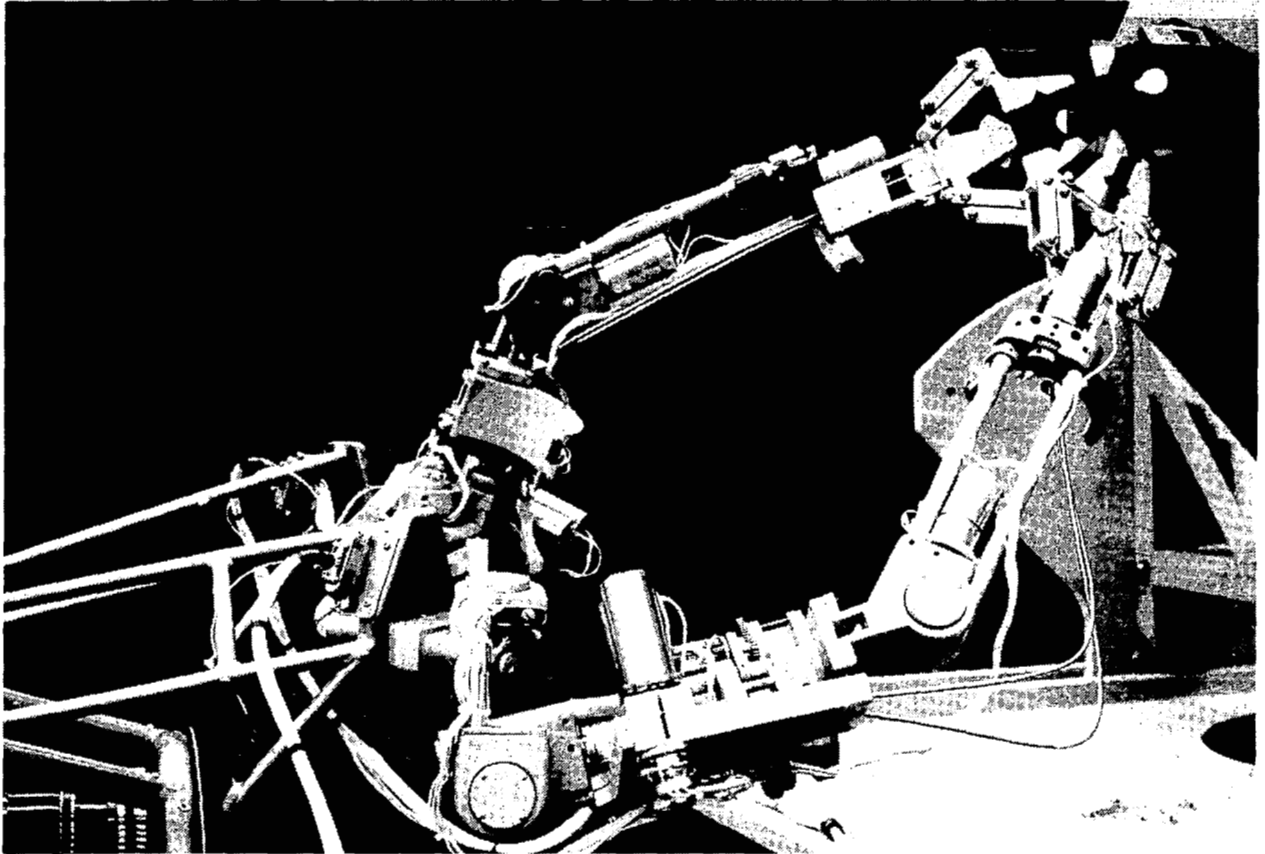


Figure 2.- The Rancho Antropomorphic Manipulator (RAM-M12) being evaluated for space applications. The primary objectives of such tests are for guidance and control studies, not work-load evaluations.

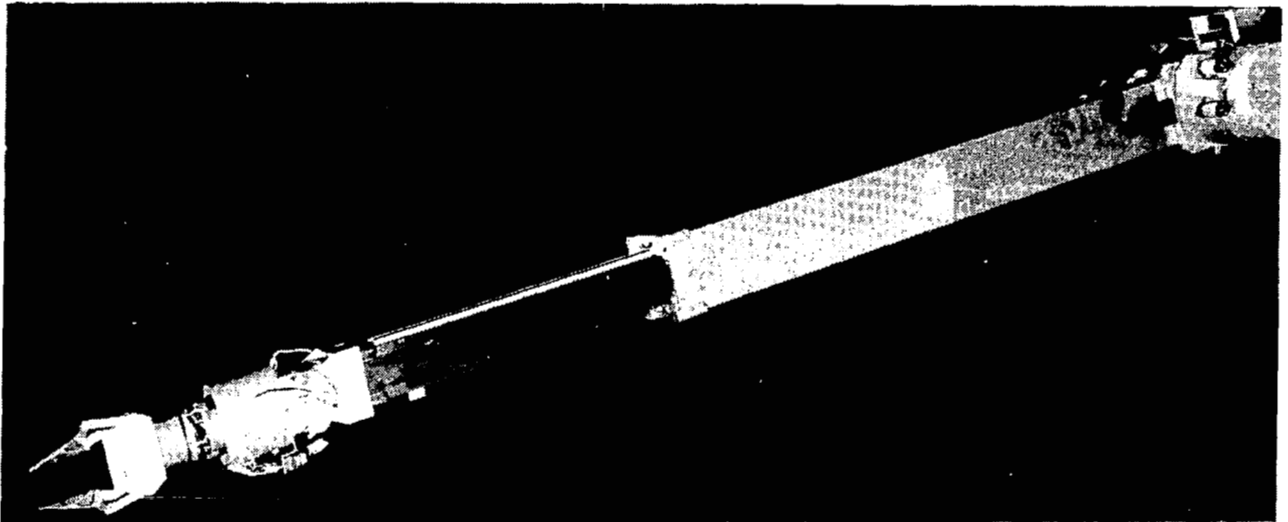
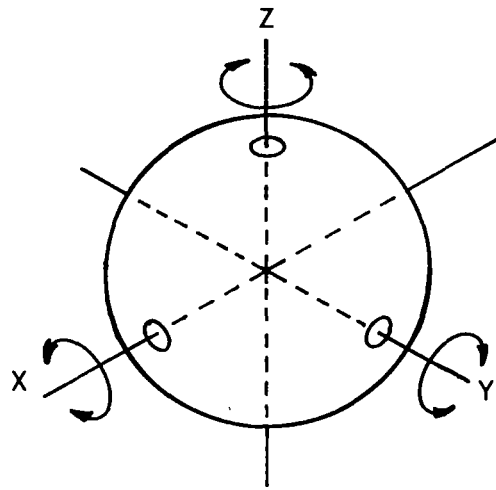
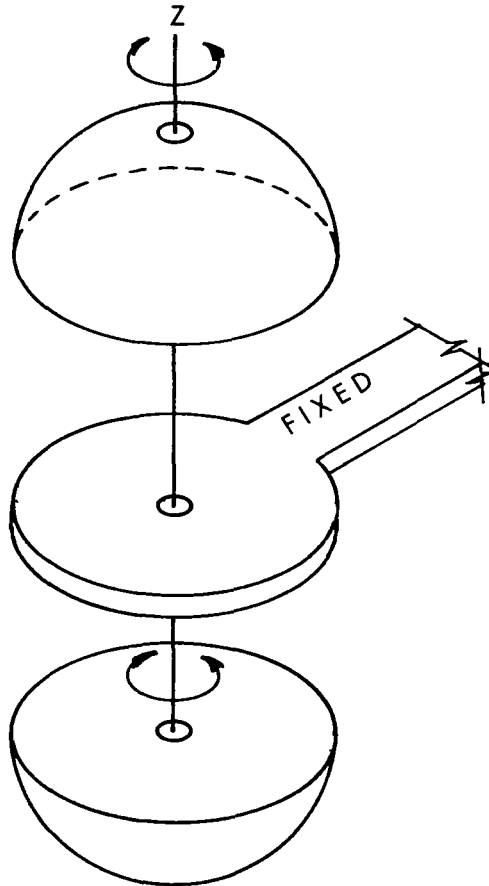


Figure 3.- The Extendable Stiff Arm Manipulator (ESAM) being tested at Marshall Space Flight Center. The wrist joint provides only Pitch and Roll where the shoulder must provide the Yaw motion.

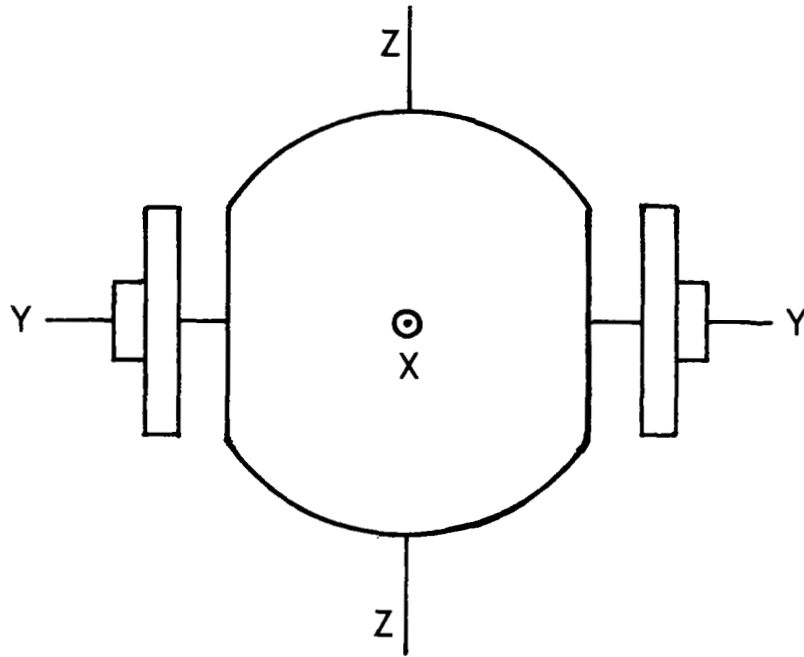


a. The triple axis concept.

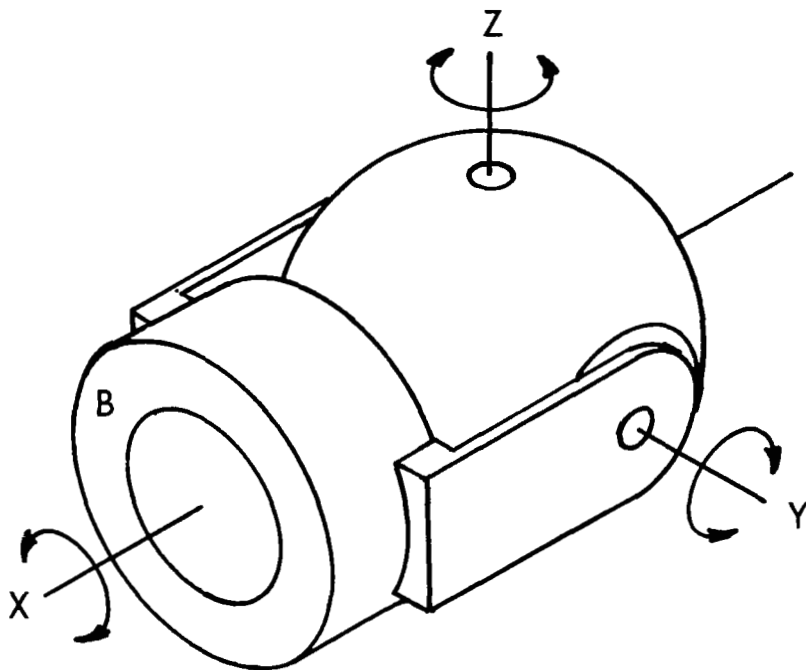


b. Implementing the concept to establish yaw motion about the Z-axis.

Figure 4.- The triple axis concept and its implementation.



c. Providing the pitch motion about the Y-axis.



d. Completing the concept by creating a continuous roll motion about the X-axis.

Figure 4.- Concluded.

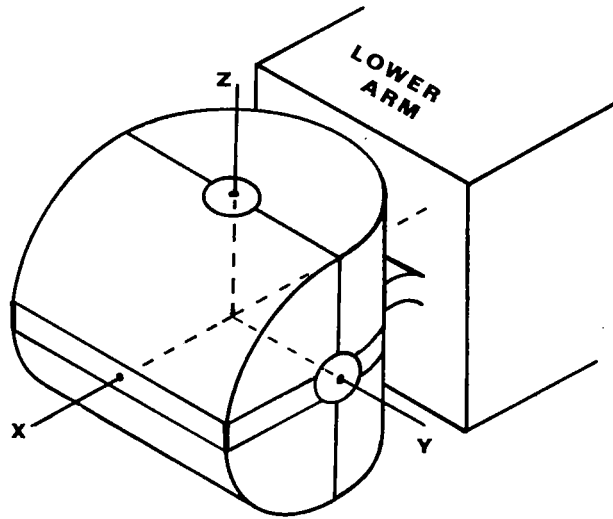


Figure 5.- The evolution from spherical shape to the more volumous double cylindrical configuration.

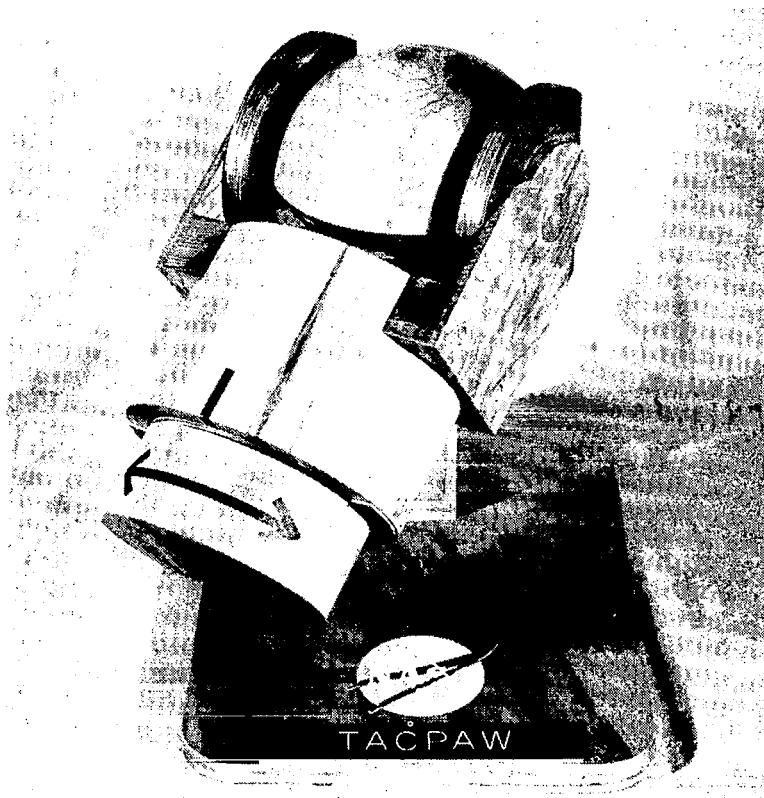


Figure 6.- A concept mock-up of TACPAW to illustrate feasibility.

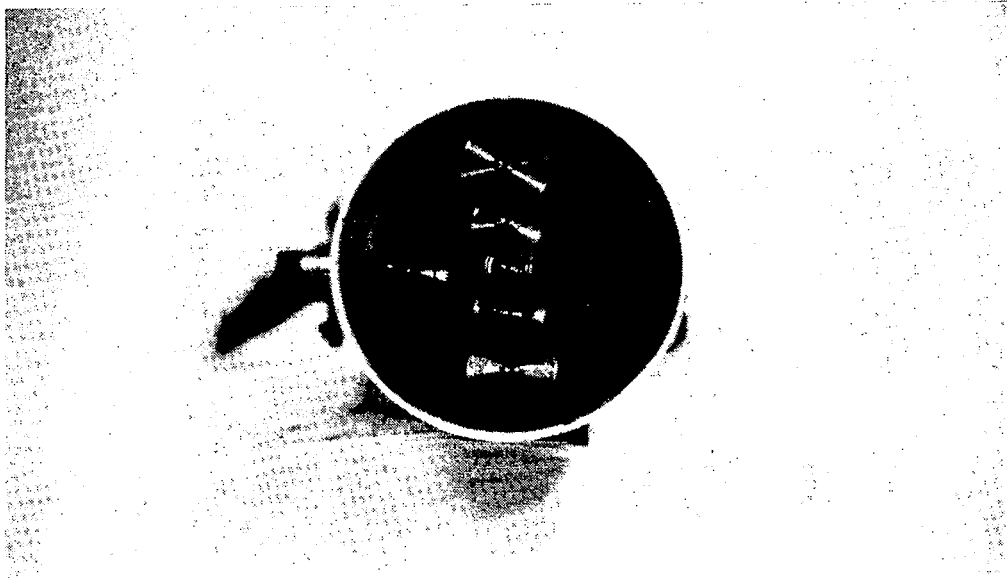


Figure 7.- The back-driveable gear train (100:1 reduction) produces a 20.5 N-m torque, while preloading in both rotational directions enables a near zero backlash.



Figure 8.- Major components of the primary embodiment for complete yaw and partial pitch motion.



Figure 9.- The assembled primary embodiment complete with wiring harnesses.  
(The sliprings on left and right and coinciding with pitch axis are longer than required as a result of an "off-the-shelf" purchase.)

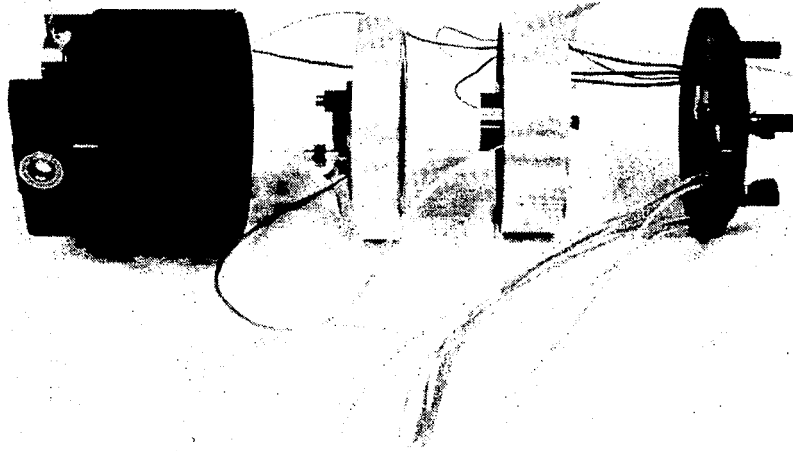


Figure 10.- Various components for the provision of pitch motion prior to complete assembly. The drive for the roll is also in this secondary embodiment.

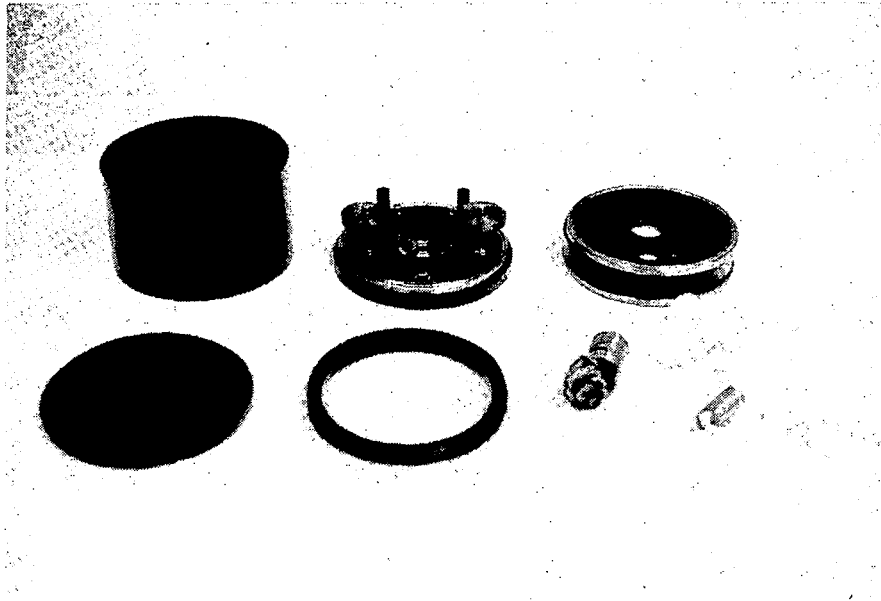


Figure 11.- Preassembly parts of the final embodiment to create continuous roll. The lower right corner shows the 21 lead slipring.

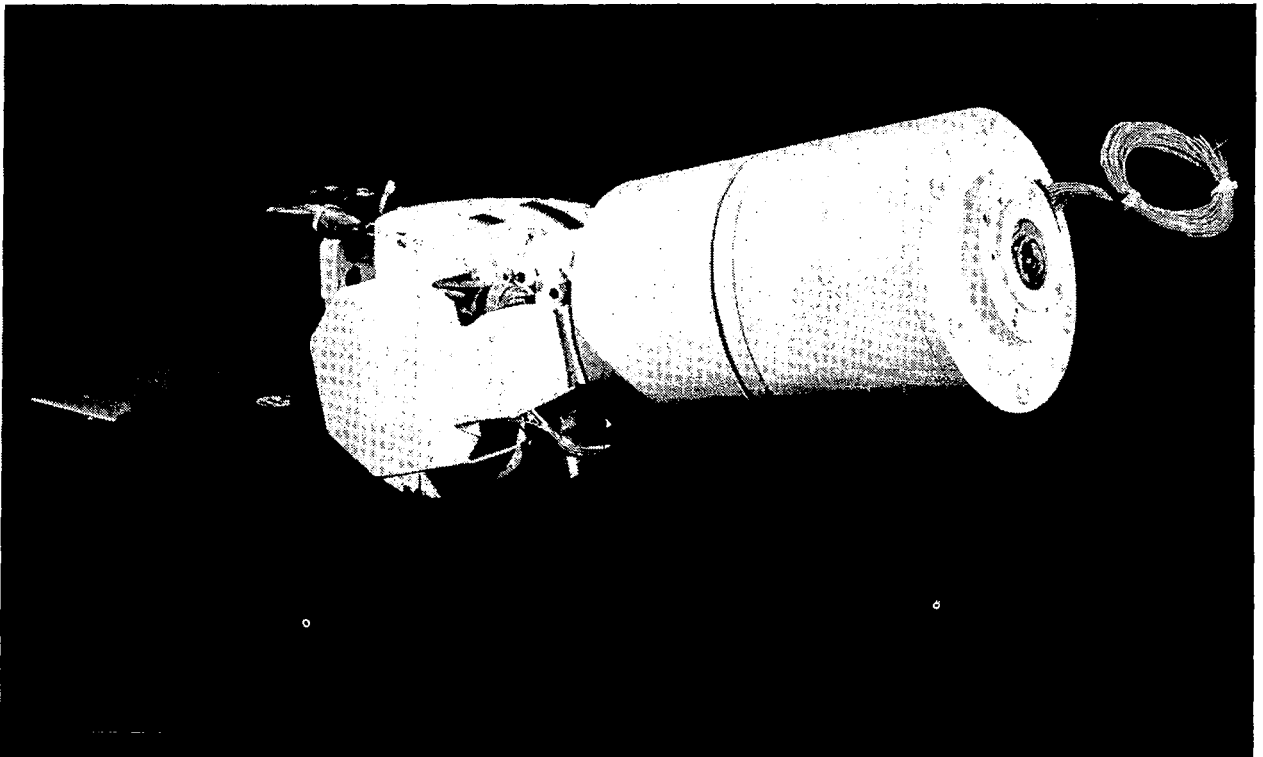


Figure 12.- The completed TACPAW (on test stand) as delivered to NASA NSFC. Note the 21 lead termination on the adapter ring.

DESIGN AND DEVELOPMENT OF THE QUAD REDUNDANT  
SERVOACTUATOR FOR THE SPACE SHUTTLE SOLID ROCKET BOOSTER  
THRUST VECTOR CONTROL

James M. Lominick  
Marshall Space Flight Center

SUMMARY

The intent of this paper is to describe the design of the servoactuator used for thrust vector control of the Space Shuttle Solid Rocket Booster. To accomplish this, a description of the design and theory of operation is accompanied by highlights from the development and qualification test programs. Specific details are presented concerning major anomalies that occurred during the test programs and the corrective courses of action pursued.

INTRODUCTION

The National Aeronautics and Space Administration (NASA)/Marshall Space Flight Center (MSFC) in Huntsville, Alabama, has had responsibility for the design, development, flight qualification testing and procurement of thrust vector control (TVC) servoactuators for many large space vehicles. These applications included all stages of the Saturn I, IB, and V vehicles, Space Shuttle Main Engine (SSME) ground tests, and the Space Shuttle Solid Rocket Booster (SRB).

With the Space Shuttle came the first demand for a TVC servoactuator with some degree of redundancy. A three-channel version was developed for the SSME TVC ground testing. This design possessed servovalve bypass capability and a return to null mechanism. Out of this configuration evolved the final design for the SRB TVC servoactuator. This design basically encompasses four servovalve channels to create a fail-operate, fail-operate redundancy scheme in those components susceptible to common contamination and electrical failures.

Not only did the Space Shuttle create a demand for redundancy, it also demanded an actuator designed for a 20-mission lifetime. Furthermore, the vibration environment for each mission was to be more hostile than any of the single-mission Saturn series TVC servoactuators. Added to these requirements, the SRB TVC servoactuator must absorb splashdown loads and remain leakproof in the saltwater environment.

## DESIGN AND PERFORMANCE CRITERIA

### Objectives

Two SRB's are attached to the Space Shuttle external tank to provide primary thrust during the flight ascent phase. To provide TVC of the booster, two servoactuators are attached to the outboard side of each of the SRB's as shown in figure 1. These actuators are mounted in the "tilt" and "rock" planes which are at  $\pi/4$  rads (45 deg) to the shuttle pitch axis. The basic objectives were to provide required thrust vector gimbaling and rate capability against loads imposed by the SRB nozzle. Unlike the fixed pivot point gimbal bearing of Saturn vehicle engines, the SRB nozzle is attached to the Solid Rocket Motor (SRM) by a flex seal gimbal bearing which is protected by an ablative boot. This design not only introduced the complexity of locating the nozzle pivot point, but also imposed the high restraining torques characteristic of the flex seal and the protective boot. A last and very important primary objective was to provide the highest degree of redundancy attainable within the given restraints of weight, envelope, cost and scheduling.

### Performance Requirements

Physical sizing of the actuator was dictated by the flexible bearing and boot nozzle restraining torque. These loads coupled with the required gimbal rates, nozzle/structure dynamics and installation geometry sized the main piston area and basic loop gain of the system. Computer simulations were used to size a dynamic pressure feedback (DPF) mechanism. From this mechanism, the load differential pressure is sensed and shaped to stabilize the first resonant mode of the gimballed nozzle mass and attaching compliances. Functional, environmental and dynamic requirements pertinent to the SRB TVC servoactuator design are summarized in Tables I, II and III.

## DESCRIPTION AND OPERATION

### General

The TVC servoactuator is a four channel proportional control device that operates normally after one or two channel failures. These failures originate from the drive electronics or within the servoactuator control channels. Figure 2 shows an assembly drawing of the TVC servoactuator, and figure 3 shows the redundant components and feedback. From these figures the major components can be located. These major components are: four servovalves (conventional torque motor/nozzle-flapper first stage with second stage spool); four differential pressure transducers; four isolation valves; four dynamic pressure feedback modules; mechanical position feedback mechanism; power stage spool; main piston; transient load relief mechanism; hydraulic supply switching and prefiltration valve (not shown) and the lock and manual bypass valve (not shown). The servovalves are arranged in a "V-4" configuration. Figure 4 shows a general

servoactuator block diagram. Figure 5 contains the simplified linear mathematical block diagram with the four servovalves lumped into one channel with the power valve. The parameter list of table III together with figure 5 define the basic linear mathematical model of the servoactuator. Figures 2 through 5 can be used in conjunction with the following discussion to understand the basic system operation.

### Normal Operation

Two pressure sources, primary (P1) and secondary (P2), are supplied from separate auxiliary power units (APU) to ports on the main actuator body. From these ports, the fluid enters a dual function, three-position hydraulic supply switching and prefiltration valve. Manual external positioning to the prefiltration mode allows flushing action for both P1 and P2 pressure sources while bypassing the critical valve components with potentially contaminated fluid. In the normal mode of operation, a compression spring and differential area allow source P1 (with both P1 and P2 present) or source P2 (with P2 only present) to pass on to the servoactuator. With normal supply source P2, supply switching will occur when P1 drops to  $1.413 \times 10^7 \pm 1.034 \times 10^6 \text{ N/m}^2$  ( $2050 \pm 150$  psi). Recovery of source P1 to  $1.689 \times 10^7 \pm 1.034 \times 10^6 \text{ N/m}^2$  ( $2450 \pm 150$  psi) will cause the valve to revert to the normal mode of operation.

From the supply switching valve, high pressure fluid is routed directly to the power valve and simultaneously through a replaceable 10 micron (nominal) filter to the redundant sections of the servoactuator (servovalves, valve pressure transducers, and isolation valves).

Filtered fluid is supplied to the four servovalves, which are of the two-stage mechanical feedback type units. The first stage consists of a 0.226 Nm (2 in. lb) torque motor and a conventional four-leg orifice bridge. Two fixed orifices and a movable flapper positioned between two nozzles make up the orifice bridge. A closed center spool with pressure feedback to a stub area on either end of the spool make up the second stage. This pressure feedback reduces the servovalve pressure gain and minimizes force fight between valves as they drive the power valve spool. Second-stage spool position is mechanically fed back to the torque motor through a wire spring element extending from the flapper into a groove on the spool. The feedback torque is proportional to spool position.

Command input currents to the torque motors cause the flapper to rotate, creating an imbalance in the orifice bridge. This imbalance produces a net driving force on the second stage spool of each servovalve creating an output differential pressure. These outputs are force summed on the large power spool. Movement of this spool meters flow to the main piston and controls piston velocity. The power spool position is mechanically fed back to the torque motors through wire springs extending from the flappers to grooves on the power spool.

The load differential pressure is developed across the ports of the power valve spool as a function of actuator load and spool position. This differential pressure is fed back through four dynamic pressure feedback modules to a set of nozzles directed onto the flappers of each servovalve. These networks provide a frequency sensitive-load damping feedback signal. The system remains stiff against static loads and dissipates energy created by the resonant frequency of the nozzle and structure.

The main power piston is located on the actuator centerline. Two bearings, one in the actuator body and the other in the cylinder, guide the piston rod. The piston position is sensed mechanically by a "scissors-like" mechanism consisting mainly of two elements pinned together producing four ends. Two ends of the scissors assembly are spring loaded to ride an internal conical cam located within the piston rod. With one end pivoted from a rigid point on the actuator body, the fourth end becomes the output member. Motion of the piston causes the feedback assembly to open and close causing movement of the output member proportional to piston position. Through a linkage, the output of the scissors mechanism drives two spring loaded cages resulting in a negative feedback torque to the servovalve flappers. The result is piston position proportional to servovalve input.

A hydraulic lock valve located in the actuator body locks the piston in a fixed position in the absence of hydraulic pressure. When system pressure exceeds  $4.14 \times 10^6 \text{ N/m}^2$  (600 psi), a spring loaded spool moves allowing fluid to pass from the power valve output ports through the lock valve to the piston.

To absorb the water impact loads during splashdown, a large transient load relief valve is located within the piston assembly. This valve senses the transient load pressure across the piston and opens to bypass flow through the piston when the load differential pressure transient exceeds  $2.48 \times 10^7 \text{ N/m}^2$  (3600 psi). The valve has an integrating mechanism incorporated to prevent opening for static or low frequency loads. This device protects the actuator and the attaching structure/SRB nozzle from splashdown loads.

Also located within the actuator are two monitoring devices, the piston position and load pressure transducers. The scissors mechanism moves the free end of a cantilevered beam instrumented with strain gages to convert piston position into a proportional output. The load pressure transducer senses the differential pressure output of the power valve.

### Redundancy Management

The primary purpose of redundancy within the SRB TVC servoactuator is to eliminate catastrophic actuator behavior resulting from in-line control component failures. Included are failures within the computer, control electronics and the servoactuator redundant components. Not included are failures of simplex servoactuator components for which redundancy was not practical. These include the power valve, main piston, mechanical position feedback mechanism

and the transient load relief valve. Such components were therefore designed for optimum reliability. These simplex components utilize large driving forces and from past experience have a record of proven reliability. In the redundant control components, the servoactuator can tolerate two failures with no significant degradation in performance.

Actuator failures are generally the results of fluid contamination which causes restricted orifices and/or excessive spool stiction. To execute the redundant capabilities of the servoactuator, differential pressure transducers are used in conjunction with a remote computer, the Ascent Thrust Vector Controller (ATVC), to detect and isolate offending servovalves. The transducers sense the pressure differential across the output ports of each servovalve. Basically, the transducer is a spring centered piston with a Linear Variable Differential Transformer (LVDT) coil mounted concentric to the piston. The piston drives the LVDT probe to produce an output voltage proportional to the differential pressure.

External to the servoactuator, the ATVC monitors the signals from these transducers. Here, the "failure detection, isolation and recovery" (FDIR) logic determines the status of the individual servovalves. If the output pressure of a given servovalve exceeds  $1.52 \times 10^7 \pm 1.38 \times 10^6 \text{ N/m}^2$  (2200  $\pm$  200 psi) a timer is started. Should the differential pressure remain above this level for 120 ms, that particular channel is isolated from the system by terminating the output of the servovalve. To accomplish isolation, a solenoid operated isolation valve (one per channel) internal to the servoactuator is utilized. Energizing the solenoid results in the application of system pressure to the end of a spring loaded spool. The spool is driven to a position which blocks the servovalve output pressure from one side of the servovalve and connects the other side to both ports on the power valve normally driven by the servovalve in question. Thus, control of the offending servovalve and force fight among valves are eliminated.

#### DEVELOPMENT AND QUALIFICATION TEST PROGRAM

Development testing of the SRB TVC servoactuator was accomplished jointly by the servoactuator vendor and MSFC. To verify the design approach, a two-phase development test program was devised and conducted at the facilities of the vendor. Phase one consisted of component and subassembly testing to verify performance, life and reliability. The components and subassemblies undergoing the vendor conducted development tests were: 4 servovalves; 8 DPF modules; 12 servovalve differential pressure transducers; hydraulic supply switching valve; hydraulic lock valve; 4 solenoid isolation valve assemblies; transient load relief valve; and the power valve assembly. These elements were subjected to the life, environmental, functional and performance criteria of MSFC document 16A03000 (SRB TVC Electro-Hydraulic Servoactuator Design and Procurement Specification). Performance was verified by determining pressure gains, feedback loop gains, stability, friction levels, linearity, null shifts, pressure switching levels and leakage. Phase two verified the performance of a complete

servoactuator assembly, the development test unit. Although representative of the deliverable actuator's functional design, the development test unit fabrication was not restricted to production unit tooling, methods or NASA quality control. Two objectives were met with the development test unit. First, the design approach was proven to meet the functional and performance requirements of 16A03000; and second, an acceptance test procedure (Moog report MR A-2237) applicable to production hardware was developed.

The first production unit of flight configuration was the engineering test unit (S/N 001). This servoactuator was delivered to MSFC and was subjected to a "prequalification" test program. The tests centered around the vibration environment imposed by 16A03000. Previously, no complete SRB servoactuator had been subjected to these vibration requirements (see Table II). The engineering test unit was periodically removed to the dynamic inertia simulator and load-flow test bench at MSFC to verify that performance criteria were maintained as specified. The purpose of this test program was to detect and modify any deficient elements and thus minimize problems with the formal qualification test program to follow.

Two servoactuators (S/N's 005 and 008) were designated to undergo the formal qualification test program as specified in MSFC's "SRB TVC In-House Qualification Test Procedure" (MSFC document MTCP-CC-SRB-529). At present these tests simulating 20 missions are approximately 5 percent complete.

Another effort, which began prior to and runs parallel with the these tests, verifies performance of the servoactuator with a hot fired APU. These tests are being conducted at the MSFC verification test stand. Initially, these tests were conducted without an active ATVC to verify compatibility of the APU and the servoactuator. Currently, these tests are utilizing an active ATVC, which integrates the APU and servoactuator with the failure detection, isolation and recovery logic in the ATVC. The objective of these tests is to verify the total system performance.

At Thiokol's Wasatch Division, the SRB motor was static test fired in the horizontal position. Four development SRM's (DM1 through DM4) and three qualification SRM's (QM1 through QM3) were to be tested. All test SRM's have been fired as of mid February 1980. Two servoactuators (S/N's 006 and 007) were used for DM3 through QM3. SRB servoactuators were not available for the DM1 and DM2 firings. A test plan for each development motor static test was jointly agreed upon by the SRB vendor and MSFC. Each test plan featured unique and extensive test duty cycles for both the tilt and rock actuators. Various amplitudes of sine wave, ramp and step commands were input to the servoactuators. A frequency response for each static firing test was conducted on the tilt servoactuator, spanning the frequency range from 0.2 to 20 Hz at an amplitude of  $\pm 6$  percent of total stroke. The commands were delivered to the servoactuator through the ATVC, however, the FDIR logic was not active. These static firing tests enabled testing of the servoactuator with the flight type mating structures. Thus, for the first time the first mode resonance of the flight type SRB nozzle and attaching structure was determined. For the final SRB Static Test (QM-3), a small

hydraulic accumulator was installed in the Rock Servoactuator fluid supply line. The frequency response normally conducted on the tilt system was conducted on the Rock Servoactuator. The effects of the accumulator on the pump and hydraulic line modes observed on prior tests were investigated.

## DEVELOPMENT AND QUALIFICATION PROBLEMS

### General

In general, the SRB TVC servoactuator development and qualification programs have been relatively trouble free. The prior development of the SSME TVC ground test servoactuator by the same vendor and MSFC are mainly responsible. Although the SSME ground test servoactuator used three control channels, many of the components shared common designs.

Most problems were of a routine nature and required minimal efforts to analyze and implement corrective action. Such problem areas include: excessive spool friction; improper frequency response; meeting the required linearity and gain criteria; adjustment of feedback gains; and external and internal leakage and seal problems. These problems are of a relatively trivial nature and will not be dealt with. The intent of this section is to address the three most significant anomalies encountered during the development and qualification programs. These three problem areas were deemed "most significant" because of the level of concern and effort devoted to the problems' natures, analyses and solutions.

### End of Stroke Instability

A major problem was detected during testing of the development test unit. A considerable vendor and NASA effort was expended to determine the problem root cause and recommended course of action.

Simply stated, a chattering or oscillation at a frequency of 45 Hz was observed as the piston was moved into or out of the stroke extremities. The oscillations occurred during operational modes only when the piston came within  $5.1 \times 10^{-4}$  m (0.02 in.) of the end of stroke (extend or retract direction) and physically bottomed on the cylinder end. The resultant response of the servoactuator output differential pressure was a 45 Hz square wave with amplitude varying from zero to full system pressure. Superimposed upon this basic wave was a higher frequency (1000 Hz) resulting from the line dynamics of several oil supplying passages. Driving the piston harder into the stops caused the oscillation to cease. The oscillation occurred also in a nonoperational mode when the actuator was pressurized with the mid-stroke locks installed. This lock is an external shipping and handling device that mechanically holds the piston in the null position. Since the mid-stroke locks are always removed for operation, this condition posed no problem.

The development test unit was instrumented with pressure transducers in all areas where pressure transients could be produced by the oscillations. High pressure spikes were detected at the ends of several long, small passage-ways terminating with small restrictions. High frequency spikes were recorded in excess of  $6.895 \times 10^7 \text{ N/m}^2$  (10,000 psi). To eliminate these spikes, orifices were installed in the lines of the four servovalves and main cylinder differential pressure transducers.

An inherent high loop gain around the dynamic pressure feedback loop at the end of stroke was determined to be the root cause of the oscillations. The gain of this loop includes the actuator-oil stiffness as well as the dynamics of the DPF mechanism, servovalves and power valve. Figure 5 shows the simplified linear block diagram of the nominal servoactuator with all four servovalves lumped into one channel. Table III defines the associated parameters. When operating normally, the actuator piston acts as a near ideal integrator, converting power valve flow into piston position. When the piston physically bottoms against the cylinder end, the error signal from the piston position feedback is driven to zero. Under these conditions, figure 6 becomes the representative block diagram of the system. The differential pressure output of the piston then becomes a function directly of the fluid bulk modulus ( $B_o$ ) and indirectly of the line volume ( $V_o$ ) from the power valve to the actuator cylinder. The quantity " $B_o/V_o$ " =  $7.384 \times 10^{12} \text{ N/m}^2/\text{m}^3$  (17,550 psi/in.<sup>3</sup>) resulting in an open loop gain of  $493 \text{ sec}^{-1}$  for figure 6. This gain is more than sufficient to drive the loop unstable.

Several factors contribute to this instability. These are the high flow gain of the total valve assembly, relatively high DPF loop gain and the frequency response of the three stage valve configuration. At the high gain encountered at the end of stroke, the servovalve dynamics are not adequate to maintain stability. This problem was never encountered on the Saturn vehicles' servoactuators. This is attributed to more common use of two stage servovalves and lower DPF gains on the Saturn vehicles.

Attempts were made to introduce damping by adding piston bypass flow at the end of stroke. The large flow quantity required, combined with the complexity and reduced overall reliability, made this approach unacceptable. Because of the modification difficulties encountered, tests were conducted at MSFC to establish the effects of the oscillation on the SRB and associated structure. These tests verified no detrimental effects were imposed by the oscillations upon the SRB, the attaching structure and the actuator itself. At the vendor's facility the servoactuator was cycled in and out of the ends of stroke for two hours with no detectable change in performance.

Because of the discrete occurrence of the oscillation within the last  $5.1 \times 10^{-4} \text{ m}$  (0.02 in.) of the end of stroke and the benign detrimental effects, a redesign of the servoactuator was not justified. A modification to the flight ATVC will limit current commands to the servovalves such that the servoactuator will not be driven into the end of stroke.

## Position Feedback Cam Failure

During prequalification vibration testing on the engineering test unit (S/N 001) at MSFC, a failure of the piston position feedback cam occurred. When the failure occurred, the servoactuator was undergoing the boost random vibration input to the rod (nozzle) end of the longitudinal axis. The cam fractured around the total periphery at the small end of the conical section where the cone blends into the end flange. A cross section of the cam is shown in figure 2. A new cam was instrumented with strain gages and accelerometers and installed into the servoactuator.

Using the data collected in subsequent tests, a fatigue failure analysis was performed by MSFC personnel. A finite element model was utilized and showed a maximum stress of  $3.158 \times 10 \text{ N/m}^2$  (4580 psi) on the inner radius of the cam. The stresses were shown to be low away from the radius. The failed cam was made from 6061 aluminum which was hard anodized. The S-N diagrams for this material showed that the fatigue strength was reduced approximately 40 percent by anodizing. Test data showed the cam/support to have a high Q resonant frequency of 1400 Hz. This mode, coupled with the reduction in the fatigue characteristics of the material, was shown to result in a fatigue failure of the cam.

An analysis by MSFC's Materials and Processes Laboratory was made of the failed part. Examination of the fracture surface showed that contact between fracture halves occurred during longitudinal oscillating applied stress. A metallurgical cross section of the cam fracture showed that initiation probably occurred in the hard anodize at the inner radius machined transition point between the cam cone and end. The fracture then propagated through the parent metal. Susceptibility of this material and configuration to fatigue induced failure was further exemplified by the presence of multiple longitudinal cracks in the hard anodize. It was recommended that the material be changed to a high strength material such as A-286 stainless steel.

The cam was redesigned using A-286 stainless steel with other modifications. Retaining guides were added to prevent the small section from significant movement should a failure occur. Secondary retention was also implemented to hold the cam in the piston. The new cam design was then tested to the vibration criteria with no problems encountered.

## Servo valve Differential Pressure Drift

The SRB static test firings at Thiokol's Wasatch Division facility identified a servo valve differential pressure drift phenomenon not observed on previous tests. The problem was detected on the DM-3 static test article, the first SRB development motor firing with flight configuration TVC servoactuators installed. The output null differential pressures of all servo valves drifted

with time, starting at near zero and increasing to the  $4.1 \times 10^6 - 5.5 \times 10^6$  N/m<sup>2</sup> (600-800 psi) range toward the end of the 120 sec duration firings. Referring to the layout of figure 3, valves "A" and "C" drifted with a positive polarity while valves "B" and "D" drifted with a negative polarity.

After observance of this phenomenon, review of previous tests from the verification test stand at MSFC revealed similar behavior. A number of special tests were conducted on MSFC's inertia simulator and flow bench to attempt reproduction of the pressure drift. However, these tests, using the facility hydraulic supply source with a large reservoir, exhibited no pressure drift with time. After review of the various tests, it became apparent that every test conducted with the APU supplying hydraulic fluid produced similar servo-valve pressure drifts.

The drift characteristics were analyzed and verified by test and analysis to be a function of the time rate of change of hydraulic fluid temperature. The rate of fluid temperature change is directly related to the power dissipation in the hydraulic fluid and the total hydraulic fluid volume. The power dissipation in the hydraulic fluid is a function of the commanded duty cycle. The fluid volume in the SRB TVC system is approximately 26.5 liters (7 gal). Since the fluid is in direct contact with the power valve body, increases in the fluid temperature causes the aluminum power valve body to expand at a different rate than the cage assembly and steel power spool. The difference in expansion of the power valve body with respect to the cage assembly causes an error torque on the flapper assembly. This error torque results in a pressure output from each of the servovalves. The expansion causes valves A and C to move in the direction opposite to valves B and D. Thus the output differential pressures of valves A and C drift with a polarity opposite to that of valves B and D. The summation of these differential pressures was always zero (within the power spool friction force levels) at any given time. Therefore, the power spool and main actuator piston positions were unaffected by the pressure drift.

Since these differential pressure outputs are sensed and utilized by the ATVC for failure detection and isolation, the impact of the pressure drift phenomenon was investigated. It was confirmed by the ATVC vendor that the magnitudes and rates of the pressure drifts observed were well within design tolerances. The development motor static firing tests and extensive testing at MSFC showed the pressure drifts to be very predictable with no detrimental effects on system performance. Also, the servoactuator test duty cycles were much more severe than those expected in flight. Therefore, a redesign was not deemed necessary.

## CONCLUDING REMARKS

As of January 1, 1980, the design and development of the SRB TVC servo-actuator is complete. The engineering test unit has undergone a 20-mission flight vibration test program at MSFC with minimal redesign. A number of verification tests at MSFC with hot-fired APU's have been successfully completed. Four SRB's equipped with flight type servoactuators have been static test fired with no failures. The final qualification test motor (QM-3) was test fired in mid February 1980. With the formal 20-mission qualification test program presently underway, it appears that the present configuration will be the final flight version of the SRB TVC servoactuator.

TABLE I. DESIGN AND PERFORMANCE REQUIREMENTS

Operating fluid	MIL-H-83282
System pressure, $N/m^2$ (psi)	$2.068 \times 10^7 - 2.241 \times 10^7$ (3000-3250)
Burst pressure, $N/m^2$ (psi)	$5.602 \times 10^7$ (8125)
Proof pressure, $N/m^2$ (psi)	$3.361 \times 10^7$ (4875)
Weight, N (lb)	$1.446 \times 10^3$ (325)
Length at null, m (in.)	1.346 (53)
Rated input signal, A (mA)	$\pm 5 \times 10^{-2}$ ( $\pm 50$ )
Stroke, m (in.)	$\pm 1.626 \times 10^{-1}$ ( $\pm 6.4$ )
Piston effective area, $m^2$ (in. <sup>2</sup> )	$2.085 \times 10^{-2}$ (32.32)
Moment arm, m (in.)	1.819 (71.6)
Output force, maximum, N (lb)	467,000 (105,000)
Rated load, N (lb)	$2.818 \times 10^5$ (63,360)
Rate at rated load, m/s (in./sec)	0.151 - 0.212 (5.95-8.33)
Frequency response:	
Bandpass, Hz	2.5 - 3.5
Phase lag at 1 Hz, rad (deg)	0.349 (20)
Load 1st mode resonant frequency, Hz	13.8
Internal leakage, $m^3/s$ (gpm)	$1.893 \times 10^{-4}$ (3)
Intersystem leakage, $m^3/s$ (gpm)	$2.145 \times 10^{-6}$ (0.034)
Null shift, A (mA)	$2.37 \times 10^{-3}$ (2.37)
Hysteresis, A (mA)	$1.15 \times 10^{-3}$ (1.15)
Threshold, A (mA)	$5 \times 10^{-4}$ (0.5)
Null bias, m (in.)	$1.397 \times 10^{-3}$ (0.055)
Pressure gain:	
Servovalve, $N/m^2/A$ (psi/mA)	$3.447 \times 10^9 \pm 8.619 \times 10^8$ ( $500 \pm 125$ )
Power valve, $N/m^2/A$ (psi/mA)	$3.448 \times 10^{10}$ (5000)
Temperature operating range, K (°F)	266.5 to 338.7 (20 to 150)
Water pressure, $N/m^2$ (psi)	$4.895 \times 10^5$ (71)
Water entry pressure, $N/m^2$ (psi)	$1.069 \times 10^6$ (155)

TABLE II. DESIGN AND TEST VIBRATION REQUIREMENTS

Criteria	Input Source	Axis	Level	Total exposure time, sec/axis
Vehicle dynamics	Nozzle	Radial Tangential Longitudinal	3.7 g peak 3.7 g peak 2.4 g peak	120
	Aft skirt	Radial Tangential Longitudinal	3.7 g peak 3.7 g peak 1.0 g peak	150
Flight random	Nozzle	All	26.5 g rms	2640
Liftoff random	Aft skirt	Radial Tangential Longitudinal	5.0 g rms 6.3 g rms 6.3 g rms	250
Boost random	Aft skirt	Radial Tangential Longitudinal	6.1 g rms 9.2 g rms 9.2 g rms	880
Re-entry random	Nozzle	Radial Tangential Longitudinal	14.7 g rms 14.4 g rms 14.4 g rms	660
	Aft skirt	Radial Tangential Longitudinal	11.2 g rms 12.7 g rms 12.7 g rms	660

TABLE III. SRB TVC SERVOACTUATOR PARAMETERS

Symbol	Description	Units	Value
$I_c$	Command input current	A (mA)	$\pm 0.05$ ( $\pm 50$ )
$K_{TM}$	Torque motor gain	N-m (in.-lb/mA)	4.519 (0.04)
$K_V$	Valve flow gain	$m^3/s/N-m$ (Cis/in.-lb)	0.212 (1460)
$\zeta$	Valve parameters		0.7
$\omega$	Valve parameters	$s^{-1}$	1571
$\zeta_o$	Valve parameters	-	0.471
$\omega_o$	Valve parameters	$s^{-1}$	310.1
$\zeta_1$	Value parameters	-	0.4
$\omega_1$	Value parameters	$s^{-1}$	1189.1
$\zeta_2$	Valve parameters	-	0.502
$\omega_2$	Valve parameters	$s^{-1}$	2880.1
A	Actuator piston area	$m^2$ (in <sup>2</sup> .)	$2.085 \times 10^{-2}$ (32.32)
$K_T$	Total system compliance	N/m (lb/in.)	$3.003 \times 10^7$ (171,500)
$K_L$	Load compliance	N/m (lb/in.)	$3.387 \times 10^7$ (193,400)
J	Gimballed moment of inertia	$N-m/s^2$ (lb-in.-sec <sup>2</sup> )	$1.491 \times 10^4$ ( $1.32 \times 10^5$ )
B	Nozzle viscous friction	N-m/s (in.-lb-sec)	$6.56 \times 10^4$ (580,590)
$K_b$	Nozzle restraining torque gain	N-m/rad (in.-lb/rad)	$3.39 \times 10^6$ ( $30 \times 10^6$ )
d	Moment arm	m (in.)	1.819 (71.6)
H	Position feedback gain	N-m/m (in.-lb/in)	1.392 (0.313)
$T_P$	DPF time constant	s	0.125
$K_P$	DPF gain	N-m/pascal (in.-lb/psi)	$2.524 \times 10^{-9}$ ( $1.54 \times 10^{-4}$ )
$B_o$	Effective bulk modulus	$N/m^2$ (psi)	$1.034 \times 10^9$ (150,000)
$V_o$	Effective end volume	$m^3$ (in. <sup>3</sup> )	$1.4 \times 10^{-4}$ (8.5)
$Q_v$	Power valve flow	$m^3/s$ (Cis)	$\pm 5.57 \times 10^{-3}$ ( $\pm 340$ )

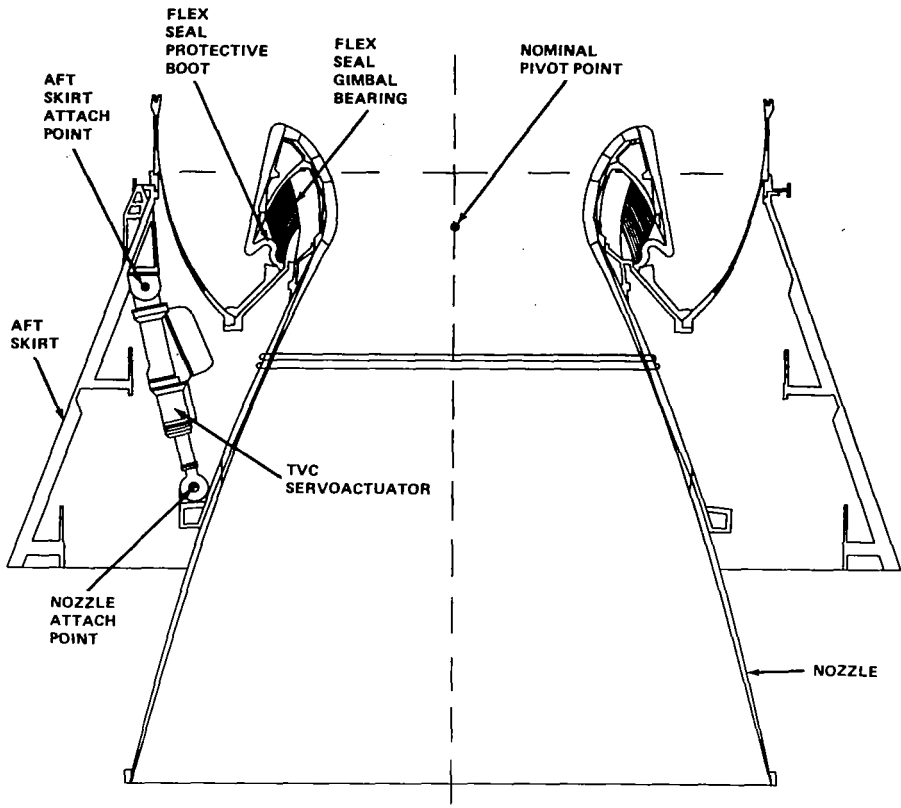


Figure 1.- SRB TVC servoactuator/nozzle installation.

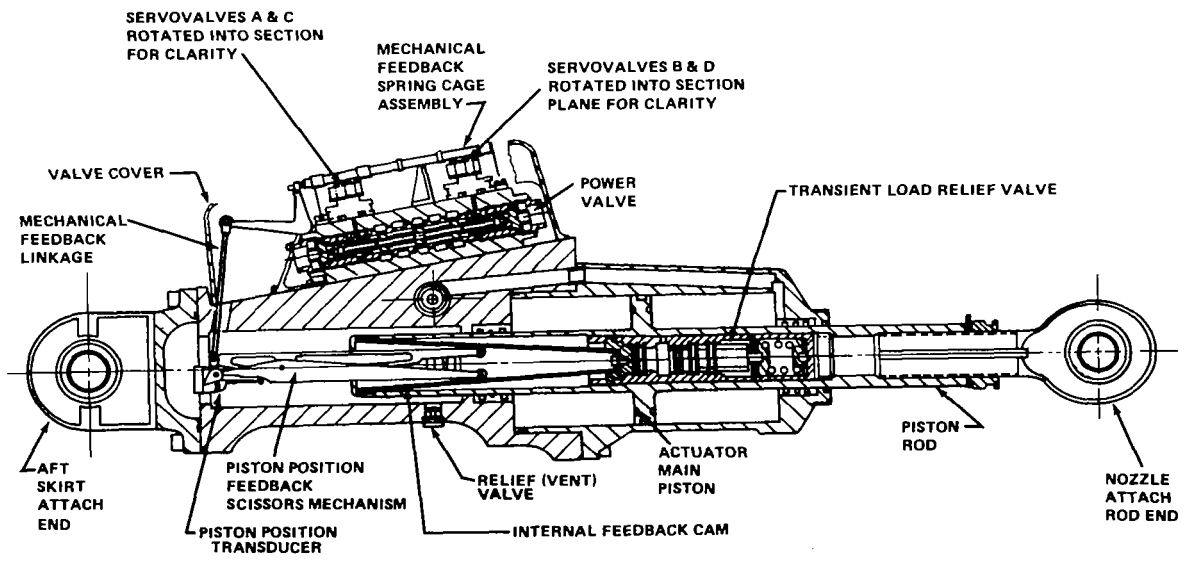


Figure 2.- SRB TVC servoactuator assembly.

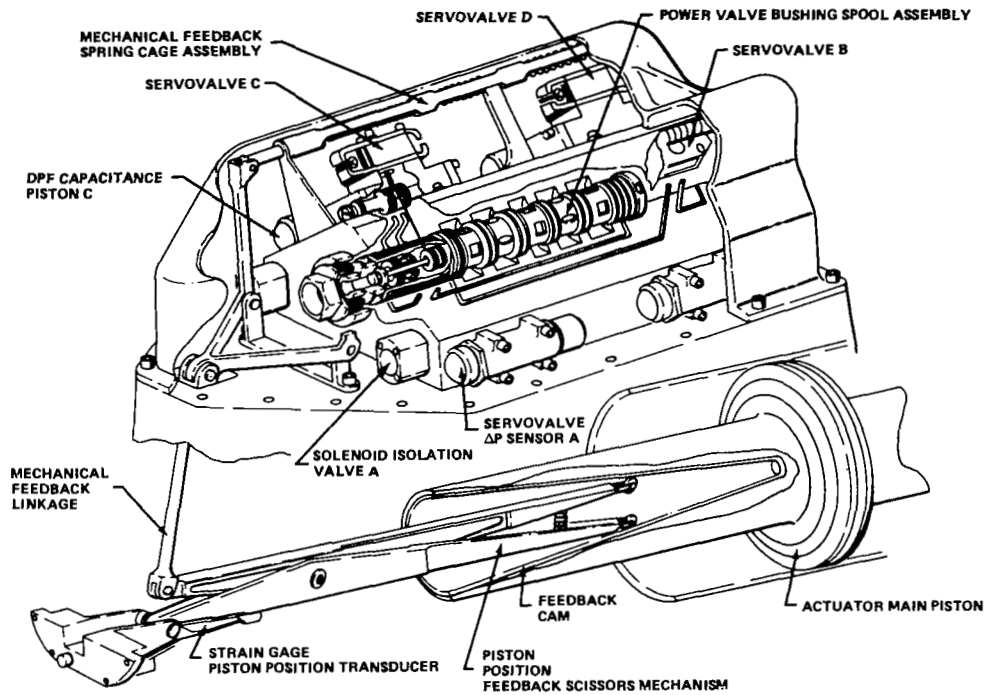


Figure 3.- SRB TVC servoactuator redundancy and feedback mechanisms.

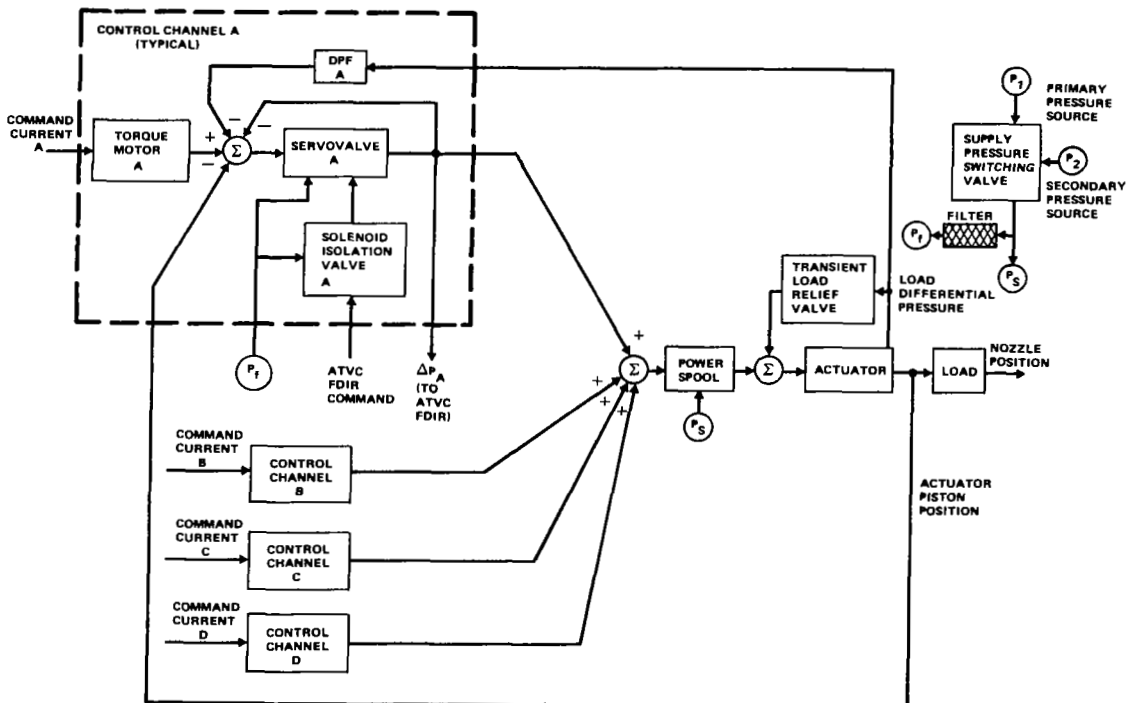


Figure 4.- SRB TVC servoactuator simplified block diagram.





A PRECISION BEARING GIMBAL SYSTEM FOR  
THE TEAL RUBY PROGRAM

Charles H. Lowry, System Project Manager  
Teal Ruby Experiment

Rockwell International  
Space Systems Group  
Seal Beach, California

SUMMARY

The Teal Ruby Experiment employs a precision bearing gimbal system that allows it to stare at points on the earth while in orbit. This paper describes that gimbal system and points out problems encountered, analytical tools and test methods used, and data applicable to users of similar systems.

INTRODUCTION

The Teal Ruby Experiment (TRE) is an earth-orbiting infrared sensor. The TRE program is being carried out by Rockwell International Corporation, Space Systems Group. The program is sponsored by the Defense Advanced Research Projects Agency and managed by the Department of the Air Force--Headquarters, Space Division. The P80-1 spacecraft provides a stable orbiting platform for the TRE sensor.

The objectives of the TRE are (1) to demonstrate that cooperative aircraft can be detected from space with an infrared-type sensor, (2) to establish a global data base in several infrared spectral bands that will be useful in defining future space surveillance systems, and (3) to demonstrate, in space, mosaic infrared sensor technology.

The TRE sensor mosaic focal plane detects infrared energy radiated to space from the earth in several spectral bands. The focal plane and interior optics of the telescope are cooled to cryogenic temperatures by a solid cryogen system, which is integral to the sensor assembly. Three electronic boxes mounted on the P80-1 spacecraft functionally support the sensor assembly. Figure 1 shows the TRE mounted on the P80-1 spacecraft; figure 2 shows the sensor equipment arrangement.

The TRE has a pointing capability in both the in-track (line of flight) and cross-track axes of the sensor. The pointing control system, under direction of stored time-tagged commands, fixes the line of sight on an earth-fixed point by using spacecraft-supplied ephemeris, attitude, and angular rate data.

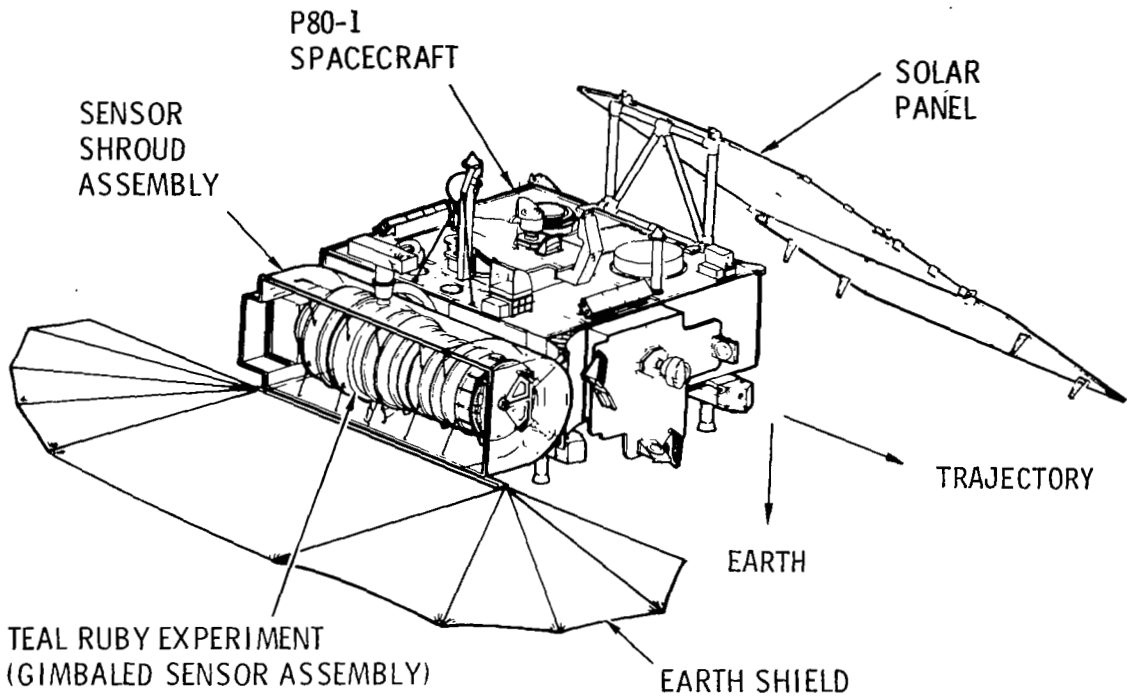


Figure 1.- Teal Ruby Experiment mounted on P80-1 spacecraft in stowed position.

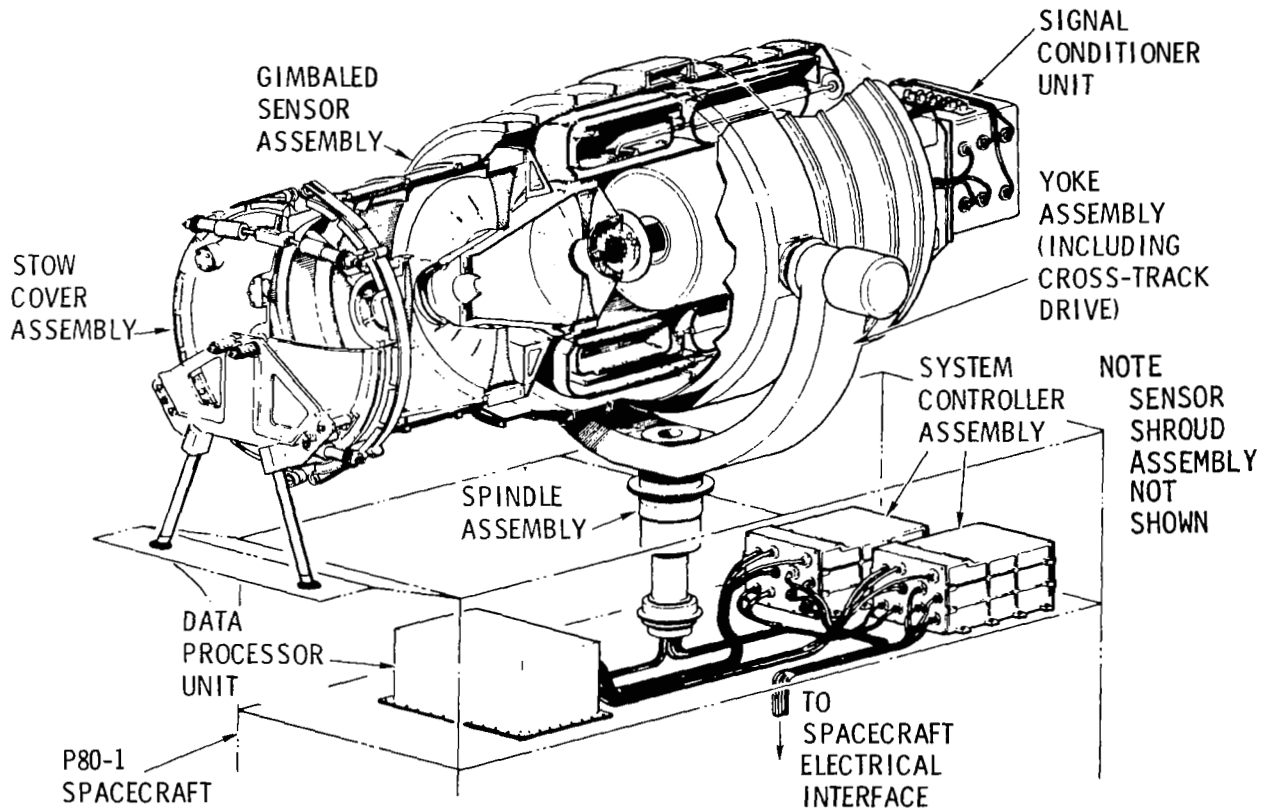


Figure 2.- Teal Ruby Experiment.

In the nominal "step-stare" operational mode, the pointing control system directs the experiment to stare at a ground point and hold that point fixed while the gimbal motion compensates for both spacecraft and earth motion. This stare operation may be repeated several times during a single data gathering period.

The TRE, mounted on the P80-1 spacecraft, is carried into low earth orbit by the Space Shuttle. After ejection from the orbiter payload bay, the spacecraft is boosted by the P80-1 propulsive stages to a final orbit altitude of approximately 740 km (400 nmi). Launch is scheduled for late 1981.

#### GIMBAL SYSTEM REQUIREMENTS

The TRE gimbal system must meet stringent structural and dynamic requirements under varying conditions. Maximum loading occurs during launch and boost. To save weight, the spindle is allowed to deflect significantly under boost loads, but no bearing "Brinelling" or other roughness is tolerable that could result in excessive gimbaling noise during on-orbit operations. Minimizing the random noise content of the gimbal system is essential to avoid perturbing and obscuring the sensor data.

After the TRE reaches operational orbit, the gimbal system represents a relatively stiff mount for the sensor and is required to perform for a year with low torque and low noise, with significant temperature differentials across the bearings, and with bearing temperatures as low as 160 K.

To facilitate the step-stare operational mode, the sensor gimbal system must have two degrees of freedom through the excursion ranges necessary to accommodate the required field of view. Table I shows gimbal requirements in terms of excursions, torques, and accuracy. The 200-arc-second accuracy shown converts to a 0.7-km accuracy at a point on the earth's surface.

The torque budget is shown in table II for on-orbit operation. This table allocates the available torque from the motors into (1) torque used to move the sensor to its excursion extremes and (2) margin. The margin values include acceleration torque plus contingency torque to overcome any possible applied external loads, such as loads caused by loose insulation. Wire harness flexing may aid or hinder gimbaling, depending on the gimbal position at the time and the direction of travel.

#### GIMBAL SYSTEM CONFIGURATION

The gimbal system arrangement is shown in figure 3. To enable the TRE to point at targets on the earth, the sensor is mounted on a gimbal system that provides two degrees of freedom for motion. This system consists of the following major components:

In-track spindle assembly

Cross-track trunnion assembly

Yoke structure assembly

Torque motor and resolver assemblies

Rate gyro assemblies

Bearing assemblies

The spindle assembly provides a low-friction rotating support for attaching the sensor to the spacecraft in a cantilevered fashion. The spindle is supported by two duplex, preloaded pairs of angular contact ball bearings. Spindle rotation is controlled with a motor-resolver assembly, rate gyro, and control electronics.

TABLE I.- GIMBAL REQUIREMENTS

Characteristic	In Track	Cross Track
Gimbal freedom (deg) operating	+80 to -60	$\pm 10$
Gimbal position (deg) stowed	-90	0
Gimbal rate (deg/s)	$\pm 1$	$\pm 1$
Motor torque, nominal (N·cm)	144	150
Pointing accuracy (arc-s)	200*	200*
Rate accuracy (arc-s/s)	0.52*	0.52*

\*Total P80-1/TRE budget

TABLE II.- TORQUE BUDGET

Torque Source	In Track (N·cm)	Cross Track (N·cm)
Bearing friction	21	14
Wire harness flexing	15	7
Margin	108	129
Total	144	150

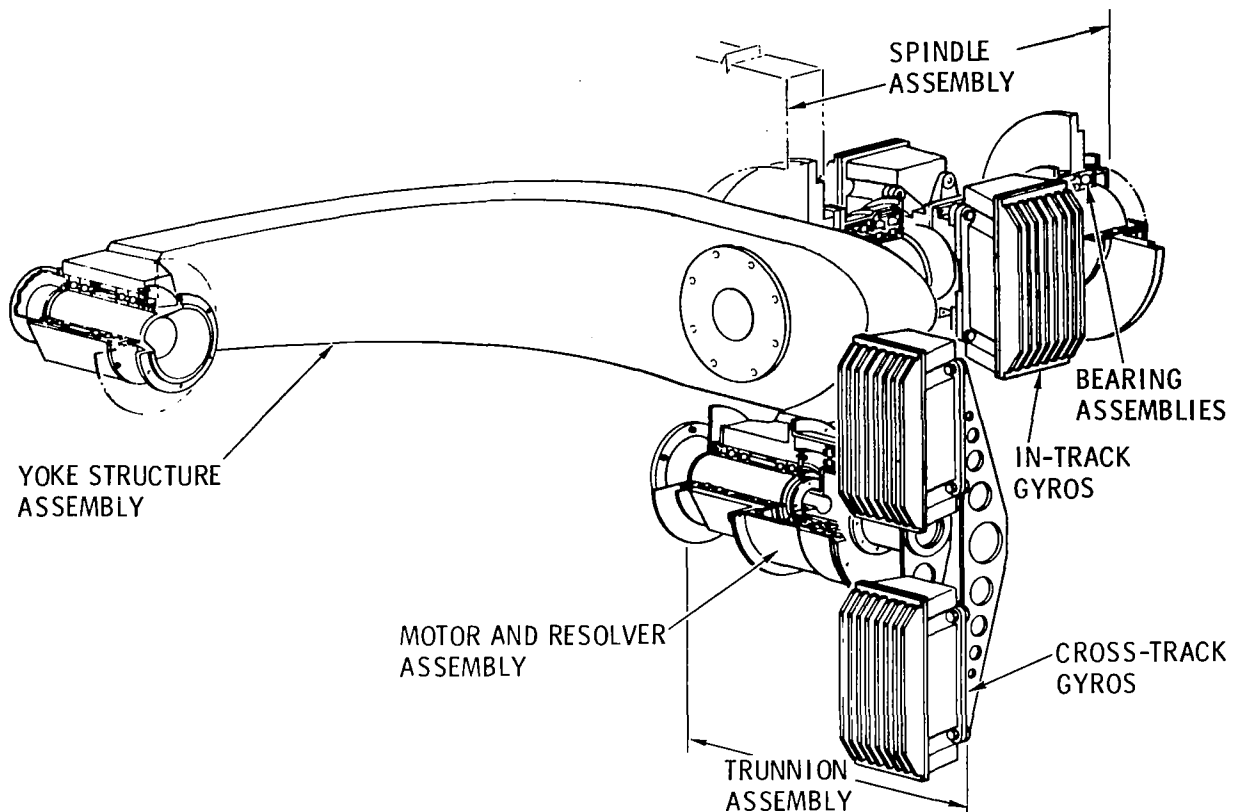


Figure 3.- Gimbal system arrangement.

The yoke is a U-shaped structure that attaches to the spindle at the base of the U. Trunnions extending from the sensor girth ring are accepted by cross-track bearings located at the ends of the yoke structure. This trunnion-to-bearing attachment of the sensor to the yoke provides the second degree of freedom for the sensor to enable cross-track viewing. Cross-track motion is similarly controlled with a motor-resolver assembly, rate gyro, and control electronics.

#### GIMBAL SYSTEM DESIGN

Primary attention is given here to the design philosophy of the spindle system, which is similar to that of the cross-track system.

The spindle bearing installation in the outboard P80-1 attachment is shown in figure 4. The spindle, made from Inconel 718, is hollow in the center for wiring to pass through, interconnecting the P80-1 and TRE. The 90-mm internal diameter bearings are heated to 121°C (250°F) so that they can be slipped over the spindle shaft, then allowed to cool and contract there when properly positioned. Next, a lock nut is torqued up to apply a compressive load between the inner races. The outer races are clamped

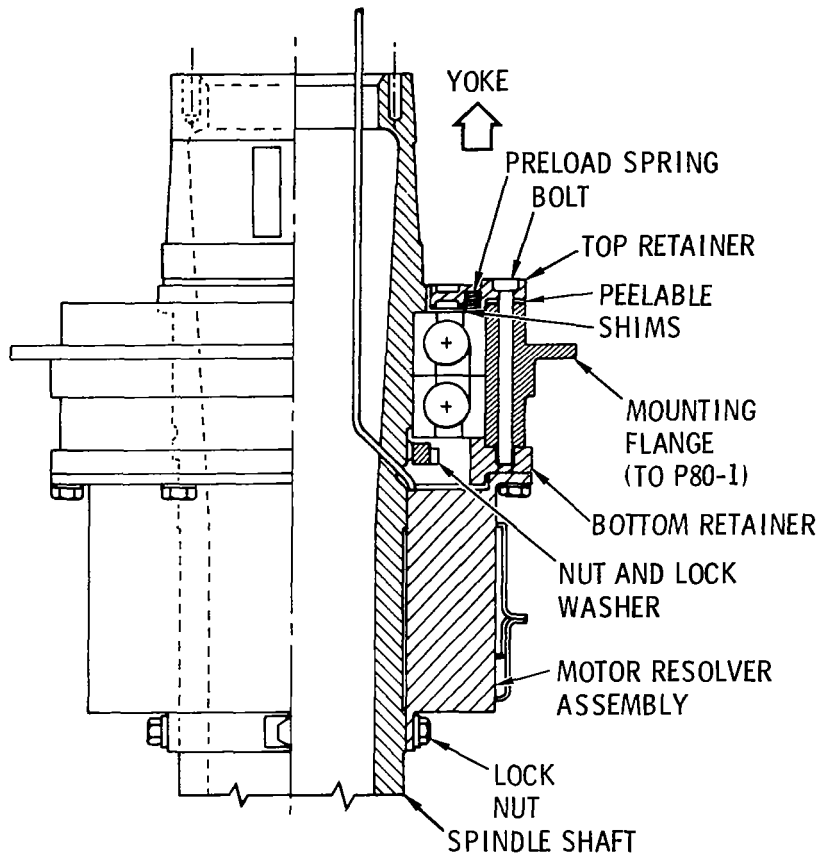


Figure 4.- 90-mm bearing installation.

between the top retainer, mounting flange, and bottom retainer. Peelable shims are positioned between the top retainer and mounting flange to control the maximum gap or interference between the outer races and the top retainer.

The design and dimensions of this installation limit looseness so that no "Brinelling" occurs during boost vibration. The maximum gap between the outer race of the top bearing and the top retainer is 0.0127-mm (0.0005-in.), and the maximum gap between the outer races and the mounting flange is 0.0102 to 0.0152 mm (0.0004 to 0.0006 in.).

On orbit, the spindle is cooled by its thermal proximity to the sensor body. Thus, the bearings shrink from their launch configuration dimensions and a looseness develops in the two areas mentioned above, allowing the outer races to "float." The preload springs now come into play to keep the prescribed value of 311 N (70 lb) on the bearings for smooth, low-friction operation during gimbaling.

The bearing installation in the inboard P80-1 location is shown in figure 5. It is similar to the outboard installation except that these bearings have an 80-mm internal diameter. No thrust loads are taken by the inboard bearings, and again the mounting flange freely floats relative to the outer bearing races after temperatures stabilize on orbit.

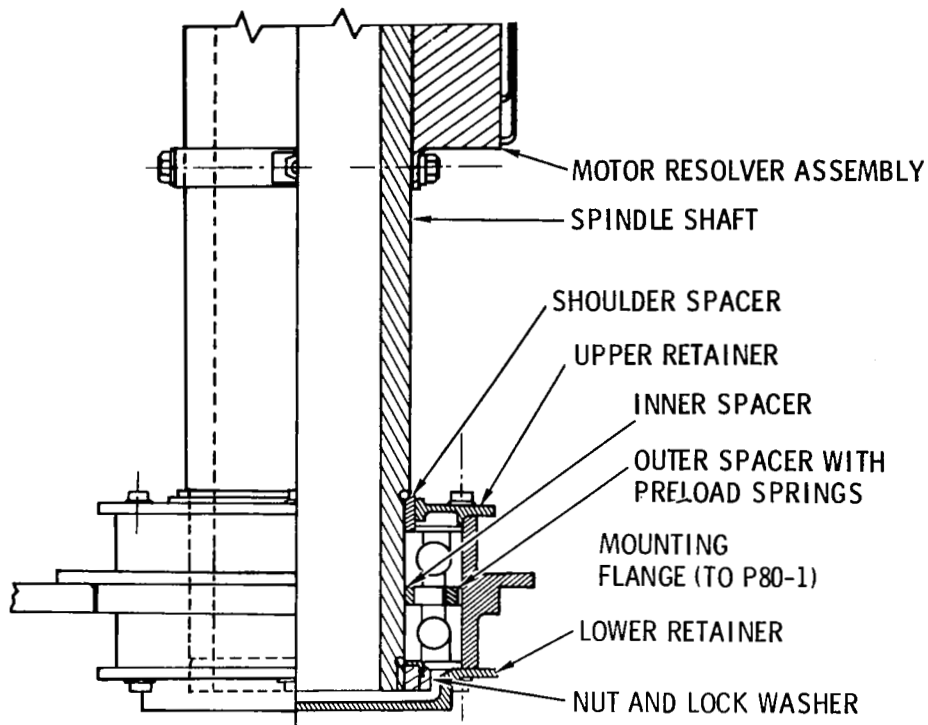


Figure 5.- 80-mm bearing installation.

The bearings themselves are of a precision design and are fabricated by the Fafnir Bearing Company for the TRE program. The material is 440C and the lubrication is applied by a unique process developed by Hughes Aircraft for spacecraft gimbal bearings.<sup>1</sup>

A dry lubricant was chosen to meet low-temperature requirements and to minimize outgassing. Similarly, a minimum thickness, maximum adhesion lubricant was needed to ensure low torque and noise. The lubricant system selected was molybdenum disulfide, applied by an RF sputtering process. The lubricant film thus applied is approximately 1200 angstroms thick. It is burnished and run in, and then the torque and noise are characterized.

#### ASSEMBLY

During assembly, parts are placed in their relative locations and allowed to "soak" to a constant temperature for 24 hours. Handling is minimized to avoid the effects of body heat and resulting expansion and distortion. All gimbal system assembly takes place in a 100,000-level clean room and assemblers wear lint-free gloves. Frequent use of a vacuum during assembly removes any loose dry lub or other contaminants.

<sup>1</sup>Christy, R.I., and Barnett, G.C.: Sputtered MOS<sub>2</sub> Lubrication System for Spacecraft Gimbal Bearings. Hughes Aircraft Company,

The spindle was assembled several times at Rockwell to support various TRE and P80-1 tests. The recorded torque in the bearings varied significantly when measured at different times. Tests and analyses were conducted to build a data baseline and to identify significant contributors to increases in torque.

Early assembly activities revealed that the process of heat-shrinking the inner race of the bearings onto the spindle shaft did not greatly affect the bearing torque. There was a general increase in torque as a function of time, however, after the bearings were removed from their protective bags and installed. This effect appeared to be a combination of contamination and atmospheric moisture. There were also apparent contributions from asymmetrical loads induced by an accumulation of component tolerances and preload variations.

An example of how torque varied throughout the history of a set of 80-mm bearings is shown below. Bearing pairs were preloaded in all cases.

<u>Sequence</u>	<u>Torque (N·cm)</u>
1. As originally accepted at Fafnir (not installed)	4.2
2. Initial test at Aerospace Corp. (not installed)	4.9
3. Early installation on spindle	29-44
4. Repeat of test at Aerospace Corp. (not installed)	14.0
5. Flushed, dried, and reinstalled on spindle	7.3

An analysis of these data showed that the torque did not change significantly between sequence 1 and 2; a change of this magnitude could be attributed to different test setups. The change from sequence 2 to 3, however, was due primarily to a combination of (1) moisture and contamination plus (2) asymmetrical loads induced in installation. The effects of moisture and contamination were isolated by sequence 4, which tested the bearings in the same configuration as sequence 2. The difference in the sequence 3 torque (29-44) and the sequence 4 torque (14) was attributed largely to asymmetrical loading in installation. This anomaly was analyzed and corrected, and sequence 5 showed a return to low torque with installation discrepancies resolved--the bearings having been flushed and dried. Separate tests were run to further isolate the effects of preload, moisture, and contamination.

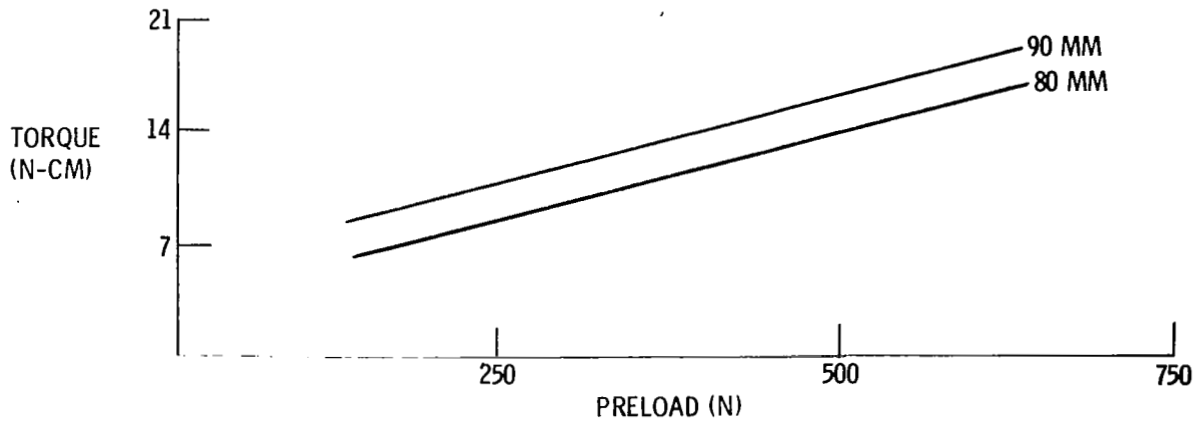


Figure 6.- Effects of preload on torque.

#### PRELOAD TESTS

Since assembly tolerances can cause excessive bearing preload, it was necessary to determine and understand the effects of preload on bearing torque. Tests were run on the 80-mm and 90-mm bearings immediately after cleaning and drying. The results, shown in figure 6, indicate a linear increase in torque as a function of preload within the range tested. Nominal preload provided by the springs is 245 N (55 lb) for the 80-mm bearings and 311 N (70 lb) for the 90-mm bearings. These data were used in analyzing the relative contributions of assembly variations.

#### MOISTURE TESTS

The effects of moisture and contamination were of primary interest because they could become extreme as a function of time and usage prior to launch. A series of tests was conducted to isolate the contribution of moisture. The following sequence of activities took place under controlled test conditions.

1. Install bearings on a spindle; run baseline torque tests.
2. Expose spindle to 85-percent relative humidity for up to eight days, conducting intermittent torque tests, until torque reaches a constant level.
3. Bake out spindle in a dry oven at 121°C (250°F) until torque reduces to a constant lower level.

The data from these tests indicate the maximum and minimum torque to be expected from a set of bearings with maximum and minimum moisture.

A related test series was then conducted to determine if bearings dry out in a space environment.

1. Conduct baseline torque tests.

2. Reintroduce moisture as in step 2, above.
3. Install spindle in a vacuum chamber and control bearing temperature to approximate on-orbit levels.
4. Conduct torque tests after prescribed time increments to verify torque reduction to budget levels.

These data dictate the degree to which atmospheric moisture can be tolerated in the bearings prior to launch and, conversely, the degree of protection required to minimize moisture accumulation. The data from these tests are being evaluated and will be presented at the symposium.

#### STRUCTURAL ANALYSIS AND TEST

Analysis of the gimbal assembly from a structural standpoint was initiated early in the design. The spindle assembly in its cantilevered loading condition was the most critical area of analysis; and the bearings were identified as the most critical structural elements within the assembly.

Rockwell used a unique program to predict bearing stresses for both rigid and flexible spindle shaft and housing. Parametric analyses gave insights into the sensitivity of bearing stresses to such factors as element stiffness and installation misalignment.

Load tests were conducted with the spindle installed on the actual flight spacecraft. Limit loads were applied to the spindle in three axes. To pass this test the spindle assembly had to remain undamaged, and bearing noise had to be within prescribed limits. After the spindle was loaded in this static test, the bearings were removed, and the total assembly was inspected. No discrepancies were noted, and bearing noise did not increase from the pretest levels.

The test was then repeated at 1.25 times limit loads. The criterion for this test was that no permanent deformation could occur; there was no noise criterion. The assembly passed the test, but the bearing noise did increase above the level allowed in the noise budget.

#### NOISE TESTING

An essential element in minimizing data disturbances induced by the sensor itself is control of the noise sources that cause line-of-sight jitter. One of the sources of noise that must be monitored and controlled is roughness in the gimbal bearings from contamination, chipped dry lube, "Brinelling" of the balls and races, etc.

Before and after vibration and static load testing, noise tests were run on preloaded sets of bearings. Basically, a sensitive torque test was conducted while the bearings were rotated several times. The torque data were then run through narrowband filters to determine the energy level in the noise versus frequency. These data were then used

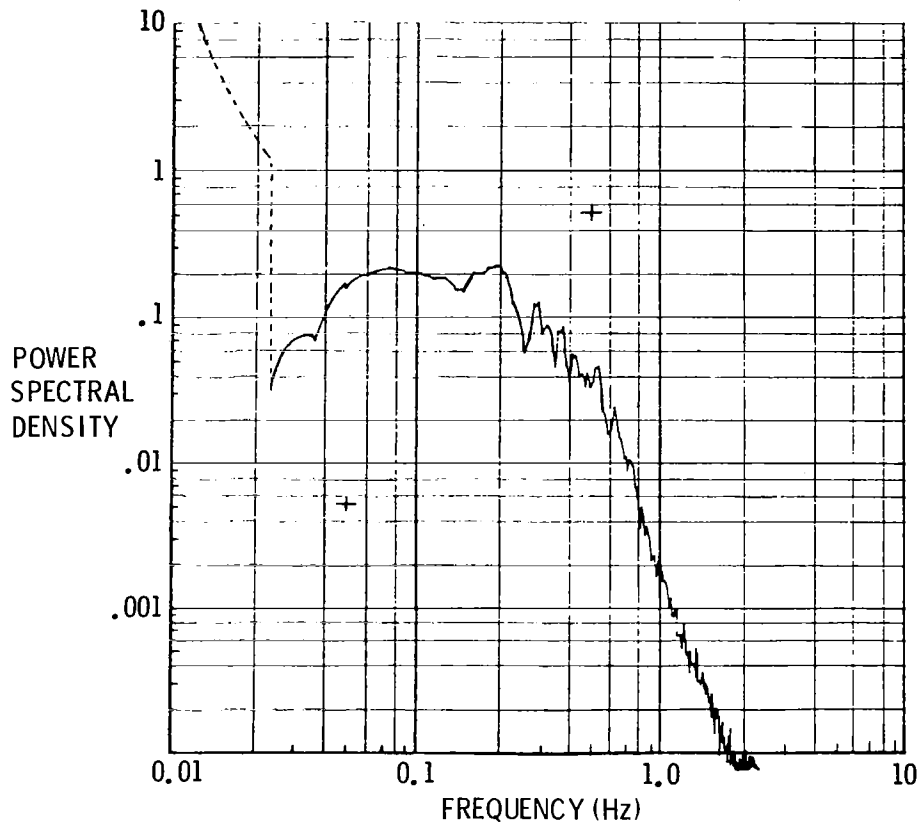


Figure 7.- Bearing noise.

in the TRE servo dynamic math model to verify that the resulting line-of-sight jitter was acceptable. Figure 7 shows a typical power spectral density plot for the 90-mm bearings.

Noise testing on the Teal Ruby program verified that qualification-level random vibration and limit-level static loads do not appreciably affect noise, but bearing contamination increases the noise level significantly.

#### CONCLUDING REMARKS

Proper use of contemporary design principles and fabrication techniques can produce a gimbal system capable of supporting a precision-pointing, low-weight, low-noise sensor. Cleanliness, moisture control, and control of component tolerances are essential to minimizing adverse effects.



# **FUEL/HYDRAULIC TRANSFER VALVE IMPROVES RELIABILITY OF ATLAS SPACE LAUNCH VEHICLE**

**M. Ogman**  
**General Dynamics Corporation — Convair Division**

## **SUMMARY**

The Atlas Fuel/Hydraulic transfer valve (FHV) design is enhancing the Atlas space vehicle launch reliability without a major redesign. The concept represents a rational evolutionary design change. General Dynamics Convair Division has designed a fuel/hydraulic transfer valve to permit controlled interfacing with the RP-1 fuel supply. The design satisfies primary goals such as fuel and oil isolation before launch in order to use existing ground support and airborne hardware and procedures. The valve will operate only after the vehicle has been committed to launch. Hydraulic system function will be maintained if the valve fails to function. Valve operation is mechanical and interfaces only with the propulsion system.

## **BACKGROUND**

The Atlas vehicle has two independent hydraulic systems, one for each stage, used to provide power for thrust vector control and to the engine propellant utilization system. As a first generation missile designed primarily as a high priority weapons delivery system, no consideration was given for designing redundancy features into the hydraulic system. As a weapon system vehicle, its development and operational flight record was tarnished by occasional hydraulic system failures attributed to system leakage.

The changeover from a weapons system to a space launch vehicle placed greater emphasis on vehicle reliability. The hydraulic system reliability was improved by critical analysis, design improvements, generous testing, and tender loving care.

The Atlas vehicle carries at liftoff approximately 47.3 cubic meters (12,500 gallons) of RP-1 fuel and the hydraulic systems carry 0.0011 cubic meters (0.3 gallons) of reserve hydraulic fluid. Leakage of the hydraulic fluid in flight in excess of reserve capacity could result in a costly mission failure. The concept of tapping the RP-1 fluid as an "infinite" reservoir for the hydraulic system became attractive. System reliability can be increased to permit the hydraulic system to become leak-tolerant. An estimated 50% of the previous hydraulic system flight failures (and mission losses) would have been prevented if the concept had been utilized.

## **CONCEPT**

The fuel/hydraulic transfer valve design uses a diaphragm to isolate hydraulic and RP-1 fluids. A ram is used to rupture the diaphragm. This event can only occur when the engines are ignited and high-pressure RP-1 fluid is generated. The high-pressure RP-1 fluid is ported to the ram which then ruptures the diaphragm. The subsequent interface attainment between low pressure RP-1 and hydraulic fluid thus makes the "infinite" supply of RP-1 available to the hydraulic system. With zero system inflight leakage, the hydraulic system functions on a low mixture of RP-1 in hydraulic fluid. If a leak is manifested, system function will continue as RP-1 flows into the hydraulic system.

## PREVIOUS DEVELOPMENT

Air Force funds were made available in 1967-68 to design and develop a similar interface valve to the subject valve. The major difference between the two designs was that the earlier version had a design feature that would not allow inflight interfacing of RP-1 fuel with hydraulic fluid under any circumstances except when a system leak developed. The valve would function by sensing an inflight pressure loss in the return or low pressure system circuit.

A valve was designed, developed, and tested to demonstrate the concept feasibility. The diaphragm-design configuration was the major hurdle to overcome. After starting with no experience, a satisfactory diaphragm configuration was attained. System tests using surplus flight hardware demonstrated all program objectives, but the program was cancelled without implementation. Fortunately, the data was used to design the current valve now in flight service.

## HYDRAULIC SYSTEM DATA

- Number of independent systems: two (one for each stage)
- Operating pressures (nominal)
  - High pressure: 205 ATM (3,015 psia)
  - Return or low pressure: 5.3 ATM (80 psia)
- Hydraulic pump flow (variable, engine driven):
  - Booster:  $0-1.45 \times 10^{-3} \text{ m}^3/\text{sec}$  (0-23 gpm)
  - Sustainer:  $0-0.50 \times 10^{-3} \text{ m}^3/\text{sec}$  (0-8 gpm)
- Hydraulic fluid: MIL-H-5606, (hydrocarbon — red color)
- Fuel: RP-1 per MIL-R-25576
- Function:
  - Booster system: Provide power to engine nozzle thrust vector servactuators
  - Sustainer system: Provide power to engine nozzle thrust vector servactuators and engine propellant control system

## OBJECTIVES AND CONSTRAINTS

The task objective was to design, test, and integrate a valve into three existing Atlas vehicle configurations requiring three different installation versions. Fortunately, the three vehicle hydraulic systems used common hardware and functioned identically. This allowed the designer to create a common valve design and envelope with port fitting configuration differences to accommodate unique installation requirements.

The Atlas SLV-3D model is manufactured for NASA under a Lewis Research Center managed contract. The Atlas SLV-3A and E/F models were manufactured and subsequently modified for the U.S. Air Force Space Division use. The U.S. Air Force Space Division and NASA jointly provided the design and testing funds for the valve basic design. All agencies participated in preliminary and critical design reviews.

The prime technical objectives were:

1. To increase booster and sustainer hydraulic system reliability by utilizing RP-1 fuel as a ready reserve fluid in the event of a hydraulic system leak to maintain system function:
  - A. With any size return system leak.
  - B. With a limited leak in the pressure system.
2. To maintain hydraulic system function if the FHV valve does not activate.

3. To achieve program economy by utilizing a wholly mechanical system and avoiding a more costly electrical system.

**Design Objectives Achieved:**

- A. System reliability has been increased.
- B. No pyrotechnic devices or electrical interfaces were used..
- C. The FHV valve uses high-pressure fuel to activate the valve. Valve integration between hydraulic and propulsion systems is not affecting either system performance.
- D. Prior to vehicle launch, there is zero leakage of hydraulic or RP-1 fluids into the alien system.
- E. Interface of RP-1 fuel and hydraulic fluid occurs only when the vehicle is committed to launch. This occurs for:
  1. Atlas E/F vehicles: at initiation of "Engine Start" sequence.
  2. Atlas SLV vehicles: at vehicle release (Post Engine Start).
- F. Valve design makes maximum use of design features of the "emergency fuel valve" design developed in 1967-68.

In Design Objective E.1 above, the E/F vehicle is a nonrestrained launch concept. The vehicle will liftoff when engine thrust exceeds vehicle weight. No launch abort is possible. The SLV vehicle, being of an earlier design, is restrained to the launcher until engine thrust has increased to a steady state level. The vehicle is then automatically released for flight after satisfying all launch control monitor functions. During the interim period between engine start and "launch release" an abort capability exists. The problem presented here is twofold: (1) how to delay valve operation past the engine start transient for E/F and SLV vehicles, and (2) how to allow an abort event for SLV vehicles without activating the valve.

In Design Objective E.2, the use of a pyrotechnic device to trigger the FHV valve with high pressure fuel would have been ideal, but this introduces an electrical interface. This concept was dropped because the E/F vehicle would have required an electrical relay box to fire the pyrotechnic squib. The qualification cost of the relay box and lot control costs of the squibs would have exceeded allocated funds.

### **HOW THE FHV VALVE FUNCTIONS**

See Figure 1. A diaphragm is used to isolate RP-1 fuel from hydraulic fluid. The diaphragm is ruptured by high pressure RP-1 that is only available upon engine ignition. When the diaphragm ruptures, low pressure RP-1 and hydraulic fluid interface. The RP-1 pressure is greater than the hydraulic return pressure by the amount of the RP-1 head pressure in the vehicle tank (about 0.4 atm, 6 psid). With no hydraulic system leakage, the hydraulic return pressure will rise to equalize with RP-1 pressure. The small extra volume of RP-1 is accommodated by the airborne hydraulic reservoir and no further mixing occurs. In case of an external leak in the hydraulic system, RP-1 fuel will flow into the hydraulic system and be directed to hydraulic pump inlet to maintain system pressure and flow. System function will be maintained with any size leak in the return portion of the circuit upstream of the FHV valve and a limited leak in the pressure circuit.

In the event the diaphragm inadvertently does not rupture at lift off, the hydraulic system will function as if the FHV valve does not exist. The airborne reservoir will maintain sufficient pump inlet pressure to feed the pump fluid.

In order to satisfy the requirement to actuate the FHV valve after the engine transient phase, a timing restrictor is installed in the high-pressure RP-1 line at the engine thrust chamber. This line normally contains no fluid and is at atmospheric pressure. At engine start, RP-1 is metered into the line

and pressure builds up thermodynamically until the ram overcomes diaphragm rupture resistance. The metering creates sufficient time delay for the engine start transient to be completed before the diaphragm will rupture. Imposing a time delay prior to diaphragm rupture is more critical for SLV vehicles which have abort capabilities. The diaphragm must not break prior to run out of time allotted for an abort period while at the same time minimizing the time wherein the FHV valve is not activated while airborne. See Figure 2. Because of the many variables involved in calculation of the thermodynamic pressure rise in the timing circuit coupled with no meaningful data associated with some of those variables, the size of the timing restrictor was determined by making reasonable assumptions for calculation purposes.

Flight data revealed that the valve was activated early, but still within acceptable limits. What had transpired, was a race between the run out of the abort timer and the diaphragm rupture event. By design, the abort timer was to run out a fraction of a second prior to the diaphragm rupture. Any abort during the abort period would maintain the diaphragm structurally intact and thereby maintain isolation between propulsion and hydraulic systems. In reality, a photo finish occurred.

### FHV VALVE DESIGN FEATURES

The valve detail elements are shown in Figure 3. The simplicity of the valve design contributed to its successful performance. A short stroke ram is the only moving part. Dual seals with an in-between vent in the body assure no intermixing of fuel or hydraulic fluid because of seal leakage. The same dual seal is also employed on the diaphragm.

A filter is located in the hydraulic section which allows hydraulic fluid to pass through its core without filtration. RP-1 fuel allowable contamination content is greater than that allowed for the hydraulic system. Consequently all RP-1 entering the hydraulic system is filtered.

Between the low-pressure fuel port and the diaphragm is installed a fine mesh screen. Its function is to prevent particles, generated when the diaphragm ruptures, from entering the fuel system.

The diaphragm design is basically a V-groove cut 360 degrees in the interior wall end of cup design. The "shear" thickness of the V-groove is controlled dimensionally. This control consists of physical dimensions, surface finish condition and anodize thickness. The choice of 5059H16 aluminum material was primarily based on its excellent corrosion characteristics. All diaphragms are leak checked with helium. Lot test consists of 2 out of 10 units being subjected to rupture tests. The allowable rupture force is 5,782 N (1,300 lb) to 7,606 N (1,710 lb).

The original diaphragm rupture force tolerance requirements were not met. This was anticipated and our design concept allowed us to open the tolerance in either direction. One lot of diaphragms failed rupture tolerance limits. This was baffling since all machining tolerances were satisfied. A metallurgical analysis of the V-groove revealed differences between thin coat anodize thicknesses of the failed and acceptable lots. This was a surprise as it was assumed that the anodized strength capability was insignificant. As a consequence, anodized thickness was subsequently controlled.

Diaphragm seal and structural integrity loss by accidental or unrecognized means was addressed during the design review phase. The problem was not so much a gross diaphragm rupture, but rather detection of a small leak. A gross rupture by pressure was remote as it would require approximately 115.6 atm (1,700 psid) to rupture the unit. Neither the low-pressure fuel or hydraulic return systems during factory or site checkout or in launch status are capable of such pressure magnitudes.

In order to detect a potential small leak, a port was designed into the low pressure fuel section to allow for leak inspection. With no fuel tanked, it was simple to open the port cap and inspect for hydraulic fluid. With fuel tanked, it was difficult to detect hydraulic fluid in fuel, since both fluids are hydrocarbons and red in color. This was resolved by using infrared spectrophotometer analysis to detect hydraulic oil in RP-1 fluid. Hydraulic oil has a viscosity improver compound and hydraulic fluid

is detectable as low as a half-percent in fuel. Fluid samples were taken on about 20 installed valves until sufficient confidence was gained to eliminate sample tests.

The ever-present potential of human error did occur at the component level. A technician failed to follow prescribed testing procedures and managed to burst a diaphragm. This has been the only adverse incident to date.

The restrictor check valve function is to minimize the back flow of RP-1 fluid in the event an external leak occurs in the return system upstream of the valve.

As installed in the system, the FHV valve is located as close to the hydraulic pumps as existing vehicle hardware would permit in order to reduce the amount and length of tubes connecting between the FHV valve and the pump. The low pressure RP-1 connection to the FHV valve is self bleeding with the vehicle erected in the vertical position.

### **FLIGHT EXPERIENCE**

The inflight performance of the hydraulic systems is monitored by low pressure (return) and high pressure transducers via telemetry. Any gross leak manifestation would be revealed by a pressure loss.

To date, 14 vehicles or 28 valves have been flown. All valves have activated properly and all hydraulic system functions were satisfactory. We have experienced no gross hydraulic system leaks during inflight operation.

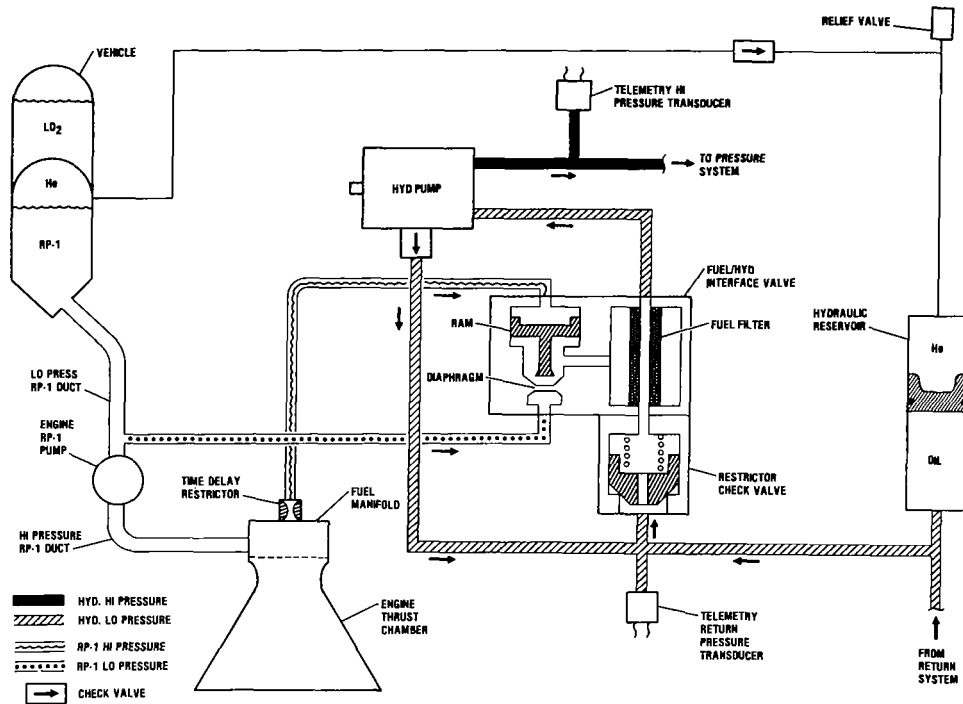


Figure 1.- System schematic with FHV valve.

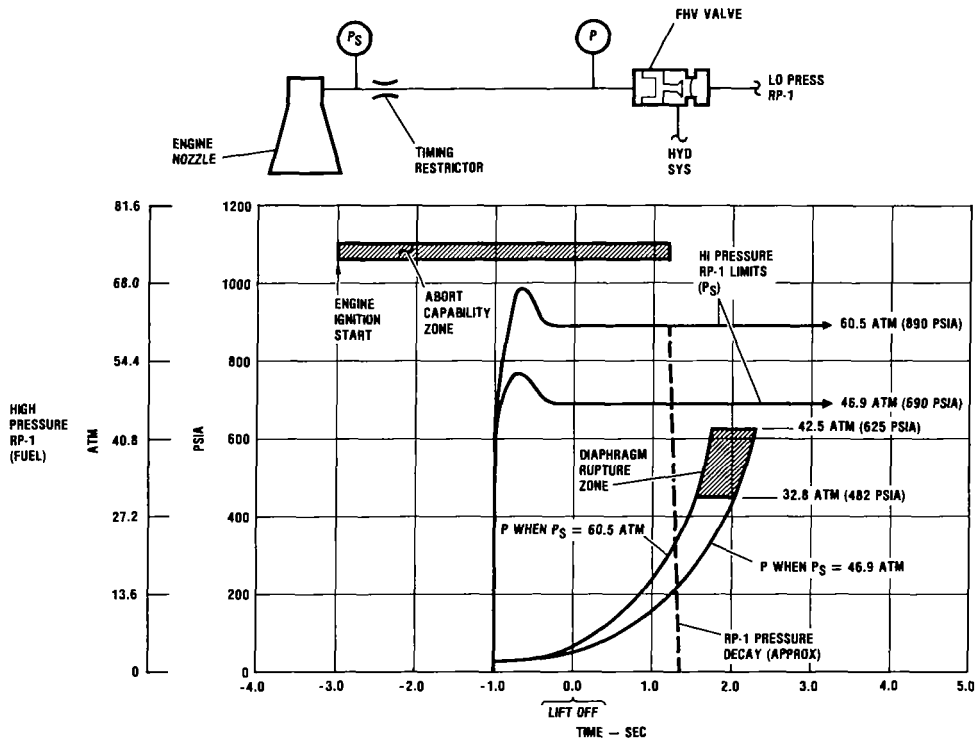


Figure 2.- FHV valve timing curve.

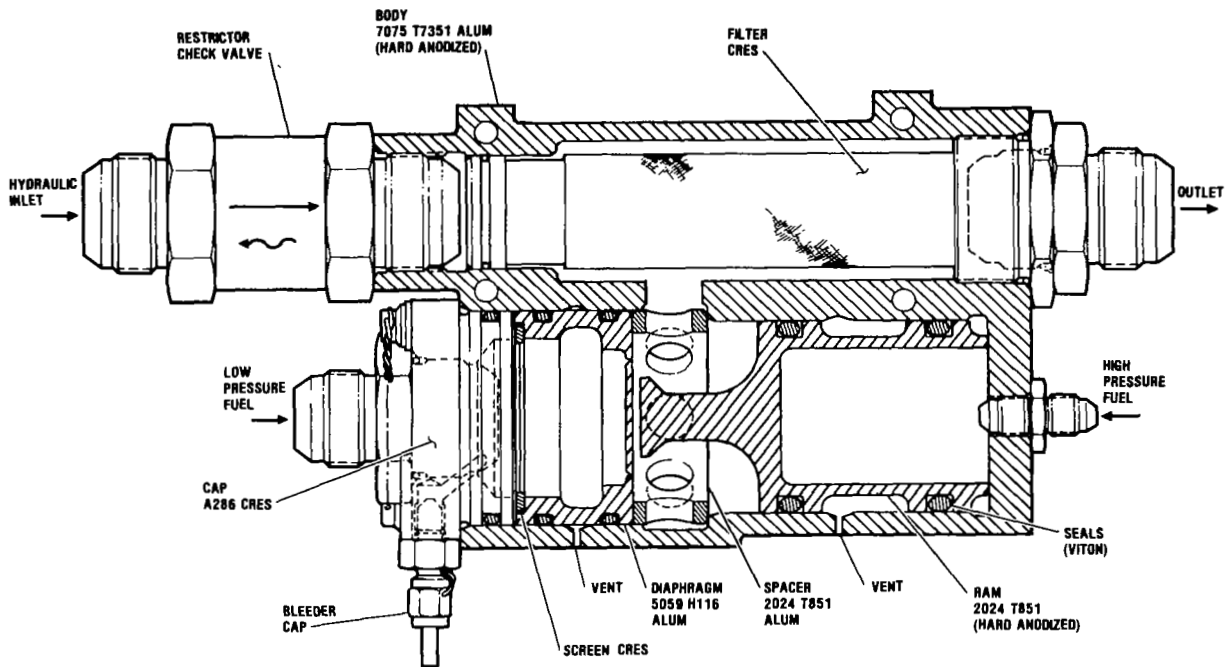


Figure 3.- FHV design details.



## KU BAND DEPLOYED ASSEMBLY AND GIMBAL\*

T. E. Deal  
Hughes Aircraft Company

### SUMMARY

Requirements for Shuttle Orbiter missions to locate satellites for servicing and to communicate when out of touch with a direct ground link are satisfied by a Ku Band deployed antenna system providing an integrated radar and communications function.

The deployed assembly comprises that portion of the system that stows in the limited space between the Shuttle door radiators and the payload volume for launch and landing, and is deployed out from the Shuttle during orbit to provide near spherical coverage by a 91.44 cm (36 inch) diameter antenna. Unique features of the gimbal assembly are:

- Edge mounted antenna to minimize stowage volume in Shuttle and maximize gain
- Unique two-axis housing and shaft arrangement to accommodate two runs of waveguide and 55 electrical conductors without requiring slip rings
- Maximum use of aluminum in gimbal structure to reduce costs
- Lubricant chosen to survive earth and space environments.

### BACKGROUND

Obtaining a good RF gain margin without using parametric amplifiers led to the selection of a 91.44 cm (36 inch) diameter antenna reflector for the Ku Band system. With this baseline antenna size, an edge mounted gimbal configuration was selected from a tradeoff study of the three configurations shown in Figure 1. The edge mount was the clear winner when weight, trunnion obscuration, peak power, and stowage considerations were compared. Disturbance torques due to Shuttle accelerations are negligible; therefore, a centered load is not an operational constraint. To test the antenna in a 1 g field, a counterbalance or offloading device would be required for any of the three configurations. This testing is simplified with the edge mount.

---

\* This task was performed under contract to Rockwell International, Space Systems Division.

ANGULAR COVERAGE. The angular coverage requirements call for maximum field of view for TDRS communication and unrestricted coverage of all points within 60 degrees of Shuttle zenith for radar rendezvous. Obscuration caused by the gimbal trunnion is minimized by locating the primary axis so that the obscuration cone falls within the Shuttle body area. The antenna is deployed as far from the Shuttle body and as high and far forward as possible to decrease overall obscuration presented by the Shuttle.

Ability to deploy the antenna is dependent upon the amount of volume available for stowage and the Shuttle hardware that the deployed assembly must clear. The allocated volume is in the forward part of the payload bay between the cabin bulkhead and the Remote Manipulator Boom. A 7.62 cm (3 inch) static clearance between the door radiators and the payload envelope is required. A full scale mockup, shown in Figure 2, was constructed to verify fit.

Ideally, the deployment hinge would be canted so that the antenna is swung up and out into an optimum location. However, stowage considerations and interference problems involving the boom and the integral Deployed Electronics Assembly (DEA) prevent the use of a canted hinge. With the vertical hinge, optimization with respect to angular coverage and obscuration was accomplished by canting the gimbal mount on the structure. A beneficial byproduct of the edge mounted antenna is that the location of the antenna beam center varies as a function of the line of sight. The antenna literally looks around the corner from the fixed gimbal axis intercept coordinate position, thus increasing total coverage. With the pole axis pointed outboard, more favorable coverage is attained and ample clearance between the antenna sweep volume and the vehicle is provided. Figure 3 shows the coverage achieved by the selected design.

DEPLOYMENT AND STRUCTURE. The deployed assembly shown in Figure 4 consists of a structural frame that attaches to the Rockwell hinge, together with the DEA and gimbal antenna assembly that attach to the frame.

Figure 5 shows details of the structural frame and the DEA mounting. Originally, a simple tubular boom to connect the gimbal to the hinge, with the DEA strapped alongside, was considered. However, it was difficult to keep the boom and box within the prescribed stowage envelope without resorting to a less than optimum boom diameter with undesirable sharp bends. The selected open frame configuration takes advantage of the structural properties of the 0.635 cm (one-fourth inch) thick thermal radiator that is part of the DEA.

ENVIRONMENTS. In addition to standard environments associated with space vehicles, the Ku Band Deployed Assembly (DA) must also be designed to withstand the unusual environment of multiple re-entry as well as aircraft type ground environments. Also, since the Shuttle is a manned space vehicle, the constraints on flammability and toxicity apply.

Materials and processes were carefully screened, therefore, to assure survival and continued operation. To avoid galvanic corrosion, sealing against humidity was required at each interface where steel screws contacted aluminum parts. Sliding closures were employed together with dessicant filled filter ports. Humidity tests were conducted to evaluate operational characteristics of bearing dry film lubricant.

Thermal environment carried one unique aspect. The location of the DA on the Shuttle places it just above and ahead of the Shuttle door radiators. These radiators are concave and covered with highly specular silvered teflon. In orbit, with the sun 30 degrees behind and 30 degrees to the right of Shuttle zenith, the DA is placed in the focus of fairly efficient collectors. Therefore, the DA is covered with silvered teflon which not only radiates heat from the DA itself, but also rejects the intense heat load from the Shuttle door radiators. Relief was granted by NASA to assure that this sun angle would not be maintained for a long period of time.

#### GIMBAL PACKAGE

The gimbal packaging arrangement is shown in Figure 6. The primary axis gimbal housing is fixed relative to the supporting structure, and its motor and bearing system rotates the inner T-shaped shaft through a full 360 degrees stop-to-stop. The secondary axis gimbal motor and bearing system rotates its housing, to which the antenna supports are attached, around the upper branch of the T shaft a minimum of 165 degrees stop-to-stop. Gimbal limits on this secondary axis are set simply by sizing the housing cutout which must clear the T shaft. For the primary axis, assuring the full 360 degree range without a blind spot at the end of travel required the incorporation of a toggle stop to allow a 1 degree minimum overlap.

Selection of the more conventional fixed housing rotating shaft configuration for the inner axis would involve the complexity of exiting the waveguide run between the axes and routing the waveguide to a juncture with the inner gimbal rotary joint. Further, the service cables that must cross the axes would have to make a similar exit and have their service loops mounted externally with several special guides, restraints, and supports to provide proper gimbal freedom. The T shaft configuration allows a much simpler waveguide, rotary joint, and cable packaging to be used by allowing the whole arrangement to move together across the axis junction. Internal cable breakouts are also avoided. Cabling which passes through the gimbal, shown in Figure 7, is a printed circuit flat ribbon that carries 55 conductors (20 shielded groupings) and two RG 178 coaxial leads. The T shaft configuration also allows a stiffer and simpler antenna attachment than would be achievable with widely separated shaft ends. Since the shaft ends are not exposed in this arrangement, the housing ends are closed off to provide environmental protection. The only open space through which contamination could enter is the area at the shaft juncture where the inner axis housing is cut away to allow gimbal freedom. In this area, a seal is provided around the bearings, and all other axis equipment is placed in enclosures beyond the bearings. The enclosures are equipped with dessicant filled filtered openings to allow the inflow of air to bypass the bearings during Shuttle descent and thus protect the overall cleanliness level of the mechanism interior.

Two precision angular contact bearings, lubricated by dry film lubricant, support the gimbal axes. One of the bearings in each set has the outer race mounted onto a diaphragm spring to provide axial compensation with temperature. This arrangement is a proven Hughes design used on several despin assemblies built for long life communications satellites. The spring mounted bearing is

located at the opposite end of the shaft from the rotary joint and encoder, precluding dimensional change of these critical gaps.

Bearing lubrication for this application has been selected from the standpoint of successful operation in a space mission over the temperature range and also from the standpoint of the ground environment to which the gimbals will be subjected. An evaluation test conducted in July 1977 showed that bearings ion plated with 1500 Å of 99 percent pure commercial grade lead provided the best and most uniform performance when tested between several cycles of humidity exposure.

The gimbal motors are 17.78 cm (7 inch) diameter, full rotation, permanent magnet brush dc motors. High torque motors are required to achieve the 400 degree/sec<sup>2</sup> accelerations associated with the radar search spiral scan. The incremental shaft angle encoders, 4096 counts per revolution together with an index pulse, use light emitting diode sources and photo transistor sensors. The basis for selection of these components is given in Table 1.

SERVO CONTROL. A Rate Sensor Assembly (RSA) containing two rate integrating gyros (RIGs) is mounted on the gimbal output. With the primary axis gyro mounted on the secondary axis output, this gyro measures the true line of sight rather than the primary axis gimbal rate. This causes a scale factor change as a function of secondary look angle that must be compensated for to achieve servo stability. Loop closure electronics for the two RIGs are located within the RSA package. This location minimizes noise in the high bandwidth loop that might be picked up on the 9.6 meter long cable between the electronics and the DA. The RSA package is also temperature controlled to assure stable operation.

A feature of the design worth noting is the absence of tachometers. By using the RIGs to provide rate damping signals, adequate servo performance can be achieved without the cost and weight penalty of tachometers.

Another prominent feature of the servo design is the coordinate conversion requirement. Since the trunnion axis is not aligned with the Shuttle X-axis, commanded designate angles are generated in Shuttle pitch and roll and must be transformed into gimbal coordinates for execution. Conversely, the gimbal angles and LOS rates must be transformed into Shuttle pitch and roll equivalents for astronaut readout. It is also necessary to transform slew commands, since a nominal pitch slew actually requires the combined motion of both gimbal axes. The coordinate conversions are performed by the control logic microprocessor, thus eliminating the need for bulky resolver chains.

GIMBAL LOCK SYSTEM. Multiple launch and re-entry use of the DA calls for a reuseable gimbal lock system. The system consists of two DC gearhead servo motors mounted on the stationary housing of the primary axis that rotate V wedges into blocks located under the two structural members extending below the secondary axis housing. This configuration is shown in Figure 8.

A single motor-driven lock was originally planned; however, attempting to lock both axes at a single point was not workable. The restricted volume around the gimbal due to the antenna size and angular coverage requirements did not allow a pinning or grasping type of lock.

#### CONCLUSION

The Shuttle DA gimbal hardware was selected from proven technology, packaged to accommodate Shuttle stowage and use. Other mechanisms with the assembly--an RF polarization switch and waveguide switch--were also designed to use state of the art components.

**TABLE 1. Ku BAND ANTENNA POSITIONER**

Item	Options	Advantages	Disadvantages
Axis location	Edge mount*	<ul style="list-style-type: none"> <li>● Lighter weight</li> <li>● Better stowage fit</li> <li>● Better deployed pole location</li> <li>● Lowest cost</li> <li>● Lowest trunnion obscuration</li> </ul>	<ul style="list-style-type: none"> <li>● Unbalance in 1 g field</li> <li>● Load inertia variation</li> </ul>
	Yoke mount	<ul style="list-style-type: none"> <li>● Less 1 g unbalance</li> <li>● More conventional approach</li> </ul>	<ul style="list-style-type: none"> <li>● Complex structure</li> <li>● Difficult stowage</li> <li>● Higher system weight</li> <li>● Higher cost</li> </ul>
Motor type	DC brush torquer*	<ul style="list-style-type: none"> <li>● Simpler electronics</li> <li>● Well proven</li> <li>● Self commutating</li> </ul>	<ul style="list-style-type: none"> <li>● Brush friction</li> <li>● Ripple torques</li> </ul>
	DC brushless torquer	<ul style="list-style-type: none"> <li>● Less friction than dc brush torquer</li> </ul>	<ul style="list-style-type: none"> <li>● Requires resolver</li> </ul>
	Stepper motor	<ul style="list-style-type: none"> <li>● Lowest power</li> <li>● Lightest weight</li> </ul>	<ul style="list-style-type: none"> <li>● Speed limitation in raster</li> <li>● Gear train wear</li> <li>● Stepping dynamics in track</li> </ul>
Position readout	Resolver	<ul style="list-style-type: none"> <li>● Absolute position indication</li> <li>● Long life elements</li> </ul>	<ul style="list-style-type: none"> <li>● Complex electronics</li> <li>● &gt;360° ambiguity</li> <li>● Complex wiring</li> </ul>
	Incremental encoder*	<ul style="list-style-type: none"> <li>● Digital output compatibility</li> <li>● No &gt;360° ambiguity</li> <li>● Small cable bundle</li> </ul>	<ul style="list-style-type: none"> <li>● LED degradation</li> <li>● Requires initial setting</li> </ul>
	Absolute encoder	<ul style="list-style-type: none"> <li>● Interrogation capability reduces LED use</li> </ul>	<ul style="list-style-type: none"> <li>● Multiple parallel bits requires large wire bundle</li> <li>● &gt;360° ambiguity</li> </ul>
Rate feedback	Separate tachometer	<ul style="list-style-type: none"> <li>● Conventional</li> </ul>	<ul style="list-style-type: none"> <li>● Additional component</li> <li>● Additional cabling</li> </ul>
	Use position readout rate of change*	<ul style="list-style-type: none"> <li>● Eliminates component</li> </ul>	<ul style="list-style-type: none"> <li>● None</li> </ul>

\*Selected design

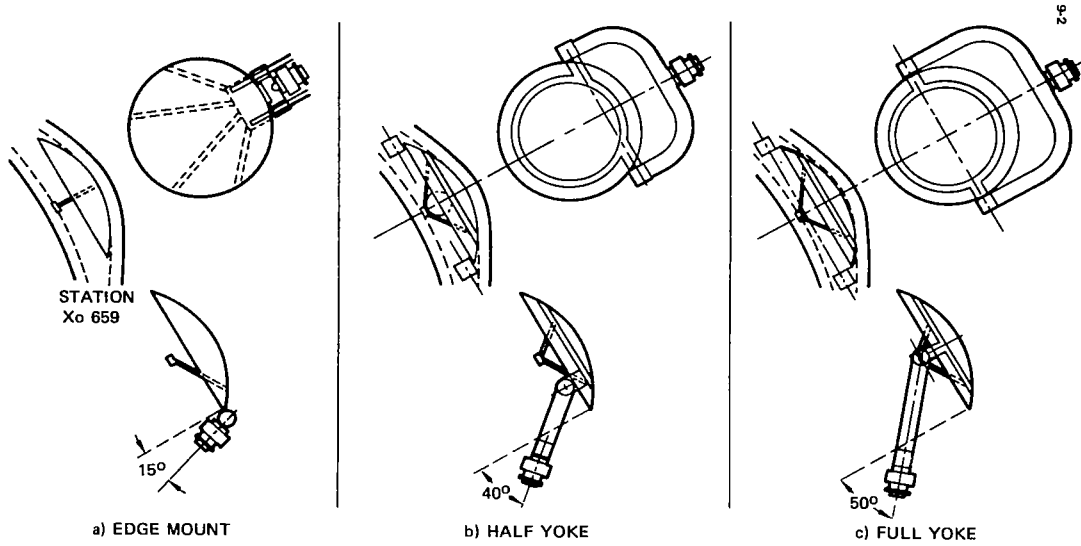


Figure 1.- Gimbal configurations considered, showing trunnion half-angle obscuration.

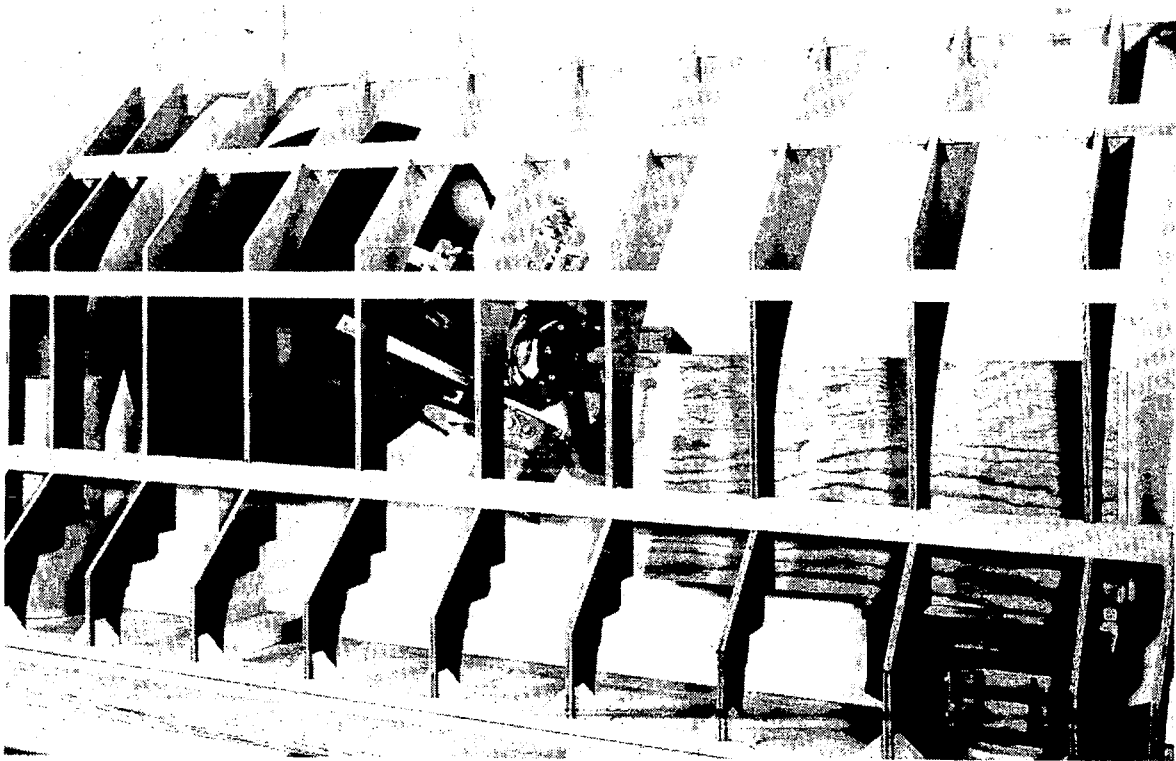


Figure 2.- Deployed assembly mockup.

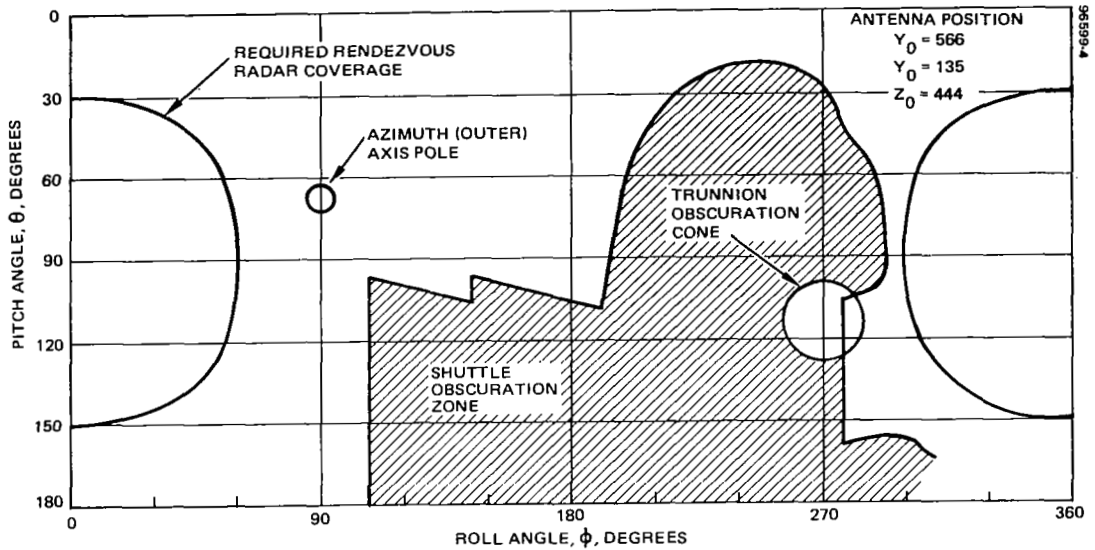


Figure 3.- Right antenna obscuration and gimbal characteristics based on 91.44 cm (36 inch) diameter antenna beam.

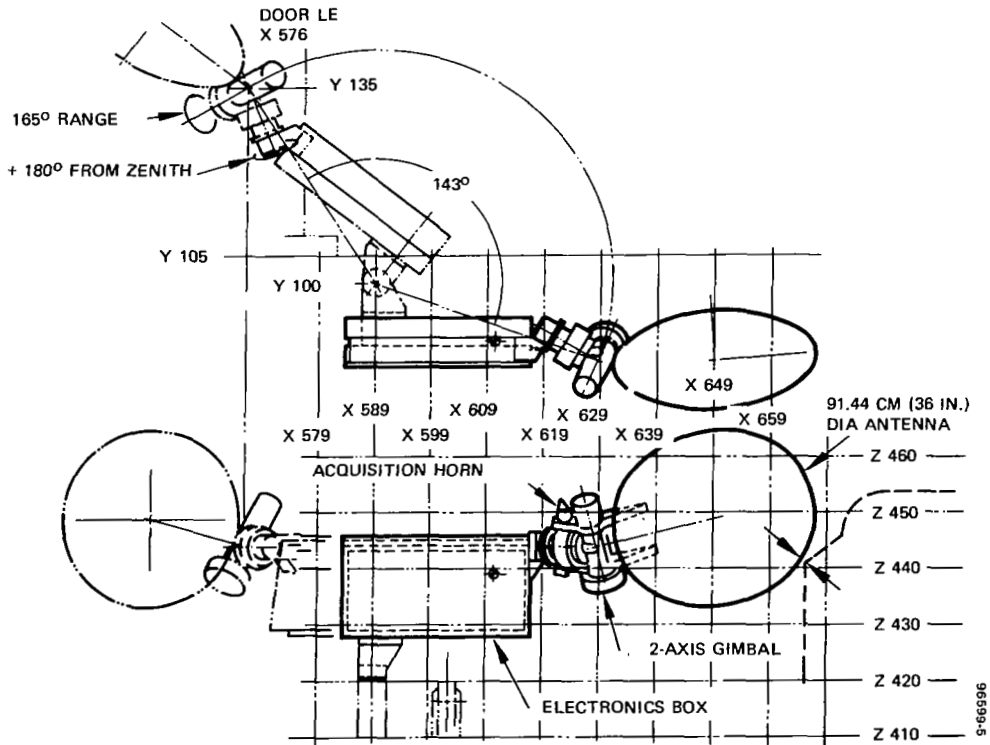


Figure 4.- Deployed mechanism assembly.

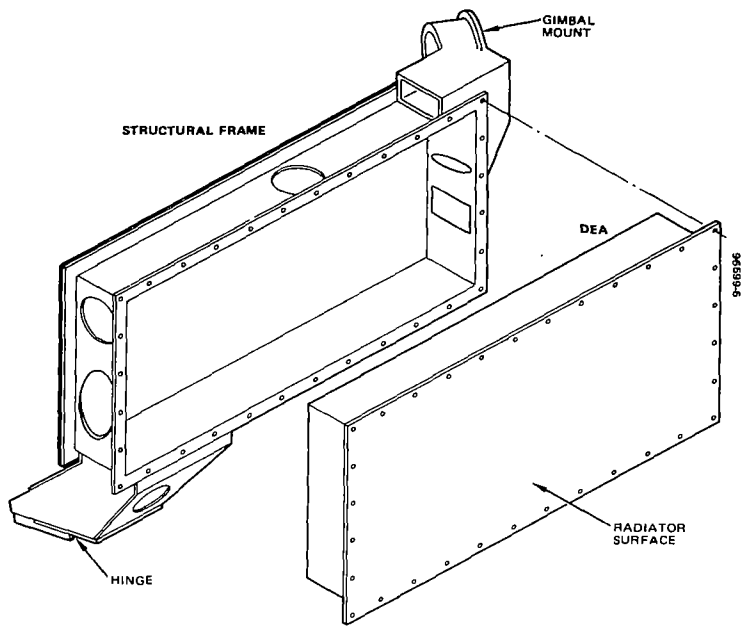


Figure 5.- Structural frame and DEA mounting.

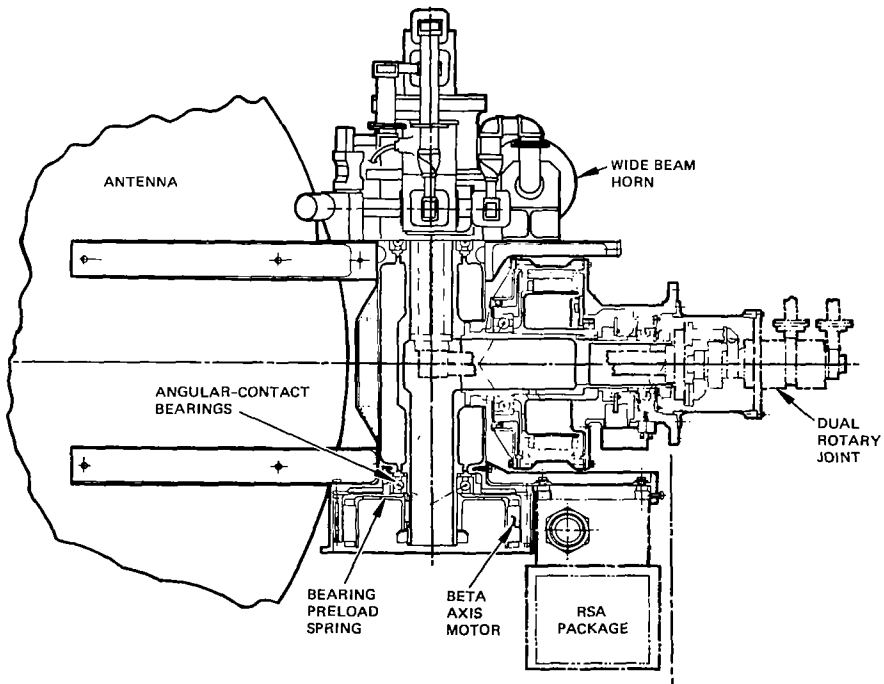


Figure 6.- Antenna gimbal.

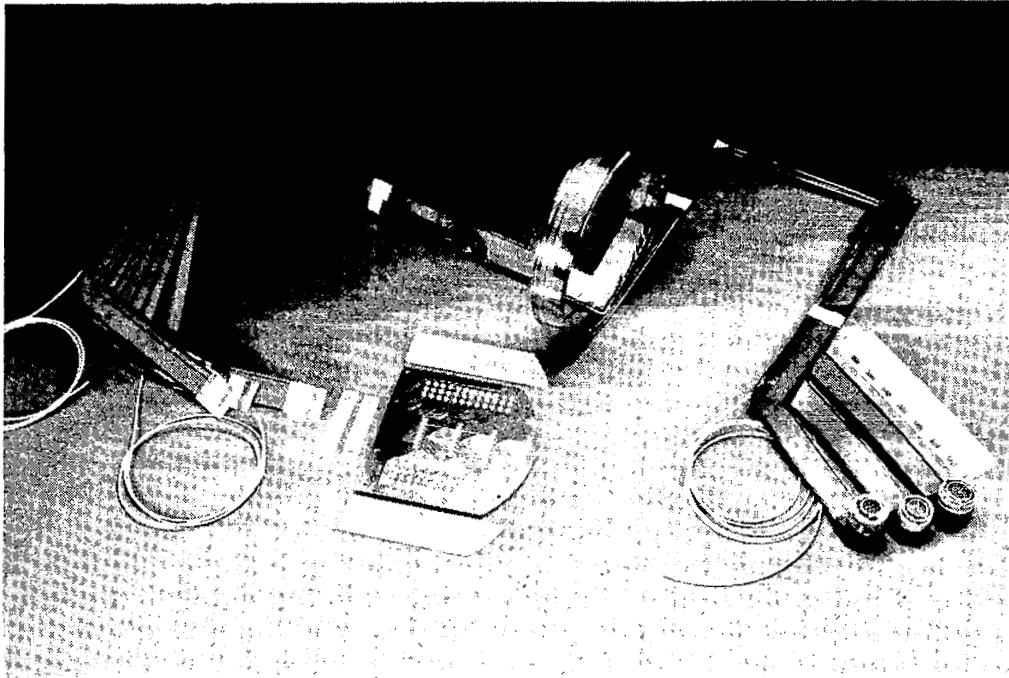


Figure 7.- Flat ribbon cable.

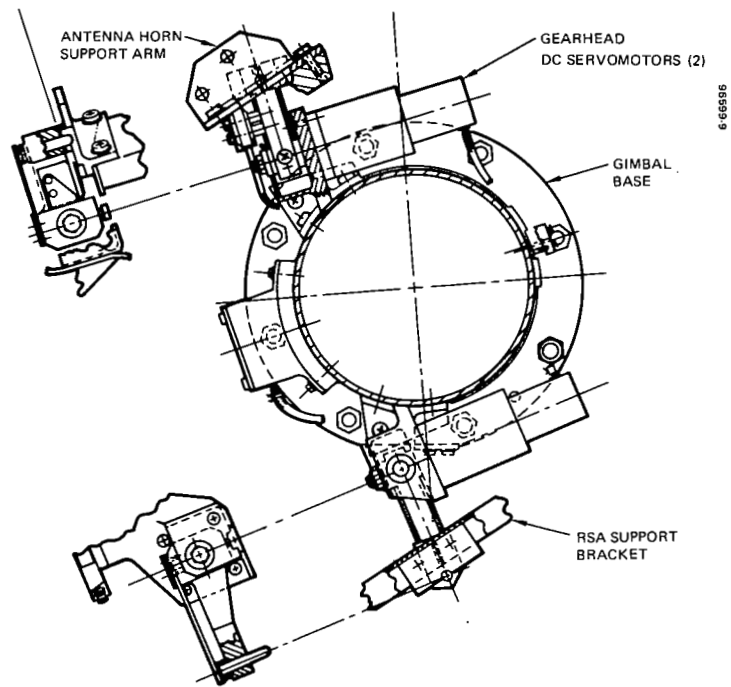


Figure 8.- Dual gimbal lock.

## EMERGENCY IN-FLIGHT EGRESS OPENING FOR GENERAL AVIATION AIRCRAFT

Laurence J. Bement  
NASA Langley Research Center

### SUMMARY

In support of a stall/spin research program at the National Aeronautics and Space Administration (NASA), Langley Research Center (LaRC), an emergency in-flight egress system is being installed in a light general aviation airplane. The airplane has no provision for egress on the left side. A left-side egress opening would greatly enhance the pilot's ability for bailout, particularly in a right spin. To avoid a major structural redesign for a mechanical door, an add-on 11.2-kg (24.6-lb) pyrotechnic-actuated system was developed to create an opening in the existing structure. The skin of the airplane will be explosively severed around the side window, across a central stringer, and down to the floor, creating an opening of approximately 76 by 76 cm (30 by 30 in.). The severed panel will be jettisoned at an initial velocity of approximately 13.7 m/sec (45 ft/sec). System development included a total of 68 explosive severance tests on aluminum material using small samples, small and full-scale flat-panel aircraft structural mock-ups, and an actual aircraft fuselage. These tests proved explosive sizing/severance margins, explosive initiation, explosive product containment, and system dynamics. This technology is applicable to any aircraft of similar construction.

### INTRODUCTION

Airplanes, upon stalling, may begin a rotating, sinking motion called a spin. Stall/spin is a prime causal factor in fatal general aviation accidents. Several light airplanes are being spin tested at NASA-LaRC in an effort to improve the stall/spin characteristics of this class of airplanes. These airplanes are equipped with tail-mounted spin recovery parachute systems in the event that the spinning cannot be stopped by the normal airplane controls. If both the airplane controls and the recovery parachute fail to stop the spin, the pilot would have to abandon the airplane. One airplane currently being readied for spin testing has a single door on the right side with no option for egress on the left side. Bailout would require the pilot to move across the aircraft to open the existing door, possibly against centrifugal loads; this is a difficult task at best. A left-side egress opening would minimize the pilot's bailout effort and time.

A pyrotechnic-actuated egress opening was developed because it proved to be more advantageous than a mechanical system on the basis of structural modification, performance, and the potential for success. A mechanical system would require considerable structural modification and reanalysis to incorporate a door and release mechanisms. A pyrotechnic approach would be an add-on system, based on previous experience gained in the F-111 and B-1 escape modules.

The pyrotechnic system developed in this effort uses a small-quantity, fully contained, explosive-shaped charge to sever and jettison a left-side panel from the airplane. The system is initiated mechanically by a bell crank pulled by the pilot. From that point, the system functions automatically. The design and development capitalized on existing pyrotechnic technology, materials, and components, and emphasized proving all aspects of functional performance. This proof of performance was accomplished analytically and functionally to show margins of capability greater than the force, strength, or energy required.

This paper describes the design, development, and functional testing of the pyrotechnic-actuated emergency in-flight egress opening for a NASA-LaRC general aviation research airplane.

## APPARATUS

This section describes the off-the-shelf components that were qualified under previous aerospace programs and the test fixtures used in this program.

### Flexible Linear-Shaped Charge (FLSC)

FLSC has been widely applied by the aerospace community in such applications as rocket vehicle staging and aircraft escape systems. Figure 1 shows a transverse cross section of FLSC. The materials used in this application are hexanitrostilbene II (organic-precipitated HNS II) explosive (3.19 g/m (15 grains/ft)) in a silver sheath. This explosive can only be initiated by a high explosive input (greater than  $5.5 \times 10^9$  N/m<sup>2</sup> (800 000 psi)); it cannot be initiated by gunfire, lightning, electromagnetic-induced radiation, or physical handling. It will burn in a fire, but cannot achieve its cutting function. On initiation, the material detonates at a linear velocity of 7250 m/sec (23 800 ft/sec), generating  $2.0 \times 10^{10}$  N/m<sup>2</sup> ( $3 \times 10^6$  psi). The expanding gases and sheath materials are focused in the chevron to effect a metal penetration and deformation/breaking action.

### FLSC Booster Tips

To assure reliable initiation of the FLSC and to seal the exposed explosive at the ends of the six lengths of FLSC, booster tips were installed. These tips are cups (4.83 mm (0.190 in.) i.d., 8.89 mm (0.35 in.) height) stamped from 0.15-mm (0.006-in.) 302 stainless steel (condition A) and loaded with hexanitrostilbene I (HNS I) at  $2.20 \times 10^8$  N/m<sup>2</sup> (32 000 psi) to a height of 3.81 mm (0.150 in.). The cups were potted on the ends of the FLSC with a non-solvent structural adhesive (Scotch-Weld Brand Structural Adhesive 2216 B/A<sup>1</sup>).

---

<sup>1</sup>Product of 3M Company.

## Lanyard-Actuated Detonator

The detonator used to initiate the FLSC is shown in figure 2. A 1.27-cm (0.5-in.) stroke compresses the linear spring to 89 N (20 lbf) resistance at release of the sear. The firing pin assembly is driven into the percussion primer to initiate the lead azide/HNS I explosive materials in the output cup. The lead azide provides an interface to develop the initiation flame to a detonation within a 2.54-mm (0.1-in.) column to properly initiate the HNS I, which in turn initiates an FLSC booster tip.

## Manifolds

To properly locate, secure, and protect the FLSC booster tips, four 6061-T6 aluminum manifolds were attached to the skin and aircraft structures, one above and below the central stringer at the forward and aft extremities of the egress area. The aft manifolds contained a close-tolerance groove to secure the tips. However, the forward manifolds contained not only a groove but also a threaded port to receive the lanyard-actuated detonators at the correct relative position to the tips (minimum gaps of 0.50 mm (0.020 in.)) to assure reliable explosive initiation.

## Internal Containment Development Fixture

To develop the internal structure required to contain the explosive blast of the FLSC, a test fixture was developed that would demonstrate performance margins. The fixture was an exact mock-up of a typical aircraft structure, but to demonstrate a containment margin, the explosive load was increased to 150 percent of the required amount and the mock-up of the aircraft skin thickness was increased to prevent any severance and venting of the explosive pressure. Further, the internal free volume within the containment structure, as well as the clearances of the FLSC to the structure, were reduced to the minimums expected in the aircraft.

## Small-Panel Test Fixture

Wood-framed panels, measuring 45.7 by 45.7 cm (18 by 18 in.) were used as mock-ups of aircraft-representative structures for explosive severance tests. The mock-up skin was attached to the frame, and the representative full-scale structural elements, with explosive components, were mounted to the skin.

Full-scale, flat-panel test fixtures.- Two full-scale, light-airplane structures were mocked-up in wood-framed, flat-panels to evaluate the egress system performance. All materials (Alclad 2024-T4), material thicknesses (1.02 mm (0.04 in.)), and structural layouts, including a 3.175-mm (0.125-in.) thick plexiglass window, were mocked-up. A 3.8-cm (1.5-in.) square-mesh stainless wire (0.5 mm (0.020 in.) thick) was used on the second test to prevent the plexiglass from moving internally. A complete assembly, except for the initiation system, was tested.

Aircraft fuselage test fixture.- A center section of a typical airplane fuselage was modified to simulate the end application research-airplane structure as closely as possible, as shown in figure 3.

The research-airplane structure is fabricated from 1.02-mm (0.04-in.) Alclad 2024-T4 aluminum. The fuselage skin panels are made up of flat stock, overlapping above and below the window and just above the floor at the stringers. The depth of the formed channel frames, stringers, and ribs is 3.8 cm (1.5 in.). The frames are made up of flat stock mounted on the ribs in the central fuselage area. The 0.317-cm (0.125-in.) thick plexiglass window has an aperture of approximately 38.1 by 76.2 cm (15 by 30 in.). The major difference in the simulation was in the depth of frames, stringers, and ribs. The research-airplane depth is 3.81 cm (1.5 in.) and the test-fuselage depth was 6.35 cm (2.5 in.).

Final aircraft-designed containment, as well as the wire mesh of the window and initiation-system hardware, was used. The explosive severance was initiated by dropping a weight to actuate the control handle through a cable/pulley system.

A plexiglass witness panel was mounted inboard of the internal containment system at a distance of 21.6 cm (8.5 in.) from the mid-waterline (center stringer) of the egress opening. Dynamic pressure was monitored by two transducers mounted on the plexiglass panel in the proximity of the expected location of the pilot's head in the experimental airplane. One transducer was mounted 5.1 cm (2.0 in.) aft of the forward internal containment, and the other was 20.3 cm (8.0 in.) aft. High-speed cameras (400 and 4000 pps) filmed the system operation and dynamics from the front, side, and rear.

#### PROCEDURE

The description of the development of the egress system can be logically broken into six phases: system selection/development considerations; materials selection/system qualification; initiation-system development; explosive severance and containment development; full-scale, flat-panel tests; and aircraft fuselage mock-up test.

#### System Selection/Development Considerations

A mechanical or pyrotechnic system could provide the required egress opening. The selection and development of this emergency in-flight egress system were based on the following:

1. Minimizing structural impact to the aircraft
2. Minimizing pilot effort and response time to actuate
3. Minimizing system weight
4. Maximizing egress opening area

5. Minimizing pilot egress interference
6. Providing jettisoning force of egress panel
7. Providing passive, low-maintenance system
8. Providing maximum system reliability

#### Materials Selection/System Qualification

The pyrotechnic materials and techniques used in this egress system were selected on the basis of previous aerospace design experience and previously qualified components and systems.

#### Initiation-System Development

The initiation subsystem was designed and developed with safety considerations paramount. The selection and development of the initiation system were based on the following characteristics:

1. Independent system, isolated from onboard systems
2. Manageable actuation force
3. Fully secure in flight
4. Additional safetying measures on the ground
5. Positive "stops" to assure that the actuation is complete
6. Accessibility and reliability

The complete initiation subsystem actuator (no detonators) was mounted on a flat-plate breadboard to evaluate the actuation forces required to overcome internal static and kinetic friction. The 89-N (20-lbf) maximum resistive force of the lanyard-actuated detonator was applied to the cable, and the pull forces necessary to overcome friction were measured.

#### Explosive Severance and Containment Development

The development of the explosive severance technology progressed through several phases:

1. Size the flexible linear-shaped charge and determine severance performance margins under worst-case conditions (a double thickness of aluminum and increasing the thickness beyond the expected limits). Also, determine the cutting performance of the FLSC and booster-cup combination inside the manifolds. Past experience indicated that any foreign material such as potting in the

chevron area of the FLSC destroys the cutting efficiency. Tests were conducted on double-thickness plates (1.016 on 1.016 mm (0.040 on 0.040 in.)).

2. Develop an external containment system to contain the explosive products outside the fuselage and provide a jettisoning force to the severed panel. A demonstration of the development was made by using small-panel test fixtures.

3. Develop a method of severing the central stringer in the egress area. Again, small-panel test fixtures were used to demonstrate the local-area performance.

4. Develop a method of containing the explosive products inside the fuselage, assuring a performance margin. By using the internal containment development fixture described in the Apparatus section, containment tests were conducted under worst-case conditions of:

a. 150 percent of the required explosive load was used, 3.19 g/m (15 grains/ft) RDX (cyclotrimethylenetrinitramine) instead of 2.13 g/m (10 grains/ft)

b. No explosive pressure venting

c. Minimum volumes

d. Filling the volume with closed-cell, flexible foam (used to preclude contamination of the containment volume)

e. Proximity of the FLSC to the aircraft and containment structure

#### Full-Scale, Flat-Panel Tests

To develop an understanding of system-level performance, tests were conducted on the full-scale, flat-panel test mock-ups described in the Apparatus section. Performance parameters to be evaluated were complete severance, neatness/uniformity of severed edges, effect on aircraft structure during severance, capability of the containment structure (particularly at the stringer) to stop explosive products internally, jettison velocities and dynamics of the severed panel, and capability of the window mesh to prevent internal entry of the plexiglass window fragments on panel jettison.

#### Aircraft Fuselage Mock-up Test

To demonstrate the final system design, a full-scale aircraft fuselage mock-up test was conducted. This test included actuating the mechanical initiation subsystem with both detonators installed, the final design of the containment system (particularly at the stringers) with closed-cell foam to prevent volume contamination, and the 3.8-cm (1.5-in.) protective wire mesh on the inside of the window to prevent the plexiglass from moving internally. Internal explosive debris and pressure were monitored with a plexiglass panel across the entire egress area.

## RESULTS

### System Selection/Development Considerations

Two candidate egress systems could meet the considerations outlined in the Procedure section - mechanical and pyrotechnic.

The mechanical system approach would require a large structural modification and design effort to incorporate a door frame and door. This would be followed by a release system, such as pulling hinge pins and actuating the latches, which could require considerable pilot effort and time. The released door may then require (according to flight conditions) manual and aerodynamic jettison. Finally, a considerable effort may be required to validate the structural design of the modified aircraft under the high-stress, spin-pullout conditions.

The pyrotechnic system approach would use a flexible linear-shaped charge (FLSC) to sever the existing skin and structure, following proven principles, applications, and materials. A minimal aircraft modification could be expected, that is, attaching the explosive and containment to the existing structure. A pyrotechnic system would require little effort to initiate and, as a completely independent energy source, would produce a highly responsive severance and jettisoning capability. Since the expected structural changes would be minimal, no new load paths or structural analysis would be expected or necessary. Based on these considerations, the pyrotechnic system was selected for development.

### Materials Selection/System Qualification

The flexible linear-shaped charge (FLSC) has been applied to several aerospace systems, including the F-111 (ref. 1) and the B-1 aircraft, in which the cockpit is severed from the fuselage. The FLSC materials, organic-precipitated hexanitrostilbene (HNS II) in a silver sheath, were developed specifically for thermal and age stability (ref. 2); applications include the F-14, F-16, and AH-1G (Cobra) aircraft. The booster tip materials, HNS I in a steel cup, are applied almost universally to aircraft explosive transfer systems. The lanyard-actuated detonator was qualified for the F-14, F-15, and the Space Shuttle Orbiter. The capability of the FLSC to withstand severe environments is demonstrated by its many applications. The functional qualification was based on component and system development, emphasizing performance margins described in subsequent sections.

### Initiation-System Development

The initiation system developed in this effort is shown in figure 4. A 40° rotational stroke of the handle assembly (9.9 cm (3.9 in.)) produces 4.95 cm (1.95 in.) pulley rotation and cable withdrawals. The cables thread through guide tubes to provide 90° redirected pulls on the lanyards of the detonators. Since a 1.27-cm (0.5-in.) stroke is required to actuate the detonator, a margin of at least 3 to 1 exists. Each cable is fitted with a

clevis fork to adapt to the detonator and a ball which is captured by a plate on the pulley. The cable lengths were adjusted to prevent simultaneous engagement/actuation of the detonators, which would result in twice the load.

Safety features were incorporated in the system to prevent inadvertent system actuation on the ground and in flight. The handle and pulley assembly is secured to the mounting plate by a ball-release bayonet safety pin for ground safety. An aluminum shear pin, again securing the handle and pulley assembly to the mounting plate, prevents inadvertent actuation without the safety pin for flight. Furthermore, the left-side cover posts (fig. 4) act as motion stops; the upper-post stop prevents forward motion of the handle, and the lower post provides a stop to assure that full actuation has occurred. A cover plate protects the entire pulley assembly and cable/tube ends. The entire assembly is mounted on the forward frame beside the pilot, just aft of the instrument console. The handle is positioned just above the lower extremity and 2.54 cm (1.0 in.) aft of the instrument panel.

The initiation-system breadboard revealed that the 3.175-mm (0.125-in.) diameter, pure-aluminum shear pin sheared at 137.9 N (31 lbf). Furthermore, the static friction of either cable (preloaded to 89 N (20 lbf)) required only 93 N (21 lbf) at the handle. Actual friction loads will be much less in the system, since an 89-N (20-lbf) load will occur only at maximum stroke of the detonator, which occurs dynamically.

#### Explosive Severance and Containment Development

The 68 explosive tests are briefly outlined in table I to establish the explosive severance and containment approaches and performance margins. The results of the explosive sizing and performance comparisons are shown in table II. In determining the ability to sever double-skin thicknesses, the FLSC, composed of 2.125 g/m (10 grains/ft) RDX (cyclotrimethylenetrinitramine), could sever/break the 1.016- on 1.60-mm (0.040- on 0.063-in.) aluminum, which provides a performance margin of 58 percent. Furthermore, a 131-percent margin is achieved by using an HNS II FLSC of 3.188 g/m (15 grains/ft) instead of the 2.125 g/m RDX, resulting in an overall performance margin approaching 100 percent.

In evaluating the performance of the booster tip/FLSC combination under manifolds, it was determined that the increased quantity of explosive (due to the tips) easily ruptured a single skin thickness and, with minimal potting, could rupture two skin thicknesses. An already initiated tear would progress through the relatively short lengths where FLSC penetration did not occur.

The effectiveness of the external containment approach in the small-panel tests is shown in figures 5 and 6. The no-containment test (fig. 5) produced ragged edges (large deflections) on both the severed panel and the aircraft skin mock-up. The containment test (fig. 6) produced smooth, neat edges on both the panel and the aircraft skin. Although the containment-test panel weighed nearly three times as much, no loss in jettison velocity occurred compared with the no-containment test. The external containment is a 1.60-mm

(0.063-in.) thick cold-rolled steel coverplate (3.81 cm (1.50 in.) wide, as required), separated from the skin by a 3.15-mm (0.125-in.) aluminum-plate standoff. The bent-down portion closes the cavity and smooths the surface, reducing aerodynamic drag. The cavity between the steel and the skin was necessary to assure adequate deflection of a double-thickness skin to allow reliable severance/fracture. A 1.60-mm (0.063-in.) cavity allowed only partial severance. The final design of the external containment is shown in figure 7 on the aircraft fuselage mock-up of the egress system.

To reliably sever the central stringer, two lengths of explosive were used. One length was laid along the skin, through a hole in the stringer (inside the bend radius of the channel), and across the leg of the channel; the other length was laid around the stringer and matched into common booster tips at each end. This arrangement introduced two problems: determining the reliability of severing the double-thickness material (stringer and skin) with the larger standoff to avoid the stringer radius, and determining how to manage the structural damage and deformation caused by the doubled quantity of explosive. Several tests with larger standoffs than required indicated sufficient energy existed to sever and tear the material with an adequate margin. The doubled quantity of explosive required doubling the structural attachment bolts (2.54-cm (1.0-in.) centers) and using steel internal containment structure on the severed panel.

The internal containment structure to protect the pilot from explosive products is shown in figure 8. The cross-sectional lines indicate the locations of subsequent structural views.

The principles of the internal explosive containment are shown in figure 9 (section A-A). The skin is severed by the explosive, causing the structure to the right to be jettisoned downward with the panel. The explosive products are contained within the free volume formed by the stringer, the angle to the right, and the cover channel. A cover channel is used to prevent a left rotation of the cover plate and stringer due to the explosive pressure. The two cover plates above the channel stiffen the channel and cover the gaps at the cover-channel interfaces. The reinforcement angle prevents shearing damage from the close proximity of the explosive. The closed-cell foam (95-percent air) prevents contamination of the free volume. If this volume were filled with water (no foam), considerable deformation of the containment structure could occur, possibly causing pilot injury.

The same approach as described above is shown in figure 10 (section B-B), except a cover angle attached to the aircraft ribs is used to prevent rotation rather than a channel. The cover angle is curved to match the aircraft contour. The severed/jettisoned portion of the structure is below the stringer.

Figure 11 (section C-C) and figure 8 show the complicated welded stainless-steel containment structure used at the forward and aft sections of the central stringer. The structure attaches to the frames above and below the stringer. In order to maintain an internal free volume to dissipate the explosive energy of the flexible linear-shaped charge around the stringer, the structure had to project inboard into the cockpit. Also, this structure had to accommodate the post-assembly installation of the detonators and initiation-cable guide tubes.

An approach similar to section B-B is shown in figure 12 (section D-D), except that the cover angle is attached to the frame. Furthermore, there is no need for a reinforcement angle; the explosive was not mounted against the frame.

### Full-Scale, Flat-Panel Tests

The full-scale, flat-panel tests confirmed a number of system principles as well as detecting system problem areas. The explosively severed edges of the skin and jettisoned panel were smooth and uniform. The dynamics of the severed panels were uniform and predictable. The panel was smoothly released and pitched horizontally; the base of the panel swung upward in the direction of motion. However, the external containment structure and skin detached from the panel in the areas beneath the doubled FLSC around the central stringer, allowing explosive gaseous products to enter the fuselage.

The gases, created on detonation of the explosive, sharply load the entire area within the internal explosive containment, causing the skin to deflect between the bolt attachments to exhaust the gases. These gases are highly visible as flame and smoke. The flame is a secondary burning of the unreacted carbon on mixing with the air. The flame duration in both tests was approximately 21 msec, an unlikely ignition source of even the most reactive materials.

The manifold attachments and the plexiglass window retention were inadequate on the first test and were corrected on the second test. The manifolds (attached only through the skin) pulled loose; attachments through the frame prevented detachment. The window broke up due to panel/frame oilcanning, tossing several pieces inboard. A 3.8- by 3.8-cm (1.5- by 1.5-in.) wire mesh was stretched across the window and attached to the internal containment structure to eliminate internal debris.

The jettison capabilities demonstrated in the flat-panel tests (small and full scale) are summarized in table III. Although the system weight increased, the amount of energy delivered per unit weight was consistent.

### Aircraft Mock-up Test

Figures 13 and 14 show the neat, predictable, severed edges of the skin and the frame around the opening created by the internal containment. No internal debris was detected by the witness panel or high-speed camera coverage (4000 pps). The internal pressures measured were  $34.5 \text{ kN/m}^2$  (5 psi) and  $17.7 \text{ kN/m}^2$  (2.5 psi) with a duration of less than 1.0 msec. These pressure levels compare favorably with measurements made on the British aircraft Jet Provost Mk.5, which employs an explosive cord-actuated overhead-canopy severance system. Measurements at the chest level of dummies indicated pressures of 50.3 to 117  $\text{kN/m}^2$  (7.3 to 17 psi). However, pressure levels at the dummy ears (inside the helmet) were approximately  $26.2 \text{ kN/m}^2$  (3.8 psi).

The flame duration and jettison velocity were considerably improved by the room temperature-vulcanizing (RTV) compound application on the external containment. The actual duration of the flame was less than 5 msec. The

improvement of the containment prevented carbon particle and air mixing and burning. Furthermore, the jettison velocity (table III) increased 28 percent due to the improved sealing of the explosive-gas pressure wave. The severed panel weighed 6.62 kg (14.6 lb) and achieved a velocity of 13.7 m/sec (45 ft/sec).

The severed panel was completely intact, except for the window, following the test (figs. 15 and 16). The wire mesh prevented any window fragments from entering the fuselage. The frame created by the external containment was smooth and uniform, and the skin was securely attached in all areas.

### CONCLUSIONS

A pyrotechnic-actuated, in-flight egress opening has been developed and qualified for use in a light, general aviation research airplane. This system will allow the pilot to bail out from the left side of the airplane.

The egress system is simple and highly responsive, requiring minimal airplane modifications to incorporate. A complete, full-scale aircraft fuselage mock-up demonstrated the ability of the system to create an opening of approximately 76 by 76 cm (30 by 30 in.), including the window, in the cabin side. The total system weight was 11.17 kg (24.6 lb). The opening was created by small-quantity explosives (flexible linear-shaped charge) which severed and jettisoned a 6.62-kg (14.6-lb) portion of the fuselage skin and structure at a velocity of 13.7 m/sec (45 ft/sec). The explosive products are contained, presenting no debris or sound/pressure hazard to the pilot. Furthermore, the opening created is neat and smooth, presenting a minimal interference potential to the pilot on egress.

System reliability has been demonstrated by previous aerospace system applications and by functional tests. The pyrotechnic components and performance principles have been qualified on aircraft systems such as the F-111 and B-1 escape modules. All functional parameters have been tested for this application to demonstrate substantial performance margins (a greater capability than required to accomplish the desired function). The system will require no maintenance, except for a 5-year replacement cycle on the detonator.

This egress system technology is applicable to any aircraft of similar construction.

#### REFERENCES

1. Schimmel, M. L.: The F-111 Crew Module: Major Challenge for Thermally Stable Explosives. McDonnell paper presented at the Symposium on Thermally Stable Explosives at the Naval Ordnance Laboratory (White Oak, Maryland), June 23-25, 1970. (Available as MDC 70-019.)
2. Bement, Laurence J.: Application of Temperature-Resistant Explosives to NASA Missions. NASA paper presented at the Symposium on Thermally Stable Explosives at the Naval Ordnance Laboratory (White Oak, Maryland), June 23-25, 1970.

TABLE I.- EXPLOSIVE DEVELOPMENT TESTS

Explosive sizing/severance tests . . . . .	23
Manifold development . . . . .	5
Containment . . . . .	29
Small-scale mock-ups . . . . .	8
Full-scale mock-ups:	
Flat . . . . .	2
Aircraft . . . . .	1
Total test specimens . . . . .	68

TABLE II.- EXPLOSIVE SEVERANCE TESTS AND COMPARISON

(a) Explosive severance tests

Explosive, g/m (grains/ft)	Material severed, mm (in.)		
	1.016 on 1.016 (0.040 on 0.040)	1.016 on 1.60 (0.040 on 0.061)	1.60 on 1.60 (0.063 on 0.063)
1.488 (7) RDX	Yes	No	
2.125 (10) RDX	Yes	Yes	No

(b) Explosive severance comparison (2024-T4 tapered plates)

2.125 g/m (10 grains/ft) RDX will cut 1.53 mm (0.0602 in.)	} 131-percent increase
3.188 g/m (15 grains/ft) HNS II will cut 2.00 mm (0.0788 in.)	

TABLE III.- PANEL JETTISON COMPARISONS

Type test	Weight of severed panel, kg (lb)	Velocity of severed panel, m/sec (ft/sec)	Energy per unit weight of severed panel J/kg (ft-lbf/lb)
Small-scale (no containment)	0.34 (0.76)	9.8 (32)	48.2 (15.9)
Small-scale (with containment)	1.00 (2.2)	10.4 (34)	53.2 (17.9)
First mock-up (flat panel)	3.40 (7.5)	10.7 (35)	58.8 (19.0)
Second mock-up (flat panel)	5.94 (13.1)	10.7 (35)	57.2 (18.9)
Fuselage mock-up	6.62 (14.6)	13.7 (45)	94.0 (31.4)

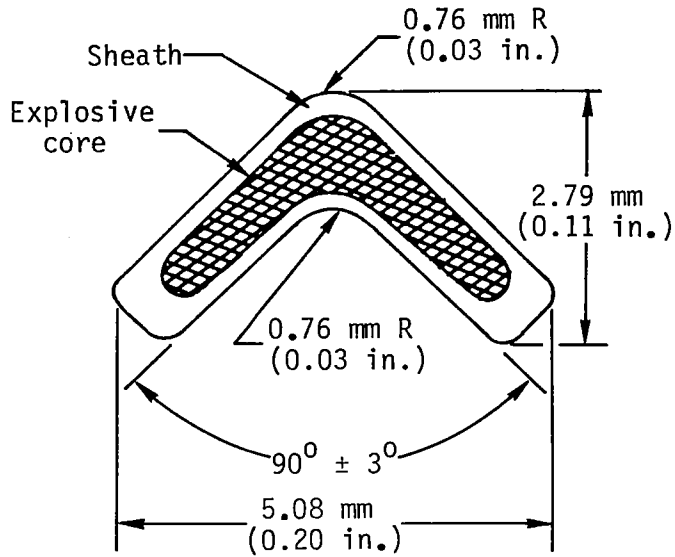


Figure 1.- Cross section of silver-sheathed HNS II flexible linear-shaped charge.

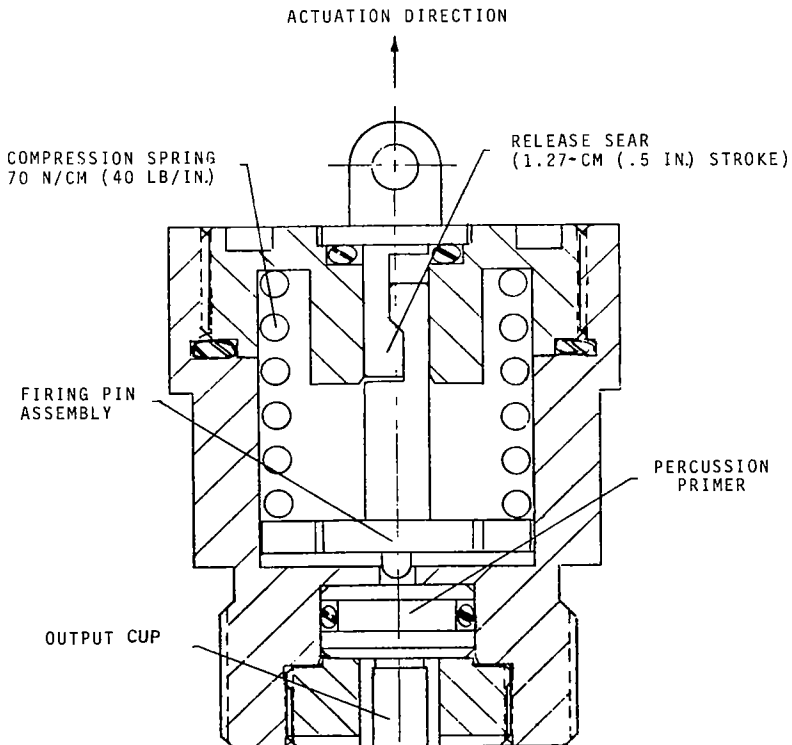
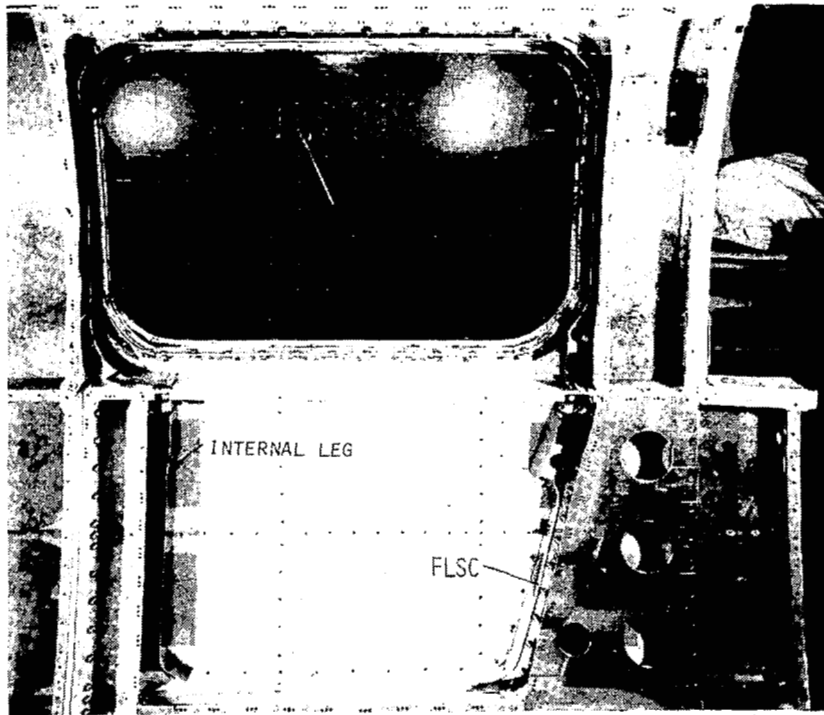
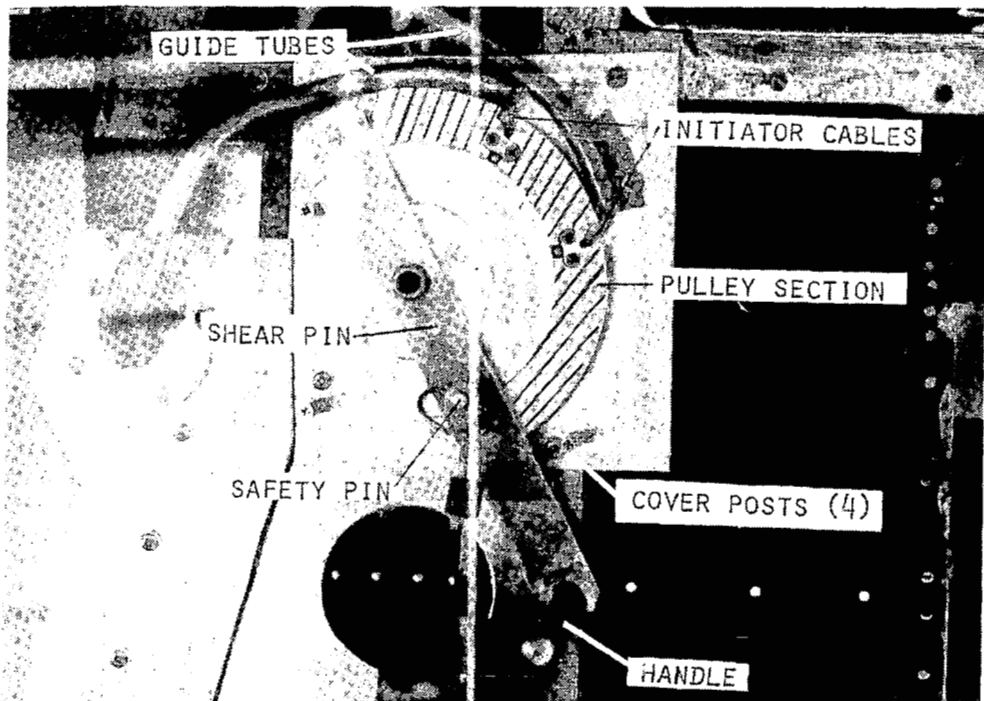


Figure 2.- Cross section of lanyard-actuated detonator.



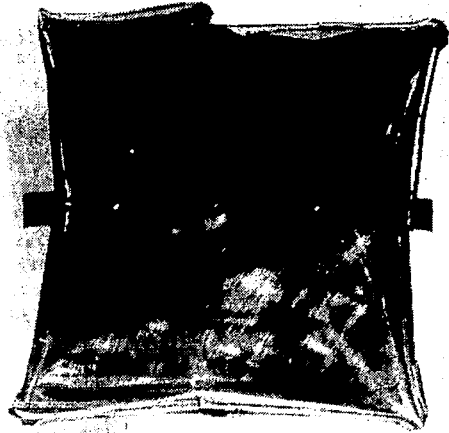
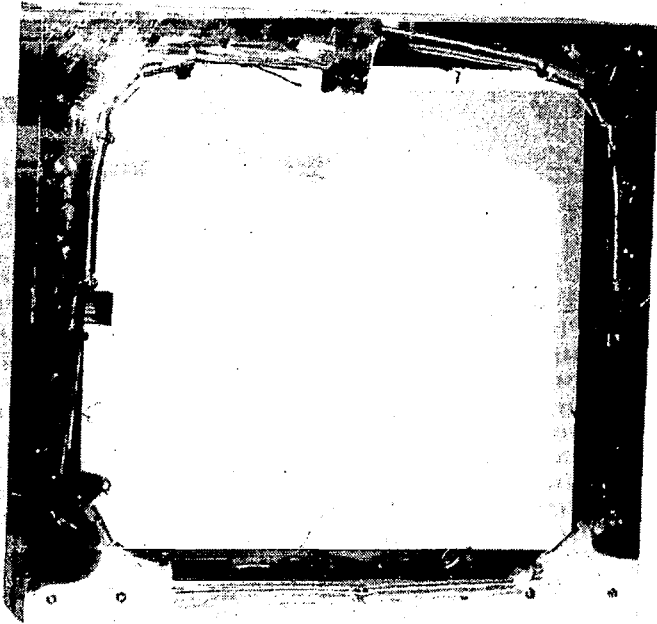
L-80-113

Figure 3.- Internal view of aircraft fuselage mock-up.



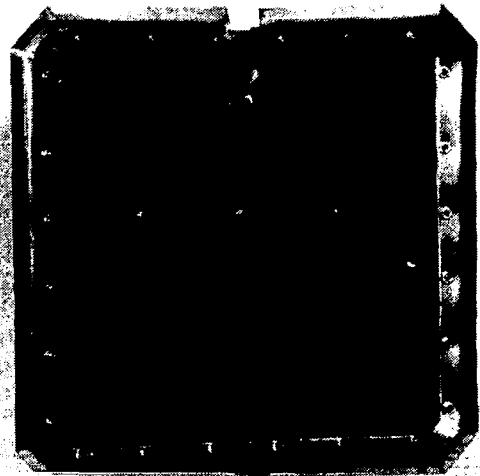
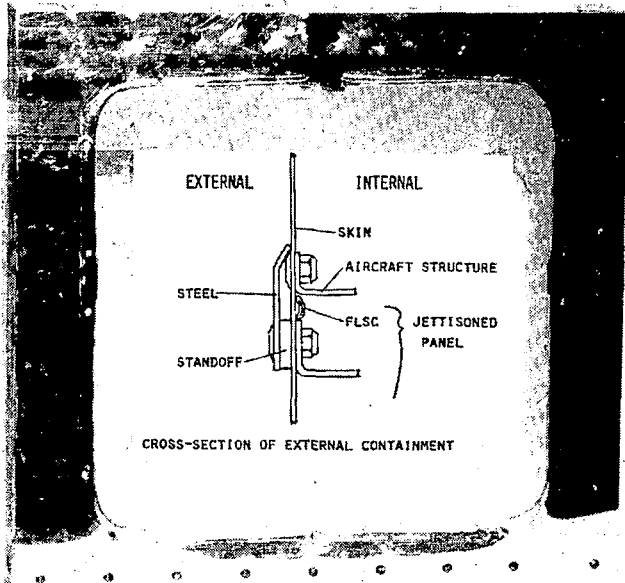
L-80-114

Figure 4.- Mechanical initiation system.



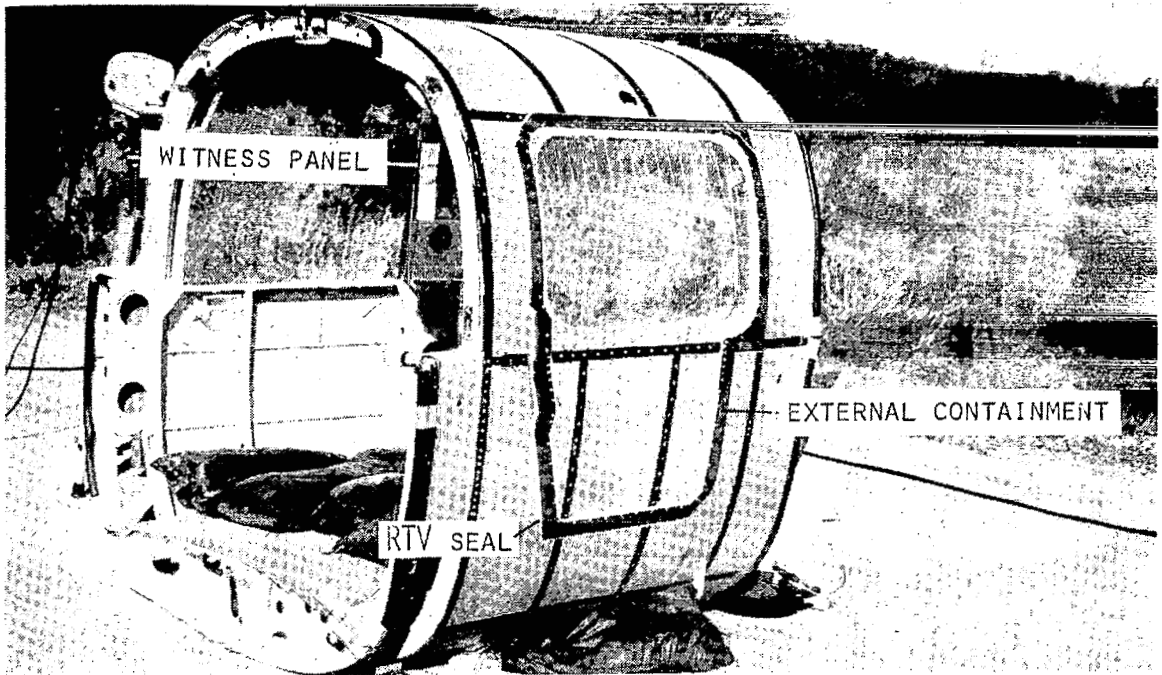
L-80-115

Figure 5.- Small-panel severance test with no external containment.



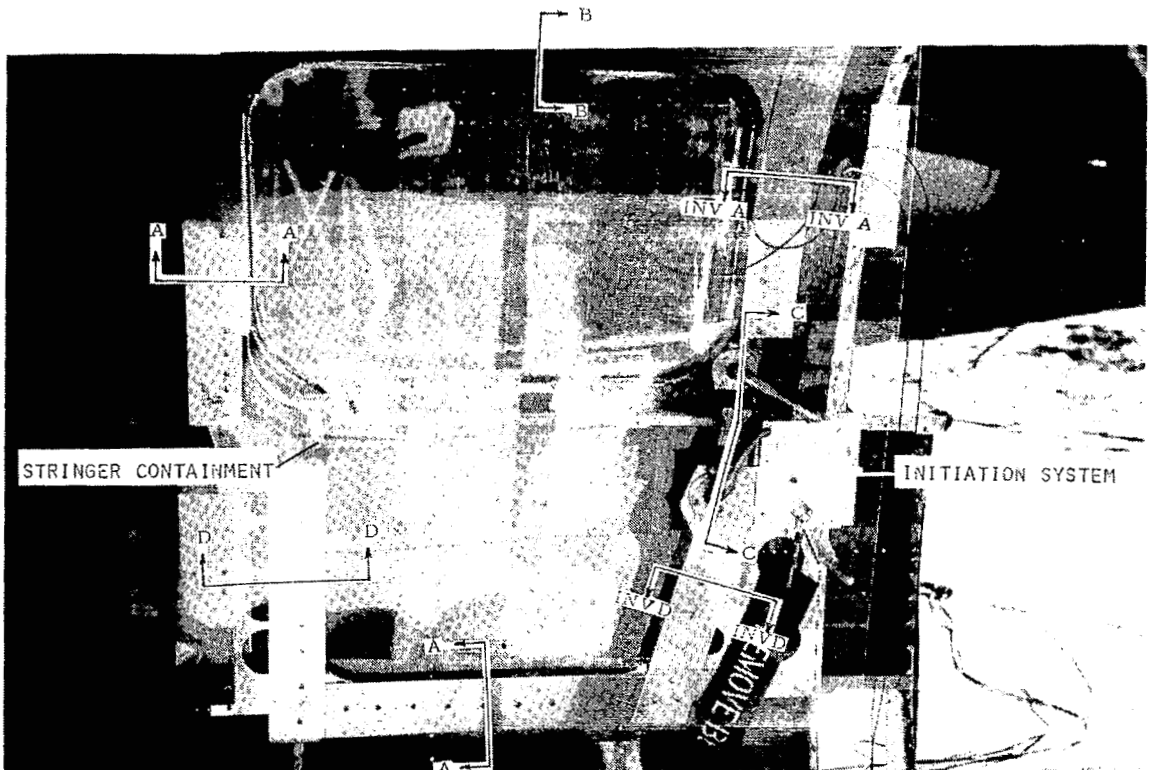
L-80-116

Figure 6.- Small-panel severance test with external containment.



L-80-117

Figure 7.- External view of fuselage mock-up of egress system.



L-80-118

Figure 8.- Internal view of fuselage mock-up of egress system.  
(Section views indicate subsequent illustrations.)

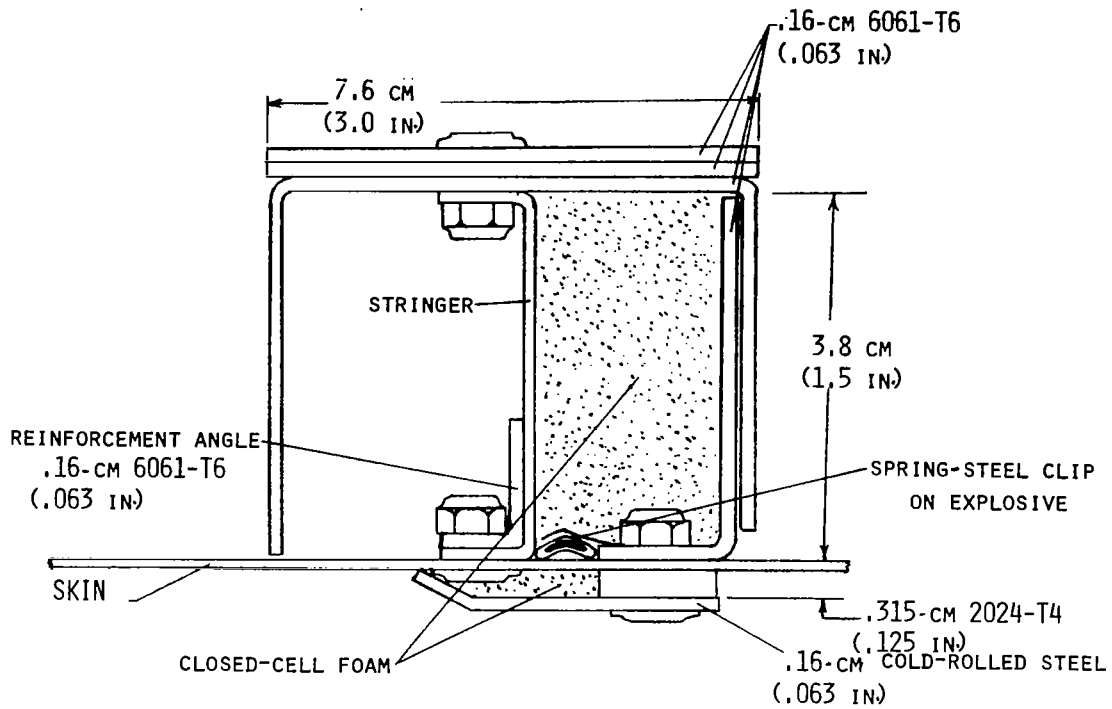


Figure 9.- A-A and inverted A-A cross section of internal containment.

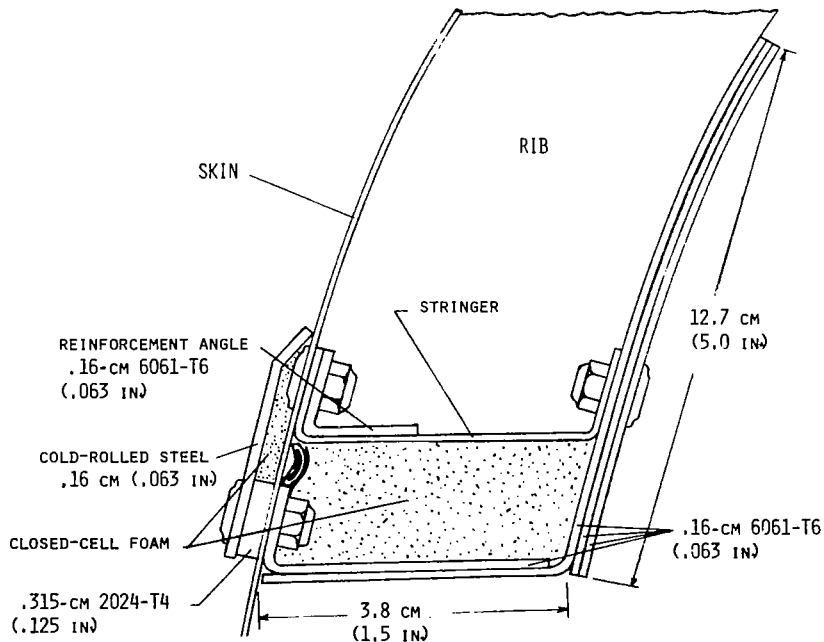


Figure 10.- B-B cross section of internal containment.

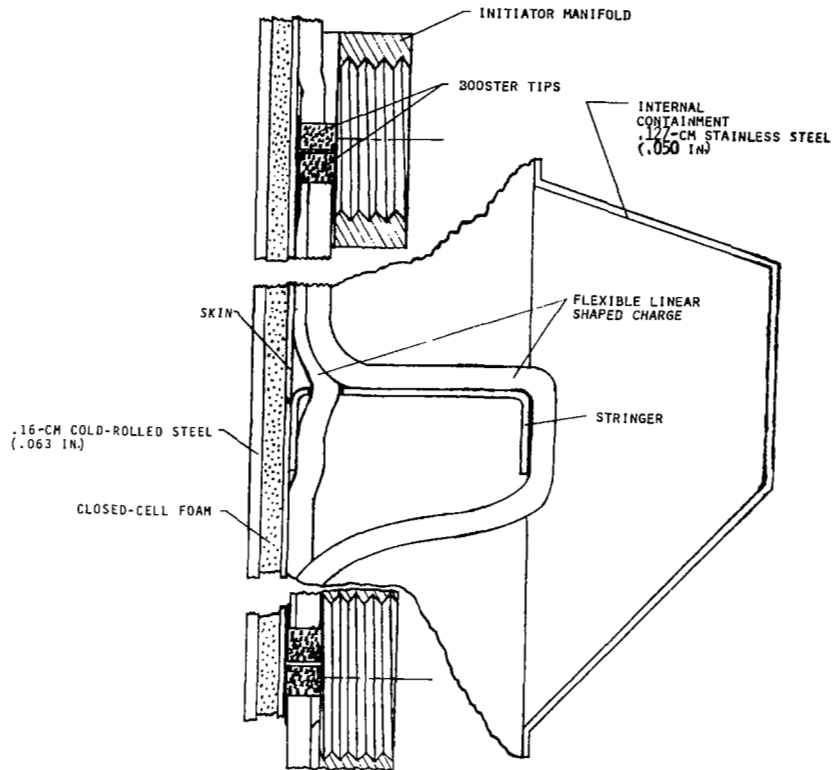


Figure 11.- C-C cross section of internal containment.

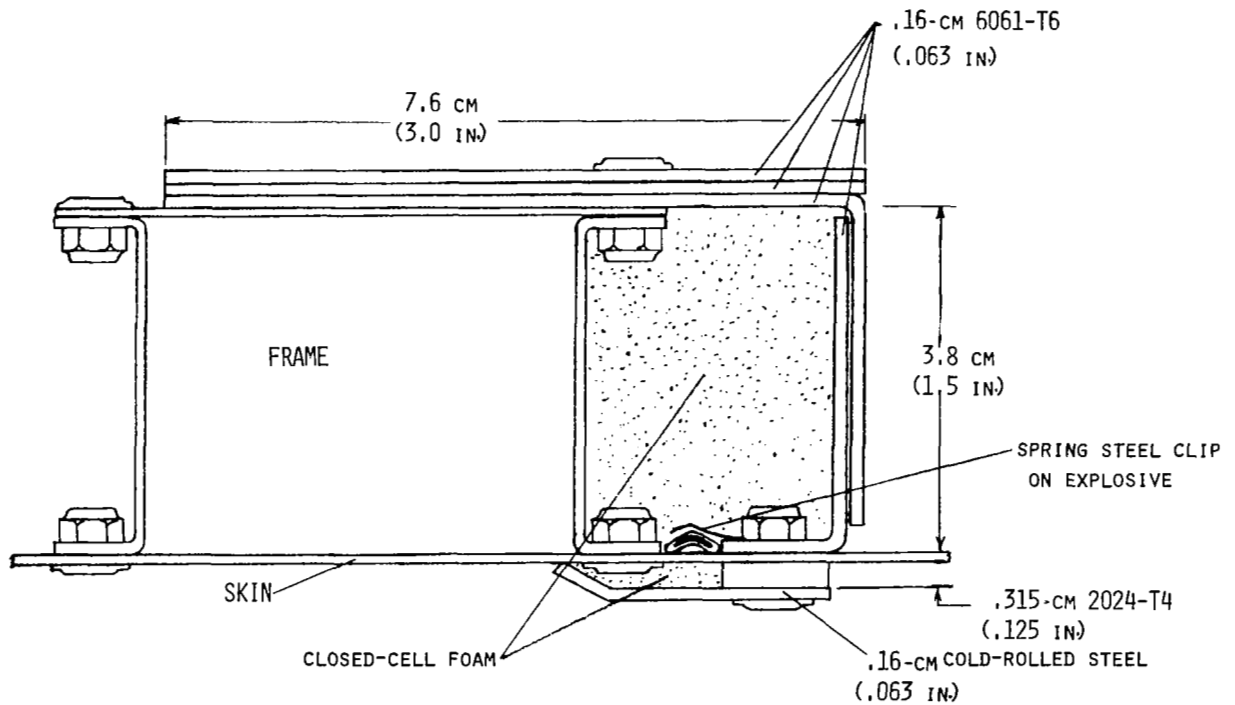
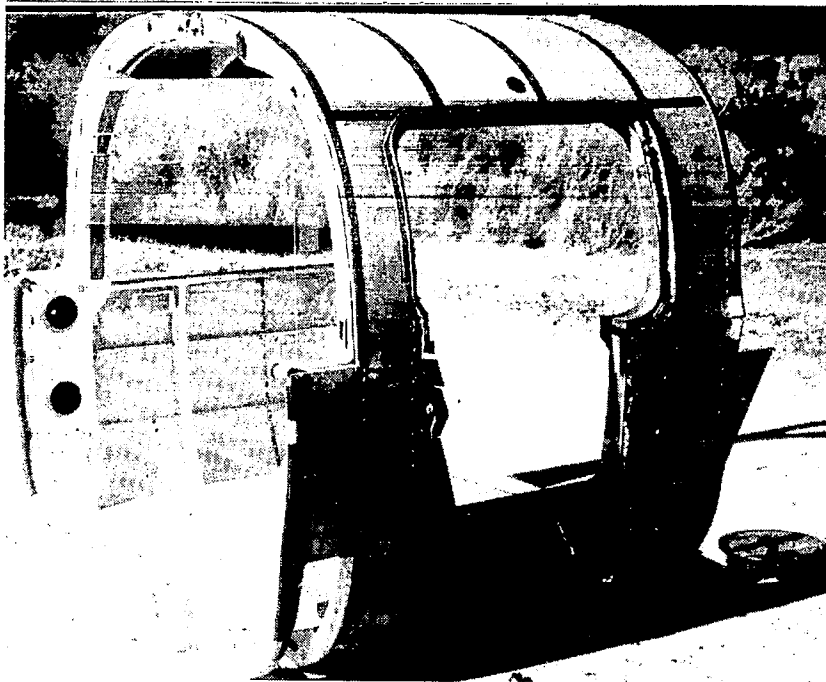
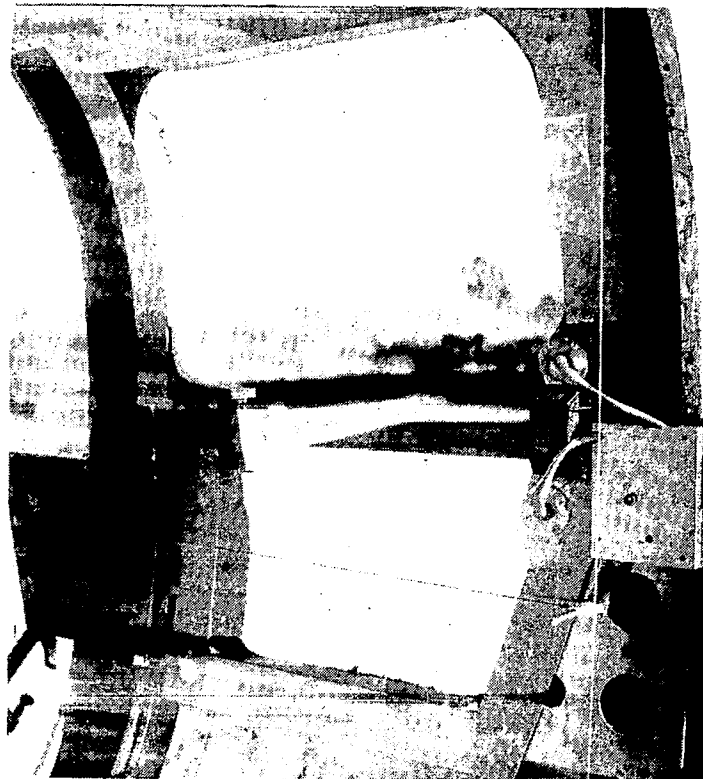


Figure 12.- D-D and inverted D-D cross section of internal containment.



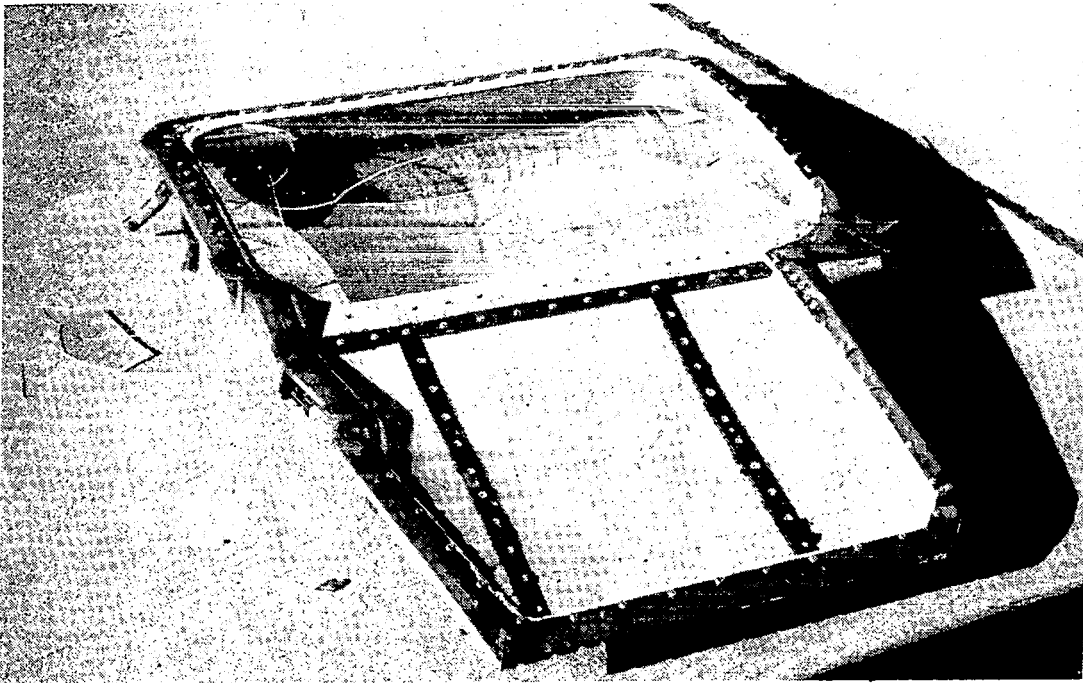
L-80-119

Figure 13.- Post-test external view of fuselage mock-up of egress system.



L-80-120

Figure 14.- Post-test internal view of fuselage mock-up of egress system.



L-80-121

Figure 15.- External view of severed panel.



L-80-122

Figure 16.- Internal view of severed panel.

# A SPIN-RECOVERY PARACHUTE SYSTEM FOR LIGHT

## GENERAL-AVIATION AIRPLANES

Charles F. Bradshaw  
Langley Research Center

### SUMMARY

A tail-mounted spin-recovery parachute system has been designed and developed by the NASA Langley Research Center for use on light general-aviation airplanes. The system was designed for use on typical airplane configurations, including low-wing, high-wing, single-engine and twin-engine designs. A mechanically triggered pyrotechnic slug gun is used to forcibly deploy a pilot parachute which extracts a bag that deploys a ring-slot spin-recovery parachute. The total system weighs 8.2 kg (18 lb). System design factors included airplane wake effects on parachute deployment, prevention of premature parachute deployment, positive parachute jettison, compact size, low weight, system reliability, and pilot and ground-crew safety. Extensive ground tests were conducted to qualify the system. The recovery parachute has been used successfully in flight 17 times.

### INTRODUCTION

Although spin-recovery parachute systems have been used for many years when conducting spin tests on light airplanes, the design, testing, and in-flight use of these systems are not thoroughly documented. As a result of the lack of design information, test guidelines, and feedback from actual flight use, accidents continue to occur during spin evaluation tests. These accidents have been attributed to improper parachute geometry and deployment and jettison failures.

The NASA Langley Research Center is currently conducting a comprehensive research program to improve the stall/spin characteristics of general-aviation airplanes (ref. 1). As part of this program, an emergency spin-recovery parachute system was designed and developed for use on the test airplanes during spin tests. Small-scale model tests (ref. 2) have been performed to determine the parachute geometry required for spin recovery of a typical single-engine low-wing airplane. Utilizing the model data, a tail-mounted spin-recovery parachute system (fig. 1) was designed, tested, and installed on the corresponding full-scale spin-research airplane. The system incorporates many safety features and stresses simplicity to ensure high reliability without redundancy and excessive weight. The system can be adapted to various airplanes, provided the parachute size and riser lengths are varied accordingly.

Design features of the system and its components are presented. Parachute sizing, loads estimation, deployment technique, attachment and release mechanism, and cockpit controls are described. Ground and flight tests are described to provide guidelines for qualifying a spin-recovery parachute system for use on an airplane. A typical deployment load time

history is presented for a flat spin recovery, and flight results are compared with qualification test results and design estimates.

## TEST AIRPLANE

The NASA general-aviation stall/spin program includes spin tests of several different airplanes; therefore, a spin-recovery parachute system was designed that could be adapted to different light-airplane configurations. The single-engine, low-wing airplane shown in figure 2 was the first to be fitted with this system. This airplane has two spin modes - a moderately flat mode and a flat unrecoverable mode. The recovery system design, installation, and testing are described using this aircraft as an example.

## SYSTEM DESCRIPTION AND DESIGN REQUIREMENTS

### Spin-Recovery Parachute

Geometry.- A ring-slot parachute was selected for the spin-recovery parachute because it has a low opening shock, a high degree of reliability, good stability (oscillations less than  $\pm 10^\circ$ ), low weight, and low bulk.

The parachute geometry necessary for airplane spin recovery was determined from tests of a dynamically scaled model in the Langley spin tunnel (ref. 2). A 3.2-m-(10.5 ft) diameter parachute canopy with a drag coefficient of 0.5, suspension line length of 3.2 m (10.5 ft), and riser length of 2.9 m (9.5 ft) was selected because it provided a rapid recovery without excessive size.

Operating environment.- The conditions under which the spin-recovery parachute must function were defined by the airplane spin modes as determined from spin-tunnel model tests and the selection of 1500 m (5000 ft) as the minimum altitude for parachute deployment. These conditions were:

Deployment altitude	1500 m (5000 ft)
Descent rate	34 to 52 m/sec (112 to 170 ft/sec)
Airplane rotation rate	36 $^\circ$ /sec to 200 $^\circ$ /sec
Dynamic pressure	622 to 1436 Pa (13 to 30 lb/ft $^2$ )

Loads.- The spin-recovery parachute geometry and operating environment were used to estimate the recovery-system limit loads. The direction of the force vector produced by the parachute may vary considerably due to the spin rate, descent rate, and attitude of the airplane during the deployment. Therefore, for design purposes, the limit parachute load envelope was represented by a moving force vector, the end of which described a semiellipsoid as illustrated in figure 3. For recovery system design (ultimate) loads, the limit loads were multiplied by a safety factor of 1.5.

A strain-gage load link (fig. 4) was installed in the spin-recovery parachute riser to measure the actual parachute loads during deployment and spin recovery. The link was also used to measure loads during ground and

flight deployment tests. To install the load link, loops were sewn to the riser to provide a parallel but shorter path through the load link. If the link failed, the continuous riser would carry the parachute load. The link was wired to an onboard instrumentation system through a connector plug on the parachute support structure. At parachute jettison, the plug disconnects from the socket.

Deployment method.- One of the more important factors to consider when selecting the deployment method for the pilot parachute and the spin-recovery parachute is the wake effect above and behind a spinning airplane. In general, the wake is nonuniform, has less than free-stream dynamic pressure, and in some areas, has airflow reversal. Any of these conditions may cause difficulty in inflation or may actually prevent inflation of the parachute. Therefore, careful consideration was given to the selection of the parachute deployment method in order to avoid these detrimental effects.

The spin-recovery parachute is deployed by the line-first method. A pilot parachute extracts the deployment bag from the parachute support structure, deploying first the riser, then the suspension lines, and finally the recovery-parachute canopy. This method provides a clean separation of the deployment bag from the airplane and insures that inflation of the spin-recovery parachute occurs away from the airplane. The possibility of the parachute fouling on the airplane is thereby reduced, and effects of the airplane wake on the parachute are minimized. The parachute snatch load (force imposed by acceleration of canopy mass at full line stretch) is also reduced because the canopy inflates after the riser and suspension lines are fully extended.

### Pilot Parachute

Geometry.- The pilot parachute must produce the force required to deploy the spin-recovery parachute from the deployment bag in a positive and orderly manner. Past experience (ref. 3) indicated that a pilot parachute should be sized to provide an initial acceleration of 39.2 to 58.8 m/sec<sup>2</sup> (4 to 6 g) on the deployment bag at the minimum expected dynamic pressure. Based on this, a 0.9-m-(3 ft) diameter, 8-gore, vane-type, solid, no-spring pilot parachute with low porosity canopy material and line length of 0.9 m (3 ft) was selected. This type pilot parachute has a high drag coefficient and a small area, which resulted in a small packing volume. The pilot-parachute bridle line, including an energy absorbing loop, was selected to be 8.8 m (29 ft) long to avoid effects of the airplane wake.

Deployment method.- To insure reliable pilot-parachute deployment regardless of the deployment method used, the pilot parachute should be ejected rearward away from the airplane wake. Three deployment methods (ref. 3) were considered: a spring-loaded system, a mortar system, and a deployment-gun system. The deployment-gun method was selected for this application because it had lower reaction loads than a comparable mortar, it provided a more positive deployment of the pilot parachute than a spring system, and a reliable deployment gun was readily available from a commercial source.

The gun projectile (slug) is attached to the pilot parachute by a short retainer line (figs. 1 and 5). When the gun is fired, the projectile pulls the pilot parachute and bridle line out to its full length. Excess projectile energy is expended by tearing out stitching in a loop installed between the pilot parachute and its bridle line (fig. 6). The energy absorbing loop was added during developmental testing as a simple means of eliminating excess slug energy to prevent spring back of the slug which could foul the pilot parachute.

### Deployment Gun

The parachute deployment gun (fig. 6) used in the spin-recovery system is a ballistic device used by the U.S. Air Force to forcibly deploy a personnel parachute. It has undergone extensive qualification tests, is flight qualified, and is manrated. It has proven to be highly reliable and has many ground-handling safety features. The gun is mechanically triggered by pulling on a cable with a force of 53.4 to 155.7 N (12 to 35 lb), whereby the initial cable movement cocks a firing pin and continued cable movement releases the firing pin. The firing pin impacts the primer of an explosive cartridge which ignites and fires the projectile. The 0.37-kg (0.81 lb) projectile leaves the gun barrel at a muzzle velocity of 46 to 67 m/sec (150 to 220 ft/sec), and a peak recoil force of 8967 N (2016 lb) is developed. After 10 firings the gun is completely refurbished. A safety pin is installed in the cable assembly to lock out inadvertent cable movement and insure safety of the deployment gun while on the ground.

### Airplane Installation

Support structure.- The deployment bag containing the parachutes, the deployment gun, and the mechanism for attaching and jettisoning the spin-recovery parachute are mounted to the support structure, as shown in figure 1.

Overall size and projected side area of the support structure were kept as small as possible to minimize aerodynamic effects which might alter the basic airplane spin modes. A parachute riser tunnel (fig. 1) was incorporated in the design to minimize changes in the airplane inertias due to the added mass of the recovery system. The riser tunnel allowed the recovery-system center of gravity to be placed closer to the airplane center of gravity, but placed the parachute riser exit far enough aft of the empennage to keep the riser from coming in contact with the tail. This design provided the maximum moment arm through which the antispin parachute force could act during the spin recovery and used the tunnel rather than the latch to react vertical and side loads from the parachute. The support structure was designed such that when the bag mounting pins are pulled, the bag is free of the support structure and automatically separates due to the centrifugal force produced by the spin.

Deployment bag.- The deployment bag and parachute system components are shown in figure 5. The bag was designed to provide an orderly and reliable deployment of the spin-recovery parachute. The bag is constructed of 203.5 g/m<sup>2</sup> (6 oz/yd<sup>2</sup>) nylon fabric reinforced with 4448-N (1000 lb) test nylon tape and is divided into three separate compartments: riser and suspension

line compartment, spin-recovery parachute canopy compartment, and pilot parachute and bridle compartment.

The spin-recovery parachute canopy is stored in an accordion-fold manner in the middle compartment. Locking flaps separate the canopy from the riser and suspension-line compartment and prevent the canopy from deploying until the riser and suspension lines are fully extended. The riser and suspension lines are stowed on a line stow flap with rubber retainer bands and packed in the front compartment.

The pilot parachute and bridle are packed in the aft compartment with the bridle attached to the aft end of the bag. Two rip cords are attached to the pilot parachute bridle for mounting the deployment bag to the support structure. A 89-N (20 lb) test break cord between the bag and the apex of the spin-recovery parachute canopy provides for extension of the canopy and separation of the pilot chute and bag before canopy inflation.

Closure flaps at each end of the bag seal off the deployment bag and protect the parachutes from damage. Nylon cords laced through mouth tie loops are used to lock the ends of the bag closed. Steel knife line cutters on the projectile retainer line and parachute riser sever the cords to open the bag ends during the deployment sequence.

The packed deployment bag is 38 cm (15 in.) long and 13 cm (5 in.) in diameter and is mounted to the support structure by loops made from shock cord which are attached to the outside of the bag. The loops pass through holes in the support structure and are held in place by the mounting pins on the two rip cords attached to the pilot parachute bridle as shown in figure 7. The mounting pins are pulled when the pilot chute and bridle line are fully extended by the deployment-gun slug during the deployment sequence.

Attachment and release mechanism.- The spin-recovery parachute riser is attached to the airplane by the attachment and release mechanism shown in figure 8. This device is mounted in the forward part of the support structure with the latch at the forward end of the riser tunnel. The mechanism is mechanically operated by cables that are connected to a control handle in the cockpit. This mechanism is a critical item in the overall system design because it attaches the parachute riser to the airplane, releases the parachute after spin recovery, and automatically releases the parachute in the event of inadvertent deployment during take-off or landing.

Automatic release of the parachute is accomplished by setting the mechanism lock arm and clamp in the jettison position, while maintaining the latch in the closed position with a small shear pin as shown in figure 8(a). The shear pin provides sufficient force to prevent the latch from vibrating open in flight before it is actually locked closed prior to spinning the airplane. If the parachute should deploy inadvertently on take-off or landing, the parachute load shears the pin and the parachute automatically separates from the airplane. A tension spring provides a force of 22 N (5 lb) to hold the clamp in the jettison position until the mechanism is manually locked.

Prior to entering a stall/spin condition, the lock arm and clamp are set in the locked position by the pilot by applying tension in cable A (fig. 8(b)) thus locking the spin-recovery parachute to the airplane. A spring locking clip prevents the lock arm from opening due to vibration. The lock arm and latch each close separate microswitches when the riser shackle is properly locked to the airplane. Both switches must close to illuminate an indicator light (fig. 9) in the cockpit verifying to the pilot that the spin-recovery parachute is properly locked to the airplane.

After deployment and spin recovery, the parachute is jettisoned by moving the lock arm to the jettison position by applying tension in cable B (fig. 8(c)). The parachute load severs the shear pin and pulls the latch open. As the shackle pulls out of the latch, the parachute load causes a rapid acceleration of the latch, swinging it against a lead stop that deforms to dissipate the latch energy. This energy absorber was required to reduce the large inertia load imposed on the leg of the latch by the rapid deceleration of the latch when it contacts the mechanism housing. The lead energy absorber is replaced after each system deployment.

### Cockpit Controls

Arrangement.- Two separate and distinct cockpit controls, a deployment handle and arm/jettison handle (fig. 9), are used to operate the spin-recovery parachute system. A "D-ring" deployment handle is located between the pilot's legs at the front of his seat, and a spherical arm/jettison handle is located immediately to the right of the pilot. The controls are positioned so that they can be reached and operated easily by the pilot under all spin conditions.

Deployment handle.- The deployment handle is similar to that used for actuating aircraft ejection seats. It can be reached with either hand and requires a pull force of 27 to 31 N (6 to 7 lb) and a travel of about 5.3 cm (2.1 in.) to fire the deployment gun. The handle is connected through a bell crank to the deployment gun by means of cables. The bell crank was sized to provide an acceptable deployment-handle travel and pull force. Metal tubing was used as a cable guide to route the cable from the bell crank through the fuselage to the deployment gun. A safety pin is installed to lock out the deployment handle during take-off, landing, and when on the ground.

Arm/jettison handle.- The arm/jettison handle is connected to the attachment and release mechanism by cables A and B in figure 8. The handle moves in a fore-and-aft direction. For take-off, landing, and ground operations, the handle is positioned aft in the jettison position. This unlocks the attachment and release mechanism so the spin-recovery parachute will separate from the airplane if inadvertently deployed.

Prior to initiating a spin maneuver, the arm/jettison handle is moved forward and to the left into a locking detent. This arms the system by locking the attachment and release mechanism which is verified by illumination of an "armed" indicator light on the instrument panel. If the spin-recovery parachute is used to recover the airplane, jettison is accomplished

by pushing the arm/jettison handle forward and to the side to clear the detent and then pulling rearward with a force of 22 to 44 N (5 to 10 lb).

### System Deployment Sequence

Prior to spin entry, the parachute is locked to the airplane by putting the arm/jettison handle (fig. 9) in the "armed" position. The spin-recovery parachute system (fig. 1) is activated by pulling the deployment handle (fig. 9) in the cockpit. This mechanically triggers the deployment gun (fig. 5), firing the projectile which starts the system deployment sequence. The spin recovery parachute-system deployment sequence is shown in figure 10.

### SYSTEM TESTING AND QUALIFICATION

To assure system reliability, a comprehensive qualification test program was performed which included static load, ground deployment, airplane taxi deployment, and flight deployment tests.

#### Static Load Tests

The parachute support structure, along with the attachment and release mechanism, was statically loaded to verify that they would withstand the limit loads and function properly under such loads. The parachute attachment and release mechanism was operated under load to determine the forces required of the pilot to operate the mechanism and to verify proper jettison operation up to the limit design load on the riser shackle. Both the magnitude and direction of the spin-recovery parachute loads (fig. 3) were simulated.

#### Ground Deployment Tests

Deployment tests from a moving truck provided a check of the deployment sequence with dynamic pressure acting on the parachutes. To avoid the wake area behind the vehicle, the recovery system was suspended 2.4 m (8 ft) from the side of the vehicle by means of a boom, as shown in figure 11. Tests were performed at dynamic pressures of 294 Pa (6.1 lb/ft<sup>2</sup>) to 919 Pa (19.6 lb/ft<sup>2</sup>), the maximum attainable with the vehicle moving into the wind. Time, dynamic pressure, and parachute load were recorded onboard the truck. High-speed cameras on the truck and in a chase helicopter filmed the deployment sequence for review of the test in slow motion.

The first two deployments from the moving truck showed that after the projectile stretched out the pilot parachute bridle line, it sprang back with the potential of fouling the pilot parachute. Additional tests were defined to develop a method of expending excess projectile energy through a smooth, slow deceleration to eliminate the spring back. This led to the incorporation of the previously described stitched energy-absorber loop. Several combinations of thread size, stitching pattern, and loop length were tested. The final configuration (fig. 12) was tested four times from the moving truck. In two of these tests, the system was deployed rearward parallel to the direction of travel, and for the last two tests, the system was deployed

pointed upward at a 45° angle and perpendicular to the direction of travel. The system functioned properly in all deployments.

### Airplane Taxi Test

An airplane taxi test provided the first operational checkout of the complete spin-recovery parachute system and controls and provided pilot familiarization with the system prior to flight test. The system was deployed with the airplane taxiing down a runway at a speed that produced the minimum design dynamic pressure (622 Pa (13 lb/ft<sup>2</sup>)). The deployment was filmed by wing-tip cameras and from a chase helicopter. An instrumentation system onboard the airplane was used to record parachute load and airplane response. Results duplicated those of deployments from the moving truck.

### Flight Deployment Test

As the final step in qualifying the spin-recovery system for flight use, the system was deployed twice in level flight. These tests provided the opportunity to check system deployment at minimum design dynamic pressure and to check system integrity near maximum design dynamic pressure. Parachute deployment loads and airplane response were recorded onboard the airplane. The deployments were filmed from wing-tip cameras and from a chase helicopter. Both level flight deployments exhibited opening loads similar to those experienced in ground tests.

## OPERATING EXPERIENCE

### Deployment in a Spin

To date, the spin-recovery system has been used 17 times to recover the airplane from otherwise unrecoverable spins. Sixteen of these were recoveries from a flat spin; one was a recovery from a steep spin.

After the first deployment of the parachute to recover the airplane from a spin, the attachment and release mechanism latch fractured when the parachute was jettisoned. The failure did not effect the jettison function of the parachute, but replacement of the broken latch was necessary. This failure was duplicated in ground tests by unlocking the latch with a dead weight suspended from the riser and shackle that was equivalent to the parachute load at the time of jettison. When the latch was unlocked, the riser shackle pulled the latch open and swung it against the body of the attachment and release mechanism, causing the latch to fracture. Previous load and jettison tests had utilized a hydraulic jack to apply the load, resulting in different loading because the force accelerating the shackle was rapidly reduced to zero after the latch was unlocked. Use of a less brittle material for the latch and addition of the previously described lead energy absorber in the attachment and release mechanism eliminated the fracture problem.

Figure 13 presents a typical load time history of a deployment to recover the airplane from a flat spin. The spin-recovery parachute stopped the spin within two turns after the deployment gun was fired. Most notable

from the load plot is the absence of the large opening load peak that characterized the ground and level flight deployment tests.. The maximum load occurred just prior to jettison, with the airplane and parachute moving at terminal velocity. The maximum vertical and side loads produced by the parachute during deployment and recovery did not exceed the vertical and side loads produced by the parachute oscillations in the terminal velocity dive prior to jettison. Loads measured during steep and flat spin recoveries were found to be much lower than the estimated load values used to design the system. The open parachute was very stable in the wake of the airplane, providing a smooth stable glide.

#### CONCLUDING REMARKS

A highly dependable spin-recovery parachute system has been developed and qualified for light general-aviation airplanes. The design, testing, and use of the system have been described. The system has been used to recover a general-aviation research airplane from 1 steep and 16 flat spins that were otherwise unrecoverable. The deployment-gun method used to deploy the pilot parachute was effective in avoiding the airplane wake and provided positive pilot-parachute inflation. The ring-slot parachute proved satisfactory for spin recovery, had low deployment loads, and was very stable in the wake of the airplane. Due to high dynamic pressure and parachute oscillations, the maximum normal and longitudinal parachute loads occurred just prior to jettison. The flight deployment data indicated that the spin-recovery parachute limit loads used for design purposes were conservative.

Langley Research Center  
National Aeronautics and Space Administration  
Hampton, VA 23665  
February 29, 1980

#### REFERENCES

1. Stough, H. Paul III; DiCarlo, Daniel J.; and Patton, James M., Jr.: Spinning for Safety's Sake. Paper presented at SAFE Association 17th Annual Symposium (Las Vegas), Dec. 2-6, 1979.
2. Burk, Sanger M., Jr.; Bowman, James S., Jr.; and White, William L.: Spin-Tunnel Investigation of the Spinning Characteristics of Typical Single-Engine General Aviation Airplane Designs. II - Low Wing Model A: Tail Parachute Diameter and Canopy Distance for Emergency Spin Recovery. NASA TP-1076, 1977.
3. Burk, Sanger M., Jr.: Summary of Design Considerations for Airplane Spin-Recovery Parachute Systems. NASA TN D-6866, 1972.

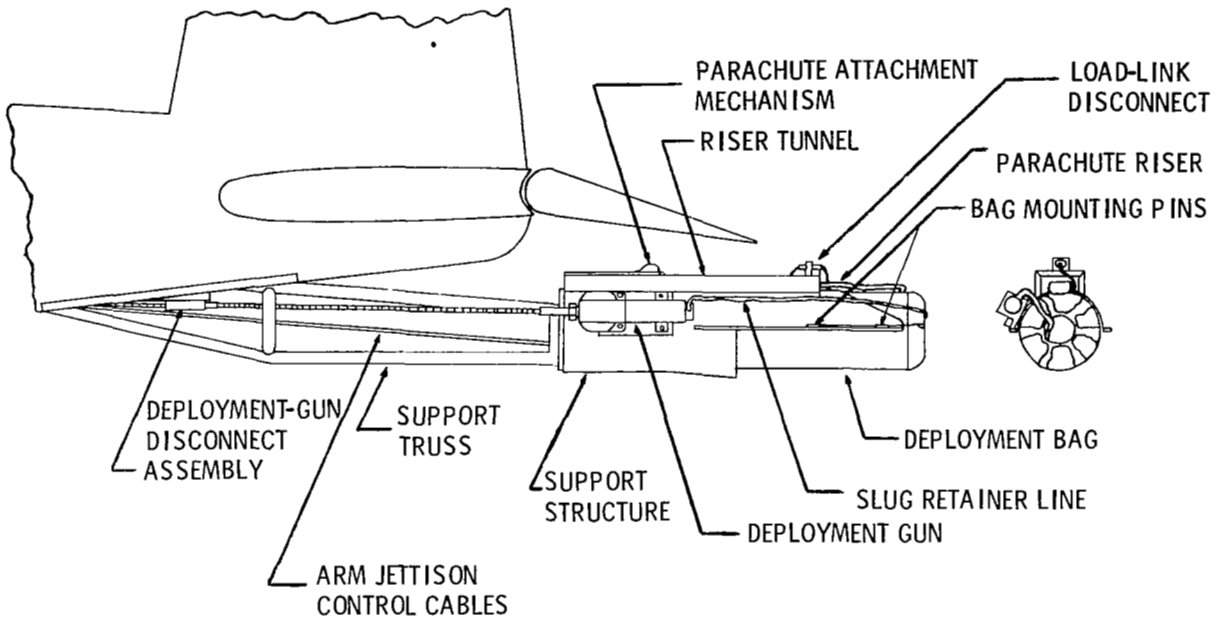


Figure 1.- Spin-recovery parachute system.

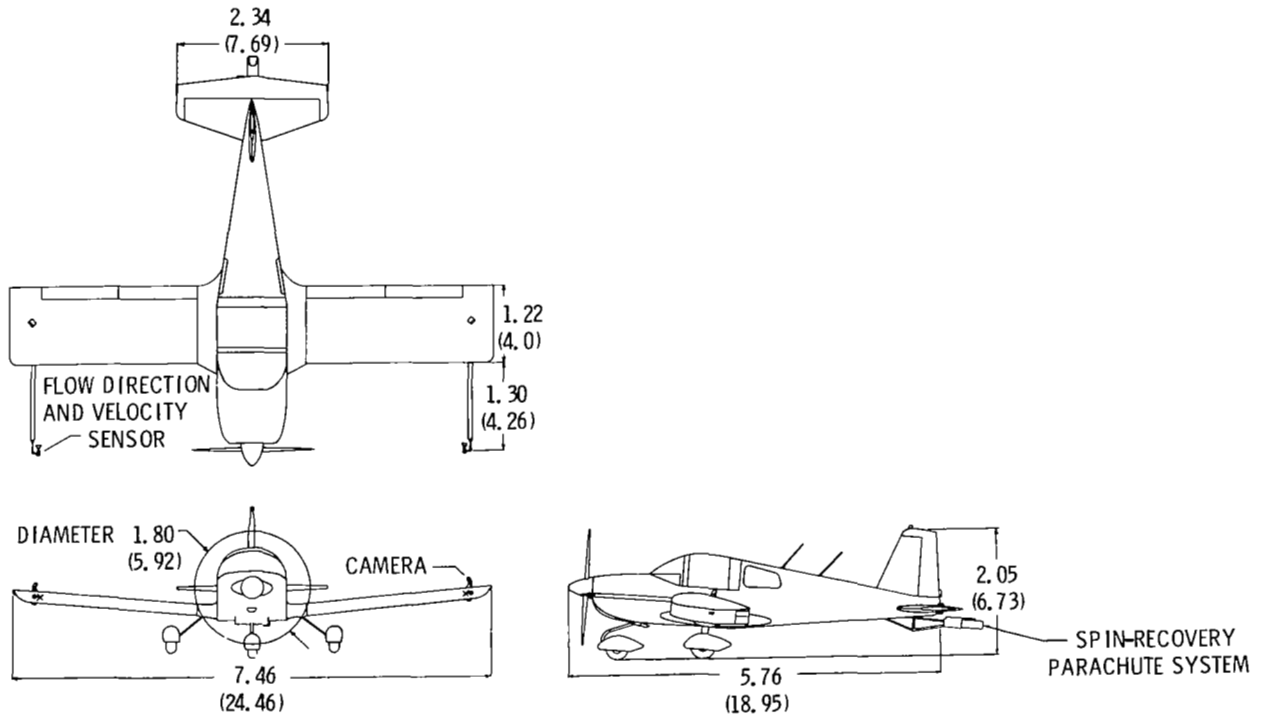


Figure 2.- Spin research airplane. Dimensions are in m (ft).

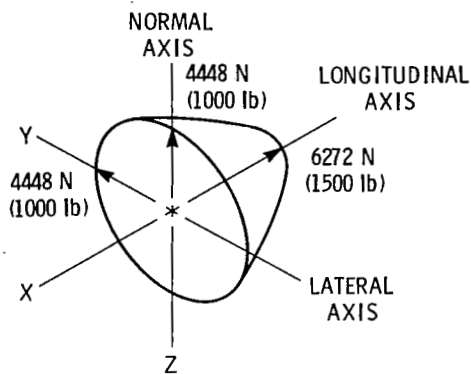


Figure 3.- Spin-recovery parachute limit-load envelope.

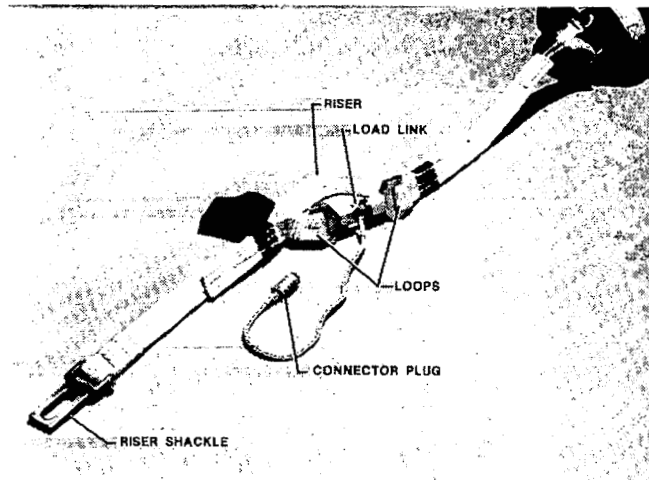


Figure 4.- Strain-gage load-link installation.

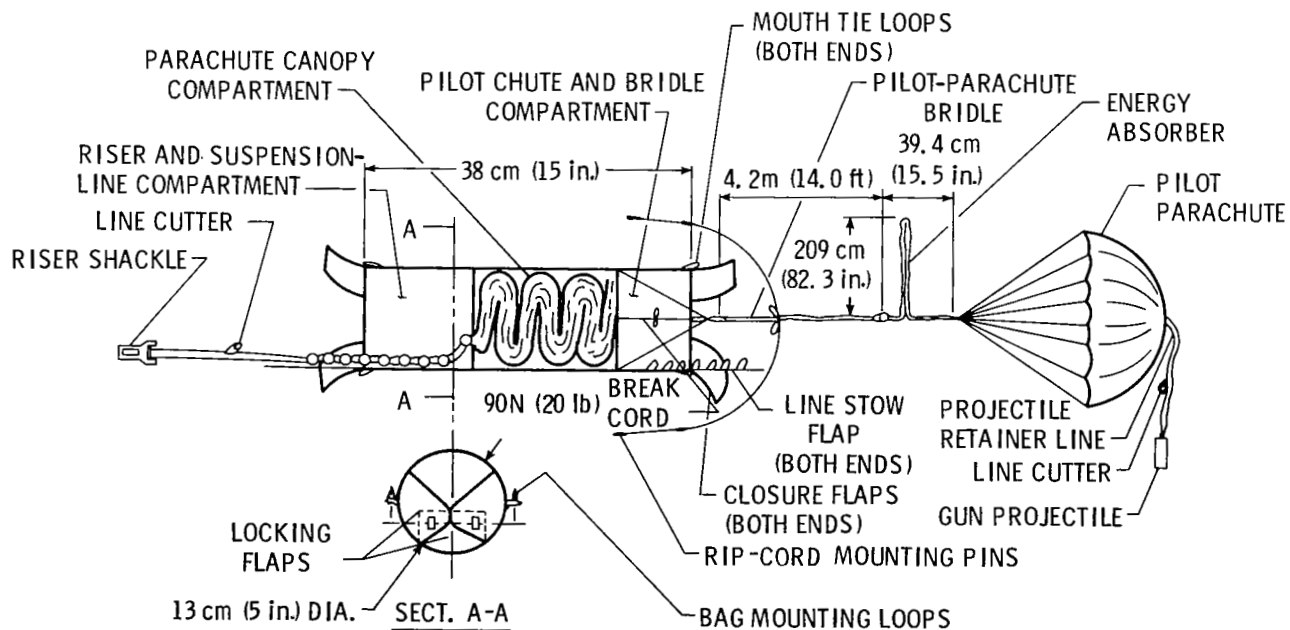


Figure 5.- Deployment bag and parachute system components. (Not to scale.)

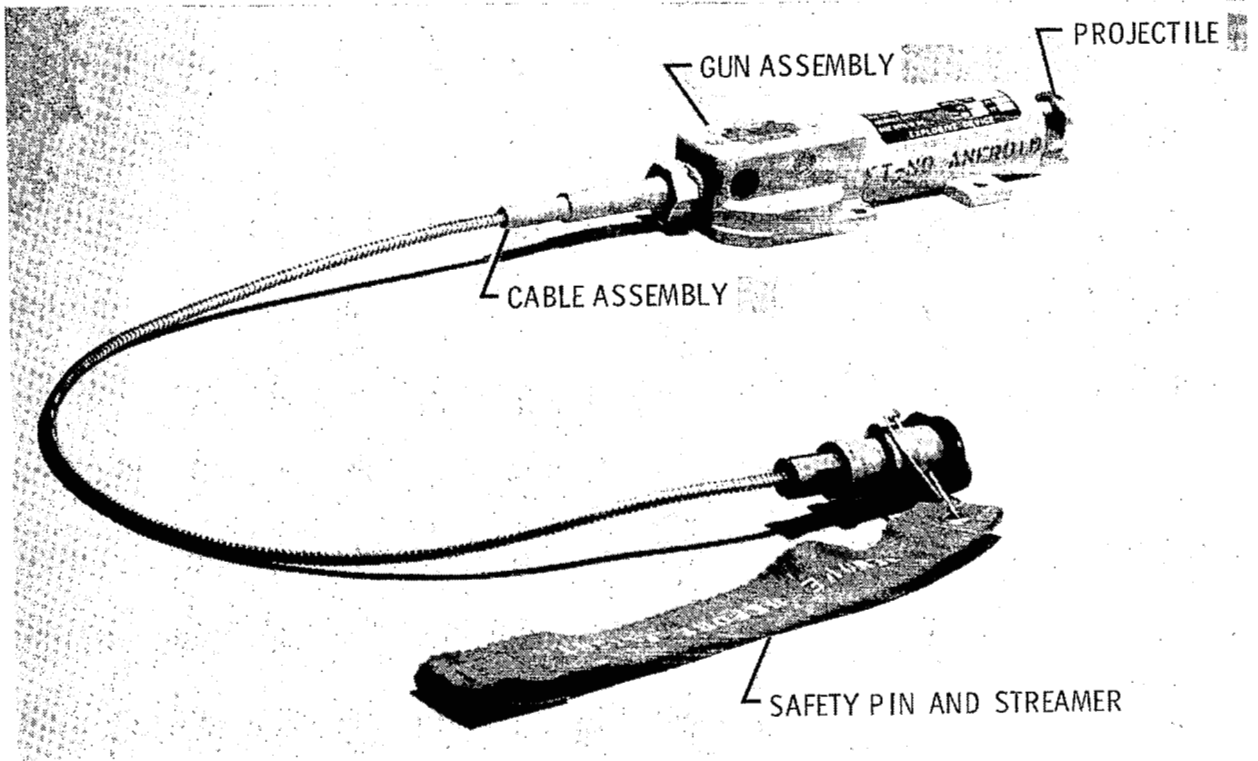


Figure 6.- Parachute deployment gun.

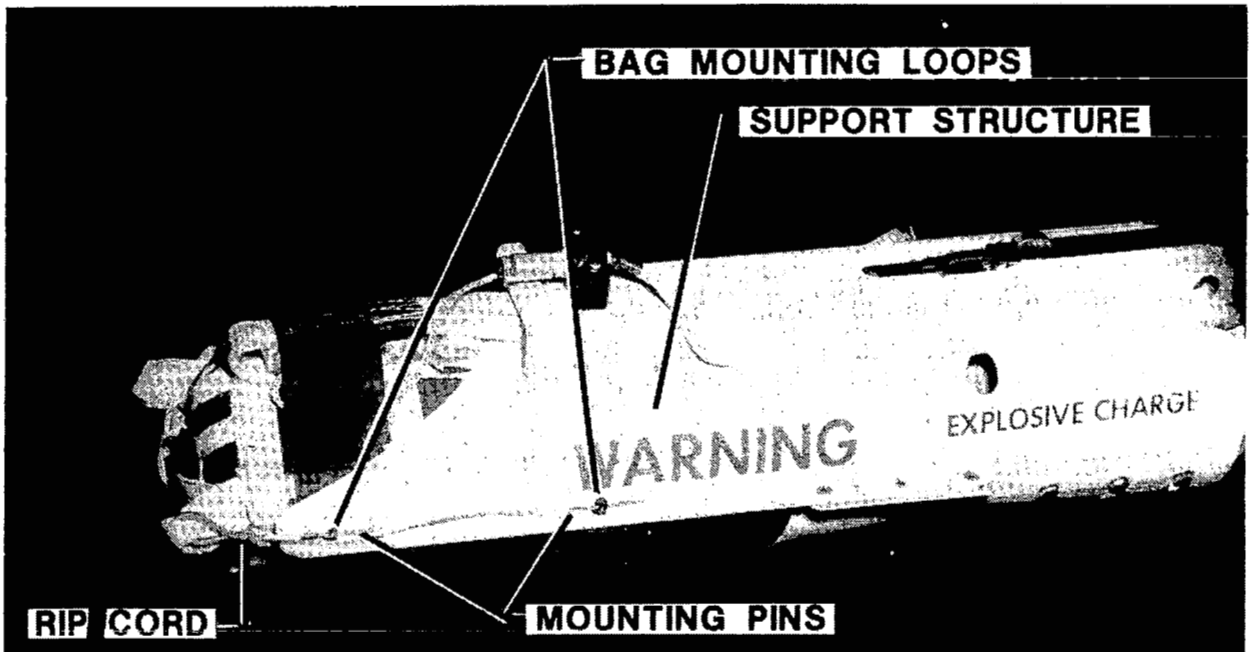


Figure 7.- Deployment bag mounted support structure.

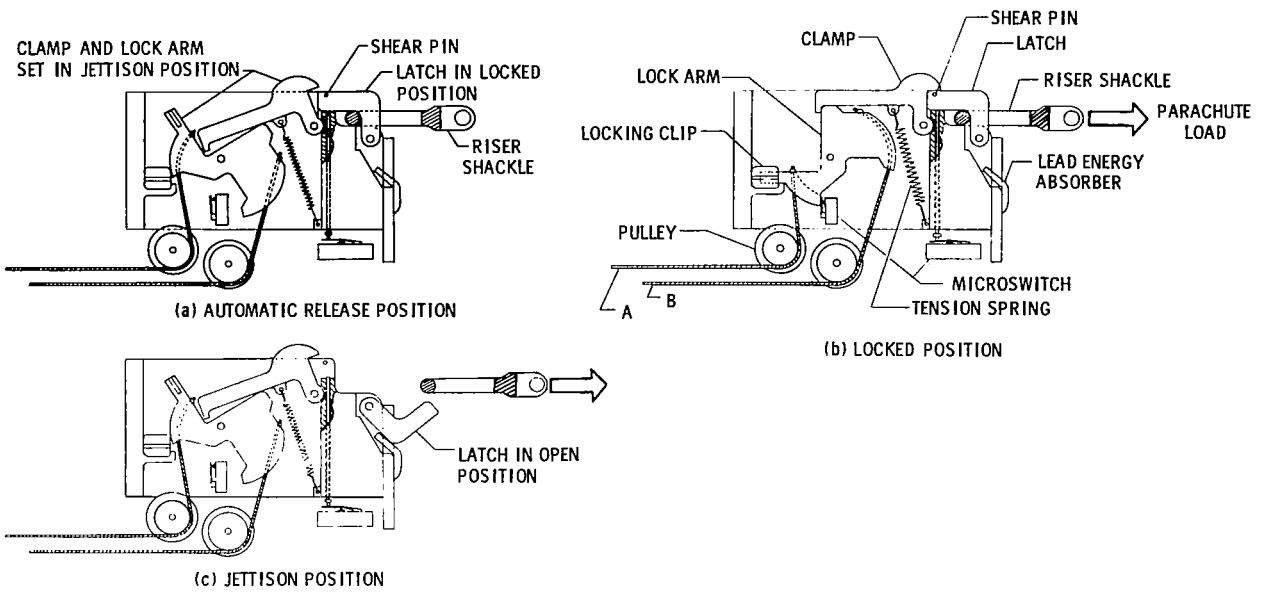


Figure 8.- Spin-recovery parachute attachment and release mechanism.

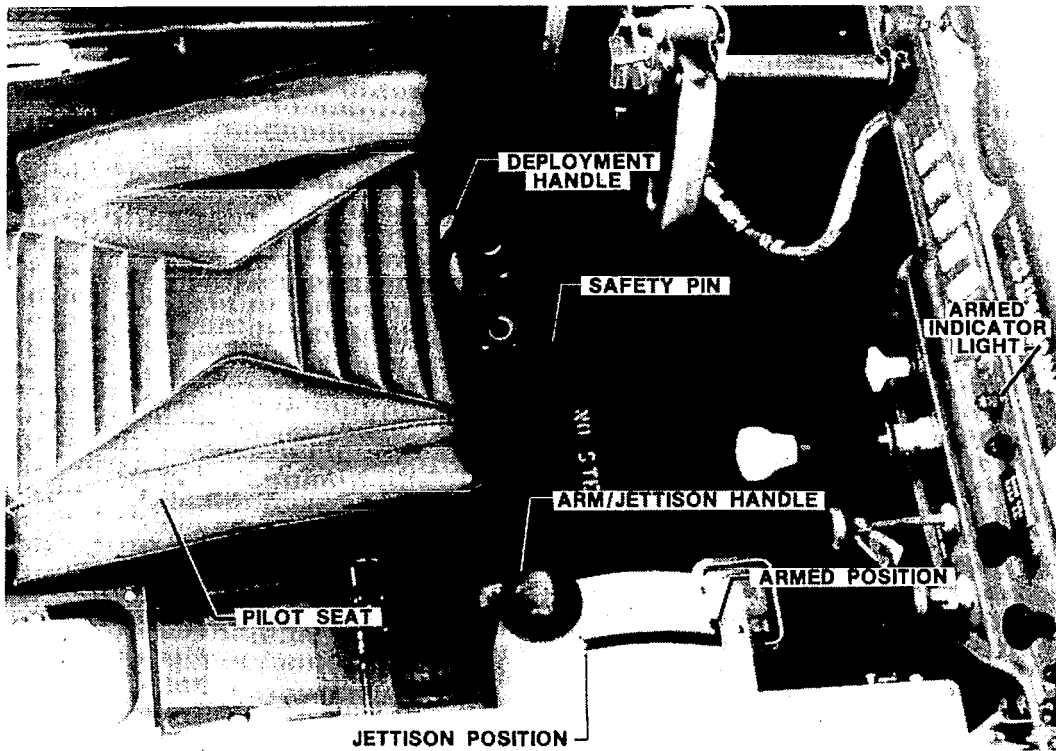


Figure 9.- Arrangement of cockpit controls.

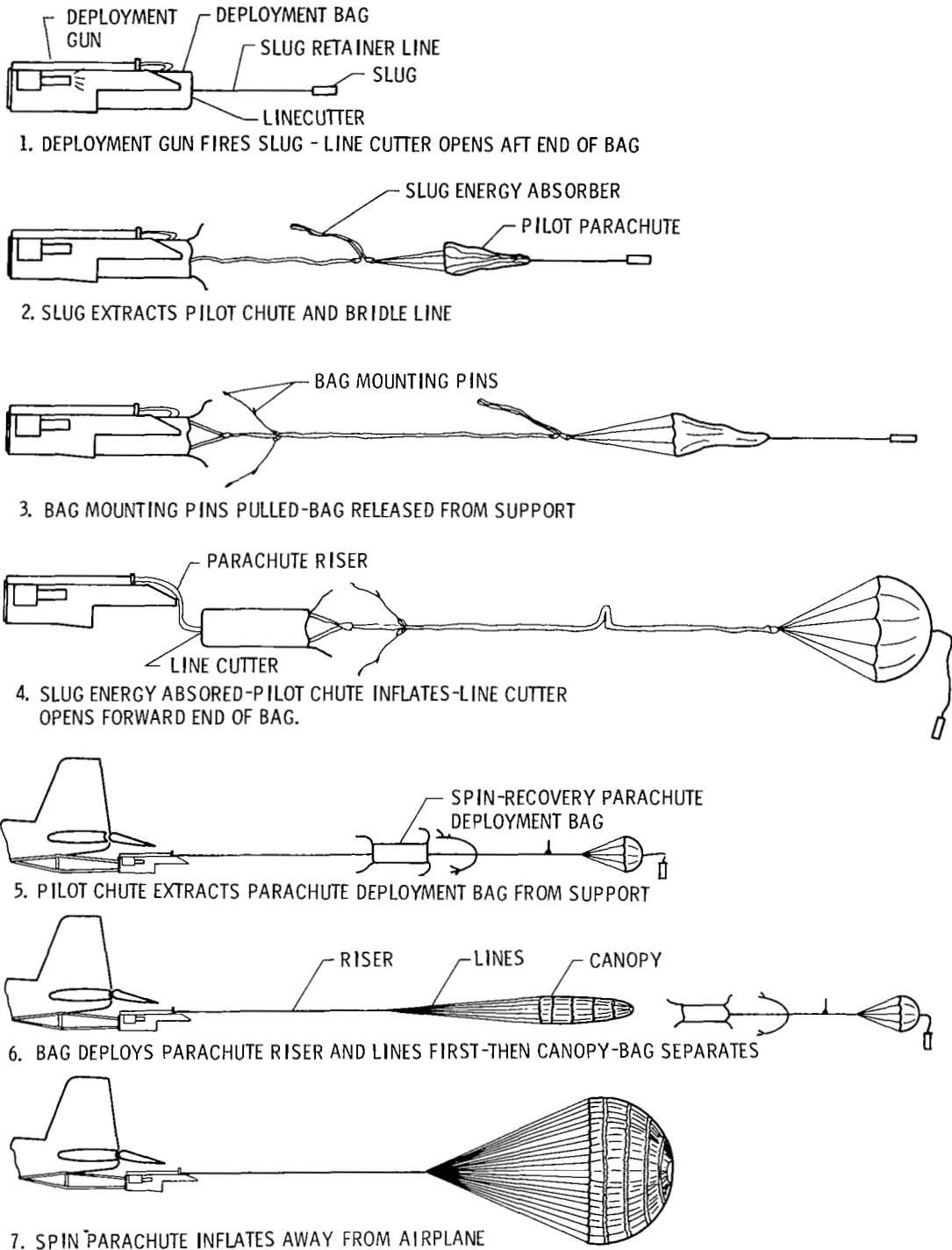


Figure 10.- Spin-recovery parachute system deployment sequence.

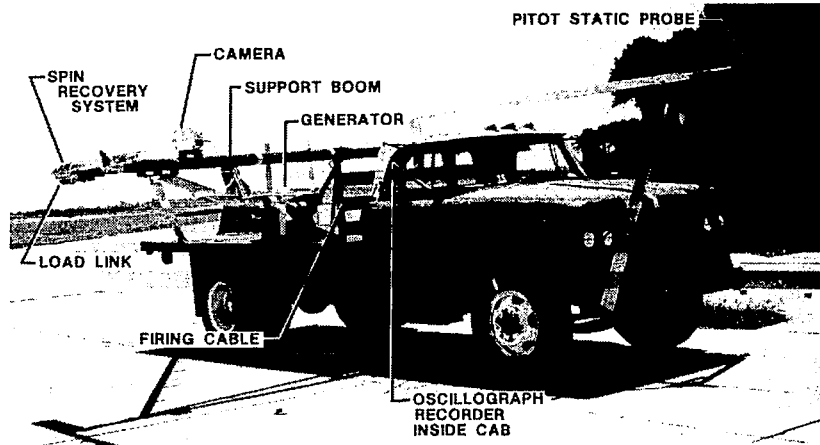


Figure 11.- Truck used for deployment tests.

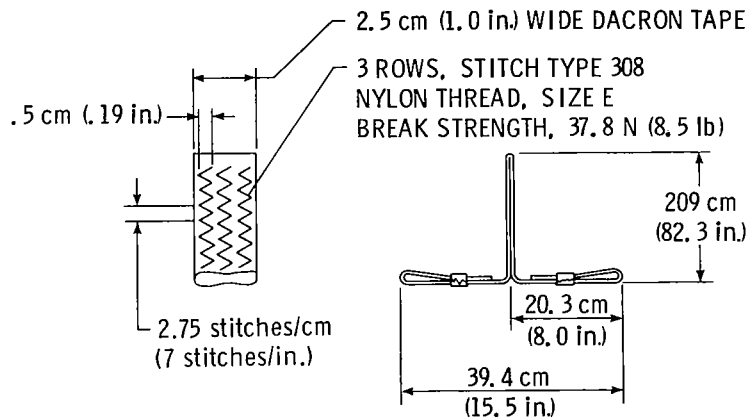


Figure 12.- Projectile energy absorber detail. (Not to scale.)

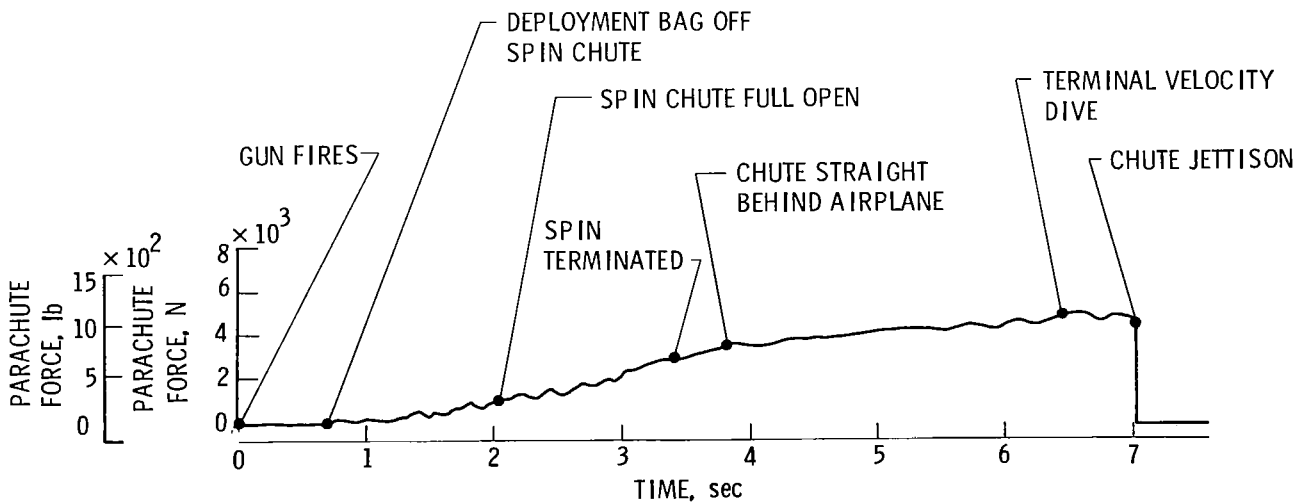


Figure 13.- Typical parachute load time history for recovery from flat spin.



# **F100 EXHAUST NOZZLE AREA CONTROL**

## **MECHANISM**

**Joseph R. Kozlin  
Design Project Engineer  
Pratt & Whitney Aircraft Group  
Government Products Division**

## **SUMMARY**

The current production F100 Turbofan Engine exhaust nozzle area control mechanism represents a highly developed mechanical device comprised of three basic elements: (1) a power driven primary nozzle area setting system, (2) a balance beam or pressure load balanced convergent nozzle system, and (3) an aerodynamically adjusting or floating divergent nozzle system. Installed in the twin engine F-15 and in the single engine F-16 aircraft (figure 1), these systems have been called upon to operate over a wide range of environmental conditions. Design requirements have been modified as a result of accumulated operational experience and changing mission requirements in both single and twin engine aircraft configurations. Durability and life cycle cost improvement without sacrifice to weight or performance are the dominant design goals today.

## **INTRODUCTION**

The convergent/divergent exhaust nozzle of the F100 Turbofan Engine (figure 2) functions primarily to accelerate exhaust gases and maximize propulsive thrust. A second and very important function of the nozzle is to minimize transient pressure fluctuations within the engine flowpath system in order to maintain internal aerodynamic stability through scheduled low pressure rotor speed control. Thirdly, the exhaust nozzle design must integrate well into the installed aircraft configuration to minimize propulsion depleting drag forces. In addition, the nozzle mechanical system must provide reliable operation in a sometimes hostile environment (see figure 3) with internal metal surface temperatures approaching 1477 K (2200°F) and external skin temperatures up to 477 K (400°F) while simultaneously being subjected to nonuniform or asymmetrical external flowfield pressures and aircraft maneuver loadings. To accommodate these requirements in an advanced high performance production engine, the F100 incorporates a sophisticated exhaust nozzle area control mechanism.

This paper highlights details of the F100 Nozzle Mechanism design, placing particular emphasis upon the evolution of design constraints or drivers from initial concept through current operational deployment. A kinematic description of the area control mechanism is given, and several environmental constraints which complicate the normal mechanism design process are discussed.

## **THE EXHAUST NOZZLE MECHANISM**

Three basic elements comprise this mechanical system: (1) a power driven primary (convergent) nozzle area setting system; (2) a balance beam or pressure load balanced convergent nozzle system; and (3) an aerodynamically adjusting or floating divergent system. These systems have been described by Reference 1.

Primary nozzle throat area ( $A_j$ ) control is achieved through an exhaust nozzle control system which senses critical engine operating parameters (inlet temperature, burner pressure, fan rotor speed, power lever

angle), integrates these into a nozzle area requirement and transmits a nozzle positioning command to an air motor. The air motor powers two 0.8 cm (0.3 in.) dia flex cables which rotate at a maximum speed of 20,000 rpm. Aft or downstream of the two airmotor cables is a series of five equally spaced ball screw actuators which extend and retract, in a synchronized system through interconnecting drive cables (see figure 4). The ball screw actuators have a stroke of 18.5 cm (7.3 in.) including adjustment. Retraction opens the nozzle and extension closes. The actuator rod extensions act together through a set of curved links (Link 1, figure 5) to axially position a synchronizing ring which is supported in each degree of freedom except axially by a bearing and track system within the nozzle support structure (see figure 6). Axial degree of freedom is controlled by the actuators. A bellcrank and linkage system is activated by Long Links (Link 2, figure 5) connected to the synchronizing ring. These transform the linear motion of the extended actuator rods into a variable diameter hoop of connecting links (Short Links 3 and 4, figure 5) that bring the nozzle system into equilibrium after changing nozzle throat area. Each Long Link transmits motion and loading to a bellcrank attached to the outer post on each of the Convergent Nozzle Flaps. The bellcrank rotation drives the two tangentially aligned Short Links connecting the bellcrank of one flap to each of the adjacent Convergent Flaps. When connected to all bellcranks and flaps, the short links form a 360 degree contiguous hoop loading element which is set into radial position by synchronized bellcrank rotation.

The balance beam or pressure load balanced convergent nozzle section is comprised of a series of Balance Flaps connected to the Convergent Flaps through a series of hinged joints. The Convergent Flaps pivot about their fulcrum points or support hinges. The Balance Flaps are supported at their forward end by an interconnecting hoop of links. Internal pressure vessel loadings are reacted out of the Balance Flap on the forward hoop of links and at the rear hinge. The hinge loads transferred from the Balance Flap react upon the Convergent Flap forward hinge to counterbalance the internal pressure induced turning moments imposed on the Convergent Flap System. Since it is not practical to null the resulting unbalanced moment for all operating conditions, some actuator loading is required to maintain equilibrium as well as overcome system friction. Spaces between both balance and convergent flaps are sealed by a series of floating seal segments which maintain internal pressures and minimize leakage. Figure 7 shows the schematic loads/reactions for this system.

The floating or divergent nozzle element is a self-adjusting nozzle expansion ratio mechanism providing distinct limits at either of two area ratio extremes (Low Mode and High Mode) for each primary nozzle area setting. Both internally and externally induced static pressures combine to produce floating divergent section static equilibrium at either of the two area ratio extremes or at some intermediate position within the float range. The relationship between  $A_e/A_j$ , or the area expansion ratio, is controlled by the pressure balancing parameters acting upon a four bar linkage (figures 7 and 8). The linkage is comprised of: (1) Convergent Flap, (2) Divergent Flap, (3) Mode Strut, and (4) Nozzle Support Structure. The Mode Struts each pivot in a slotted bracket attached to the rear of the Nozzle Support Structure.

## HIGHLIGHTS/FEATURES

### Weight

The F100 exhaust nozzle system weighs approximately 159 Kg (350 lb), or about half of that for the TF30 P100 engine exhaust nozzle, a similar thrust class engine of 1960's vintage used to power the F111 aircraft. Extensive design trades were made before choosing a cooled inner flowpath configuration with titanium structural flaps as opposed to an uncooled system with heavier higher temperature capability superalloys such as INCO 718 and Waspaloy. TF30 operational experience was factored into that trade-study process. The result was the current F100 balance beam concept with a sealed and cooled inner gas path surface, permitting extensive use of titanium structure for both Balance and Convergent Flaps. Further significant weight improvements over the TF30 were made possible through use of the airmotor driven ball screw actuators as opposed to the TF30's hydraulic system and through use of the balance beam concept

which greatly reduced actuation load requirements. The TF30 blow in door ejector and tail feather concept for reduced installed drag was not used in the F100 in favor of the integral floating divergent nozzle system.

Since aircraft center of gravity location is highly sensitive to nozzle weight, weight remains a significant consideration in F100 nozzle design modifications, even today.

### **Bellcrank System**

Positive throat positioning, nozzle stability and minimum actuation system loading is enhanced by placement of the bellcrank actuation system near the nozzle throat. This minimizes throat changes due to pressure loading and temperature changes, and reduces actuation system loads.

### **The Balance Flap**

The purpose of the Balance Flap, as mentioned earlier, is to minimize actuator loads required to vary nozzle throat area. The Balance Flap functions to counterbalance gas loads and moments acting on the convergent/divergent portion of the nozzle. The forward end of the Balance Flap is connected to each adjacent flap by a link with a spherical bearing at each end, thereby forming a contiguous hoop. (See figures 7 and 9.)

### **Convergent Flap**

This element is the major structural flap in the nozzle. Its primary function is to provide variable throat area ( $A_j$ ). This is accomplished by pivoting the flap from the static structure and varying the convergence angle of the flap. Convergence angle is varied by the actuation system through the bellcrank and linkages described above. (See figure 5.)

### **Divergent Flap**

The Divergent Flap forms the divergent portion of the nozzle and provides for complete internal aerodynamic expansion over a wide range of operating conditions. The flap positions itself in low, high or intermediate mode depending upon gas pressures and system friction loadings. (See figures 7 and 8.)

### **External Flap and Mode Strut**

The External Flap acts as the external aerodynamic contour which is exposed when installed in the respective aircraft. External loadings, both static and dynamic, are therefore highly dependent on specific aircraft flowfield conditions. A separate strut (Mode Strut) is used to limit the resultant divergent section position to two extremes — High or Low Mode — or to some intermediate or floating position between those extremes. The Mode Strut is the structural support link for the divergent nozzle section during all operating conditions except when operating in the float range. For relative F-15 and F-16 flight envelope float characteristics see figure 10. Figure 9 shows the External Flap relationship to Mode Strut and Divergent Flap.

### **Static Structure**

The static Nozzle Support Structure or nozzle case (see figure 6) is the major structural element of the balanced beam nozzle. The forward end is flanged and connects the nozzle system to the rear of the cantilevered Augmentor Duct. The center section of the static structure supports the actuator and Synchronizing Ring track loads while forming an aerodynamic external surface. The aft end of the static structure supports both the forward ends of the divergent Mode Struts and the forward ends of the External

Flaps. This section incorporates two rings which support the flap system by transferring radial loads into hoop loads and axial loads into the support case. (Rings A and B, figure 6.)

### **Flap Liners/Seals**

To maintain internal pressurization and avoid hot exhaust gas radial outward flow through the nozzle flap system, a series of seals and flap liners are utilized. These seals (Balance, Convergent and Divergent elements) are hinged together axially (see figure 9) to overlap and fill the gaps between the hinged internal flap system. The Convergent Section liners create the coolant flow passage.

## **ENVIRONMENTAL CONSTRAINTS**

The F100 Exhaust Nozzle is a convergent/divergent system. Exhaust gases from fan and core engine flow streams mix in the Augmentor Duct, are further heated to temperatures approaching stoichiometric during Augmentor operation, and discharge from the rear of the Augmentor into the Convergent Nozzle Section. The Convergent Nozzle accelerates the internal gases to a choked flow or sonic velocity condition at its minimum area constriction,  $A_j$ , located at the convergent section aft end. From the choke plane area  $A_j$ , a partially constrained aerodynamic expansion takes place to further accelerate the exhaust gases through the Divergent Nozzle Section. Aircraft aerodynamic flowfields pass rearward over the exposed engine External Nozzle Flaps contour to join with engine exhaust gases aft of the Divergent Section exit plane,  $A_e$ . Internal aircraft nacelle airflows pass from the engine inlet duct region aft in the cavity between engine and airframe to discharge rearward through openings in the Divergent Nozzle Section, External Nozzle Flap Section, or through Nozzle Support to Air Frame seal openings. These airflow systems comprise the fundamental aerodynamic loading environments in which the exhaust nozzle mechanism must operate. It is an extremely complex flow condition and the resulting pressure loads are hard to predict.

Further environmental constraints in the nozzle system are imposed by mechanical loadings due to aircraft maneuvers (g's and gyro's) and system vibrations fed by rotor induced harmonics and installed acoustical excitations.

In order to control rotor speed and maintain internal engine aerodynamic stability at all operating conditions within the specified flight envelope, the nozzle mechanical system must be extremely quick in response to engine control system command. Response rate cannot be compromised by a sluggish design which is not tolerant of all combinations of integrated system loading constraints. The F100 nozzle capability includes excursions from full open to full closed, or the reverse, in less than one second elapsed time. This high response rate is fully compatible with the very short engine acceleration/deceleration capability required for high performance. The F100 engine accelerates from idle to full intermediate power in only 2.2 seconds and the nozzle must be compatible.

Mechanical friction effects play a major role in the total system design. Increased friction loadings generally aid in damping induced vibratory responses, while at the same time reducing system operational life due to increased wear rates. Heavy wear can result in a loose system which could become more susceptible to structural fatigue and distress. Fits, clearances, and wear resistant coatings therefore become critical design concerns in a highly functional and durable nozzle mechanism design. Trade-offs had to be made between an extremely "loose" system with benefits of high response rate and adaptability to manufacturing tolerance variation; versus a "tight" system with lower response rate due to higher system friction, and minimized flow leakage. The resulting production F100 nozzle configuration is a compromise between the two extremes.

Under conditions of asymmetric pressure (see figure 11) and maneuver loading where the nozzle can become ovalized or distorted, several design considerations are introduced. From a mechanisms design point of view, the most obvious is the distortions under loading conditions which could override the simple kinematic model through which design link loadings are derived. Special consideration must also be given to linkage stability in all actuating environments while in a distorted nozzle condition. Also, aerodynamic excitations of External Flaps are of particular concern since this portion is exposed not only to engine acoustics but aircraft flows as well. A transonic high "G" turn with nozzle in the float range could present a severe mechanisms design point, for example.

The F100 nozzle mechanical system was initially designed with a power driven two position Divergent Section. The originally qualified and produced power driven configuration was attractive from a durability standpoint, providing excellent Divergent System stability but at a higher weight and cost. After performance, cost and weight trades were redone and a successful redesign and test program completed, the current floating system was incorporated. Aerodynamically actuated systems that have reversal of load must go through a null state where the sum of the loads acting on the system is zero. In the region near zero loading, small cyclic loads can drive the system into vibration or instability which can produce accelerated wear or structural damage from high inertia loads. The two-position Divergent Section Actuator restricted the system freedom by providing positive stabilizing loads at the Low and High Mode extremes while eliminating float range positioning.

Successful flight and sea level static testing of the YF100, and the F100 floating nozzles, resulted in removal of the Divergent Exhaust Nozzle Control and actuation system in favor of the floating Divergent Nozzle. This basic change in design resulted in a savings of 10.4 Kg (24 lb) of engine weight, significantly reduced the engine cost, and introduced a new design trade-off for future balanced beam nozzles.

### **WEAR AND DIRT ACCUMULATION**

Wear and dirt accumulation can act in conjunction with system friction to further complicate the nozzle mechanism. As stated above, a worn, or loose nozzle might have a faster response rate due to reduced system friction, while sacrificing leakage and some degree of system damping and inviting increased hardware fatigue and distress. Dirt acts in the same way as increased system friction to inhibit system response time and increase mechanism loadings.

Most of the F100 nozzle mechanism joints utilize uniballs (figure 5). Radial clearance is such that either dirt or surface spalling can accumulate to jam the uniball driving motion and generate wear in the attaching pin and sleeve members. These conditions are further aggravated by the high local environmental temperatures (up to 561 K/550°F) which limit lubrication to a dry film approach. Coatings to seal out foreign materials and corrosives in these environments and to provide increased durability are being successfully developed in an on-going challenge to extend joint service life. Several promising choices such as Nickel-Boron are currently being studied on a life cycle cost trade basis.

Another example of wear problem is at the External Nozzle Flap attachment hinge joints where pins and retaining rings fretted. High speed F-15 flight movies recently showed an External Flap pounding mode of vibration not previously identified. Initial nozzle design requirements called for a symmetrical external static flowfield loading. Later reduced scale model test data were obtained from wind tunnel testing. The design static loads were then modified but kept symmetrical. Further instrumented testing in F-15 flight indicated significant static load increase and a non-uniform flowfield. Of particular significance was speed brake deployment effects. Later, instrumented testing in the F-16 showed even higher loadings. The design loadings history to date is given in figure 12. Dynamic data acquisition is now in the F-15 flight test plan for 1980 since it is likely that operational dynamic loads have exceeded the original design allowables.

The External Flaps are themselves a classic example of advantages and disadvantages of system looseness and friction. When loose in an unstable external aerodynamic environment, the hinges pound and wear until looseness becomes excessive enough to eliminate effective friction damping. Service life can then be substantially reduced through impact loading. Shaker rig tests of External Flaps with simulated flap support systems (figure 13) are currently being conducted at GPD for durability testing in conjunction with the forthcoming measured F-15 dynamic flight test data. Results will be evaluated against the most recent design improvements to upgrade the durability of the External Flap System.

### **ENGINE/AIRFRAME INTEGRATION EFFECTS**

An integrated propulsion system is subjected to the constraints of the installed environment. For the F100 engine, the environments within which the exhaust nozzle mechanism must perform differ significantly between the F-16 single engine installation and the F-15 twin engine configuration (figure 1). Close engine location and spacing to minimize overall installed afterbody drag, as in the case of the F-15 (Reference 2), can result in extraordinary and unstable engine external flap environments, as well as increased sensitivity to engine-to-engine and engine-to-airframe acoustical excitations.

### **TRADE-OFF FACTORS**

The self positioning exit area system resulted from design trade-off studies to provide a desirable balance between weight, cost and performance.

Weight and c.g. concerns were and continue to be the prime driver in the design and optimization of the F100 exhaust nozzle mechanism. These concerns conflict with a pure durability approach which might favor a heavier system. Tradeoffs between durability, weight, cost and performance are continually made in attempt to further increase system life. Current efforts are focused on reducing nozzle mechanism wear and increasing overall life without sacrificing weight or cost objectives. An extensive laboratory wear rig and coatings evaluation program is under way and all system fits and clearances have been reevaluated to optimize damping and minimize wear. A further objective of these efforts is to maintain or improve nozzle response capability while reducing system life cycle cost.

### **CONCLUDING REMARKS**

The F100 nozzle area control mechanism was initially designed to operate in a symmetrical aerodynamic loading environment. A series of design and development iterations followed which produced a current production configuration which is highly tolerant of the sometimes severely compromised kinematic symmetry. Further dynamic and static flight test data will be obtained and reduced during 1980 in an on-going program to further understand and optimize the installed system.

### **REFERENCES**

1. Bonner, George A., "Effect of F-15 Aircraft Induced Aerodynamic Loads on the Evaluation of the F100 Balanced Beam Nozzle," Paper No. 76-733, AAIA/SAE 12th Propulsion Conference, Palo Alto, California/July 26-29, 1976.
2. Martens, Richard E., "F-15 Nozzle/Afterbody Integration," Journal of Aircraft, Vol. 13, No. 5, May 1976, pp 327-333.

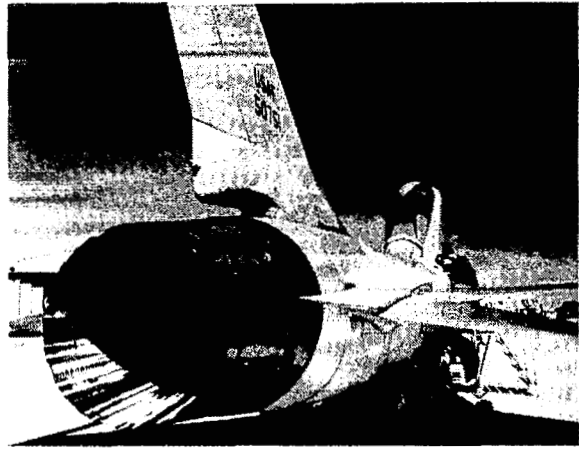
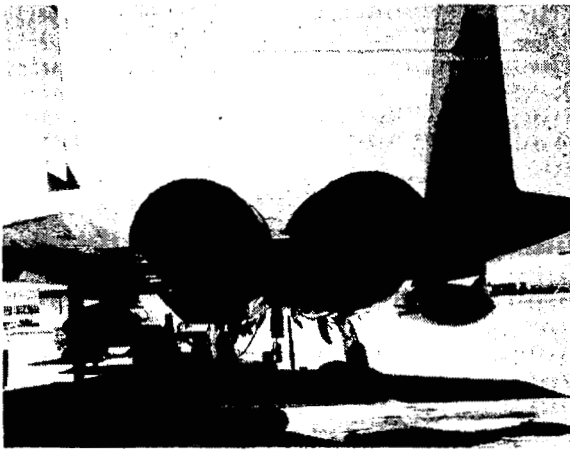


Figure 1.- Rear views of F-15 and F-16 aircraft showing F100 orientation.

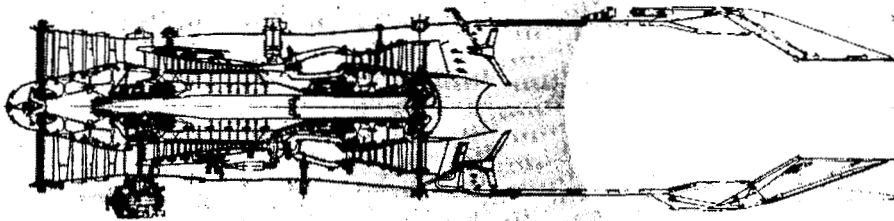


Figure 2.- F100 turbofan - highlighting nozzle mechanism.

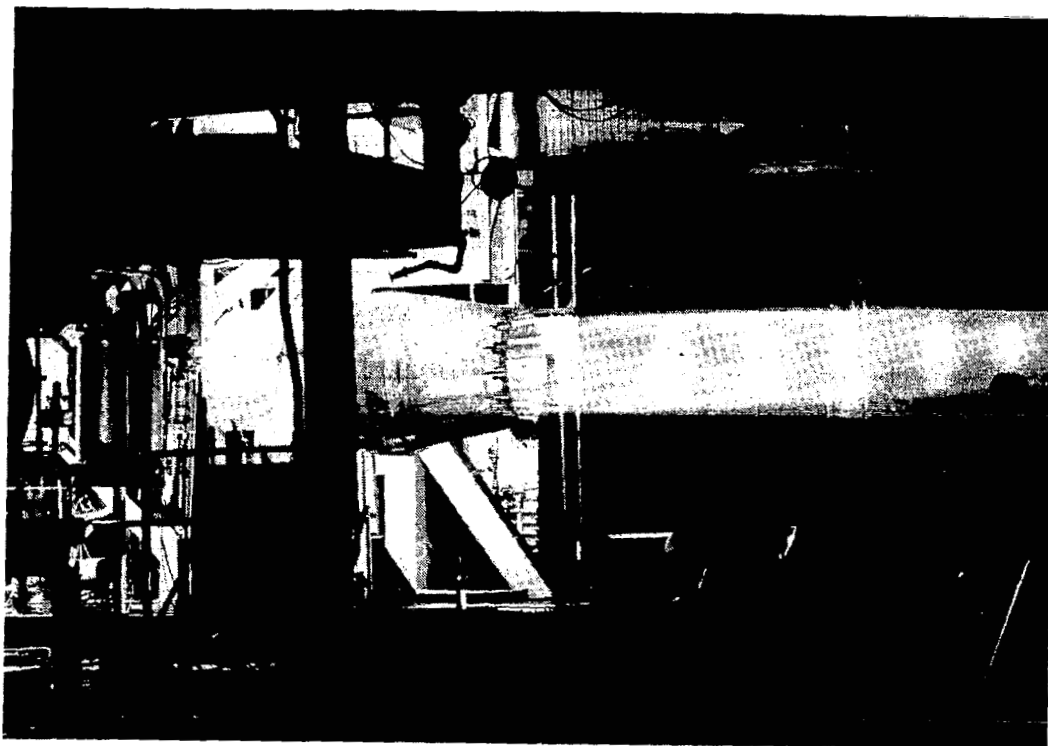


Figure 3.- F100 nozzle during test stand run.

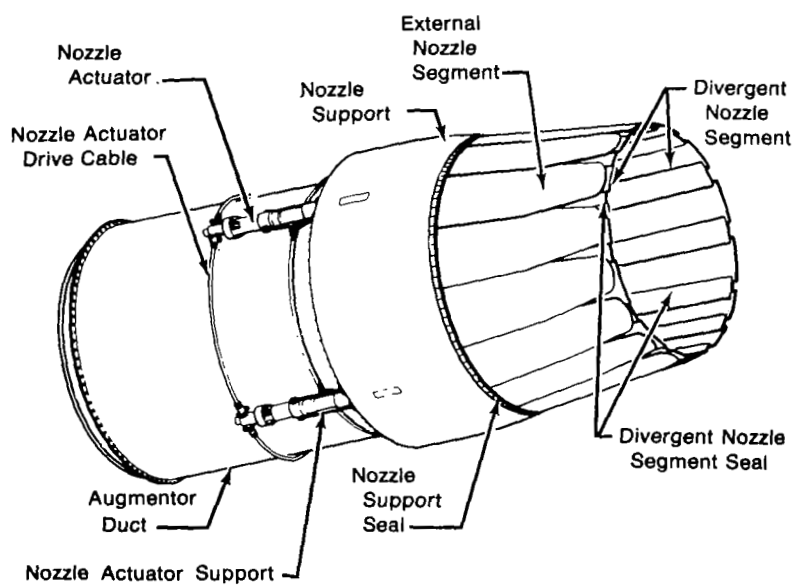


Figure 4.- External duct and nozzle view.

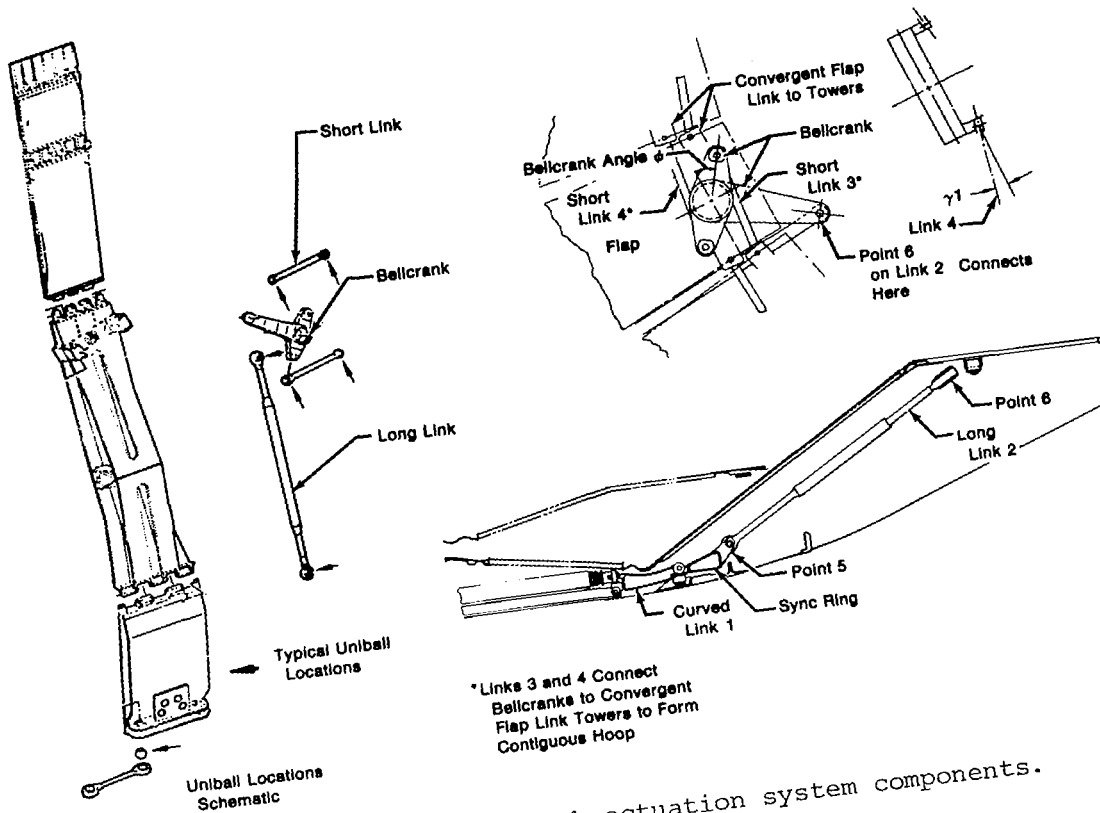


Figure 5.- F100 bellcrank actuation system components.

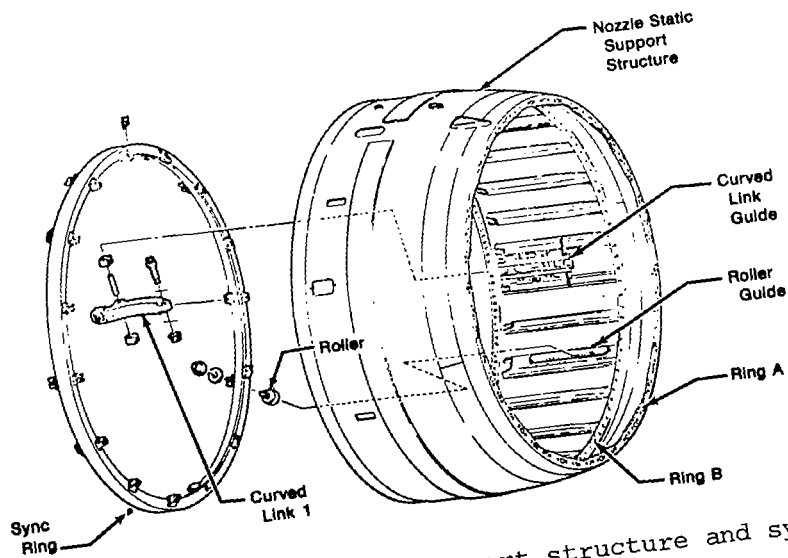


Figure 6.- Exploded-view static support structure and sync ring.

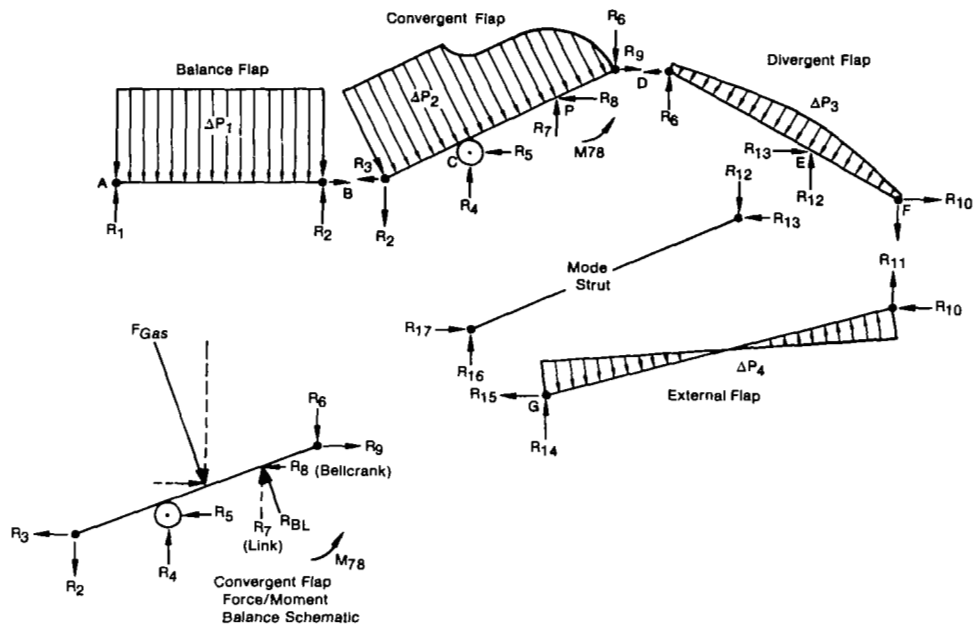


Figure 7.- Free body diagram of flap and mode strut elements.

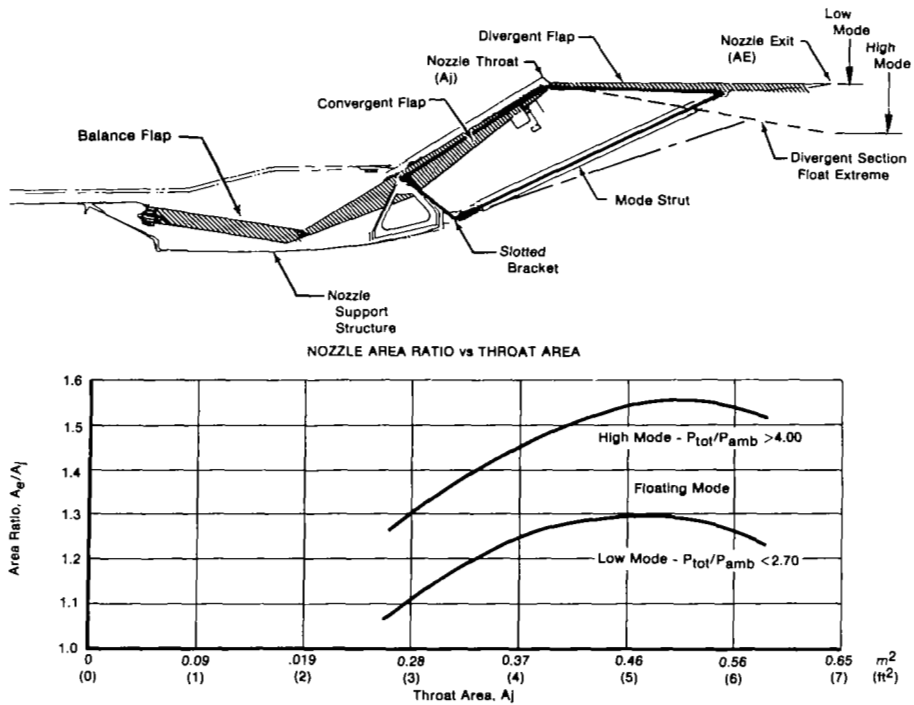


Figure 8.- Four bar linkage and area ratio relationships.

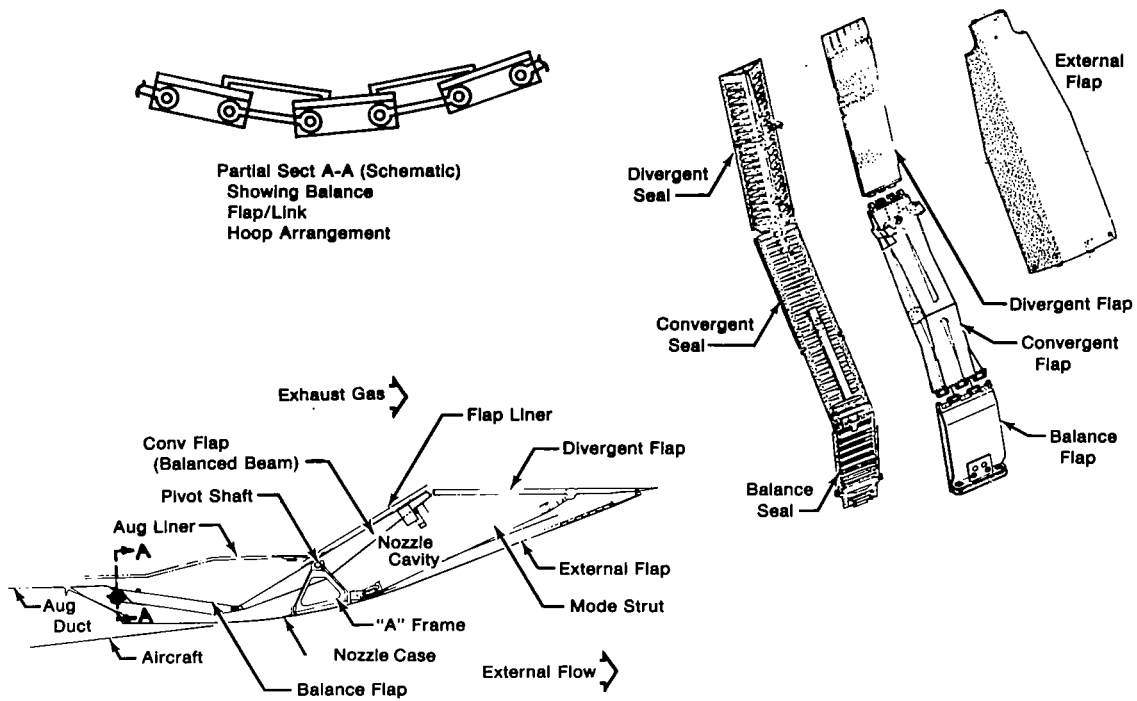


Figure 9.- F100 exhaust nozzle structural components.

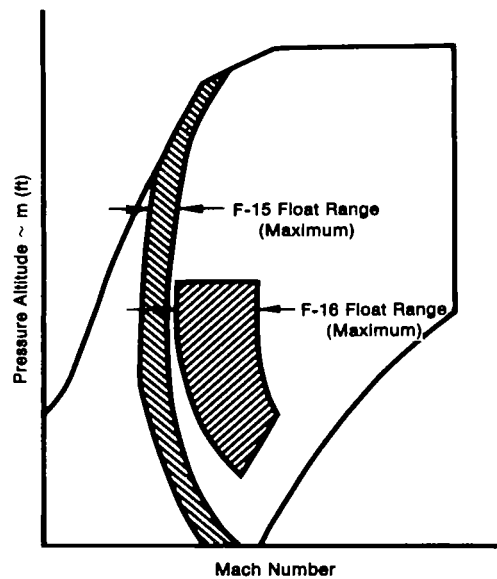


Figure 10.- F100 floating nozzle F-16 float envelope compared to the F-15 estimated float envelope based on test data.

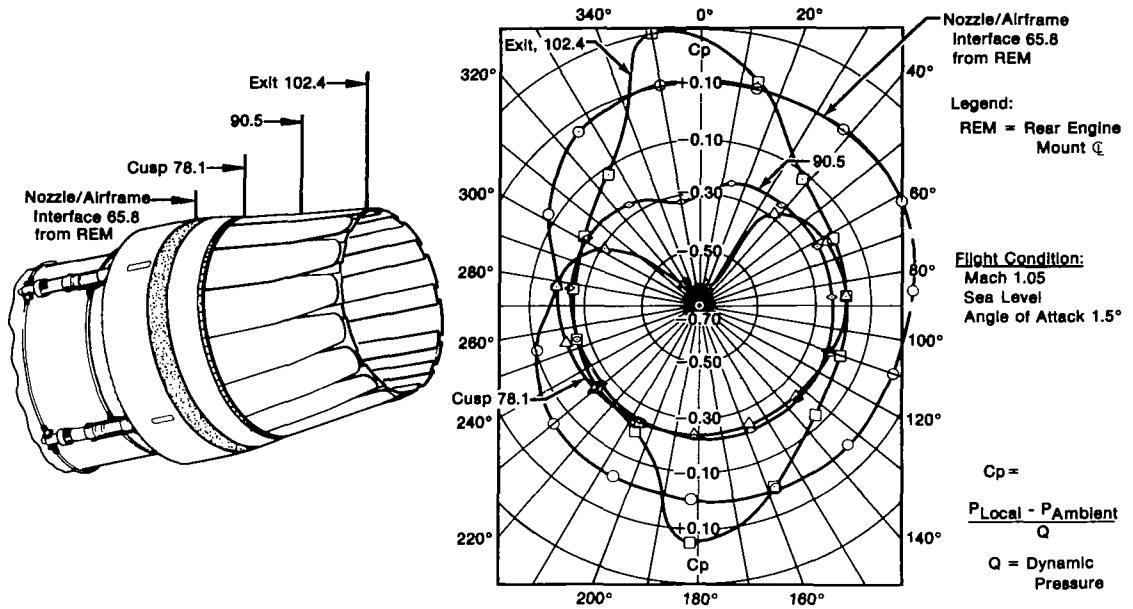


Figure 11.- External flow field pressure coefficient ( $C_p$ ) distribution.

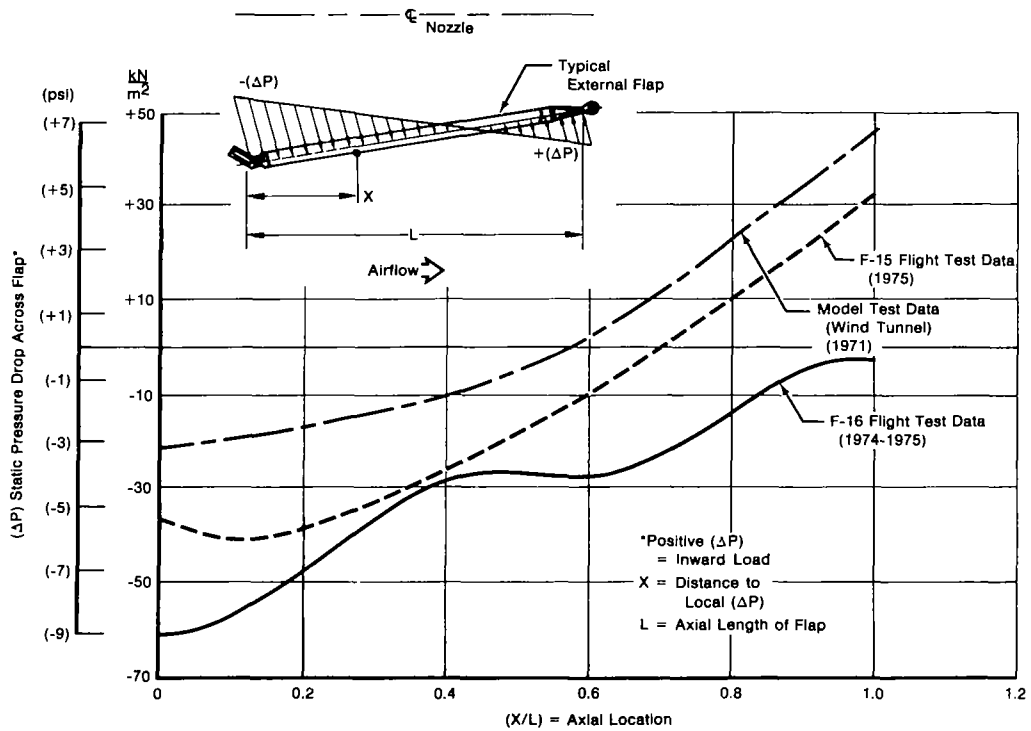


Figure 12.- External flap design loadings history.

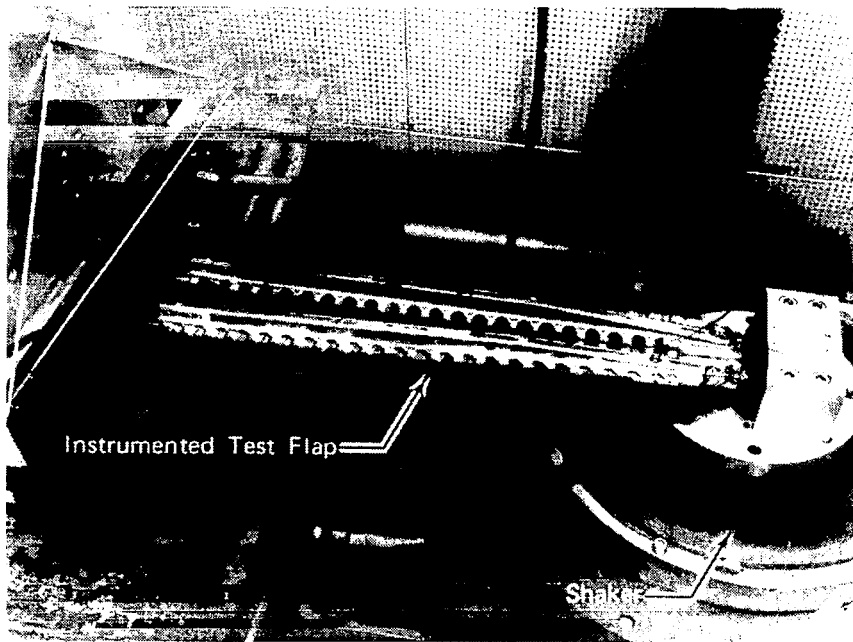


Figure 13.- External flap shaker test.



# AIRPLANE WING LEADING EDGE VARIABLE CAMBER FLAP

James B. Cole  
Boeing Commercial Airplane Company

## SUMMARY

A design solution to an aerodynamic high lift problem was effected by the application of "flexible skin" and "dynamic structure" concepts. Mechanisms and structures were invented to implement these concepts and provide the desired solution.

The paper covers the following subject matter: 1) Problem Solved 2) Scope 3) Definition 4) Invention and Design Evolution 5) Flexible Skin Technology 6) Actuation Scheme 7) Vibration and Flutter Considerations 8) Operating Experience 9) Applications and Usage 10) Concluding Remarks.

## PROBLEM SOLVED

This paper deals with the invention and design of an aerodynamic high lift device which provided a solution to an aircraft performance problem. The performance problem in general was that of converting a high speed cruise airfoil into a low speed aerodynamic shape that would provide landing and take-off characteristics superior to those available with contemporary high lift devices. More specifically, the need was for an improved wing leading edge device that would complement the high lift performance of a triple slotted trailing edge flap. The solution provided was the invention of the wing leading edge variable camber flap.

## SCOPE

This paper will deal primarily with the mechanical and structural aspects of the variable camber flap and will present the aerodynamic performance aspects only as they relate to the invention and design of the device.

## DEFINITION

What is a variable camber flap? For the purposes of this paper, a variable camber flap is the patented device which was invented and designed for use on the Boeing 747 airplane.

In order to eliminate any misunderstanding regarding the term "variable camber" as applied to this device, the term is used to describe the camber change that occurs to the flap panel as it is extended from its relatively flat shape, when stowed as part of the wing lower surface to its fully cambered shape in the extended high lift position, and not to describe a change in camber after it is extended to its operating position. In other words this device is a two position device that does not have the ability to vary its camber once it is extended. This latter feature, however, is very attractive from an aerodynamic standpoint, and an invention which provides such a feature is described in Patent No. 4,159,089 Three Position Variable Camber Flap. This paper, however, will be restricted to the two position concept.

## INVENTION AND DESIGN EVOLUTION

The quotation from Plato, "Necessity is the mother of invention," certainly applies to this invention. It was invented to satisfy an aerodynamic need. The need was for a leading edge device that was more powerful than the familiar leading edge slat and Krueger flap. (See Figures 1 and 2.) Such a device was needed to complement the powerful 747 triple slotted trailing edge flaps in order to provide an airfoil configuration that would have a sufficiently high coefficient of lift to meet landing and take-off requirements. Exactly what was required to accomplish this was not initially clear. However, the shortcomings of the slat and Krueger flap were pretty well known, and it was felt that the correction of these should result in a configuration that would improve the wing stall characteristics at high angles of attack. The needed improvements were as follows: (See Figure 3.)

1. A contour with a larger leading edge nose radius whose shape is similar to a logarithmic spiral.
2. Good extension to provide an increase in wing area.
3. Elimination of any breaks or cut-outs on the wing leading edge upper surface.

In evaluating these improvements and experimenting with various mechanical concepts it became evident that a new approach would be required in order to provide an increase in the upper surface camber. The slat and the Krueger flap are essentially devices that deploy rigid sections of the wing leading edge structure which do not have adequate camber or the right camber when they are deployed as high lift devices. Some means of tailoring the camber of these surfaces was needed. If the shape of the surface was to be changed, it followed that the surface skin would have to be flexible. If the skin was flexible, a means of shaping and supporting it would be required. Some sort of dynamic structure that would simultaneously support the skin and control its camber was required. These "flexible skin" and "dynamic structure" concepts could be applied to either a slat or Krueger flap; however, the flap seemed to be a more promising candidate for the following reasons: 1) It doesn't produce a break in the upper wing surface. 2) There is no loss in the overall chord of the fixed wing structure as with a slat. 3) The cambering and support mechanisms for a flap would penetrate the lower surface of an airfoil, while the mechanism for a slat would penetrate the critical upper surface, creating potential air flow separation problems. 4) A flap is rotated into position providing good relative motion for mechanism slaving purposes. A slat is essentially translated into position providing little slaving motion potential.

A process of design, test and evaluate was initiated in an effort to turn the "flexible skin" and "dynamic structure" concepts into a hardware design that would not only solve the aerodynamic problem, but also would be structurally sound, safe and reliable. Figures 4 through 7 show some of these designs. They are only a portion of the designs involved in this effort, but they are representative of the design evolution. Out of this effort certain requirements and criteria were established. (See Figure 8.) The following is a list of these:

1. The flexible skin panel camber must not exceed the limits imposed by the combination of bending strength, fatigue strength and stiffness requirements.
2. Good extension and nose radius requirements are best met by combining a flexible skin panel with a separate folding nose structure.

3. In order to produce and maintain a given aerodynamic shape the flexible panel thickness must be tailored and the panel curvature must be controlled by at least 3 spanwise supports.
4. The panel must be positively supported throughout its extension and retraction cycles.
5. The panel should not be part of the support load path.
6. The support mechanism should not flex the skin panel to a tighter bend radius during extension than the bend radius at full extension in order to prevent reduction of its fatigue life.
7. The kinematics of the "dynamic structure" mechanism must simultaneously position and camber the flap panel while rotating the folding nose into its extended position to satisfy the aerodynamic angle, gap and shape requirements.
8. The kinematics must move the flap panel parallel to the undersurface of the wing during initial extension to ensure a good panel fair and prevent seal damage.
9. The actuator must be capable of rotating the flap approximately  $135^{\circ}$ .
10. The flap mechanism must provide maximum flap extension without penetrating the wing nose structure which contains a thermal anti-icing duct.
11. The kinematic solution and flap geometry should be developed so that the same flap hardware can be used on as much of the wing span as possible in order to reduce fabricating and maintenance costs.
12. The retracted flap mechanism must fit into and be compatible with the fixed leading edge structure and must accommodate the systems passing through this area (electrical, flap drive, controls, anti-icing, etc).

Figure 9 shows the mechanism that evolved to fulfill the "dynamic structure" concept. This mechanism, in conjunction with a flexible skin panel and folding nose, was able to meet all of the foregoing requirements and criteria. This mechanism consists essentially of three four-bar mechanisms in a series arrangement. In addition, there is a crank arm and link which program the motion of the center flap panel support. The first four-bar mechanism consists of those members connected at points A, B, C and D, the second at points B, E, H and G, and the third at H, K, M and N. The crank arm is part of the member GHJK which is one solid part, and the center link is JL.

The kinematic solution for this mechanism was obtained primarily by using graphical techniques in conjunction with a computer program. The computer program is essential for a precise solution and for the contour matching process that is required to adapt one common mechanism to an ever-changing wing surface. This process consists of solving for the coordinates of points A, D and C so that the panel attachment points F, L and N will cause the flap panel to fair with the lower wing surface. This obviously is a very important economic feature since it allows one common mechanism to be used in a number of places along the wing span. On the 747 the same mechanism is used in 20 different locations. This would increase to 40 if the same flap chord length was used for all 20 variable camber flaps. Such economies are not possible with a slat or Krueger flap because, as previously stated, they are devices that deploy rigid structural sections of the wing whose cross sections constantly vary.

A kinematic solution by computer alone is certainly possible, but the constraints imposed by the structural envelope are not exact and, therefore, the number of solutions is almost limitless. The problem of defining constraints for a computer program is the most difficult for linkage points in the retracted position. As can be seen in Figure 9 the mechanism is confined in a very compact area. The only points that can be defined exactly are points F, L and N in the extended positions. All other points are free to move within the limits imposed by: 1) the structural envelope; 2) interference with other members; 3) size of the members; and 4) the limits imposed by kinematic requirements 6, 7, 8 and 9.

Needless to say, a great deal of kinematic visibility is required in order to work out a satisfactory solution. It is needed not only in the extended and retracted positions, but also throughout the cycle. A computer combined with a cathode ray tube display can provide this visibility; however, computer simulation of panel flexing is very difficult. Graphical solutions not only provide the required visibility, but with modeling techniques the simulation of skin panel flexing is easily accomplished. Graphical solutions in this application are also more economical from both a time and equipment standpoint. However, once a solution is established, its conversion into a computer program is a must for the reasons previously stated.

### FLEXIBLE SKIN TECHNOLOGY

A separate paper is required to make a rigorous presentation of this subject. For this reason, only the highlights of the problem involved and its solution will be discussed. The problem essentially consists of finding a material and its dimensional proportions that will satisfy the previously stated bending strength, fatigue strength and stiffness requirements imposed on a flexible skin panel by air loads, bending loads and aerodynamic shape.

In the retracted position the skin panel stiffness (thickness and modulus of elasticity) must be sufficiently high to prevent deflections that exceed aerodynamic smoothness requirements when the panel is exposed to cruise airloads. In the extended position the panel thickness ( $t$ ) and modulus of elasticity ( $E$ ) must be sufficiently low and the bend radius ( $R$ ) sufficiently high so that the resulting bending stress ( $s$ ) does not exceed the allowable fatigue strength of the panel material. This is reflected by the equation

$$s = Et/2R. \quad (1)$$

At the same time this stress should be higher than the stress imposed by air loads in the extended position to prevent distortion of the aerodynamic shape. To compound the problem, the panel thickness proportions must be tailored to produce the desired aerodynamic shape. This shape is obtained by varying the thickness ( $t$ ) in accordance with the equation

$$t = (12 RFx/E)^{1/3} \quad (2)$$

which is derived from the equation

$$R = EI/M \quad (3)$$

where ( $R$ ) is the radius of the elastic curve, the moment of inertia  $I = t^3/12$  for a one unit wide strip and the bending moment  $M = Fx$  where ( $F$ ) is the force acting on the panel at a

distance (x) from the support point. The force (F) is determined from the transposed equation (2)

$$F = Et^3/12Rx \quad (4)$$

where the thickness (t) at the critical section (smallest radius of curvature) is determined by the allowable fatigue stress, Eq (1).

The best material evaluated for this application was a solid epoxy fiberglass laminate where, as a rule of thumb, the panel thickness was not less than 1/100th of the bend radius. This material and the foregoing dimensional tailoring were successful in solving the strength and stiffness problems of the flexible skin panel.

#### ACTUATION SCHEME

The means of actuating the multiple four-bar mechanism was initially an item of concern because linear actuators in the form of either a hydraulic cylinder or ball screw were not able to provide adequate rotation of the main support member ABG. The 135° requirement is a great deal of rotation for a linear actuator acting on a simple crank arm. The moment arms at the ends of a 135° crank arm stroke are so small that the resulting loads are impractical to handle. On previous Boeing aircraft the high lift devices were actuated with linear actuators, but it was apparent that a departure was needed for this application. The solution was a rotary actuator as shown in Figure 10. This actuator is a planetary gear box with an approximate 240:1 gear reduction. The adoption of this new actuator for this application turned out to be a blessing in disguise since its compact design and high torque resulted in both a space saving and significant weight reduction.

#### VIBRATION AND FLUTTER CONSIDERATIONS

Because of the many joints in the flap support mechanism plus the high degree of extension and air loading, vibration and flutter were items of initial concern. To satisfy this concern, both laboratory and flight tests were conducted on the variable camber flaps. These tests had a very happy ending and revealed some unanticipated virtues of the design.

Vibration tests were conducted in the laboratory by attaching shaker pots to the flap structure in order to determine its natural frequency. The frequency band was very broad, with no critical peaks. The dampening effect was provided by the flexible fiberglass panel which acts as a large spring under tension. This spring tension preloads the joints of the linkage mechanism, thereby removing any play due to tolerances and wear. In the retracted position, the panel spring effect is replaced by preloading the mechanism against up-stops.

Flight tests were conducted on a Boeing 707 by replacing the Krueger flaps between the engines with variable camber flaps. The Krueger flaps outboard of the engine were left intact for comparison purposes. These tests confirmed the laboratory tests and demonstrated their freedom from vibration and flutter. The variable camber flaps demonstrated excellent stability under all flight conditions tested, including stall. Their stability was visibly superior to that of the Krueger flaps.

During these flight tests the flap and wing surfaces were tufted in order to observe the aerodynamic flow of the air. Air flow separation occurred on the Krueger flaps and, of

course, on the wing at very high angles of attack, but there was no separation on the variable camber flaps even at stall, attesting to their superior aerodynamic shape.

### OPERATING EXPERIENCE

Because of the limited nature of this paper, the operating experience will be confined to the following comments:

The 747 has been in operation over 12 years. The overall operating performance of the flap mechanism and structure has been excellent.

Because over one thousand bearings are used in the 747 variable camber flap mechanisms, a self-lubricating bearing design was adopted in place of one requiring grease fittings for periodic lubrication. The self-lubricating feature is provided by a TFE (tetrafluorethylene) fabric liner. Because of some early unsatisfactory experience with TFE bearings it was felt that they might not provide the required service life. However, these bearings have given excellent service to date with little or no replacement required. We feel the following two items have contributed to this good performance: 1) a low bearing stress design; and 2) the elimination of cyclic loading from vibration and flutter provided by the flap panel camber preload.

### APPLICATION AND USAGE

The variable camber flap is in use on the following aircraft:

- All Boeing 747 models
- Boeing YC-14 prototype

It was incorporated in the following aircraft designs:

- Boeing B-1 design proposal
- Boeing 727-300 design proposal
- Boeing 7N7 design proposal
- Boeing 7X7 design proposal

Because of the emphasis on fuel economy it is not being used on the initial models of the Boeing 757 and 767 airplanes, but it may be used on short-field versions of these aircraft if Boeing decides to offer them at a later date.

### CONCLUDING REMARKS

The wings of a bird are beautiful examples of the "flexible skin" and "dynamic structure" concepts. If we can approach their sophistication and reliability in the design of future aerodynamic high lift devices, then, perhaps, we will realize the aerodynamic versatility required to successfully combine high and low speed flight.

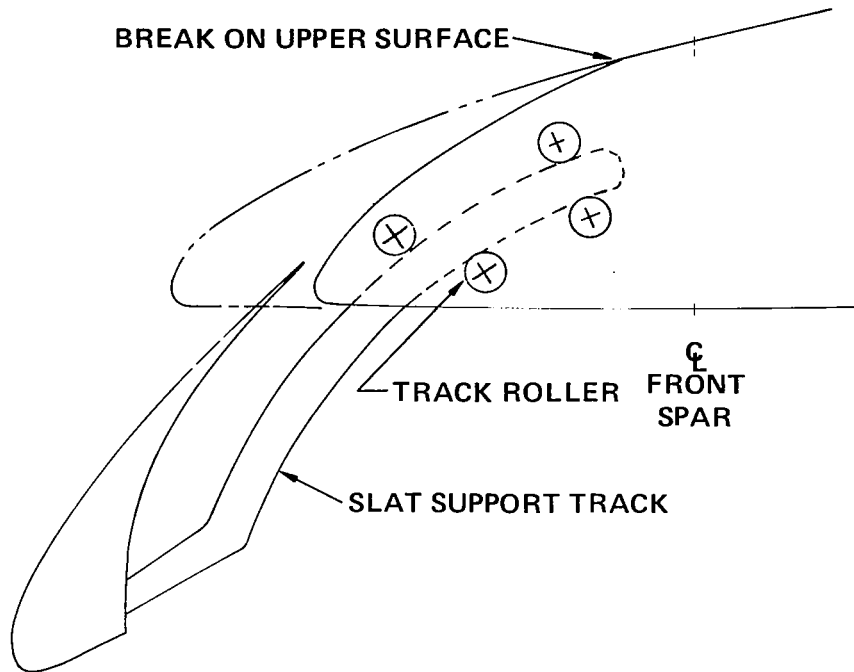


Figure 1.- Wing leading edge slat.

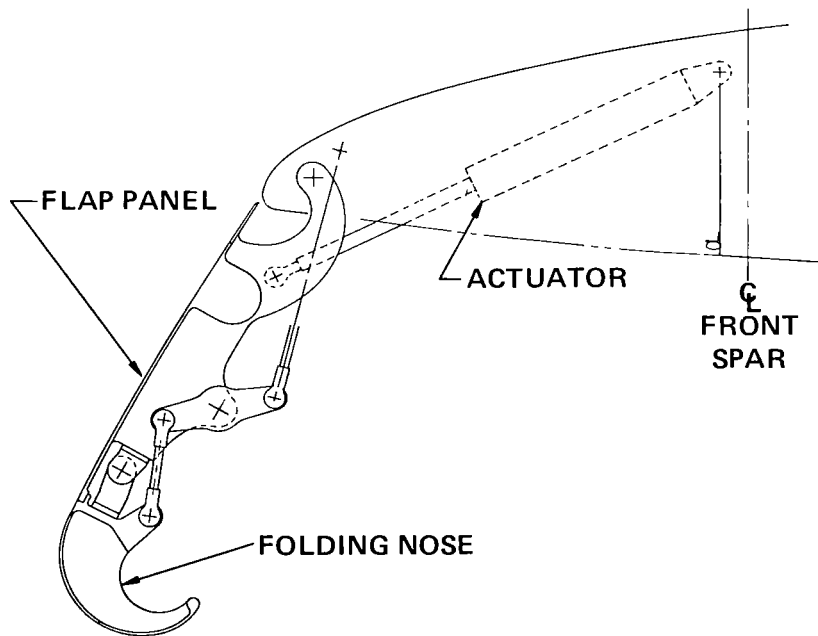


Figure 2.- Wing leading edge flap.

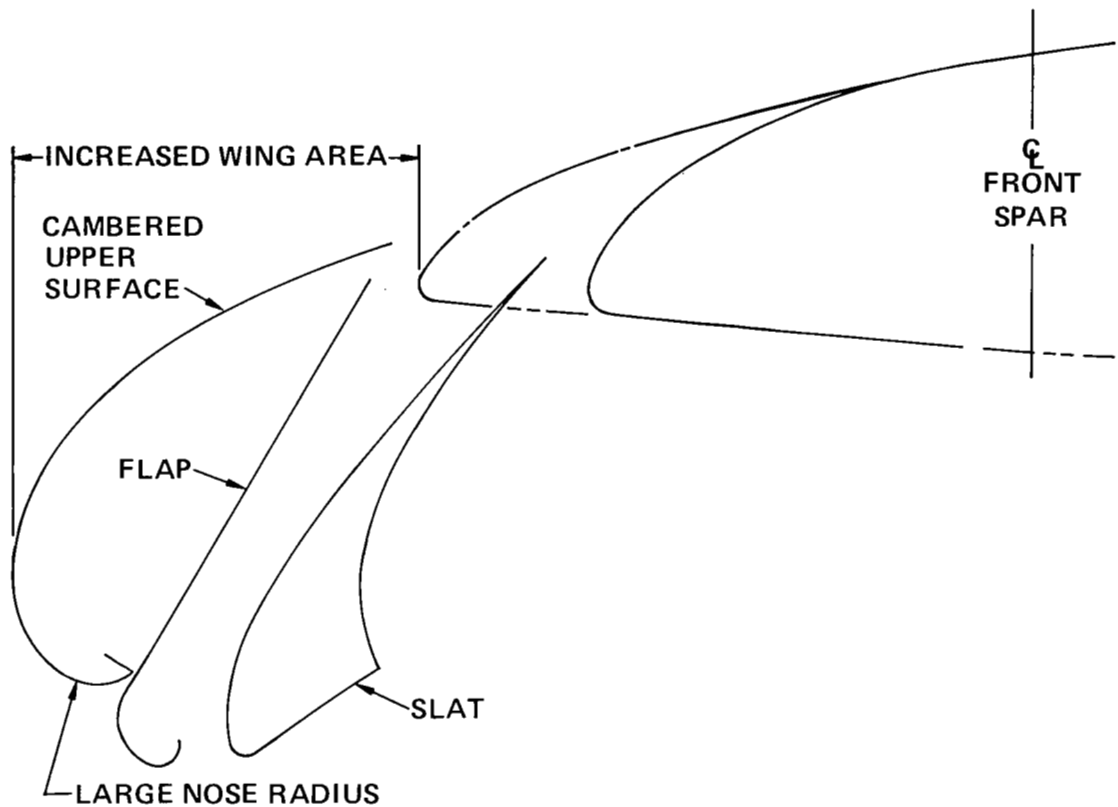


Figure 3.- Aerodynamic improvements.

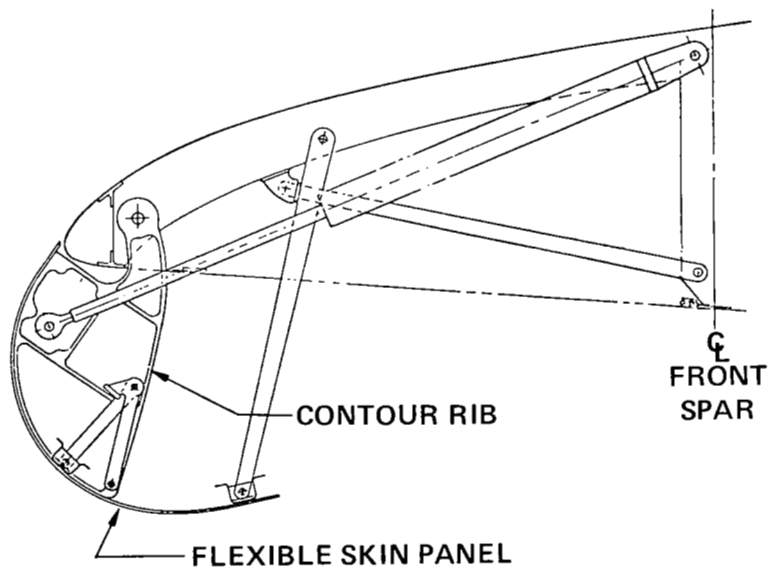


Figure 4.- Flexible Krueger flap.

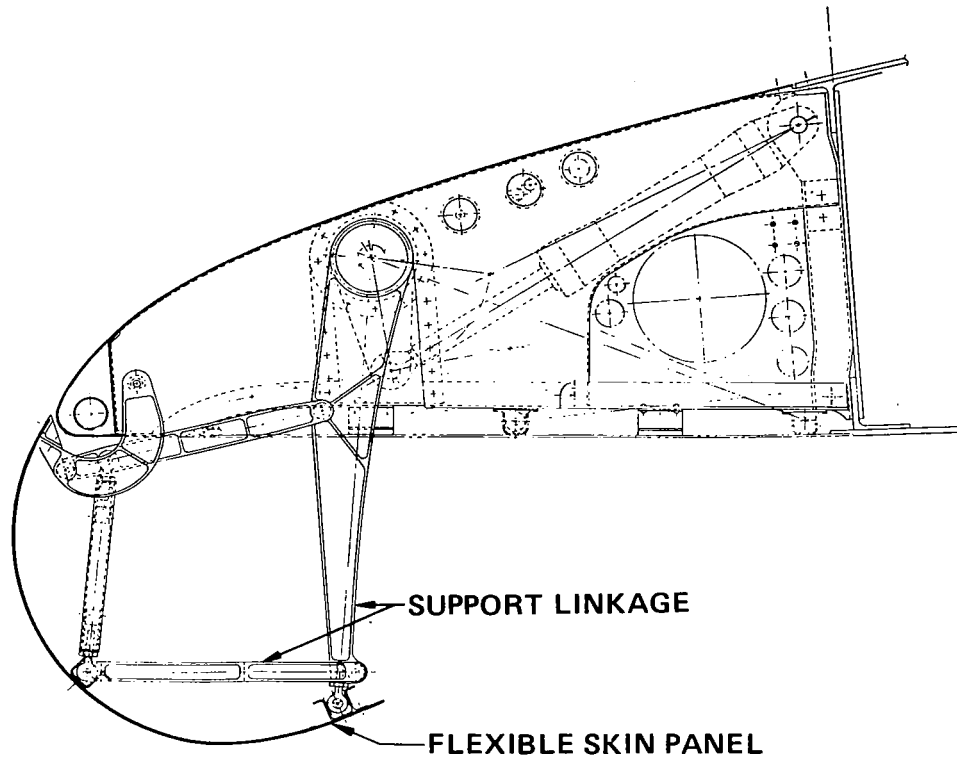


Figure 5.- Flexible Krueger flap.

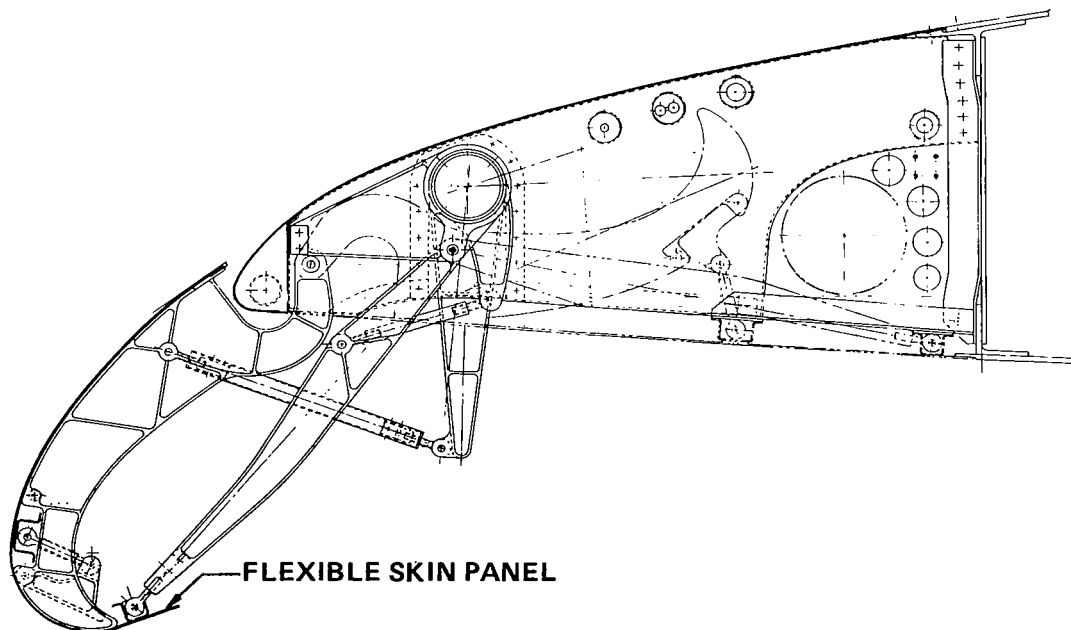


Figure 6.- Flexible Krueger flap.

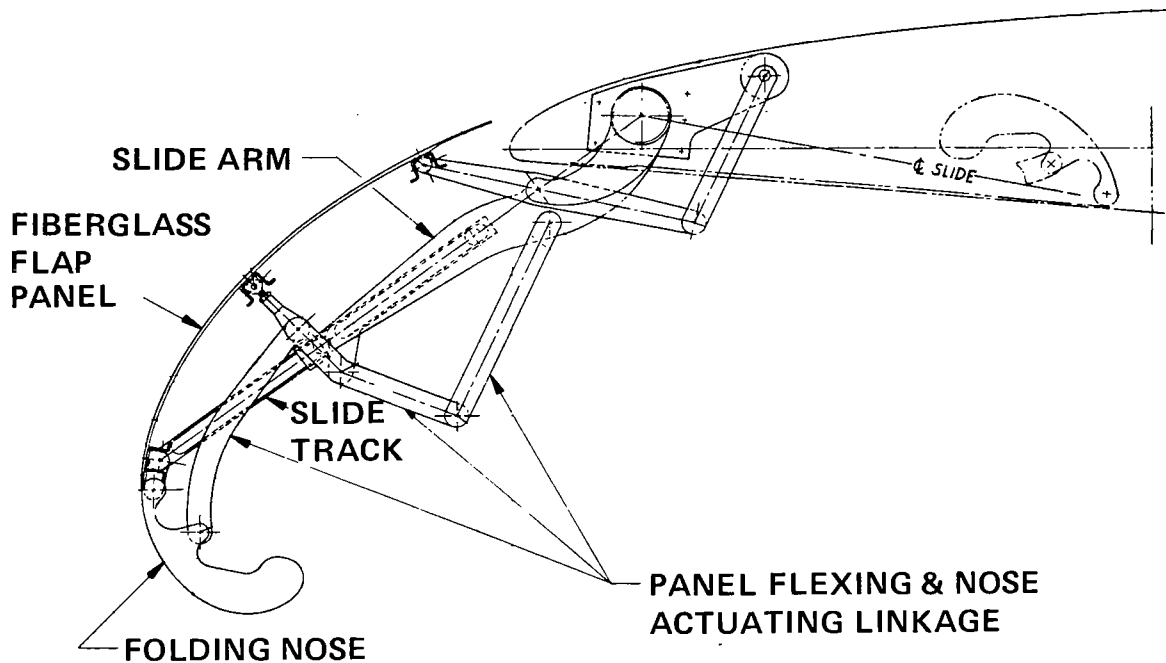


Figure 7.- Variable camber flap with slide.

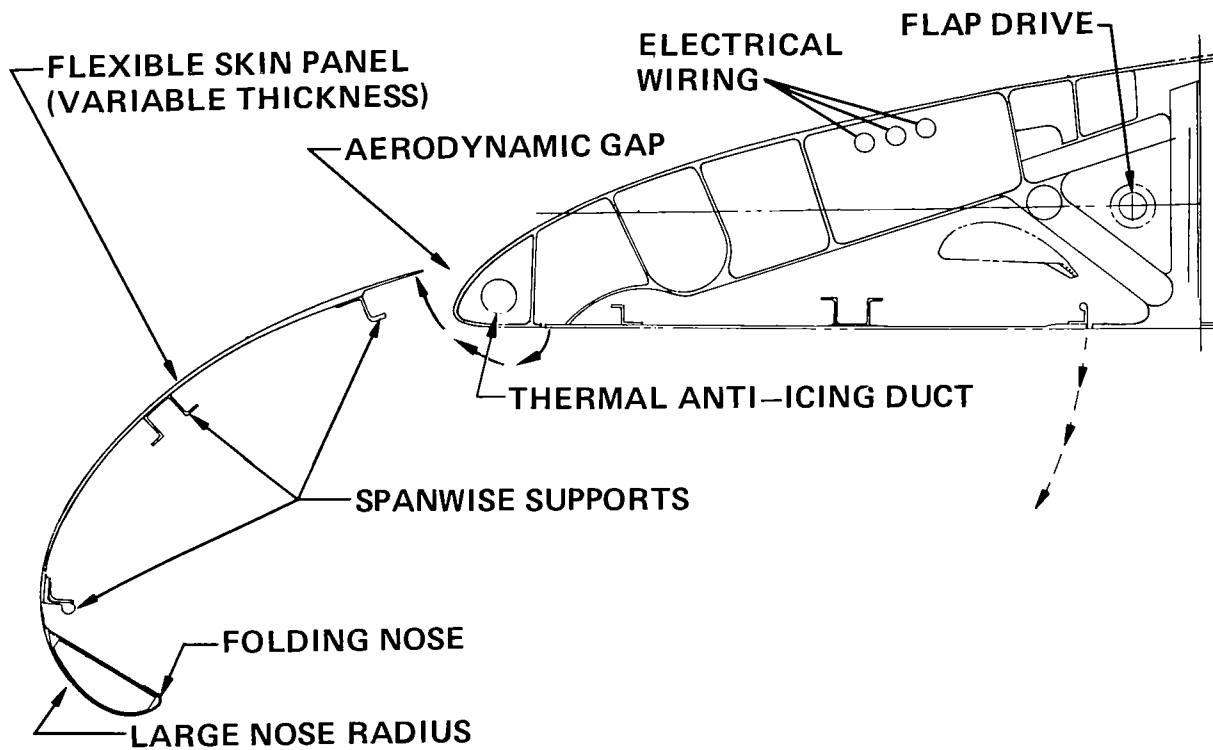


Figure 8.- Leading edge flap requirements.

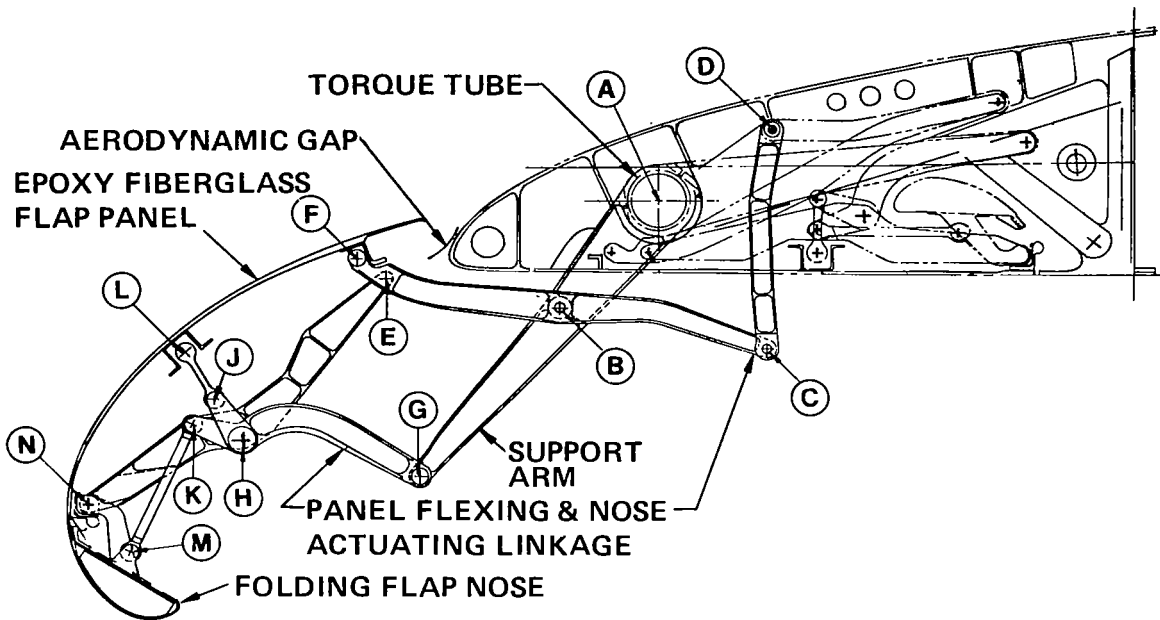


Figure 9.- Wing leading edge variable camber flap.

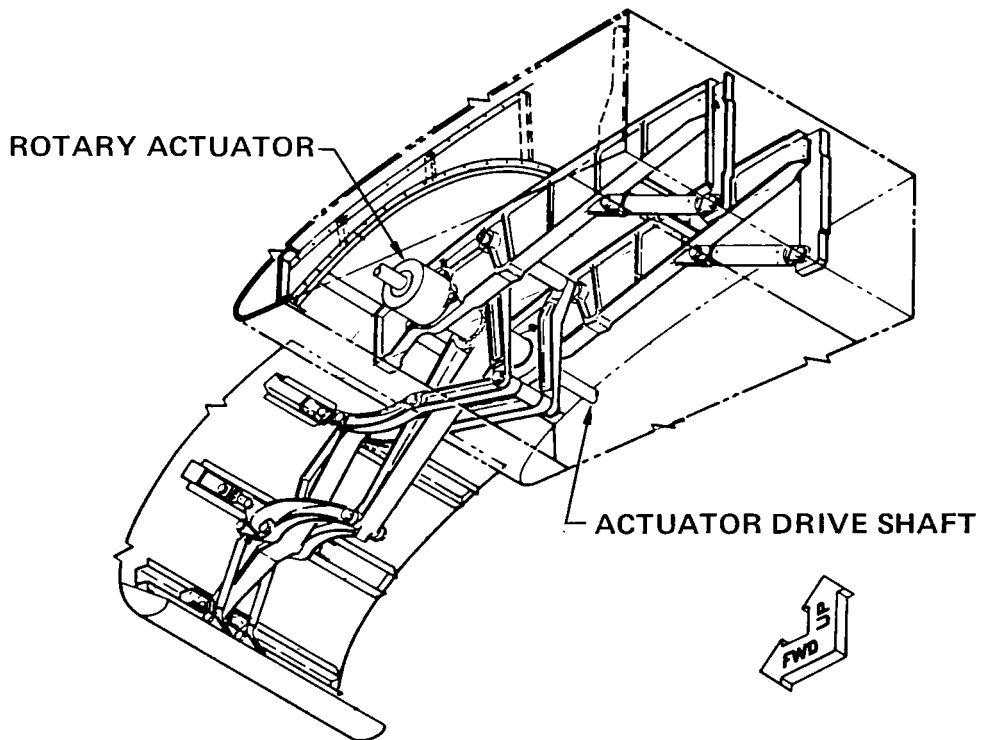


Figure 10.- Variable camber flap with rotary actuator.



A MECHANICAL ADAPTER  
FOR INSTALLING MISSION EQUIPMENT  
ON LARGE SPACE STRUCTURES

A. LeFever and R. S. Totah  
Members of the Technical Staff  
Space Operations & Satellite Systems Division  
Rockwell International Corporation  
Downey, California

ABSTRACT

In the construction of large space systems, the installation of mission equipment and payloads on structural platforms poses a serious challenge to space construction operations. For such operations, attachment mechanisms are required that promote simple and quick mate and demate capabilities and provide a rigid connection during mission operations. While under contract to the National Aeronautics and Space Administration (NASA), Rockwell International has designed, constructed, and tested such a mechanical attachment adapter in NASA's Neutral Buoyancy Simulator (NBS) at Marshall Space Flight Center, Huntsville, Alabama. The adapter was included in a simulation program that investigated techniques for assembling erectable structures under simulated zero-g conditions by pressure-suited subjects in a simulated EVA mode. The adapter was utilized as an interface attachment between a simulated equipment module (SEM) and one node point of a tetrahedral structural cell. The mating performance of the adapter, a self-energized mechanism, was easily and quickly demonstrated and required little effort on the part of the test subjects.

INTRODUCTION

In the study of large space systems, initial emphasis has been placed on beams and joining concepts for various structural configurations. Since equipment installations are considered basic and routine operations even on the earliest of missions utilizing large space structures, interface concepts must be generated to promote "easy" mate and demate capabilities with positive verification in the orbital environment.

An operational concept for installing mission equipment on a large space platform was investigated by Rockwell International during a study of Erectable Large Space Systems for Langley Research Center. A subsequent effort by Rockwell while under contract to Langley Research Center and Marshall Space Flight Center concerned, among other objectives, the design of a self-energized mechanical adapter that could function as the interface between mission equipment and structure.

This paper discusses the fundamental requirements of such mechanical interfaces and presents two concepts considered during the study. One of the

concepts underwent a proof-of-concept design, and a prototype unit was fabricated and tested. The design will be described, along with the test and its results.

### FUNDAMENTAL REQUIREMENTS

The main function of the adapter is to provide a structurally sound interface between any two assemblies. For illustration, let us assume the assemblies of interest are a large space truss platform structure and mission equipment made up of individualized modules, as shown in figure 1. The adapter is the structural connection that couples each module to the platform. In that function, the adapter must be rigid and capable of supporting loads imposed on it throughout the life of the mission. These include impact loads during construction, orbit transfer loads, and operational loads caused by dynamic modules.

The adapter must also satisfy several important operational requirements and features. A simple and easy engagement mechanism on the adapter is essential to facilitate its attachment manually or remotely. The initial insertion must be forgiving in terms of alignment and orientation, but once engaged, the attachment must be rigid and provide a specific orientation (clocking) in all three axes. The adapter must also provide a positive indication of engagement, and a disengagement capability for contingency and maintenance operations.

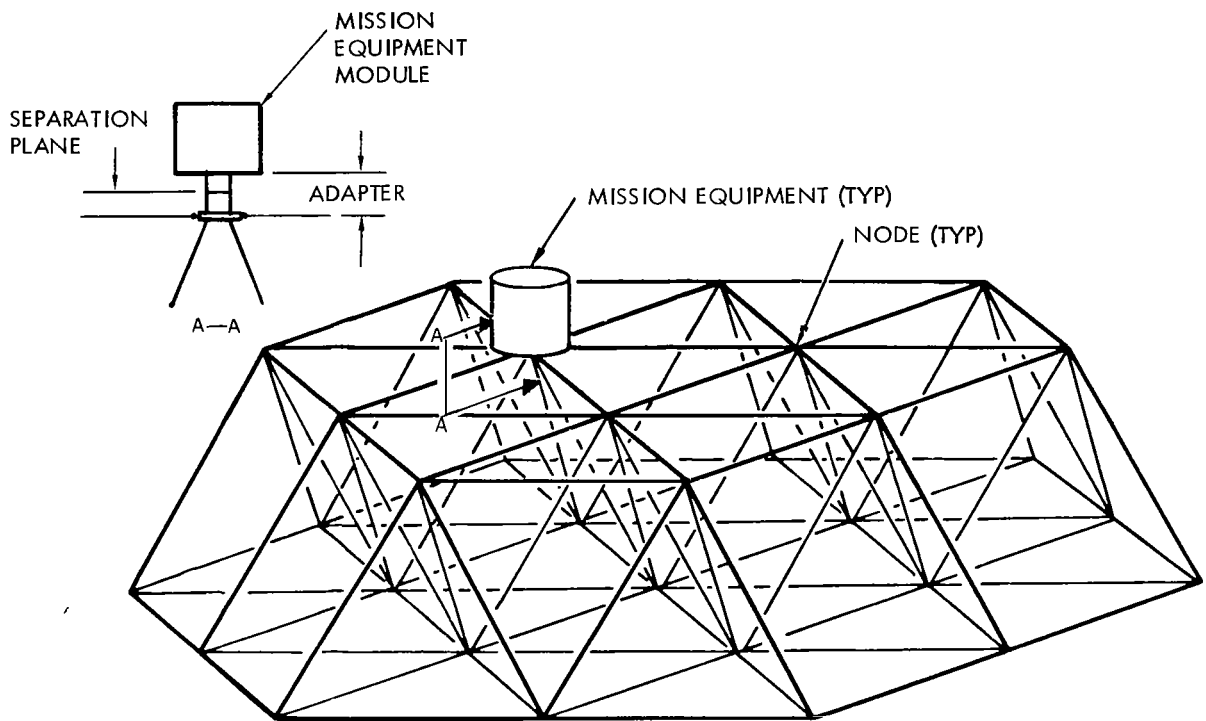


Figure 1. Representative Structure

## DESIGN CONCEPTS

To satisfy the fundamental requirements, two adapter concepts were generated during the design of the test hardware. The concepts, a ball-socket adapter and a self-energized screw adapter, were subjectively evaluated, and the latter emerged as the best candidate for further detail design. Both concepts are described in this section, along with discussions of their operational features that had a bearing on the final selection. It should be emphasized that, although the following discussions and illustrations show the female half of the adapter as part of an erectable structure node union, its application is by no means limited to a node point or to the erectable structure.

### Ball Socket Adapter

The first adapter concept to be considered for the test is based on a ball socket joint design developed for the joining of structural elements during space construction (reference 1). The main advantage of the ball socket joint was its operational ease which was verified during ground simulations involving both remote and EVA assembly techniques (references 2 and 3). The ball socket adapter, illustrated in figure 2, is essentially a probe drogue coupling where the probe is part of the module and the drogue is incorporated within the cavity of the node union.

The probe is engaged in a two-step latching procedure. First, as the module is positioned "over" the node union and slowly "lowered" into posi-

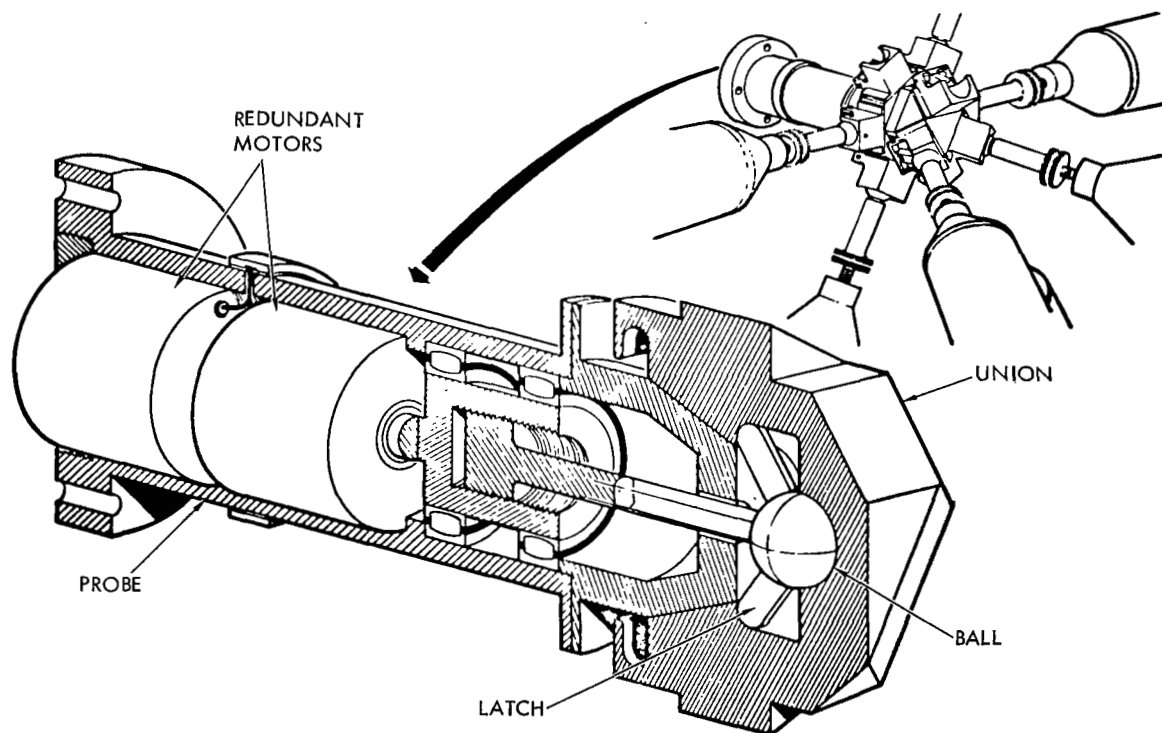


Figure 2. Ball Socket Adapter

tion, the ball end of the probe engages the drogue and its latches. In the second step, the drogue's redundant motors are activated to drive the tapered shell of the probe into the cavity of the union and effect a rigid interface. The motors could be torque-limited and reversible so that disengagement would be effected, if warranted. Power for the motors could be supplied by the manipulator or by EVA astronauts through hand tools, depending on which module installation method is employed.

The two-step engagement operation of the ball socket adapter is an advantage. However, it requires external power which is not easily supplied by either the manipulator or EVA astronauts. While disengagement of the tapered shell can be achieved, the ball disengagement is a more difficult task because of its inaccessibility.

### Self-Energized Mechanical Adapter

This adapter is a self-energized coupling that promotes the quick attachment of relatively large modules on the surface of a large space platform. The active half of the coupling, which drives an Acme threaded screw, forms a part of the module. The other half incorporates a receiving nut into a structural union which represents a node point on the surface of a truss-configured space platform. As depicted in figure 3, the energy source for the adapter is a set

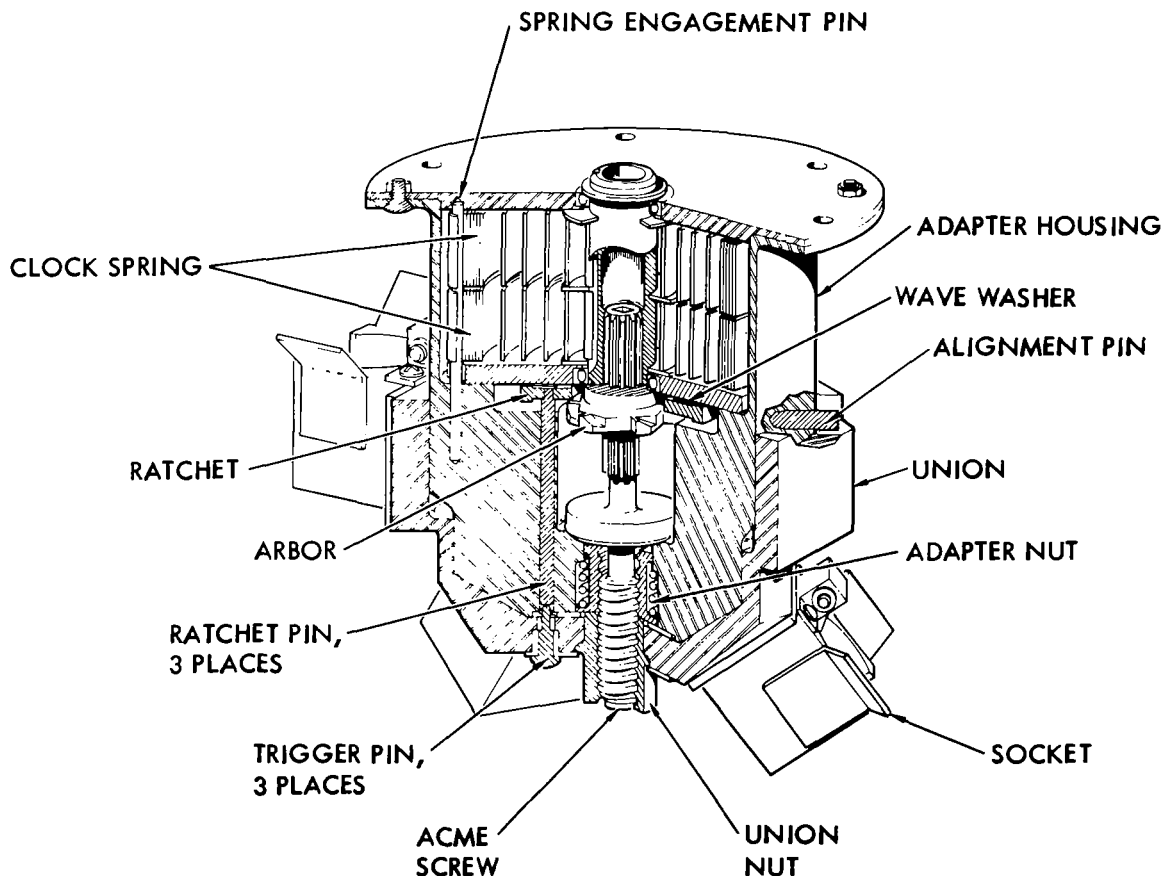


Figure 3. Self-Energized Adapter

of two clock springs that drive the Acme threaded screw into the receiving nut on the mating union. The screw is held in the energized position by a ratchet until triggered by the insertion of the adapter into its union and the application of a slight compressive force on it.

To disengage the adapter, a square-nosed speed wrench can be inserted into a socket at either end of the screw shaft to rewind the screw; this disengages the adapter and reenergizes it at the same time.

This concept fulfills most of the requirements that are expected in such a device. Therefore, it was selected for inclusion in the test. A detailed design and operational description of the adapter is presented in the next section.

#### DESIGN AND OPERATION

The module half of the adapter is a probe that houses all the active components to energize and drive the probe into a rigid attachment with the structural platform. A photograph of the adapter probe and the module is shown in figure 4. The major active components of the probe are:

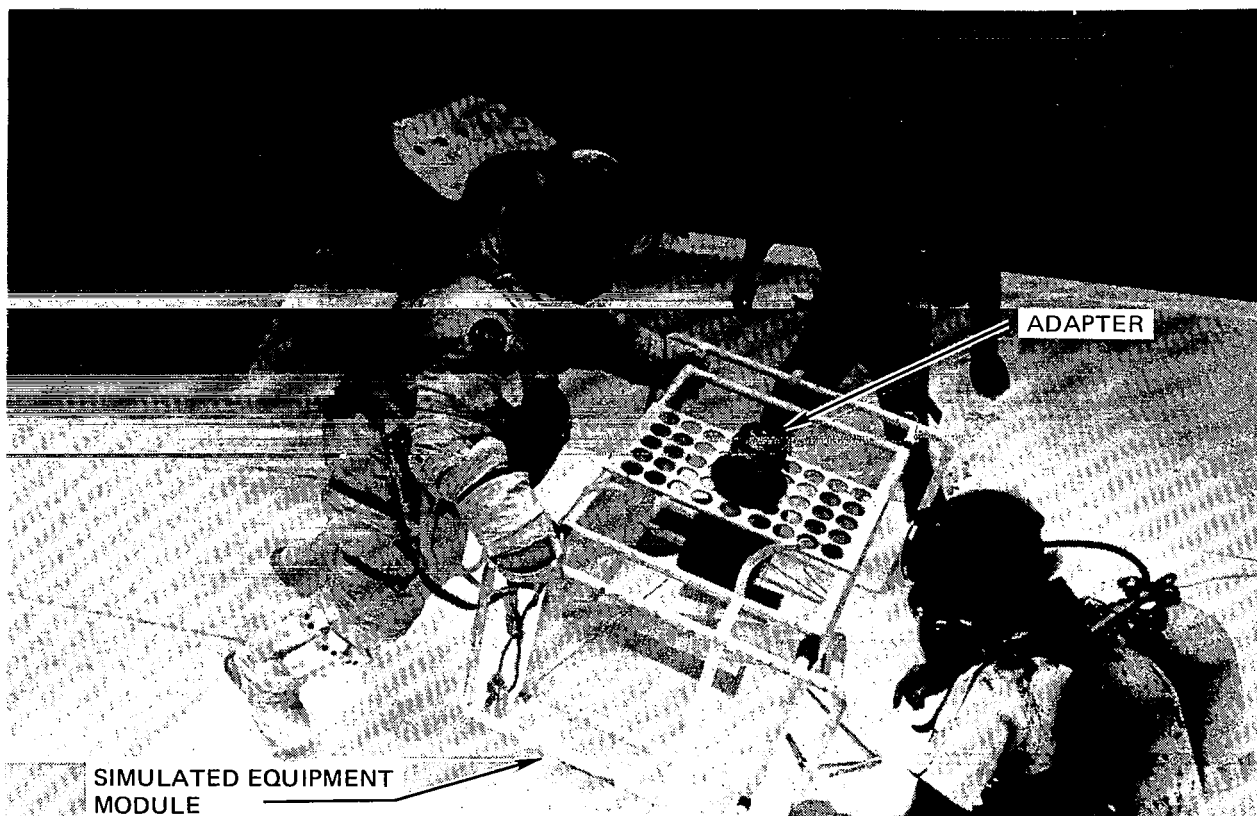


Figure 4. Simulated Equipment Module (SEM)

- Two clock springs which provide the energy for the adapter. The outside lips of both springs are anchored to a single engagement pin. Internally, both springs interface with a rotating arbor.
- An arbor that rotates freely on Teflon journals. Externally, it incorporates a groove for capturing the internal lips of the two clock springs. On one end, there are six teeth for engaging the ratchet. Internally, it contains a spline to couple with the screw shaft in torsion only. The screw shaft is free to slide axially.
- A ratchet that retains the arbor in the energized position until triggered. It accepts the arbor teeth and prevents the arbor from rotating in the clockwise direction only. Three pins are attached to the ratchet which protrude to the leading end of the adapter. The ratchet pins form a part of the trigger mechanism.
- An Acme screw which is partially engaged in an adapter nut. It features a central flange to control its travel by bearing against an adapter housing internal shoulder, and a splined end that couples, torsionally only, with the arbor spline.

The platform half of the adapter is a union that accepts the probe half. The union features a slot to accept the adapter housing alignment pin, three trigger pins that align with the ratchet pins and a captive floating nut to accept the screw when triggered.

Operationally, a module with an energized adapter attached is brought to the node point and "lowered" into it. As the adapter guide pin rides over the lip of the union, the module is rotated until the pin "drops" into its slot and, in the process, the trigger pins are aligned with the ratchet pins. A slight compressive force on the module causes the trigger pins to depress the ratchet pins which disengage the ratchet from the arbor. At that point, the stored energy in the clock springs is released by rotating the arbor and, in turn, the screw. Since the screw is already partially engaged in the adapter nut, it drives itself through to the captive union nut until the flange on the screw shaft seats itself inside the adapter. At that position, sufficient residual energy remains in the springs to assure a positive engagement at all times.

#### TEST METHOD

The mechanical adapter was tested in the Neutral Buoyancy Simulator (NBS) at Marshall Space Flight Center, Huntsville, Alabama, as a portion of the Large Space Systems Erectable Structures Assembly Simulations in which an entire truss cell was constructed under simulated zero-g conditions. As a final task of the construction, a simulated equipment module (SEM) was installed at the node of the truss cell. The SEM was attached by the self-energized mechanical adapter described herein. Two pressure-suited test subjects in a simulated EVA mode manipulated the SEM into position, oriented it, and inserted it to the point where installation was effected. The assembled test article is shown in figure 5.

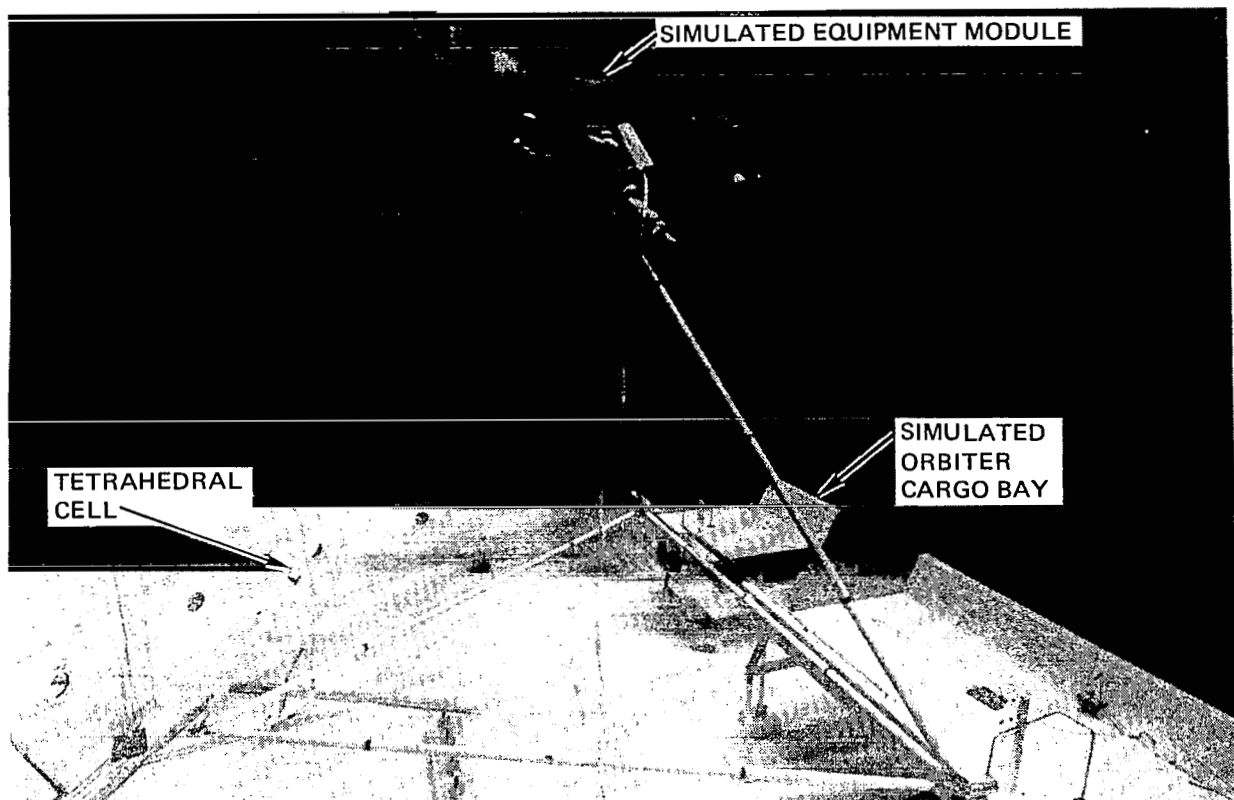


Figure 5. Assembled Test Article

## RESULTS

In the initial series of tests, operational and design difficulties surfaced which resulted in unsatisfactory performance of the adapter. After modification, the adapter operated satisfactorily, and repeated tests showed that the attachment of equipment to a structural platform could be performed by EVA subjects in less than 35 seconds. The relatively easy attachment was rigid and permanent, and imposed no undue loads on the structure.

The first difficulty was encountered in attempting to orient and level the SEM relative to its mating union. In performing that task, the actions of the test subjects seem uncoordinated. Figure 6 illustrates the leveling difficulty, which was eliminated in subsequent tests by adding a work station adjacent to the node of the truss cell.

Once leveling was achieved, the test subjects were unable to trigger the adapter. When repeated attempts resulted in partial engagements at best, the adapter was modified to the configuration shown in figure 7. The major corrective actions included the following:

1. The interfacing surfaces of the union and the adapter were reconfigured to a conical shape to eliminate a suspected binding of the original stepped cylindrical surfaces.

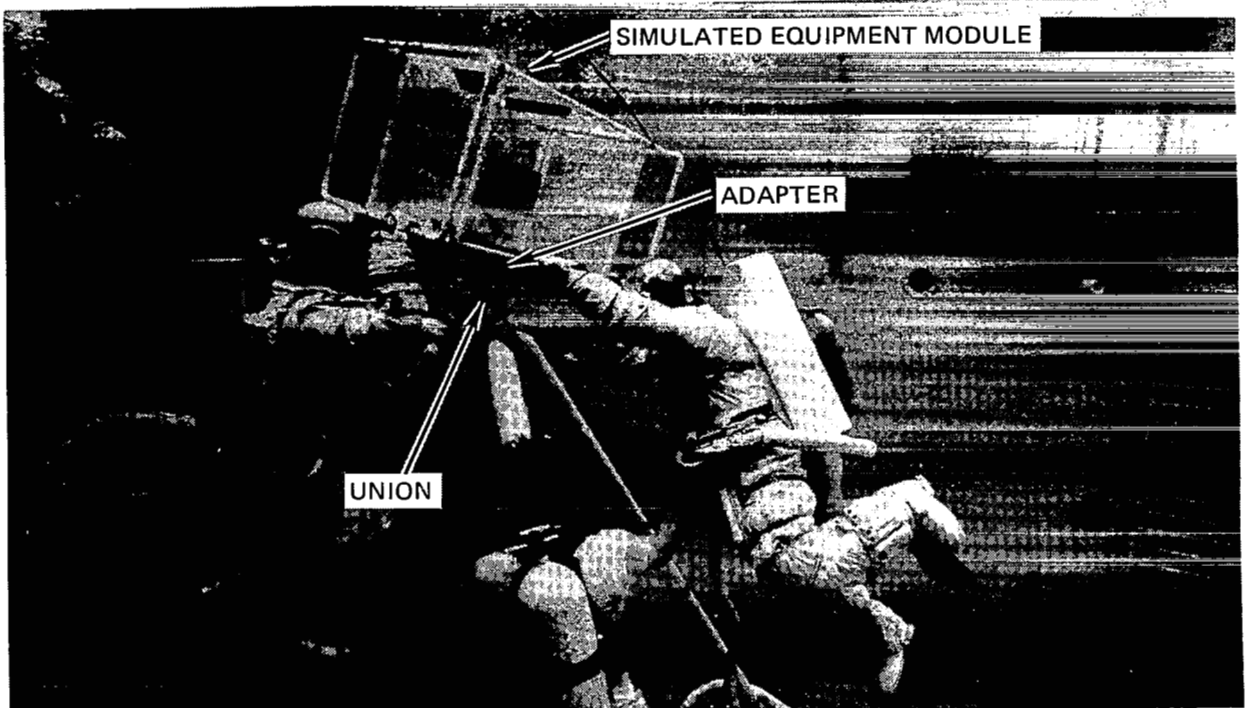


Figure 6. SEM Installation

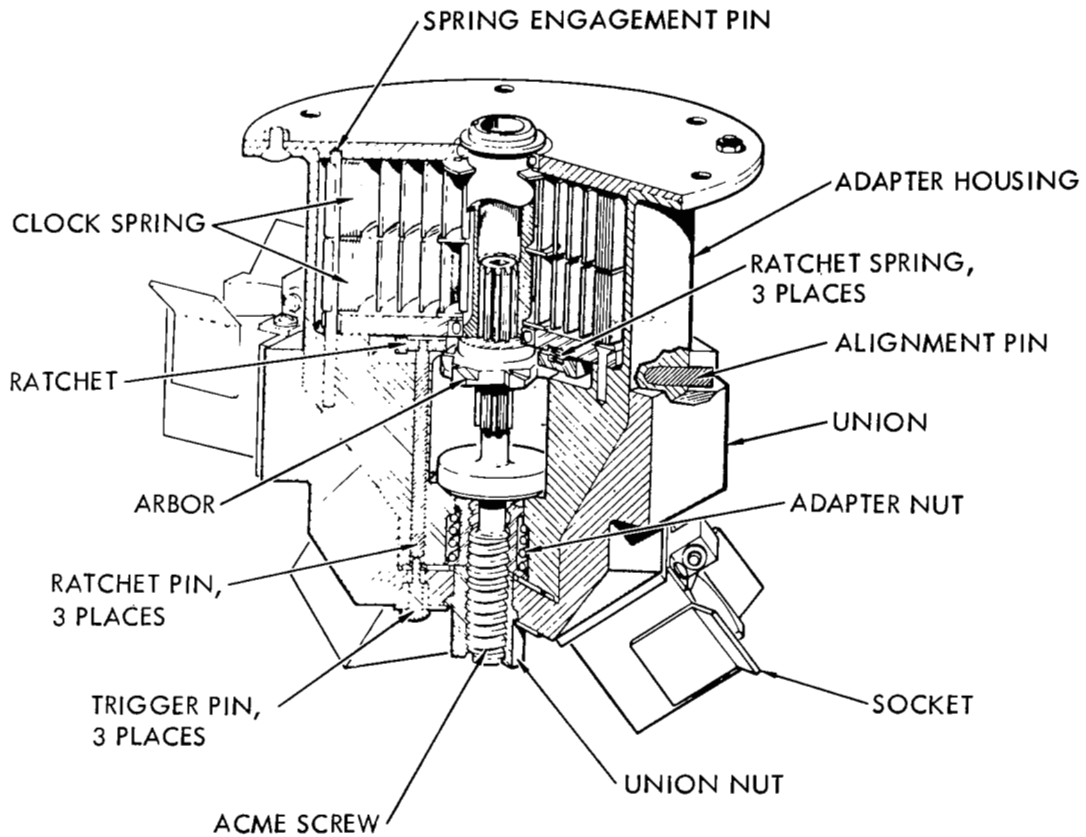


Figure 7. Modified Self-Energized Adapter

2. The captive receiving nut was slightly countersunk to accept misalignment of the screw, and shortened slightly to allow the screw to protrude through it for visual verification of engagement.
3. The ratchet wave washer was replaced by three softer compression springs to bring the triggering force from 178N (40 lb) down to 124N (11 lb).

After modification, another series of tests was conducted in which the module was satisfactorily and reliably attached with relative ease.

Disengagement of the adapter by EVA subjects was another objective of the tests. The task required one subject to insert a square nose speed wrench into a socket at the end of the screw and rewind it until the probe disengaged. The initial attempt indicated that the subjects were unable to reach the adapter from outside the cell, and consequently, could not disengage it.

#### CONCLUSIONS

The self-energized mechanical adapter is a feasible concept for the structural attachment of mission equipment or subsystems to a large platform. However, improvements in its disengagement features will be required before the adapter can be productively used.

Another important finding is that equipment to be operated in the foreign environment of space must be tested and refined under simulated space conditions to verify the equipment configuration.

#### REFERENCES

1. Advanced Technology Laboratory Program for Large Space Structures, Parts 1 and 2, Final Report, NASA CR-145206 (SD76-0210), Contract NAS1-14116, Mod. 1 (May 1977).
2. Totah, R. S., "Joints and Implications on Space Construction," Paper No. 78-1653, AIAA Large Space Platforms Conference, Los Angeles, CA (September 27-29, 1978).
3. Totah, R. S., Large Space Systems Erectable Structural Assembly Simulations, Final Report, Rockwell International Corporation, SSD 79-0215, Contract NAS8-33420 (December 1979).



## AUTOMATED BEAM BUILDER

Walter K. Muench  
Grumman Aerospace Corporation  
Bethpage, New York 11714

### SUMMARY

With an eye on the future, NASA has been funding study and development contracts to determine the feasibility of constructing large volume, light weight structures in space. This would include deployable, erectable and fabricatable space structures, depending upon the size of the structure to be constructed and its ultimate utilization. One such approach, space fabrication of large space structures, has been under study by several aerospace companies. Early in 1977, Grumman Aerospace Corporation was awarded a contract (Ref. 1) to design, develop, manufacture and test a machine which would automatically produce a basic building block aluminum beam (Fig. 1). This paper discusses the results of that effort and the work which still continues today, including:

- Aluminum Beam Builder, which was completed and delivered to NASA-MSFC in October, 1978
- Composite Beam Builder, for which technology development is still underway.

### INTRODUCTION

In-house study efforts at Grumman during the early 1970's indicated that a machine which could automatically produce beams in space would be a likely candidate requirement for construction of large space structures, such as a solar power satellite. Further study under a seven month contract with NASA (Ref. 2) indicated that near-term feasibility demonstration of such a machine which would produce aluminum beams was possible. Next, a competition was held to build such a machine, and Grumman was named the winner. The work performed, including designing, developing, manufacturing and testing of the first ground demonstration aluminum "beam builder", is discussed in some detail below.

When the effort associated with this aluminum beam builder was well underway, recognition of the need for a machine which would produce composite beams encouraged us to start investigating the technological development necessary to do this. Grumman has been conducting various significant critical process development tests from mid-1977 to the present time. These are also discussed below.

## ALUMINUM BEAM BUILDER

The approach to providing a ground demonstration machine entailed two significant steps, i.e.:

- Design and Development - several approaches to solving problems associated with various subsystems were investigated, including:
  - Beam cap forming
  - Brace storage, dispensing and transporting
  - Beam component fastening
  - Beam cut-off
- Manufacture and Test - problems, encountered and solved, were also associated with several subsystems, including:
  - Beam cap roll forming machinery
  - Brace dispensing mechanisms
  - Control devices.

## DESIGN AND DEVELOPMENT

Basic to the design of the beam builder was the idea that the machine must be capable of transforming high density, low volume material brought into space into lightweight, high volume structural beams in space. Ideally, this would apply to the production of all the structural members to be formed and assembled to fabricate a beam. Therefore, initial design concepts included six machine components to fabricate the beam components, three to continuously form the beam caps and three with appropriate cut-off and handling devices to form the braces and bring them into assembly position. Cost restraints and the desire to have the demonstration machine fit within the Orbiter payload bay accounted for the present configuration of the beam builder: three cap forming machines and preformed brace storage, dispensing and handling devices (Fig. 2).

### Beam Cap Forming

Two approaches to forming the open beam cap shown in Fig. 1 were considered: roll forming and step pressing. Development tests were conducted utilizing available production equipment (Figs. 3 and 4). Both approaches formed acceptable caps. However, it became clear that while the roll forming required more tooling, the length within which the beam cap could be formed

was considerably less than that of the step press, with its finite forming station lengths and required step to step transition zone.

### Brace Storage, Dispensing and Transporting

The initial approach was to have the brace storage, dispensing and transporting all performed in one package (Fig. 5). The concept had the entire package moving to the brace fastening position, picking off one brace and camming it into position on the beam cap for the clamp and fastening mechanism to hold it while the entire package retracted to its clear position. At the PDR (preliminary design review), it was decided that it would be undesirable to have these packages (three vertical and three diagonal brace cannisters) moving due to their mass. Therefore, a separate pivoting, pick-up and transporting device was developed (Fig. 6). The figure only shows two arms on the development cannister, although the plan was to have four arms in order to assure positive brace gripping and transportation.

Mechanization of the concept as it developed and the desirability to either reload or replace empty cannisters led us to consider another approach (Fig. 7). This final approach divorced the transportation function from storage and dispensing. Transportation is now accomplished by a separate brace gripping and carriage mechanism (Fig. 8) which has simplified overall mechanization of all brace storage and dispensing functions.

### Fastening Beam Components

A number of approaches to fastening the braces to the caps to construct the 1 m beam were explored, some simply on paper and others by development testing. Concepts which required pre-finished holes and insertion of rivets, screws or other similar fastening devices were eliminated due to inherent alignment problems which could exist, depending upon the size of the parts being assembled. Concepts which would result in metal vaporization, such as electron beam or laser welding, were also eliminated. Concepts which involved punching or punch and bending were attempted and eliminated for one of two reasons: (1) they produced debris (self-piercing rivets or screws) or (2) the fastening technique produced cracking in either the brace or cap material at the fastening points (punch and upset in a fashion similar to a grommet or tab and bend). Ultrasonic welding (Fig. 9) and resistance spot welding (Fig. 10) seemed to be the only readily available approaches which satisfied all design conditions. Ultrasonic welding yielded inconsistent results and was therefore abandoned.

Development tests of series resistance spot welding (Fig. 11) gave consistent, predictable results, which led to the clamp and weld mechanisms utilized in the machine (Fig. 12) and shown conceptually in Fig. 13. Each pair of electrodes is actuated individually by a separately driven cam within each weld block. To minimize peak power, each pair of welds is made sequentially after a set of braces has been clamped in place, first the verticals and then the diagonals, to complete each beam bay.

Because the peak power required for resistance welding exceeds the peak power capability of the Orbiter, a separate power supply will be required, unless another less demanding fastening approach is developed. This possibility is presently being explored.

#### Beam Cut-off

The first approach attempted to provide beam cut-off once the desired length had been fabricated was a simple single shear device (Fig. 14). This proved to be unacceptable, since it produced severe rippling of the beam end away from the cutting edge. (This rippling would impair the installation of a beam end tripod used to attach one beam to another, as well as providing a possible safety hazard to the astroworker assembling the beams or installing equipment on them.)

The solution, although it did produce debris, was a double shear mechanism which not only sliced cleanly through the cap but also caught the debris in a self-contained storage box (Fig. 15).

#### MANUFACTURE AND TEST

Considering the complexity of the machine, the actual manufacture of the detail parts and assembly of the beam builder, as well as its preacceptance debugging and testing, went very well. There were, however, several areas in which problems did occur, as discussed in the following paragraphs.

#### Beam Cap Roll Forming Machinery

The lower right rolling mill (when looking at the machine from the material feed end) produced beam caps with pronounced flange waviness. Although structural compressive load tests demonstrated that this waviness was not detrimental to the strength of the part, it was still considered unacceptable since the other two machines were producing beam caps without waviness. No amount of adjustment of the roll tooling or subsequent weld block shunt bars which guide the beam caps through the brace fastening section of the beam builder eliminated the problem. Finally, all the roll form tooling from the three rolling mills were removed and shipped back to the manufacturer for comparative measurements on a forming station by forming station basis. It was found that the roll tooling from the lower right rolling mill was slightly different from that of the other two rolling mills, although it was still within the manufacturer's tolerances. The tooling was reworked to match precisely, and since its reinstallation in the beam builder, it has given no further problems.

#### Brace Dispensing Mechanisms

In the original brace storage and dispensing device (Fig. 5) there was a tendency to pick off more than one brace from time to time. This was solved

by careful design and placement of brace spacers which maintain brace flange alignment and also transmit the stacking spring load through the stack of braces to the retaining/pick-off surface of the present helical brace dispenser (Fig. 7).

Presently, there are occasions when a brace fails to dispense. It has been determined that this has been caused by improper installation of the braces when loading the cannister. Care must be taken to assure that all braces are properly stacked and aligned, and free within the cannister, i.e., clear of the dispensing helix drive rod and not bound against any of the brace guide surfaces within the cannister.

### Control Devices

There are 173 operational detection devices located throughout the machine to monitor every function of the machine. They provide start and operation complete signals to the machine as the beam cap is rolled for one bay length of 1.5 m and stopped, braces are dispensed and transported into place, clamped and welded (first the verticals and then the diagonals), with each sequence repeated until the preprogrammed length of beam is produced, cut-off and the next beam started. Of these devices, 162 are limit switches, with the remainder being encoders, tachometers, photo-optical detectors and electrical pulse sensors. The limit switches are all alike. With regard to size, they are small enough to fit within the limited space available in a mechanism, such as the brace clamp and weld device. They provide no difficulty where protected within the particular mechanism with which they are associated, but where they are exposed and subject to accidental damage by technicians servicing the beam builder, they have been a source of beam builder malfunction. Although one can override a malfunction indicated by the control computer during operation, it is still a source of concern. Where possible, shielding has been provided to protect the most vulnerable limit switches. This has minimized the problem but has not eliminated it. Under consideration is the possible replacement of those limit switches which are still subject to damage by larger units, either photo-optical or magnetic proximity switches, where possible, to eliminate this troublesome problem altogether.

### COMPOSITE BEAM BUILDER

As the development efforts associated with the aluminum beam builder were nearing completion, attention was focused on what it would take to modify the design of the primary machine subsystems in order to produce composite beams. This new development effort focused on three items, as noted in Fig. 16, while the remaining subsystems were considered to be usable as is or with slight modification to handle the new material.

#### Beam Cap Processing Development

In mid-1977, work began with a brute force approach of trying to roll form a graphite/polyethersulfone laminate using the aluminum beam cap development

tooling with heaters added to soften the thermoplastic composite to forming temperature (Fig. 17a). Figure 17d shows the result of these efforts. Disastrous, burnt toast aptly describe the product, but at the same time, much was learned; such things as temperature control (polyethersulfone softens at about 260°C and has a forming range before it begins to sublime of about 10°C), bend zone heating (heating the whole part resulted in severe rippling and deformation) and speed control between stations (the part must be kept in tension as it passes through the mill to prevent any rippling or folding in the bend area).

Following a thorough evaluation of the results, we decided to work with a lower forming temperature material that also had a broader working range. The material selected was graphite/acrylic which forms at 140°C with a 30°C range. The selection process and criteria are discussed further below (see Material Evaluation). Still recognizing the need for higher working temperature material, our intent was "to crawl before we walk and walk before we run". Using the same machine previously used but now modified to provide some temperature control, heating along the bend zone only and with a uniform drive (Fig. 17b), encouraging results were obtained (Fig. 17d). Although there was notable flange rippling and some twist, as well as skewing of the finished part, we were encouraged enough to ask corporate management for funding to design and build a composite structural component forming process development tool, since we had been tying up a piece of production machinery with our experiments (Fig. 17a and b).

Having received a go-ahead, the machine was designed and built (Fig. 17c). Figure 17d shows the results. After having successfully formed a good graphite/acrylic cap we tried graphite/polyethersulfone once again. An acceptable product resulted (Fig. 18). With the composite industry supplying continuous strip stock (not available at the time of writing this paper) we hope to report on successful graphite/polyethersulfone beam cap production at the symposium.

#### Fastening of Composite Beam Components

As work on beam cap processing began to progress satisfactorily, development effort on fastening braces to beam caps began. Many approaches were considered; those listed in Fig. 19 were subjected to limited development testing and evaluation. Briefly:

- Ultrasonic Weld - Joint was acceptable but the ultrasonic vibrating horn tended to bore a hole in the part. Packaging presented a problem due to the horn size. Power consumption was higher than the other processes investigated.
- RF Welding - Joint appeared to be good. Arcing of the laminate to the test fixture away from the joint being made indicated a potentially difficult material quality control problem.
- Stapling (Cold) - Joint produced was excellent. However, uncontrollable debris was produced.

- Stapling (Hot) - Heating the parts at the fastening location eliminated the debris problem and still produced an excellent joint. Size and shape of the staple cartridge presents a packaging problem.
- Adhesive - Joint produced was good. Outgassing may be a problem (no measurements were attempted at this time).
- Induction Weld - Excellent joint was produced. Induction currents heat the part at the joint interface until the resin melts and fuses together. Packaging presents no problem and power consumption is extremely low. RFI may be a problem, although this is still to be investigated.

### Material Evaluation

As discussed earlier, our first composite processing development efforts met with somewhat disastrous results. After reviewing our goals, we decided to try some alternate approaches. The material to be investigated had to satisfy the following simple requirements:

- Structurally sound in a space environment, including vacuum, thermal and radiation exposure
- No outgassing during forming in space or during its operational lifetime
- Simple to preprocess into the required strip stock laminate
- Long ground storage life
- Easy to handle.

Thermoplastics seemed to satisfy these general requirements (Ref. 3). (Thermosets present strip laminate processing, storage and handling problems since they have to remain in their uncured state until formed.) Figure 20 shows the thermoplastic composite materials which were evaluated. Acrylic was selected because it not only met our structural baseline (strength and modulus of elasticity to be as close to or better than that of aluminum) but also because it is a resin system which lends itself to continuous preprocessing of graphite and strip laminate production, including:

- Monomer/polymer blend liquid at room temperature
- Excellent fiber wetting characteristics
- Monomer and polymer are readily available - in tank car quantities, if required
- Monomer and polymer are relatively low in cost - a factor which makes them attractive for research, development, and production.

The other materials tested did not, in general, meet the performance requirements. For example:

- Structural - much lower strength and modulus of elasticity than desired
- Preprocessing - poor fiber wetting. Press forming of strip stock required, thus limiting length available.

Woven graphite was chosen as the fiber medium because it is readily available and easy to handle. When processed as a graphite/acrylic composite, it gives good strength and stiffness properties and also forms easily.

The thermal performance of this particular composite is also quite good for passive structure in low earth orbit (Fig. 21). Through testing, we have demonstrated that though the strength of the material begins to fall off somewhat at the elevated temperature, compressive load testing at room temperature indicated a load carrying capability 180% greater than aluminum at room temperature and 120% at the elevated temperature. The coefficient of thermal expansion of this woven graphite/acrylic is 10% of that of aluminum. Recent electron bombardment testing in Grumman's Van de Graff facility has indicated that the material would have about a forty year life in low earth orbit (LEO). Ultraviolet exposure testing is still to be conducted.

While the graphite/acrylic satisfies the structural requirements for a passive structure (one which carries non-heat generating or radiating components or experiments), there still exists a need for a composite which could operate in a higher temperature regime. Work has therefore been continued with determining the forming process parameters associated with graphite/polyether-sulfone laminates. The preliminary results have been encouraging (Fig. 18), although further study is required.

## CONCLUSION

The automatic fabrication of basic building block aluminum beams has been ground demonstrated with the aluminum beam builder now operating at NASA-MSFC.

The automatic fabrication of basic building block composite beams still is to be demonstrated. Machine elements, composite beam cap forming and brace to cap fastening have been ground demonstrated. A composite beam builder still needs to be constructed.

To date, composite efforts have demonstrated the need for real improvements in basic thermoplastic composite processing in order to obtain better fiber wetting and continuous laminate strip stock. Short (1 to 3 m), press formed strips have been used for process development and demonstration purposes, but the real need is for a continuous strip up to 300 m long (the beam builder storage reel capacity). Material suppliers have been given this challenge.

Further effort is required to improve the structural characteristics, ease of preprocessing and final forming of graphite reinforced thermoplastics. Other resin systems and graphite fiber orientations need to be examined. The performance of these materials in both vacuum and radiation environments also needs to be determined.

Finally, once all ground feasibility tests have been completed and the choice has been made between aluminum and composite for the first space flight demonstration, a flight beam builder will be built and integrated aboard the Orbiter and a still to be determined mission flown (Fig. 22).

#### REFERENCES

1. Space Fabrication Demonstration System. Rep. no. NSS-SFDS-RP013, Grumman Aerospace Corp., Mar. 15, 1979. (Available as NASA CR-161286.)
2. Space Fabrication Techniques. Rep. no. NSS-SF-RP004, Grumman Aerospace Corp., Dec. 15, 1976. (Available as NASA CR-150202.)
3. Lubin, G., Marx, W., Poveromo, L., "Reinforced Thermoplastic Composites for Space Beam Fabrication," SPI Reinforced Plastics/Composites Institute, 34th Annual Conference, New Orleans, Louisiana, February 1979.

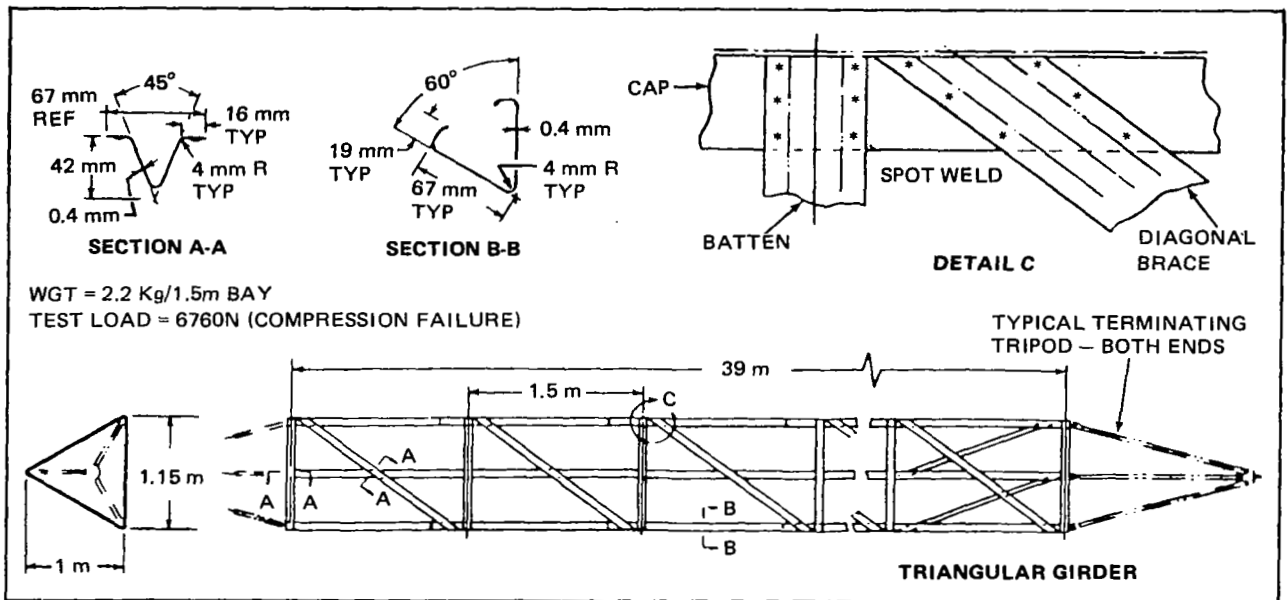


Figure 1.- Basic building block 1 m beam.

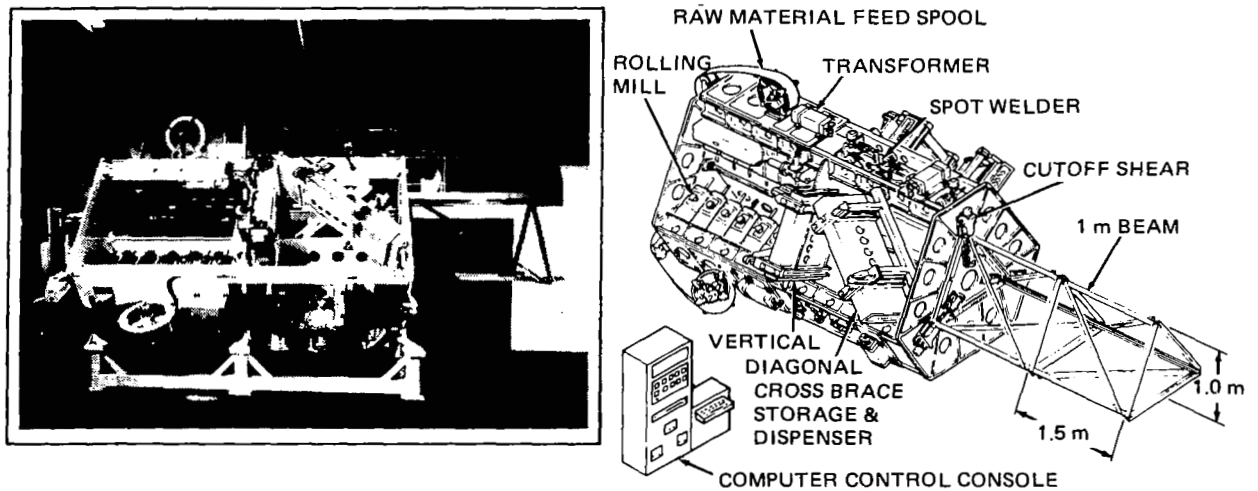


Figure 2.- Aluminum beam builder.

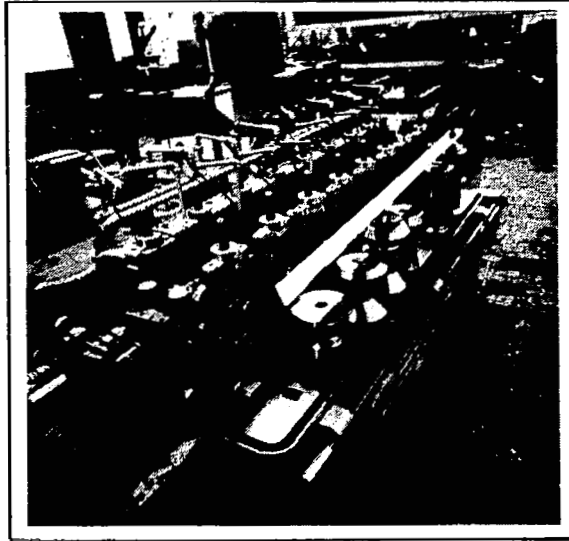


Figure 3.- Rolling mill with 1 m beam cap forming tools.

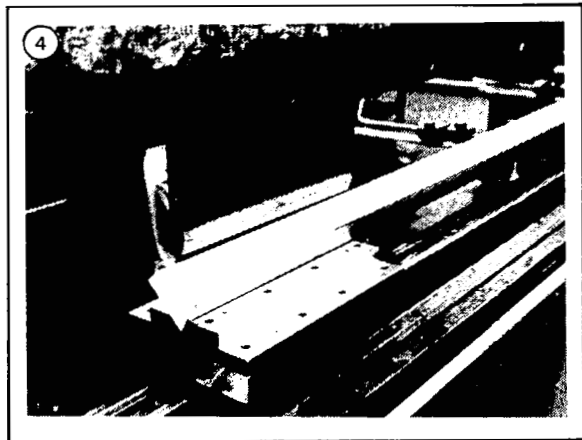
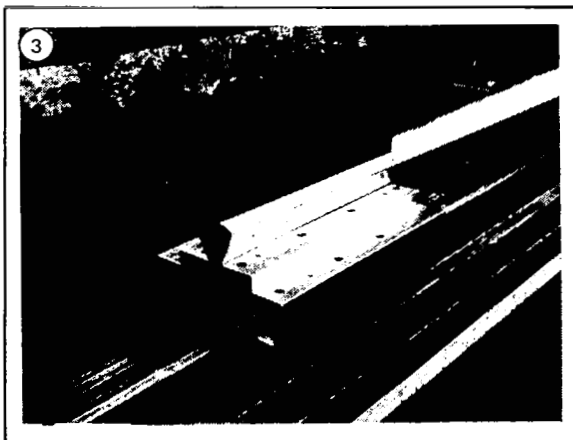
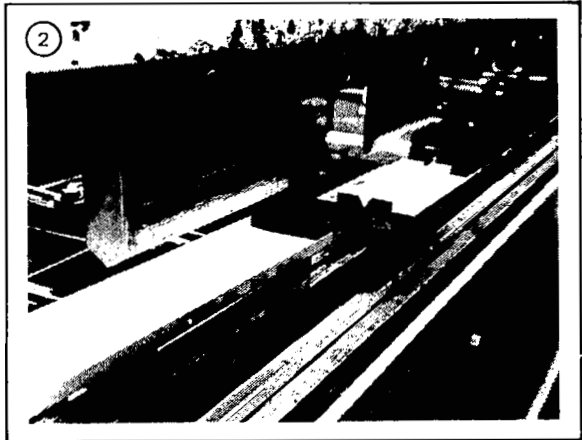
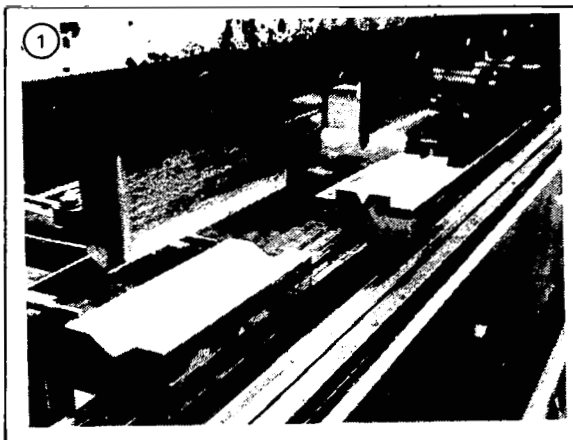


Figure 4.- Step press 1 m beam cap forming.

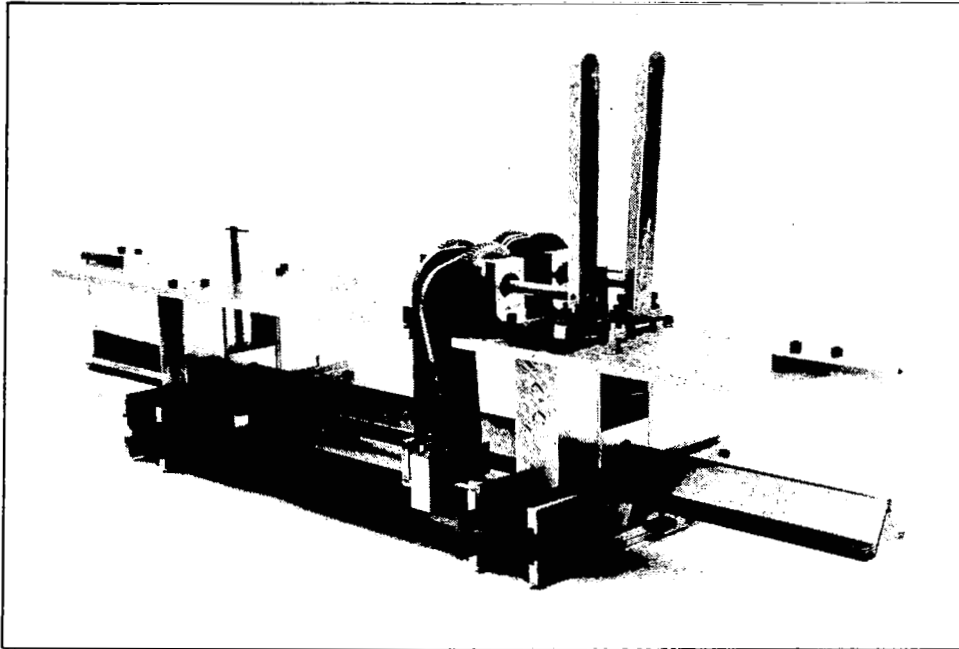


Figure 5.- Brace storage and dispensing device.

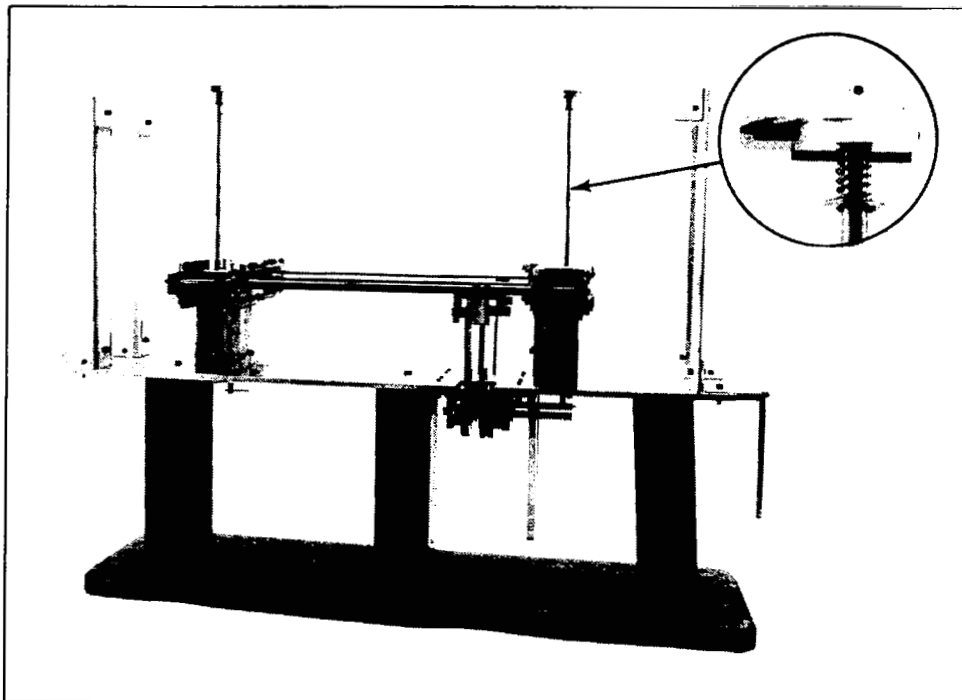
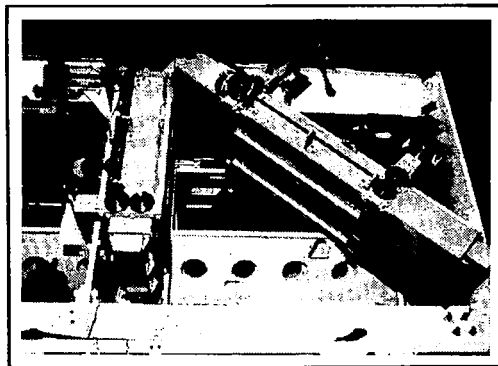
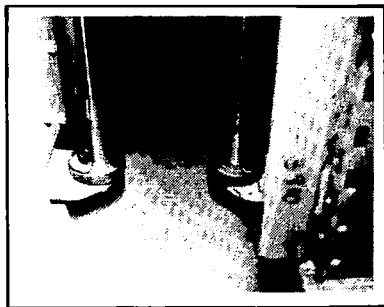


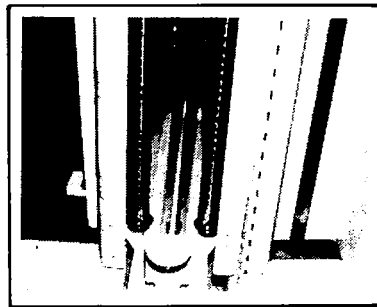
Figure 6.- Brace pivoting pick-up transport arm.



CANNISTERS



PICK-OFF HELIX



DRIVE RODS

Figure 7.- Final brace storage and dispensing device.

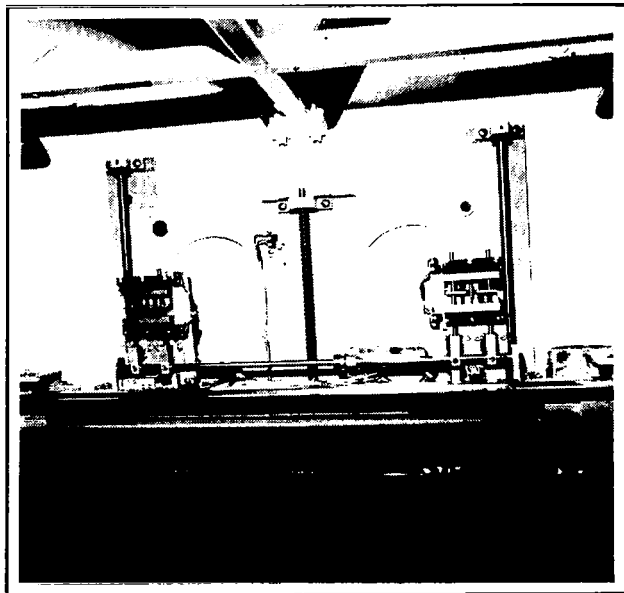
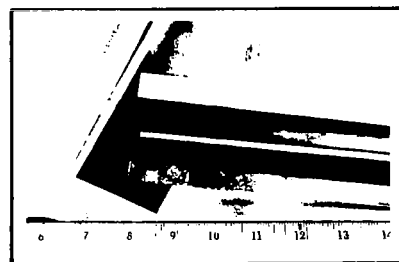


Figure 8.- Brace gripping and carriage mechanism.



(BRANSON)



(SONOBOND)

Figure 9.- Ultrasonic weld sample.

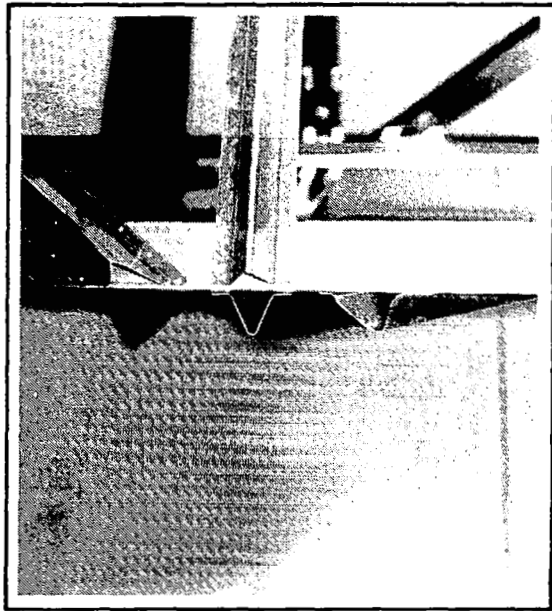
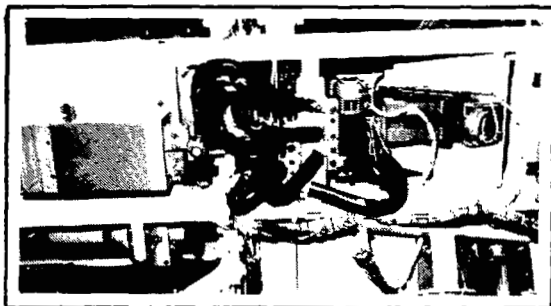


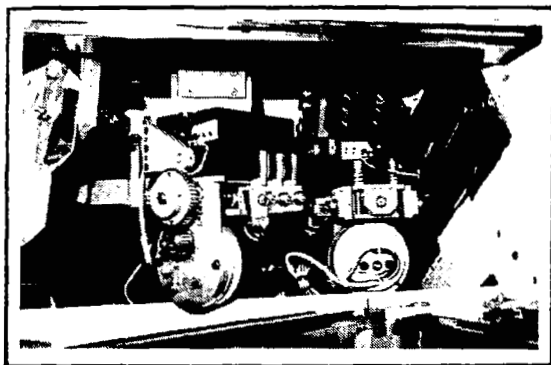
Figure 10.- Resistance spot welded brace to cap.



Figure 11.- Series resistance spot welding development set-up.



OUTBOARD



INBOARD

Figure 12.- Clamp and weld block mechanism.

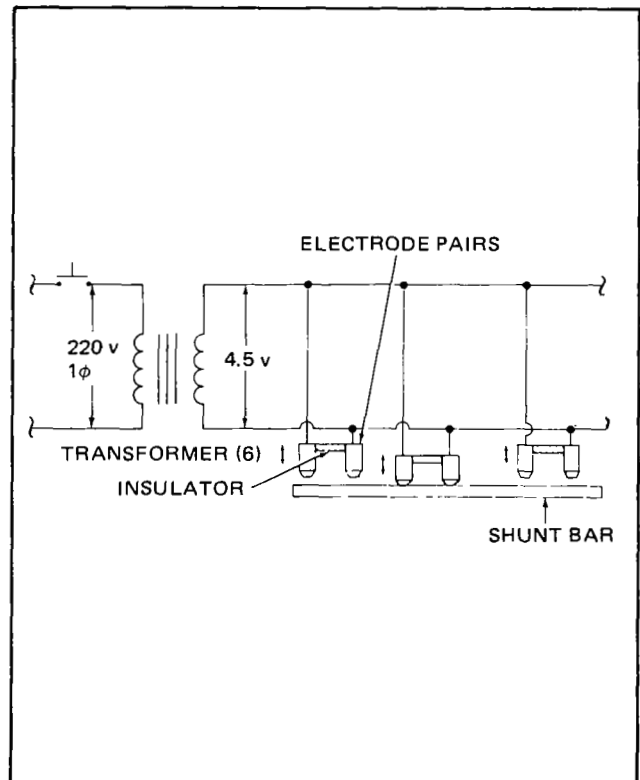


Figure 13.- Series resistance spot weld schematic.

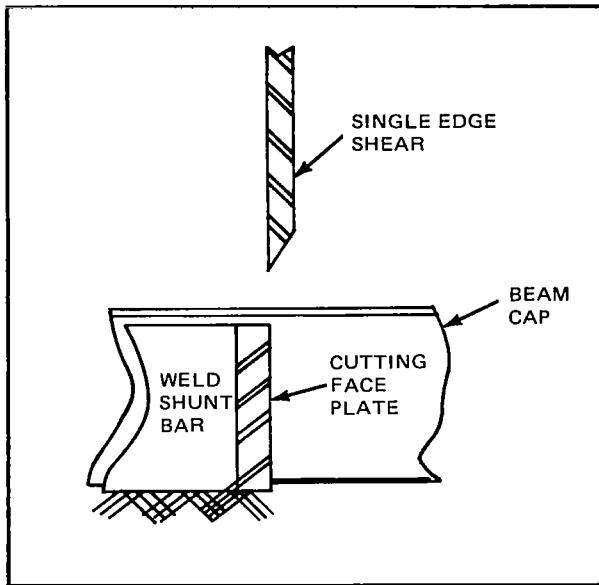


Figure 14.- Single edge shear cut-off schematic.

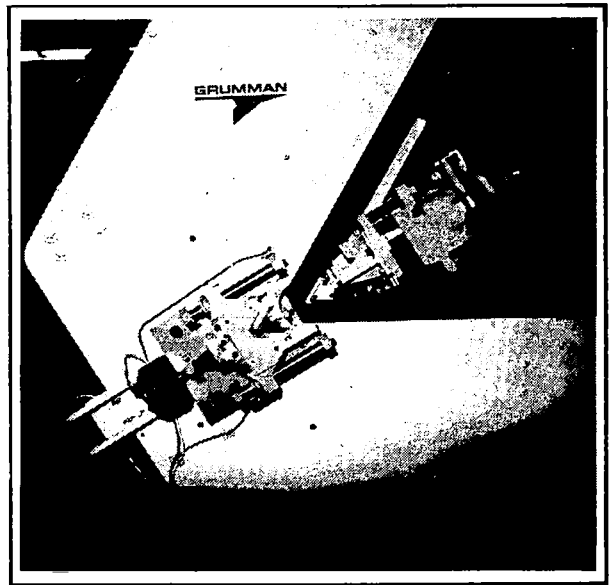


Figure 15.- Double edge shear cut-off mechanism.

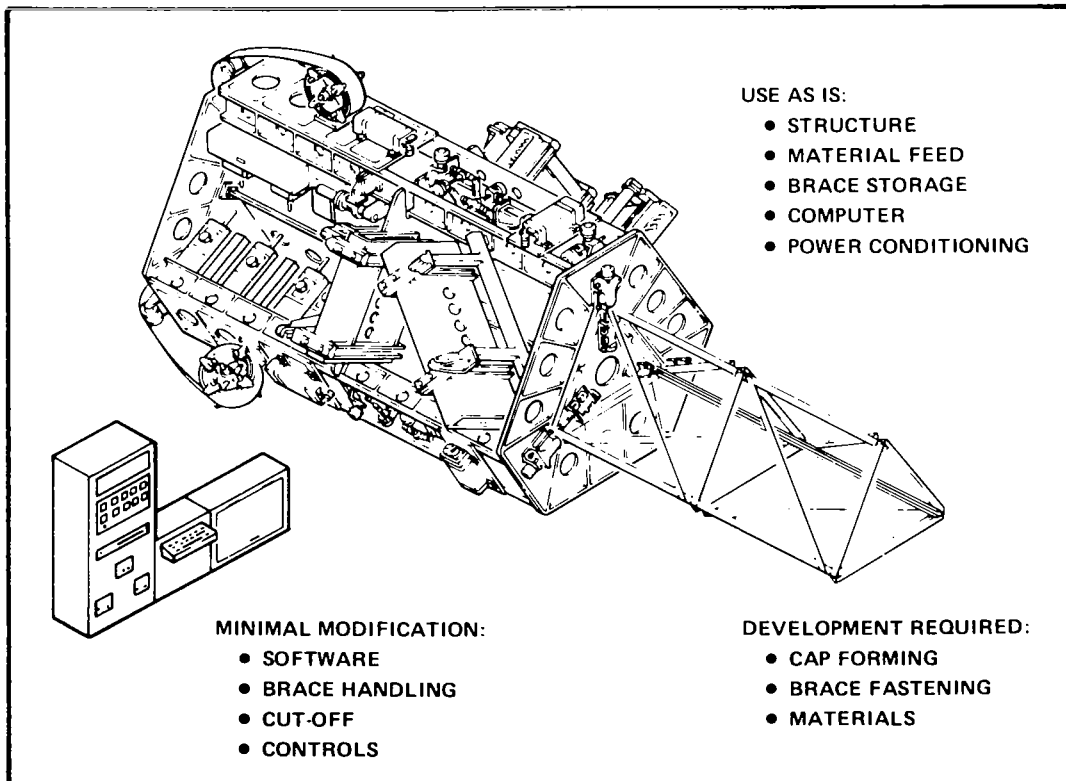
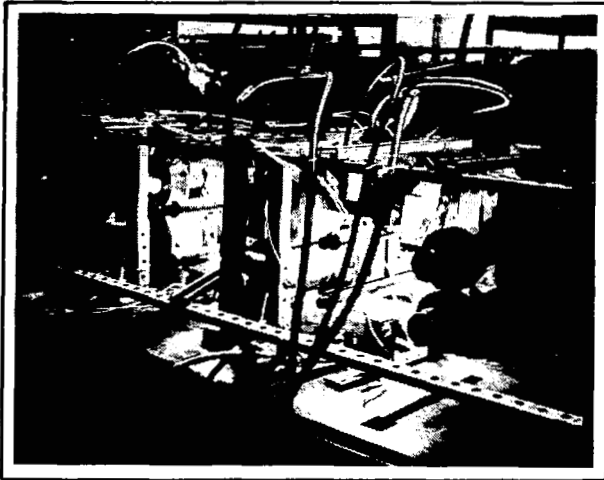
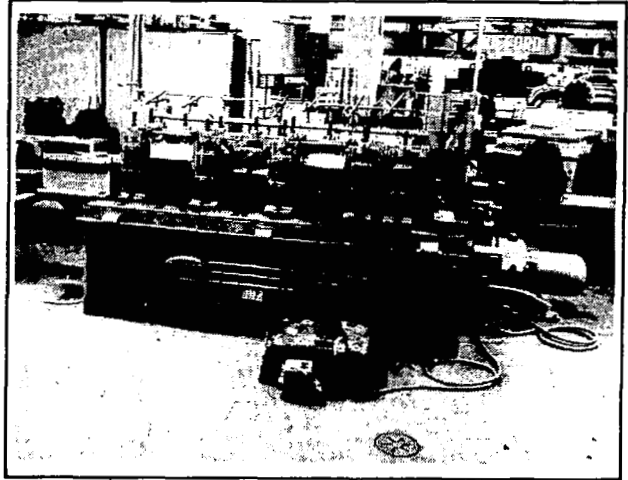


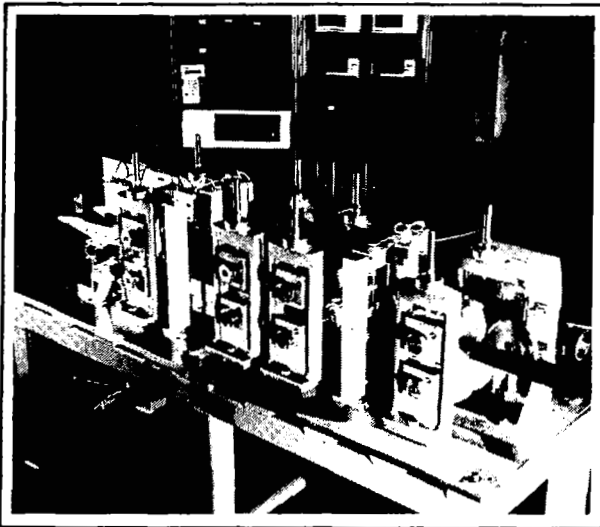
Figure 16.- Composite beam builder technology development.



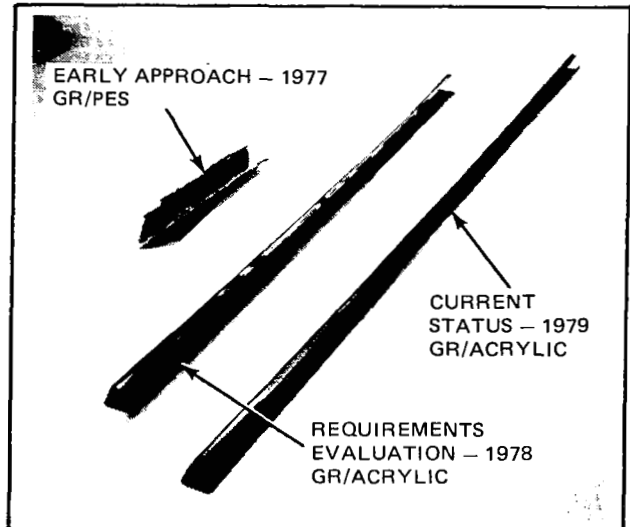
a) EARLY APPROACH - 1977



b) REQUIREMENTS EVALUATION - 1978



c) CURRENT STATUS - 1979



d) RESULTS

Figure 17.- Composite beam cap forming process development and results.

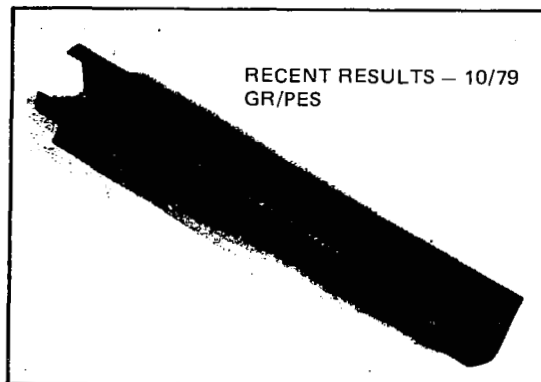


Figure 18.- Graphite/polyethersulfone beam cap sample.

METHOD	RESULT	PROBLEM	RECOMMENDATION	STATUS
ULTRASONIC WELD	ACCEPTABLE	POWER SIZE	DROP	—
RF WELDING	LIMITED SUCCESS	ARCING	DROP	—
STAPLING (COLD)	LIMITED SUCCESS	DEBRIS	DROP	—
STAPLING (HOT)	EXCELLENT	SIZE	MORE WORK (BACK-UP)	ON HOLD
ADHESIVE	GOOD	OUTGASSING	MORE WORK (BACK-UP)	ON HOLD
INDUCTION WELD	EXCELLENT	RFI	MORE WORK (PRIME)	NAS8-32472

Figure 19.- Composite fastening process development summary.

PHYSICAL/MECHANICAL PROPERTIES										
LAMINATE IDENT	MFG	RESIN	CLOTH REINFORCEMENT	PROCESS PARAMETERS			LONG. TENS. STRESS (MPa)	LONG. TENS. MODULUS (GPa)	RESIN CONT (%)	THICKNESS (mm)
				TEMP (°K)	PRESS (KPa)	TIME (min)				
201P	3M	Polycarbonate	Gr. 2423	533	690	30	333.7	43.2	—	1.0
102PH	Hexcel	Phenoxy	Gr. 1313	450	690	30	341.3	39.4	—	0.6
101A	GAC	Acrylic	Gr. 1212**	422	690	30	469.5	62.7	48.3	0.8 **
201A	GAC	Acrylic	Gr. 2423	422	690	30	444.7	58.3	35.4	0.8
301A	GAC	Acrylic	Gr. 2423/ Glass Scrim	422	690	30	427.5	42.8	—	1.1
302A	GAC	Acrylic	Gr. 2423	422	690	30	433.0	50.1	—	0.9
102PL	Hexcel	Polyester	Gr. 2424	—	—	—	281.3	30.1	—	1.5
303A	GAC	Acrylic	GR. 2423	422	690	30	284.1 @ 350° K	36.1 @ 350° K	—	0.7
501A	Hexcel	Acrylic	Gr. 2423	477	1380	2	451.6	47.4	—	0.9
501A	Hexcel	Acrylic	Gr. 2423	477	1380	2	270.3 @ 350° K	39.9 @ 350° K	—	0.9

\* LAMINATES — 2 PLYS THICK EXCEPT AS NOTED  
\*\* LAMINATES — 4 PLYS THICK

Figure 20.- Thermoplastic materials requirements evaluation.

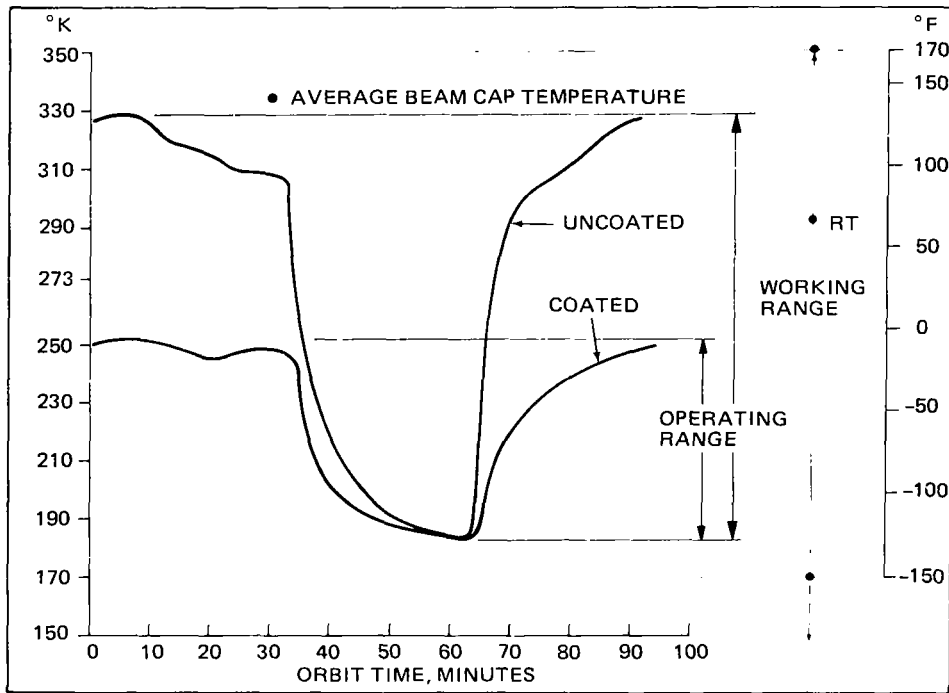
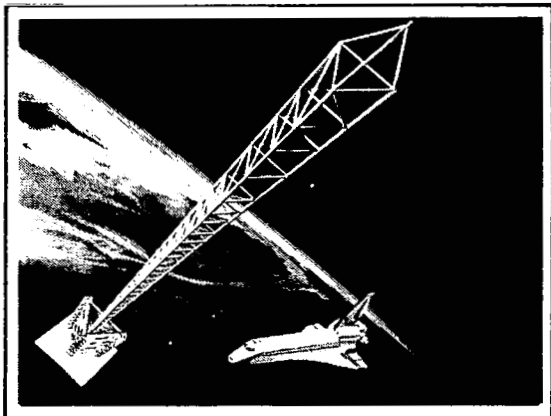


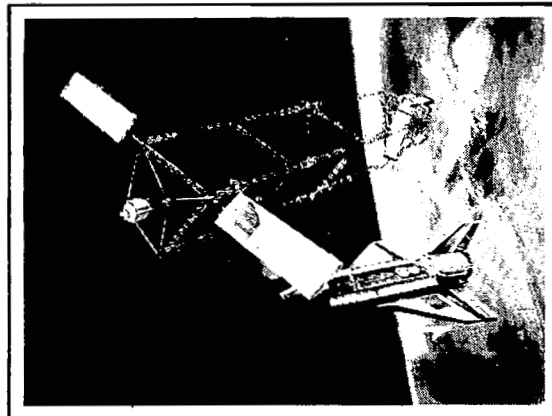
Figure 21.- Graphite/acrylic thermal gradient in low earth orbit.



BEAM BUILDER



GRAVITY GRADIENT RADIOMETER



TRIBEAM PLATFORM

Figure 22.- Early Orbiter beam builder mission possibilities.



## THE MAGSAT MAGNETOMETER BOOM

James F. Smola, Wade E. Radford, and Marcus H. Reitz  
The Johns Hopkins University  
Applied Physics Laboratory

### SUMMARY

A continuing requirement exists for lightweight extendable structures that can precisely position magnetically sensitive instruments safe distances from magnetic sources in a spacecraft. Presented herein is a brief description of one such device - The MAGSAT Magnetometer Boom System - and an overview of the major areas of concern that played dominant roles in its development. Weight, packaging volume, thermal distortion, mechanical misalignments, dimensional instability, launch environments, and low temperature functioning were areas that presented some formidable obstacles. The ways in which these obstacles were dealt with are offered here to those involved in the development of similar aerospace mechanisms with equally restrictive requirements.

### INTRODUCTION

The need for a simple, lightweight, precisely alignable, virtually distortion-free, extendable structure capable of overcoming the stiffness of sizeable multiconductor electrical cabling arose during the development of the TRIAD (1972) satellite by the Johns Hopkins University's Applied Physics Laboratory. Similar devices - all of which utilized the scissors concept - were developed for GEOS-C (1975) and TIP II and III (1975, 1976). The experience acquired during these programs provided the background that was necessary for the undertaking that became the MAGSAT Magnetometer Boom.

MAGSAT's (Magnetic Field Satellite) mission was to provide global vector magnetic field data which would be used to create new maps of the earth's magnetic field and to detect large scale anomalies in the magnetic field for use in planning resource exploration strategy. Data collected during the spacecraft's low altitude phase following 5 months of expected life prior to re-entry, was to be especially desirable for the latter objective. In addition to these principal objectives, the data was to be used for core/mantle studies, magnetospheric and ionospheric research, marine and other studies.

Measurements of the three vector components of the earth's magnetic field were the task of an ultrastable, high accuracy vector magnetometer and a pair of star cameras. Providing redundancy and an independent confirmation of total field magnitude were the roles of a companion instrument--a scalar magnetometer.

Magnetic contamination of the magnetometer sensors was avoided by locating the fairly magnetic star cameras on an optical bench in the spacecraft instrument module (I/M). The sensors of both magnetometers were mounted on a platform with passive and active temperature control, which was attached to the end of the magnetometer boom. Upon command the boom was to uncage and displace the sensor platform 6 meters distant from the (I/M). To satisfy requirements imposed by an Attitude Transfer System (ATS) which measured vector magnetometer tilt relative to the star cameras, the boom was to maintain the platform position such that the center of an ATS plane mirror, precisely attached to the backside of the vector magnetometer sensor, remained within a  $\pm 1.91$  cm ( $\pm 0.75$  in) square target zone. This zone was centered on an optical axis defined by an ATS infrared light beam emanating from the I/M. In addition the plane mirror was to remain orthogonal to the optical axis within 3 arc minutes. (See ref. 1.)

#### SYSTEM DESCRIPTION

Figure 1 illustrates the MAGSAT spacecraft's operational configuration. Shortly after injection into a  $96.76^\circ$  inclination, 352 km by 561 km sun synchronous orbit, the spacecraft was three-axis stabilized with its Z-axis near the orbit normal and the magnetometer boom trailing aft. This orientation was maintained by an attitude control system consisting of a reaction wheel with an infrared horizon scanner, a three-axis magnetic torquing system, a pitch axis gyro system for pitch rate sensing, an attitude signal processor for semi-autonomous roll/yaw control, momentum wheel dumping and pitch loop dynamics compensation, and a second adjustable boom for aerodynamic trimming.

The magnetometer boom system consisted of a 14 link scissors boom, a three axis gimbal and the sensor platform (S/P). The S/P was connected to the I/M electrically with multiconductor cabling that was routed through the interior of each boom link. Two independent pyrotechnically actuated caging systems were used to contain and protect the boom and S/P in their stowed configurations during launch. The three-axis gimbal located at the boom base provided the boom with pitch, yaw, and roll capabilities of  $\pm 2^\circ$ ,  $\pm 2^\circ$ , and  $\pm 5^\circ$  for ATS acquisition. The drivers for each gimbal actuator, consisting of a 491 cycle square wave inverter powering

2 phase synchronous-hysteresis gearmotors coupled to gearboxes, provided average pitch, yaw, and roll scan rates of 30 arc sec/sec. A pair of tension springs attached to the drive base and I/M structure eliminated all unrestrained play in the gimbal actuator adjusting screws. Rotary potentiometers geared to the output shafts of each of these gearboxes were calibrated to give S/P angular orientation. (See Figure 2)

The boom drive consisted of a right and left handed ball screw which was similarly driven. A rotary potentiometer geared to the output shaft of the gearbox was calibrated to give boom length during deployment. Confirmation of total extension was given by a second pot made of non-magnetic materials and pinned to one of the boom hinges closest to the S/P. Total runout time was about 20 min.

Weight and thermal distortion dictated the use of graphite epoxy for the boom links. The basic link was 0.94 meters (37.125 in) long and measured 1.07 cm x 5.08 cm (0.42 in x 2.00 in) in cross-section. Magnesium fittings were fastened to the ends and the center of each link with a semi-rigid epoxy to prevent interface cracking due to differential expansion. Each link was a hollow box with a .076 cm (0.030 in) thick wall and was covered internally and externally with an aluminum foil moisture barrier. (The hygroscopic nature of graphite epoxy is a source of dimensional instability). A final wrapping of aluminized Kapton\* with an aluminum oxide overcoat was added for temperature control. The links were hinged to each other with pins that were forced through compliant undersized bushings which permitted rotation, but eliminated all unrestrained mechanical side play.

The aluminum foiled, graphite epoxy S/P was attached to the tip of the boom through a hollow graphite epoxy, box-like spacer and a "figure-eight" mechanism that enabled the S/P to translate while maintaining its attitude normal to the boom axis as the boom extended. Attached to the S/P with a kinematic suspension was the temperature controlled vector magnetometer base (VMB) which in turn had attached to it the vector magnetometer sensor, the remote plane and dihedral ATS mirrors, and a precision sun sensor. The kinematic suspension provided a compliant mount for the VMB and isolated it from thermally induced structural distortions that would be detrimental to the alignment of the vector magnetometer and the remote mirrors. The scalar magnetometer was attached to a 1.27 cm (0.50 in) thick epoxyglass thermal isolator which was fastened to the side of the graphite epoxy spacer.

The weight breakdown for the boom system is shown in Table 1.

\*Kapton, polyimide film manufactured by E. I. duPont deNemours and Co. Inc.

## AREAS OF MAJOR CONCERN

Although the precision scissors boom was a flight-proven concept, the remote, precisely aligned S/P was not. Magnetic considerations disallowed electrically powered adjusting mechanisms at the S/P end. Consequently S/P tilt adjustments could only be achieved by gimbaling the boom at its base which caused the S/P to translate. This side effect coupled with the ATS's narrow field of view severely limited tilt adjusting capability. For this reason considerable engineering analysis and testing were necessary to demonstrate that the SCOUT launch environment, uncaging, deployment, thermal distortions and attitude control disturbances would not compromise the ability to achieve the precise alignments that were required.

The discussion that follows focuses on three major areas of concern that received considerable attention.

### CONTROL OF THERMAL DISTORTION

The requirement here was to limit initial boom thermal distortion-due to broadside solar illumination - sufficiently to permit acquisition of the ATS remote mirrors by gimbaling the boom at its base. Although the gimbals were adjustable  $\pm 2^\circ$  in pitch and yaw and  $+5^\circ$  in roll, any tilting of the boom at its base would translate as well as rotate the remote mirrors. Since the target zone was  $\pm 1.91$  cm ( $\pm 0.75$  in) square, any mirror tilting that was necessary for acquisition had to be achieved within  $0.33^\circ$  once the mirrors entered the target zone. This made the initial tilt angle of the mirrors and direction of tilt extremely important. If, for instance, the mirrors were perfectly centered within the target zone initially, acquisition would have to be achieved within  $0.16^\circ$  or 9.6 arc min.

The  $\pm 3$  arc min requirement on mirror angle limited the permissible transverse offset of boom tip position to  $\pm 0.51$  cm ( $\pm 0.20$  in) for simple mechanical misalignment and  $\pm 0.25$  cm ( $\pm 0.10$  in) for misalignments caused by thermal distortion. It was important then that the system was free of play and that the boom elements were made of some material that was virtually immune to thermal distortion. (Active temperature control was ruled out because of the complexity required to implement it in the time that was available, and lack of sufficient electrical power).

The thermal problem narrowed the field of materials down to a very few. The goal was to find a material whose coefficient

of thermal expansion (CTE) would remain very close to zero over a temperature range of 0°C to 40°C. Once other considerations such as weight, strength, stiffness and availability were thrown in, the only material that remained suitable was graphite fiber reinforced plastic (graphite epoxy).

Design analysis concluded that graphite epoxy GY 70/X30 (co-cured foil, 0, 54, -54, -54, 54, 0, foil) would be the optimum selection. The average CTE for the 14 links in the MAGSAT boom was  $+0.34 \times 10^{-6}/^{\circ}\text{C}$ .

The thermal coating selected to control link temperatures and temperature gradients in the presence of the solar and earth infrared environments was vapor deposited aluminum with an  $\text{Al}_2\text{O}_3$  overcoat on a Kapton substrate. It was attached to the aluminum moisture barrier with an acrylic, pressure sensitive adhesive. The coatings 0.11/0.16=0.69 ratio of solar absorptance to infrared emittance was chosen to give link equilibrium temperatures close to 25°C. This temperature was dictated by the fact that all mechanical alignments would be done and checked at room temperature.

Thermal distortion tests conducted in the NASA/GSFC solar simulator on a four link version of the flight boom provided temperature data that was fed into a NASTRAN model of the test boom. Tip deflections in pitch, yaw and roll that evolved were then compared against those measured during the test. Satisfactory correlations gave a high degree of confidence in the NASTRAN model of the flight boom which was three times as long. This model indicated that the transverse and angular displacements of the S/P due to boom thermal distortion would be well within the ATS allowable range.

#### UNCAGING, SEPARATION, AND EXTENSION

The fact that the boom and sensor platform were to trail behind the I/M and base module in orbit made stowing for launch rather elaborate. To preserve mechanical alignments and to prevent the 7.03 kg (15.5 lb) S/P from transmitting sizeable launch loads into the more delicate boom structure, two independent caging systems were provided. The S/P was held securely by two separate chains of latches each consisting of three latches interconnected by two pullrods. Pyrotechnic piston-type actuators were used to open each latch chain by command.

A second caging system consisting of two "T-rods" strapped the folded boom links and drive base securely to the vertical bulkhead of the I/M. The lower ends of these T-rods were inserted into anchor posts that were mounted to the same vertical bulkhead.

Two pyrotechnically actuated pullrods beneath the drive base pinned each T-rod to its anchor post. An adjustable nut at the other end of each T-rod was then torqued to preload the folded boom at two points 0.59 m (23.25 in) apart to 1067.6 nt (240 lbs). The preload was required to keep the boom links and gimbal actuators from chattering and to prevent the links and drive base from rolling over when subjected to side loads during vibration testing and launch. Boom uncaging preceded S/P uncaging in the boom deployment scenario.

The stowed system abounded with potential hangups. Multi-layer insulation in regions of tight clearance and extremely cold temperatures at separation gave great cause for concern. Eight 150 ohm 7.5 watt resistors were attached to the drive base to provide about 15 watts of heat which kept the drive mechanism in a temperature range that would prevent it from loading up and possibly seizing due to differential contraction. The heat also kept the drive lubricants in an acceptable operating range.

Since the boom system was located in an external cavity which was shadowed from the sun prior to uncaging not much more could be done simply to keep certain parts from growing very cold. Temperature predictions for link ends that protruded from the cavity were as low as  $-70^{\circ}\text{C}$ . Telemetry indicated that cavity side wall temperatures dropped to  $-6^{\circ}\text{C}$  while the drive base dropped to  $-10^{\circ}\text{C}$  at the time of heater turn on. After 100 minutes of preheating the drive base temperature reached  $13^{\circ}\text{C}$ , after which the S/P was uncaged. Boom extension followed.

Early in the development effort there was great concern over the ability of the boom to overcome the stiffness of the multi-conductor cabling that was routed through the interior of each boom link and across 16 hinges. This cable consisted of 52 electrical conductors insulated with Durad-coated Teflon\* and woven into a flatpack. Two such flatpacks ran between the S/P and I/M. With so much cabling present, it was feared that cable stiffness would become a critical factor at temperatures as low as  $-70^{\circ}\text{C}$ . Cold temperature tests demonstrated that the increased stiffness of the cable was manageable. Torsion springs operating at each link pivot were of sufficient capacity to overcome cold cable stiffness as well as hinge frictional moments.

\*Durad, fluorocarbon polyimide, manufactured by Haveg Industries, Winooski, Vermont  
Teflon, tetrafluoroethylene, manufactured by E.I.duPont deNemours Co. Inc.

## PRE-LAUNCH MECHANICAL ALIGNMENTS

The objective here was to bring the remote mirrors mounted on the S/P into the fields of view of the ATS pitch/yaw and roll optical heads and then to bring them into the linear region of the ATS by fine adjustment. How this was to be accomplished with a 6.02 m separation between them was not immediately apparent at the outset. A way had to be found to eliminate the one-g bias which would overwhelm any boom system biases that might be present.

The idea that turned out to be the best of those proposed was one that utilized a pair of 6.1 m long water troughs - Figure 3. Specially designed floats with gimballed pulleys were attached to the boom link pivots. The idea here was to simulate a zero-g condition in a plane parallel to the plane of the water. Remote mirror transverse and/or angular offset could then be corrected by gimbaling the boom at its base and/or introducing shims at the VMB-S/P interface. The boom system was installed in a special fixture which was attached to a rotary table, the purpose of which was to rotate the boom into its pitch and yaw-planes for orthogonal plane zero-g measurements and adjustments. With the aid of an autoreflecting telescope, a theodolite, and numerous mirrors to measure the transverse and angular offset of the plane remote mirror, the data in Table 2 was generated.

Tests I and V were the baseline and final tests. Tests II through IV (not shown) were performed to check alignment repeatability following numerous boom extensions and retractions, removal of the boom from and its reinstallation in the flotation system, and vibration testing. These test results indicated that errors introduced by the test system were slight and that the aligned boom system had sufficient margin to accommodate the remote mirror tilting and displacement that could be expected from thermally induced structural distortions. Following this the boom system was installed in the I/M and aligned for flight.

The boom was extended from 1.52 m to fullout and back 30 times during alignment testing at room temperature and never exhibited any functional abnormalities whatsoever. Complete retractions were not easily achievable due to limitations imposed by the flotation system. Consequently only 10 total extensions and retractions were performed.

## OPERATIONAL PERFORMANCE

MAGSAT was launched on 30 Oct 79. By 1 Nov 79 the spacecraft attitude was stabilized and at 23:27:53UT, following S/P uncaging, the magnetometer boom was extended. Telemetry in the form of

potentiometer readouts - converted to boom length - of the drive screw rotations and the angle between the last hinged set of links, indicated that the boom extended properly. The final readings were practically identical to the readings obtained during the deployment tests. ATS telemetry surprisingly indicated that the remote mirrors were within sight of the ATS optical heads. This obviated the need for extensive gimbals searching for ATS acquisition. The following day slight gimbals adjustments were made to bring the remote mirrors into the linear range of the ATS. Subsequent gimbals adjustments were unnecessary.

Figure 4 - one orbit of data 28 days into mission life - shows ATS roll, pitch, and yaw angles relative to orbital time and boom link temperatures as measured by thermistors attached directly opposite one another on a boom link. The plots indicate that the remote mirrors were oscillating slightly in pitch, yaw, and roll, but well within the  $\pm 180$  arc sec pitch and yaw and  $\pm 300$  arc sec roll limitations of the ATS. These oscillations had periods approximately equal to the spacecraft orbital period. Interestingly the boom link temperatures exhibited this same characteristic. The variations in temperatures were caused primarily by the once per orbit coning of the solar vector. Their magnitudes were functions of the boom link angle relative to the sun which was established by the link angle relative to the boom axis and the seasonal variation of the solar vector. The near cyclical coincidence of these curves led to the inference that the boom was being thermally excited at the orbital frequency.

Bulk temperatures ran somewhat hotter than expected. The design goal - about  $25^{\circ}\text{C}$  - was exceeded by temperatures that ran as high as  $32^{\circ}\text{C}$  early into mission life. Twenty-four and 43 days later, readings as high as  $38.6^{\circ}\text{C}$  and  $40.5^{\circ}\text{C}$  were observed and were representative of a general uptrend that started shortly after boom extension. This is symptomatic of degradation in the link thermal control surface.

Hot-to-cold side temperature differences cycled with bulk temperatures and typically fell into the  $2.0^{\circ}\text{C}$  to  $2.5^{\circ}\text{C}$  range. Analysis predicted a range of  $4.0^{\circ}\text{C}$  to  $4.6^{\circ}\text{C}$ .

#### CONCLUDING REMARKS

The ability of this boom system to maintain the precise position and angular inclination required of the sensor platform is an endorsement of the concept and the special precautions that were exercised to guarantee its successful utilization.

#### REFERENCE

1. Mobley, F. F.; Eckard, L. D.; Fountain, G. H.; and Ousley, G. W.: MAGSAT - A New Satellite to Survey the Earth's Magnetic Field. Johns Hopkins paper presented at IEEE INTERMAG Conference (Boston), Apr. 21-23, 1980.

TABLE 1 - BOOM SYSTEM WEIGHT BREAKDOWN

Link Structure	2.72 kg	6.00 lbs
Drive Ass'y	2.93	6.45
Gimbal Actuators (3)	3.09	6.82
Caging Subsystems	<u>1.13</u>	<u>2.50</u>
	9.87 kg	21.77 lbs
Inverters (2)	0.62	1.37
Electrical Subsystem	<u>0.76</u>	<u>1.68</u>
	1.38 kg	3.05 lbs
Sensor Platform Ass'y	7.03	15.50
Boom Cable	<u>2.72</u>	<u>6.00</u>
	9.75 kg	21.50 lbs

TABLE 2 - ALIGNMENT TEST RESULTS

TEST NO.	MIRROR TILT ANGLE(1) (arc min)	MIRROR POSITION OFFSET(2) (cm)	TRANSVERSE DISPLACEMENT TO CORRECT MIRROR TILT (cm)	SUM OF POSITION OFFSET AND TRANSVERSE DISPLACEMENT(3) (cm)
A. Rotary Table at 0° (Pitch)				
I	+ .75	0	-.128	-.128
V	+1.12	0	+.191	+.191
B. Rotary Table at 180° (Pitch)				
I	+1.87	+.064	+.317	+.381
V	-4.12	+.128	-.699	-.571
C. Rotary Table at 90° (Yaw)				
I	+3.75	0	+.635	+.635
V	-1.12	+.381	-.191	+.191
D. Rotary Table at 270° (Yaw)				
I	-4.87	+.128	-.826	-.699
V	-.75	+.191	-.127	+.064

(1) Mirror is normal to ATS optical axis when tilt angle is 0.0 arc min.

(2) Mirror is centered on ATS optical axis when position offset is 0.0 cm.

(3) Operation of the pitch (or yaw) gimbal to produce a displacement of this magnitude reduces tilt angle to zero and leaves this position offset. Size of target zone for position offset is +1.91 cm in both pitch and yaw.

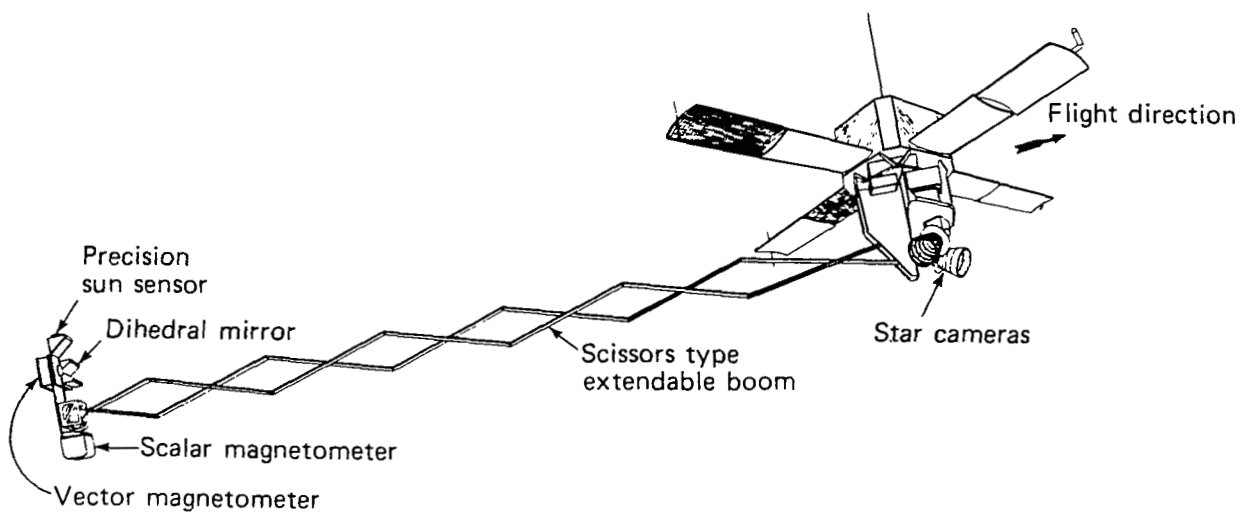


Figure 1.- MAGSAT orbital configuration.

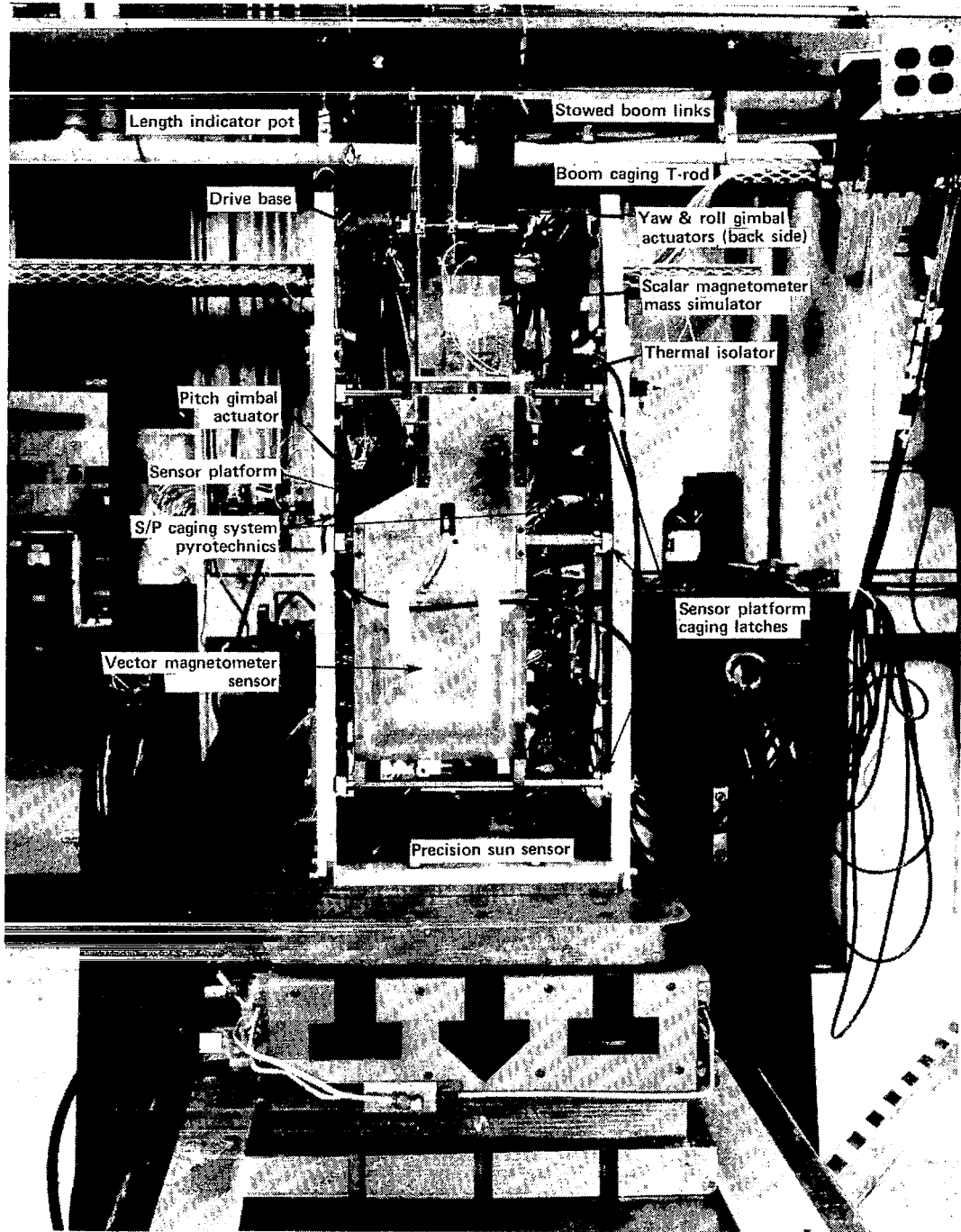


Figure 2.- Magnetometer boom system.

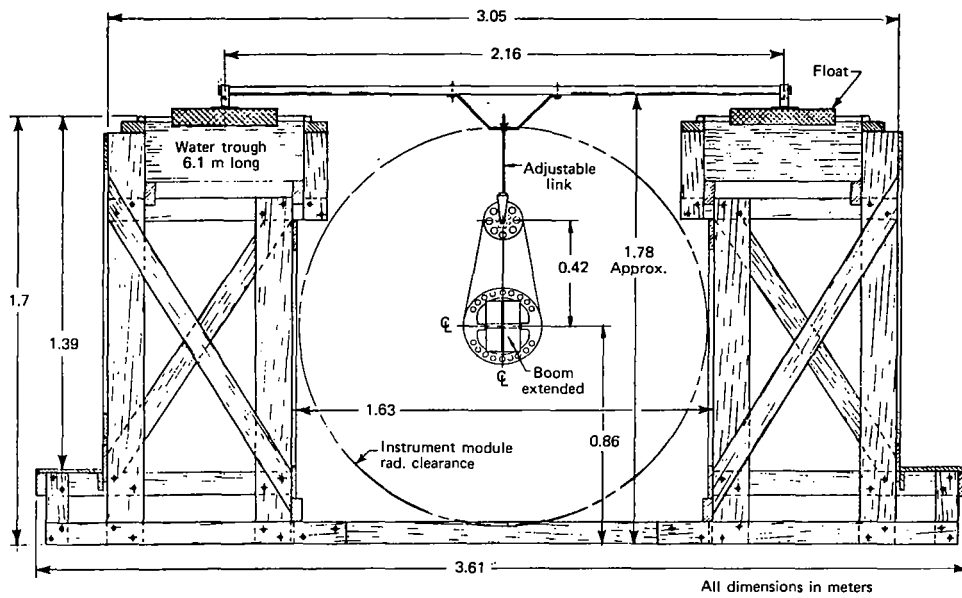


Figure 3.- MAGSAT boom flotation system.

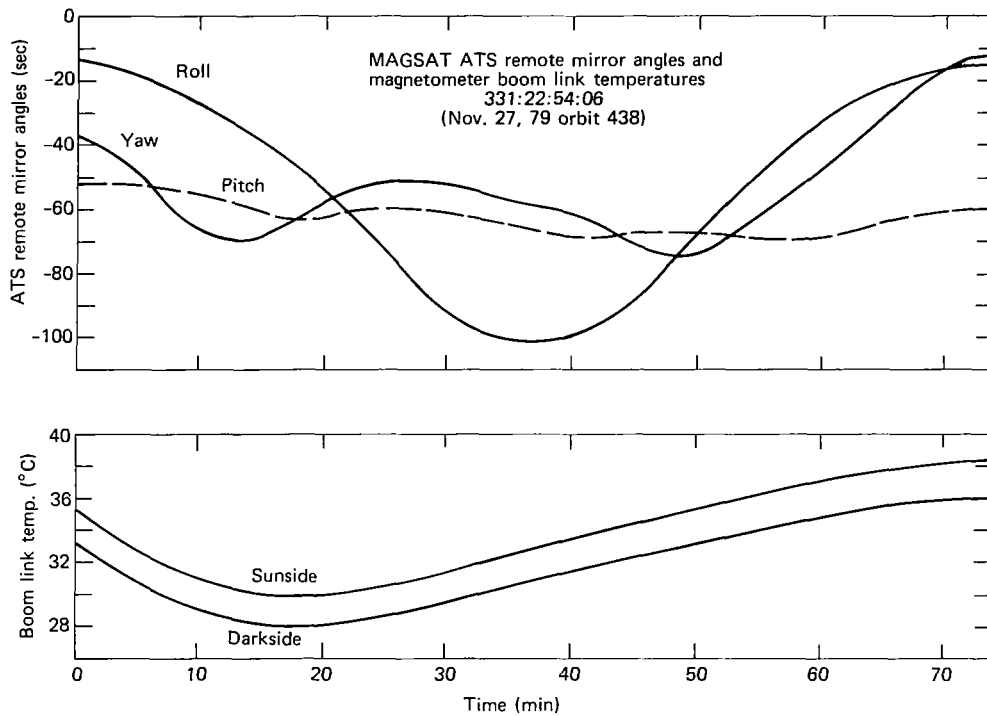


Figure 4.- Mirror angles and link temperatures.

# DRAWER DRIVE FOR SPACE SHUTTLE VACUUM CANISTER<sup>1</sup>

Kenneth E. Werner  
General Electric Company  
Re-entry Systems Division

## SUMMARY

A sliding drawer type canister was designed to contain LDEF experiments which require vacuum storage before and after space exposure. The elastomeric seals require high closing loads which are generated thru camming levers and transmitted thru a spring loaded pressure plate. Lubrication was provided by various dry surface coatings. Higher than expected friction required some redesign after which the assembly functioned well and provided good sealing.

## INTRODUCTION

A conceptual study for a Vacuum Exposure Control Canister (VECC) for NASA's Space Shuttle Long Duration Exposure Facility (LDEF) resulted in the sliding drawer concept depicted in figure 1. The experiment is carried in a tray or drawer which upon closing, slides into the Vacuum chamber and the "drawer-front" seals against the face of the chamber. The entire assembly is designed to occupy one third of an LDEF experiment frame and to a 15.2-cm (6-in.) depth. The assembly measures 83.8 x 41.3 x 15.2 cm; the chamber is 37.5 x 37.6 x 9.5 cm; while the experiment drawer measures 35.6 x 34.0 x 4.8 cm deep. The application requires that the drawer may be opened and closed several times in the preparation, exposure, and evaluation of an experiment. This requirement eliminated the use of metallic or ceramic sealing elements in favor of elastomeric sealing elements, despite the knowledge that such seals could not maintain a hard space vacuum in the chamber. It was also decided that the prototype design phase would include a full scale evaluation of three candidate "Gasko-Seal" designs as manufactured by Parker Seal.

## SPECIAL DESIGN REQUIREMENTS

In addition to the usual aerospace design constraints the following requirements were special to the LDEF and VECC usages.

---

<sup>1</sup>Work performed under contract NAS-1-14375

## General Requirements

The unit must meet the Space Shuttle environment which was found to be typical of aerospace flight. The most significant single requirement is that the mechanism must function at ambient conditions, in a hard vacuum at 1 g, and after long periods in a hard vacuum at zero g. This means that all sliding members must be provided with lubrication that will be sustained for long periods in space vacuum. The other general requirement impacting the design is that nonmagnetic materials be used in the mechanism and structure.

## Specific Requirements

### Space

The total volume for the VECC sounds large; however the upper 9.5 cm of the total height of 15.2 cm is occupied by the vacuum chamber or is swept out by the drawer motion. The mechanism must operate in the lower 5.7 cm. The space under the chamber must house the motor with gearing and the mechanism in the closed position along with all electrical connectors and wiring, the programmer, support structure and an experiment data wire trough.

### Seals and Loads

The candidate seals are shown in figure 2 along with the face plate configuration. The seals, variants of Parker Seal's "Gasko Seal" design, all are embedded directly into the seal plate, rather than being fabricated into a separate carrier piece as is often practiced. The integral design approach eliminates an extra leak path. The single and double seals were carried thru to tests, while the double lipped single seal was dropped on the recommendation that this seal offered no sealing advantage and sometimes is troubled by gases trapped between the lips. All the seal configurations were to use Parker V720-75 compound, which is a variant of DuPont "Viton" fluorocarbon and is considered to provide the best vacuum sealing.

The required force to close the seal is a function of seal geometry and the seal material characteristics. The gasko seal design requires that the seal is compressed so that it occupies a very high percentage of the volume available in the seal groove. The Viton is a very tough material which resists being compressed into a confined groove. Whereas the preliminary design of the drawer drive was based on a more typical closing load of 6130 N/m (35 lb/in) of seal, the Viton gasko-seal combination requires a load of 20,315 N/m (116 lb/inch). This significant increase of design load required a re-thinking of the drive design. Although a low power drive targeted at 25 watts was desirable, this requirement was not hard. A firmer limitation was the space available for the motor. This condition is somewhat alleviated by a loose requirement for closing and opening time. Initially the design was targeted toward the 3-4 minute range, but any time within half an hour was acceptable. Energy was more critical than time.

## SEAL EVALUATION

The program plan was to evaluate the seals at the earliest possible date while the design and fabrication of the remainder of the unit were in progress. Accordingly the chamber, face plate, and pressure plate assemblies were designed first. Face plates as shown in figure 2 were fabricated with blank faces and shipped to the seal manufacturer where the grooves were cut and seals molded. The chamber was designed and fabricated with a thick bottom which could be later modified to mount and accommodate the drawer drive elements. The pressure plate assembly including the stacks of Belleville washer springs were designed. Individual springs were loaded to a recommended 67% of deflection to the flat state. The washers were stacked in parallel to provide the necessary load and these stacks were used in series to provide a deflection judged necessary for good load distribution. The total seal load for the single seal is 18,237 N (4100 lbs) and for the double seal 36,474 N (8200 lbs). Nominal location for the three spring stacks had been established in the early design release. An examination of deflections in the face plate revealed that the ends deflected well in excess of the allowable .008 cm (.003 inch) flatness to assure good sealing. Side stacks of springs were introduced to closely match the distribution of the applied spring load with the seal loading. A breadboard pressure plate was made up for seal evaluation testing. Figure 3 shows the spring stack arrangements used and the tie bolted test setup. The belleville springs were lubricated with dry film  $\text{MoS}_2$  to avoid binding between individual washers. The tie bolts were tightened to provide the computed spring deflections. The face plates - chamber face gap was measured before loading and was found to conform to the seal height tolerance .061 to .066 cm (.024 to .026 in). When loaded, the design fully satisfied the seal manufacturer's recommendations that the seal plate faces shall be closed within .008 cm (.003 in).

Helium leak rate testing is shown in figure 4. Six tests were run using two single seal face plates and one double seal plate. Leak rates were obtained as follows:

Run No.	Seal Plate S/N	Leak Rate SCC/Sec (He)	
		Single Seal	Double Seal
51	2	4.28 x 10 <sup>-5</sup>	
52	2	5.38 x 10 <sup>-5</sup>	
53	1	5.17 x 10 <sup>-5</sup>	
54	1	4.13 x 10 <sup>-5</sup>	
D1	1		3.56 x 10 <sup>-5</sup>
D2	1		5.74 x 10 <sup>-5</sup>

Although the double seal tests took up to 50 minutes to arrive at steady state while it took up to 17 minutes for the single seals, the steady state leak rates show no significant difference. In the application, the steady state leak rate is the significant criterion. Accordingly, all subsequent work was with the single seal which required a 18,237 N (4100 lb) rather than a

36,474 N (8200 lb) closing load. These tests validated the pressure plate and spring stack design and demonstrated seal leak rates compatible with predictions.

### MECHANISM DESIGN

The design approach was driven by the duty cycle. The drawer must traverse its full length, 33.3 cm (13.1 inches), at a very nominal loading, overcoming only friction and in the final .439 cm (.173 inches), the load increases to the final value of 18,237 N (4100 lb). This suggests a drive of modest load capability to traverse the distance and which then operates a load multiplying mechanism to develop the high terminal load. The basic drive consists of a gear motor driving an Acme lead screw engaging a trunnion nut. The nut drives the tray thru a pair of actuating arms as shown in Figure 5. These arms are held in disengaged position by latches. As the drawer approaches the closed position the operating arms pass thru an opening in a reaction plate, and then are unlatched so that further movement of the trunnion nut rotates the actuator arms. The trunnion nut and slide blocks slide in the arms, and a cam surface on each actuating arm bears against a reaction surface on the reaction plate. The actuator arms are mounted to the pressure plate by support fittings which pull the pressure plate home. Trade offs include gear ratio, lead screw pitch and diameter, Acme nut vs. ball nut, and lever ratio. A ball nut was rejected as being too bulky and unnecessary. Low friction coatings promised high efficiency of the drive. A load limited 7/16-12 Acme lead screw was used after analysis of shaft resonance frequencies showed that heavier shafts still resonated within the 60-300 Hz vibration requirement. A 218.4:1 commercial gear motor with a nominal 13 RPM no load speed and a stall torque of .71 N·m (100 oz·in.) was chosen to match the loads and provide a closing or opening time of approximately 12 minutes. The chosen motor performance was characterized by test and found to closely match catalog data. It was found that this motor offered good performance while the cost of purchasing it and modifying it for space operation was much less than for purchasing an aerospace motor.

The actuating arms were designed to give the maximum ratio consistent with the geometry constraints, which proved to be 5:1. This trade off involved the Hertz stress at the camming surface. The radius of the surface was kept as large as possible, but at 2.54 cm (1.0 in.), the Hertz stress was 1,275,000 kPa (185,000 psi) for the double seal and 896,000 kPa (130,000 psi) for the single seal. This stress in combination with the requirement for non-magnetic materials posed a problem which was solved by fabricating the arms and the reaction plate of A286 steel.

In the vertical plane the support fittings pull on the pressure plate at a line below the center of the sealing forces, creating a moment of 2083 N·m (18,450 lbf·in). This moment is reacted out thru the pressure plate arms as shown at  $R_1$  and  $R_2$  in figure 6. These arms were originally envisioned as lightweight support and guiding members, but to carry the large moment, they were beefed up and provided with reaction surfaces. The top of the far end of each arm slides on the bottom of the vacuum chamber, and a shelf at the pressure plate end engages a mating shelf on the reaction plate. This engagement occurs just prior to seal closure.

In addition to the drawer drive, trigger type mechanisms were designed and built to operate shades which protect the elastomeric seals from strong solar radiation while the drawer is in the fully open position during space exposure. These appear in Fig. 1.

A programmer was also developed to control the operation of the unit. This component appears in figure 6. Although it required a considerable effort it is not discussed further in this paper.

### MATERIALS AND FRICTION COATINGS

The structure used aluminum to a maximum degree. Nuts, cap screws, and various pins, slide blocks and small slippers are of 300 series CRES. The high stress members, i.e., the trunnion nut, drive screw, the actuator arms and the reaction plate are all of A286. This alloy provides the necessary strength in a nonmagnetic material, and it is the least expensive and most readily available material meeting these requirements.

For the VECC to be used conveniently, it is required that all sliding surfaces be self lubricated. The need to operate after extended space exposure further emphasizes the need for relatively permanent lubricated surfaces. Dry film MoS<sub>2</sub> and a number of proprietary surface treatments were used. These were various grades of "Tufram", "Nedox" and "Hi-T-Lube" developed by General Magnaplate Corporation. Tufram is a form of anodize impregnated with Teflon. Nedox is a form of nickel plate impregnated with Teflon, and Hi T - is a dry film lubricant developed for temperatures above 587 K (600°F). The design was reviewed with the intent of choosing finishes so that in each sliding contact a relatively hard surface bears against a relatively soft surface.

A few of the major parts and the finishes used are as follows:

#### Lubricant Surfaces

Component	Material	Surface	Thickness cm
Drive Worm	A286	Hi-T-LUBE	.0013
Trunnion Nut	A286	NEDOX SF-2	.0018
Slider Blocks	304 CRES	NEDOX SF-2	.0013
Actuator Arms	A286	Hi-T-LUBE	.0013
Reaction Plate	A286	NEDOX SF-2	.0013
Guide Slipper	7075-T651 aluminum	TUFRAM H-2	.0025
Rail	6061-T4 aluminum	TUFRAM L-4	.0038

The drive performance was predicted on the basis of a 70% lead screw efficiency which is approximately equivalent to a coefficient of friction of 0.15. A torque margin of 1.01 was available for the double seal and 3.02 for the single seal.

Adapting the motor for space operation was a separate effort. The manufacturer provided silver graphite brushes and then the gearbox was lubricated with a high vacuum grease containing MoS<sub>2</sub>.

### SYSTEM TESTS

The complete VECC was assembled and operation of various elements attempted. The seal shades were adjusted to accommodate asymmetric tolerance build up. The drawer suspension slippers and rails appeared to function well.

The first serious trouble developed when trying to unlock the actuator arm latches. They did not unlock; rather when the adjustment screws contacted the reaction plate, the drive motor stalled. After some tinkering with adjustment, it became evident that the trouble was more fundamental. Geometrically, the latch looks good and with the "low" nominal friction expected in all parts it should work very well. Accordingly, it breezed thru all the entire design review gamut without a careful force analysis. In actual operation, the low friction surfaces are effective, but friction is still of a significant value. This fact coupled with the moment arm ratio of the trunnion nut to the latch pin approximating 12:1 made the force on the latch pin so high that the latch could not slide off the pin. The latches were replaced by a single latch arm as shown in figure 7, which operates satisfactorily.

The general level of friction proved higher than predicted including the drive screw friction. In cycling the unit, the drive motor was dragged down to near stall before the actuator arm contacted the shut off switch. This demonstrated that the available motor torque was marginal. Fortunately, a higher torque motor was available, which could easily fit into the design and this was later incorporated.

Leak testing of the chamber when closed by the VECC drawer drive produced leak rates equal to those of the earlier tie bolt tests. The unit was cycled thru more than 50 complete openings and closings, demonstrating the durability of the design and the seals. The unit has since successfully passed environmental testing to Space Shuttle levels, and several units have been built for use on LDEF.

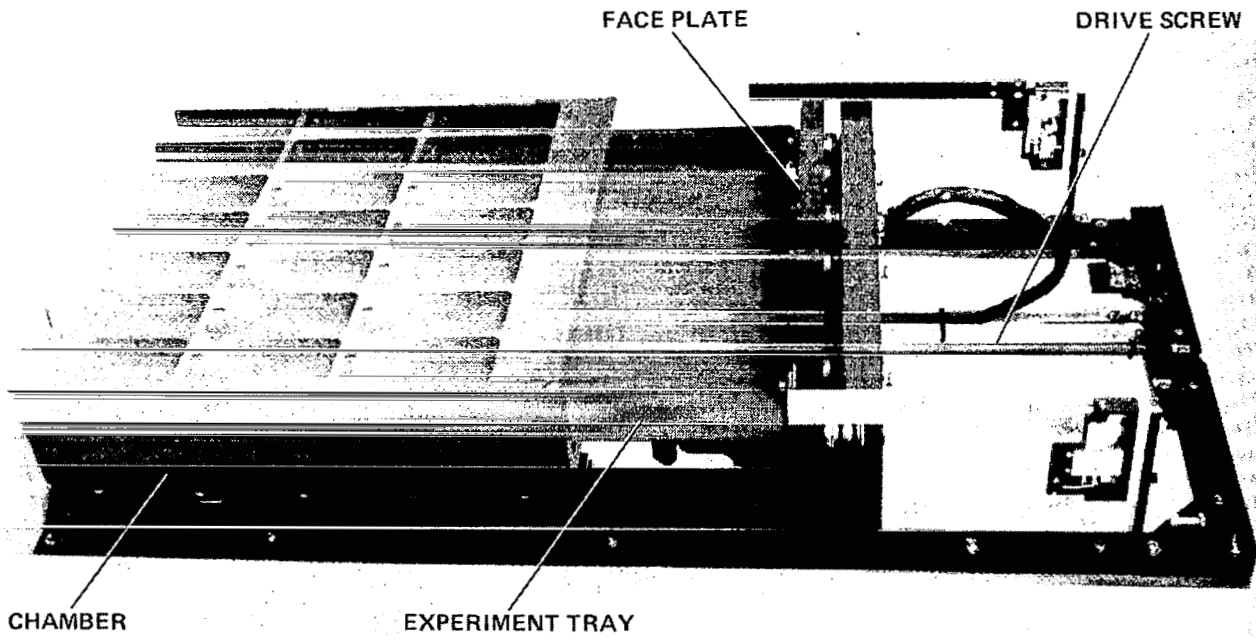


Figure 1.- Sliding tray Vacuum Experiment Control Canister.

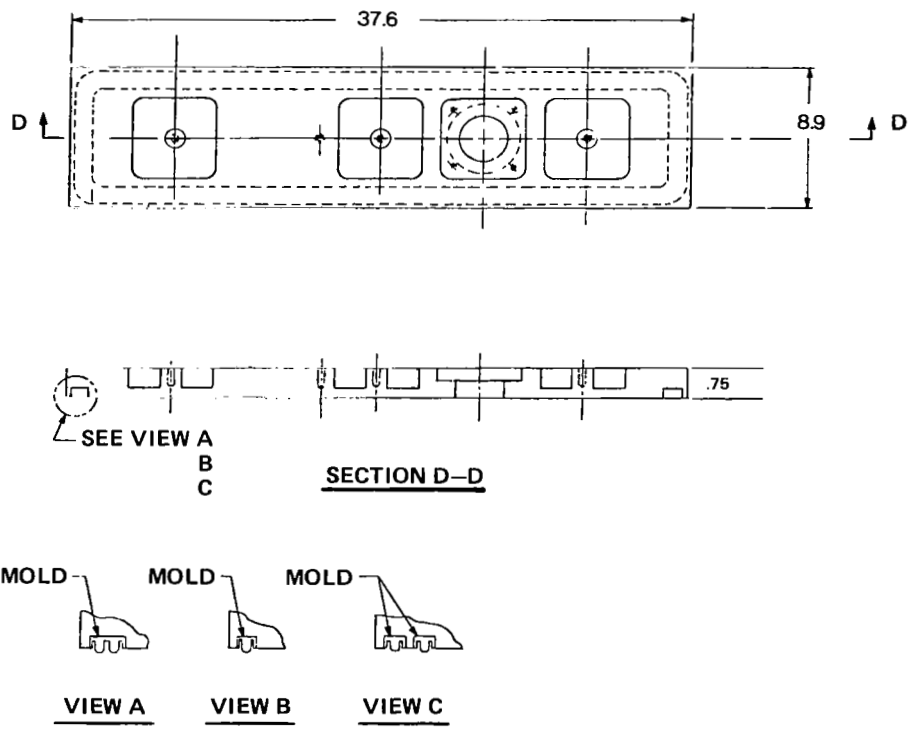


Figure 2.- Face plate. Dimensions are in centimeters.

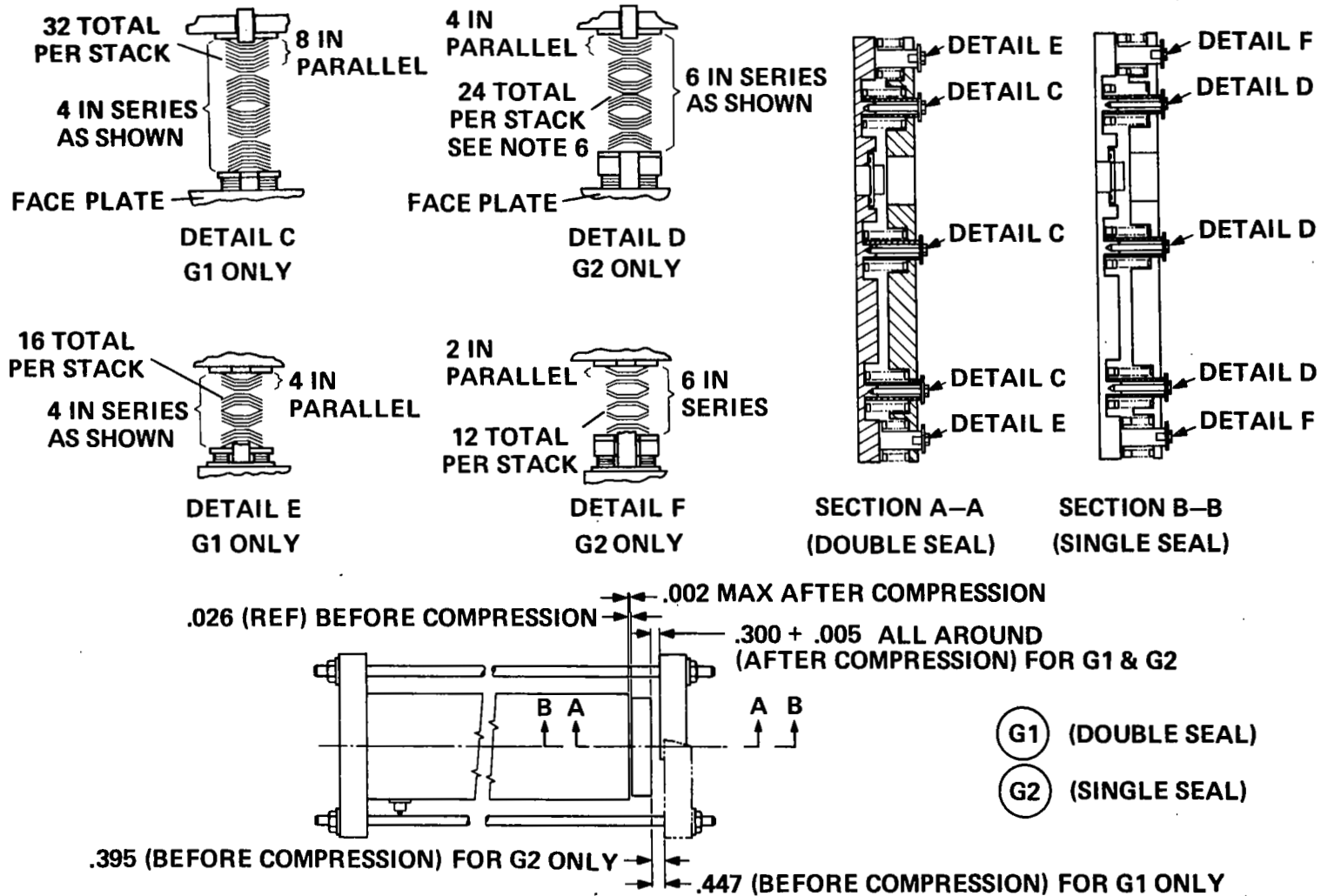


Figure 3.- Spring stacks and test setup.

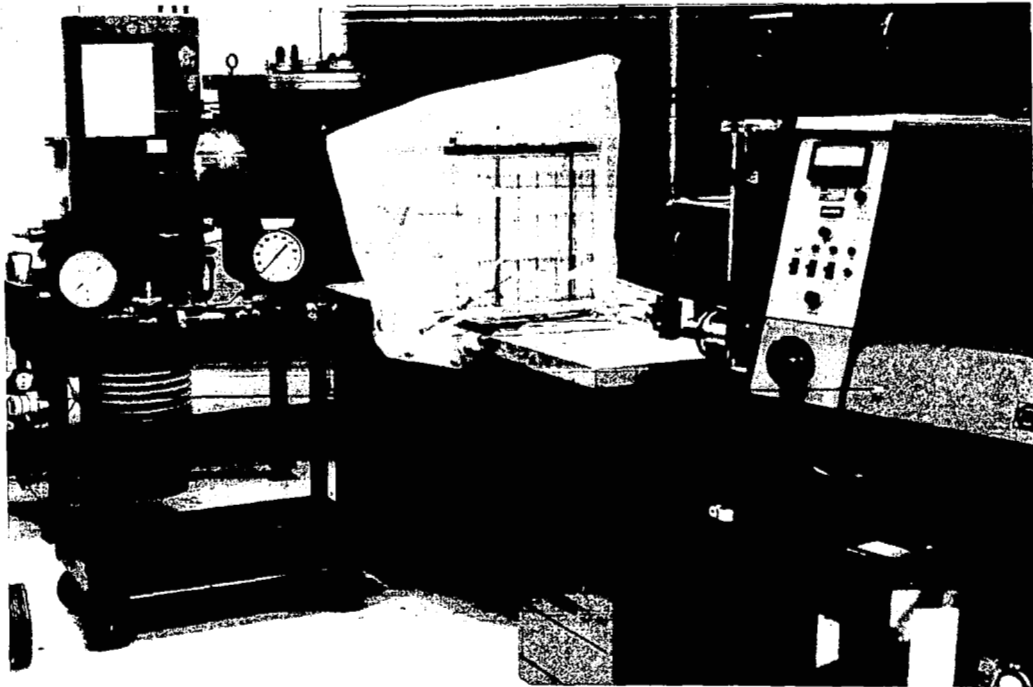


Figure 4.- VECC leak rate test configuration (cannister enclosed for helium fill).

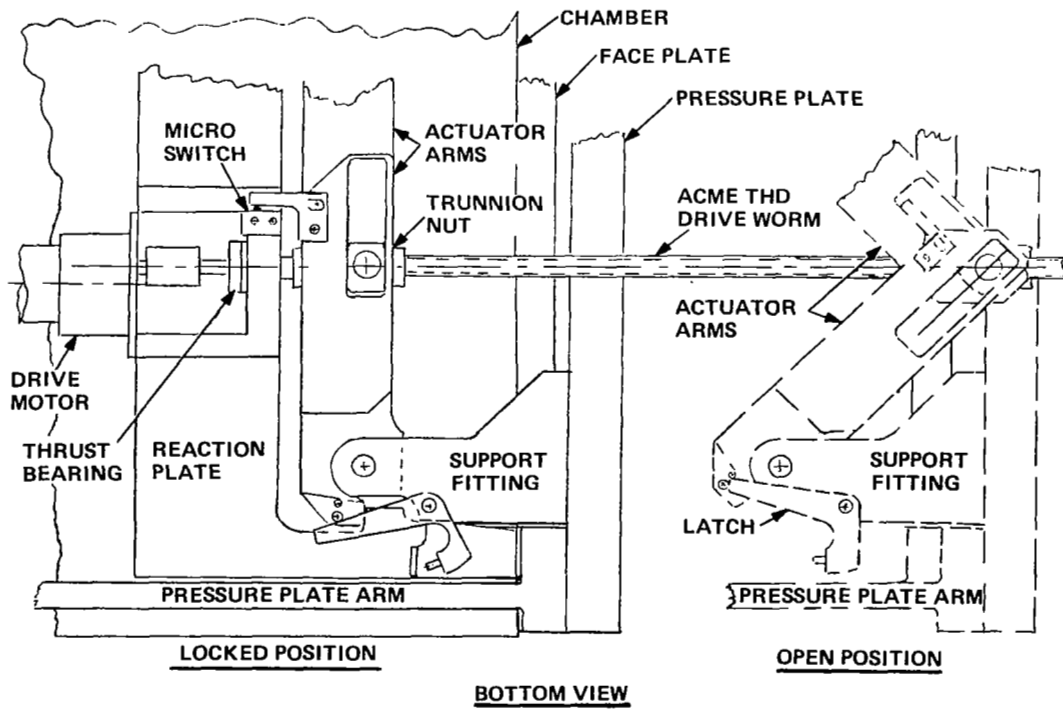


Figure 5.- Tray drive design.

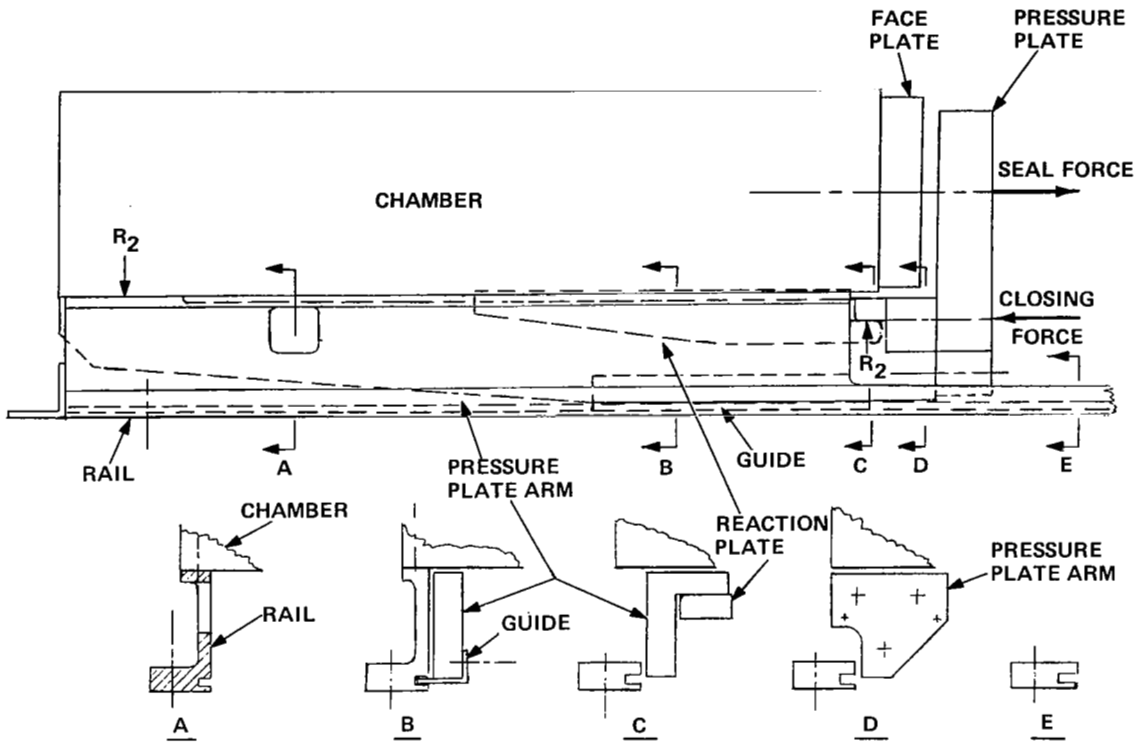


Figure 6.- Tray and chamber support.

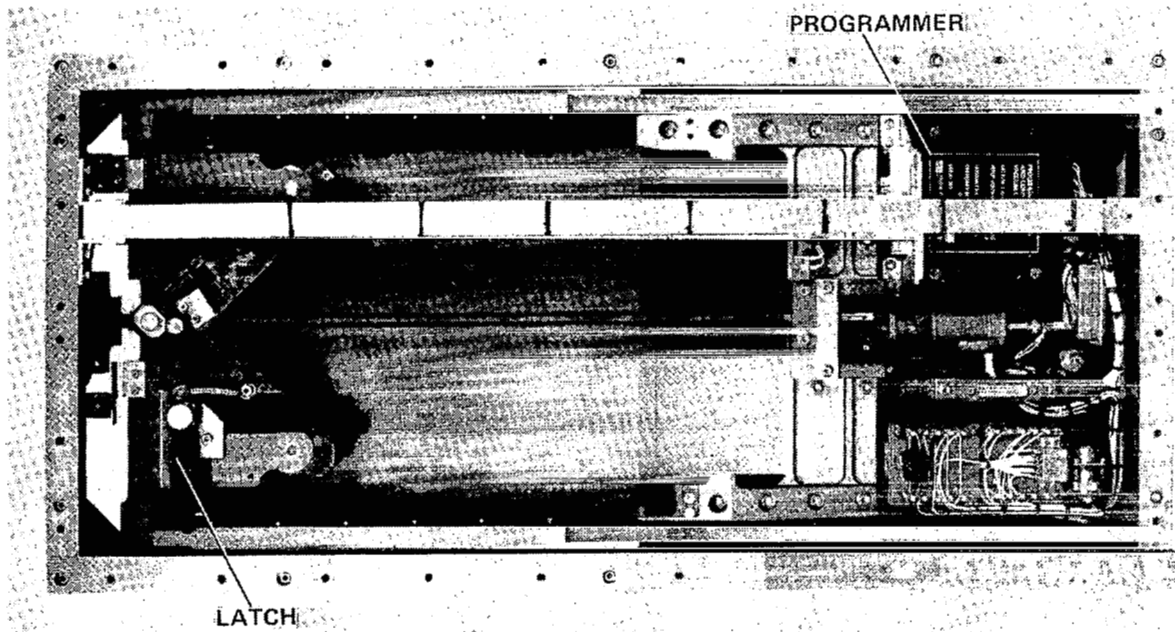


Figure 7.- VECC bottom view.

DESIGN OF AN ATMOSPHERIC SOUNDING RADIOMETER  
FOR THE GOES METEOROLOGICAL SATELLITE SYSTEM\*

Robert G. Jensen

Santa Barbara Research Center  
Goleta, California

ABSTRACT

Each of the U. S. Geostationary Operational Environmental Satellites (GOES) has as the principal on-board sensor a spin-scan radiometer called a "VISSR" (Visible Infrared Spin Scan Radiometer). An advanced version of the VISSR will add a vertical dimension to the instrument's infrared atmospheric images through the addition of a rotating filter wheel and an oscillating calibration shutter. The following presentation gives an overview of the radiometer design with a close look at the filter wheel and calibration shutter mechanisms and their pre-flight test performance.

INTRODUCTION

Six VISSR's have been placed in synchronous orbits at various locations around the world. From their geostationary orbital positions, the VISSR instruments sense energy radiated from earth in the broad-band visible and infrared spectrums, thus enabling ground-based operational terminals to produce day and night pictures of the earth's cloud cover.

An advanced version of the VISSR called a VAS (VISSR Atmospheric Sounder) is now under development and will be flown on future GOES spacecraft. With the addition of twelve selectable narrow-band filters and more precise in-flight calibration of the infrared detectors, the VAS will provide increased data to help determine the earth's atmospheric temperature and water vapor distribution.

---

\*The work reported in this paper was conducted at Santa Barbara Research Center, Goleta, California, under contracts NAS5-21139 and NAS5-20769 sponsored by the National Aeronautics and Space Administration.

## VAS SYSTEM DESCRIPTION

The completed VAS Scanner is shown in Figures 1 and 2, while a cross section of the scanner is shown in Figure 3. For purposes of discussion, the instrument can be divided into three major subassemblies:

- Telescope (Three-Mirror System and Scanner Housing)
- Aft Optics Assembly (Visible Light Sensing Devices)
- Radiative Cooler (Infrared Sensing Detectors)

The VAS Telescope Assembly is a lightweight, all beryllium structure consisting of a scan mirror, primary mirror and secondary mirror mounted in a cylindrical housing. The plane scan mirror is mounted at  $45^\circ$  to the scanner spin axis and is elliptically shaped so as to reflect collected energy into the 40 cm diameter entrance aperture of the Ritchey-Chretien primary and secondary mirrors. In scanning the earth from North to South, the scan mirror is servo-positioned through 1820 steps (0.192 mr/step) by the twin torque-motor drives which support it. East-West scanning is provided by the 100 rpm spacecraft spin.

Mounted just behind the telescope is the Aft Optics Assembly. Energy collected in the visible spectral region is focused on a fiber optics array and transmitted from the telescope focal plane to eight photomultiplier tubes mounted radially on the Aft Optics Plate. The Aft Optics assembly contains a lens system which relays the infrared spectral energy from the telescope focal plane through the optical bandpass filters and on to the infrared detectors located in the Radiative Cooler at the rear of the instrument. The calibration shutter and a blackbody reference source are also contained in the Aft Optics Assembly as well as focusing gear-motor mechanisms which can be stepped to reposition the Visible and IR optical elements axially.

A passive radiative cooler is used to cool the long-wavelength detectors of the infrared channels to a controlled temperature of  $95^\circ\text{K}$  for optimum detector performance. The Cooler Assembly consists of an external sunshield, first stage cooler and a second stage cooler with the latter supporting the evacuated infrared detector package. Each stage of the cooler is thermally isolated from its surroundings and is cooled by a honeycomb high-emissivity radiator which views space. The satellite subpoint resolution varies from 0.9 km in the visible channels to 6.9 km in the infrared.

## FILTER WHEEL ASSEMBLY

### Filter Wheel Design Requirements

As mentioned earlier, the expanded infrared data acquisition capabilities of the VAS system are made possible mainly by the addition of twelve optical filters within the Aft Optics Assembly. When operated in the infrared atmospheric "sounding" mode, the instrument scans the earth scene from West to East with one of the twelve filters in the optical beam. The same scan line is then retraced on the next spacecraft spin with the second filter in the optical beam and so on for all twelve filters. The scan mirror is then stepped from North to South to the next scan line and the filter sequencing is repeated.

In keeping time with the 100 rpm spacecraft spin rate and to allow some time for detector calibration, any one of the filters must be inserted in the optical beam and settled within a 350 milli-second allotted time period for each spacecraft spin. Power consumption must be less than 5 watts. The flat filters must be parallel to each other within 0.5 mrad. Additionally, the mechanism which holds and positions the filters must withstand the environmental requirements of launch vibration induced by the Thor Delta 3914 booster vehicle and then operational temperature extremes of  $-15^{\circ}\text{C}$  to  $+45^{\circ}\text{C}$  in space vacuum. All functional elements must be dual redundant so as to have high reliability over the five year operational design life of the instrument.

### Filter Wheel Design Description

An 11.2 cm diameter magnesium wheel provides accurately machined cells for the circular filters with a minimal moment of inertia ( $2.8 \times 10^{-4}$  newton-meter-sec<sup>2</sup> total including filters).

The wheel is mounted on a shaft which is suspended between two preloaded duplex bearing pairs mounted in series such that if either bearing set fails, the other set will still turn freely. The bearings are dry-lubricated by a molydisulfide film on all contacting surfaces and teflon-impregnated retainers. Wheel positioning is accomplished using a direct drive six-pole brushless torque motor together with a 5-bit optical position encoder.

A second similar motor (mounted in tandem with first) is normally used as a tachometer to assist in the control loop for settling the wheel in any given filter position. This second motor can be driven together with the first, thereby doubling the available torque should this failsafe measure ever become necessary to move a particular filter into the optical beam.

The mechanism arrangement can be seen in the cross section and photograph shown in Figures 4 and 5. Since the different-mass filters are arranged around the wheel for best mechanical balance, the electronic drive logic must step the wheel back and forth in a complicated sequence which depends on filter wavelength. However, the maximum single-step rotation is never more than  $180^\circ$ . The filter wheel acceleration and deceleration rate is then approximately  $1000 \text{ rad/sec}^2$  with a peak velocity of  $20 \text{ rad/sec}$ . The wheel and housing external surfaces are finish-coated with high emittance flat black and low emittance gold for purposes of filter thermal control.

#### Filter Wheel Problem Areas

During testing of an engineering model filter wheel assembly, two problems arose, one in the motor design and one in the position encoder.

The tandem redundant motor concept led to the development of a torque motor which could be used for both the primary drive and the tachometer. Ease of production and simplicity of electronic drive circuitry were both reasons for pursuing a single interchangeable motor design. The 6-pole, 2-phase torquer provided 12 magnetic detents for holding the wheel in any position without power. In order for the drive motor to step the wheel, it needed to have a torque sensitivity high enough and with the proper angular distribution to overcome the unpowered detent torque of both motor rotors. Although the motor performance was specified in order to achieve tandem operation, the motor manufacturer was unable to meet the specified torque sensitivity curves and as a result, the engineering model motors would not drive the wheel reliably between certain filter positions. A new motor was built which had the twelve stator pole pieces skewed at an angle to the motor axis but with the rotor pole pieces still aligned axially (Figure 6). By skewing the stator pole pieces, the magnetic flux from each rotor pole piece is spread among several stator pole pieces and the unpowered magnetic detent is reduced to nearly zero with a negligible reduction in powered torque sensitivity. The combination of a primary drive motor with skewed stator poles and a tachometer motor with straight stator poles (original design) resulted in a tandem pair with a total magnetic detent torque that was half of what it was originally yet still retaining the double total powered torque required for failsafe operation.

The position encoder problem arose during radiation testing intended to simulate radiation exposure in space. The encoder consists of 12 light-emitting-diode / phototransistor pairs and a

thin intervening metal disc with cutouts in 5 tracks. When exposed to a  $1 \times 10^5$  rad dose of Cobalt 60 radiation, the output of the LED's was reduced to a level which rendered the encoder inoperable. Correction of the problem was achieved by adding a radiation shield made of tantalum around the entire encoder area. There were no failures of this kind after subsequent radiation tests.

### Filter Wheel Testing

Once the drive motor problems were solved using the engineering model, a second filter wheel assembly was built using all new parts. Testing on this "reliability model" started with qualification vibration exposure followed by a functional check-out and then long-term operation in a vacuum chamber. An operational extreme was simulated wherein the filter wheel was automatically stepped back and forth  $180^\circ$  rather than in the normal filter sequence. Continual 24 hour operation accelerated the duty cycle to about 4 times that which would ever be experienced in space. This test was allowed to continue for a simulated space lifetime of eleven years. Periodic measurements of the time required for each step were used together with measurements of rolling and static bearing torque to evaluate bearing life expectancy. Bearing torque increased with time for both the inner and outer bearing sets as shown in Figure 7. Interestingly, the static torque required to turn each bearing separately did not equalize with time but rather exhibited a leapfrog increase at first and then a large difference for the duration (Figure 7). After approximately 7 million cycles of the filter wheel, the stiction in the larger outer bearings rose substantially so that the inner bearings were turning nearly all of the time.

The bearing torque increases were attributed to the formation of small bumps in the raceway lubricants as the teflon retainer material became unevenly distributed on contacting surfaces. Once the large bearing set became stuck in a particular spot, the repeated vibration created by operation of the small bearings caused the large bearings to become increasingly mired in that spot. Although the step time increased with the bearing stiction, it never exceeded 250 milliseconds, and since the test lasted more than double the design lifetime, no redesign was necessary and the subsequent flight model assemblies were built exactly like the reliability model.

## CALIBRATION SHUTTER ASSEMBLY

### Shutter Design Requirements

In-flight radiometric calibration of the scanner's infrared detectors is required for each spacecraft spin. A heated conical blackbody mounted within the Aft Optics Assembly serves as a constant-temperature IR reference source when viewed by the detectors through a 45° reflective mirror. Since 100% field-of-view coverage is required for calibration, the 2 x 3.5 cm rectangular mirror must be completely inserted into the optical beam within 50 msec, maintain blockage for 33.3 msec, and then be completely removed in 50 msec prior to earth view. After surviving the launch vibration mentioned earlier, the shutter mirror mechanism must operate continuously in the same environment as the filter wheel with minimal power consumption and must not block the optical beam whenever power is removed.

### Shutter Design Description

Since shutter power consumption was to be minimized, the design concept evolved around mounting the mirror on a torsional spring so that it would oscillate at a natural frequency in time with the spacecraft spin. Then only a slight amount of input power would be required from a drive motor to maintain the amplitude and to occasionally correct frequency for spacecraft spin rate variations.

As shown in the photographs and cross section in Figures 8, 9 and 10, two flex pivot devices are mounted in series to provide the proper spring rate at sufficiently small deflection amplitude to insure nearly infinite spring life. The rotor of a two-pole brushless torque motor is coupled to the oscillating mirror portion of the mechanism. Attached to the same arm as the mirror is a chopper flag which actuates a 2-bit optical encoder for amplitude and frequency control. The shutter was designed to oscillate at twice the satellite rotation frequency to meet the insertion timing requirement without increasing the oscillation amplitude or swing radius beyond those allowed by the available space within the VAS Aft Optics area. Shutter mirror motion is then expressed as

$$\theta_m = 18^\circ \sin 2 (\theta_s - 5.17^\circ)$$

where  $\theta_m$  is mirror position and  $\theta_s$  is satellite angular position relative to earth nadir. Static balancing of the rotating mass is accomplished by simply changing the thickness of a counterbalance weight.

Precise adjustment of the shutter natural frequency is then accomplished by adding thin rings to the shutter hub, thereby increasing the moment of inertia of the oscillating portion in accordance with the torsional pendulum relationship:

$$f = \frac{1}{2\pi} \sqrt{\frac{K}{J}}$$

where f = frequency

K = total spring rate

J = polar moment of inertia

The rings are mounted so as to have no effect on the static balance of the shutter arm.

#### Shutter Problem Areas and Testing

A major oversight was made in the mathematical analysis of the dynamic forces acting on the shutter during operation in the spinning scanner. The shutter assembly is mounted in the scanner about 7 centimeters off the scanner spin axis. Since the Scanner's optical axis is nearly coincident with the spin axis, the shutter mirror moves on and off the spin axis in a plane that is tilted 45° to the spin axis. When the scanner is spinning, three types of dynamic forces affect the sinusoidal shutter arm motion:

1. Centrifugal force on the shutter arm CG resulting from static imbalance.
2. Forces resulting from Coriolis acceleration of the shutter mass as it moves in a rotating inertial reference frame.
3. Forces that are the result of any inertial imbalance in the shutter arm.

Static balancing of the shutter arm reduces the effects of the centrifugal force to negligible levels. The analysis also showed that since the shutter oscillates in one plane, the Coriolis forces always act on the arm in a direction intersecting the shutter rotation axis, thereby producing no torque about the shutter axis. The analysis stopped at that point, and consequently the first shutter assembly was built with a 6:1 imbalance ratio between the principle non-polar moments of inertia of the shutter arm. The unit worked fine until the scanner was spun, and then shutter motion was uncontrollable at spin rates over 30 rpm due to the inertial imbalance.

Corrective action was accomplished by redistributing the mass along the shutter arm by material density changes and the addition of two inertial balance weights at 90° to the axis of the shutter arm. Inertial balance between the two principle axes was thereby achieved, and a retrofitted unit operated flawlessly throughout the maximum electronic control range with scanner spin rates ranging from 80-120 RPM.

Just as with the Filter Wheel Assembly, a "reliability model" of the shutter assembly was built and tested in the laboratory. After being subjected to the launch vibration environment, the shutter was placed in a vacuum chamber and allowed to operate on a real-time basis for a period of 3 years. Periodic measurements of spring rate and natural frequency showed no change. Since the shutter assembly is a resonant-frequency device, no acceleration of the test is possible and it will therefore continue until five years of operation have been accumulated.

#### CONCLUDING REMARKS

In retrospect, the basic design approach was sound for both the Filter Wheel and Calibration Shutter assemblies. If requirements arise in the future for longer mechanism lifetime, some changes will have to be made to improve the Filter Wheel bearing lubrication. Research has already been performed on the bearing lubrication scheme in the scan mirror drives where the partial rotation creates a bearing "bump" problem much more rapidly than in the Filter Wheel Assembly. Perhaps a thinner RF sputter coating of molydisulfide would reduce the teflon transfer rate and thereby improve Filter Wheel bearing longevity as it did in the scan mirror drives.

The Calibration Shutter design concept was adopted for use in two shutter assemblies in the Thematic Mapper instruments now under development for the Landsat program. An improvement to the VAS design was made in the Thematic Mapper Shutters by supporting the oscillating mass between two side-mounted flex pivots rather than in a cantilever arrangement as in VAS. This prevents bending loads from being exerted on the pivots by the drive motor and affords better control of the rotor-stator air gap. Although this design was considered for VAS, the VISSR retrofit requirement left insufficient space for the bulkier side-mount flex pivots.

Three VAS Systems are currently being built. The first of these has successfully completed all of the scanner-level acceptance tests and is now being installed on the GOES 'D' spacecraft. Launch of the GOES 'D' is scheduled for August of 1980 with GOES 'E' and GOES 'F' following at six-month intervals.

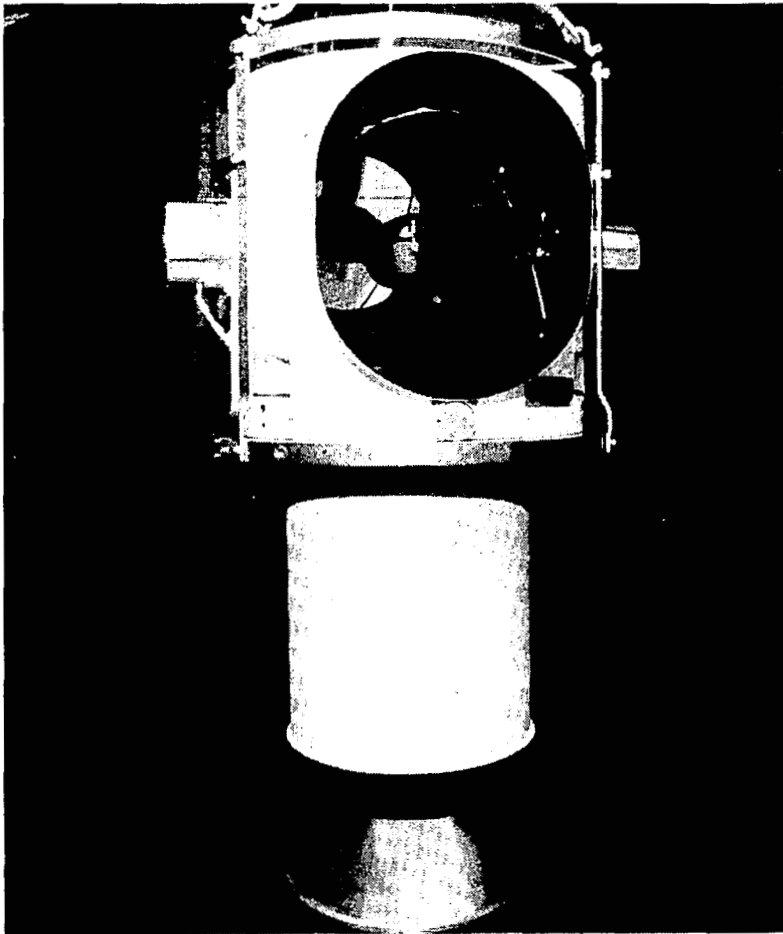


Figure 1.- VAS Scanner.

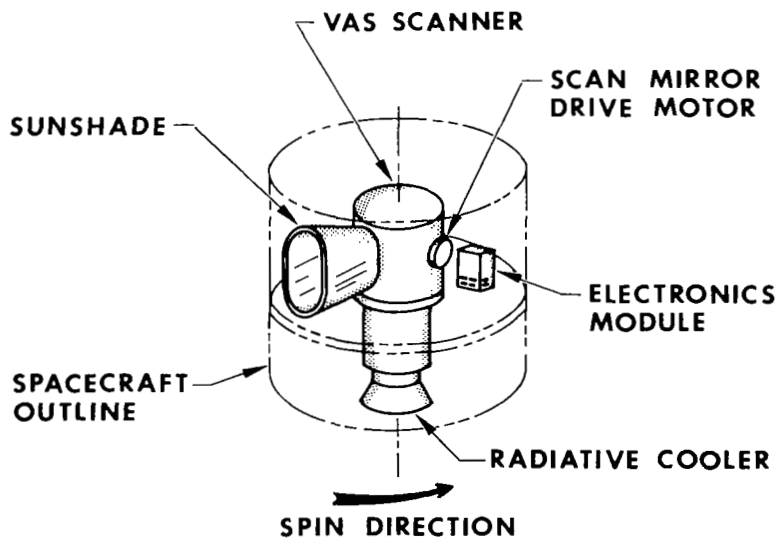


Figure 2.- VAS mounting in GOES spacecraft.

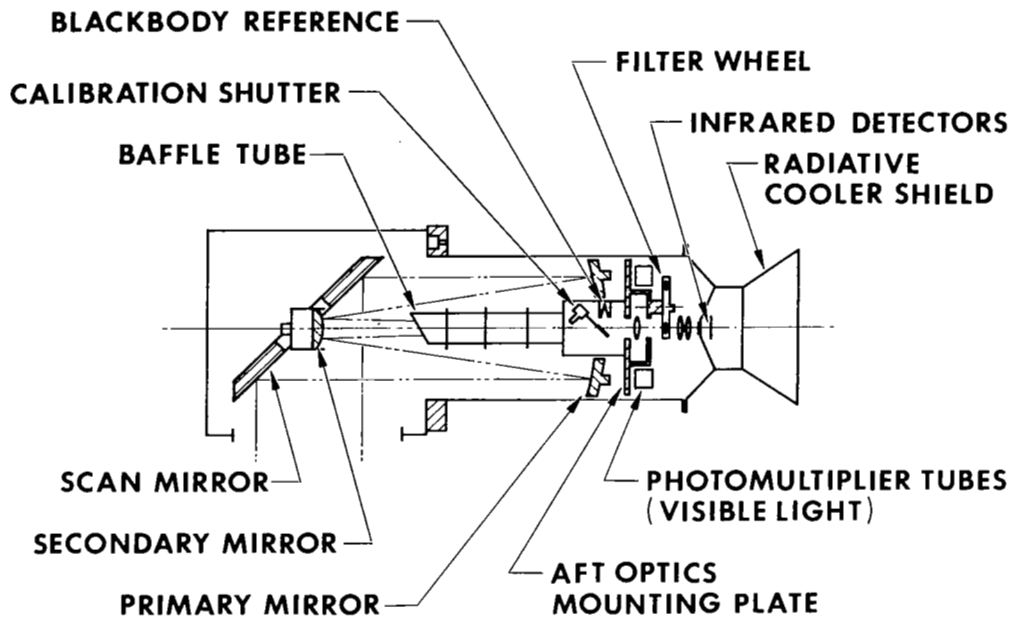


Figure 3.- VAS schematic cross section.

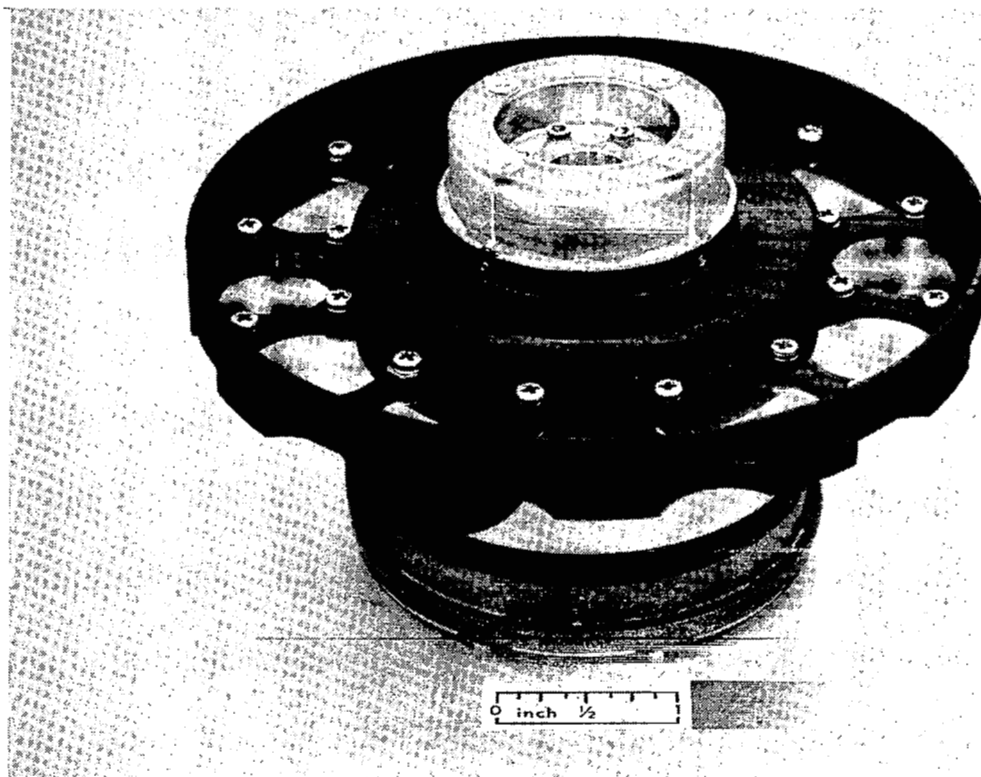


Figure 4.- Filter wheel assembly.

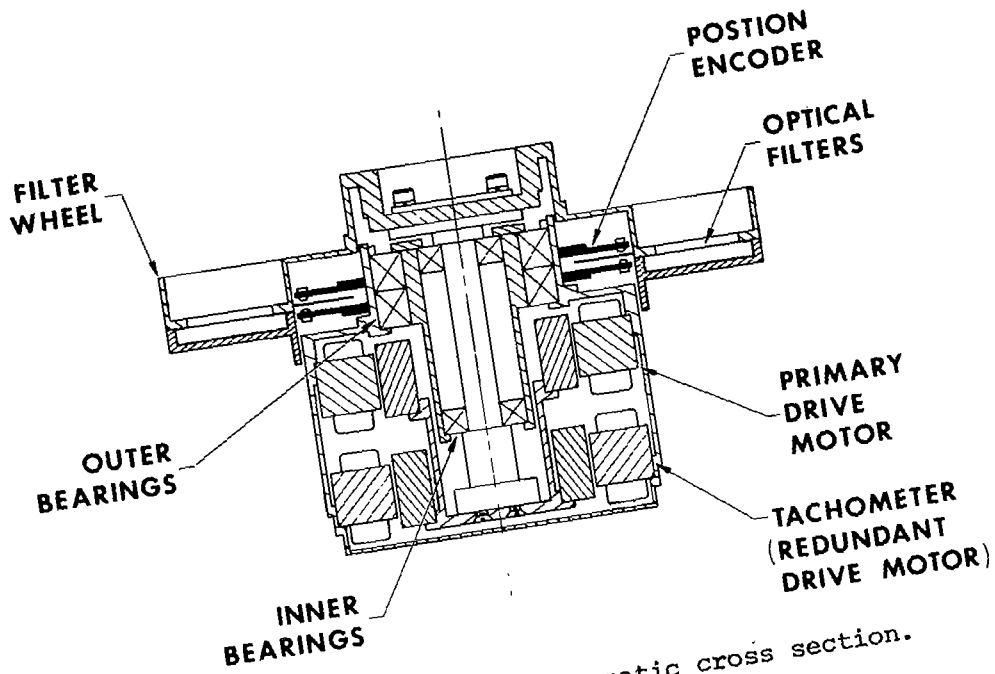


Figure 5.- Filter wheel schematic cross section.

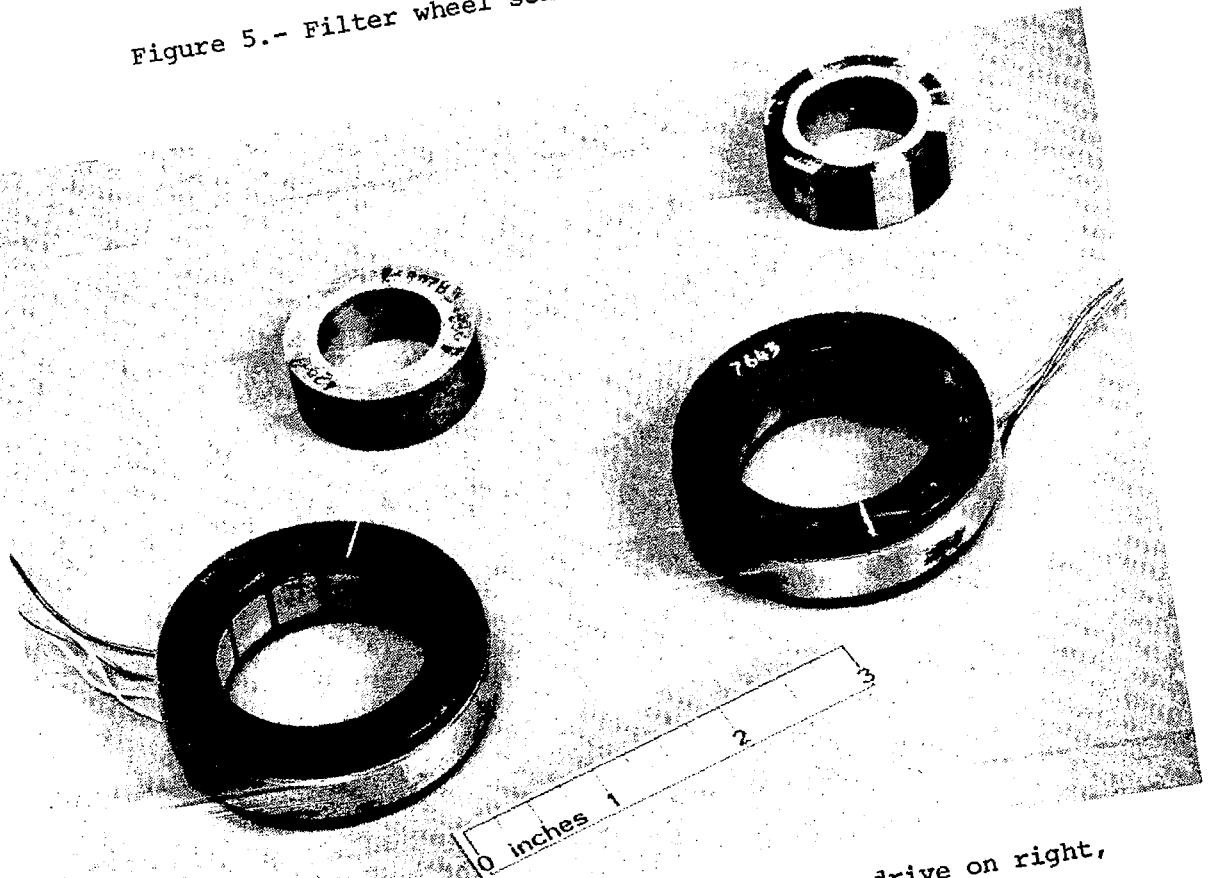


Figure 6.- Filter wheel motors - primary drive on right, tach (redundant drive) on left.

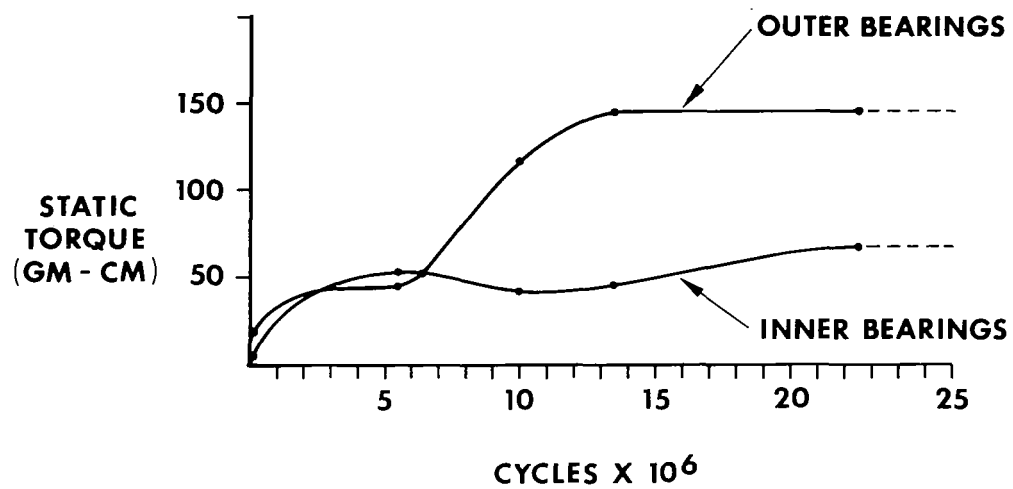


Figure 7.- Filter wheel life test - bearing torque vs. accumulated operation.

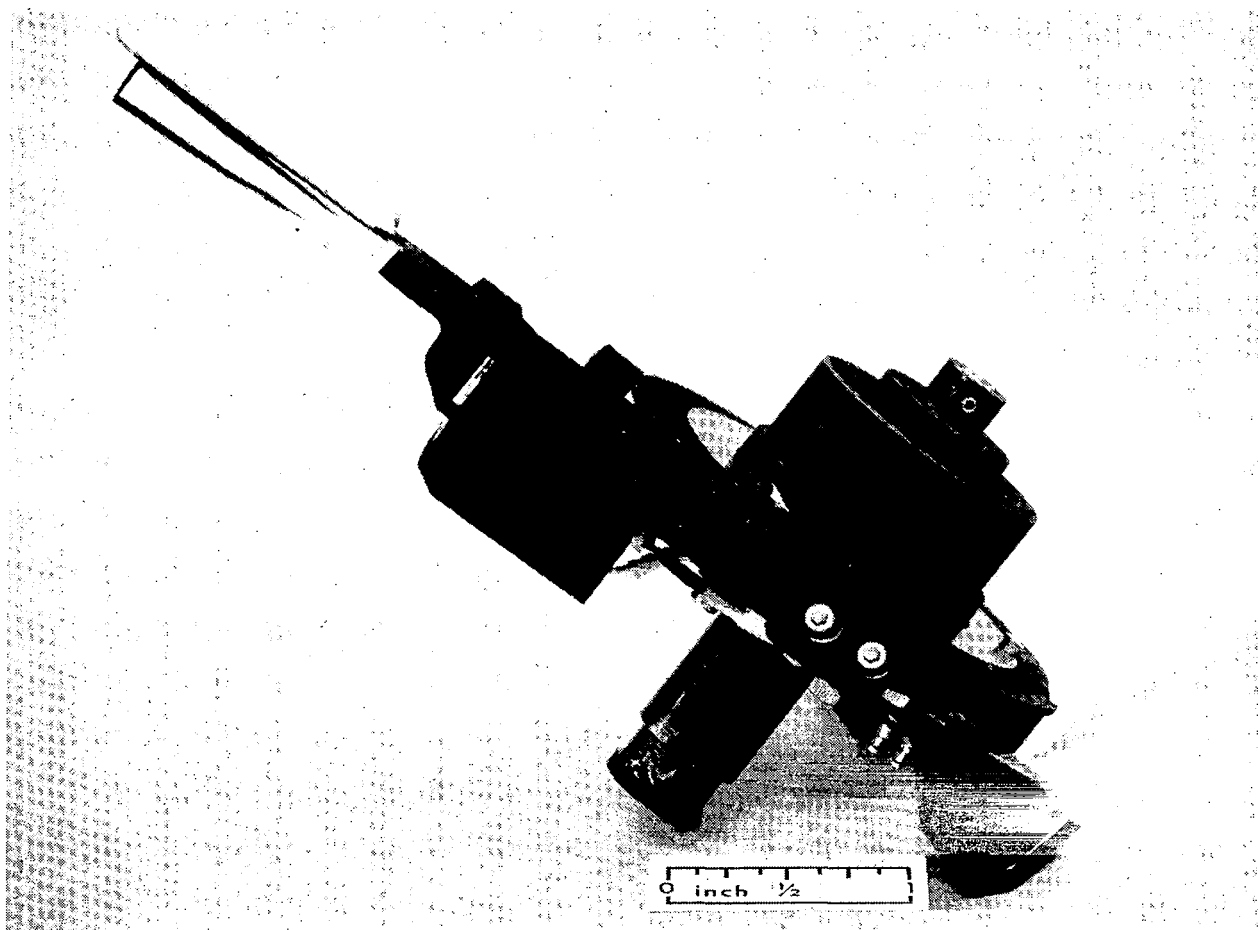


Figure 8.- Calibration shutter assembly.

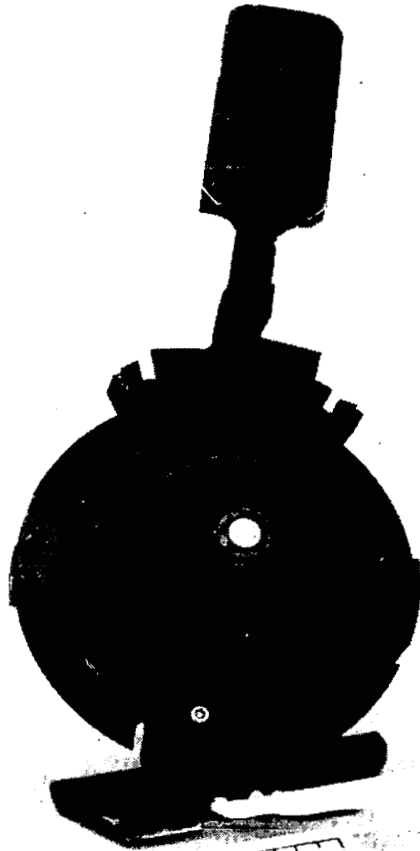


Figure 9.- Calibration shutter assembly.

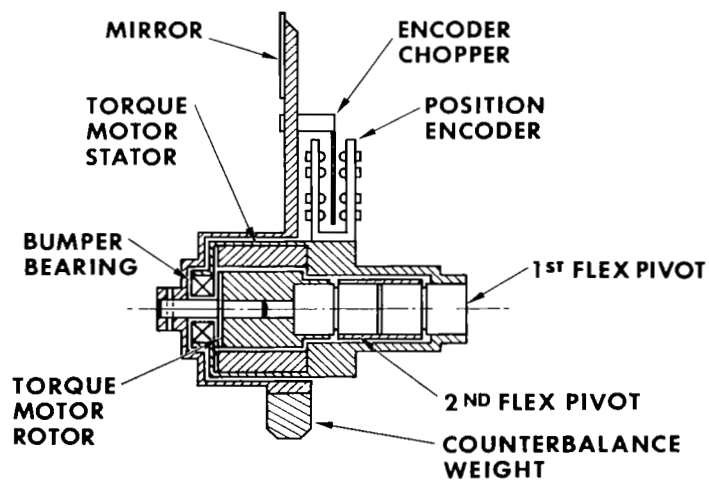


Figure 10.- Calibration shutter schematic cross section.



## A POLARIMETER FOR THE HIGH RESOLUTION

### ULTRAVIOLET SPECTROMETER/POLARIMETER

John A. Calvert  
George C. Marshall Space Flight Center

#### INTRODUCTION

The High Resolution Ultraviolet Spectrometer/Polarimeter (HRUVSP) is an experiment to be launched aboard the Solar Max Mission sometime in early 1980. The HRUVSP will allow the study of active solar regions through ultraviolet polarimetry and spectroscopy. The polarization capability, along with other modifications, was added to an existing engineering model of the OSO-8 High Resolution Spectrometer.

The High Resolution Ultraviolet Spectrometer/Polarimeter is depicted in Figure 1. The polarimeter ( $\lambda$  wave plate) is shown enclosed by a heavy line.

This paper will deal specifically with the mechanical design, testing, and operation of the polarimeter for the HRUVSP.

#### DESIGN REQUIREMENTS

The design requirements of the polarimeter were established by the scientific optical objectives of the experiment. The polarization of the light is accomplished by a rotating magnesium fluoride quarter wave plate. The quarter wave plates are rotated in  $22\frac{1}{2}$ -degree steps about an axis coincidental with the light beam. As the light beam passes through the wave plate, the transformation that occurs can be expressed by mathematical equations. By having the wave plates calibrated, the data obtained from solar flares can be analyzed and meaningful information provided to the investigators. The polarimeter has two wave plates with different optical characteristics to provide both redundancy and versatility. A four-mirror polarizer was added behind one wave plate to provide additional polarization.

#### MECHANICAL DESIGN

The polarimeter mechanical design was required to provide three positions for the wave plates: either one of the wave plates in the light path or both wave plates out of the light path. When the wave plate is in the light path, rotation in  $22\frac{1}{2}$ -degree steps is necessary. To provide the quality of data

required, the centerline of rotation of the wave plates was not to be over 1.8 mm from centerline of the light path; and the deviation from the desired  $22\frac{1}{2}$ -degree rotation of the wave plates was to be less than  $\frac{1}{2}$  degree.

In addition to the above optical criteria, the design was required to:

1. Provide mechanical and electrical redundancy;
2. Have low electrical power usage;
3. Maintain cleanliness for wave plates and other optics in the experiment;
4. Fit into an existing cavity (12.7 cm wide x 11.4 cm long x 8.9 cm high);
5. Operate intermittently for one year in space; and
6. Provide a data feedback system to indicate wave plate position and rotation.

#### DESCRIPTION

The polarimeter is shown in artist's conception in Figures 2 and 3.

#### WAVE PLATE ROTATION SYSTEM

The quarter wave plates are two layers of magnesium fluoride optically bonded together to a total thickness of .600 mm and an open diameter of 7.0 mm. The plates are fragile and cannot be easily handled alone. A structural holding ring was designed to provide a safe method of handling and a means of securing the wave plates into the barrel assembly. The complete wave plate-holding ring assembly is shown in Figure 4. The holding ring was made of a non-outgassing plastic material .051 mm thicker than the recess in the barrel. This additional thickness insured that the quarter wave plates were securely held, and vibration would not cause the plates to move. After initial installation and rotational alignment of the wave plates, the plastic holding rings and keeper rings were drilled for installation of an alignment pin so the wave plate assemblies could be removed and reinstalled precisely.

The limited volume available to house the polarimeter dictated the use of small stepper motors (Figure 5). The available running torque of 44.6 cm-gm (.62 oz-in) and precision optical alignment requirements made a precision gear mesh, low friction system mandatory. Four motors, as depicted by Figure 5, were used in the polarimeter.

Each of the two wave plate rotation systems consisted of a stepper motor driving through a 96 pitch, 31 tooth spur gear pinned to its shaft and the barrel assembly (Figure 4) with a 96 pitch, 124 tooth spur gear. Both barrel assemblies and their respective drive motors were held by a single machined aluminum housing. This housing gave the best opportunity for maintaining the tolerances required for proper gear tooth operation and also for maintaining the alignment required for the optics. This design approach required close tolerancing and precision machining operations; but because of the limited volume available for the polarimeter, there was no space available for adjustments if separate assemblies had been used.

The wave plates had to be rotated (one direction only) in  $22\frac{1}{2}$ -degree steps at 7.8 steps/second with data being taken while the wave plates were at rest. It was required that the plates complete one rotation every two seconds. The step pulse width of the wave plate rotation motor was 23 milliseconds, and oscillation of the plate was to be less than  $\frac{1}{2}$  degree after 20 milliseconds. The usual procedure of sending a pulse to the motors and allowing the friction to damp out the oscillations of the wave plate required too much of the time allocated for each step. A special control circuit was designed so that after the motor steps the motor windings were shorted to make use of viscous damping caused by the generated EMF. This gave two improvements to the design: it shortened the step-oscillation time and also gave a more repeatable positioning of the wave plates. During design of the barrel assembly, the inertia was kept as low as possible to help in the damping of the oscillations and to decrease the time to step the wave plates. During assembly of the barrel assembly into the machined housing, care was taken to have the minimum preload possible on rotational bearings to give stability but have minimum friction possible.

#### WAVE PLATE POSITIONING SYSTEM

As indicated previously, the wave plate positioning system has three positions: wave plate "A" in the light path, both wave plates out of the light path, and wave plate "B" in the light path. The insertion-retraction system is capable of placing either wave plate into or out of the light beam.

The system has two stepper motors (Figure 5) identical to the wave plate rotation motors, both driving through a 31 tooth spur gear to a 124 tooth spur gear. One stepper motor is fixed to the support plate, the other is movable about the worm gear (Figures 2 and 3). For the movable motor to operate, the worm gear and supporting shaft are held fixed by the magnetic detent of the stepper motor and the non-backdrive characteristic of a single thread worm. The movable motor is pulsed 140 steps at a rate of 15.625 steps/second and, through a 280:1 total gear reduction (4:1 spur gear, 70:1 worm gear), the movable motor and worm move  $\pm 45^\circ$  around the worm gear. Depending upon motor rotation direction, either wave plate will be placed into the light path. The outer assembly rotates about the supporting shaft on four bearings. For the fixed motor to operate, the outer rotational assembly was fixed to the worm gear; and the fixed motor rotated the worm gear, supporting

shaft, and rotational assembly as a unit. The supporting shaft rotated in bearings in the support posts at either end of the shaft.

This arrangement had the advantage of mechanical redundancy (either motor could place either wave plate into the light path without having to backdrive the other; and completely separate sets of bearings were provided for each mode of operation) without having to have a differential in the drive system.

The method of operation of the insertion-retraction motors was to select either motor for operation, designate direction of rotation, and the electronics would send 140 pulses at a rate of 15.6 steps/second to the designated motor. This would place the selected wave plate into the light path. A feedback system, to be discussed later, would then send a signal to indicate the wave plate was in the proper position. The signal also served as a redundant cutoff in case of electronic malfunction, and more than 140 step commands were given.

The insertion-retraction motors (IRM) did not have the non-oscillating requirements of the wave plate rotation motors, but more torque was required. Also the IRM was to be operated only a short period of time, so electrical power consumption was not as important a consideration. For these reasons a pulse width of .030 second was used. This gave more assurance that a step would not be missed, and the wave plates would be in position for data taking.

Both the wave plate rotational system and the insertion-retraction system had a method of position feedback (reference Figures 2 and 3). Each wave plate had rotational sensors that indicated once per revolution. The sensors were photodiodes and phototransistors. A hole was provided in the spur gear on the barrel assembly for the phototransistor to sense the light emitted by the photodiode. The photodiode is pulsed rather than powered constantly to provide additional electrical power savings. The insertion-retraction position sensors were required to provide a one motor step resolution so the wave plates could be positioned to within 1.8 mm (one step accuracy) about the optical light path. The position plate is fixed to the wave plate holder machining. It has one slot .2 mm wide in the center to correspond to the out of light path position. On each side of the position plate a sharp edge is used for reference. An edge was used as it allowed fitting at assembly to achieve the minimum possible deviation from the light path. The low light level of the photodiode and the small hole (.2 mm diameter) in the mask required the phototransistor be placed as close as possible to the photodiode.

#### LUBRICATION

The cleanliness requirements of the optics made the lubrication an important design consideration. Any coating of the optics due to outgassing would reduce the ultraviolet light throughput of the wave plates. Both gears and bearings were lightly loaded, but the bearings and spur gears of the wave plate rotational system had a possible  $6.3 \times 10^7$  cycle lifetime requirement.

Tests were conducted to compare low outgassing grease and also dry lubricant. It was found the grease contaminated the optics and could not be used. The dry lubricant was applied to all bearings and all spur gears. It was still necessary to shield the optics from line of sight relationship to the open spur gears to prevent any dry lubricant which might separate during operation from being deposited onto the optics.

The worm-worm gear interface was a special consideration. Dry lubrication was not considered satisfactory because of the sliding action of the gears. The worm gear was manufactured from polyimide so no lubrication would be required. An anti-backlash worm was considered, but because of the added friction and low torque available from the motors, it was not used.

#### PROBLEMS ENCOUNTERED DURING DEVELOPMENT TESTING

1. It was found that the insertion-retraction system would not operate consistently. The unit would operate satisfactorily one afternoon, then the next morning with the same electrical configuration the unit would not give consistent operation. After investigation it was found the polyimide worm gear was hygroscopic, and an increase of humidity over 50% would cause interference between the worm and worm wheel. The qualification unit was installed into a thermal-humidity chamber and tested for both temperature and humidity tolerance. It was found that within  $\pm 20^{\circ}$  C. (specified design temperatures) and below 30% relative humidity, no problems were encountered with the insertion-retraction system. Humidity in-flight will not be a problem.

2. The thickness of the dry lubricant applied to the spur gears was also a problem. The added thickness of the lubricant and the build-up of dry lubricant between the spur gear teeth caused binding between the spur gears. This problem was solved by brushing the spur gears with a soft wire brush and removing all dry lubricant except a thin film. Due to the light loading of the gears, no breakdown of the lubricant was experienced.

#### CONCLUSION

Three complete units of the polarimeter have been built, one prototype and two flight units. The prototype unit was used for development and qualification testing. One flight unit was delivered to GSFC in January of 1978 for integration into the flight experiment. The flight polarimeter has undergone system testing (vibration, vacuum, and optical alignment) and has met design requirements to this date.

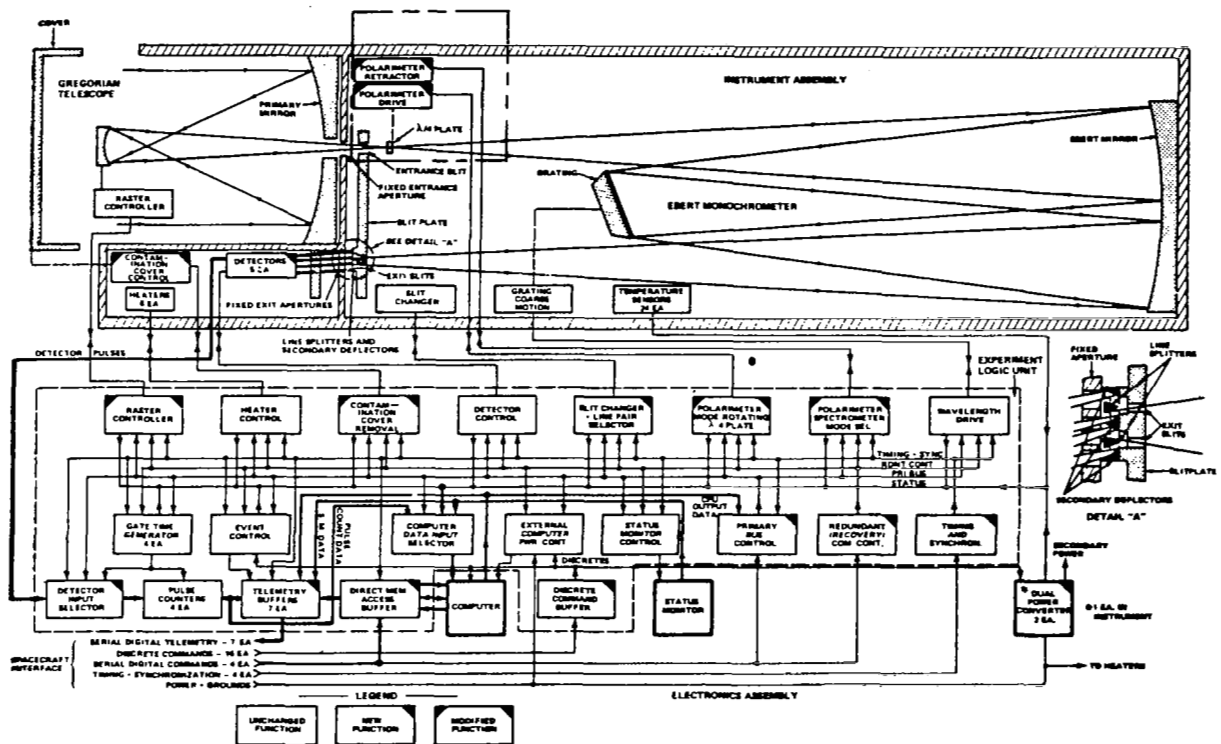


Figure 1.- Block diagrams of HRUVSP.

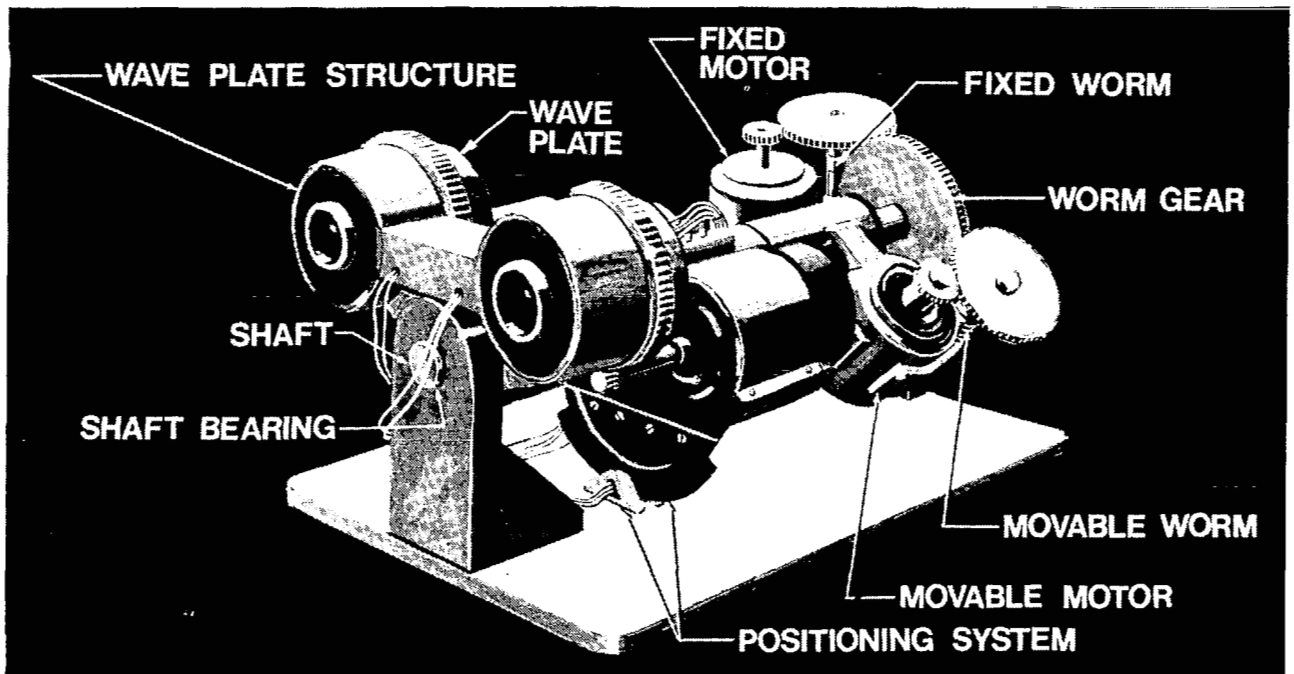


Figure 2.- Polarimeter, showing movable motor side.

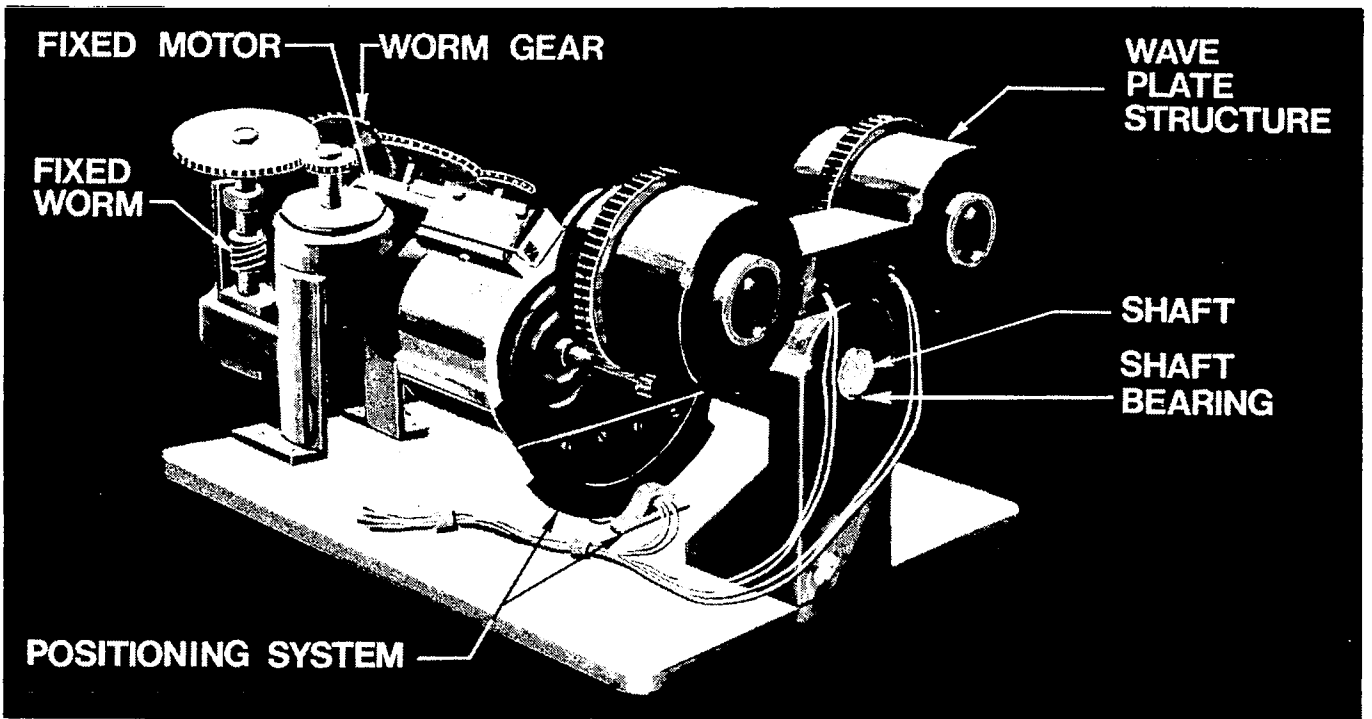


Figure 3.- Polarimeter, showing fixed motor side.

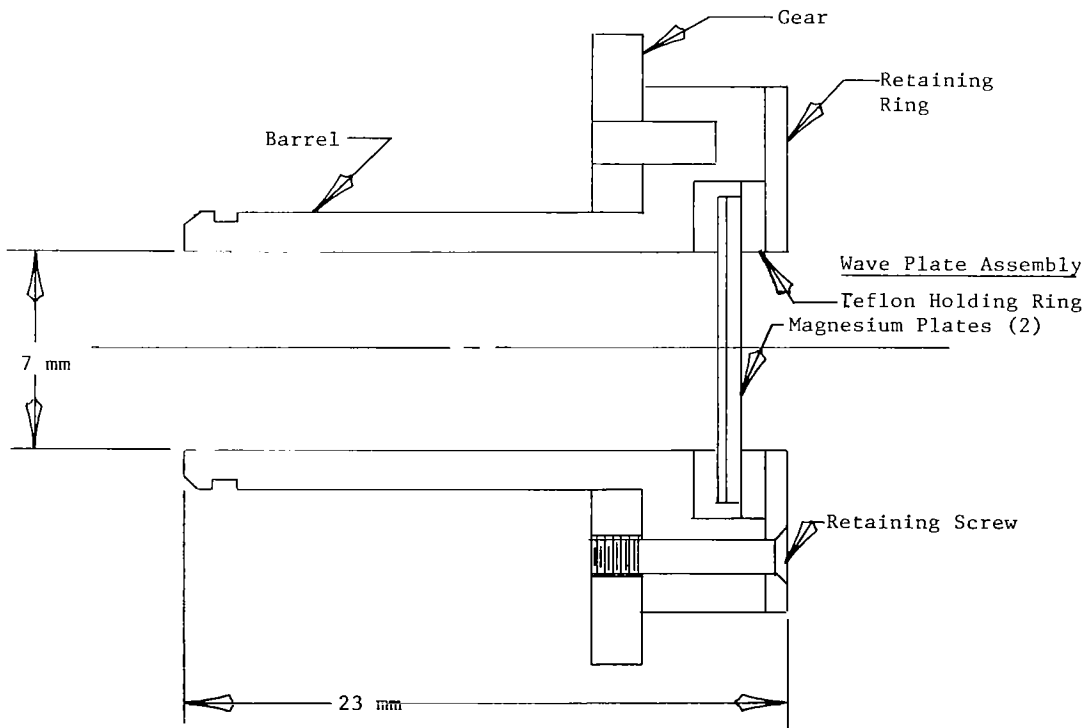
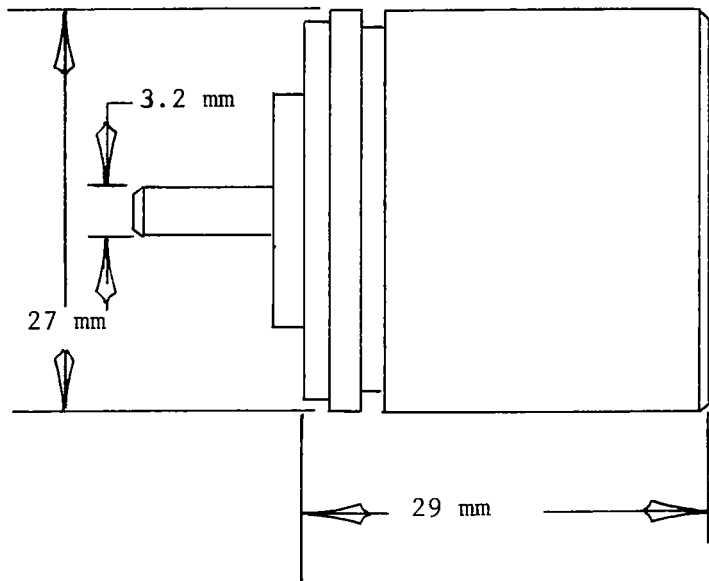


Figure 4.- Barrel assembly.



- (1) 90° Step Angle
- (2) 44.6 cm-gm Running Torque  
(.62 oz-in)
- (3) Weight 96 gm (3.4 oz)

Figure 5.- Stepper motor.

THE DESIGN AND APPLICATION OF AN ANTENNA POSITIONER MECHANISM  
FOR INTELSAT-V SERIES COMMUNICATION SATELLITE

Big Szeto  
Ford Aerospace and Communication Corporation  
Western Development Laboratories Division

SUMMARY

A two-axis Antenna Positioner Mechanism (APM) has been designed and qualified for use on the Intelsat-V series communication satellite. The APM will be used for positioning of Spot Beam Reflectors during the seven year mission.

INTRODUCTION

In operation, the East/West Spot Beam Reflectors on the Intelsat-V series communication satellite are required to satisfy; i) Initial precise-pointing to particular earth locations; ii) Repositioning and pointing to different earth locations as traffic changes dictate during the seven years mission.

Two 2-axis Antenna Positioner Mechanisms are utilized in fulfilling these requirements. The APM is specifically designed, developed and tested by Ford Aerospace and Communication Corporation, Western Development Laboratories Division (FACC).

The APM is comprised of three components which consist of one center pivot and two linear actuators rather than an integral two-axis gimbal design. The step resolution of the APM can be adjusted as required with the present design, at a step resolution of 0.002865 degrees.

In this paper, the design philosophy and considerations, test program and test results are discussed. Also, some major problems encountered during the course of testing along with their resolutions are detailed.

GENERAL DESCRIPTION

The APM which is shown in Figure 1 consists of three components which are:

- a. One Center Pivot: A passive universal joint device which is capable of movement about two orthogonal axes in the same plane.
- b. Two Linear Actuators: Two linear actuators are located at a distance of 25.4 cm (10 inches) and 90° apart from each other. Each actuator can be moved independently and linearly to provide rotary motion when coupled with the center pivot. The linear actuator consists of a stepper motor driving a jack-screw system which is supported by a pair of ABEC-7 ball bearings, ball joints at structure interface and reflector interface and a linear potentiometer for position telemetry.

The schematic arrangement of these components is illustrated in Figure 2.

The components of the APM are mounted to the same spacecraft structure at one end while the other interface is connected via the spot beam reflector to formulate the two-axis configuration. In operation, the actuators will be moved, one at a time, to locate the reflector at any location within the design constrained pattern. For this particular APM, the pattern is bounded within a square of 6.4 degrees which results in a square of 12.8° beam motion. The location of the reflector is fed back to ground via telemetry through the voltage readout of a linear potentiometer.

#### DESIGN PHILOSOPHY AND CONSIDERATION

The APM is designed, fabricated and tested to satisfy the primary and derived requirements as listed below:

- a. Operational during the 7 year mission time.
- b. Operational at extreme temperatures ranging between -85°C and +66°C with non-operating temperature ranging between -180°C and +100°C.
- c. Withstand high launch loads without detrimental effect on the performance.
- d. Minimum weight.

In the initial design stage, two design concepts were studied and traded off against each other. These two concepts were 1) APM and 2) Integral two-axis gimbals mechanism which utilized gear train to obtain high output torque. The APM concept was chosen because of the following reasons:

- a. Higher load capacity with same mass property.

- b. Simplicity in design.
- c. Simplicity in fabrication.
- d. Simplicity in assembly.

### Linear Actuator Design

The external actuator configuration is shown in Figure 1. The actuator consists of a stepper motor driving a power screw which is supported by a pair of ABEC-7 ball bearings. The power screw as it turns drives a mating nut up and down in a linear motion. Ball joints are utilized at reflector interface and structure interface to allow pivotal movements required for self-alignment. Solid lubrication, Molybdenum Disulfide, is used on the ball bearings, ball joints, screw-nut interface and other rubbing interfaces to provide low friction coefficient. The major design areas and considerations are described in the following paragraphs:

- a. **Driving Motor:** A stepper motor is used to provide driving motion. This motor provides more than three-to-one running torque margin over the operating temperature range; also, detent torque is provided to prevent any potential back driving in one "g" condition. This motor is a dual, separately wound permanent magnet motor to provide redundancy with a step size of 1.8 degrees. The stepper motor was chosen over a DC motor because of relative simple control electronics required. This motor is designed and built by American Electronics, Inc.
- b. **Linear Motion Area:** The heart of the linear motion is a jack screw principle. An ACME threaded power screw which is supported by a pair of ball bearings is connected to the motor's shaft, a mating power nut is moved in an up-and-down linear motion through a linear guide. For this particular design, a pitch of 0.254 cm (0.1 inch) is used. Thus, for each step of the motor, the linear movement is 0.00127 cm (0.0005 inch), with a corresponding angular motion of 0.002865 degree. The choice of the ACME threaded system over a ball screw system is based on; i) Lighter weight; ii) Less volume and iii) simplicity in design.
- c. **Self-aligning pivots** at the reflector interface and the structure interface are provided to allow rotary motion. Spherical bearings are used for this purpose.
- d. **Position Indication:** The approximate position of the reflector is fed back to telemetry by means of the voltage readout of a linear potentiometer. This potentiometer has very high resolution with the linearity being  $\pm 0.35\%$ . It is designed and fabricated by Vernitech, a division of Vernitron Corporation.

- e. Lubrication Scheme: Because of extreme temperature requirements, especially at the cold end (-85°C operating, -180°C non-operating), solid lubrication is used throughout the actuator and preferred over liquid lubrication. Molybdenum Disulfide,  $\text{MOS}_2$ , is used.
- f. Materials Selection and Compatibility: The materials chosen for the actuator are based on; i) Light weight; ii) High strength and iii) Similar thermal expansion coefficients. Titanium Alloy, Ti-6 AL-4V, is used for main structure, with 440C stainless steel for bearing materials and 17-4 PH stainless steel for other interfacing parts with Titanium.

#### Center Pivot

The center pivot external configuration is shown in Figure 1. The center pivot is a passive two-orthogonal-axis gimbal. Each axis of movement is supported by two spherical bearings which are lubricated with  $\text{MOS}_2$ . The usage of spherical bearings over ball bearings and roller bearings is because of compact size yet very high load carrying capability.

#### QUALIFICATION ENVIRONMENTS AND TEST PROGRAM

##### Qualification Environment

The APM was designed to withstand the following qualification environments:

- a. Barometric Pressure: Between sea level and  $1 \times 10^{-10}$  torr.
- b. Random Vibration: 22.6 grms in three orthogonal axes, for 4 minutes per axis.
- c. Static Load: 170 Newton-Meter (1500 in-lb); 890 Newton (200 lbs).
- d. Temperatures: Operating: -85°C to +66°C  
Non-Operating: -180°C to +100°C

##### Qualification Test Program

The APM has been qualified by means of a qualification test program which included the following test sequence:

- a. Initial functional test.
- b. Random vibration - non-operating.
- c. Static load test - non-operating.
- d. Post vibration functional test.
- e. Thermal vacuum test.
- f. Final functional test.

The step resolution and potentiometer voltage resolution were tested in each functional test to detect any discrepancy.

## TEST RESULTS AND DISCUSSION

Typical results on step resolution and potentiometer voltage resolution for different test conditions are shown in Figures 3 and 4 respectively. The variations of these results are presented in Tables 1 and 2.

### Step Resolution

The measurement of step resolution is from the actual angle of movement which is obtained by making optical measurements. The results show that the change of the actual angle of movement at different environments is by no more than 3.7%. It indicates a well repeated movement of the APM at different environmental conditions.

### Potentiometer Voltage Resolution

The potentiometer voltage resolution as shown in Figure 4 and Table 2 shows a greater variation than the actual step resolution. The maximum variation at different environments is 13.5%. This high variation is attributed to the induced misalignment within the potentiometer due to the assembly which creates non-uniform friction at different conditions. This result indicates that the voltage output per step should be used as a guide and approximation only. For precise usage of the potentiometer voltage output, calibration during the ground test is incorporated. A better indication of the utilization of the potentiometer is also tested as hysteresis and repeatability as described below in the other test results.

## Other Test Results

Other measurements have been performed on the APM. A few of these results are described here:

- a. Repeatability and Hysteresis: This test is to measure the angle repeatability of the APM using the potentiometer voltage as reference. The actuator is initially set at nominal location with the voltage and angle as a reference. The actuator is then moved the whole operating range in an upward or downward direction and returned to the original voltage reading. The actual angle is measured and compared to the reference angle with the angle difference being repeatability and hysteresis. The maximum deviation has been found to be within 1.5 arc minutes.
- b. Backlash: This measurement is to find the inherent backlash of the APM when reversing the direction of movement. The maximum has been found to be 1.7 arc minutes.
- c. Motor Redundant Operation: Motor redundant operation has been performed satisfactorily under different environmental conditions.
- d. Weight: Weight of the APM is measured to be 3.45 Kilograms.

## PROBLEMS AND RESOLUTIONS

In the course of testing, two major problems surfaced which required some redesign of the actuator and potentiometer. These problems and their resolutions are described below.

### Jamming Problem

After vibration, the linear actuator was found to be stuck at one particular location in the linear range which was away from the position during vibration. After extensive evaluation, the causes of the problem were determined to be:

- a. The surface finish at the rubbing interface between the power nut and linear guide was not smooth enough.

- b. The lubrication film was too thin.
- c. The rubbing interface between the power nut and linear guide was used both to constrain linear motion and provide dynamic load carrying capability.
- d. The material for power nut and linear guide was the same (Ti-6 AL-4V). Thus, when the lubrication film breaks down, galling action is introduced and jamming action occurs.

The resolutions of this problem were:

- a. Create a very smooth surface finish for the interface between the power nut and guide.
- b. Apply a much thicker lubrication film at the interface.
- c. Separate the load carrying function from the moving interface by creating a new load carrying interface.
- d. Change the material of the guide to stainless steel so that any potential galling effect is minimized.

With the incorporation of the above changes, the APM has successfully passed the qualification test.

#### Potentiometer Problem

After vibration, the potentiometer indicated an open circuit at the vibrated location even though the actual movement of the APM was normal when measured by an optical instrument. This problem has been diagnosed as:

- a. The material of the resistance substrate within the potentiometer was made of plastic material.
- b. This material was indented at the repeated hammering action by the wiper during vibration and open circuit at this location is created.

This open circuit problem was solved by replacing the plastic substrate with ceramic material.

#### CONCLUSIONS

The two axis Antenna Positioner Mechanism (APM) has been successfully qualified for use to precisely position the spot beam reflectors on the



Intelsat-V series communication satellite.

The APM has been tested under extreme dynamic and environmental conditions and the results indicate good correlation between the actual data and the design analyses.

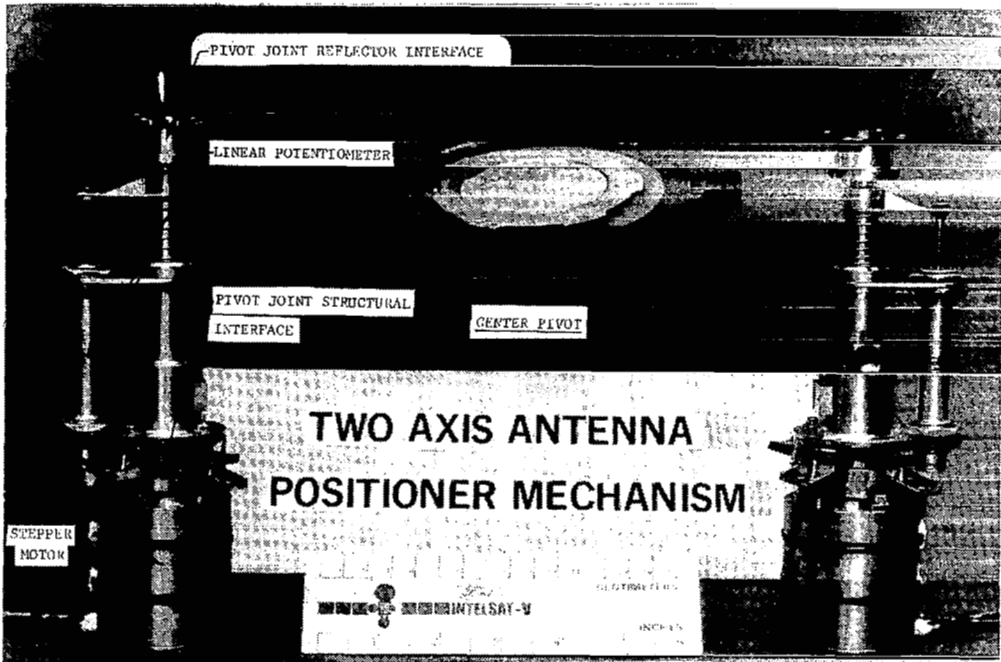
The APM has been designed and developed for this particular application. However, this APM can be used for other applications as well, such as one axis motion. Higher and lower step resolution can be obtained by adjusting the corresponding distance. With the same design, the measurement accuracy can be increased by tightening controls on the tolerances of the parts.

TABLE 1 - VARIATION IN STEP RESOLUTION

Description	Variation
Maximum variation in same functional test.	5.3%
Maximum variation in the same location.	3.7%
Maximum variation from theoretical value.	+1.7%
	-3.6%

TABLE 2 - VARIATION IN POTENTIOMETER VOLTAGE RESOLUTION

Description	Variation
Maximum variation in same functional test.	17.7%
Maximum variation in the same location.	13.5%
Maximum variation from theoretical value.	+11.3%
	-11%



Linear actuator #1

Linear actuator #2

Figure 1.- Two-axis antenna positioner mechanism.

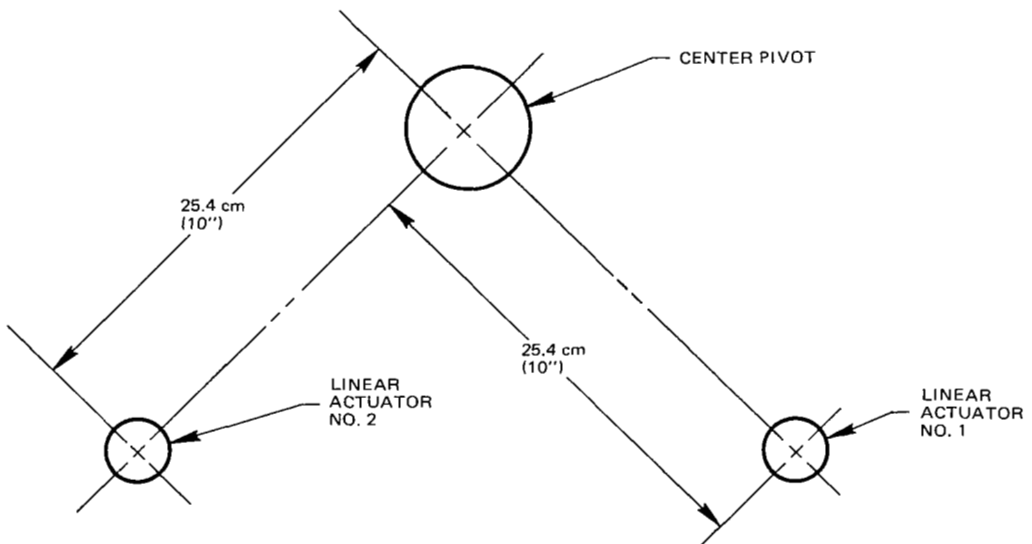


Figure 2.- APM schematic arrangement.

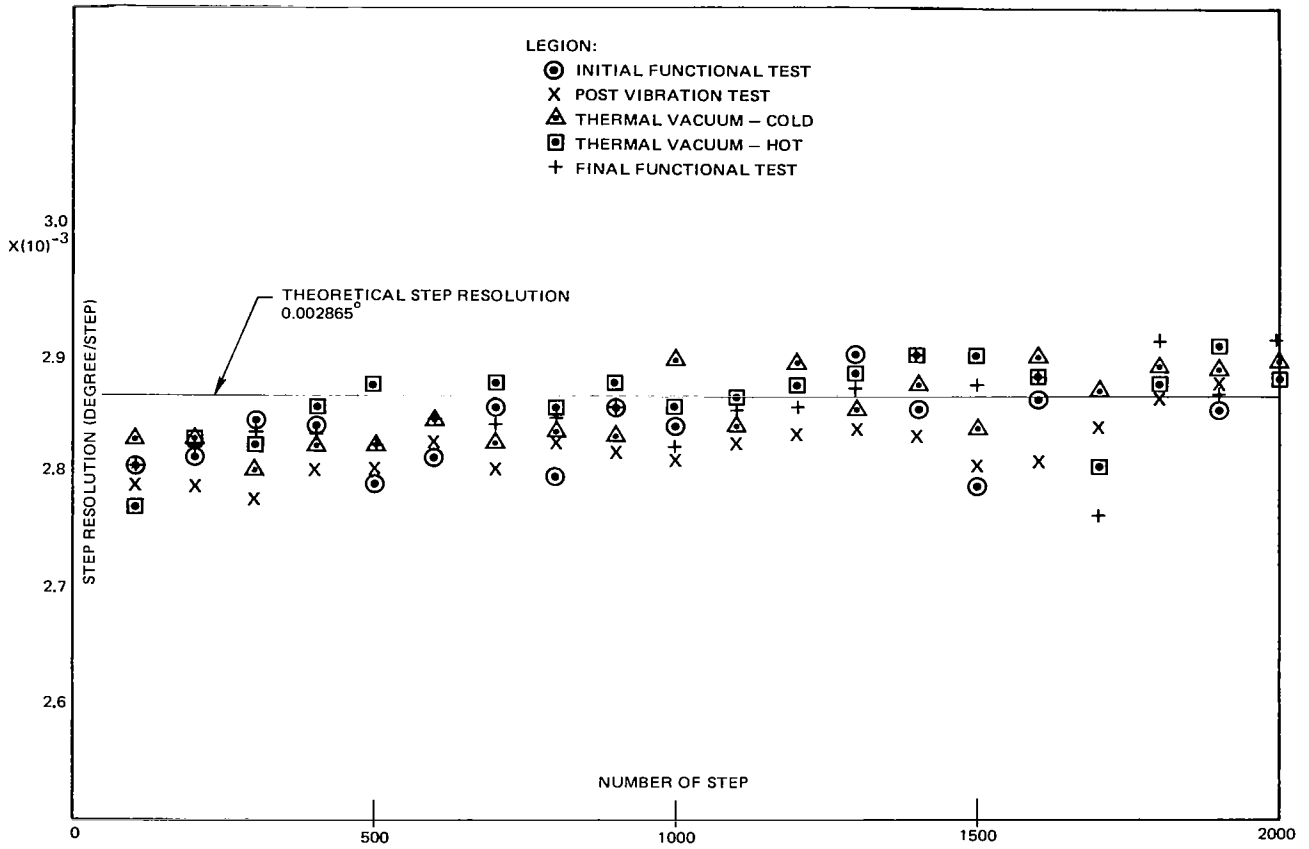


Figure 3.- Step resolution.

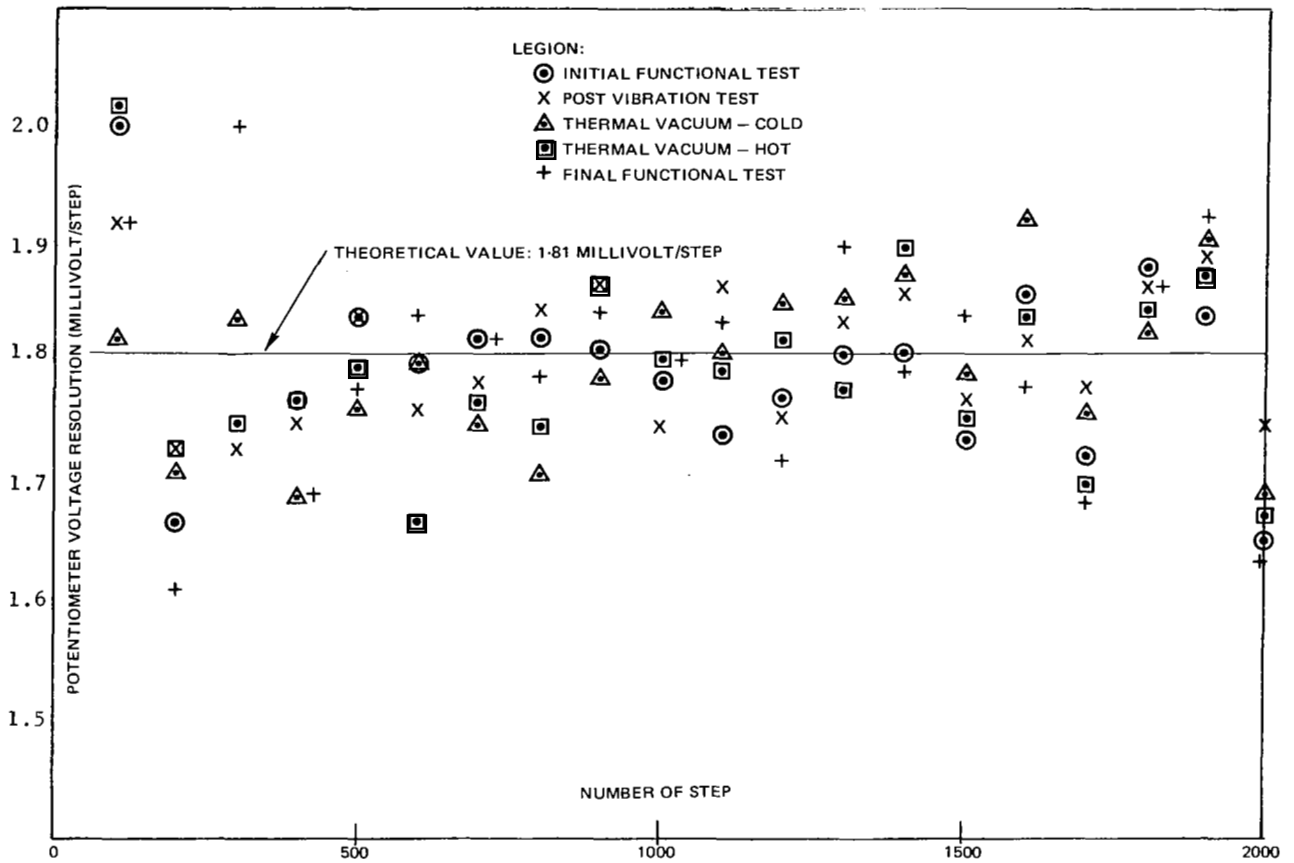


Figure 4.- Potentiometer voltage resolution.

THE MECHANISMS OF THE SAMS EXPERIMENT FLOWN ON NIMBUS 7  
WITH PARTICULAR REFERENCE TO THE 2 AXIS SCANNING MIRROR

H. Hadley  
Rutherford and Appleton Laboratories  
Science Research Council U.K.

SUMMARY

The Stratospheric and Mesospheric Sounder (SAMS) experiment on Nimbus 7 which was launched in October 1978 includes a 2 axis scanning mirror and 7 pressure modulator cells. The SAMS experiment is a limb sounding instrument to measure the temperature profile and minor constituents of the atmosphere. The limb scan requires small mirror steps over a  $3^\circ$  range, while the scan in azimuth is in larger steps over a  $15^\circ$  range. The mirror is plane, 20 cm in diameter, and of zero expansion glass-ceramic. It is supported on two tilt tables, fitted one on the other, with the axes at right angles. The angle of tilt is adjusted by means of recirculating ball screws which are ion plated with lead for lubrication and driven by stepper motors.

The seven gas filled cells are each pressure modulated by a 3 cm diameter, 0.3 cm stroke piston which is supported by diaphragm springs and driven electromagnetically at the system's mechanical resonant frequency. The mean pressure of the filling gas, which is the atmospheric constituent being measured, is changed by varying the temperature of a suitable molecular sieve.

INTRODUCTION

This paper describes the mechanisms of an infrared radiometer called the Stratospheric and Mesospheric Sounder (SAMS), which is flying in Nimbus 7 and which was devised by the Department of Atmospheric Physics - Oxford University under Professor J. T. Houghton. It is a development from the Nimbus 6 Pressure Modulated Radiometer which is described in a companion paper (Ref. 1). The Rutherford Laboratory of the Science Research Council provided the engineering design, the mechanisms and the management for this project. The sensor housing and electronics unit was made by British Aerospace (Dynamics Group).

The pressure modulator technique, more correctly called gas correlation spectroscopy, uses cells filled with  $\text{CO}_2$  for the temperature measurement, based upon the known distribution of  $\text{CO}_2$  in the atmosphere. With the temperature accurately known, other cells filled with gases which are constituents of the atmosphere and stable under pressure modulation will provide a signal which is related to their presence in the atmosphere. This leads the way to a further family of instruments to measure the ozone chemistry of the atmosphere, water vapour, methane and various pollutants such as carbon monoxide.

To obtain the highest resolution, the sounding instrument should look through the limb of the atmosphere to deep space, (i.e., parallel to the horizon) so that the path length is very long and the slice thickness being observed is as thin as possible. The SAMS instrument does this and has 7 pressure modulator cells filled with 6 different constituents. (See Fig. 1 and Ref. 2).

#### THE SAMS SCANNING REQUIREMENT

To scan the limb of the atmosphere from a satellite at a height of 1000 km, a path length of 3700 km to the tangent is required. A 10 km slice of the atmosphere requires a field of view of  $0.16^\circ$ , which is extended by a factor of 10 in azimuth. The limb scan step is half this, requiring a movement of the mirror of  $0.04^\circ$ . In total, a movement of  $1.5^\circ$  is required for complete cover of the atmosphere, including a view to space for calibration purposes. This movement is doubled to allow for uncertainties in the orbit and attitude achieved.

The limb scan must be normal to the direction of flight and therefore is greatly affected by the roll error and the roll rate of the spacecraft. The error is likely to be more than 3 times the step size specified. However, provided the roll rate is slow enough, the experiment itself, using its CO<sub>2</sub> reference channel, is able to measure the tangent height of its field of view to an accuracy of 0.1 km over the range 43 - 47 km, and is sufficiently accurate down to 30 km. If the scan is wholly outside this range then the roll rate determines how often the mirror is moved within this range and its position measured in order to make a check.

The scan in the azimuth direction is a doppler scan and image motion compensation of  $\pm 15^\circ$ , requiring a mirror motion of  $\pm 7.5^\circ$  over a period of 250 seconds. This motion must be very smooth and continuous or in steps at 2 second intervals between signal integrations, which makes the mechanism similar to that of the limb scan system. The step rate required is thus 125 steps, totalling  $15^\circ$  (i.e.,  $0.12^\circ/\text{step}$  with a flyback rate the fastest possible). When no doppler scan is commanded, only complete scans are required with the mirror facing the half way or zero position.

#### The SAMS Scanning Mirror

The scanning mirror is a "Zerodur" (similar to CER-VIT) glass-ceramic plane mirror 20 cm in diameter, 1.5 cm thick at its support ring and hollowed out at its rear face to weigh only 450 gm. The flatness tolerance requirement of 2 fringes (Na) per cm is not difficult to achieve. The support arrangement is 3 sectors of invar. Each is bolted with 3 screws and silicone rubber bushes to the inside of the mirror support ring and then moulded in place with silicone rubber, filling the 0.05 cm gap left for this purpose. The invar sectors carry 3 radial titanium pins ( $120^\circ$  spacing), each burnished with MoS<sub>2</sub> and clamped to a thick aluminium tube fitted with a small clearance inside the invar sectors, thus forming a kinematic mount. The curing of the silicone rubber distorts the flatness by one or two fringes per cm but the final assembly can be repolished before gold coating without any difficulty. The complete mirror weighs 600 gm.

## Scanning Mirror Mechanism

The two axis mirror mechanism consists of two tilting tables, one mounted on top of the other, with the main pivots at right angles to each other as shown in figures 2 and 3. The mirror carrier is an inverted triangular frame, top hung from two pivots at the corners and a jack screw at the lower apex. The stationary nut of the jack screw is flexibly coupled to the carrier and the screw is driven by a stepper motor, moving the nut along the screw and adjusting the tilt angle. The driving motor is connected to the screw via a single dog and is thus readily removable. The motor is supported by pivots to an intermediate frame which also supports the other half of the top hung pivots mentioned above. The limb scan moving assembly weighs 1.7 kg.

The intermediate frame, which is the top of the second tilt table, is supported by trunnions on one side, with the trunnion base fixed to the radiometer housing. The other side of the frame supports the nut of the second jack screw, while the driving motor is supported from the structure in a similar manner to that of the limb scan, thus providing the azimuth or doppler scan. The weight of this moving assembly is 3.4 kg.

All the pivots used are Bendix Flexural Pivots Cantilever Series (crossed-leaf spring flexi-pivots), with the top hung and trunnion pivots being 1.59 cm (5/8 in.) dia., 100-kg zero deflection load units. For the limb scan loads and deflections, these units have a life of over  $10^7$  cycles and for the azimuth scan loads,  $2.5 \times 10^5$  cycles, which is many years at the duty cycle envisaged. The spring rate for the pair is 3 Nm/radian. The motor support pivots are 1.27 cm (1/2 in.) dia., 64-kg zero deflection load with 1.5 Nm/radian/pair. The nut pivots are 1.27 cm dia. 6.4-kg zero deflection load with 0.2 Nm/radian/pair. The latter were originally specified to be the same type as the motor pivots, but at the maximum azimuth angle the twisting load on the nut was sufficient to back drive the jack screw against the detent torque of the motor. The small load capacity of the nut pivots is not a problem since loads greater than 10 kg or so will cause the motor to back drive. All the 1.27 cm pivots were mounted in bushes arranged so that radial motion was limited to 0.01 cm. The main 1.59 cm dia. pivots were clamped at one end with a key at the other end and burnished with MoS<sub>2</sub>, which allowed axial motion with a PTFE thrust washer between the two housings. The key-ways were spark eroded into the thicker walls of the flexi-pivot. This design relieves the pivots of all axial loadings which would cause the spring leaves to buckle. In addition, pegs adjacent to the jack screws enter slots with clearances of 0.03 cm at the position chosen for the launch configuration. The pivots are assembled so that their zero deflection position occurs at this launch position, which is about 40% of maximum travel. Vibration testing for all prototype mechanisms was 20 g sine wave and 13.4 g rms random ( $0.09g^2/Hz$ ), with the sine wave level reduced to 6.7 g for the complete flight sensor unit but with the same random excitation level.

### Mirror Mechanism - Jack Screw and Nut

The limb scan step of  $0.04^\circ$  using the longest lever arm possible resulted in a step size of about 0.15 mm so that 8 steps from a  $45^\circ$  stepper motor would give a pitch of 1.25 mm (or 0.05 in). Ball screws are available for these

pitch dimensions, and also standard screw threads provide this pitch if nuts of self lubricating materials are used.

Tests were carried out on a ball screw with the screw shaft and nut burnished with MoS<sub>2</sub>, but this was not satisfactory. An ESRO report then available confirmed that it could not meet the lifetime required (reference 3). A number of self lubricating plastic materials were tested and the best results and the lowest torque were obtained using PB03 loaded with 47.5% PTFE by weight and 2.5% MoS<sub>2</sub> by weight. This material available from Yorkshire Chemicals is a loaded aromatic polybenzoxazole. This would work as a second choice using two half nuts, spring loaded, with due allowance for wear and thermal expansion compared to stainless steel.

The solution adopted was to use 1.25 mm pitch ball screws (type ED513/V501 from RMB Switzerland), which use two half nuts in a housing, each with 1½ tracks of 1 mm stainless steel balls (440 C). The half nuts are machined from beryllium copper (hardness Rockwell C39-44) since they cannot have their tracks ground. Each half can be rotated and locked against the other to reduce backlash to a specified value. The shaft is stainless steel (440) and is lead coated to provide long life lubrication. The disadvantage of lead coating is that all testing must be done either in vacuum or with a dry nitrogen purge, since in air oxidation occurs. For each axis of the scanning mirror a cumulative maximum total of 1 hour use in air for setting up and adjustment checks was allowed.

Lead lubrication of ball races for space use is well established using electroplating or vacuum deposition of lead onto the raceways (ref. 4) so ESTL (European Space Tribology Laboratory) was asked if they could apply their ion plating technique to the ball screw to give a coating of lead 0.3 to 0.6 µm thick to the screw thread. We were considering coating the nut as well as the screw, but the nut material (Berylco 33-25) is a good bearing material. Also reference to some other development work then being completed in the UK (ref. 5) showed that the torque is increased by about a factor of two with the nut and screw plated compared with the screw only.

The ion plating process at ESTL Risley uses oil free vacuum pumps and gives a final clean to the screw by ion bombardment for a period of 30 mins followed by lead evaporation for 1 minute. The throwing power of the method is high because the plating is done at a pressure of ≈1Pa(≈7.6µm Hg) of argon. With the screw in a horizontal position under the electrode, it was found that due to gas scattering the thickness limits specified could be achieved without the necessity of rotating the screw into a second 180° position. Dummy shafts were coated to establish the optimum ion current, times and accelerating potential, while electron probe analysis provided the thickness measurements. If the design had been able to allow a 1.5 cm length of screw which was not travelled by the nut when in service, it would have been possible to coat an assembled ball screw unit with the nut moved to the unused portion and masked off. In our case the shaft and nut had to be returned to RMB in Switzerland for reassembly.

After reassembly the ball screws felt lumpy, rough and 'gritty' with peak torque figures of 2.8 mNm (28 gcm) and minimum figures of 0.2 mNm (2 gcm).

After running in air slowly for 10 complete travels of the nut up and down the screw in an unloaded condition, the torques were reduced to an average of less than 0.4 Nm (4 gcm) with peaks reduced by at least 2 but with little difference in the actual 'feel' of the assemblies. Some black powder (no doubt lead and lead oxide) could then be seen on the screw. All work was done under Class 100 clean conditions, and it is a fault in the design that space did not allow the ball screws to operate inside of bellows or telescopic tubes since it is a prime design requirement to protect the ball screw from external contamination and from wear debris from the bearing assemblies. Unfortunately one unit was damaged after initial use by being jammed by a sliver of 'Solithane' compound used to lock access panel screws, and the unit allocated to a life test program was installed in its place.

These ball screws can be supplied with backlash as little as 2  $\mu\text{m}$ . For the above use the backlash specified was 10  $\mu\text{m}$  since the spring loading of the main flexi-pivots over the limb scan range, where it mattered, was all in one direction to take up any clearance. This provided repeatability of each step position. The 3<sup>o</sup> limb scan movement required from this ball screw was extended by a further 2<sup>o</sup> so that a quasi-vertical earth view position (actually 70<sup>o</sup> to the local earth vertical) could be selected. This is a single commanded position and no scanning is required over this additional movement.

#### Stepper Motor

The requirement for the stepper motor is: 45<sup>o</sup> per step; running torque at 40 steps per second 0.085 Nm (1.2 oz in) min; stall torque 0.127 Nm (1.8 oz in) min; zero input detent torque from permanent magnet rotor at least 0.02Nm (0.3 oz in) to resist flexi-pivot loads plus normal gravity loads during all test orientations. The rotor inertia plus the ball screw inertia is the major component of the accelerating torque, and motors are available with rotor inertias of less than 1.2 gm cm<sup>2</sup>. The above ratings are based upon a 24 volt 4 phase system. The mirror must be able to step at least 4 limb steps (i.e., half a rev of the screw) in 175 ms including settling time.

Two motors met these requirements and were tested, but the more efficient motor of the two (65 ohms/phase compared to 30 ohms/phase) had a difference of about 3<sup>o</sup> between the energised and the non-energised detent positions, and this movement occurred at the end of the 175 ms period. The other motor was therefore used (IMC 011-869) and supplied with 'BarTemp' bearings and spring washers to provide some preload and differential expansion take up. No axial load is carried by the motor because of the driving dogs coupling the shaft to the screw. Thrust of the screw is carried by a preloaded duplex 'BarTemp' bearing at the motor end of the screw.

#### Mirror Position Control

The position of the mirror is monitored in each axis by means of a linear variable differential transformer (LVDT) coupled alongside each ball screw. The maximum and minimum limits of travel are controlled by optotransducers with mechanical stops outside these limits. The limb LVDT is connected to a 14 bit triple-slope integration type analogue-to-digital converter and, when corrected against the LVDT's temperature coefficient, gives a system resolution

of  $7 \times 10^{-6}$  radians (1.5 arc secs) in mirror position (i.e., 1/100th of a step). The azimuth LVDT is a simpler system to give a resolution of  $2.5 \times 10^{-4}$  radians (1 arc min) independent of temperature over the range 10 to 20°C.

The scan is controlled in each axis by stored programs which can be loaded into a memory by ground control, and a back-up mode allows the mechanism to respond to single step relay commands. The program instructions are converted to "step and settle" pulses to the stepper motors under control of clock signals, and the limb motion can be set to any position within the 3° range or down to the earth view opto-controlled stop. Periodically (usually ten times per orbit), the mirror is driven to the other end of the scan for a space calibration and the drive is limited by the opto stop. Should any steps be lost, the control will reset correctly to this position. Full travel excursions are also introduced to even out the lead coating. Scans always commence at the end of the 1.8 second signal integration period, and if the number of steps is such that they exceed 0.2 seconds, then the data from the next period(s) is ignored. The block diagram for these controls is shown in figure 4 which is a schematic of the complete radiometer.

#### PRESSURE MODULATED CELLS

The SAMS radiometer incorporated 7 pressure modulator cells filled with 6 different gases operating with mean pressures up to 60 mbar. The design is a development of the Nimbus 6 PMR units. However, the higher pressures demand a more efficient drive system, so a moving coil with an internal ring permanent magnet not unlike a loud speaker drive unit is used. With the higher pressures, a smaller head path can be used so that compression ratios of up to 3 are obtainable. The pistons are 3 cm dia and a peak stroke of 0.3 cm is required. The drive shaft is supported by two beryllium copper diaphragm springs but the constant stress springs used before do not provide sufficient radial stiffness so that the reduction in radial width is limited to a ratio of 2:1 (max. to min.) and this, with a radial gap at the piston of 0.005 cm, allows the cells to operate normally for bench testing with the cylinder axis horizontal.

The pressure modulator assembly is shown in section in figure 5. An extension to the shaft that carries the piston and the coil is seen, which carries a soft iron slug. This extension passes into the end plate where it is surrounded with a coil system which constitutes a differential transformer position sensor. Oscillation is maintained at constant amplitude and at the resonant frequency, which varies from 25 Hz (evacuated) to 50 Hz (40 mbar pressure), by a control loop coupled to the position sensor. The loop can also be switched into a negative feedback mode to inhibit piston motion since up to three PMCs are in the same optical path to a single detector and only one is measured at a time. The mean gas pressure is again controlled by molecular sieve material with the thermostat settings controlled by the program control unit. Piston frequency is used to monitor cylinder pressure and is measured and telemetered to 1 part in 6000. The various gases used demanded extensive development to determine the choice of adhesives and materials that will not outgas, will not absorb, and will not corrode with the individual filling gas. Molecular sieve materials had to be found that with a volume of a few  $\text{cm}^3$  (2 to 6 gms) would give the pressures required

for the various gases within a temperature range of 30°C to 100°C. Finally, each assembled PMC has an extensive schedule of bakeout, vacuum pumping, leak testing and filling.

#### OTHER COMPONENTS

The other mechanisms included in this radiometer are a vibrating reed chopper driven by redundant pairs of piezo-electric ceramic plates and covering 10% of the view. A small black body target is switched into the focus of the primary optics by means of a 90° stepper motor (IMC 008-845) with a spring and powered return. The cooler door release latches are operated by rotary solenoids. The Sensor and electronics module weighs 26 kg and consumes 25 watts.

#### CONCLUSION

Nimbus 7 was launched on 24 October 1978 and now after 14 months the SAMS mechanisms are still operating faultlessly. The mirror was operated only in the limb scanning mode for the first six months and then the azimuth scan was operated for the first time apart from the centering operation after launch. The repeatability and precision of the mirror movement has exceeded our expectations and meets its specification more than adequately.

The limb scan has now executed over 30 million steps mostly over a 25% length of the ball screw. The use of ion-plated lead as a solid lubricant for use in space, particularly for recirculating ball screws or for ball races for rotation over small angles, has been proved satisfactory provided that occasional excursions to the maximum limits are made to even out the lead coating.

The use of crossed spring flexi-pivots has been demonstrated, but the design must incorporate mechanical stops to limit motion under launch and test conditions. Vibration loads at launch must be accurately predicted or the chosen pivots must be very conservatively rated, well within the manufacturers recommendations. The fatigue lifetime must be many times the experiment life required. It may be necessary to clamp the pivots during launch or otherwise off load any axial loads from the flexi-pivots.

#### REFERENCES

1. Hadley, H.: Mechanisms of UK Radiometers Flown on Nimbus 5 and 6 with Particular Reference to Bearings, Pivots and Lubrication. 14th Aerospace Mechanisms Symposium, NASA CP-2127, 1980. (Paper 10 of this compilation.)
2. Drummond, J.R.; Houghton, J.T.; Peskett, C.D.; Rodgers, C.D.; Wale, M.J.; Whitney, J.; & Williamson, E.J.: The Stratospheric & Mesospheric Sounder (SAMS) Experiment. The Nimbus 7 Users Guide NASA 139-174. Oct. 1978.
3. Lansdown, A.R.: Molybdenum Disulphide Lubrication. ESRO-CR402 (1974) and CR 764 (1976).

4. Harris, C.L.; et al: Life Test evaluation of Solid Film Lubricated ball bearings at  $10^{-10}$  torr. JASLE (Lubrication Engineering) 131-138 (1968).
5. Stewart, D.E.; & Bentall, R.H.: Procurement, Treatment & Evaluation of Recirculating Ball Screws for use in Vacuum. ESA. SP111 267-276 (1975).



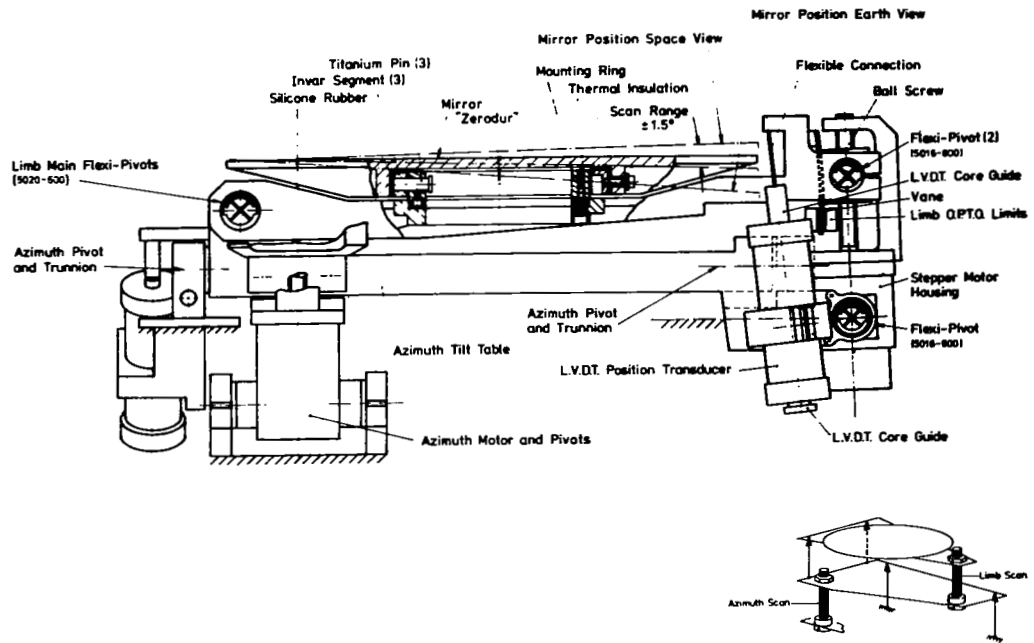


Figure 3(a).- Details of limb scan movement.

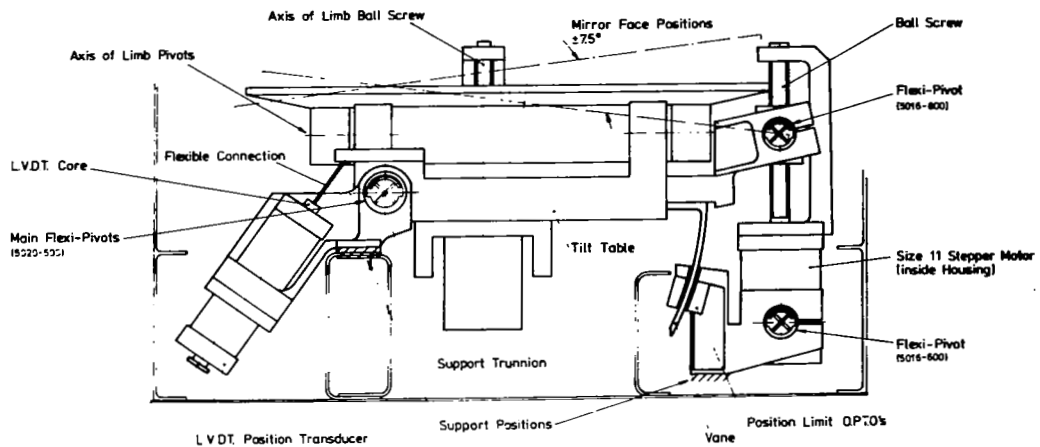


Figure 3(b).- Details of azimuth scan movement.

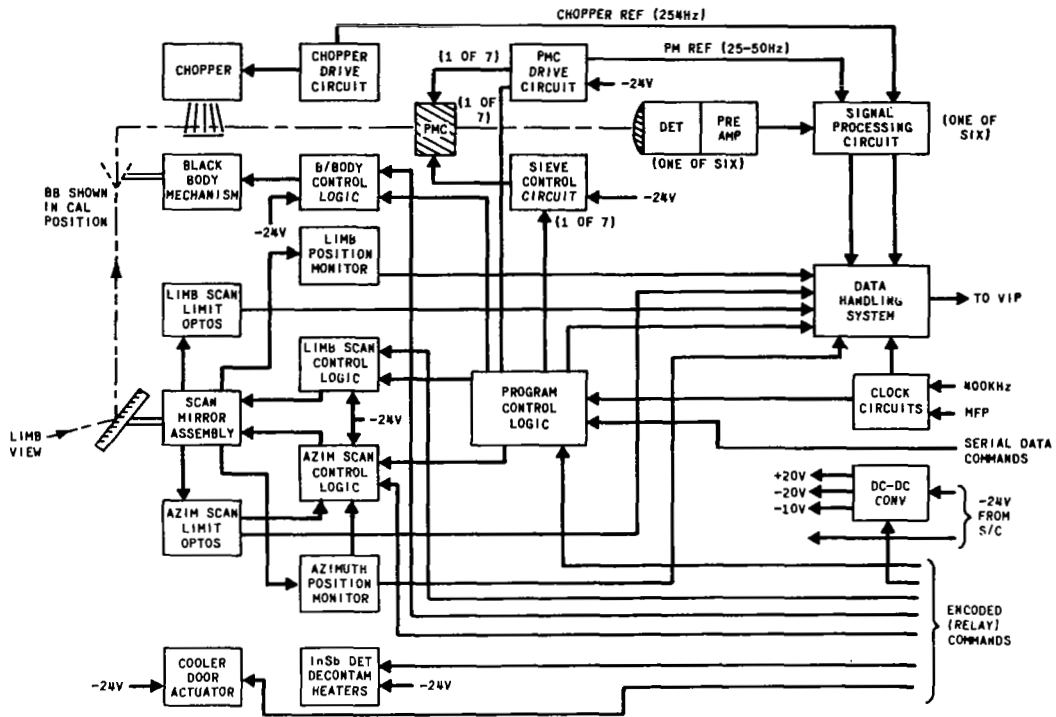


Figure 4.- Block schematic of SAMS radiometer.

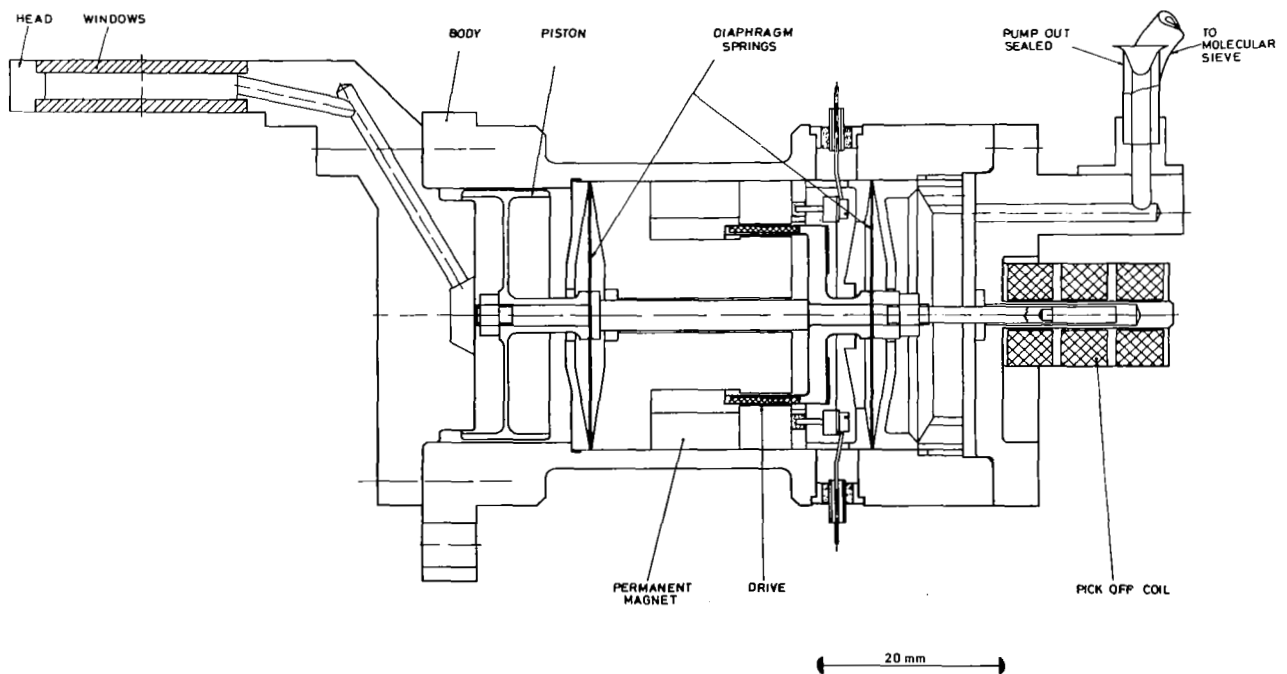


Figure 5.- Pressure modulating cylinder for SAMS.

1. Report No. <b>NASA CP-2127</b>		2. Government Accession No.		3. Recipient's Catalog No.	
4. Title and Subtitle <b>14th Aerospace Mechanisms Symposium</b>				5. Report Date <b>May 1980</b>	
				6. Performing Organization Code	
7. Author(s)				8. Performing Organization Report No. <b>L-13610</b>	
				10. Work Unit No.	
9. Performing Organization Name and Address <b>NASA Langley Research Center Hampton, VA 23665</b>				11. Contract or Grant No.	
				13. Type of Report and Period Covered <b>Conference Publication</b>	
12. Sponsoring Agency Name and Address <b>National Aeronautics and Space Administration Washington, DC 20546 and California Institute of Technology Pasadena, CA 91109 and Lockheed Missiles &amp; Space Company, Inc. Sunnyvale, CA 94088</b>				14. Sponsoring Agency Code	
15. Supplementary Notes					
16. Abstract <p>The proceedings of the 14th Aerospace Mechanisms Symposium held at the Langley Research Center on May 1-2, 1980, are reported in this NASA Conference Publication. Technological areas covered include aviation propulsion, aerodynamic devices, and crew safety; space vehicle propulsion, guidance, and control; spacecraft deployment, positioning, and pointing; spacecraft bearings, gimbals, and lubricants; and large space structures. Devices for payload deployment, payload retention, and crew EVA on the Space Shuttle Orbiter are also described. A new concept in actuation, described as the "Eccentuator," is presented. A novel fluid circulating pump for a solar collector is discussed, and the development of a unique actuated latch pin is described.</p>					
17. Key Words (Suggested by Author(s))			18. Distribution Statement		
<b>Actuators                      Emergency escape Latching devices              Circulating pump Deployment devices              Shuttle Orbiter Drive systems                    Valve Adapter                            Bearing gimbal Exhaust nozzle                   Thrust vector control</b>			<b>Unclassified - Unlimited</b>  <b>Subject Category 39</b>		
19. Security Classif. (of this report) <b>Unclassified</b>		20. Security Classif. (of this page) <b>Unclassified</b>		21. No. of Pages <b>339</b>	22. Price* <b>\$12.00</b>